FINITE-TIME STABILITY CRITERIA

FOR SUN-PERTURBED PLANETARY SATELLITES

by

Bonita Alice Steves

Thesis submitted

to the University of Glasgow

for the degree of Ph. D.

Department of Physics and Astronomy,
The University,
Glasgow G12 8QQ

December 1990

ProQuest LLC.
789 East Eisenhower Parkway
P.O. Box 1346
Ann Arbor, MI 48106 – 1346

For

Mom & Dad

and Pete

The Land of Beyond

Have ever you heard of the Land of Beyond,
That dreams at the gates of the day?
Alluring it lies at the skirts of the skies,
And ever so far away;
Alluring it calls: O ye the yoke galls,
And ye of the trail overfond,
With saddle and pack, by paddle and track,
Let's go to the Land of Beyond!

Have ever you stood where the silences brood,
And vast the horizons begin,
At the dawn of the day to behold far away
The goal you would strive for and win?
Yet ah! in the night when you gain to the height,
With the vast pool of heaven star-spawned,
Afar and agleam, like a valley of dream,
Still mocks you a Land of Beyond.

Thank God! there is always a Land of Beyond
For us who are true to the trail;
A vision to seek, a beckoning peak,
A fairness that never will fail;
A pride in our soul that mocks at a goal,
A manhood that irks at a bond,
And try how we will, unattainable still,
Behold it, our Land of Beyond!

by Robert Service

Acknowledgements

I would like to thank all the students and staff of the Astronomy Unit in the Department of Physics and Astronomy, University of Glasgow. Not only did I benefit from their enthusiasm for Astronomy, but the family atmosphere they created made me feel instantly at home in Scotland.

In particular, my special thanks go to my supervisor Professor Archie Roy. Over the years he has been many people to me: a respected teacher, an intriguing seeker of the unknown (psychic phenomena, stone circles, haunted houses, poltergeists, corn circles, you name it!), a fascinating storyteller and writer, a father away from home, an ever enthusiastic colleague at work, a wicked but trusted travelling companion in mischief and adventure, and above all a deeply cherished friend.

I have also learned many things of value to my research through discussions with Dr. Victor Szebehely, Dr. Andrea Milani, and Dr. Anna Nobili. I would particularly like to thank my colleagues, Dr. Giovanni Valsecchi and Dr. Ettore Perozzi, for the many enthusiastic hours spent together discussing and working on the fascinating mysteries of the Saros cycle. I would also like to thank Colin McInnes for his collaboration on the research found in Section 5.4.

Thanks go also to the University of Glasgow and to the Committee of Vice-Chancellors and Principals of the Universities of the United Kingdom for their financial support in the form of a University of Glasgow postgraduate award and an Overseas Research Students ORS award, respectively. Thanks also to CNR, Rome, Italy for inviting me and for making it financially possible for me to work with Dr. Giovanni Valsecchi and Dr. Ettore Perozzi at the Instituto di Astrofisica Spaziale, Reparto Planetologia, CNR.

This thesis is written for Anneke who always had faith in me and for my brothers, sisters and grandmothers whose company I missed constantly throughout my years away from home. It is written for my mother who never stopped listening to my incessant questions and who taught me the joy of searching for the answers. It is written for my father who showed me that nothing is impossible to learn or do, if you only set your mind to it. And finally, it is written for Pete who stuck with me and spent many hours proofreading this thesis despite all the frustrations created by my having to spend all my spare time writing up "the DREADED thesis"!

Bonnie Steves

December, 1990

CONTENTS

Summary

The inability of the c^2H stability criterion in the general three-body problem to guarantee Hill (or hierarchical) stability in the case of a planetary satellite perturbed by the Sun when the planet's orbital eccentricity is non-zero, leads to the search for a finite-time stability criterion applicable to such cases. Instead of looking for a stability criterion that guarantees stability for all time, a search is made for one which is valid for a finite length of time and which provides an estimate of that finite time.

The finite-time stability method involves applying a series of increasingly less pessimistic stability criteria that are each valid for finite lengths of time. The successive levels of the finite-time stability method are based on the natural periodic cycles found in the planet-satellite-Sun system. At each level the stability criteria method takes the most pessimistic viewpoint. Choosing the eccentricity to be the best indicator of an approaching unstable situation, it assumes that the worst possible change in the satellite's eccentricity over the specified cycle is added on to the satellite's eccentricity every period of that cycle. When the eccentricity accumulates to some arbitrarily chosen upper limit, the system is taken to be approaching an unstable situation. The time required for the eccentricity to reach this upper limit is then a measurable minimum lifetime for the satellite system.

The finite-time stability method is developed for both a circular and elliptical coplanar restricted three-body model of planet-satellite-Sun systems. Applications of the method to the main satellites of Jupiter, Saturn and Uranus produce minimum durations ranging from $1x10^6$ to $1x10^9$ years for Jupiter's satellites, $7x10^5$ to $1x10^{10}$ years for Saturn's satellites and $1x10^9$ to $9x10^{11}$ years for Uranus's satellites.

Extension of the finite-time stability method to include the elliptic coplanar restricted three-body model for planetary satellites, produces minimum durations that are similar to the equivalent results for the circular case, only slightly smaller. The failure of the c^2H criterion in the general three-body problem to guarantee the stability of any of the satellites found in the solar system when the eccentricity of the planet is included in the problem, suggests that the c^2H criterion is far too stringent a test for most of the real cases of interest in the solar system.

Application of the finite-time stability method failed to provide useful results for several highly Sun-perturbed outer satellites, such as the Earth's Moon, Jupiter's outer satellites and Saturn's Phoebe. In the case of the Earth's Moon, a search is made for a larger natural period which will produce more reasonable results.

A description is given of certain historically known cycles associated with high-number near commensurabilies among the synodic, anomalistic and nodical lunar months and the anomalistic year. In particular, the properties of the Saros cycle are studied. The Saros is a period of 6,585.32 days or approximately 18 years and 10 or 11 days, depending on the number of leap years in the interval. The Saros has been known since Babylonian times as the time that elapses between successive repetitions of a particular sequence or family of solar and lunar eclipses. It is a cycle formed by high-number commensurabilities between the synodic, anomalistic and nodical lunar months.

Using eclipse records and the JPL ephemeris, any dynamical configuration of the Earth-Moon-Sun system (within the framework of the main lunar problem) is shown to repeat itself closely after one Saros period. The role played by mirror configurations in reversing solar perturbations on the lunar orbit is examined and it is shown that the Earth-Moon-Sun system moves in a nearly periodic orbit of period equivalent to the Saros. The Saros cycle is therefore the logical base period to use in the application of the finite-time stability method to the lunar problem. The Saros cycle is also the natural averaging period of time by which solar perturbations can be most effectively removed in any search into the long term evolution of the lunar orbit.

The Saros cycle, with its ability to reverse solar perturbations, may have relevance to the stability of any system which contains a saros-like cycle. Since tidal evolution affects the periods which form the commensurabilites within the Saros cycle, the Moon's orbit may not have had in the past and possibly will not have in the future a saros-type cycle to cancel solar perturbations. Also studied therefore is the probability that a dynamical three-body system will contain a saros-like cycle (ie that a set of commensurabilities between the three periods can be found to within a given accuracy and with integer multiples of less than a given upper limit). Unfortunately, the Moon has only about a 25% chance of finding a saros-like cycle within its orbital dynamics. A possible sequence of saros cycles that the Moon's orbit might evolve through is calculated, if only tidal friction is considered.

Preface

The Mesopotamian seer could pick out five in all. All were important deities in the pantheon of the sky gods. And as such they wandered the sky at will, refusing to be confined by the laws and restrictions that governed mere mortals.

"The most brilliant was Venus - Ishtar, to the Babylonian seers - star of both morning and evening, who sometimes shone forth even when the sun was up. Since here brightness fluctuated in an enticing manner, she was seen as the goddess of youth, beauty and amorous love. But Ishtar was also known as the Lady of Battles and was depicted riding on a lion with a weapon in her hand. Jupiter was another intensely bright planet, whose regal and steadfast glow the seer associated with Marduk, king of gods. Marduk could unleash storms and cataclysms, but he was generally gracious, and he presaged worldly power and renown. Mars, on the other hand, with his red, malevolent light, was known as the war god Nergal, harbinger of death and destruction. The remote, slow-moving Saturn - Ninurta to the seer - reigned as the pale and flickering deity of time, old age, and scholarly pursuit. With a cycle around the heavens of almost thirty years' duration, Ninurta took the long view of things. His opposite in personality and effect was Mercury, or Nebu, as fast as quicksilver, whose darting path earned him a reputation for foxlike trickiness." (Time-Life Books, 1988, pp 16-17)

Their movements puzzled the seer. What was the meaning behind Nergal's sudden decision to reverse his path, linger in the vicinity of the King - the King being Regulus, the brightest star in Leo - and then return to his original course?

"The planets appeared to roam the sky at will, with no logical relationship to one another or to anything else. Mercury danced back and forth in the vicinity of the sun. Saturn might linger in a single constellation for years on end, as though chained in place. Sometimes a

> planet would march ahead in good order, then pause or even reverse itself and move backward. The seers referred to these whimsical orbs as *bibbus*, or wild goats - an oddly irreverent term for the gods of human destiny. But their movements were recorded meticulously . . ." (Time-Life Books, 1988, p 17).

Wild goats cavorting in the skies, powerful deities laying out the destinies of humankind or mere lumps of rock and gas moving under the influence of mysterious forces, the movements of the planets through the heavens have fascinated people from all ages.

Modern scientists now know that the planets do not actually suddenly reverse their courses. They only appear to do so when observed from the Earth. As early as the 18th century astronomers could even construct elegant analytical theories consisting of long strings of trigonometric terms describing the positions of the planets thousands of years into the past or present. But there were limits to these series. Poincaré proved in 1893 that in general such series are divergent.

The question remains: Will the present hierarchy of planets and satellites remain intact forever? More recently through the use of high-speed computers, attempts have been made to integrate directly the equations of motion of the planets over time intervals as long as 10^8 years. Unfortunately again, due this time to round-off error accumulation, the results beyond 10^8 years are meaningless.

Through various scientific means such as dating lunar samples and meteorites, the age of the solar system is at present thought to be approximately 4.5 to 5 $\times 10^9$ years. Fossils indicate that the Earth has been inhabited by complex life forms continuously for about 2×10^9 years, suggesting that the Sun's radiation and, by implication the Earth's orbital elements, have remained relatively unchanged for at least this period of time. Yet despite the knowledge gained through the use of geophysics and solar astrophysics on the age and stability of the solar system, the field of celestial mechanics is still unable to provide any definite statements on the dynamical age and long-term stability of the solar system.

The following work is an attempt to put a finite-time limit on the durations of planetary satellites perturbed by the Sun. Chapter 1 contains a description of the

present structure of the solar system and a review of the various means of studying the stability of the bodies found in the Solar System. A summary of the procedure and the restrictions used to find minimum durations of sun-perturbed planet-satellite systems is found in Chapter 2. This procedure requires the analytical derivation of the changes in the satellite's orbital elements over one synodic period for each three-body model studied.

Chapter 3 contains the above derivation for the case where the Sun is assumed to move in a fixed circular orbit about the planet, while perturbing the orbit of a coplanar planetary satellite of negligible mass. Chapter 4 contains the equivalent derivation for the case where the Sun is assumed to move in a fixed elliptical orbit about the planet, while perturbing the coplanar orbit of the same satellite of negligible mass.

In the first case, the model - the circular coplanar restricted three-body problem - has a hierarchical stability guarantee, based on the c^2H criterion, for most of the planet-satellite systems found within the Solar System. It is therefore used as a verification that our method is working well. In the second case, the c^2H criterion applied to the elliptic coplanar restricted three-body problem provides no guarantee of hierarchical stability for any of the Sun-perturbed planetary satellites in the Solar System.

Chapter 5 describes the increasingly less pessimistic levels of the finite-time stability method and gives the resulting minimum durations for the majority of the satellites of Jupiter, Saturn, Uranus and Mars.

Application of the finite-time stability method to the Earth's Moon, Jupiter's outer satellites and Saturn's Phoebe fails to give any useful results. Another larger natural period of the planet-satellite-Sun system besides the synodic period is required in order for the finite-time stability method to succeed with the above satellites. Such a possible period for the Earth's Moon called the Saros is studied in Chapter 6.

The Saros cycle appears to be able to reverse solar perturbations, resulting in the approximate return after one Saros period of the Moon to its original orbital position relative to that of the Sun's. It therefore becomes important to discover the effect that tidal evolution has on the existence of the Saros cycle. Also of interest is

the probability that another Saros-like cycle can be found by the Moon's orbit, if the present Saros cycle is disrupted. These questions are addressed in Chapter 7.

Chapter 8 describes possible lines of future research that follow from the studies completed in the previous chapters. Appendix A contains the statistical tables required for the statistical verification of the probability formulae derived in Sections 7.2 and 7.4.

Two papers which are partially formulated from research found in this thesis are included as supplementary material. The first paper (Roy and Steves, 1988) entitled "*A Finite-Time Stability Criterion for Sun-Perturbed Planetary Satellites*" consists of work based on Chapters 2 to 5, although the procedure and results found in the thesis have been refined since the publication of the paper. Paper 2 (Perozzi, Roy, Steves and Valsecchi, submitted to Celest. Mech. Oct. 1990) entitled "*Significant High Number Commensurabilities in the Main Lunar Problem* I. *The Saros as a Near-Periodicity of the Moon's Orbit*" constitutes work from Chapter 6, plus a description of the results of several new lines of research that are mentioned in Chapter 8.

The original work of this thesis is found in Chapters 2 through to 8. The work of Section 5.4 was partially explored with the help of Colin McInnes, a summer student working under a Carnegie Summer Studentship, while the research found in Chapters 6 and 7 was produced under the teamwork of Dr. Ettore Perozzi, Dr. Giovanni Valsecchi, Professor Archie Roy and myself over several visits to the CNR in Rome, Italy.

Parts of Chapters 2 to 5 are in preparation as an updated version of Paper 1, while Chapter 6 already forms the greater part of a paper entitled "*Significant High Number Commensurabilities in the Main Lunar Problem*" by Perozzi, Roy, Steves and Valsecchi, accepted for publication in Predictability, Stability and Chaos in N-Body Dynamical Systems (1991). The materials described in Chapter 7 and part of Chapter 8 should form the basis for two more papers entitled "*Significant High Number Commensurabilities in the Main Lunar Problem* II. *Saros-Like Cycles for Varied Lunar Orbits*" and "*A Postscript to a Discovery of the Ancient Chaldeans*" by the same authors.

CHAPTER 1

METHODS OF STUDYING THE STABILITY OF THE SOLAR SYSTEM

thesis

"I always take my ~~diary~~ with me on journeys, so that I have something sensational to read!"

A parody of Oscar Wilde

1.1 The Structure of the Solar System

The majority of the bodies found in the planetary and satellite systems of the Solar System move in nearly circular, nearly coplanar orbits that are well spaced. Of the nine planets which form the Solar System, the only exceptions to the above rule are Mercury with an eccentricity of ~ 0.21 and an inclination of ~7°, and Pluto with an eccentricity of ~0.25 and an inclination of ~17°. All the planets revolve in the same direction about the Sun. Most of them also rotate on their axes in this same direction. The only exceptions are Venus and Uranus, whose equatorial planes are inclined at ~177° and ~98° respectively to their orbits.

Most of the planetary orbits can be easily ordered in increasing size without any of the orbits having to cross each other. Thus, by definition the planetary system nearly forms a hierarchical dynamical system. Only the orbits of Neptune and Pluto intersect each other; however the large inclination of Pluto's orbit makes any close encounters of the two bodies unlikely. Also, numerical experiments suggest that there may be several dynamical mechanisms acting which serve to ensure that the two bodies are always far apart when one of the bodies approaches a possible close encounter point. Such mechanisms can involve near commensurabilites between the mean motions of the two bodies about their primary. Neptune and Pluto exhibit a 3:2 commensurability between their mean motions, while Jupiter and Saturn display a mean motion commensurability of 5:2. Table 1.1 lists the planets in order of increasing distance from the Sun, along with some of their basic orbital details.

With the advent of the discoveries of Voyagers 1 and 2, there are now known to be over fifty natural satellites in the Solar System. Table 1.2 lists the satellites that were known to exist as of 1988, along with the orbital data currently accepted at that time. The satellites are listed under their respective planets in order of increasing distance from their primary. The orbital data for both the satellites and the planets

are taken from the 1988 Nautical Almanac.

Planet	Mass Ratio μ	Eccentricity e_1	Inclination i (°)	Sidereal period T_1 (yrs)	Resonances n_{inner}/n_{outer}
Mercury	6.02×10^6	0.206	7.00	0.240845	
Venus	4.08×10^5	0.007	3.39	0.615197	
Earth	3.33×10^5	0.017	0.0	1.000019	
Mars	3.08×10^6	0.093	1.85	1.880850	
Jupiter	1.05×10^3	0.048	1.31	11.861976	5:2
Saturn	3.50×10^3	0.056	2.49	29.457090	
Uranus	2.28×10^4	0.047	0.77	84.011514	
Neptune	1.93×10^4	0.009	1.77	164.78993	3:2
Pluto	1.3×10^8?	0.250	17.17	247.681	

Table 1.1 Orbital data for the planets found in the Solar System.

The mass ratio is defined as the ratio of the mass of the Sun to that of the planet. The major resonances found amongst the planets are given in terms of the ratio of the mean motion of the inner planet to that of the outer planet.

The above data is taken from the 1988 Nautical Almanac.

The satellite systems are similar to the planetary system, except that they exhibit a wider range of eccentricities and inclinations. Most move prograde in nearly circular orbits within the equatorial plane of their primaries. These type of satellites are called 'regular' satellites. Only seven satellites: Triton, Charon, the four outermost satellites of Jupiter and Phoebe, the outermost satellite of Saturn move retrograde, ie in the opposite direction to the other satellites. Many scientists

Planet	Satellite		Orbital radius	Eccentricity	Inclination	Orbital period	Resonances
	No.	Name	$\alpha=a/a_1$	e	i (°)	(days)	n_{inner}/n_{outer}
Earth		Moon	2.571×10^{-3}	0.05490	18.28 -28.58	27.322	
Mars	M1	Phobos	4.117×10^{-5}	0.015	1.0	0.319	
	M2	Deimos	1.030×10^{-4}	0.0005	0.9-2.7	1.262	
Jupiter	J16	Metis	1.65×10^{-4}	?	?	0.295	
	J15	Adrastea	1.66×10^{-4}	?	?	0.298	S
	J5	Amalthea	2.326×10^{-4}	0.003	0.40	0.498	
	J14	Thebe	2.85×10^{-4}	0.015	0.8	0.675	
	J1	Io	5.424×10^{-4}	0.004	0.04	1.769	triple
	J2	Europa	8.625×10^{-4}	0.009	0.047	3.551	
	J3	Ganymede	1.375×10^{-3}	0.002	0.21	7.155	7:3
	J4	Callisto	2.420×10^{-3}	0.007	0.51	16.689	
	J13	Leda	1.426×10^{-2}	0.14762	26.07	238.72	
	J6	Himalia	1.476×10^{-2}	0.15798	27.63	250.566	
	J10	Lysithea	1.506×10^{-2}	0.107	29.02	259.22	
	J7	Elara	1.509×10^{-2}	0.20719	24.77	259.653	
	J12	Ananke	2.72×10^{-2}	0.16870	147	631	
	J11	Carme	2.90×10^{-2}	0.20678	164	692	
	J8	Pasiphae	3.02×10^{-2}	0.378	145	735	
	J9	Sinope	3.05×10^{-2}	0.275	153	758	

Continued ...

Planet	Satellite		Orbital radius	Eccentricity	Inclination	Orbital period	Resonances
	No.	Name	$\alpha=a/a_1$	e	i (°)	(days)	n_{inner}/n_{outer}
Saturn	S15	Atlas	9.654×10^{-5}	0.000	0.3	0.602	S
	S16	Prometheus	9.772×10^{-5}	0.003	0.0	0.613	S
	S17	Pandora	9.937×10^{-5}	0.004	0.0	0.629	S
	S10	Janus	1.062×10^{-4}	0.007	0.14	0.695	1:1 S
	S11	Epimetheus	1.062×10^{-4}	0.009	0.34	0.695	S
	S1	Mimas	1.301×10^{-4}	0.0202	1.53	0.942	2:1
	S2	Enceladus	1.669×10^{-4}	0.00452	0.00	1.370	2:1
	S3	Tethys	2.066×10^{-4}	0.00000	1.86	1.888	1:1
	S13	Telesto	2.066×10^{-4}	?	?	1.888	
	S14	Calypso	2.066×10^{-4}	?	?	1.888	
	S4	Dione	2.647×10^{-4}	0.00223	0.2	2.737	1:1
	S12	1980 S6	2.647×10^{-4}	0.005	0.0	2.737	
	S5	Rhea	3.696×10^{-4}	0.00100	0.35	4.518	
	S6	Titan	8.568×10^{-4}	0.029192	0.33	15.945	4:3
	S7	Hyperion	1.039×10^{-3}	0.104	0.43	21.277	
	S8	Iapetus	2.497×10^{-3}	0.02828	14.72	79.330	
	S9	Phoebe	9.083×10^{-3}	0.16326	177.°	550.48	
Uranus		1986 U7	1.735×10^{-5}	<0.001	?	0.335	
		1986 U8	1.876×10^{-5}	0.01	?	0.376	
		1986 U9	2.063×10^{-5}	<0.001	?	0.435	
		1986 U3	2.154×10^{-5}	<0.001	?	0.464	
		1986 U6	2.185×10^{-5}	<0.001	?	0.474	
		1986 U2	2.244×10^{-5}	<0.001	?	0.493	
		1986 U1	2.304×10^{-5}	<0.001	?	0.513	
		1986 U4	2.439×10^{-5}	<0.001	?	0.558	
		1986 U5	2.624×10^{-5}	<0.001	?	0.624	
		1985 U1	2.999×10^{-5}	<0.001	?	0.762	
	U5	Miranda	4.512×10^{-5}	0.0027	4.2	1.413	triple
	U1	Ariel	6.660×10^{-5}	0.0034	0.3	2.520	
	U2	Umbriel	9.285×10^{-5}	0.0050	0.36	4.144	
	U3	Titania	1.520×10^{-4}	0.0022	0.14	8.706	
	U4	Oberon	2.035×10^{-4}	0.0008	0.10	13.463	

Continued ...

Planet	Satellite		Orbital radius $\alpha=a/a_1$	Eccentricity e	Inclination i (°)	Orbital period (days)	Resonances n_{inner}/n_{outer}
	No.	Name					
Neptune	N1	Triton	7.884×10^{-5}	<0.01	159.00	5.877	
	N2	Nereid	1.226×10^{-3}	0.7483	27.6**	360.2	
Pluto	P1	Charon	3.34×10^{-6}	?	94.**	6.387	

Table 1.2 Orbital data for the satellites found in the Solar System.

The satellite orbital radius is given in terms of the ratio between the semi-major axis of the satellite 'a' and its primary a_1. Except where noted, the satellites' orbital inclinations are measured with respect to their planetary equators.

The major resonances found amongst the satellites are given in terms of the ratio between the mean motions about their primary of the inner satellite n_{inner} to that of the outer satellite n_{outer}.

The following are the triple resonances:

(1) $n_I - 3n_E + 2n_G \approx 0$

where I=Io, E=Enceladus, G=Ganymede and n denotes the mean motions of the satellites.

(2) $n_M - 3n_A + 2n_U \approx 0$

where M=Miranda, A=Ariel, U=Umbriel

'S' in the last column denotes a shepherd satellite in resonance with the boundary of a ring.

The above data is taken from the 1988 Nautical Almanac.

* Measured relative to the ecliptic plane.

** Measured relative to the equator of 1950.0.

believe that the outermost retrograde satellites are actually captured asteroids and are therefore not part of the original satellite system which presumably evolved together. See Kuiper (1956), Bailey (1971) and Heppenheimer (1975).

The Moon is sometimes considered to be one of the irregular satellites because it has an anomalously high mass ratio to that of the Earth.

The two satellites of Mars: Phobos and Deimos, are both regular satellites. They are named after the attendents of the war god Mars as described in the Illiad. Phobos means fear and Deimos means panic. Phobos, the innermost satellite is thought to be spiralling in towards Mars.

Most of the satellites of Jupiter are named for lovers of the chief Roman god, Jupiter. Not much is known about the orbits of the two innermost satellites of Jupiter, Metis and Adrastea. Adrastea appears to be acting as a shepherd satellite creating the outer boundary of Jupiter's ring. The next innermost satellites: Amalthea, Thebe and the Galilean satellites of Io, Europa, Ganymede and Callisto, all move in nearly coplanar, nearly circular orbits. The Galilean satellites also exhibit commensurabilities between their mean motions, which may help to stabilize their orbital motions. See Section 1.7 for further details.

The remaining satellites of Jupiter can be clustered into two major groups according to their orbital elements. These groups are called: the 'outer satellites' of Jupiter comprised of Leda, Himalia, Lysithea and Elara; and the 'retrograde satellites' of Jupiter comprised of Ananke, Carme, Pasiphae and Sinope. The outer satellites move in prograde orbits of moderate eccentricities and inclinations, which range respectively from approximately 0.11 to 0.21 and 25° to 29°. The retrograde satellites move in retrograde orbits with similar ranges in eccentricites and inclinations above the jovian orbital plane of approximately 0.17 to 0.38 and 16° to 35° respectively.

Most of the names of the satellites of Saturn were suggested by Sir John Herschel at the beginning of the nineteenth century and generally refer to brothers or sisters of the Roman god Saturn, some of which were members of a family of giants called Titans. All of Saturn's satellites out to and including Titan, move in nearly circular orbits close to the equatorial plane of Saturn. Of these satellites the innermost five: Atlas, Prometheus, Pandora, Janus and Epimetheus, act as shepherd

satellites for some of the rings of Saturn. The rest of the regular satellites, with the exception of Rhea, exhibit a complicated network of commensurabilites between their mean motions. Titan has its own atmosphere and as such is a possible abode for primitive life.

The three outermost satellites of Saturn: Hyperion, Iapetus and Phoebe, form the irregular group of satellites orbiting Saturn. Hyperion moves in an orbit of moderately high eccentricity, locked in a strong orbital commensurability with Titan. Iapetus moves in a nearly circular orbit of high inclination, while Phoebe moves retrograde in an orbit of moderately high eccentricity and inclination.

The satellites of Uranus form the most regular satellite system in the Solar System. Most of the satellites are named after fairies described in the prose of Pope or Shakespeare. All the satellites revolve prograde in almost perfectly circular, coplanar orbits. The only exception, Miranda, exhibits a small orbital inclination of about 4°. The inclinations of the orbits of the newly discovered satellites are unknown as of 1988.

Neptune has two irregular satellites orbiting it. Triton, the innermost satellite and the largest one, moves in a highly inclined, almost circular, retrograde orbit. It is thought to be spiralling in towards Neptune. Nereid moves prograde in the most eccentric orbit of any known satellite in the Solar System. These two satellites were named after the creatures who attended the Roman god of the oceans, Neptune.

Finally, Pluto's satellite Charon moves retrograde in the most highly inclined orbit found in the Solar System. Its orbital eccentricity is not well-known. Charon is the name of the boatkeeper who ferried the dead across the river Styx to the underworld ruled by the Roman god Pluto.

The remaining structure found in the Solar System consists of the planetary rings and the minor bodies such as the asteroids, comets and meteor streams. Four planets are now known to exhibit ring structure. These are Jupiter, Saturn, Uranus and Neptune. The rings are made of small particles which move in nearly circular orbits within the primary's equatorial plane. Noticeable gaps between the rings, where a relatively low number of particles exist, are apparently caused by resonances or mean motion commensurabilities with nearby satellites. For example in Saturn's ring structure, the largest gap called Cassini's Division is in a 2:1 mean

motion commensurability with Mimas, a 3:1 commensurability with Enceladus and a 4:1 commensurability with Tethys, while the boundary between the B and C rings called the Encke's Division is in a 3:1 commensurability with Mimas.

The asteroid belt also exhibits similar gaps and preferred locations, which are related to commensurabilities of their mean motions about the Sun with the mean motion of Jupiter about the Sun. The major gaps, called the Kirkwood gaps, occur at mean motion commensurabilities with Jupiter of 3:1, 5:2 and 7:3. The main part of the belt is cut off abruptly at a 2:1 resonance (the Hecuba gap). Then, two further clusters of asteroids appear at the 3:2 (the Hilda group) and 1:1 (the Trojans) resonances with Jupiter. Most of the asteroidal orbits are nearly circular, existing between Mars and Jupiter. Other families, such as the Hidalgo group and the objects Apollo and Amor have orbits of higher orbital eccentricities that enable them to cross planetary orbits.

Generally, for most of the major bodies found in the Solar System little change is exhibited in their orbital semi-major axes, eccentricities and inclinations over many periods of their revolution. The changes that do occur appear to be purely periodic. No secular trends have been observed. Does this mean that the planetary and satellite systems have been and will continue to remain for some very long time span in much the same arrangements that are seen today? Or will the gravitational interaction of the bodies cause some of the bodies to collide, escape the system or simply cross orbits to form a different hierarchical arrangement of the bodies? The honest answer is that no one knows.

There have been many different approaches formed in an attempt to answer the above questions. The following is a brief summary of the most important approaches and the results that were gained from them.

1.2 General Perturbation Methods

The problem of n number of point masses acting under their mutual gravitational forces alone was first formulated by Newton. The equations of motion can be written as 3n second order differential equations, representing the motions of each body in each of the three dimensions. Thus, 6n integrals representing the constants in the second order differential equations are required in order to solve the problem. Only ten general integrals have been found. Even if time is eliminated as the independent variable and the "elimination of the nodes" procedure used by Jacobi is implemented, the problem still requires 6n - 12 integrals. The n-body problem therefore cannot be solved exactly for any values of n greater than two. However the ten integrals do provide the following information: the total energy H and the total angular momentum c of the system are always constant and the centre of mass of the system moves with a constant velocity.

Special solutions to the three-body problem were found by Lagrange. Fixing the positions of two of the bodies in a coordinate space which rotates with the mean motion of the two bodies about their centre of mass, the third body may be located at five points in the above phase space. Two points form two equilateral triangles with the line joining the two fixed bodies, while three points are located on the same line joining the two fixed bodies, one on either side of the two bodies and one at a specified location between the two bodies. The equilateral triangular solutions are traditionally labelled as the L_4 and L_5 points, while the collinear solutions are labelled as the L_i points where i is 1,2 or 3 depending on which of the masses m_1, m_2 or m_3 is located at the centre of the collinear arrangement. To find the exact positions of each of the collinear solutions relative to the two fixed bodies, three different quintic equations must be solved. Each quintic equation is formulated using one of the three unique possible collinear arrangements of the masses (ie m_1-m_2-m_3 or m_1-m_3-m_2 or m_2-m_1-m_3). See Roy (1988, p 121) for mathematical derivations of the special Lagrangian solutions to the three-body problem.

The stability of the Lagrangian points can be analyzed using standard linear stability procedures. See Roy (1988, p 135). The collinear solutions are unstable,

in the sense that small displacements from the Lagrangian point can result in the third body wandering away from the point. The equilateral triangular solutions are stable, in the sense that small displacements merely cause the third body to oscillate about the Lagrangian point, provided that the ratio of the least massive of the two fixed bodies to the sum of the masses of the two fixed bodies is less than 0.0385. Examples of real bodies in the Solar System existing at the equilateral triangular Lagrangian points are the Trojan asteroids with the Sun and Jupiter as the other two bodies; Telesto (L_4) and Calypso (L_5) with Tethys and Saturn as the other two bodies; and 1980 S6 (L_4) with Dione and Saturn as the other two bodies.

Lagrange, Laplace, Poisson, Leverrier, and many others since the 18th century have produced planetary perturbation theories. These theories involve expanding analytically the equations of motion into long series of sine, cosine and secular terms (ie terms that contain powers of time when integrated). These series are then integrated to give very accurate values of the orbital elements for each of the bodies in the problem over thousands of years in the past or future. See Section 2.3(iii) for further details on how the above procedure is accomplished.

In the past, scientists sought to answer the question of the Solar System's stability by studying the long-term changes in the semi-major axes of the planets. Laplace found that to first order in the disturbing masses, the series solution for changes in the semi-major axes contained no secular terms. Thus, he concluded that each planet was confined to an annulus of size equal to the amplitude of the periodic variations occurring in its semi-major axis. He calculated the widths of these annuli and showed that they do not cross each other. Since collisions or escapes of the planets were therefore impossible, the planetary system was thought to be stable for at least the first order solution.

Poisson studied the same problem to second order in the disturbing masses and produced what is known today as Poisson's theorem, ie no secular terms exist due to gravitational interactions between planets in the expression for the change in the semi-major axes for both the first and second order perturbation theories.

Haretu (1885) and Eginitis (1889) later discovered secular terms in the expansion for changes in the semi-major axes for the third order perturbation theory. This result seemed to indicate that the Solar System was not stable since the

semi-major axes of the planetary orbits grew or shrank consistently with time, which would inevitably lead to collisions of the planets or escape of some of the planets from the system all together. However, such secular terms could be more a result of the method of expansion chosen than a result of the solution itself. For example, Taylor expansions of periodic terms will result in secular terms containing powers of time, suggesting evolution with time where no such secular evolution occurs.

The problem was finally resolved by Message (1976, 1982) who showed that if the theory is expanded in a particular way, no secular terms exist within the series for the changes in the semi-major axes to any order of the disturbing masses.

Newcomb (1876) generalized the method of Laplace and showed that a multiple-periodic, trigonometric, infinite series solution existed for an n-body system where the central mass is assumed to be very large compared to the rest of the masses, and where the orbits of the other masses about the central mass have small inclinations and eccentricities. Unfortunately, Poincaré (1893) proved rigorously that Newcomb's series, and consequently all series expansions like it, were generally divergent. This result effectively dismissed the general perturbation methods as a possible means of studying the long-term stability of the Solar System.

1.3 The Kolmogorov-Arnol'd-Moser Theorem

The work of Kolmogorov (1954), Arnol'd (1963) and Moser (1966,1973), known collectively as the KAM theorem, showed that the approaches of Laplace, Lagrange and Poisson could produce series expansions which are convergent. However, the perturbations acting on the system had to be small and the natural frequencies of the system had to be poorly approximated by rational numbers. Only then would the series solutions be valid for all time.

Essentially the KAM theorem uses the idea that unperturbed two-body motion can be represented as a flow on a torus (Szebehely, 1984). The question of stability or convergence then becomes: Will the motion remain as a flow on a torus when it is distorted by outside perturbations or resonances? If the flow covers the torus completely but the torus remains, the system is quasi-periodic with irrational commensurabilities. If the flow joins itself after a finite number of revolutions, then the system is periodic. Finally, if the torus disappears altogether, the system is chaotic. For certain parameter values, the n-body problem was shown to exhibit quasi-periodic motion and to therefore be stable in the sense that such a perturbed motion is bounded for all time. Convergence proofs developed by Moser (1974) placed limits on the size of the perturbing masses, below which bounded motion could still occur.

Unfortunately, the planets found in the Solar System are too massive relative to the Sun and the perturbations are therefore too large for any series expansion of the equations of motion to be proved convergent by the KAM theory. Also, the ratios of the natural frequencies are not known to infinite accuracy, making it difficult to decide whether or not the ratios can be represented by rational numbers. The KAM theorem is therefore not a very useful tool for studying the stability of the Solar System.

1.4 The c^2H Criterion

Using the hierarchical arrangement of the bodies found in the Solar System, the planetary and satellite systems can be easily divided into subsets of three bodies for stability analysis in isolation from the rest of the Solar System. In a three-body hierarchical dynamical system the two closest bodies form a binary system, while the third body moves in a larger, non-crossing orbit about the centre of mass of the binary. See Figure 1.1 for an illustration of a three-body hierarchical dynamical system.

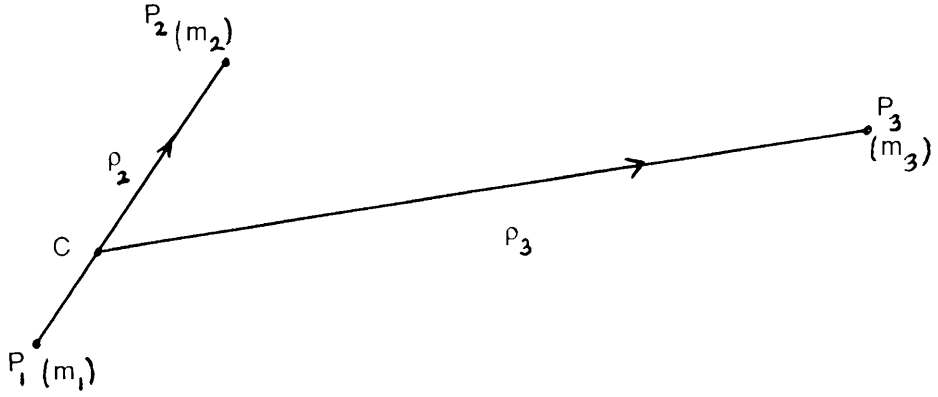

Figure 1.1 A three-body hierarchical dynamical system.

m_i are the masses of the bodies P_i, for i=1 to 3. C is the centre of mass of the binary formed by P_1 and P_2, the two closest bodies. ρ_2 is the distance separating the binary, while ρ_3 is the distance between point C and the body P_3. $\rho_2 \leq \rho_3$.

Although the general three-body problem cannot be solved exactly, the topology of the regions of forbidden motion for the three bodies can be examined for Hill-type stability (or hierarchical stability). A hierarchical dynamical system is said to exhibit Hill-type stability if the third body is confined to the same region of

configuration space relative to the other two bodies for all time. A hierarchical dynamical system exhibits hierarchical stability, if the hierarchical arrangement of its orbits does not change.

In 1878, Hill discovered a means of using surfaces of zero velocity to find regions of allowed motion for a simplified version of the three-body problem called the circular restricted three-body problem. In this problem one of the bodies is assumed to have negligible mass compared to the other two bodies. As a result, the two massive bodies move in circular orbits about their centre of mass, unperturbed by the third body. The problem is to ascertain the effect of the two massive bodies on the orbit of the third body.

The ten integrals that were discovered for the general n-body problem are no longer applicable; however Jacobi (1836) derived another integral of motion specific to the circular restricted three-body problem. 'Jacobi's integral' is a constant C related to the total energy of the system. It can be written as

$$C = 2U - V^2$$

where U and V are functions of the positional coordinates of the third body in a coordinate space which rotates with the primaries about their centre of mass. In this coordinate system the two masses are fixed in space to lie along the x-axis, with their centre of mass at the origin. U is also a function of the masses of the two fixed bodies and V is the velocity of the third body in this rotating coordinate system. For a complete derivation of Jacobi's integral, please see Roy (1988, p 127) or any other text on elementary celestial mechanics.

Since V^2 must always be greater than zero in order for the system to be real,

$$2U \geq C \qquad (1)$$

Thus, for a given three-body system with a given constant C, there are regions in the rotating coordinate space where the third body can exist and regions where it cannot. The boundary between these regions is given by

$$V^2 = 0 \quad \text{or} \quad 2U = C \qquad (2)$$

Equation (2) can therefore describe surfaces of zero velocity as the value of C is varied. Some examples of these surfaces are given in Figure 1.2. In parts (a) to (f) of Figure 1.2, the two massive bodies of masses m_2 and m_3 are located at the same fixed points along the x-axis. The negligible mass m_1 can exist in orbit about one or both of these two points in only the unshaded regions of the coordinate space. The shaded regions are the regions of motion forbidden by the criteria of Equation (1). In this particular example $m_1<m_2<m_3$.

Figure 1.2(a) represents a dynamical system whose constant $C = C_1>>1$. It contains three distinct regions of allowed motion: one bounded region surrounding each primary and one unbounded region surrounding the forbidden regions of motion. If the hierarchical system is arranged so that the third negligible mass forms a binary with one of the two massive bodies, it will be confined to orbit that primary for all time. It can never reach the other primary, nor can it escape from the system. It therefore exhibits Hill-type stability. Nothing, however, can be said about the type of orbit found within the region or how closely the body approaches its primary. It is still considered to have Hill-type stability even if it falls into its primary.

If the hierarchical system is arranged so that the third negligible mass orbits the centre of mass of a binary formed by the two massive bodies, it must be located in the unbounded region outside the forbidden regions of motion. As such, it can never approach an individual primary. Therefore it too exhibits Hill-type stability, even though it can still escape the system. In both of the above hierarchical systems, the hierarchy of the system is preserved for all time. Both systems are therefore also hierarchically stable.

In Figure 1.2(b) C has been decreased to C_2. The bounded regions are now touching at a common tangent point L_1. As C is decreased still further to C_3 (Figure 1.2 (c)), the bounded regions coalesce to form a dumb-bell shape. If the negligible mass forms a binary with one of the two massive bodies, it is now free to cross-over

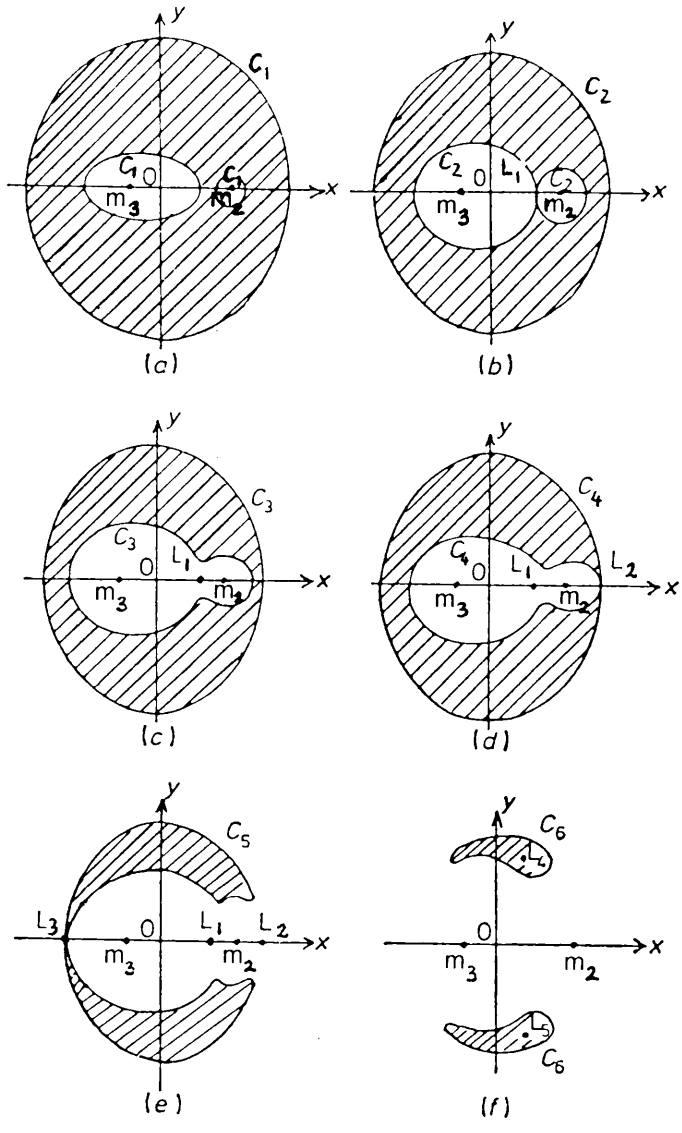

Figures 1.2(a) to (f) Hill's surfaces of zero-velocity in the x-y plane for the case where $m_1 < m_2 < m_3$.

The bodies of masses m_2 and m_3 are taken to be fixed along the x-axis. The body of mass m_1 can exist only in the unshaded regions. This diagram is taken from Roy (1988, p 133).

and orbit the other binary. It doesn't have to cross-over, but it no longer has a guarantee of Hill-type stability. It still cannot escape the system altogether. If the negligible mass orbits a binary formed by the two massive bodies, it remains in the same situation as described for Figure 1.2(a) and therefore maintains its Hill-type stability guarantee.

At a value of C decreased still further to C_4, the two remaining regions of allowed motion touch at a common point L_2 (Figure 1.2(d)). In Figure 1.1(e), with an even smaller value of $C = C_5$, the regions of allowed motion coalesce. The negligible mass is now free to approach either primary or to escape the system, no matter which part of the hierarchical system it originated from. There are no longer any cases where the negligible mass is guaranteed Hill-type stability.

Finally, Figure 1.2(f) shows that the forbidden region eventually breaks into two disconnected regions surrounding the points L_4 and L_5. As C is decreased further, these regions eventually shrink to these points.

The critical value of the Jacobi integral for Hill-type stability is C_2 or C_4, depending on the part that the negligible mass plays in the hierarchical arrangement of the three-body system. In the case of the negligible mass forming a binary with one of the massive bodies, the negligible mass will remain orbiting its primary forever as long as $C > C_2$. In the case of the negligible mass orbiting a binary formed by the two massive bodies, the negligible mass will not approach either of the massive bodies individually as long as $C > C_4$. Both cases guarantee Hill-type stability.

The value of the Jacobi constant C can be calculated for any three-body dynamical system using the initial positions and velocities of the bodies. The critical values C_2 and C_4 are found using Lagrange's collinear solution to the three-body problem. Studying the mathematics of the problem, the points L_1, L_2, L_3, L_4 and L_5 turn out to be none other than the Lagrangian points which form the collinear and equilateral triangular solutions to the three-body problem. See Roy (1988, p 132) for rigorous proof of this characteristic. The value of C_2 can therefore be evaluated using the masses of the bodies and the positional coordinates of the negligible mass

located at the Lagrangian point L_1, while the value of C_4 can be evaluated using the positional coordinates of the negligible mass located at the Lagrangian point L_2.

Attempts were made to generalize the above method of stability analysis to the elliptic restricted three-body problem. In this problem, the two primary bodies are allowed to describe elliptical orbits about their centre of mass. Unfortunately, there is no longer any Jacobi-type integral for this problem. Ovenden and Roy (1961) did derive expressions for the angular momentum and Jacobi integrals; however, these integrals were explicitly dependent on time. It is therefore possible to form zero-velocity curves which vary with time, but Hill-type stability can then no longer be guaranteed for all time.

A generalization of the use of Hill-type stability to the general three-body problem was put forth by Marchal and Saari (1975) and Zare (1976, 1977). They discovered that a combination of the angular momentum integral **c** and the energy integral H could be used in much the same way as the Jacobi integral is used in the restricted problem. Like the value of the Jacobi integral C, the value of the constant c^2H for a particular dynamical system can be used to determine regions of forbidden motion in the configuration space. Particular values of c^2H may also produce regions of forbidden motion which totally enclose each of the binaries for all time and thus may preserve the hierarchical arrangement of the three bodies.

Again surfaces giving the boundaries of these forbidden regions in configuration space can be found for different values of c^2H. The major difference between the two problems is that there are no longer two masses fixed in configurational space, with a negligible mass moving around them. Instead, there are three ways of studying the c^2H contours, depending on which body's position is being studied relative to the other two bodies' positions. Figures 1.3 show the c^2H contours from the three different perspectives for a three-body system where $m_1<m_2<m_3$. Recall that the Lagrangian points L_i, where i=1,2 or 3 are labelled according to which mass is located at the centre of the collinear arrangement of the three bodies when the mass with the varying position is taken to be located at the Lagrangian point L_i.

The surfaces look much the same as they did for the restricted problem. They have similar forbidden regions which, as c^2H is increased, open out at the saddle

Figures 1.3 (a) to (c) The c^2H contours in the configuration space for the case where $m_1 < m_2 < m_3$.

Each diagram descibes the possible positions of one of the bodies relative to the other two, depending on the value of c^2H for the three-body system. Labels A to E denote the contours for five successively larger values of c^2H.

In part (a) m_3 and m_2 are fixed, while the position of m_1 is varied. In part (b) m_3 and m_1 are fixed, while the position of m_2 is varied. In part (c) m_2 and m_1 are fixed, while the position of m_3 is varied.

These diagrams are taken from McDonald (1986, p. 76-78)

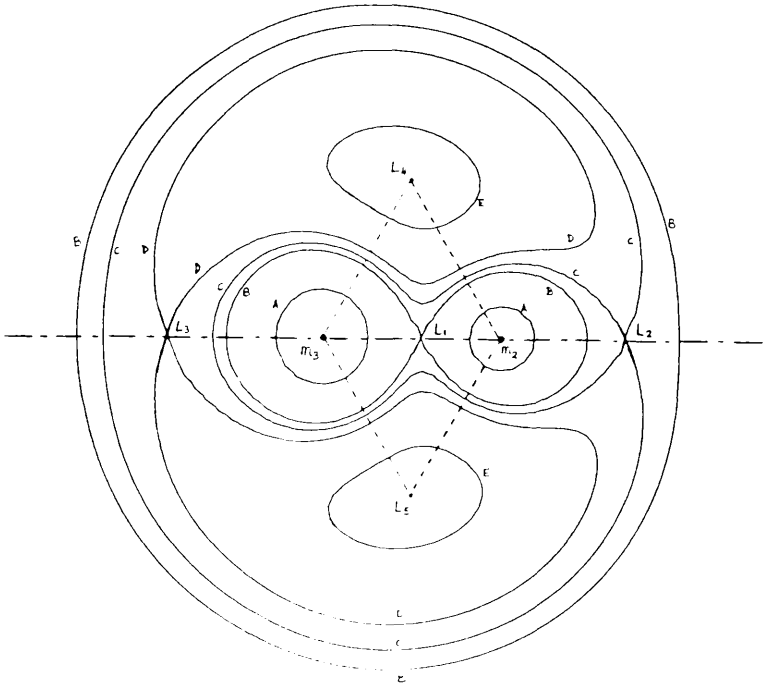

(a)

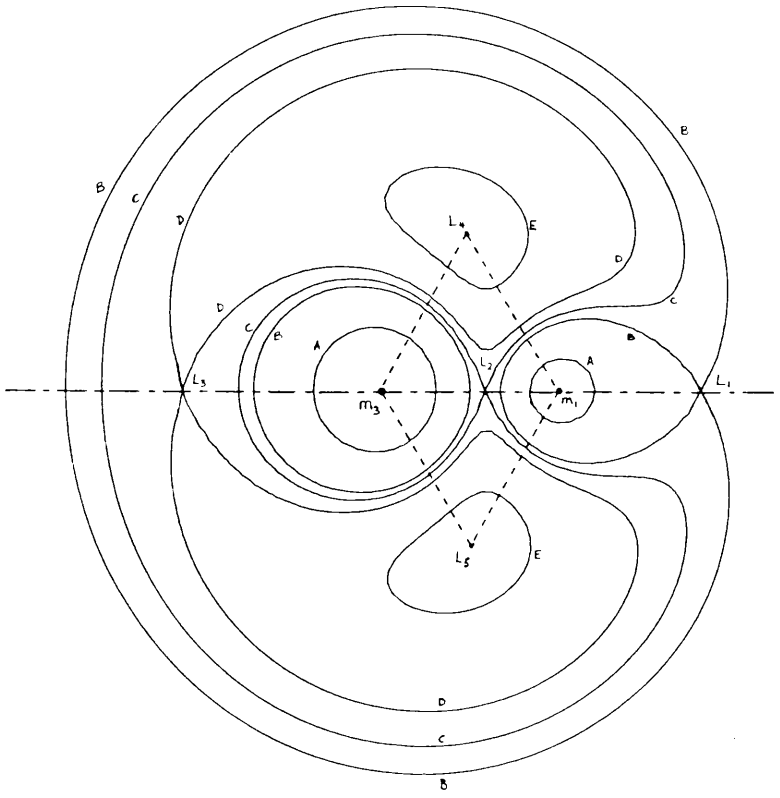

(b)

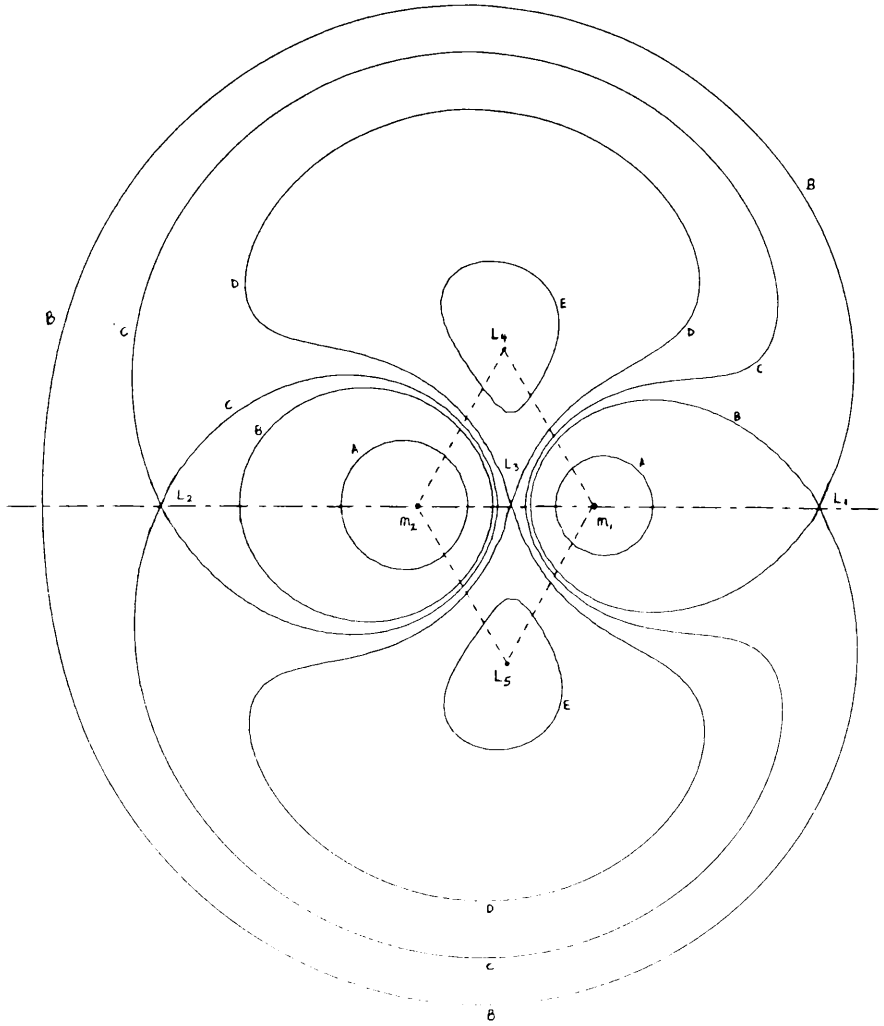

(c)

points L_1, L_2 and L_3 and which finally disappear at the Lagrangian points L_4 and L_5. In fact Figure 1.3(a) appears to be almost identical to the contours of Figures 1.1 because it describes a similar situation where the possible motions of the smallest mass are studied relative to the positions of the two larger masses.

Figure 1.3 (b) shows the c^2H contours for the case where the position of the middle-sized mass m_2 is studied in relation to the positions of the other two masses. If the hierarchical arrangement is one where m_2 forms a binary with m_3, the critical value of c^2H occurs at the Lagrangian point L_2. As long as the value of c^2H for the dynamical system is less than this critical value, the hierarchical dynamical system will remain hierarchically stable for all time.

If the hierarchical arrangement is one where m_2 forms a binary with m_1 or if it is one where m_2 orbits a binary formed between the other two masses, the critical value of c^2H occurs at the Lagrangian point L_1. In general, the critical value of c^2H (c^2H_{crit}) occurs at the Lagrangian point L_i (where i=1 or 2) which corresponds to the collinear configuration where the smaller of the two masses in the binary is located at the centre of the configuration.

To summarize, if $c^2H \leq c^2H_{crit}$, the hierarchical general three-body system will be hierarchically stable for all time. c^2H_{crit} is evaluated using the positional coordinates of the appropriate collinear Lagrangian point and the masses of the three bodies, while c^2H, being a constant of the dynamical system, can be evaluated using the initial positions and velocities of the bodies.

Many people including Szebehely (1977), Szebehely and McKenzie (1977a,b), Szebehely and Zare (1977), Roy (1979), Walker et al (1980), Valsecchi et al (1984), Roy et al (1984), etc. have studied the c^2H stability criterion for both fictitious and real systems. Szebeheley (1978) showed that the Moon in an (Earth-Moon)-Sun system has no Hill-type stability guarantee for the general three-body problem. The brackets denote the binary in the hierarchical arrangement of the three bodies. This result is in contrast to Hill's original result (Hill, 1878) using the Jacobi integral and the restricted problem.

All three-body subsystems of the Solar system of the form Sun-Jupiter-planet are found to be stable, except for Mercury, Mars, Pluto and any of the asteroids. It seems unlikely that a system containing larger perturbations such as Sun-Jupiter-Saturn would be stable under this criterion, while smaller planets like Mercury or the asteroids are not. The failure of the c^2H criterion here is probably due more to the possibility that the criterion becomes meaningless as the mass of one of the bodies becomes too small relative to the other bodies.

In the case of (planet-satellite)-Sun systems, all the satellites in the Solar System except the retrograde satellies of Jupiter are guaranteed hierarchical stability against solar perturbations as long as the Sun is assumed to move in a fixed circular orbit (Walker et al, 1980). When the eccentricity of the Sun's orbit is included in the problem, only Triton retains its guarantee of hierarchical stability (Valsecchi et al,1984).

1.5 The Empirical Stability Parameter Method

Although the c^2H stability criterion is sufficient for Hill-type stability to exist, it is not a necessary condition for such stability. For example, even if one of the bodies was allowed to cross-over from an orbit about one primary to an orbit about the other, such a situation may never occur, particularly if the neck forming the dumb-bell shaped region of motion around the primaries is very narrow.

In a recent set of papers, Roy (1979, 1982), Walker et al (1980), Walker and Roy (1981, 1983a,b), Walker (1983) and Roy et al (1985) demonstrate, through extensive numerical integrations of the three-body problem, the existence of a considerable region of empirical stability where the c^2H stability criterion is violated. For given mass ratios between the three bodies (μ and μ_3), they calculated numerically the lifetimes of the systems as the ratio of the semi-major axes α_{23} is increased. The sharp transition from very long lifetimes (stable) to measurable short lifetimes (unstable) occurs at a value of the ratio of the semi-major axes greater than that expected by the c^2H criterion.

Nacozy (1977) found that the Sun-Jupiter-Saturn system was empirically stable even when the planetary masses were augmented by a factor of up to thirty times. The c^2H stability criterion, however, only guarantees hierarchical stability for planetary masses that are up to twenty-five times as massive as their actual values. The c^2H stability criterion appears to be far too strict in its measure of the stability of three-body dynamical systems.

The statistical or empirical stability method provides a statistical estimate of the time taken for half the members of a family of particles with similar initial conditions to escape through the neck of the dumb-bell. The best way to estimate the size of the perturbations acting on the masses in an n-body system is to use the empirical stability parameters ϵ_{ij} and ϵ^{kj} (Roy, 1979). These measure the disturbance of the elliptic motion of the j^{th} body by the remainder of the bodies. ϵ_{ij} describes the disturbance of the j^{th} body by a superior body, while ϵ^{kj} describes the disturbance of the j^{th} body by an inferior body. As an example, in the three-body problem these parameters become:

$$\epsilon^{23} = \mu (1 - \mu) \alpha_{23}^{2}$$

$$\epsilon_{32} = \mu_3 \alpha_{23}^{3}$$

where

$$\mu = \frac{m_2}{m_1 + m_2}, \quad \mu_3 = \frac{m_3}{m_1 + m_2}, \quad \alpha_{23} = \frac{\rho_2}{\rho_3}$$

where the masses are arranged in the hierarchical arrangement $(P_1\text{-}P_2)\text{-}P_3$ as depicted in Figure 1.1. m_i are the masses of the bodies P_i, respectively for i = 1 to 3. ρ_2 is the distance between the bodies forming the binary and ρ_3 is the distance from the centre of mass of the binary to the third body.

"ϵ_{32} is a measure of the ratio of the disturbance by P_3 on the orbit of P_2 about P_1, to the central two-body force between P_2 and P_1. Likewise, ϵ^{23} is a measure of the ratio of the disturbance by P_1 and P_2 on the orbit of P_3 about the centre of mass of P_1 and P_2, to the central two-body force between P_3 on the one hand and P_1 and P_2, assumed to lie at their mass-centre" (Roy, 1988, p 272-273).

Instead of using the ratio of the masses (μ's) and the ratio of the separations of these masses (α's) as the parameters which describe a particular three-body system, Roy and Walker use the empirical stability parameters (ϵ's) and the α's. Dynamical systems with similar values for their ϵ's and α's form families of dynamical systems, which have similar lifetimes before hierarchical stability is disrupted. A family of hierarchical dynamical systems will therefore also have an average half-life T, where T is the time taken for half the hierarchical dynamical systems to change their hierarchy either by cross-over orbits, close encounters or escapes.

Using a large number of numerical experiments, Roy and Walker have completed half-life contours for both three-body and four-body systems. These contours can then be used to make reliable predictions for the durations of given three or four body hierarchical dynamical systems. Although their work is incomplete, they conclude that the planetary and satellite systems in the Solar System have empirical stability parameters which lie in the contour regions where the half-life is of astronomical duration.

1.6 The Milani and Nobili Method

Even though the discovery of the c^2H stability criterion was a huge breakthrough for studying the stability of the Solar System, no three-body subsystem actually exists totally unperturbed by other bodies. Milani and Nobili (1983a,b), however, showed that it is possible to treat four or more body systems as sets of disturbed three-body subsets. Using the Roy-Walker empirical stability parameters, they related the hierarchical stability lifetime of the four-body hierarchical dynamical system to the rate of change of the c^2H stability criteria for each of the three-body subsets as they are disturbed by the fourth body.

The result was a set of minimum times, one for each subset of three bodies, that the perturbations would take to increase c^2H to c^2H_{crit}. If the subsets were no longer hierarchically stable, then the four or more body system comprised of the subsets could no longer be stable either. Using this procedure, they found that the four-body system of Sun-Mercury-Venus-Jupiter was hierarchically stable for at least 1.1×10^8 years, that being the minimum lifetime of the subset Sun-Mercury-Venus. The minimum lifetime of the subset Sun-Mercury-Jupiter was found to be at least 3×10^9 years.

It is interesting to note that the isolated system of Sun-Mercury-Jupiter has no hierarchical guarantee of stability. Yet the existence of Venus between Mercury and Jupiter allows the two three-body subsets to have hierarchical guarantees of stability, thus enabling a minimum lifetime to be placed on the four-body system comprised of the two subsets.

The Milani and Nobili method has two problems. Jupiter's perturbations on Saturn are so large that if both of these planets are included in the four-body system, the resulting minimum lifetimes to first order in the ϵ's are too short to be of use. The first order theory is therefore only useful in the case of the inner planets and Jupiter. The second problem arises when resonances occur. The minimum lifetimes are found by averaging over the angular variables. This procedure may no longer be valid if small divisors in the coefficients to these angular variables cause these terms to have very long periods. See Section 2.3 (iv) for further discussion of the problem of small divisors.

1.7 Orbital Resonances

Greenberg (1984) in his paper on "Orbital Resonances Among Saturn's Satellites" gives a short explanation of the terminology and kinematics involving resonances. He states that resonances will occur in any dynamical system when "the natural frequency of the system is matched by the frequency of a periodic force or a harmonic of that force" (Greenberg, 1984, p 596). Natural oscillations in a satellite's orbital motion can be either oscillations relative to a circular reference orbit (ie epicyclic motion) caused by the orbital eccentricity e or oscillations out of the reference plane caused by the orbital inclination i or a combination of both. The periodic force acting on the satellite's motion can be, as in the case of the three-body problem, the perturbing force of a third body. The period of this force is then simply the synodic period of the two bodies $T_S=2\pi/(n-n_1)$, where n and n_1 are the mean motions of the satellite and the third perturbing body, respectively.

In a two-body system, the natural oscillation of the one body with respect to the other is simply the sidereal period of its orbit T_{si}. Therefore, exact resonance occurs when the sidereal period is equal to an integer multiple of the synodic period or when

$$n = j\,(n - n_1) \qquad \text{where j is an integer}$$

Since the epicyclic or vertical motion is not exactly sinusoidal, except to the first order in e or i, a resonance will occur when any multiple of the natural frequency matches any multiple of the forcing function. Hence

$$k\,n = j(n - n_1) \qquad \text{where j, k are integers}$$

or

$$\frac{n}{n_1} = \frac{j}{j - k}$$

and the mean motions are exactly commensurable.

In a three-body coplanar system where the orbit of the perturbing body is assumed to be circular, the natural frequency of the perturbed body is now given by the epicyclic frequency κ or the frequency at which the perturber causes the perturbed body's orbit to precess.

$$\kappa = n - \dot{\varpi}$$

where $\dot{\varpi}$ is the rate of change of the longitude of pericentre for the satellite. See Section 2.3(i) and Figure 2.2 for a more detailed description of the orbital parameters of a body moving in space, such as the orbital eccentricity e, the inclination i, the longitude of the pericentre ϖ and the longitude of the ascending node Ω.

An exact resonance then occurs when

$$k\ (n - \dot{\varpi}) = j\ (n - n_1) \qquad \text{where j, k are integers} \qquad (3)$$

This relation gives rise to the expression

$$0 = (j - k)\ n - j\ n_1 + k\ \dot{\varpi} \qquad (4)$$

or the e resonance criterion.

If we now look at a three-body system where the orbits are largely circular but no longer coplanar, the natural frequency of the system now becomes the vertical frequency κ_V or the frequency at which the perturber causes the perturbed body to oscillate out of the reference plane. Thus, an exact resonance occurs when

$$k\ \kappa_V = k\ (n - \dot{\Omega}) = j\ (n - n_1) \qquad \text{where j, k are integers}$$

$\dot{\Omega}$ is the rate of change of the satellite's longitude of the ascending node. This equality can also be expressed as the i resonance criterion

$$0 = (j - k)\, n - j\, n_1 + k\, \dot{\Omega}$$

If the perturbed body's orbit is both inclined and elliptical, while the perturber's orbit remains circular, both natural frequencies are included to produce a general e-i resonance criterion of the form

$$k\,(n - \dot{\Omega}) = j\,(n - n_1) \qquad (5)$$

$$l\,(n - \dot{\varpi}) = m\,(n - n_1) \qquad (6)$$

or if Equation (5) and (6) are added together:

$$0 = (j + m - k - l)\, n - (j + m)\, n_1 + k\dot{\Omega} + l\dot{\varpi} \qquad (7)$$

Note that for all the cases described so far, the coefficients of the resonance arguments used here always add up to zero. This is the "D'Alembert relation".

If a general three-body system is studied, then both natural frequencies for both bodies would have to be included and the general resonance criterion becomes

$$0 = j_1 n + j_2\, n_1 + j_3\, \dot{\varpi} + j_4\, \dot{\varpi}_1 + j_5\, \dot{\Omega} + j_6\, \dot{\Omega}_1$$

$$\text{where} \sum_{i=1}^{6} j_i = 0 \quad \text{and} \quad j_i \text{ are integers} \qquad (8)$$

In Section 2.3(iv), we show that if Equation (8) is valid, any integration of periodic terms from an expansion of the equations of motion which contain multiples of the argument

$$\phi = j_1\, \lambda + j_2\, \lambda_1 + j_3\, \varpi + j_4\, \varpi_1 + j_5\, \Omega + j_6\, \Omega_1$$

where j_i for i = 1 to 6 are integers

will produce secular-like terms with infinite periods. In other words, the coefficients of these integrated periodic terms tend to infinity when Equation (8) is

true. They can therefore dominate any series expansion solution to the motions of bodies which exhibit resonant motion.

The existence of resonant motion in a system can sometimes ensure the stability of the system. For example, the Saturn-Titan-Hyperion system moves in an e type resonance where

$$0 = 4n_1 - 3n - \dot{\varpi}_1$$

A subscript of 1 denotes a parameter of the outer perturbing body or Hyperion in this case. As a result, Equation (3) becomes

$$-(n_1 - \dot{\varpi}_1) = 3\,(n - n_1)$$

which ensures that the conjunction of the two bodies (ie the conjunction line) always occurs at the same position in Hyperion's orbit relative to its semi-major axis. In reality the conjunction line librates about a constant position located at the apocentre of Hyperion's orbit with an amplitude of 36° and a period of 1.75 years. In other words, the resonant argument is

$$\phi = 4\,\lambda_1 - 3\,\lambda - \varpi_1 \approx 180°$$

Since the conjunction of the two satellites always occurs near the apocentre of the outer satellite Hyperion's orbit, the resonance mechanism ensures that the closest approach of the satellites to each other occurs with the largest possible separation. The high perturbations which occur near conjunction are therefore kept to a minimum, resulting in a greater likelihood that the system will remain stable in the sense that the dynamical system does not undergo any collisions, escapes or changes in its hierarchy.

A resonant system is only stable, however, if the enhanced perturbations which occur at the repeated configuration of the conjunction line can maintain the resonance against outside disruptive forces. In the Saturn-Titan-Hyperion system example, let us assume that the conjunction line is slowly varying due to outside influences. Since Hyperion's mass is negligible compared to that of Titan, we ignore

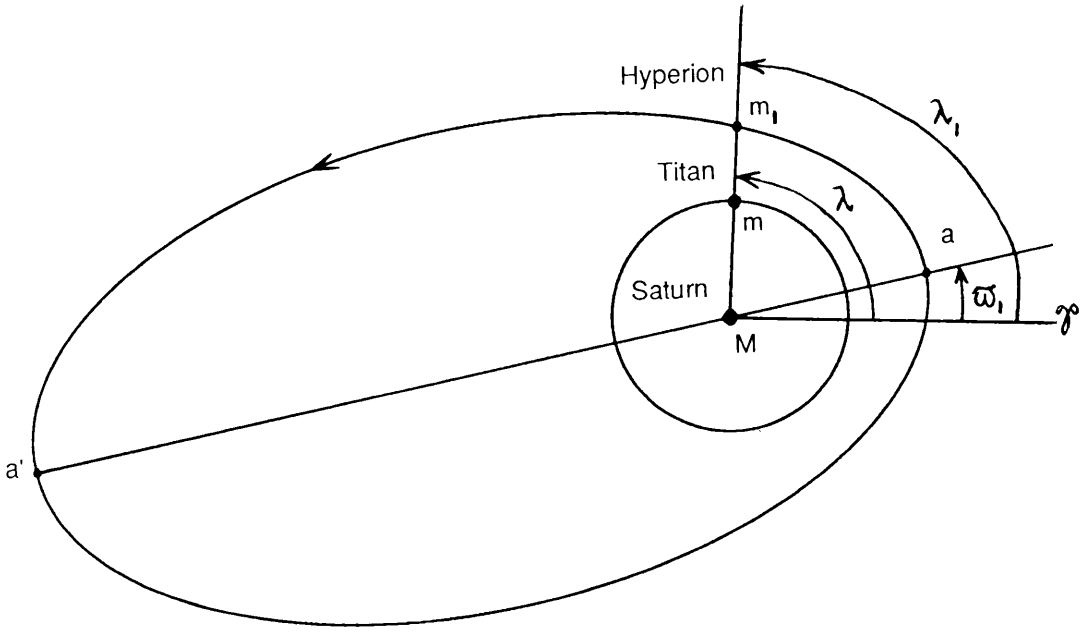

Figure 1.4 The 4:3 resonant locking mechanism of Titan and Hyperion where the resonant angle $\phi = 4\lambda_1 - 3\lambda - \varpi_1$ librates about 180°.

A subscript of 1 describes a parameter of the outer body Hyperion. No subscript denotes a parameter of the inner body Titan. $\overline{aa'}$ is Hyperion's orbital semi-major axis. Point a is Hyperion's pericentre and point a' is its apocentre. γ is some specified reference direction.

any effect that Hyperion has on Titan's orbit and consider only the effects of Titan on Hyperion's orbit when the two satellite's approach each other. Let the conjunction line occur after Hyperion's pericentre but before its apocentre. See Figure 1.4 for a diagram of the orbits of Hyperion and Titan.

When the two satellites are in conjunction, Titan exerts a force on Hyperion directed radially towards Saturn, while Hyperion moves radially away from Saturn moving from its pericentre to its apocentre. As a result, energy is being removed from Hyperion's motion.

The closest approach of the two satellites actually occurs just before the conjunction shown in Figure 1.4. At this closest approach, Titan with the greater angular velocity will be behind Hyperion. It therefore puts a dragging force on Hyperion in its orbit, causing Hyperion to lose energy. A loss of energy decreases Hyperion's period. The effect is small at each conjunction, but because the approximate position of the conjunction is repeated at every conjunction, the effect is enhanced.

As Hyperion's period decreases, the next conjunction occurs slightly closer to Hyperion's apocentre. Hyperion can now move further towards its apocentre before Titan overtakes it. If the conjunction line were to occur after Hyperion's apocentre but before its pericentre, the same effects occur but in reverse. Thus, the enhanced perturbations near the conjunction configuration serve to move the conjunction line towards Hyperion's apocentre no matter where it is originally located. The conjunction line therefore librates about the stable configuration located at Hyperion's apocentre and the Saturn-Titan-Hyperion resonant system is stable.

The Saturn-Enceladus-Dione system displays a 2:1 e type resonance where the conjunction line librates about the pericentre of the inner body Enceladus with an amplitude of less than 1° and a period of 12 years. ie

$$0 = n - 2n_1 + \varpi$$

$$\phi = \lambda - 2\lambda_1 + \dot{\varpi} \approx 0^\circ$$

where a subscript 1 denotes the outer body Dione and no subscript describes the inner body Enceladus. The resonant mechanism serves to ensure that conjunction doesn't

occur when the inner body is at its apocentre and the separation between the two satellites in conjunction is a minimum.

The Saturn-Mimas-Tethys system exhibits an inclination type resonance where the conjunction line librates about the midpoint of the ascending nodes of the two satellites on Saturn's equatorial plane with an amplitude of about 48° and a period of 71 years. Thus,

$$0 = n - 2n_1 + \frac{1}{2}(\Omega + \Omega_1)$$

$$\phi = \lambda - 2\lambda_1 + \frac{1}{2}(\dot{\Omega} + \dot{\Omega}_1) \approx 0°$$

Rigorous analysis of inclination type resonances show that the enhanced perturbations produced near conjunction tend to maintain the conjunction line at 90° from the mutual nodes of the satellites.

The three inner satellites of Jupiter: Io, Europa and Ganymede, exist in a stable resonance which prevents all the satellites from lining up on the same side of Jupiter. ie

$$0 = n_1 - 3n_2 + 2n_3$$

where the subscripts 1, 2 and 3 correspond to Io, Europa and Ganymede respectively. Adjacent pairs of these satellites also exhibit 2:1 commensurabilities in their mean motions.

The three inner satellites of Uranus: Miranda, Ariel and Umbriel exist in a nearly identical relation

$$-0.08°/\text{day} = n_1 - 3n_2 + 2n_3$$

where the subscripts 1, 2 and 3 correspond to Miranda, Ariel and Umbriel respectively. There is no evidence, however, that this system is locked into a stable resonance. This could be a result of the fact that in this case the pairs of mean motions are not commensurable.

Roy and Ovenden (1954) demonstrated that there are greater number of mean

motion commensurabilities existing in the Solar System than would be expected by mere chance. Goldreich (1965) proposed that tidal forces between the planet and the satellites could bring the system in to one that is in resonance. Tidal friction transfers angular momentum from the spinning planet to the two satellites. This results in an increase in their semi-major axes. The effect on the inner satellite is greater, causing it to move outward from the planet at a faster rate. Thus, the ratio of the mean motions of the two satellites changes and may eventually approximate a ratio of small whole numbers.

Once a commensurability exists, Goldreich (1965) showed that, if the gravitational interaction between the two satellites was strong enough, it was possible for the two satellites to share the increase in angular momentum from the planet in such a manner as to maintain the commensurability. The resonant structure is then stable against the continued influence of the tidal forces.

1.8 The Mirror Theorem

The repeated conjunction configuration found in stable resonances not only keeps the satellites apart, but as a "mirror configuration", it also reverses the perturbances acting on the system in such a way that the behavior after the mirror configuration is a mirror image of the previous behavior (Roy and Ovenden, 1955). This characteristic may also help stabilize the resonant system.

In a system of n gravitationally interacting point masses, a mirror configuration is defined by Roy and Ovenden (1955) to be a configuration where all the relative velocity vectors of the masses are perpendicular to all their relative radius vectors. The radius and velocity vectors are measured relative to the assumed stationary centre of mass of the system. If a mirror configuration occurs at a certain epoch, the mirror theorem (Roy and Ovenden, 1955) states that "the behavior of each of the point-masses under the internal gravitational forces of the system after that epoch will be a mirror image of its behavior prior to that epoch".

Roy and Ovenden (1955) pointed out that in practice only two different kinds of mirror configurations are possible. In one configuration, the bodies occupy a plane with all their velocity vectors perpendicular to that plane (ie the velocity vectors are parallel to each other). See Figure 1.5(a). In the other configuration, the bodies are positioned along a straight line with all their velocity vectors perpendicular to that line (ie the velocity vectors are not necessarily parallel to each other). See Figure 1.5(b). The repeated conjunction described in the case of the Titan-Hyperion stable resonance is of the latter type.

The corollary to the mirror theorem is obvious. If a dynamical system passes through two mirror configurations then the system is periodic. One mirror configuration is not sufficient for periodicity since particles in parabolic or hyperbolic orbits can pass through one mirror configuration.

That a dynamical system moving through two mirror configurations is periodic does not necessarily mean that the dynamical system is stable. Left to itself, the system will last forever, but even very small external perturbations may disturb the system irrevocably. However, Roy and Ovenden (1955) suggest that frequent occurrence of mirror configurations in the dynamical system, producing frequent

"mirror" reversals of the perturbations, will result in a more stable system against external forces. If, however, a mirror configuration does not occur in a sufficiently short time interval after the previous one in order to "reverse" perturbations, the disturbances to the system may accumulate enough to disrupt the current hierarchical arrangement of the system.

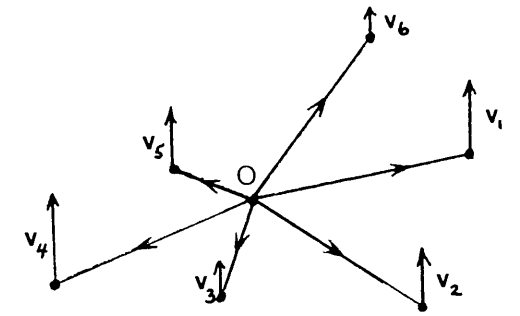

(a)

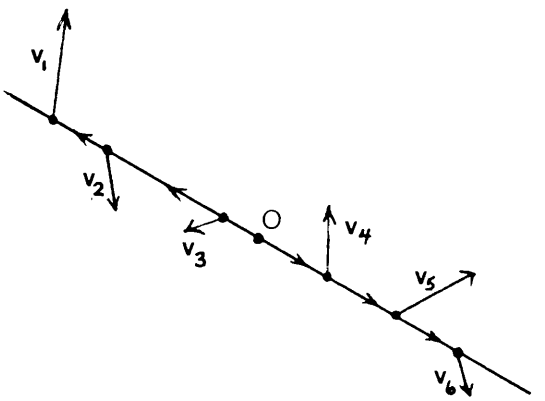

(b)

Figure 1.5 The two possible types of mirror configurations.

In part (a), the bodies lie in a plane with their velocity vectors perpendicular to that plane. In part (b), the bodies lie in a line with their velocity vectors perpendicular to that line.

1.9 Numerical Integration Methods

With the advent of high-speed computers, the many difficulties found in the analytical theories can be avoided by numerically integrating the equations of motion directly. Numerical integration has its own problems however. The solutions are limited by the uncertainty in the starting conditions, the amount of machine time available, error accumulation and the amount of storage space available for the huge data output. There have been many different procedures tried over the last few decades in an attempt to reduce the errors and difficulties caused by the above limitations.

Because an increase in the number of bodies requires longer integration times per step and because the greater speed of the inner bodies of the Solar System necessitates the use of smaller step sizes, an integration of the whole Solar System for very long time spans is very difficult. The mass of the inner planets is therefore usually added to that of the Sun and only the motions of the five outer planets are considered.

The first major attempt at numerically integrating the equations of motion for the Solar System was performed by Cohen, Hubbard and Oesterwinter. See Cohen and Hubbard (1965) and Cohen, Hubbard and Oesterwinter (1967, 1972). They integrated the motions of the five outer planets of the Solar System over a time span of 10^6 years centred on the epoch of 1941, Jan. 6.0. Their final calculation used Cowell's numerical method to twelth order with a fixed step size of 40 days.

Cowell-type numerical methods generally refer to methods which require no prior knowledge of the orbital behavior. Encke-type numerical methods measure the real orbit relative to a fixed reference orbit which is usually a keplerian ellipse. When the difference between the real orbit and the reference orbit becomes too large, a new reference orbit described by the current osculating elements of the real orbit is chosen. Encke-type methods are more accurate than Cowell-type methods and allow the use of a greater step size as long as the reference orbit remains close to the real orbit. If the difference grows quickly, the Cowell-type methods are more efficient. Cowell-type methods are easier to implement and have wider applications.

The Cohen, Hubbard and Oesterwinter computer had a 48 bit mantissa,

providing a precision to 14 decimal places. The total computing time was eventually less than 20 computer hours. The huge amounts of data output in the form of positions and velocities for the five planets at given time steps were converted to plots of the orbital elements of the planets as functions of time.

From these plots, Cohen et al found no evidence of secular trends in any of the semi-major axes, eccentricities or inclinations of the planets. The evidence was inconclusive for the orbital elements of Pluto. They also discovered much about the interaction of the outer planets, in particular, that a stable resonance exists between Neptune and Pluto, ie

$$\phi = 3\lambda_P - 2\lambda_N - \varpi_P \qquad \text{where N = Neptune, P = Pluto}$$

The resonant angle ϕ librates about 180° with an amplitude of 80° and a period of 19,440 years, ensuring that the two planets never approach each other within the vicinity of Pluto's pericentre.

Kinoshita and Nakai (1984) performed a similar numerical integration of the five outer planets over a time span of 5×10^6 years. They also used Cowell's method and a fixed step size of 40 days; however, with improved computers, the calculation only took 4 computer hours to complete. The output was later processed by Milani and Nobili (1984,1985) to show the existence of yet another resonance mechanism locking the pericentre of Uranus to the apocentre of Jupiter. The resonant angle librates about 180° with an amplitude of about 70° and a libration period of 1.1×10^6 years.

In an effort to integrate the equations of motion for still longer time intervals, two scientific groups were formed. One group, Applegate et al(1986), built their own parallel computer called the Digital Orrery designed especially for solving n-body problems. The other group, Roy et al (1988), brought together some of the leading celestial mechanicians from the U.K. and Italy to work on a project they called LONGSTOP (LONg-term Gravitational STudy of the Outer Planets).

The Digital Orrery group integrated the outer planets of the Solar System for 2×10^8 years using a Cowell-type numerical method and time steps near 40 days . The LONGSTOP consortium used an Encke-type numerical method to integrate the five

outer planets for a total time span of 10^8 years. The inner planets were simulated by a ring of equivalent mass around the Sun. Relativistic effects were also included. In both cases, the results were compared with standard secular perturbation theory. Some discrepancies were found, but no instabilities were observed in these time scales.

The LONGSTOP group also integrated the Uranian satellite system for 10^6 orbits of Miranda (Murray et al, 1988). The discovery of some near-resonant terms led to a few modifications of the classical secular perturbation theory.

In order to handle the enormous output, the LONGSTOP group developed a synthetic secular perturbation theory which filters all the short period terms up to 4,900 years in length from the output (Carpino et al, 1987). The secular perturbation theory is 'synthetic' because it is obtained from numerical and not analytical results. It is however compared and checked with other analytic secular perturbation theories. The final data gives the secular periods of the planets' pericentres, nodes and any combinations of these. It also gives the secular periods of the semi-major axes, eccentricities and inclinations of the planets.

Milani and Nobili (1988) showed that the main limit to increasing the time span of the numerical integrations of the planetary orbits was no longer the availability of computer resources, but rather the accumulation of integration error. In particular, round-off error caused by the computer's inability to represent real numbers with infinite precision is the dominant source of error and currently places the limit of integration at about the order of 10^8 years for the outer planets.

They also discovered that the spectrum of frequencies contains many multiplets of lines which cannot be identified by the synthetic theory as allowed combinations of the fundamental frequencies of the dynamical system. From this, Milani (1988) suggested that the solution to the problem may not be quasi-periodic and that therefore it may not be possible to predict the motions of the outer planets for time spans much longer than 10^8 years even with the use of better computers or better numerical algorithms. A slight change in the starting conditions could produce an entirely different solution to the problem over such a time span.

More recently, the Digital Orrery group (Sussman and Wisdom, 1988) completed a 8.45×10^8 year integration of the Solar System. They showed that the

orbit of Pluto is chaotic. They took two very similar sets of starting conditions for Pluto and discovered that the two orbits diverged with a Liapunov exponent of 1 per 20 million years.

Direct proof of chaotic motion can be found by computing the positions of two different systems with very similar starting condtions. If the rate of increase of separation between the two solutions is exponential with time, then the orbit that can be described by both of the two similar sets of starting conditions is chaotic. The coefficient of the exponential is called the maximum Liapunov exponent. See Szebehely (1984) for a mathematical definition of Liapunov exponents.

In 1989 after the research in this thesis had been completed, Laskar showed that the orbits of the inner planets are also chaotic. He used a conventional supercomputer and the computer algebra processors developed at the Bureau des Longitudes in Paris to complete an extensive analytical averaging of the equations of motion for the eight main planets, accurate to second order in the planetary masses and to fifth order in the eccentricity and inclination (Laskar, 1988). Corrections for general relativity and the Moon were also included.

He then numerically integrated this system of averaged equations of motion backward for 2×10^8 years. He discovered that the solution was chaotic with a maximum Liapunov exponent of 1 per 5 million years. He therefore concluded that the Solar System exhibits chaotic and not quasiperiodic motion, with the predictability of the inner planetary orbits being lost within the order of 10^7 years (Laskar, 1989).

That the Solar System's planetary system is chaotic does not mean that irrevocable changes in the hierarchy of the planetary system will occur within 10^7 years. It simply means that any of the traditional methods of analysis which begin with a given set of initial conditions and go on to derive a unique solution to the problem will fail to predict any of the catastrophic changes which might occur in the system. If the orbits are chaotic, the problem cannot be solved by following the changes in just one given dynamical system over the required time span. Solutions derived from similar sets of initial conditions can no longer be guaranteed to produce similar solutions over these time spans.

In future, the whole problem of the stability of the Solar System will have to

be restudied in light of the knowledge that the planetary system is chaotic. This means using probabilistic or qualitative dynamical methods to find and study the regions of chaotic and stable motion within the planetary and satellite systems of the Solar System. Many solutions with slightly different initial conditions will have to be computed in order to investigate the qualitative behavior of the Solar System's motion in each part of the phase space. We need to understand how bodies such as Pluto and the inner planets can move in chaotic orbits, yet still remain stable for timescales far longer than the inverse of their maximum Liapunov exponent.

CHAPTER 2

AN INTRODUCTION TO THE FINITE-TIME STABILITY CRITERIA

2.1 Introduction

2.2 A Brief Outline of the Finite-Time Stability Method

2.3 Traditional Developments of the General Three-Body Problem Written in Terms of the Orbital Elements

- (i) The orbital elements
- (ii) Lagrange's planetary equations of motion
- (iii) Different expansions of the disturbing function
- (iv) Dominant terms in R
- (v) The solution to Lagrange's planetary equations

2.4 Development of the Coplanar Restricted Three-Body Problem

- (i) Derivation of $\partial R/\partial a$
- (ii) Derivation of $\partial R/\partial r$ and $\partial R/\partial L$
- (iii) An exact form of Lagrange's planetary equations with respect to time
- (iv) An exact form of Lagrange's planetary equations with respect to the true anomaly
- (v) A more convenient form of Lagrange's planetary equations in preparation for their numerical integration and analytical expansion

2.5 The Validity of the Assumptions Made in the Previous Development of the Coplanar Restricted Three-Body Model

"He said, 'Cheer up. It could be worse.' So I cheered up and it did get worse."

2.1 Introduction

The previously described theoretical calculations for the problem of the stability of Sun-perturbed planetary satellites have at least one common feature. They all involve a search for a stability criterion which is valid for all time. The various limitations of these solutions have already been discussed; but, in general, an attempt to find a theoretical stability guarantee that is valid for all time appears to produce results which are far more restrictive on the planet-satellite system than reality would suggest is necessary for stability of the system to exist.

In an attempt to avoid the problem of using a possibly over-restrictive model, long-term numerical integrations of the equations of motion are performed and estimates of the length of time for which individual three-body systems remain stable are found. However, over the time span required, numerical investigations of this kind have the disadvantage of taking up enormous amounts of machine time and of accumulating enough computer round off errors to cause some doubt as to the validity of the results (Milani and Nobili, 1988).

In this thesis we seek a different approach to the problem, an approach which combines characteristics of both the numerical and analytical methods discussed so far. Instead of searching for a stability criterion which is valid for all time, we look for one which holds, in any particular case, for a finite length of time and which also provides us with an estimate of that finite time.

Section 2.2 outlines briefly this method of finding finite-time stability criteria for a given model and explains how minimum durations of the planet-satellite systems can be calculated. The scope of this thesis involves only an application of our finite-time stability criteria to a coplanar restricted three-body model of a Sun-perturbed planet-satellite system, but the method could easily be extended to include more general three-dimensional models.

In order to understand the restrictions made in the coplanar restricted three-body problem, we first describe in Section 2.3, the general three-body

problem. The equations of motion for this general model are specified in terms of the orbital elements. The orbital parameters which are commonly used as the orbital elements are then defined in detail so that it is easily seen which parameters are independent of each other and which are dependent. This information becomes very important later when we transform the equations of motion to a more manageable form for our purposes. Traditional developments of the disturbing function located within the equations of motion are discussed and the standard procedures used to solve the equations of motion for a particular three-body system are outlined.

In Section 2.4, we describe the coplanar restricted three-body model, which we will be using throughout most of the thesis. The relevant formulae from Section 2.3 are simplified to fit the new model and our method of expanding the equations of motion is described and compared with the more traditional methods. Finally, we derive the specific form of the equations of motion which is best suited for use with our finite-time stability criteria method. The validity of the assumptions made in the coplanar restricted three-body model within the context of our solar system are discussed in Section 2.5.

2.2 A Brief Outline of the Finite-Time Stability Method

The finite-time stability method involves applying successively to the three-body problem a series of increasingly less pessimistic stability criteria which are valid for finite lengths of time. Estimates of these finite times during which the satellite system is clearly stable can then provide us with minimum durations of the satellite system perturbed by the Sun. If the minimum lifetime obtained from the first most pessimistic stability criterion is long enough to allow the next less pessimistic stability criteria to take effect, then the minimum duration of the system using the second stability criterion can be found. If this second minimum duration is long enough to enable the third stability criterion to be applied, a third, even longer, minimum duration can be calculated, and so on. In this manner, we can keep extending the minimum lifetime of the planetary system until all the possible stability criteria have been invoked.

The successive levels of the stability criteria are based on the natural periodic cycles found in the planet-satellite-Sun system. In the coplanar case these cycles are: the synodic, the conjunction and the mirror configuration cycles. The synodic cycle involves a repetition of the Sun and satellite positions with respect to each other. The conjunction cycle involves a repetition of the Sun and satellite positions with respect to each other and with respect to a fixed reference point. The mirror configuration cycle involves a repetition of the Sun and satellite positions with respect to each other and with respect to the apsidal line of the satellite's orbit in the circular case or the apsidal lines of both the satellite and the Sun's orbits in the elliptical case.

Note that the conjunction and the mirror configuration cycles simply consist of a specific number of synodic cycles. We use the synodic cycle as the basis for our periodic cycles because it is the smallest cycle involving both the Sun and satellite, that repeats a conjunction of these two bodies. This last point is of particular importance because perturbations caused by the Sun are greatest at conjunctions and therefore conjunctions provide the best chances for instabilities to occur.

We can therefore think of the minimum lifetimes of planet-satellite systems acting under solar perturbations as being the minimum number of synodic cycles or conjunctions that the satellites can survive without any dramatic changes occurring in

their orbital hierarchy.

For the stability criterion itself, we choose an orbital parameter which can indicate when the system is approaching an unstable situation. We show later in Sections 3.4 and 4.4 that for both the circular and elliptical coplanar restricted three body problems, the best orbital element for this purpose is the eccentricity of the satellite's orbit. As the satellite's eccentricity increases to a value of one, the system approaches an unstable situation where the satellite will either collide with its planet or escape from its gravitational influence.

At each level the stability criteria takes the most pessimistic viewpoint. It assumes that the worst possible change in the satellite's orbital eccentricity over the specified cycle is added on to the satellite's eccentricity every period of that cycle. This procedure is highly pessimistic since the changes in the eccentricity over any one of the three cycles vary in a cyclic manner about zero and depend on the position of the initial satellite-Sun conjunction with respect to the apsidal lines of the two orbits. However taking this most pessimistic view, the eccentricity is allowed to accumulate in this manner until some arbitrarily chosen upper limit for the eccentricity is reached, say $e_u = 0.5$. At this point we take the system to be approaching an unstable situation.

Attaining an eccentricity of $e_u = 0.5$ does not necessarily imply that the planetary system will become unstable. The eccentricity could either continue to increase to a value of one where the system would become unstable, or at some future date it could decrease to remove the system from the unstable situation. In either case, the time taken to reach the arbitrarily chosen upper limit of the eccentricity provides a measurable minimum lifetime for the satellite system.

The number of cycles needed to increase the eccentricity of the satellite's orbit from its original value to the upper limit is computed. The minimum duration of the satellite system then becomes the number of cycles the system is known to definitely survive unchanged, multiplied by the period of the cycle.

If this minimum duration is long enough to allow the satellite to move through at least several of the next longer periodic cycles, the next level of the finite-time stability criteria method can be applied. A new longer minimum duration using the maximum possible change in the eccentricity over the new periodic cycle is then

calculated. This procedure is continued until one of three events occur: either all the natural periodic cycles of the planetary system are exhausted; or the minimum duration of the system is no longer much greater than the period of the next largest cycle; or the eccentricity of the satellite grows beyond the arbitrarily chosen upper limit e_u within one of the cycles, even though the total eccentricity may subsequently decrease to give a very small change in the eccentricity over the whole cycle.

This description presents only a bare outline of the method. We shall explain the method in greater detail in Chapter 5, when we apply the method to the circular and elliptical coplanar restricted three-body models of Sun-perturbed satellite systems. But first, in order to do the above analysis, we must define the equations governing the general three-body problem and give the simplications which produce the circular and elliptical coplanar restricted three-body problems. We do this in the following sections.

2.3 Traditional Developments of the General Three-body Problem Written in Terms of the Orbital Elements

Here we describe the orbit of a satellite of mass m about a planet of mass M_p, where the motion of both bodies are affected by the gravitational influence of an external body, in this case the Sun, of mass m_1. We assume that the bodies act as point masses and that they are only undergoing orbital perturbations due to their mutual gravitational interactions. In other words, we assume that the effects of the shape and size of each body are negligible and that no other bodies affect the orbits of the three bodies appreciatively.

In the general three-body system so far described, the two closest bodies to each other of masses m and M_p can be thought of as moving in disturbed keplerian elliptical orbits about their common centre of mass, while the third body of mass m_1 can be thought of as moving in a much larger disturbed keplerian orbit about the centre of mass of the first two bodies.

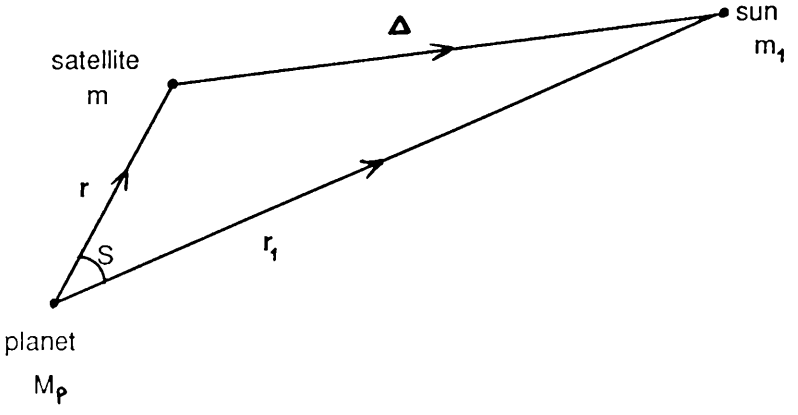

Figure 2.1 Using the general three-body model to describe a planet-satellite system perturbed by the Sun.

If **r** and $\mathbf{r}_1$ denote the position vectors of the masses m and m_1 relative to the

position of mass M_p (See Figure 2.1), the equations of motion for the masses m and m_1 are

$$\ddot{\mathbf{r}} + G(M_p + m)\frac{\mathbf{r}}{r^3} = G\,m_1\left(\frac{\mathbf{r}_1 - \mathbf{r}}{\Delta^3} - \frac{\mathbf{r}_1}{r_1^3}\right) \tag{1}$$

$$\ddot{\mathbf{r}}_1 + G(M_p + m_1)\frac{\mathbf{r}_1}{r_1^3} = G\,m\left(\frac{\mathbf{r} - \mathbf{r}_1}{\Delta^3} - \frac{\mathbf{r}}{r^3}\right)$$

where $r_1 > r$ and Δ is the distance between the two masses m and m_1.

$$\Delta = [\,(\mathbf{r}_1 - \mathbf{r}) \cdot (\mathbf{r}_1 - \mathbf{r})\,]^{1/2} \tag{2}$$

The derivations of these two equations can be found in any introductory text to celestial mechanics (eg Roy, 1988; Brouwer and Clemence, 1961; etc.). They can also be rewritten in the following form

$$\ddot{\mathbf{r}} = \nabla U = \nabla(U_0 + R)$$

$$\ddot{\mathbf{r}}_1 = \nabla U_1 = \nabla(U_{01} + R_1)$$

where

$$U_0 = \frac{G(M_p + m)}{r}$$

$$U_{01} = \frac{G(M_p + m_1)}{r_1}$$

$$R = G\,m_1\left(\frac{1}{\Delta} - \frac{\mathbf{r} \cdot \mathbf{r}_1}{r_1^3}\right) \tag{3}$$

$$R_1 = G\,m\left(\frac{1}{\Delta} - \frac{\mathbf{r}_1 \cdot \mathbf{r}}{r^3}\right)$$

and $$\nabla \equiv \mathbf{i}\frac{\partial}{\partial x} + \mathbf{j}\frac{\partial}{\partial y} + \mathbf{k}\frac{\partial}{\partial z}$$

R and R_1 are commonly known as the disturbing functions for the bodies m and m_1.

In the above equations, the coordinates of the satellite or mass m are given in terms of the positional vector $\mathbf{r} = (x, y, z)$, the velocity vector $\dot{\mathbf{r}} = (\dot{x}, \dot{y}, \dot{z})$ and time. A similar set of coordinates describes the location of the Sun or mass m_1.

(i) The orbital elements

For our purposes, it is more convenient to give the coordinates of the masses m and m_1 in terms of orbital elements which describe the orbit in space and the position of the body within that orbit. To do this, we require six orbital parameters corresponding to the six position and velocity coordinates: three to define the orientation of the orbit with respect to a set of axes (ie Ω, i, and ϖ); two to define the shape and size of the orbit within the orbital plane (ie a and e); and one to define a reference point within the orbit (ie τ or ϵ). The exact position of the body within the orbit can then be specified by giving the body's position in time or space relative to this reference point (ie using t, f, l, M, E or L).

Thus, if we study the celestial sphere in Figure 2.2(a), we see that the longitude of the ascending node Ω and the inclination i are sufficient to orient the orbital plane with respect to the ecliptic reference plane. Ω is the angular distance from the vernal equinox to the ascending node where the two planes intersect. It is measured eastward along the ecliptic plane and ranges from 0° to 360°. i is the angle between the ecliptic and orbital planes. It varies between 0° and 180°, where values greater than 90° indicate a body with retrograde motion.

The orientation of the orbit within the orbital plane is usually specified by the longitude of the pericentre ϖ. This parameter is the sum of two angular distances Ω and ω which exist in two different planes, the ecliptic and the orbital plane respectively.

$$\varpi = \Omega + \omega$$

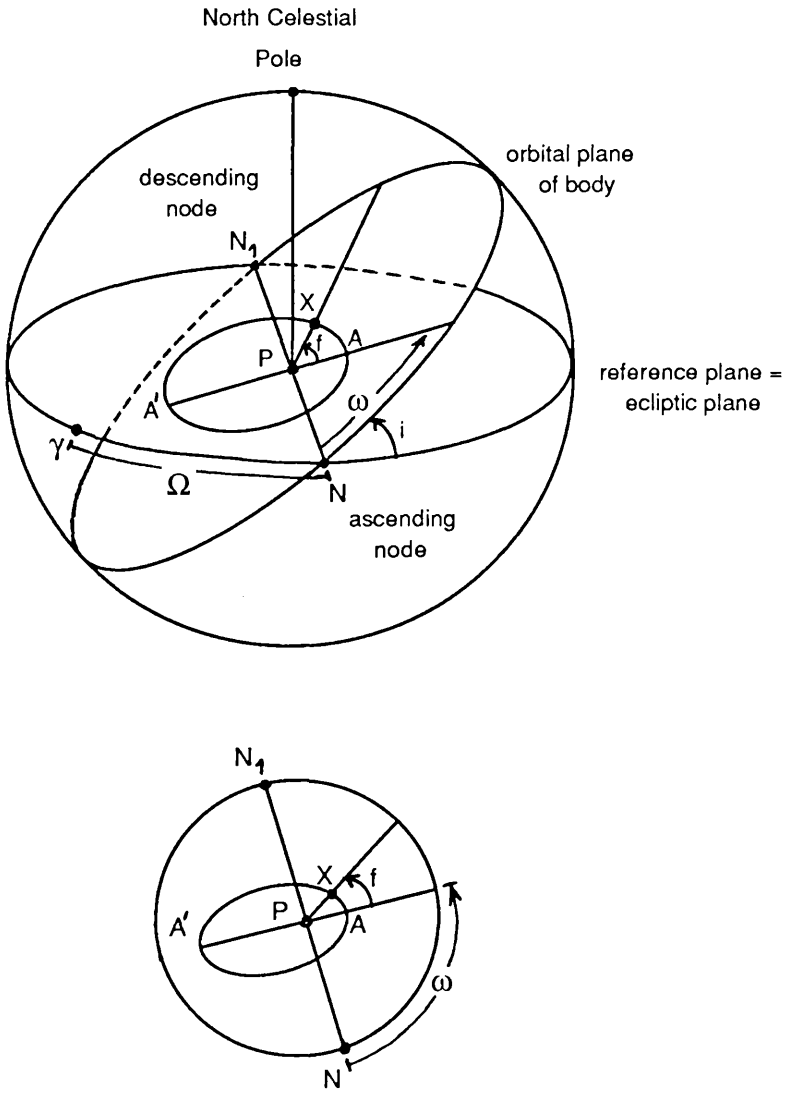

Figure 2.2 An illustration of the orbital elements which describe the elliptical orbit and position of a body X moving about its primary P.

γ is the position of the vernal equinox in the ecliptic plane. $\overline{NN_1}$ is the line of nodes where the ecliptic and orbital planes intersect, while $\overline{AA_1}$ is the line of apses of the elliptical orbit.

(a) is the three-dimensional view of the orbit referred to a celestial sphere whose equatorial plane is the ecliptic.

(b) is a two-dimensional view of the orbit seen within a great circle of the celestial sphere or the orbital plane.

ω, the argument of the pericentre, is the angle between the direction of the ascending node and the orbit's periapsis and is measured in the direction of motion. For an illustration of the angle ω and the following orbital elements found within the orbital plane see Figure 2.2(b).

The size of the elliptical orbit is described by the semi-major axis a and the shape of the orbit is stipulated by the ellipse's eccentricity e. Finally τ, a particular time at which the body passes through the pericentre of its orbit, gives a reference point within the orbit which can be used along with any other time t to fix the body's position within the orbit at that time.

At any instant in time, τ remains the time that the body arrived at its pericentre, but for convenience τ can be updated to correspond to later pericentre passages. If the orbit's orientation, shape or size are perturbed, then the scheduled arrival of the body at pericentre will also be changed.

Any one of the changing orbital angles such as the mean longitude l, the mean anomaly M, the eccentric anomaly E, the true anomaly f and the true longitude L can also be used instead of the variable time t.

The mean longitude l of the body is defined to be:

$$l = \varpi + n\,(t - \tau) \qquad (4)$$

where l specifies the position vector of the body in its orbit with respect to a combination of the periapsis and the vernal equinox, if the body were assumed to be moving at a constant angular velocity n. The mean motion n is given by:

$$n = 2\pi / T$$

where T is the orbital period.

The mean anomaly M is the angle swept out by a radius vector which rotates about the primary mass with a mean motion n and leaves pericentre with the real body.

$$M = n\,(t - \tau) \qquad (5)$$

The eccentric anomaly E is the angle swept out by a radius vector rotating about the centre of the ellipse where the eccentric anomaly and the mean anomaly are related to each other by Kepler's Equation:

$$M = E - e \sin E \qquad (6)$$

The true anomaly f is the angle beween the periapsis and the position vector of the body and is measured in the direction of motion. It is related to the eccentric anomaly by:

$$\tan \frac{f}{2} = \left(\frac{1 + e}{1 - e} \right)^{1/2} \tan \frac{E}{2} \qquad (7)$$

And finally, the true longitude L of the body gives the actual position of the body with respect to the vernal equinox by:

$$L = \varpi + f$$

These angular variables are all functions of time.

Similar to τ, the value of one of these changing angles at some special configuration of the bodies can also be used as a reference point to fix the satellite's position within its orbit. In a two body system the most obvious special configuration is the pericentre passage. Unfortunately by definition most of the angles previously mentioned are zero at this time. To avoid this problem, the reference point is often chosen to be the value of one of the changing angles at some given time, say $t = 0$, if τ is taken to be the time of pericentre passage.

Thus, for example, the mean longitude ϵ at the epoch (ie the mean longitude of the body's position at time $t = 0$, if τ is taken to be the time of pericentre passage) is often used as a reference point within the orbit.

ϵ is described by:

$$\epsilon = \varpi - n\tau \qquad (8)$$

and represents a fixed reference position within the body's orbit. However, mean longitudes are measured with respect to the vernal equinox, which is a fixed point outside the changing orbit. They are also dependant on the mean motion of the body and its expected time of arrival at pericentre. Therefore, the mean longitude ϵ of this specific reference point will change as the orientation, size and shape of the orbit change. Once ϵ is known, the position of the body within its orbit can be completely described for any time t by giving the body's mean longitude

$$l = n\,t + \epsilon \qquad (9)$$

We describe these orbital parameters at great length because later it becomes very important to understand clearly which parameters are independent and therefore sufficient to describe the body's orbit, and which are dependent and therefore can be eliminated. In summary, six orbital elements (Ω, i, ϖ, e, a, τ) and time t are necessary to describe a body's elliptical orbit and position within that orbit fully. The orbital parameters τ, ϵ and any other specific values of the time variables t, f, l, M, E and L are all dependent on each other, just as the time variables themselves are equivalent to each other.

(ii) Lagrange's planetary equations of motion

Equations (1) can be rewritten in terms of the orbital elements by applying the method of variation of parameters where the position and velocity coordinates are taken to be functions of the six orbital elements. This calculation was first performed by Lagrange to produce what are known today as Lagrange's planetary equations. See Brouwer and Clemence (1961), Chapter XI for a complete derivation of these equations.

The following are one form of Lagrange's planetary equations:

$$\frac{da}{dt} = \frac{2}{na}\frac{\partial R}{\partial \epsilon} \tag{10a}$$

$$\frac{de}{dt} = -\frac{\sqrt{1-e^2}}{na^2 e}\left(1-\sqrt{1-e^2}\right)\frac{\partial R}{\partial \epsilon} - \frac{\sqrt{1-e^2}}{na^2 e}\frac{\partial R}{\partial \varpi} \tag{10b}$$

$$\frac{d\epsilon}{dt} = -\frac{2}{na}\frac{\partial R}{\partial a} + \frac{\sqrt{1-e^2}}{na^2 e}\left(1-\sqrt{1-e^2}\right)\frac{\partial R}{\partial e} + \frac{\tan\frac{i}{2}}{na^2\sqrt{1-e^2}}\frac{\partial R}{\partial i} \tag{10c}$$

$$\frac{d\Omega}{dt} = \frac{1}{na^2\sqrt{1-e^2}\,\sin i}\frac{\partial R}{\partial i} \tag{10d}$$

$$\frac{d\varpi}{dt} = \frac{\sqrt{1-e^2}}{na^2 e}\frac{\partial R}{\partial e} + \frac{\tan\frac{i}{2}}{na^2\sqrt{1-e^2}}\frac{\partial R}{\partial i} \tag{10e}$$

$$\frac{di}{dt} = -\frac{\tan\frac{i}{2}}{na^2\sqrt{1-e^2}}\left(\frac{\partial R}{\partial \epsilon} + \frac{\partial R}{\partial \varpi}\right) - \frac{1}{na^2\sqrt{1-e^2}\,\sin i}\frac{\partial R}{\partial \Omega} \tag{10f}$$

where the mean motion n is a function of the semi-major axis 'a' through Kepler's third law:

$$n^2 a^3 = G\,(M_p + m) = \mu \tag{11}$$

and R is the disturbing function given by Equation (3), but expressed in terms of the orbital elements. An equivalent set of first order differential equations exist for the orbital elements of the external mass m_1, where its orbital elements and disturbing function are distinguished from those of mass m by using a subscript 1. Note that Equations (10a) to (10f) are exact.

In order to solve Lagrange's planetary equations, the disturbing function R needs to be expressed in terms of the orbital elements. This can be done by writing

$$R = G\,m_1\left(\frac{1}{\Delta} - \frac{r\cos S}{r_1^2}\right) \tag{12}$$

where S is the angle between the two radius vectors **r** and $\mathbf{r}_1$. See Figure 2.1. Then, using the law of cosines for a plane triangle whose vertices are the locations of the bodies M_p, m and m_1, Equation (2) becomes

$$\Delta = (r^2 + r_1^2 - 2\, r\, r_1 \cos S)^{1/2} \tag{13}$$

where r is given by the polar equation of an ellipse expressed in terms of the orbital elements.

$$r = \frac{a(1 - e^2)}{1 + e \cos f} \tag{14}$$

There is a similar equation for r_1 in terms of the orbital elements of m_1. Note that the angles S and f are related to each other and that both are functions of time.

(iii) Different expansions of the disturbing function

In the case of a planetary satellite disturbed by the Sun, the terms r/Δ and r/r_1 in Equation (12) are much smaller than 1. The disturbing function R can therefore be expanded into a rapidly converging series. This expansion can still be performed even if the above restriction is not valid, but convergence may be very slow and many terms are required in the expansion.

Typically, the disturbing function is expanded in a series containing increasing powers of $\alpha = a/a_1$, e, e_1, i and i_1 since these orbital elements are generally small for the majority of the satellites found in the solar system. Once expanded, the disturbing function has a general form similar to the following

$$R = G\, m_1 \sum_{i=1}^{n} P_i(a, a_1, e, e_1, i, i_1) \cos \phi_i \tag{15}$$

where $$\phi_i = j_1\, l + j_2\, l_1 + j_3\, \varpi + j_4\, \varpi_1 + j_5\, \Omega + j_6\, \Omega_1 \tag{16}$$

j_k are integers for k = 1 to 6.

Any equivalent orbital elements can be used instead of a, e, i, l, ϖ and Ω, as long as six independent elements and a time variable are included. Some parameters are better than others, depending on the three-body system being integrated.

Time is used as the independent variable for the majority of the older methods of expanding the disturbing function. This necessitates the use of the mean anomalies M and M_1 in the angle ϕ, so that the angle can be written as a function of time. The disturbing function R can be expressed in terms of M and M_1 either directly or indirectly. In the indirect method R is first written in terms of the true anomalies f and f_1 or the eccentric anomalies E and E_1. It is then expanded and finally expressed in terms of the mean anomalies.

Laplace was the first to produce a literal development of the disturbing function. He expanded it to third order in e, e_1, i and i_1. Pierce (1849) carried the expansion out to sixth order, while Leverrier (1855) extended the development to include seventh order terms and provided a list of all the possible arguments ϕ and their corresponding coefficients by classifying them according to the sum of the coefficient of their mean longitudes or their order $N = | j_1 + j_2 |$.

In an amazing effort to describe analytically the orbital coordinates of the Moon as functions of time, Delaunay (1867) expanded the disturbing function to seventh order, performing over 500 canonical transformations to reduce the function term by term. After twenty years of work, he finally found analytical expressions for the Moon's ecliptic latitude, ecliptic longitude and sine parallax. His work is totally analytic and can therefore be applied to any satellite problem; however, his final series are only slowly convergent.

In order to save time and effort, people began substituting numerical values for some or all of the elements of the elliptical orbit before expanding R. With this method, only the remaining elements are left in the literal form to be expanded analytically. Such a mixed numerical and analytical expansion was first published by Hansen (1831) and applied to the mutual perturbations of Jupiter and Saturn. Later, Hansen (1843) derived a numerical expansion using the eccentric anomaly as the

time variable and applied it to the perturbations of the asteroids. Hill (1890) developed a further modification to Hansen's theory on the Jupiter-Saturn-Sun system by using the mean anomaly of one planet and the eccentric anomaly of the other. Newcomb generated to sixth order two literal developments of R, one in terms of the eccentric anomalies and one in terms of the mean anomalies. He applied these expansions to the motions of Uranus and Neptune (Newcomb,1865 and 1874) and to the secular perturbations of the four inner planets (Newcomb, 1891, 1895a and 1895b).

There is a vast literature on the different methods of expanding the disturbing function. See for example Plummer (1918), Brown and Shook (1933), Smart (1953), Brouwer and Clemence (1961), Hagihara (1972a, 1972b) and Cook (1988). Brouwer and Clemence included in their introductory text on celestial mechanics a fourth order expansion in e, e_1, i and i_1 for arguments ϕ of order equal to zero and a third order expansion for the remaining terms. Terms of order zero or the secular terms are those terms whose arguments contain only the slowly varying parameters ϖ, ϖ_1, Ω and Ω_1. They therefore can accumulate in any expansion of R, making it necessary to know them to higher order, in order to obtain the same degree of accuracy as with the other terms.

(iv) Dominant terms in R

Here lies the chief difficulty in any expansion of the disturbing function. Depending on the particular three-body system being studied, certain combinations of the angles forming ϕ can dominate the expansion of R. Thus, in order to get the same degree of accuracy as for the rest of the terms, the coefficients of these dominant terms are required to a higher order in α, e, e_1, i and i_1. Therefore, it becomes important to be able to distinguish which terms will make significant contributions to R over the integration time period and which will not, so as to avoid expanding every term to the same high degree of accuracy and wasting much time and effort.

We have already seen that secular terms in the expansion of R will dominate any integration of Lagrange's planetary equations, but there can also exist a set of terms containing a special combination of the orbital angles, which have a similar

effect. If the ratio of the mean motions of the two bodies m_1 and m is very close to a perfect small numbered fraction:

$$\frac{n_1}{n} = \frac{b}{c}$$

where b and c are small integers, then any terms containing the argument ϕ where $j_1/j_2 = - b/c$ will result in

$$0 \approx j_1 \, n + j_2 \, n_1$$

which may produce large amplitude terms.

This can easily be seen by writing Equation (10a) in terms of the mean motion and mean longitude using Equations (9) and (11).

$$\frac{d n}{d t} = - \frac{3}{a^2} \frac{\partial R}{\partial l} \tag{17}$$

Then, if we substitute Equation (15) into Equation (17), we get:

$$\frac{d n}{d t} = \frac{3 \, j_1}{a^2} G \, m_1 P \sin \phi \tag{18}$$

As a first approximation to the solution of Equation (18), we can substitute Equation (9) into Equation (16) and assume the angles ϖ, ϖ_1, Ω, and Ω_1 to be so slowly varying with time as to be almost constant.

$$\phi = (j_1 \, n + j_2 \, n_1) \, t + \text{constants} \tag{19}$$

Then, if to a first approximation the orbital elements on the right hand side of Equation (18) are assumed to be constant with respect to time, Equation (18) can be

easily integrated using Equation (19). The result

$$n - n_0 \cong - \frac{1}{j_1 n + j_2 n_1} \frac{3 j_1}{a^2} G m_1 P \cos \phi$$

clearly shows that if j_1 and j_2 are such that $0 \approx j_1 n + j_2 n_1$, the integrated term will be large enough to dominate the rest of the terms in the expansion of R. These type of terms are called resonant terms.

Unfortunately, because any ratio of mean motions n_1/n can always be approximated by a ratio of two integers to arbitrary accuracy, there should be an infinite number of resonant terms which could be significant in the expansion of the disturbing function. However, since the strength of the lowest order term involving e, e_1, i, and i_1, is given by:

$$P = \frac{f(\alpha)}{a_1} e^{|j_3|} e_1^{|j_4|} \left(\sin \frac{i}{2}\right)^{|j_5|} \left(\sin \frac{i_1}{2}\right)^{|j_6|} \qquad (20)$$

the dominant resonant terms are only those whose arguments involve the smallest values of j_3, j_4, j_5 and j_6. Equation (20) is found by expanding the disturbing function using Legendre polynomials, where $f(\alpha)$ is some known function of the ratio of the semi-major axes. See Kaula (1962), Allan (1969) and Dermott, Malhotra and Murray (1988).

Thus, if the ratio of the semi-major axes $\alpha = a/a_1$ is ever equivalent to a ratio of the mean motions n_1/n that is nearly equal to a low numbered fraction b/c, resonant terms may dominate the disturbing function. Those terms containing the argument $\phi = j_1 l + j_2 l_1 + \ldots$, where $j_1/j_2 = -$ b/c will therefore have to be expanded to a higher order to attain the same degree of accuracy as that found for the rest of the terms.

If α is never a value which produces a low numbered integer fraction for the

ratio n_1/n, then there is no need to worry about resonant terms dominating the expansion of R. It is necessary in this case, only to guarantee that the secular terms are expanded to a sufficiently high degree of accuracy.

Thus as a final conclusion, the most efficient method of expanding R, and the degree to which individual terms in R should be expanded in order to obtain a specified accuracy, both depend very much on the particular problem being studied.

(v) The solution to Lagrange's planetary equations

Once the disturbing function R has been expanded using whichever method suits the problem best, the expansion is substituted into Lagrange's planetary equations. A first order approximation to the solution is obtained by treating the orbital elements a, e, i, Ω, ϖ and ϵ as constants on the right hand sides of Lagrange's planetary equations. These equations are then integrated with respect to the chosen independent time variable, to get the first order perturbations.

Second order perturbations can be included by replacing the orbital elements on the right hand side of Equations (10) with the results of the first order theory. Likewise, a third order approximation can be made by substituting into Equations (10) the results of the second order theory, and so on. These higher order approximations are only necessary, however, if higher powers of the ratio m/M_p are required in order to obtain the desired accuracy.

The solutions found by expanding Lagrange's planetary equations in a Taylor series of sines and cosines were unfortunately proven to be generally divergent by Poincaré in 1893. The solutions can, however, provide accurate measurements of the changes in the orbital elements for time intervals spanning as much as thousands of years in the past or future. This accuracy is sufficient for our purposes.

2.4 Development of the Coplanar Restricted Three-Body Problem

We now simplify the problem by assuming that the mass m of the satellite is negligible compare to the masses of the planet M_p and the Sun m_1. The satellite's mass therefore has no disturbing effect on the planet's or Sun's orbit, and the centre of mass of the planet-satellite system is located at the planet's centre. The planet-Sun system can now be treated as a simple two body problem where, in a planetocentric system, the Sun moves in a fixed keplerian orbit about the planet. In the literature, this three-body model is referred to as the restricted three-body problem.

We simplify the model even further by assuming that the satellite moves only within the orbital plane of the other two bodies, thus reducing the problem to the coplanar restricted three-body problem. Because the three-body system is assumed to be coplanar, both the inclination i and the longitude of the ascending node are no longer needed in order to describe a body's orbit fully. Therefore, if we take $i=\Omega=0$, then the orbital plane becomes the ecliptic plane, the longitude of the perihelion ϖ is equal to the argument of the pericentre ω, and the reference direction is now solely given by the vernal equinox. See Figure 2.3.

The equations of motion for the mass m now simplify to:

$$\frac{da}{dt} = \frac{2}{na}\frac{\partial R}{\partial \epsilon} \tag{21 a}$$

$$\frac{de}{dt} = -\frac{\sqrt{1-e^2}}{na^2 e}\left(1-\sqrt{1-e^2}\right)\frac{\partial R}{\partial \epsilon} - \frac{\sqrt{1-e^2}}{na^2 e}\frac{\partial R}{\partial \varpi} \tag{21 b}$$

$$\frac{d\varpi}{dt} = \frac{\sqrt{1-e^2}}{na^2 e}\frac{\partial R}{\partial e} \tag{21 c}$$

$$\frac{d\epsilon}{dt} = -\frac{2}{na}\frac{\partial R}{\partial a} + \frac{\sqrt{1-e^2}}{na^2 e}\left(1-\sqrt{1-e^2}\right)\frac{\partial R}{\partial e} \tag{21 d}$$

while the motion of the external body m_1 can be completely described in terms of the two body problem, where r_1 is simply given by the polar equation of a conic section.

$$r_1 = \frac{p}{1 + e_1 \cos f_1} \qquad p = \text{constant}$$

In addition use can be made of the standard auxiliary two body equations, such as Kepler's equation.

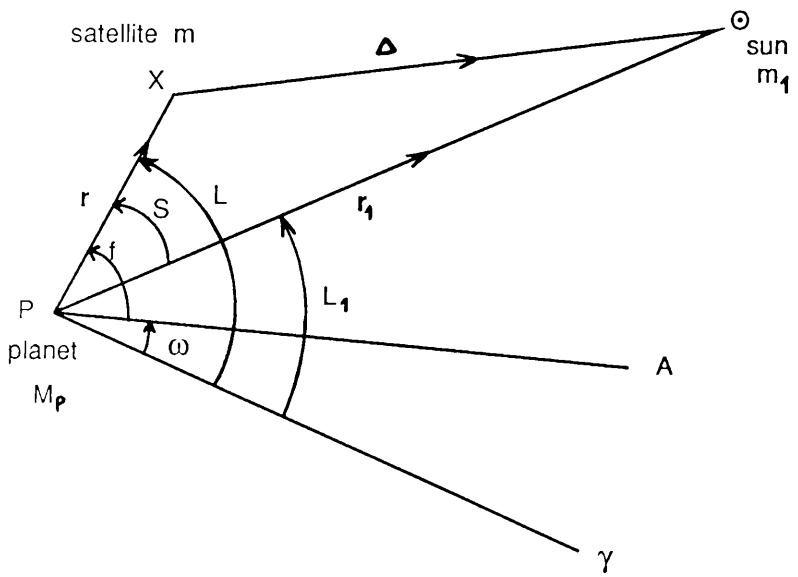

Figure 2.3 Using the coplanar three-body model to describe a planet-satellite system perturbed by the sun.

The orbital plane of the satellite is now the ecliptic plane and $\overline{PA}$ lies in the direction of the periapsis of the satellite's orbit.

We need now only choose the most efficient method, for our particular problem, of expanding the disturbing function and integrating the equations of motion.

Our sole purpose for integrating Lagrange's planetary equations of motion is to find an expression for the change in the orbital elements of the satellite over one synodic period, so that we can then begin to apply the first level of our finite-time stability criteria. With this in mind, the obvious independent time variable to use is S, the angle between the two radius vectors $\mathbf{r}$ and $\mathbf{r}_1$.

The passing of one synodic period is then just the movement of S through an angle of 2π. For mathematical convenience, we take the initial value of S to be $-\pi$. The initial configuration is then one where the two bodies m and m_1 are at opposition. Moving through one synodic period, the two bodies reach conjunction at S = 0 and their final configuration at S = $+\pi$, where they are at opposition again.

The change in the orbital elements $\Delta\sigma$ over one synodic period where σ = a, e, ϖ or ϵ is then:

$$\Delta\sigma = \int_{-\pi}^{+\pi} \frac{d\sigma(S)}{dS}\, dS \qquad (22)$$

We therefore need only find expressions for $d\sigma/dS$ and integrate with respect to S.

In order to express Lagrange's planetary equations (21) in terms of the angle S, it is easier to first express them in terms of the true anomaly f. Most of the variables in Equations (21) involve r and therefore can be easily written in terms of f using Equation (14). The remainder of this section is spent performing this transformation.

To write Equation (21) in terms of f, we use Brouwer and Clemence's (1961) expressions for $\partial R/\partial e$, $\partial R/\partial \epsilon$, and $\partial R/\partial \varpi$ written as functions of the radial distance r and the true longitude L of the perturbed body. See Figure 2.3.

$$\frac{\partial R}{\partial e} = -a \cos f \frac{\partial R}{\partial r} + \left(\frac{1}{1 - e^2} + \frac{a}{r} \right) \sin f \frac{\partial R}{\partial L} \tag{23a}$$

$$\frac{\partial R}{\partial \epsilon} = \frac{a\, e \sin f}{(1 - e^2)^{1/2}} \frac{\partial R}{\partial r} + \frac{a^2}{r^2} (1 - e^2)^{1/2} \frac{\partial R}{\partial L} \tag{23b}$$

$$\frac{\partial R}{\partial \varpi} = \frac{-a\, e \sin f}{(1 - e^2)^{1/2}} \frac{\partial R}{\partial r} + \left[1 - \frac{a^2}{r^2} (1 - e^2)^{1/2} \right] \frac{\partial R}{\partial L} \tag{23c}$$

These formulae are easily derived using the standard two-body problem equations. Using a similar procedure, we now derive an expression for the remaining partial derivative $\partial R/\partial a$.

We do not use the Brouwer and Clemence (1961) version of $\partial R/\partial a$ because it involves the orbital parameter ϵ' instead of ϵ, where $l = \int n dt + \epsilon'$ replaces $l = nt + \epsilon$. They make this adustment in order to avoid having the variable 'a' present both explicitly in the coefficients of the expanded terms of the disturbing function, and implicitly in their arguments through $l = nt + \epsilon$ and $n^2 a^3 = \mu$. Converting ϵ to ϵ' eliminates the possibility of having mixed terms containing t both outside and inside the arguments, and hence simplifies the integration of the terms with respect to t. In our development, mixed terms of S are not difficult to integrate and we prefer to keep the development as close to first principles as possible. We therefore do not make the simplification of using ϵ'.

When ϵ' is used instead of ϵ, the variable n in the expression for $\partial R/\partial a$ is not taken to be a function of 'a' during the partial derivation. We do however keep the use of the orbital element ϵ, and therefore retain the mean motion's dependence on the semi-major axis. Thus we must derive $\partial R/\partial a$ ourselves.

(i) Derivation of $\partial R/\partial a$

Beginning with Equation (12) and (13), we differentiate R with respect to 'a' to get:

$$\frac{\partial R}{\partial a} = G m_1 \left\{ \left[-\frac{r}{\Delta^3} + \left(\frac{1}{\Delta^3} - \frac{1}{r_1^3} \right) r_1 \cos S \right] \frac{\partial r}{\partial a} - \left(\frac{1}{\Delta^3} - \frac{1}{r_1^3} \right) r\, r_1 \sin S \frac{\partial S}{\partial a} \right\}$$

The partial derivatives of r and S with respect to the semi-major axis 'a' can be found as follows. Differentiating Equation (14), $\partial r/\partial a$ becomes

$$\frac{\partial r}{\partial a} = \frac{1 - e^2}{1 + e \cos f} + \frac{r^2 e \sin f}{a(1 - e^2)} \frac{\partial f}{\partial a}$$

where the true anomaly f is a function of the semi-major axis 'a' through the two-body relations Equations (7), (6), (5) and (11). ie

$$f = F(E) = F_1(M) = F_2(n, t) = F_3(a, t)$$

$\partial S/\partial a$ can also be expressed in terms of $\partial f/\partial a$ through:

$$S = f + \varpi - L_1$$

$$\frac{\partial S}{\partial a} = \frac{\partial f}{\partial a}$$

$\partial f/\partial a$ may be found by differentiating Equation (7) to get

$$\frac{\partial f}{\partial a} = \frac{1 - e}{(1 - e) \cos^2 \frac{E}{2} + (1 + e) \sin^2 \frac{E}{2}} \left(\frac{1 + e}{1 - e} \right)^{1/2} \frac{\partial E}{\partial a}$$

Differentiation of Equations (5) and (6) with respect to 'a' gives

$$\frac{\partial E}{\partial a} (1 - e \cos E) = t \frac{\partial n}{\partial a}$$

where $\partial n/\partial a$ is simply

$$\frac{\partial n}{\partial a} = -\frac{3}{2}\frac{n}{a}$$

by Kepler's third law. Hence, if we use the two-body relation r = a(1-ecosE), $\partial E/\partial a$ simplifies to

$$\frac{\partial E}{\partial a} = -\frac{3}{2}\frac{n}{r}t$$

Substitution of $\partial E/\partial a$ into our equation for $\partial f/\partial a$ gives

$$\frac{\partial f}{\partial a} = -\frac{3}{2}\frac{a\sqrt{1-e^2}}{r^2}\,n\,t$$

and as a result, $\partial r/\partial a$ and $\partial S/\partial a$ become

$$\frac{\partial r}{\partial a} = \frac{r}{a} - \frac{3}{2}\frac{e\,n\,t\,\sin f}{\sqrt{1-e^2}}$$

$$\frac{\partial S}{\partial a} = \frac{\partial f}{\partial a} = -\frac{3}{2}\frac{a\sqrt{1-e^2}\;n\,t}{r^2}$$

Finally, if we now substitute these two equations into our original expression for the partial derivative of the disturbing function R with respect to the semi-major axis 'a', we get, after some simplification:

$$\frac{\partial R}{\partial a} = Gm_1\left\{ r_1\left(\frac{1}{\Delta^3} - \frac{1}{r_1^3}\right)\left[\left(\frac{r}{a} - \frac{3}{2}\frac{e\,n\,t\,\sin f}{\sqrt{1-e^2}}\right)\cos S + \frac{3}{2}\frac{a\sqrt{1-e^2}\;n\,t}{r}\sin S\right] - \frac{r}{\Delta^3}\left(\frac{r}{a} - \frac{3}{2}\frac{e\,n\,t\,\sin f}{\sqrt{1-e^2}}\right)\right\} \qquad (24)$$

(ii) Derivation of $\partial R/\partial r$ and $\partial R/\partial L$

Returning to Brouwer and Clemence's partial derivatives of the disturbing function with respect to the orbital elements e, ϵ, and ϖ, we now express the derivatives $\partial R/\partial r$ and $\partial R/\partial L$ found within these equations in terms of the true anomaly f through r and Δ.

Differentiating Equations (12) and (13) with respect to r gives

$$\frac{\partial R}{\partial r} = G m_1 \left[r_1 \left(\frac{1}{\Delta^3} - \frac{1}{r_1^3} \right) \cos S - \frac{r}{\Delta^3} \right] \qquad (25)$$

$\partial R/\partial L$ can be rewritten as follows

$$\frac{\partial R}{\partial L} = \frac{\partial R}{\partial S} \frac{\partial S}{\partial L} = \frac{\partial R}{\partial S}$$

since $L = S + L_1$. Then differentiating Equations (12) and (13) with respect to S gives

$$\frac{\partial R}{\partial L} = -G m_1 \left(\frac{1}{\Delta^3} - \frac{1}{r_1^3} \right) r r_1 \sin S \qquad (26)$$

(iii) An exact form of Lagrange's planetary equations with respect to time

We are now ready to substitute our complete set of partial derivatives of R with respect to 'a' (ie Equation 24), e, ϵ, and ϖ (ie a combination of Equations (23), (25) and (26)) into Lagrange's planetary Equations (21).

Substitution of Equations (23) into Lagrange's planetary Equations (21 a to c) produces, after some simplification:

$$\frac{de}{dt} = \frac{\sqrt{1 - e^2}}{n a^2 e} \left\{ a e \sin f \frac{\partial R}{\partial r} + \left[(1 - e^2) \frac{a^2}{r^2} - 1 \right] \frac{\partial R}{\partial L} \right\}$$

$$\frac{da}{dt} = \frac{2}{na}\left\{ \frac{a\,e\,\sin f}{(1-e^2)^{1/2}}\frac{\partial R}{\partial r} + \frac{a^2}{r^2}(1-e^2)^{1/2}\frac{\partial R}{\partial L} \right\}$$

$$\frac{d\varpi}{dt} = \frac{\sqrt{1-e^2}}{na^2 e}\left\{ -a\,\cos f\frac{\partial R}{\partial r} + \left(\frac{1}{1-e^2} + \frac{a}{r}\right)\sin f\,\frac{\partial R}{\partial L} \right\}$$

Equations (25) and (26) for $\partial R/\partial r$ and $\partial R/\partial L$ can now be substituted into the above equations to give the first three rates of change of the orbital elements with respect to time. The fourth, the rate of change of the mean longitude at the epoch, is found by substituting Equation (24) into the appropriate Lagrange's planetary equation (21d) rewritten in terms of ϖ or

$$\frac{d\epsilon}{dt} = -\frac{2}{na}\frac{\partial R}{\partial a} + \left(1-\sqrt{1-e^2}\right)\frac{d\varpi}{dt}$$

Hence

$$\frac{de}{dt} = G m_1 \frac{\sqrt{1-e^2}}{na^2 e}\left\{ r_1\left(\frac{1}{\Delta^3} - \frac{1}{r_1^3}\right)\left[a\,e\,\sin f\cos S - \left((1-e^2)\frac{a^2}{r^2} - 1\right) r\sin S\right] - \frac{a\,e\,r\,\sin f}{\Delta^3}\right\} \tag{27a}$$

$$\frac{da}{dt} = \frac{2\,G m_1}{na}\left\{ r_1\left(\frac{1}{\Delta^3} - \frac{1}{r_1^3}\right)\left[\frac{a\,e\,\sin f\cos S}{(1-e^2)^{1/2}} - \frac{a^2}{r}(1-e^2)^{1/2}\sin S\right] - \frac{a\,e\,r\,\sin f}{(1-e^2)^{1/2}\,\Delta^3}\right\} \tag{27b}$$

$$\frac{d\varpi}{dt} = -\frac{G m_1\sqrt{1-e^2}}{na^2 e}\left\{ r_1\left(\frac{1}{\Delta^3} - \frac{1}{r_1^3}\right)\left[a\,\cos f\cos S + r\left(\frac{1}{1-e^2} + \frac{a}{r}\right)\sin f\sin S\right] - \frac{a\,r\,\cos f}{\Delta^3}\right\} \tag{27c}$$

$$\frac{d\epsilon}{dt} = -\frac{2 G m_1}{n a}\left\{ r_1\left(\frac{1}{\Delta^3} - \frac{1}{r_1^3}\right)\left[\left(\frac{r}{a} - \frac{3}{2}\frac{e\,n\,t\,\sin f}{\sqrt{1-e^2}}\right)\cos S + \frac{3}{2}\frac{a\sqrt{1-e^2}\,n\,t}{r}\sin S\right]\right.$$
$$\left. -\frac{r}{\Delta^3}\left(\frac{r}{a} - \frac{3}{2}\frac{e\,n\,t\,\sin f}{\sqrt{1-e^2}}\right)\right\} + \left(1 - \sqrt{1-e^2}\right)\frac{d\varpi}{dt} \qquad (27d)$$

Finally, we express r in terms of the true anomaly f using Equation (14), simplify, and get the following rates of change of the orbital elements with time:

$$\frac{de}{dt} = G m_1 \frac{\sqrt{1-e^2}}{n a}\left\{ r_1\left(\frac{1}{\Delta^3} - \frac{1}{r_1^3}\right)\left[\sin f \cos S - \left(\frac{e(1+\cos^2 f) + 2\cos f}{1 + e\cos f}\right)\sin S\right]\right.$$
$$\left. -\frac{r\,\sin f}{\Delta^3}\right\} \qquad (28a)$$

$$\frac{da}{dt} = \frac{2 G m_1}{n\sqrt{1-e^2}}\left\{ r_1\left(\frac{1}{\Delta^3} - \frac{1}{r_1^3}\right)[e\sin f\cos S - (1 + e\cos f)\sin S]\right.$$
$$\left. -\frac{e\,r\,\sin f}{\Delta^3}\right\} \qquad (28b)$$

$$\frac{d\varpi}{dt} = -\frac{G m_1\sqrt{1-e^2}}{nae}\left\{ r_1\left(\frac{1}{\Delta^3} - \frac{1}{r_1^3}\right)\left[\cos f\cos S + \left(\frac{2 + e\cos f}{1 + e\cos f}\right)\sin f\sin S\right]\right.$$
$$\left. -\frac{r\,\cos f}{\Delta^3}\right\} \qquad (28c)$$

$$\frac{d\epsilon}{dt} = -\frac{2 G m_1}{n a\sqrt{1-e^2}}\left\{ r_1\left(\frac{1}{\Delta^3} - \frac{1}{r_1^3}\right)\left[\left(\frac{(1-e^2)^{3/2}}{1 + e\cos f} - Ne\sin f\right)\cos S + N(1 + e\cos f)\sin S\right]\right.$$
$$\left. -\frac{r}{\Delta^3}\left(\frac{(1-e^2)^{3/2}}{1 + e\cos f} - Ne\sin f\right)\right\} + \left(1 - \sqrt{1-e^2}\right)\frac{d\varpi}{dt} \qquad (28d)$$

where $N = \frac{3}{2} n t$

(iv) An exact form of Lagrange's planetary equations with respect to the true anomaly

It remains only to transform the derivatives with respect to time to ones with

respect to the true anomaly f. This is easily done using Kepler's second law

$$r^2 \frac{df}{dt} = n a^2 \sqrt{1 - e^2}$$

$$\frac{d\sigma}{df} = \frac{d\sigma}{dt} / \frac{df}{dt}$$

Hence,

$$\frac{d\sigma}{df} = \left(\frac{r}{a}\right)^2 \frac{1}{n\sqrt{1 - e^2}} \frac{d\sigma}{dt}$$

where σ is one of the orbital elements a, e, ϖ or ϵ.

Lagrange's planetary equations now become

$$\frac{de}{df} = \frac{Gm_1}{n^2 a} \left(\frac{r}{a}\right)^2 \left\{ r_1 \left(\frac{1}{\Delta^3} - \frac{1}{r_1^3}\right) \left[\sin f \cos S - \left(\frac{e(1 + \cos^2 f) + 2\cos f}{1 + e\cos f}\right) \sin S\right] - \frac{r}{\Delta^3} \sin f \right\} \tag{29a}$$

$$\frac{da}{df} = \frac{2Gm_1}{n^2 (1 - e^2)} \left(\frac{r}{a}\right)^2 \left\{ r_1 \left(\frac{1}{\Delta^3} - \frac{1}{r_1^3}\right) [e \sin f \cos S - (1 + e \cos f) \sin S] - \frac{e\, r}{\Delta^3} \sin f \right\} \tag{29b}$$

$$\frac{d\varpi}{df} = -\frac{Gm_1}{n^2 a e} \left(\frac{r}{a}\right)^2 \left\{ r_1 \left(\frac{1}{\Delta^3} - \frac{1}{r_1^3}\right) \left[\cos f \cos S + \left(\frac{2 + e\cos f}{1 + e\cos f}\right) \sin f \sin S\right] - \frac{r}{\Delta^3} \cos f \right\} \tag{29c}$$

$$\frac{d\epsilon}{df} = -\frac{2Gm_1}{n^2 a (1 - e^2)} \left(\frac{r}{a}\right)^2 \left\{ r_1 \left(\frac{1}{\Delta^3} - \frac{1}{r_1^3}\right) \left[\left(\frac{(1 - e^2)^{3/2}}{1 + e\cos f} - Ne \sin f \right) \cos S + N(1 + e\cos f) \sin S \right] \right.$$

$$\left. - \frac{r}{\Delta^3} \left(\frac{(1 - e^2)^{3/2}}{1 + e\cos f} - Ne \sin f \right) \right\} + \left(1 - \sqrt{1 - e^2}\right) \frac{d\varpi}{dt} \tag{29d}$$

where $N = \frac{3}{2} n t$

In order to work with a totally dimensionless set of parameters we make the following simplification. Since we have assumed that $m_1 >>> M_p$, the constant Gm_1/n^2 found in Equations (29) can therefore be rewritten in terms of a ratio of the mean motions and ultimately in terms of a ratio of the semi-major axes. By Kepler's third law

$$a_1^3 n_1^2 = G(M_p + m_1) \approx G m_1$$

Hence,

$$\frac{G m_1}{n^2} \approx a_1^3 \nu^2 \qquad \text{where } \nu = \frac{n_1}{n} \qquad (30)$$

ν is simply a function of $\alpha = a/a_1$ and a ratio of the masses μ through Kepler's third law.

$$\nu^2 = \alpha^3 \mu \qquad \text{where } \mu = \frac{m_1}{M_p + m} \qquad (31)$$

If we now substitute the dimensionless Equations (30) and (31) into Lagrange's planetary Equations (29) and regroup terms into ratios of a, a_1, r and r_1 so that terms can be expressed as functions of the dimensionless α, we obtain

$$\frac{de}{df} = \nu^2 \left(\frac{r}{a}\right)^2 \left\{ \frac{r_1}{a} \left(\frac{a_1^3}{\Delta^3} - \frac{a_1^3}{r_1^3} \right) \left[\sin f \cos S - \left(\frac{e(1+\cos^2 f) + 2\cos f}{1 + e\cos f} \right) \sin S \right] \right.$$

$$\left. - \frac{a_1^3}{\Delta^3} \frac{r}{a} \sin f \right\} \qquad (32a)$$

$$\frac{d\alpha}{df} = \frac{2\nu^2}{1-e^2} \left(\frac{r}{a}\right)^2 \left\{ \frac{r_1}{a_1} \left(\frac{a_1^3}{\Delta^3} - \frac{a_1^3}{r_1^3} \right) [e \sin f \cos S - (1 + e\cos f) \sin S] \right.$$

$$\left. - e \frac{a_1^3}{\Delta^3} \frac{r}{a_1} \sin f \right\} \qquad (32b)$$

$$\frac{d\varpi}{df} = -\frac{\nu^2}{e} \left(\frac{r}{a}\right)^2 \left\{ \frac{r_1}{a} \left(\frac{a_1^3}{\Delta^3} - \frac{a_1^3}{r_1^3} \right) \cos f \cos S + \left(\frac{2 + e\cos f}{1 + e\cos f} \right) \sin f \sin S \right]$$

$$- \frac{a_1^3}{\Delta^3} \frac{r}{a} \cos f \} \qquad (32c)$$

$$\frac{d\epsilon}{df} = -\frac{2\nu^2}{1-e^2} \left(\frac{r}{a}\right)^2 \left\{ \frac{r_1}{a} \left(\frac{a_1^3}{\Delta^3} - \frac{a_1^3}{r_1^3} \right) \left[\left(\frac{(1-e^2)^{3/2}}{1 + e\cos f} - Ne \sin f \right) \cos S + N(1 + e\cos f) \sin S \right] \right.$$

$$\left. - \frac{a_1^3}{\Delta^3} \frac{r}{a} \left(\frac{(1-e^2)^{3/2}}{1 + e\cos f} - Ne \sin f \right) \right\} + \left(1 - \sqrt{1-e^2} \right) \frac{d\varpi}{df} \qquad (32d)$$

where $N = \frac{3}{2} n t$

Because the Sun is assumed to be moving in a fixed planetocentric orbit, a_1 is a constant and da/df can be converted to $d\alpha/df$ by the relation $da/df = a_1 \, d\alpha/df$.

Note that these equations of motion written with respect to the true anomaly of the perturbed body describe exactly the motion of a perturbed body in a restricted coplanar three-body system. They are not dependent on an expansion about any assumed small parameters such as α, e, e_1, etc.

The only assumptions we have added to the general three-body problem at this point are that

(1) the three body system is coplanar

(2) $m_1 >> M_p >> m$ so that the Sun moves in a fixed Keplerian orbit unperturbed by the satellite.

Also at this point in our analysis, the fixed orbit of the Sun remains general. Later we will study individually the two cases where, firstly, the Sun is assumed to move in a fixed circular orbit and then, secondly, in a fixed elliptical orbit.

(v) A more convenient form of Lagrange's planetary equations in preparation for their numerical integration and analytical expansion

We rewrite Equations (32) in the following simpler form so that we can easily study the various components of each of the equations.

$$\frac{de}{df} = \frac{\nu^2}{\alpha} R_2 \{ A F_e - B \sin f \} \tag{33a}$$

$$\frac{d\alpha}{df} = \frac{2\nu^2}{1-e^2} R_2 \{ A F_\alpha - e B \sin f \} \tag{33b}$$

$$\frac{d\varpi}{df} = -\frac{\nu^2}{e\alpha} R_2 \{ A F_\varpi - B \cos f \} \tag{33c}$$

$$\frac{d\epsilon}{df} = -\frac{2\nu^2}{\alpha(1-e^2)} R_2 \{ A F_\epsilon - B K \} + \left(1 - \sqrt{1-e^2}\right) \frac{d\varpi}{df} \tag{33d}$$

where:

$$R_j = \left(\frac{r}{a}\right)^j \qquad \text{for } j = 1 \text{ to } 3 \tag{33e}$$

$$A = \left(\frac{r_1}{a_1}\right) a_1^3 \left(\frac{1}{\Delta^3} - \frac{1}{r_1^3}\right) \tag{33f}$$

$$B = \left(\frac{a_1}{\Delta}\right)^3 \frac{r}{a_1} \tag{33g}$$

$$F_e = \sin f \cos S - \left(\frac{e(1 + \cos^2 f) + 2 \cos f}{1 + e \cos f}\right) \sin S \tag{33h}$$

$$F_\alpha = e \sin f \cos S - (1 + e \cos f) \sin S \tag{33i}$$

$$F_\varpi = \cos f \cos S + \left(\frac{2 + e \cos f}{1 + e \cos f}\right) \sin f \sin S \tag{33j}$$

$$N = \frac{3}{2} n t \tag{33k}$$

$$K = \frac{(1 - e^2)^{3/2}}{1 + e \cos f} - N e \sin f \tag{33l}$$

$$F_\epsilon = K \cos S + N(1 + e \cos f) \sin S \tag{33m}$$

Upon studying Equations (33), we see that they contain singularities at $a = 0$, $e = 0$ and 1, and $\Delta = 0$. Numerical integration or analytical expansion of these equations can therefore be subject to large errors in accuracy if any of these singularities are approached. All these singularities, except $e = 0$, imply collision or escape of one or more of the bodies. Generally, as long as we begin with values of e greater than zero, the finite-time stability criteria method will not involve values of a, e and Δ close to these singularities. Our methods ensure that when any of these singularities, except $e = 0$, are approached, the system is said to be approaching an unstable situation and the calculations are halted. For example, our method involves only a growth of e up to a stipulated upper limit $e_u < 1$.

There is however one major area of difficulty for any numerical integration of Equations (33), namely that the term A contains a difference of two nearly equal values ($1/\Delta^3 - 1/r_1^3$), which will cause both a loss of accuracy and speed in the integration. To avoid this problem we expand the terms A and B about the small

parameter $(\rho^2 - \rho \cos S)$, where $\rho = r/r_1$. We are therefore assuming that r is much smaller than r_1, which is equivalent to the assumption that α is small.

The expansion is completed as follows. Let $A=(r_1/a_1)A_1$ where $A=a_1{}^3(1/\Delta^3-1/r_1{}^3)$. A_1 can be rewritten as

$$A_1 = \left(\frac{a_1}{r_1}\right)^3 [\,(1 + \rho^2 - \rho \cos S)^{-3/2} - 1\,]$$

using Equation (13). If we now expand A_1 about the small parameter $(\rho^2 - \rho \cos S)$ to fourth order in ρ, using a binomial expansion, we obtain

$$A_1 = \left(\frac{a_1}{r_1}\right)^3 \rho Q$$

$$Q = 3\cos S + \frac{3}{2}\rho(5\cos^2 S - 1) + \frac{5}{2}\rho^2(7\cos^3 S - 3\cos S) + \frac{15}{8}\rho^3(1 - 14\cos^2 S + 21\cos^4 S) + \ldots \qquad (34)$$

A then becomes

$$A = \left(\frac{a_1}{r_1}\right)^2 \rho Q$$

and B rewritten in terms of A becomes

$$B = A\rho + \rho\left(\frac{a_1}{r_1}\right)^2 = \rho\left(\frac{a_1}{r_1}\right)^2 [\,\rho Q + 1\,]$$

We now substitute the expansions of A and B into Lagrange's planetary equations (33) and simplify to arrive at

$$\frac{de}{df} = \nu^2 \left(\frac{\rho}{\alpha}\right)^3 \{ Q(F_e - \rho \sin f) - \sin f \} \tag{35a}$$

$$\frac{d\alpha}{df} = \frac{2\nu^2}{1-e^2} \alpha \left(\frac{\rho}{\alpha}\right)^3 \{ Q(F_\alpha - e\,\rho \sin f) - e \sin f \} \tag{35b}$$

$$\frac{d\varpi}{df} = -\frac{\nu^2}{e} \left(\frac{\rho}{\alpha}\right)^3 \{ Q(F_\varpi - \rho \cos f) - \cos f \} \tag{35c}$$

$$\frac{d\epsilon}{df} = -\frac{2\nu^2}{1-e^2} \left(\frac{\rho}{\alpha}\right)^3 \{ Q(F_\epsilon - \rho K) - K \} + \left(1 - \sqrt{1-e^2}\right) \frac{d\varpi}{df} \tag{35d}$$

The final steps for obtaining the change in the elements $\Delta\sigma$ over one synodic period are the conversion of $d\sigma/df$ to $d\sigma/dS$ and the integration of $d\sigma/dS$ to get $\Delta\sigma$.

For the numerical analysis, it is more accurate to integrate the exact Equations (35) with respect to the true anomaly by converting the integral limits of $S = -\pi$ and $S = +\pi$ to limits in f using a complicated set of transcendental equations. Of course, it is still necessary to use the inexact expansion for Q in the numerical integration. Hence

$$\Delta\sigma = \int_{f_{-\pi}}^{f_{+\pi}} \frac{d\sigma}{df}\, df$$

where $f_\pi = f(S = \pi)$ and $f_{-\pi} = f(S = -\pi)$.

For the analytical work we must, in any case, expand the components of the differential equations (35) about the small parameters α, e, e_1, $\nu = f(\alpha)$ to the required degree of accuracy. The most efficient procedure is therefore to begin with an immediate expansion of the set of transcendental equations in order to get f and f_1 as functions of S. The Equations (35) are then transformed into differential equations with respect to S and integrated. We follow these procedures in the next two chapters.

It remains now only to confirm that the assumptions we make in our analysis are reasonable for the range of orbital parameters that are found in the satellite systems of our solar system. We do this in Section 2.5.

2.5 The Validity of the Assumptions Made In the Previous Development of the Coplanar Restricted Three-Body Model

In Sections 2.3 and 2.4, we make the following assumptions:

(1) the three bodies act as point masses

(2) the only forces acting on the three bodies are gravitational

(3) no other bodies interact gravitationally with the three bodies

(4) the mass m of the satellite is negligible compared to the masses of the planet M_p and the Sun m_1

(5) the three bodies move in the same orbital plane (ie i = 0)

(6) the eccentricity of the satellite is never exactly equal to zero

(7) e, e_1, $\alpha=a/a_1$ and $\nu=[\alpha^3 m_1/(M_p+m)]^{1/2}$ are small parameters of value much less than 1

(8) the orbital elements of the satellite a, e, ϖ and ϵ change so slowly over one synodic period, that a first order perturbation theory is sufficiently accurate to describe the perturbations in the orbital elements.

Generally, for most of the planet-satellite-Sun systems found in the solar system, the effects of the shape and sizes of the bodies (assumption (1)), the effects of the gravitational influence of other bodies (assumption (3)) and the effects of other forces acting in the solar system (assumption (2)) are negligible compared to the gravitational effects of the Sun and the relevant planet on the satellite. For example, the effect of solar perturbations on the Moon's orbit about the Earth is approximately four orders of magnitude greater than the effect of any other perturbing force acting on the Earth-Moon system.

The only exceptions to assumptions (1) to (3) may be the gravitational effect of a very closely orbiting satellite and the effect of tidal friction. The gravitational influence of a nearby satellite can become important if two satellites approach each other very closely. Such an event occurs regularly in the co-orbit of Janus and

Epimetheus, where the two satellites appear to revolve in opposite directions around Saturn at the same radial distance to within the radius of their bodies. They do not, however, collide with each other. The gravitational influence of each satellite on the other as they approach an apparent collision point causes them to move away from each other in a horseshoe shaped orbit (See Figure 2.4) in such a manner that they never collide (Dermott and Murray, 1981a,b). When the two satellites are not close to each other, each satellite follows a normal Keplerian elliptical orbit unaware of the other satellite's existence. Such cases where satellites approach close enough to each other to cause mutual gravitational perturbations in their orbits are, however, rare in the solar system.

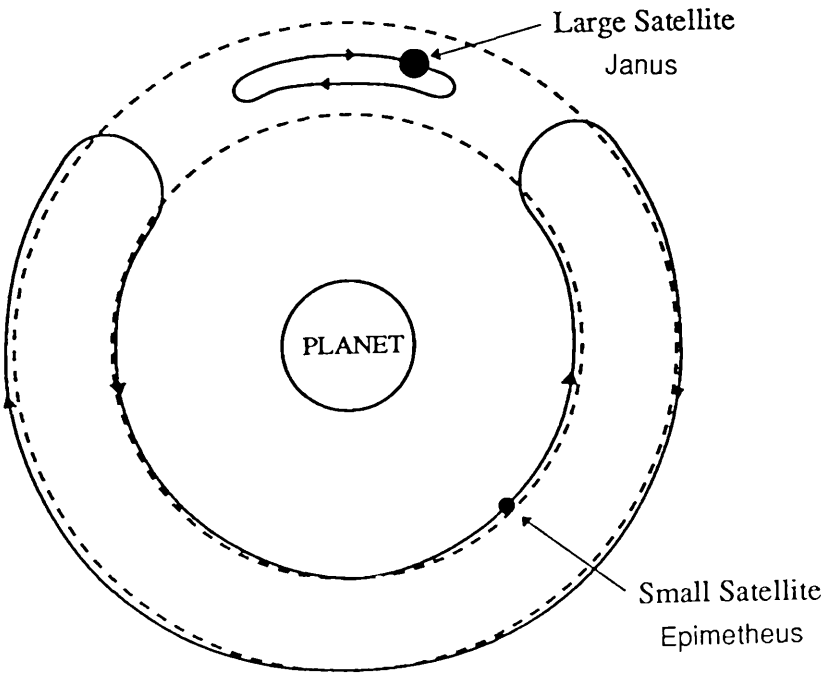

Figure 2.4 The horse-shoe shaped orbit of Janus and Epimetheus about Saturn. This partly schematic diagram is taken from Dermott and Murray (1981b). The radial widths of the horseshoe paths have been exaggerated for clarity.

The effect of planetary and solar tidal friction on the satellite is relatively small compared to gravitational effects; however, tidal friction can cause secular or very long period changes in the orbital elements of the satellite and therefore can play a very important role in the long-term evolution of the satellite's orbit. In order to make our model more manageable, we do not deal with this problem except in the case of the Earth-Moon-Sun system (See Chapter 7).

At the 1987 Nato Advanced Study Institute entitled Long-Term Dynamical Behavior of Natural and Artificial N-Body Systems, Victor Szebehely, in an unpublished lecture, demonstrated a method for analyzing the applicability of the restricted three-body model to the problem being studied. We use his method to test the validity of assumption (4) for the Sun perturbed planet-satellite systems found in the solar system.

The application of the restricted three-body model to a three body system is identical to assuming that one of the bodies has a mass so small that its gravitational effect on the other two bodies is negligible. Szebehely pointed out that this assumption results in a non-zero error which can be measured by evaluating the magnitudes of the neglected terms relative to those terms which are saved. Because these neglected terms involve functions of the distances separating the bodies, he showed that these distances could therefore be used as a criteria for the applicability of the restricted three body problem to the system being studied.

His analysis proceeds as follows. The equations of motion of the three bodies with respect to a fixed reference point O are found, taking into account all their mutual gravitational forces. If we use the notation shown in Figure 2.5, these equations of motion are

$$\ddot{\mathbf{r}}_1 = -G\left[m_2 \frac{\mathbf{r}_1 - \mathbf{r}_2}{\Delta_{12}^3} + m_3 \frac{\mathbf{r}_1 - \mathbf{r}_3}{\Delta_{13}^3} \right]$$

$$\ddot{\mathbf{r}}_2 = -G\left[m_3 \frac{\mathbf{r}_2 - \mathbf{r}_3}{\Delta_{23}^3} + m_1 \frac{\mathbf{r}_2 - \mathbf{r}_1}{\Delta_{12}^3} \right]$$

$$\ddot{\mathbf{r}}_3 = -G\left[m_1 \frac{\mathbf{r}_3 - \mathbf{r}_1}{\Delta_{13}^3} + m_2 \frac{\mathbf{r}_3 - \mathbf{r}_2}{\Delta_{23}^3} \right]$$

If we now assume that $m_1 > m_2 > m_3$, the error caused by neglecting the effect of the third body on the more massive bodies is given approximately by the ratios of the neglected term to the dominant term in each equation of motion $\ddot{\mathbf{r}}_1$ and $\ddot{\mathbf{r}}_2$. The neglected terms are underlined.

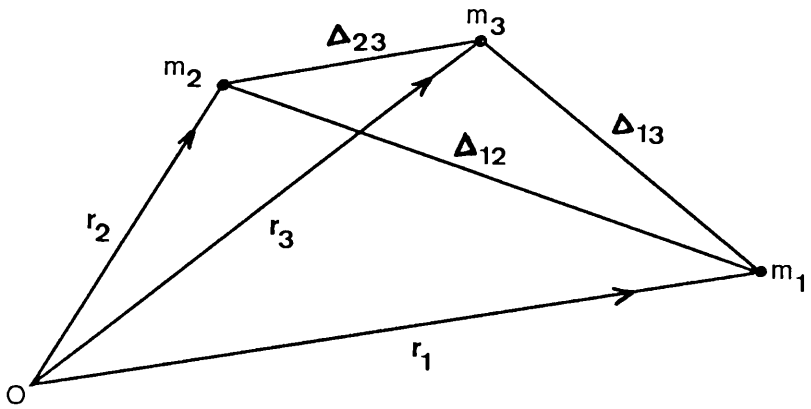

Figure 2.5 A three-body system moving with respect to a fixed reference point O, where Δ_{23}, Δ_{13}, Δ_{12} are the magnitudes of the separations between the bodies of masses m_1, m_2 and m_3 and $\mathbf{r}_1$, $\mathbf{r}_2$ and $\mathbf{r}_3$ are the radius vectors denoting the positions of these bodies.

Thus C_1, the neglected effect of the third body on the first body relative to that of the second body is

$$C_1 = \frac{m_3}{m_2}\left(\frac{\Delta_{12}}{\Delta_{13}}\right)^2$$

and C_2, the neglected effect of the third body on the second body relative to that of the first body is

$$C_2 = \frac{m_3}{m_1}\left(\frac{\Delta_{12}}{\Delta_{23}}\right)^2$$

Szebehely pointed out that in order for the restricted three body problem to be applicable to the system being studied, C_1 and C_2 must therefore be very much less than one and should happily be of the order of less than 0.01 or 1%.

When the above method is applied to planet-satellite systems disturbed by the Sun, with m_1 equalling the mass of the Sun, m_2 equalling the mass of the planet and m_3 equalling the mass of the satellite, C_1 and C_2 simplify to

$$C_1 \approx \frac{m_3}{m_2}$$

$$C_2 = \frac{m_3}{m_1}\left(\frac{\Delta_{12}}{\Delta_{23}}\right)^2$$

where Δ_{12} is the distance between the Sun and the planet and Δ_{23} is the distance between the planet and the satellite.

Szebehely (1987) gave examples of the maximum and minimum values of C_1 and C_2 which result for each planetary system. An expansion of his table is given in Table 2.2. Besides the maximum and minimum values of C_1 and C_2, Table 2.2 also includes the values of C_1 and C_2 for all the satellites which are near the limitations of the restricted three body model.

From the table we can see that the orbital dynamics of Jupiter's Io, Saturn's Titan, Uranus' Ariel and Titania, Neptune's Triton and Pluto's Charon are such that the restricted three-body problem is not strictly applicable. Our own Moon, Ganymede and Europa in the Jupiter system, and Oberon, Umbriel and Miranda in the Uranian system all lie on the border of applicability of the restricted three-body model to their orbital dynamics. The remaining satellites, viz. two for Mars, thirteen for Jupiter, sixteen for Saturn, ten for Uranus and one for Neptune, lie well within the

Planet	No. of known satellites	Satellite	C_1	C_2
Earth	1	Moon	0.0123	0.0056
Mars	2	Phobos	1.5×10^{-8}	2.86×10^{-6}
		Deimos	3.0×10^{-9}	9.13×10^{-8}
Jupiter	16	Io	4.68×10^{-5}	0.152
		Ganymede	7.80×10^{-5}	0.039
		Europa	2.52×10^{-5}	0.032
		Leda	3.0×10^{-12}	1.41×10^{-11}
Saturn	17	Titan	2.38×10^{-4}	0.093
		Phoebe	7.0×10^{-10}	2.43×10^{-9}
Uranus	15	Ariel	1.8×10^{-5}	0.177
		Titania	6.8×10^{-5}	0.129
		Oberon	6.9×10^{-5}	0.073
		Umbriel	1.2×10^{-5}	0.061
		Miranda	2.0×10^{-6}	0.043
Neptune	2	Triton	0.0013	10.83
		Nereid	2.0×10^{-7}	6.89×10^{-6}
Pluto	1	Charon	0.125?	93.?

Table 2.2 The relative errors caused by neglecting the effect of the satellite's mass on the Sun's orbit (C_1) and the effect of the satellite's mass on the planet's orbit (C_2) for various satellites in the solar system.

Only those satellites which have values of C_1 or C_2 greater than 0.01 or 1.0 % and the satellites in each planetary system which have approximately the smallest values for C_1 and C_2 are listed in this table. Those values of C_1 or C_2 which are underlined indicate a possible inapplicability of the restricted three-body model to that particular planetary-satellite system.

A question mark denotes that the masses of the bodies are uncertain and that therefore the values of C_1 and C_2 are also uncertain.

The physical data for the satellites and the planets are taken from the 1988 Nautical Almanac.

scope of the restricted three-body problem.

Due to the complexity of dealing with three-dimensional three-body systems, we have confined our attention to the coplanar case (assumption (5)). However, the application of our finite-time stability method to the circular and elliptical coplanar restricted three-body problem shows that there is no reason why it cannot be expanded to include the non-coplanar case as well. This analysis is however, outside the scope of this thesis.

In our analytic expansion of Lagrange's planetary equations, we require that the eccentricities e and e_1, the ratios of the semi-major axes $\alpha = a/a_1$ and the ratios of the mean motion $\nu = n_1/n$ be small. The eccentricities found in the solar sytem are generally much less than 0.1, while the largest values of α and ν found in the solar system are of the order of 3×10^{-2} and 5×10^{-3} respectively. Hence, assumption (7) is not too unreasonable when applied to the solar system.

A few exceptional cases, such as some of the outer Jovian satellites (ie Pasiphae and Sinope) and Pluto have eccentricities of greater than 0.25. Nereid, in the Neptune system, is especially noticeable with an eccentricity of 0.7483. Generally, numerical evaluations of the disturbing function expansion for values of eccentricity greater than 0.5 are useless and give doubtful results for values of eccentricity greater than 0.3.

Thus, in summary, our model can be applied to most of the planet-satellite systems of the solar system. Notable exceptions are Io, Titan, Ariel, Titania, Triton and Charon because they have marked gravitational effects on their primary's orbit and Nereid because of its high eccentricity. Our restricted three body model may possibly be applicable to the Moon, Ganymede, Europa, Oberon, Umbriel and Miranda, all of which might have a measurable gravitational effect on the orbits of their planets or the Sun, and to those outer jovian satellites of higher eccentricity. The rest of the planetary satellites of the solar system, numbering around forty, lie well within the scope of our model.

CHAPTER 3

THE CHANGES IN THE ORBITAL ELEMENTS OVER ONE SYNODIC PERIOD FOR THE CIRCULAR COPLANAR RESTRICTED THREE-BODY PROBLEM

3.1 The Circular Model

3.2 A Numerical Integration of the Problem

- (i) The elongation S as a function of time t and the true anomaly f
- (ii) The variable time t as a function of the true anomaly f
- (iii) Numerical integration of Lagrange's planetary equations with respect to f

3.3 An Analytical Development of the Problem

- (i) Expansion of the components of Lagrange's planetary equations found in both the circular and elliptical cases
- (ii) Expansion of the components of Lagrange's planetary equations found only in the circular case
- (iii) The expanded form of Lagrange's planetary equations $d\sigma/df$
- (iv) The expanded form of Lagrange's planetary equations $d\sigma/dS$
- (v) General form of the integration of the equations $d\sigma/dS$
- (vi) The integration of Lagrange's planetary equations $d\sigma/dS$

3.4 Discussion of the Analytic Theory, its Implications and Limitations

"Murphy's Law: If anything can go wrong, it will."

3.1 The Circular Model

We begin with the simplest case in the coplanar restricted three-body problem and take the Sun to be moving in a fixed circular planetocentric orbit. The eccentricity of the Sun's orbit is assumed to be $e_1 = 0$ and the magnitude of its radius vector $\mathbf{r}_1$ now becomes a constant a_1. See Figure 3.1.

These two simplifications result in the following changes to Lagrange's planetary equations and their subsidiary equations. The ratio of the radius vectors $\rho = r/r_1$ simplifies to

$$\rho = \alpha \ (r/a)$$

and therefore ρ^j is

$$\rho^j = \alpha^j R_j \qquad \text{where } j = 1,2, \ldots \qquad (1)$$

Lagrange's planetary Equations (35) of Chapter 2 become

$$\frac{de}{df} = \nu^2 R_3 \{ Q(F_e - \rho \sin f) - \sin f \} \qquad (2a)$$

$$\frac{d\alpha}{df} = \frac{2\nu^2}{1-e^2} \alpha R_3 \{ Q(F_\alpha - e\rho \sin f) - e \sin f \} \qquad (2b)$$

$$\frac{d\varpi}{df} = -\frac{\nu^2}{e} R_3 \{ Q(F_\varpi - \rho \cos f) - \cos f \} \qquad (2c)$$

$$\frac{d\epsilon}{df} = -\frac{2\nu^2}{1-e^2} R_3 \{ Q(F_\epsilon - \rho K) - K \} + \left(1 - \sqrt{1-e^2}\right) \frac{d\varpi}{df} \qquad (2d)$$

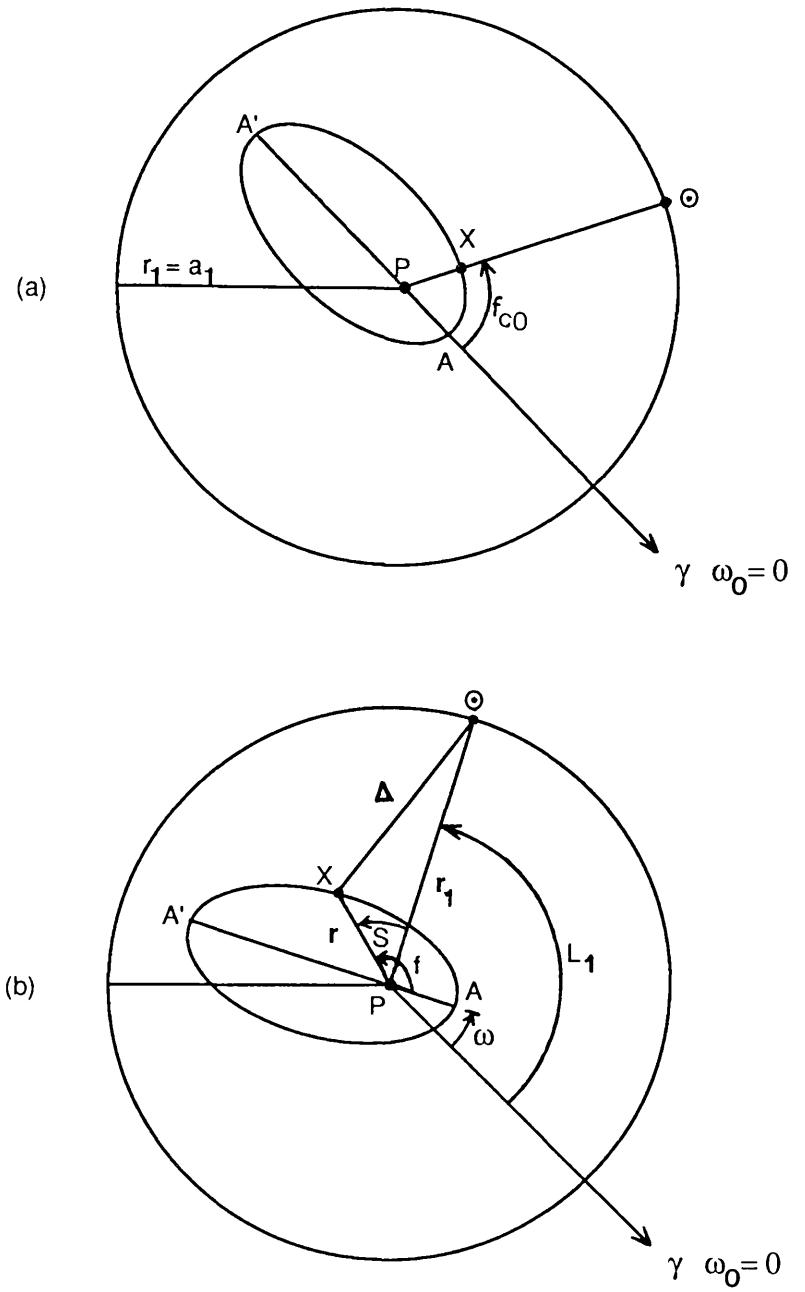

Figure 3.1 The circular coplanar restricted three-body problem, where the planet P - satellite X system is disturbed by the sun ⊙, which is assumed to be moving in a fixed circular orbit of radius $r_1 = a_1$.

The initial configuration (a) of the planet-satellite-sun system is chosen to be a conjunction. At this time t=0, the longitude of the satellite's pericentre ϖ_0 is arbitrarily chosen to be zero, so that $\overline{PA}$ lies in the reference direction $\overline{P\gamma}$. Figure (b) describes the configuration some time t later.

Parameters with a zero subscript denote values of the specified parameter at t=0, while parameters with no subscript denote values of the specified parameter at some time t.

The other components of the above differential equations remain the same as those given in Equations (33e), (33h to 33m) and (34) of Chapter 2, viz.

$$R_j = \left(\frac{r}{a}\right)^j \qquad \text{for } j = 1 \text{ to } 3 \tag{2e}$$

$$Q = 3\cos S + \frac{3}{2}\rho(5\cos^2 S - 1) + \frac{5}{2}\rho^2(7\cos^3 S - 3\cos S) + \frac{15}{8}\rho^3(1 - 14\cos^2 S + 21\cos^4 S) + \ldots \tag{2f}$$

$$F_e = \sin f \cos S - \left(\frac{e(1 + \cos^2 f) + 2\cos f}{1 + e\cos f}\right)\sin S \tag{2g}$$

$$F_\alpha = e \sin f \cos S - (1 + e\cos f)\sin S \tag{2h}$$

$$F_\varpi = \cos f \cos S + \left(\frac{2 + e\cos f}{1 + e\cos f}\right)\sin f \sin S \tag{2i}$$

$$N = \frac{3}{2} n t \tag{2j}$$

$$K = \frac{(1 - e^2)^{3/2}}{1 + e\cos f} - N e \sin f \tag{2k}$$

$$F_\epsilon = K\cos S + N(1 + e\cos f)\sin S \tag{2 l}$$

We now have the appropriate equations of motion ready for integration. It remains only to specify the starting conditions required for the integration. The satellite's orbit and position in its orbit at any time t are completely described by the orbital elements α, e, ϵ, ϖ and time t. The bodies themselves can be solely described by a ratio of their point masses $\mu = m_1/(M_p + m)$, while a complete description of the Sun's orbit relative to the satellite's orbit is found in the parameter $\alpha = a/a_1$.

The ratio of the masses is, of course, a constant of the three-body problem. We need therefore only choose a starting epoch and specify the orbital elements for this time. Since we have centred the integration from an opposition at S = $-\pi$ to an opposition at S = $+\pi$ on a conjunction, let for simplicity sake the time at which the satellite and the Sun pass through conjunction be arbitrarily t = 0.

At this time, the satellite's orbit is completely described by the four orbital

elements α_0, e_0, ϵ_0, ϖ_0 where a subscript denotes a value of the specified parameter at time t = 0.

The choice of ϖ_0 is purely arbitrary because all orientations of the satellite's elliptical orbit with respect to the Sun's circular orbit at a conjunction of the satellite and Sun, produce identical configurations. We therefore choose ϖ_0 to be zero, so that at time t = 0 the satellite's periapsis lies in the same direction as the reference direction.

Since we work with Lagrange's planetary equations written in terms of both the true anomaly f and the angle S between the two radius vectors **r** and $\mathbf{r}_1$, the most logical choice of an orbital parameter which fixes the position of the satellite within its orbit is not ϵ, but one involving the true anomaly. The time at which a conjunction occurs is a unique configuration or reference point in the satellite's orbit over one synodic period. Therefore, the true anomaly f_c of the satellite at conjunction is an equivalent parameter to ϵ. Like ϵ, it changes with time as the satellite's orbital orientation, size and shape change.

Since ϵ is the more commonly used parameter, we shall use f_c as an initial orbital parameter only, converting f_c to ϵ for the integration. Let f_{c0} be the true anomaly of the satellite at the conjunction which occurs at time t = 0. Note that the true anomaly f_{1c0} of the Sun at this time can be arbitrarily taken to be $f_{1c0} = f_{c0}$ since the Sun's motion is assumed to be circular.

In summary, the problem contains four independent initial parameters which need to be specified in order to integrate Lagrange's planetary equations. These are: the ratio of the semi-major axes of the satellite and the Sun at time t = 0 or $\alpha_0 = a_0/a_1$; the eccentricity of the satellite's orbit at time t = 0 or e_0; the true anomaly of the satellite or the Sun in the conjunction which occurs at time t = 0 or f_{c0}; and the ratio of the masses μ.

We are now ready to integrate the problem to find the changes in the orbital elements σ over one synodic period, where $\sigma = \alpha$, e, ϖ or ϵ. This is done both

analytically and numerically, in order to confirm the validity and to ascertain the limitations of the analytic theory.

In Section 3.2, we describe the numerical method used to integrate Equations (2), while in Section 3.3, we derive an analytic expansion and the subsequent analytic integration of the same equations. Section 3.4 contains a comparison of the analytic and numerical results for a range of the four initial conditions α_0, e_0, f_{c0} and μ. It also includes a discussion of the limitations of the analytic theory and gives the implications of the results for any question about the stability of planet-satellite systems against solar perturbations.

3.2 A Numerical Integration of the Problem

The most accurate method of numerically integrating Lagrange's planetary equations over one synodic period is to integrate the exact form of the equations written in terms of the true anomaly (ie Equations 2). The only approximation necessary is therefore the expansion of the components Q, which originally contained the difference of two very small quantities.

In order to have an integration time interval of one synodic period centred on a conjunction, we must now integrate from the true anomaly of the satellite at opposition ($S = -\pi$) or $f_{-\pi}$ to the true anomaly of the satellite at the next opposition ($S = \pi$) or f_{π}. Hence the changes in the orbital elements $\Delta\sigma$ are simply found by

$$\Delta\sigma = \int_{f_{-\pi}}^{f_{+\pi}} \frac{d\sigma}{df}\, df$$

To integrate numerically Equations (2) or $d\sigma/df$, we need to know each of the components of $d\sigma/df$ as a function of f. In particular, we need the relationships between the three time variables t, f, and S.

(i) The elongation S as a function of time t and the true anomaly f

S expressed as a function of f and t is easily found using Figure 3.1(b) which depicts the positions of the satellite X, the planet P and the sun ⊙ at some time t within the synodic period interval. From the diagram, we can see that

$$S = f + \varpi - L_1 \qquad (3)$$

Since ϖ is one of the independent variables, we need only find L_1 in terms of f. Because we have assumed the sun's orbit to be circular, the true longitude and the mean longitude of the sun are identical quantities at all times. Hence, using Equation (4) of Chapter 2

$$L_1 = l_1 = \varpi_1 + n_1 (t - \tau) \qquad (4)$$

At time t = 0, Equation (3) simplifies to

$$L_{10} = f_{c0} + \varpi_0 \qquad (5)$$

while Equation (4) gives

$$L_{10} = \varpi_{10} - n_1 \tau \qquad (6)$$

Using Equation (6), Equation (4) can therefore be rewritten as

$$L_1 = L_{10} + \varpi_1 - \varpi_{10} + n_1 t$$

Since the sun's orbit is assumed to be fixed $\varpi_1 - \varpi_{10} = 0$ and thus

$$L_1 = L_{10} + n_1 t$$

This last equation can be written in terms of the initial conditions f_{c0} and ϖ_0 through Equation (5) to get

$$L_1 = f_{c0} + \varpi_0 + n_1 t \qquad (7)$$

And finally substitution of Equation (7) into Equation (3) for S gives

$$S = f - f_{c0} + \varpi - \varpi_0 - n_1 t$$

Over one synodic period, we assume that the changes in the orbital elements are very

small. Therefore $\varpi - \varpi_0$ is essentially zero. Hence

$$S = f - f_{c0} - n_1 t \qquad (8)$$

Thus, if the orientations of the two orbits with respect to each other do not change very much in one synodic period, the angle S between the radius vectors **r** and $\mathbf{r}_1$ a time t after a conjunction is simply: the angle between the satellite's original position f_{c0} and its current position f, minus, the angle swept out by the sun's radius vector in that time.

(ii) The variable time t as a function of the true anomaly f

We now find time t as a function of the true anomaly f. Once this relationship is obtained we can then write both t and S completely in terms of f.

From Equation (5) of Chapter 2 we get t as a function of the mean anomaly

$$n t = M - M_0 \qquad (9)$$

where M_0 is the mean anomaly at t = 0. Equation (9) combined with Equation (6) of Chapter 2, gives t as a function of the eccentric anomaly E

$$n t = E - e \sin E - M_0 \qquad (10)$$

and hence t as a function of the true anomaly through Equation (7) of Chapter 2.

Thus in summary, given f we can find both S and t by solving the following sequence of equations for the listed variables:

$$E : \tan \frac{E}{2} = \left(\frac{1 - e}{1 + e} \right)^{1/2} \tan \frac{f}{2} \qquad (11a)$$

$$t : \quad nt = E - e \sin E - M_0 \qquad (11b)$$

$$S : \quad S = f - f_{c0} - n_1 t \qquad (11c)$$

The initial mean anomaly M_0 is simply a function of the initial condition f_{c0} through

$$M_0 = E_0 - e \sin E_0 \tag{12a}$$

$$\tan \frac{E_0}{2} = \left(\frac{1 - e}{1 + e} \right)^{1/2} \tan \frac{f_{c0}}{2} \tag{12b}$$

The initial mean longitude at the epoch ϵ_0 is also a function of f_{c0} through M_0. Using Equations (5) and (8) of Chapter 2

$$\epsilon_0 = M_0 + \varpi_0 \tag{13}$$

Then since $\varpi_0 = 0$, ϵ_0 equals M_0.

The limits of the integral are found by substituting $S = -\pi$ or $S = +\pi$ into Equation (11c), writing the equation solely as a function of f using Equations (11a) and (11b), and solving numerically for f.

Now that the limits of the integral and all the components of Lagrange's planetary equations are known as functions of f and the initial conditions α_0, e_0, f_{c0} and μ, Equations (2) can be easily numerically integrated with respect to f.

(iii) Numerical integration of Lagrange's planetary equations with respect to f

The Equations (2) are integrated numerically using NAG routine D01AKF, a one-dimensional quadrature adaptive integrator suitable for oscillating non-singular integrands. Subroutines were developed to find the proper quadrant for E given f, using Equation (11a) and

$$\cos E = \frac{\cos f + e}{1 + e \cos f} \tag{14a}$$

$$\sin E = \frac{\sqrt{1-e^2}\,\sin f}{1 + e \cos f} \tag{14b}$$

which are products of the two-body problem.

The integration limits are evaluated in another subroutine to a required accuracy of six decimal places, using a Newton-Raphson method to solve Equations (11) for the transcendental variable f. The results of the numerical integration are compared with the results of the analytical theory in Section 3.4.

3.3 An Analytical Development of the Problem

The analytical integration of Lagrange's planetary Equations (2) over one synodic period is most efficiently done by first, expanding the differential equations dependent on f about the small parameters α, e and ν to the required degree of accuracy, and then transforming them into functions of S. Integration over the time interval of one synodic period centred on a conjunction is then simply given by

$$\Delta\sigma = \int_{S=-\pi}^{S=+\pi} \frac{d\sigma}{dS}\, dS$$

We assume that the eccentricity of the satellite e, the ratio of the semi-major axes $\alpha = a/a_1$, and the ratio of the mean motions $\nu = n_1/n$ are all small parameters. The smallness of ν, of the order of 5×10^{-3} at its largest in the solar system, is of particular importance because it implies that there will be no dominant resonant terms in the resulting series which require expansion to higher powers of α, e and ν in order to obtain the same degree of accuracy as with the other terms. A very small ratio of mean motions cannot be approximated by a fraction of small valued integers $\nu=b/c$ where b and c are integers. Therefore, only secular terms dominate our expansion.

Because we are not interested in discovering the exact positions of the bodies at any time, but only in the minimum time taken for the satellite to be "noticeably" disturbed, an expansion to third order is more than sufficiently accurate for most of the satellites in the solar system. In the elliptical case, we therefore expand Lagrange's planetary equations to third order. Because the circular case is, however, the first use made of our finite-time stability criteria method, we keep the analysis simple and therefore expand it only to second order. Thus in the circular case expansion, we retain all terms which have $\alpha^I e^J \nu^K$ where $I+J+K \leq 2$ and I, J, K are integers.

Equations (2) are expanded into a series of cosine and sine terms whose arguments consist of

$$\phi = j\,f + k\,S$$

where j and k are integers and whose coefficients involve powers of α, e and v. The argument as a function of S alone is found later using a relation still to be developed between f and S.

The expansion is accomplished using a Taylor series expansion for sine and cosine terms and a binomial series expansion about small x, where x is a function of α, e and v. The following trigonometric identities are also useful in transforming the expanded terms into the standard form described previously, which consists of solitary trigonometric functions of power one whose arguments are of the form ϕ.

$$\cos^2\theta = \frac{1 + \cos 2\theta}{2}$$

$$\sin^2\theta = \frac{1 - \cos 2\theta}{2}$$

$$\cos^3\theta = \frac{3}{4}\cos\theta + \frac{1}{4}\cos 3\theta$$

$$\sin^3\theta = \frac{3}{4}\sin\theta - \frac{1}{4}\sin 3\theta$$

$$\cos^4\theta = \frac{3}{8} + \frac{1}{2}\cos 2\theta + \frac{1}{8}\cos 4\theta$$

$$\sin^4\theta = \frac{3}{8} - \frac{1}{2}\cos 2\theta + \frac{1}{8}\cos 4\theta \qquad (15)$$

$$\sin A \sin B = \frac{1}{2}\{\cos\overline{A-B} - \cos\overline{A+B}\}$$

$$\cos A \cos B = \frac{1}{2}\{\cos\overline{A-B} + \cos\overline{A+B}\}$$

$$\sin A \cos B = \frac{1}{2}\{\sin\overline{A-B} + \sin\overline{A+B}\}$$

$$\cos A \sin B = \frac{1}{2}\{-\sin\overline{A-B} + \sin\overline{A+B}\}$$

Note that a bar over a set of terms indicates that the set of terms form the argument of a trigonometric function.

(i) Expansion of the components of Lagrange's planetary equations found in both the circular and elliptical cases

We first expand all those components of Lagrange's planetary Equations (2) which are common to both the circular and elliptical problems. We do this to third order in preparation for the elliptical problem and then reduce the series to a second order expansion to be used in the circular case.

Using Equation (14) of Chapter 2, $R_j = (r/a)^j$ becomes

$$R_j = 1 + \left[\frac{j(j+1)}{4} - j\right]e^2 + \left\{\left[j^2 - \frac{j(j+1)(j+2)}{8}\right]e^3 - je\right\}\cos f + \frac{j(j+1)}{4}e^2\cos 2f - \frac{j(j+1)(j+2)}{24}e^3\cos 3f$$

where j is a positive integer. To second order, we therefore get

$$R_1 = \frac{r}{a} = 1 - \frac{1}{2}e^2 - e\cos f + \frac{1}{2}e^2\cos 2f$$

$$R_2 = \left(\frac{r}{a}\right)^2 = 1 - \frac{1}{2}e^2 - 2e\cos f + \frac{3}{2}e^2\cos 2f$$

$$R_3 = \left(\frac{r}{a}\right)^3 = 1 - 3e\cos f + 3e^2\cos 2f$$

$$\alpha R_3 = \alpha\,(1 - 3e\cos f)$$

F_e, F_α and F_{ϖ} are as follows

$$F_e = -\left(\frac{1}{2}e + \frac{1}{8}e^3\right)\sin S + \left(\frac{3}{2} - \frac{1}{8}e^2\right)\sin\overline{f-S} - \left(\frac{1}{2} - \frac{1}{8}e^2\right)\sin\overline{f+S} + \frac{1}{4}e\,[\sin\overline{2f+S} - \sin\overline{2f-S}\,] - \frac{1}{8}e^2\,[\sin\overline{3f+S} - \sin\overline{3f-S}\,] + \frac{1}{16}e^3\,[\sin\overline{4f+S} - \sin\overline{4f-S}\,] \qquad (16)$$

$$F_\alpha = e \sin \overline{f-S} - \sin S \tag{17}$$

$$F_\varpi = \left(\frac{3}{2} + \frac{1}{8}e^2\right) \cos \overline{f-S} - \left(\frac{1}{2} + \frac{1}{8}e^2\right) \cos \overline{f+S}$$
$$- \left(\frac{1}{4}e + \frac{1}{8}e^3\right)[\cos \overline{2f-S} - \cos \overline{2f+S}] + \frac{1}{8}e^2 [\cos \overline{3f-S} - \cos \overline{3f+S}]$$
$$- \frac{1}{16}e^3 [\cos \overline{4f-S} - \cos \overline{4f+S}] \tag{18}$$

To second order they become

$$F_e = -\frac{1}{2}e\sin S + \left(\frac{3}{2} - \frac{1}{8}e^2\right) \sin \overline{f-S} - \left(\frac{1}{2} - \frac{1}{8}e^2\right) \sin \overline{f+S}$$
$$+ \frac{1}{4}e [\sin \overline{2f+S} - \sin \overline{2f-S}] - \frac{1}{8}e^2 [\sin \overline{3f+S} - \sin \overline{3f-S}]$$

$$F_\alpha = e\sin \overline{f-S} - \sin S$$

$$F_\varpi = \left(\frac{3}{2} + \frac{1}{8}e^2\right) \cos \overline{f-S} - \left(\frac{1}{2} + \frac{1}{8}e^2\right) \cos \overline{f+S}$$
$$- \frac{1}{4}e [\cos \overline{2f-S} - \cos \overline{2f+S}] + \frac{1}{8}e^2 [\cos \overline{3f-S} - \cos \overline{3f+S}]$$

nt is found using Equation (9) and a series for the mean anomaly M expressed in terms of f, developed by Brouwer and Clemence (1961, pg. 64-65). Brouwer and Clemence give

$$M = f - 2\left[\beta(1 + \cos\vartheta) \sin f - \beta^2\left(\frac{1}{2} + \cos\vartheta\right) \sin 2f + \beta^3\left(\frac{1}{3} + \cos\vartheta\right) \sin 3f \ \ldots\right]$$

where $\sin\vartheta = e$

$\cos\vartheta = \sqrt{1 - e^2}$

$\beta = \frac{1}{e}[1 - (1 - e^2)^{1/2}]$

Thus to third order in e, the series for M in terms of f reduces to

$$M = f - 2e\sin f + \frac{3}{4}e^2\sin 2f - \frac{1}{3}e^3\sin 3f + \ldots \tag{19}$$

nt then becomes

$$n\,t = M - M_0$$
$$= f - M_0 - 2e\sin f + \frac{3}{4}e^2\sin 2f - \frac{1}{3}e^3\sin 3f$$

or to second order

$$n\,t = f - M_0 - 2e\sin f + \frac{3}{4}e^2\sin 2f$$

The series expansions for K, F_ϵ and Q are therefore

$$K = 1 + \frac{1}{2}e^2 + \left(-e + \frac{3}{16}e^3\right)\cos f - e^2\cos 2f + \frac{5}{16}e^3\cos 3f - \frac{3}{2}e(f - M_0)\sin f \qquad (20)$$

$$F_\epsilon = \left(1 + \frac{1}{2}e^2\right)\cos S + \frac{3}{2}(f - M_0)\sin S - \frac{3}{2}(f - M_0)e\sin \overline{f-S} + \left(-2e + \frac{3}{8}e^3\right)\cos \overline{f-S} + \left(e - \frac{3}{16}e^3\right)\cos \overline{f+S} - \frac{11}{16}e^2\cos \overline{2f-S} - \frac{5}{16}e^2\cos \overline{2f+S} + \frac{3}{16}e^3\cos \overline{3f-S} - \frac{1}{8}e^3\cos \overline{3f+S} \qquad (21)$$

$$Q = \frac{9}{4}\rho + \frac{225}{64}\rho^3 + \left(3 + \frac{45}{8}\rho^2\right)\cos S + \left(\frac{15}{4}\rho + \frac{105}{16}\rho^3\right)\cos 2S + \frac{35}{8}\rho^2\cos 3S + \frac{315}{64}\rho^3\cos 4S \qquad (22)$$

Note that Q is not completely expanded into our standard form, since the coefficients of the trigonometric functions involve ρ, which is still a function of f. We transform Q into the standard form in Section 3.3 (ii).

For now, the second order expansions of K, F_ϵ and Q are

$$K = 1 + \frac{1}{2}e^2 - e\cos f - e^2\cos 2f - \frac{3}{2}e(f - M_0)\sin f$$

$$F_\epsilon = \left(1 + \frac{1}{2}e^2\right)\cos S + \frac{3}{2}(f - M_0)\sin S - \frac{3}{2}(f - M_0)e\sin \overline{f-S}$$
$$-2e\cos \overline{f-S} + e\cos \overline{f+S} - \frac{11}{16}e^2\cos \overline{2f-S} - \frac{5}{16}e^2\cos \overline{2f+S}$$

$$Q = \frac{9}{4}\rho + \left(3 + \frac{45}{8}\rho^2\right)\cos S + \frac{15}{4}\rho\cos 2S + \frac{35}{8}\rho^2\cos 3S$$

(ii) Expansion of the components of Lagrange's planetary equations found only in the circular case

Next we expand to second order the components of Equations (2) which are found in the circular problem alone. Thus, since $\rho^j = \alpha^j R_j$ where j is an integer, Q becomes

$$Q = \frac{9}{4}\alpha - \frac{9}{4}\alpha e\cos f + \left(3 + \frac{45}{8}\alpha^2\right)\cos S + \frac{15}{4}\alpha\cos 2S$$
$$-\frac{15}{8}\alpha e[\cos \overline{f-2S} + \cos \overline{f+2S}] + \frac{35}{8}\alpha^2\cos 3S$$

Likewise, $\rho\sin f$, $\rho e\sin f$, $\rho\cos f$ and ρK are as follows

$$\rho\sin f = \alpha\sin f - \frac{1}{2}\alpha e\sin 2f$$

$$\rho e\sin f = \alpha e\sin f$$

$$\rho\cos f = \alpha\cos f - \frac{1}{2}\alpha e(1 + \cos 2f)$$

$$\rho K = \alpha\left[1 - 2e\cos f - \frac{3}{2}e(f - M_0)\sin f\right]$$

(iii) The expanded form of Lagrange's planetary equations $d\sigma/df$

The series of cosine and sine terms for each component of Lagrange's planetary equations can now be substituted into Equations (2) to get $d\sigma/df$ in their expanded form. The necessary multiplication of several complicated series of sines and cosines

is most easily done using a tabular form. For example, R_3 and Q can be rewritten as

$R_3 =$

Coeff.	f	S
1	0	0
$-3e$	1	0
$3e^2$	2	0

cos

$Q =$

Coeff.	f	S
$\frac{9}{4}\alpha$	0	0
$3 + \frac{45}{8}\alpha^2$	0	1
$\frac{15}{4}\alpha$	0	2
$\frac{35}{8}\alpha^2$	0	3
$-\frac{9}{4}\alpha e$	1	0
$-\frac{15}{8}\alpha e$	1	2
"	1	-2

cos

The column headed "Coeff." contains the coefficient of the sine or cosine term, while the other columns contain the coefficents of the arguments of the cosine or sine terms given at the top of the column. Thus, another way to write the bottom term in Q is $-(15/8)\alpha e \cos \overline{f-2S}$.

It now becomes possible to multiply R_3 by Q and apply the trigonometric identities (15) in one step. The table is then collated to give

$R_3Q =$

Coeff.	f	S
$\frac{9}{4}\alpha$	0	0
$3 + \frac{45}{8}\alpha^2$	0	1
$\frac{15}{4}\alpha$	0	2
$\frac{35}{8}\alpha^2$	0	3
$-9\alpha e$	1	0

cos

+

Coeff.	f	S
$-\frac{9}{2}e$	1	1
"	1	-1
$-\frac{15}{2}$	1	2
"	1	-2
$\frac{9}{2}e^2$	2	1
"	2	-1

cos

Ideally, these lengthy multiplications of series containing sines and cosines could have been completed much more quickly using an algebraic computing package such as REDUCE; however, as such software was not available to us at the time, we found the tabular method the next most efficient method of performing the necessary calculations. Using the tabular form of multiplying successive strings of tables of sine and cosine terms, de/df, dα/df, dϖ/df and dϵ/df are found to be

$$\frac{de}{df} = \nu^2 \left[\begin{array}{|l|c|c|}\hline \text{Coeff.} & f & S \\ \hline \frac{21}{16}\alpha e & 0 & 1 \\ \frac{1}{2}+\frac{9}{16}\alpha^2-\frac{3}{4}e^2 & 1 & 0 \\ \frac{3}{16}\alpha & 1 & 1 \\ \frac{15}{16}\alpha & 1 & -1 \\ -\frac{9}{32}\alpha e & 2 & 1 \\ -\frac{63}{32}\alpha e & 2 & -1 \\ \frac{15}{4}e & 0 & 2 \\ -\frac{3}{4}-\frac{21}{8}e^2 & 1 & 2 \\ \frac{9}{4}+\frac{3}{8}e^2+\frac{5}{4}\alpha^2 & 1 & -2 \\ \frac{3}{2}e & 2 & 2 \\ -\frac{3}{4}e & 2 & 0 \\ \hline \end{array}\right]_{\sin} + \nu^2 \left[\begin{array}{|l|c|c|}\hline \text{Coeff.} & f & S \\ \hline -\frac{15}{4}e & 2 & -2 \\ -\frac{15}{8}e^2 & 3 & 2 \\ \frac{3}{4}e^2 & 3 & 0 \\ \frac{33}{8}e^2 & 3 & -2 \\ \frac{105}{16}\alpha e & 0 & 3 \\ \frac{45}{16}\alpha & 1 & -3 \\ -\frac{15}{16}\alpha & 1 & 3 \\ \frac{75}{32}\alpha e & 2 & 3 \\ -\frac{195}{32}\alpha e & 2 & -3 \\ -\frac{35}{32}\alpha^2 & 1 & 4 \\ \frac{105}{32}\alpha^2 & 1 & -4 \\ \hline \end{array}\right]_{\sin} \qquad (23a)$$

$$\frac{d\alpha}{df} = 2\nu^2\alpha \text{ sin}$$

Coeff.	f	S
$-\frac{3}{8}\alpha$	0	1
$-\frac{3}{2}$	0	2
$-\frac{15}{8}\alpha$	0	3

$$+ \; 2\nu^2\alpha \text{ sin}$$

Coeff.	f	S
$\frac{1}{2}e$	1	0
$\frac{9}{4}e$	1	2
$-\frac{3}{4}e$	1	-2

(23b)

$$\frac{d\varpi}{df} = -\frac{\nu^2}{e} \text{ cos}$$

Coeff.	f	S
$\frac{1}{2}+\frac{9}{16}\alpha^2+\frac{3}{4}e^2$	1	0
$\frac{3}{16}\alpha$	1	1
$\frac{15}{16}\alpha$	1	-1
$-\frac{9}{32}\alpha e$	2	1
$-\frac{63}{32}\alpha e$	2	-1
$-\frac{9}{4}\alpha e$	0	1
$-\frac{3}{4}+\frac{21}{8}e^2$	1	2
$\frac{9}{4}+\frac{5}{4}\alpha^2-\frac{3}{8}e^2$	1	-2
$\frac{3}{2}e$	2	2
$-\frac{3}{4}e$	2	0
$-\frac{15}{4}e$	2	-2
$-\frac{15}{8}e^2$	3	2

$$+ \; -\frac{\nu^2}{e} \text{ cos}$$

Coeff.	f	S
$\frac{3}{4}e^2$	3	0
$\frac{33}{8}e^2$	3	-2
$-\frac{15}{16}\alpha$	1	3
$\frac{45}{16}\alpha$	1	-3
$\frac{75}{32}\alpha e$	2	3
$-\frac{195}{32}\alpha e$	2	-3
$-\frac{35}{32}\alpha^2$	1	4
$\frac{105}{32}\alpha^2$	1	-4
$-\frac{3}{4}e$	0	0
$-\frac{9}{4}e$	0	2
$-\frac{15}{4}\alpha e$	0	3

(23c)

$$\frac{d\epsilon}{df} = \frac{d\epsilon_1}{df} + \frac{d\epsilon_2}{df} + \frac{1}{2}e^2\frac{d\varpi}{df} \qquad (23d)$$

where

$$\frac{d\epsilon_1}{df} = -2\nu^2$$

Coeff.	f	S (cos)
$\frac{1}{2}+\frac{9}{16}\alpha^2+\frac{3}{2}e^2$	0	0
$\frac{9}{8}\alpha$	0	1
$-\frac{9}{4}\alpha e$	1	1
$-\frac{27}{8}\alpha e$	1	-1
$\frac{3}{2}+\frac{5}{4}\alpha^2+\frac{9}{2}e^2$	0	2
$-\frac{3}{4}e$	1	2
$-2e$	1	0
$-\frac{21}{4}e$	1	-2

$+ \; -2\nu^2$

Coeff.	f	S (cos)
$-\frac{15}{32}e^2$	2	2
$\frac{7}{4}e^2$	2	0
$\frac{183}{32}e^2$	2	-2
$\frac{15}{8}\alpha$	0	3
$-\frac{15}{8}\alpha e$	1	3
$-\frac{15}{2}\alpha e$	1	-3
$\frac{35}{16}\alpha^2$	0	4

$$\frac{d\epsilon_2}{df} = -2\nu^2(f - M_0)\ \{$$

Coeff.	f	S (sin)
$\frac{9}{16}\alpha$	0	1
$\frac{9}{4}+\frac{15}{16}\alpha^2-\frac{9}{8}e^2$	0	2
$-\frac{27}{16}\alpha e$	1	1
$-\frac{3}{4}e$	1	0
$\frac{9}{8}e$	1	-2
$\frac{45}{16}\alpha$	0	3

$+$

Coeff.	f	S (sin)
$\frac{45}{16}\alpha e$	1	-3
$\frac{105}{32}\alpha^2$	0	4
$-\frac{27}{8}e$	1	2
$\frac{9}{8}e^2$	2	0
$-\frac{45}{8}\alpha e$	1	3
$\frac{27}{8}e^2$	2	2

$\}$

(iv) The expanded form of Lagrange's planetary equations $d\sigma/dS$

We now have Lagrange's planetary equations written with respect to f and S in the form of a series of sines and cosines

$$\frac{d\sigma}{df} = \sum_{i=1}^{N} A_i \sin(j_i f + k_i S) + \sum_{l=1}^{M} B_l \cos(j_l f + k_l S) + (f - M_0) \sum_{p=1}^{W} D_p \sin(j_p f + k_p S)$$

where σ is any one of the orbital elements e, α, ϖ or ϵ; j_i, k_i, j_l, k_l, j_p and k_p are integers for i = 1 to N, l = 1 to M and p = 1 to W; N, M and W are the number of terms retained in each series expansion and the coefficients of each term A_i, B_l and D_p are functions of e, α and ν.

The final steps before integration with respect to the time variable S are to convert all the functions of f in the differential equations to functions of S, and to transform the derivatives with respect to f to ones with respect to S.

To complete the first requirement, it is necessary to find f as a function of S. Recall from Section 3.2 that

$$S = f - f_{c0} - n_1 t$$

Using Equation (9), we can write

$$n_1 t = \frac{n_1}{n} (M - M_0)$$

Thus

$$S = f - f_{c0} - \nu (M - M_0)$$

We can then use Brouwer and Clemence's (1961) series expansion for the mean anomaly M in terms of the true anomaly f or Equation (19) to get

$$S = f - f_{c0} - \nu\left(f - 2e\sin f + \frac{3}{4}e^2\sin 2f - \frac{1}{3}e^3\sin 3f + \ldots - M_0 \right) \qquad (24)$$

Unfortunately, this equation gives us S as a function of f. To reverse the relationship let

$$m(f) = M - f = -2e\sin f + \frac{3}{4}e^2\sin 2f - \frac{1}{3}e^3\sin 3f + \ldots$$

Thus

$$S = (1 - \nu)f - \nu m(f) - f_{c0} + \nu M_0$$

and hence

$$f = \frac{1}{1-\nu} S + \frac{\nu}{1-\nu} m(f) + \frac{1}{1-\nu} (f_{c0} - \nu M_0)$$

Expanding about small ν gives

$$f = (1 + \nu + \nu^2)\, S + (\nu + \nu^2)\, m(f) + \frac{1}{1-\nu} (f_{c0} - \nu M_0)$$

If we now separate f into a sum of constants K_0, small terms g and large terms G, we get

$$f = G + g + K_0$$

where $G = S$

$$g = (\nu + \nu^2)\,(S + m(f))$$

$$K_0 = \frac{1}{1-\nu} (f_{c0} - \nu M_0) \qquad (25)$$

We do this so that in future we can expand about the small terms g. Expanded to second order g becomes

$$g = (\nu + \nu^2)S - 2e\nu\sin f \qquad (26)$$

We still need to write g totally as a function of S. When Equation (25) is substituted into Equation (26) for g, we get a transcendental equation involving g

$$g = (\nu + \nu^2)S - 2e\nu\sin (S + g + K_0) \qquad (27)$$

An explicit equation for g can be found iteratively by repeatedly substituting Equation (27) for g into the right hand side of itself and expanding about the small parameter g until Equation (27) for g is no longer a function of itself to the required order.

ie $g_1 = F(g_0)$

$g_2 = F(g_1)$

$g_3 = F(g_2)$

- etc-

Using a Taylor expansion to expand about small g, the sine function can be rewritten to second order in α, e and ν as

$$\sin (S + K_0 + g) = \sin \overline{S+K_0} + g\cos \overline{S+K_0}$$

g then becomes a function solely of S, viz.

$$g = (\nu + \nu^2)S - 2e\nu\sin \overline{S+K_0}$$

In other words, the term containing g on the right hand side of the equation is of third order and is therefore ignored.

In summary, we have f as a function of S given by

$$f = S + g + K_0 \tag{28a}$$

where $$g = (\nu + \nu^2)S - 2e\nu \sin \overline{S+K_0} \tag{28b}$$

$$K_0 = \frac{1}{1-\nu}(f_{c0} - \nu M_0) \tag{28c}$$

The second step required before integration is the transformation of $d\sigma/df$ into $d\sigma/dS$.

$$\frac{d\sigma}{dS} = \frac{d\sigma}{df} \Big/ \frac{dS}{df}$$

dS/df to second order is found by differentiating (24) and replacing f with Equations (28). The result is

$$\frac{dS}{df} = 1 - \nu(1 - 2e\cos \overline{S+K_0+g})$$

And hence, with some expansion about the small parameters, $d\sigma/dS$ becomes

$$\frac{d\sigma}{dS} = (1 + \nu + \nu^2 - 2e\nu\cos \overline{S+K_0+g}) \frac{d\sigma}{df} \tag{29}$$

We use the original equations S(f) instead of differentiating f(S) directly, so that the arguments of the sine and cosine terms will contain similar components to those found in Lagrange's equations $d\sigma/df$. This procedure will simplify the multiplication of $d\sigma/df$ by the factor $1/(dS/df)$.

We can now write Lagrange's planetary equations solely as a function of S by using Equations (28) and (29). To second order, they are

$$\frac{de}{dS} =$$

Coeff.	S	K_0+g	sin
$\frac{15}{16}\alpha(1+\nu)$	0	1	
$-\frac{15}{4}e - 6e\nu$	0	2	
$\frac{21}{16}\alpha e$	1	0	
$\frac{1}{2}(1+\nu+\nu^2) + \frac{9}{16}\alpha^2 - \frac{3}{4}e^2$	1	1	
$-\frac{63}{32}\alpha e$	1	2	
$\frac{33}{8}e^2$	1	3	
$-\frac{9}{4}(1+\nu+\nu^2) - \frac{3}{8}e^2 - \frac{5}{4}\alpha^2$	1	−1	
$\frac{195}{32}\alpha e$	1	−2	
$\frac{15}{4}e + \frac{27}{4}e\nu$	2	0	
$\frac{3}{16}\alpha(1+\nu)$	2	1	
$-\frac{3}{4}e - \frac{5}{4}e\nu$	2	2	

+

Coeff.	S	K_0+g	sin
$-\frac{45}{16}\alpha(1+\nu)$	2	−1	
$\frac{105}{16}\alpha e$	3	0	
$-\frac{3}{4}(1+\nu+\nu^2) - \frac{21}{8}e^2$	3	1	
$-\frac{9}{32}\alpha e$	3	2	
$\frac{3}{4}e^2$	3	3	
$-\frac{105}{32}\alpha^2$	3	−1	
$-\frac{15}{16}\alpha(1+\nu)$	4	1	
$\frac{3}{2}e + \frac{9}{4}e\nu$	4	2	
$\frac{75}{32}\alpha e$	5	2	
$-\frac{15}{8}e^2$	5	3	
$-\frac{35}{32}\alpha^2$	5	1	

(30a)

$$\frac{d\alpha}{dS} = 2\nu^2\alpha$$

Coeff.	S	K_0+g	sin
$-\frac{3}{8}\alpha$	1	0	
$-\frac{3}{2}(1+\nu)$	2	0	
$-\frac{15}{8}\alpha$	3	0	

+ $2\nu^2\alpha$

Coeff.	S	K_0+g	sin
$\frac{1}{2}e$	1	1	
$\frac{9}{4}e$	3	1	
$\frac{3}{4}e$	1	−1	

(30b)

$$\frac{d\varpi}{dS} = -\frac{\nu^2}{e}\{$$

cos

Coeff.	S	K_0+g
$-\frac{3}{4}e-\frac{5}{4}e\nu$	0	0
$\frac{15}{16}\alpha(1+\nu)$	0	1
$-\frac{15}{4}e-6e\nu$	0	2
$-\frac{9}{4}\alpha e$	1	0
$\frac{1}{2}(1+\nu+\nu^2)+\frac{9}{16}\alpha^2+\frac{3}{4}e^2$	1	1
$-\frac{63}{32}\alpha e$	1	2
$\frac{33}{8}e^2$	1	3
$\frac{9}{4}(1+\nu+\nu^2)+\frac{5}{4}\alpha^2-\frac{3}{8}e^2$	1	−1
$-\frac{195}{32}\alpha e$	1	−2
$-\frac{9}{4}e-\frac{15}{4}e\nu$	2	0
$\frac{3}{16}\alpha(1+\nu)$	2	1
$-\frac{3}{4}e-\frac{5}{4}e\nu$	2	2

+

cos

Coeff.	S	K_0+g
$\frac{45}{16}\alpha(1+\nu)$	2	−1
$-\frac{15}{4}\alpha e$	3	0
$-\frac{3}{4}(1+\nu+\nu^2)+\frac{21}{8}e^2$	3	1
$-\frac{9}{32}\alpha e$	3	2
$\frac{3}{4}e^2$	3	3
$-\frac{15}{16}\alpha(1+\nu)$	4	1
$\frac{3}{2}e+\frac{9}{4}e\nu$	4	2
$\frac{75}{32}\alpha e$	5	2
$-\frac{15}{8}e^2$	5	3
$-\frac{35}{32}\alpha^2$	5	1
$\frac{105}{32}\alpha^2$	3	−1

$\}$ (30c)

$$\frac{d\epsilon}{dS} = \frac{d\epsilon_1}{dS} + \frac{d\epsilon_2}{dS} + \frac{1}{2}e^2\frac{d\varpi}{dS} \qquad (30d)$$

where

$$\frac{d\epsilon_1}{dS} = -2\nu^2 \{\text{cos}\} + -2\nu^2 \{\text{cos}\}$$

Coeff.	S	K_0+g
$\frac{1}{2}(1+\nu+\nu^2)+\frac{9}{16}\alpha^2+\frac{3}{2}e^2$	0	0
$-\frac{27}{8}\alpha e$	0	1
$\frac{183}{32}e^2$	0	2
$\frac{9}{8}\alpha(1+\nu)$	1	0
$-2e-3e\nu$	1	1
$-\frac{21}{4}e-\frac{27}{4}e\nu$	1	−1
$\frac{3}{2}(1+\nu+\nu^2)+\frac{5}{4}\alpha^2+\frac{9}{2}e^2$	2	0
$-\frac{9}{4}\alpha e$	2	1

Coeff.	S	K_0+g
$\frac{7}{4}e^2$	2	2
$-\frac{15}{2}\alpha e$	2	−1
$\frac{15}{8}\alpha(1+\nu)$	3	0
$-\frac{3}{4}e-\frac{9}{4}e\nu$	3	1
$-\frac{15}{8}\alpha e$	4	1
$-\frac{15}{32}e^2$	4	2
$\frac{35}{16}\alpha^2$	4	0

$$\frac{d\epsilon_2}{dS} = 2\nu^2(S + K_0 + g - M_0)$$

$$\{\text{sin}\} + \{\text{sin}\}$$

Coeff.	S	K_0+g
$-\frac{9}{16}\alpha(1+\nu)$	1	0
$\frac{3}{4}e(1+\nu)$	1	1
$\frac{9}{8}e+\frac{27}{8}e\nu$	1	−1
$-\frac{9}{4}(1+\nu+\nu^2)-\frac{15}{16}\alpha^2+\frac{9}{8}e^2$	2	0
$\frac{27}{16}\alpha e$	2	1
$-\frac{9}{8}e^2$	2	2

Coeff.	S	K_0+g
$\frac{45}{16}\alpha e$	2	−1
$-\frac{45}{16}\alpha(1+\nu)$	3	0
$\frac{27}{8}e+\frac{45}{8}e\nu$	3	1
$\frac{45}{8}\alpha e$	4	1
$-\frac{27}{8}e^2$	4	2
$-\frac{105}{32}\alpha^2$	4	0

(v) General form of the integration of the equations $d\sigma/dS$

We now have Lagrange's planetary equations written in the general form

$$\frac{d\sigma}{dS} = \sum_{i=1}^{N'} E_i \sin [j_i' S + k_i'(K_0 + g)] + \sum_{l=1}^{M'} F_l \cos [j_l' S + k_l'(K_0 + g)]$$
$$+ (S + K_0 + g - M_0) \sum_{p=1}^{W'} G_p \sin [j_p' S + k_p'(K_0 + g)]$$

where $K_0 = \frac{1}{1-\nu} (f_{c0} - \nu M_0)$

$g = (\nu + \nu^2) S - 2e\nu \sin \overline{S+K_0}$

where j_i', k_i', j_l', k_l', j_p' and k_p' are integers for i = 1 to N', l = 1 to M' and p = 1 to W', and E_i, F_l and G_p are functions of α, e and ν. For greater clarity, let it be understood that the integers j' and k' have different values for each trigonometric term in $d\sigma/dS$ and are different from the values j, k found in $d\sigma/df$. We therefore drop the primes and subscripts.

$d\sigma/dS$ is a complicated integrand involving sine functions within sine and cosine functions. To avoid the difficulty of integrating such expressions, we again expand about the small parameter g. Thus, sin (jS + kK_0 + kg) can be rewritten as

$$\sin (jS + kK_0 + kg) = \sin (jS + kK_0) \cos kg + \cos (jS + kK_0) \sin kg$$

and expanded about small g to give

$$\sin (jS + kK_0 + kg) = \sin (jS + kK_0) + k(\nu+\nu^2) S \cos \overline{jS+kK_0}$$
$$+k\nu e [-\sin \overline{(j+1)S + (k+1)K_0} + \sin \overline{(j-1)S + (k-1)K_0}]$$
$$-\frac{k^2\nu^2}{2} S^2 \sin \overline{jS+kK_0} \qquad (31)$$

This part of the integrand of $d\sigma/dS$ now involves three types of easy integrals

$$\int_{-\pi}^{+\pi} \sin (jS+kK_0)\, dS$$

$$\int_{-\pi}^{+\pi} S \cos (jS+kK_0)\, dS$$

$$\int_{-\pi}^{+\pi} S^2 \sin (jS+kK_0)\, dS$$

In the same manner

$$\cos (jS + kK_0 + kg) = \cos (jS + kK_0) - k(\nu+\nu^2)\, S \sin \overline{jS+kK_0}$$
$$+k\nu e\, [-\cos \overline{(j+1)S+(k+1)K_0} + \cos \overline{(j-1)S+(k-1)K_0}]$$
$$-\frac{k^2\nu^2}{2} S^2 \cos \overline{jS+kK_0} \qquad (32)$$

This part of the integrand also involves three types of easy integrals

$$\int_{-\pi}^{+\pi} \cos (jS+kK_0)\, dS$$

$$\int_{-\pi}^{+\pi} S \sin (jS+kK_0)\, dS$$

$$\int_{-\pi}^{+\pi} S^2 \cos (jS+kK_0)\, dS$$

And finally, the last sum containing terms of the type

$$(S + K_0 + g - M_0)\sin (jS+ kK_0 + kg)$$

can be rewritten as

$$(S+K_0+g-M_0)\,H = (1+\nu+\nu^2)\,SH + (K_0-M_0)\,H - 2e\nu H\sin(S+K_0)$$

where $H = \sin(jS + kK_0 + kg)$

Then, using the previously derived expansion for H or Equation (31), we expand the above equation to second order to get

$$\begin{aligned}
(S+K_0+g-M_0)\,H = {} & (K_0-M_0)\sin\overline{jS+kK_0} \\
& + ke\nu(K_0-M_0)\,[-\sin\overline{(j+1)S+(k+1)K_0} + \sin\overline{(j-1)S+(k-1)K_0} \\
& - e\nu\,[-\cos\overline{(j+1)S+(k+1)K_0} + \cos\overline{(j-1)S+(k-1)K_0} \\
& + S\{\,(1+\nu+\nu^2)\sin\overline{jS+kK_0} \\
& \quad + ke\nu[-\sin\overline{(j+1)S+(k+1)K_0} + \sin\overline{(j-1)S+(k-1)K_0} \\
& \quad + k(\nu+\nu^2)\,(K_0-M_0)\cos\overline{jS+kK_0}\,\} \\
& + S^2\{\,k(\nu+2\nu^2)\cos\overline{jS+kK_0} \\
& \quad - \frac{k^2\nu^2}{2}\,(K_0-M_0)\sin\overline{jS+kK_0}\,\} \\
& - S^3\,\frac{k^2\nu^2}{2}\sin\overline{jS+kK_0}
\end{aligned} \tag{33}$$

This part of the integrand for $d\epsilon/dS$ contains seven types of integrals: the six integrals mentioned on the previous page and the following one

$$\int_{-\pi}^{+\pi} S^3 \sin(jS+kK_0)\,dS$$

Table 3.1 gives a summary of the values of these integrals depending on the j,k integer coefficients of the variable S and constant K_0 respectively. The benefit of choosing the variable S as the integration variable and the synodic period as the integration interval now becomes apparent. Many of the integrals, depending on the value of j, conveniently disappear when integrated over 2π.

Type	Integral	Solution	
(a)	$\int_{-\pi}^{+\pi} \sin(jS + kK_0)\, dS$	$= \begin{cases} 2\pi \sin kK_0 & \\ 0 & \end{cases}$	$j = 0$ $j \neq 0$
	$\int_{-\pi}^{+\pi} \cos(jS + kK_0)\, dS$	$= \begin{cases} 2\pi \cos kK_0 & \\ 0 & \end{cases}$	$j = 0$ $j \neq 0$
(b)	$\int_{-\pi}^{+\pi} S\sin(jS + kK_0)\, dS$	$= \begin{cases} 0 & \\ -\frac{2\pi}{j} \cos j\pi \cos kK_0 & \end{cases}$	$j = 0$ $j \neq 0$
	$\int_{-\pi}^{+\pi} S\cos(jS + kK_0)\, dS$	$= \begin{cases} 0 & \\ +\frac{2\pi}{j} \cos j\pi \sin kK_0 & \end{cases}$	$j = 0$ $j \neq 0$
(c)	$\int_{-\pi}^{+\pi} S^2 \sin(jS + kK_0)\, dS$	$= \begin{cases} \frac{2}{3}\pi^3 \sin kK_0 & \\ +\frac{4\pi}{j^2} \cos j\pi \sin kK_0 & \end{cases}$	$j = 0$ $j \neq 0$
	$\int_{-\pi}^{+\pi} S^2 \cos(jS + kK_0)\, dS$	$= \begin{cases} \frac{2}{3}\pi^3 \cos kK_0 & \\ +\frac{4\pi}{j^2} \cos j\pi \cos kK_0 & \end{cases}$	$j = 0$ $j \neq 0$
(d)	$\int_{-\pi}^{+\pi} S^3 \sin(jS + kK_0)\, dS$	$= \begin{cases} 0 & \\ +\frac{2\pi}{j^3} \cos j\pi \,[6 - j^2\pi^2] \cos kK_0 & \end{cases}$	$j = 0$ $j \neq 0$
	$\int_{-\pi}^{+\pi} S^3 \cos(jS + kK_0)\, dS$	$= \begin{cases} 0 & \\ -\frac{2\pi}{j^3} \cos j\pi \,[6 - j^2\pi^2] \sin kK_0 & \end{cases}$	$j = 0$ $j \neq 0$

Table 3.1 A list of the general integrals and corresponding solutions needed for the integration of Lagrange's planetary equations $d\sigma/dS$, where $\sigma = e, \alpha, \varpi$ or ϵ.

(vi) The integration of Lagrange's planetary equations $d\sigma/dS$

It remains only to integrate each of the Lagrange's planetary equations using the expansions given in Equations (31) to (33) and the table of integrals Table 3.1. For example, our expression for de/dS contains sin $(jS+kK_0+kg)$ and therefore consists of three types of integrals: the sine integral of type (a), the cosine integral of type (b) and the sine integral of type (c), all from Table 3.1.

From Equation (31), we can see that type (a) integrals will be non-zero if either j=0, j+1=0 or j-1=0. Only the following terms are non-zero and of order less than or equal to two

$\frac{de}{dS}$: ν^2

		sin	
Coeff.	S	K_0	
$\frac{15}{16}\alpha(1+\nu)$	0	1	j = 0
$-\frac{15}{4}e - 6e\nu$	0	2	"
$\frac{9}{4}e\nu$	0	-2	j - 1 = 0

Hence, using the integration Table 3.1

Δe: $\nu^2\pi$

	sin	
Coeff.	K_0	
$\frac{15}{8}\alpha(1+\nu)$	1	
$-\frac{15}{2}e - \frac{33}{2}e\nu$	2	

The type (b) integrals will produce non-zero results if $j\neq 0$. The following are all the non-zero terms of order ≤ 2.

$\frac{de}{dS}$: $\nu^2 S$ {

		cos				cos	
Coeff.	S	K_0	+	Coeff.	S	K_0	}
$\frac{1}{2}(\nu+2\nu^2)$	1	1		$\frac{45}{16}\alpha\nu$	2	-1	
$\frac{9}{4}(\nu+2\nu^2)$	1	-1		$-\frac{3}{4}(\nu+2\nu^2)$	3	1	
$\frac{3}{16}\alpha\nu$	2	1		$-\frac{15}{16}\alpha\nu$	4	1	
$-\frac{3}{2}e\nu$	2	2		$3e\nu$	4	2	

Upon integration, the terms become

Δe: $\nu^2\pi$

	sin
Coeff.	K_0
$4(\nu+2\nu^2) - \frac{99}{32}\alpha\nu$	1

And finally, the type (c) integrals give two different answers depending on whether j=0 or j≠0. There are no j=0 terms of order ≤ 2. The following are the rest of the terms of order ≤ 2, where j≠0

$\frac{de}{dS}$: $\nu^2 S^2$

	sin	
Coeff.	S	K_0
$-\frac{1}{4}\nu^2$	1	1
$\frac{9}{8}\nu^2$	1	-1
$\frac{3}{8}\nu^2$	3	1

They integrate to give

Δe: $\nu^2\pi$

Coeff.	sin K_0
$\frac{16}{3}\nu^2$	1

And thus, the final collated answer gives a change in the eccentricity e over one synodic period of

$\Delta e = \nu^2\pi$

Coeff.	sin K_0
$\frac{15}{8}\alpha - \frac{39}{32}\alpha\nu + 4\nu + \frac{40}{3}\nu^2$	1
$-\frac{15}{2}e - \frac{33}{2}e\nu$	2

$d\alpha/dS$, $d\varpi/dS$ and $d\epsilon/dS$ are integrated in the same manner, using Equations (31), (32) and (33) respectively and Table 3.1. Thus, for a restricted circular coplanar three-body problem, the changes in the orbital elements of a Sun-perturbed satellite over one synodic period centred on a conjunction, are as follows

$\Delta e = \nu^2\pi$

Coeff.	sin K_0
$\frac{15}{8}\alpha - \frac{39}{32}\alpha\nu + 4\nu + \frac{40}{3}\nu^2$	1
$-\frac{15}{2}e - \frac{33}{2}e\nu$	2

(34a)

$$\Delta\alpha = 0 \tag{34b}$$

$$\Delta\varpi = \frac{\nu^2\pi}{e}$$

cos

Coeff.	K_0
$\frac{3}{2}e(1+\nu)$	0
$-\frac{15}{8}\alpha + \frac{39}{32}\alpha\nu - 4\nu - \frac{40}{3}\nu^2$	1
$\frac{15}{2}e + \frac{33}{2}e\nu$	2

(34c)

$$\Delta\epsilon = \nu^2\pi$$

cos

Coeff.	K_0
$\frac{5}{2} + 7\nu + \frac{23}{2}\nu^2 - \frac{15}{2}e^2 - 6\alpha(1+2\nu) + \frac{93}{32}\alpha^2$	0
$-\frac{33}{16}\alpha e + 46e\nu + 12e$	1
$-\frac{27}{2}e^2$	2

(34d)

$$+\nu^2\pi$$

sin

Coeff.	K_0
$-12e\nu(K_0 - M_0)$	1

where K_0 is a constant given by

$$K_0 = \frac{1}{1-\nu}(f_{c0} - \nu M_0) \tag{34e}$$

and the initial mean anomaly M_0 is given by the initial true anomaly f_{c0} of the satellite located at a conjunction through the following equations

$$\tan\frac{E_0}{2} = \left(\frac{1-e}{1+e}\right)^{1/2}\tan\frac{f_{c0}}{2} \tag{35a}$$

$$M_0 = E_0 - e\sin E_0 \tag{35b}$$

3.4 Discussion of the Analytic Theory, its Implications and Limitations

From Equations (34), giving the changes in the orbital elements of the satellite over one synodic period centred on a conjunction, we can gain much insight into the factors which affect the stability of a planet-satellite system against solar perturbations.

The first important item to notice is that $\Delta\alpha$ is zero to second order in α, e and ν. Not only does this result agree with Poisson's theorem that no secular terms exist in the first or second order perturbation expansions for α, but it also shows that $\Delta\alpha$ is very small. For example, for typical Jupiter-Gallilean satellite values of the orbital elements ($e = 0.01$, $\alpha = 0.0025$ and $\mu = 1100$), the neglected terms of our second order series expansion are of the order of 10^{-11} to 10^{-10} depending on f_{c0}. For confirmation of this range of error, see the third order circular solution of $\Delta\alpha$ (ie Equations (27) of Chapter 4). Thus, any dangers to the satellite's stability will not arise from changes in α.

Changes in the mean longitude at the epoch $\Delta\epsilon$ merely describe the shifts in the satellite's scheduled appearance at its orbital pericentre, while changes in the longitude of the pericentre $\Delta\varpi$ only alter the orientation of the satellite's orbit. Such changes may bring the satellite into a configuration which might result in an unstable situation, but $\Delta\varpi$ cannot directly indicate approaching instability. Changes in the orbital eccentricy Δe on the other hand, can cause the eccentricity to reach unity, an unstable situation where the satellite will either escape or collide with its planet. Thus, if the eccentricity is approaching 1, the satellite is approaching an unstable situation. Of the four orbital elements studied, the eccentricity is therefore the only orbital element which can indicate impending instabilities. As a result, in our stability analysis of planetary satellites perturbed by the Sun we concentrate on studying the behavior of Δe.

We now sample the size of $\Delta\sigma$ where $\sigma = e, \alpha, \varpi$ or ϵ, for different starting values of the true anomaly at the conjunction f_{c0}. This sampling is done for a range of values of the initial parameters typical of the satellites found in the solar system.

e_0 is taken to vary from 0.005 to 0.30, α_0 from 0.0003 to 0.003, and μ is chosen to be either 1.1×10^3, 3.5×10^3, 2.28×10^4, 3.33×10^5 or 3.08×10^6 corresponding to the five satellite systems of Jupiter, Saturn, Uranus, Earth and Mars. Note that this analysis is done for both our numerical and analytical solutions, so that later the two solutions can be compared and the accuracy of the analytic solution can be measured.

The general shapes of each curve Δe, $\Delta\alpha$, $\Delta\varpi$ and $\Delta\epsilon$ as a function of f_{c0} are similar throughout the complete range of values studied for the parameters. The only major change in shape is seen in $\Delta\alpha$ and $\Delta\epsilon$ when the eccentricity is increased from its smallest value to its largest value. Figures 3.2 and 3.3 give fairly typical examples of the variations in the values of $\Delta\sigma$ for f_{c0} values ranging from 0° to 360°. In particular, Figures 3.2 show the results for an approximation of the Jupiter-Callisto system, where e, α and μ are taken to be 0.01, 0.0025 and 1100 respectively.

Figures 3.2(a) to (d) The variation in the changes in the satellite's

(a) eccentricity e

(b) semi-major axis $\alpha = a/a_1$

(c) mean longitude at epoch ϵ

(d) longitude of pericentre ϖ

over one synodic period for different starting values of the initial true anomaly at conjunction f_{c0}.

The data used here is that of a typical Jupiter-Gallilean satellite system where $e=0.01$, $\alpha=0.0025$ and $\mu=1100$. Both numerical (dashed curves) and analytical (solid curves) solutions for $\Delta\sigma$ are shown here to be virtually indistinguishable.

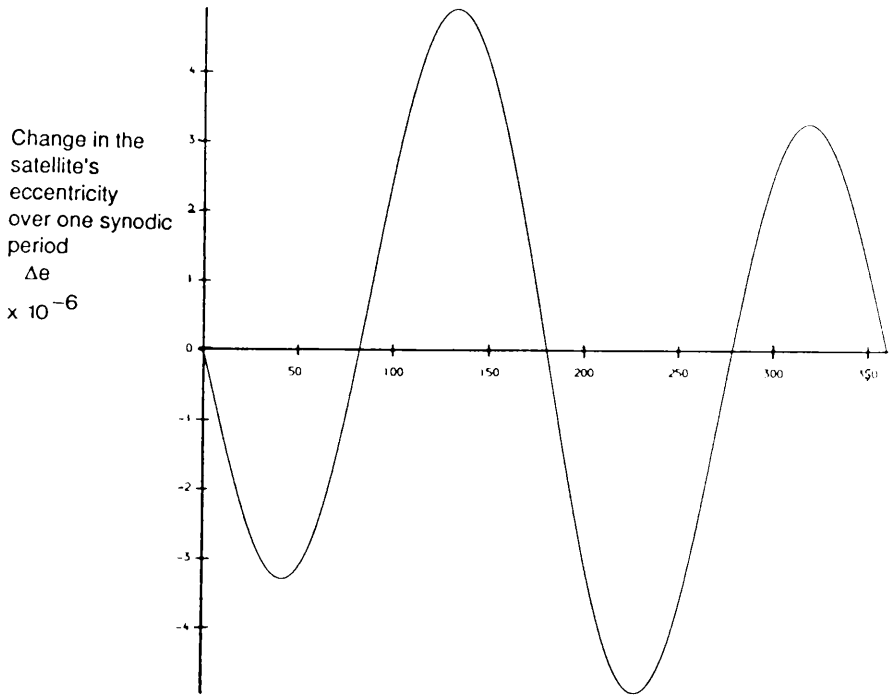
Change in the satellite's eccentricity over one synodic period
Δe
x 10 −6
4
3
2
1
0
-1
-2
-3
-4
50
100
150
200
250
300
350
Initial true anomaly at conjunction f_{c0} (in degrees)

(a)

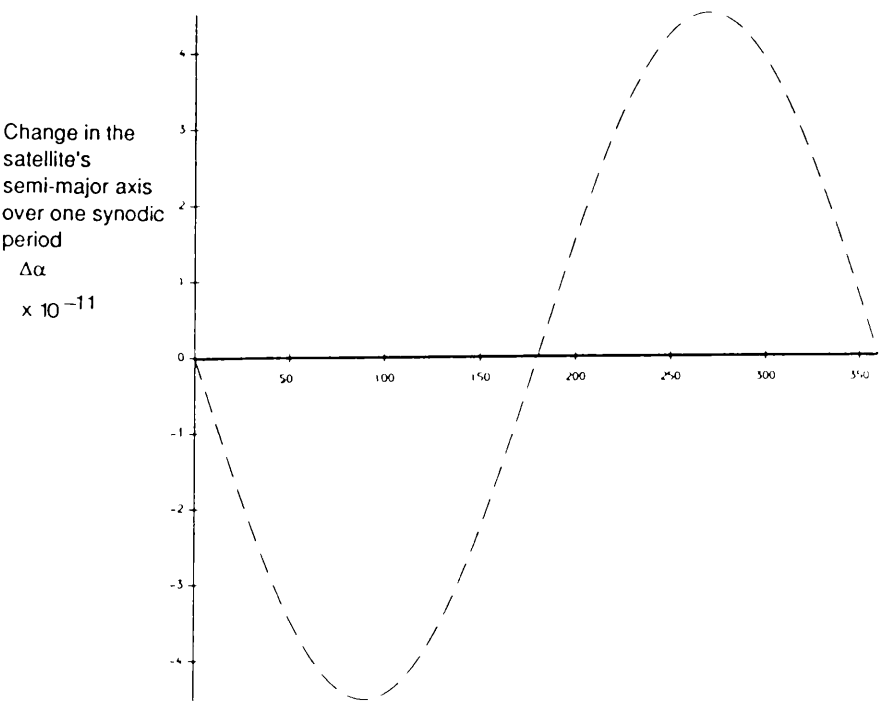
Change in the satellite's semi-major axis over one synodic period
Δα
x 10 −11
4
3
2
1
0
-1
-2
-3
-4
50
100
150
200
250
300
350
Initial true anomaly at conjunction f_{c0} (in degrees)

(b)

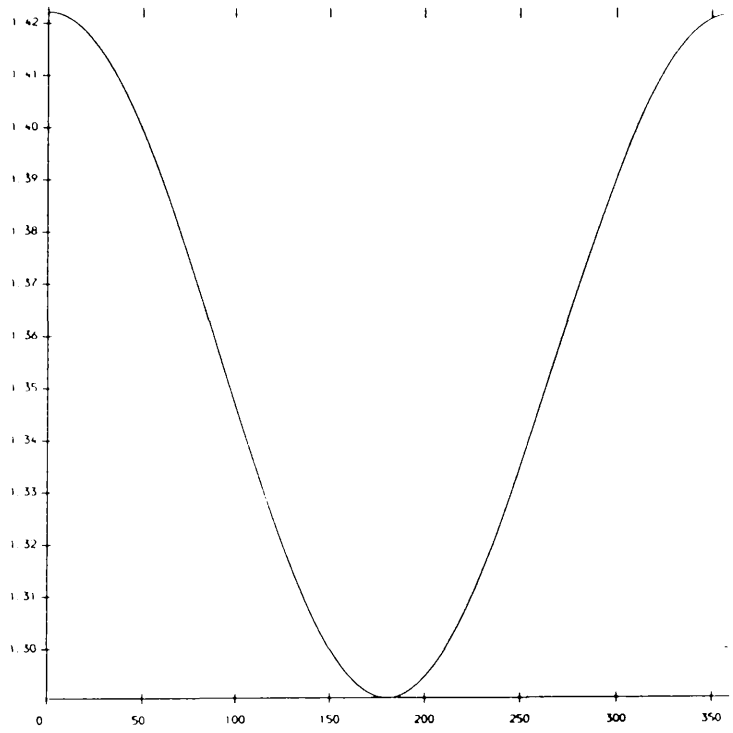
Change in the satellite's mean longitude at epoch over one synodic period
Δϵ
(in radians)
x 10⁻⁴
1.42
1.41
1.40
1.39
1.38
1.37
1.36
1.35
1.34
1.33
1.32
1.31
1.30
0
50
100
150
200
250
300
350
Initial true anomaly at conjunction f_c0 (in degrees)

(c)

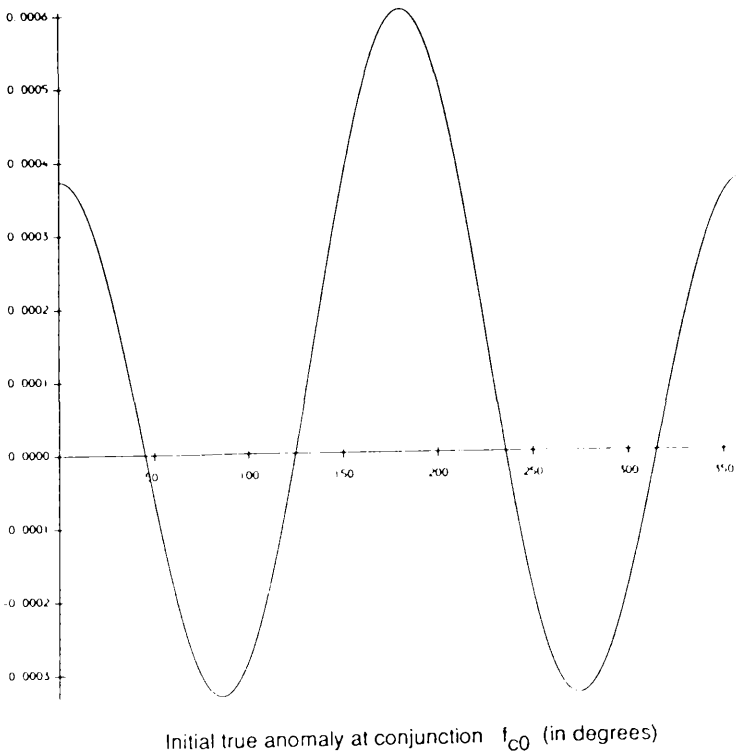
Change in the satellite's longitude of pericentre over one synodic period
Δϖ
(in radians)
0.0006
0.0005
0.0004
0.0003
0.0002
0.0001
0.0000
0.0001
-0.0002
0.0003
100
150
200
Initial true anomaly at conjunction f_c0 (in degrees)

(d)

Figures 3.3 show the variations of $\Delta\sigma$ as a function of f_{c0} for the same Jupiter-Callisto system, with the exception that now the eccentricity of the satellite's orbit has been increased to e = 0.30. The dashed lines depict the numerical solution, while the solid lines depict the analytical solution.

Note that in Figures 3.2, the analytical solution is virtually indistinguishable from the numerical solution, while in Figures 3.3, the differences between the two solutions have become apparent. The average relative difference between the two solutions in Figures 3.2 is about 0.1%, while in Figures 3.3 it is about 4.0%.

Both Figures 3.2(a),(b) and 3.3(a),(b) clearly show that the changes in the eccentricity and the semi-major axis over one synodic period are zero when the synodic period is centred on a conjunction located at the orbit's pericentre or apocentre (ie $f_{c0}=0°$ or 180°). In fact, this characteristic occurs throughout the range of values of the initial parameters studied. Substitution of $f_{c0}=K_0=0°$ or 180° into Equation (34a), confirms that Δe is zero regardless of the values of the initial parameters.

Figures 3.3(a) to (d) The variations of $\Delta\sigma$, where σ = e, α, ϵ and ϖ, as a function of f_{c0} for the same Jupiter-Gallilean satellite system as found in Figures 3.2, with the exception that the satellite's eccentricity is now taken to be e=0.3.

The numerical solutions for $\Delta\sigma$ (dashed curves) are now noticeably different from the analytical solutions for $\Delta\sigma$ (solid curves).

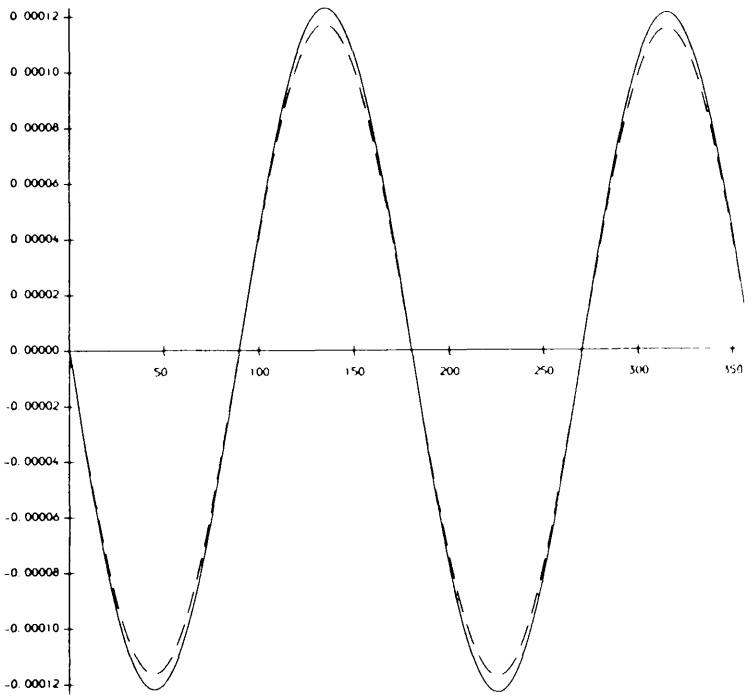
Change in the satellite's eccentricity over one synodic period
Δe
0.00012
0.00010
0.00008
0.00006
0.00004
0.00002
0.00000
-0.00002
-0.00004
-0.00006
-0.00008
-0.00010
-0.00012
50
100
150
200
250
300
350
Initial true anomaly at conjunction f_{c0} (in degrees)

(a)

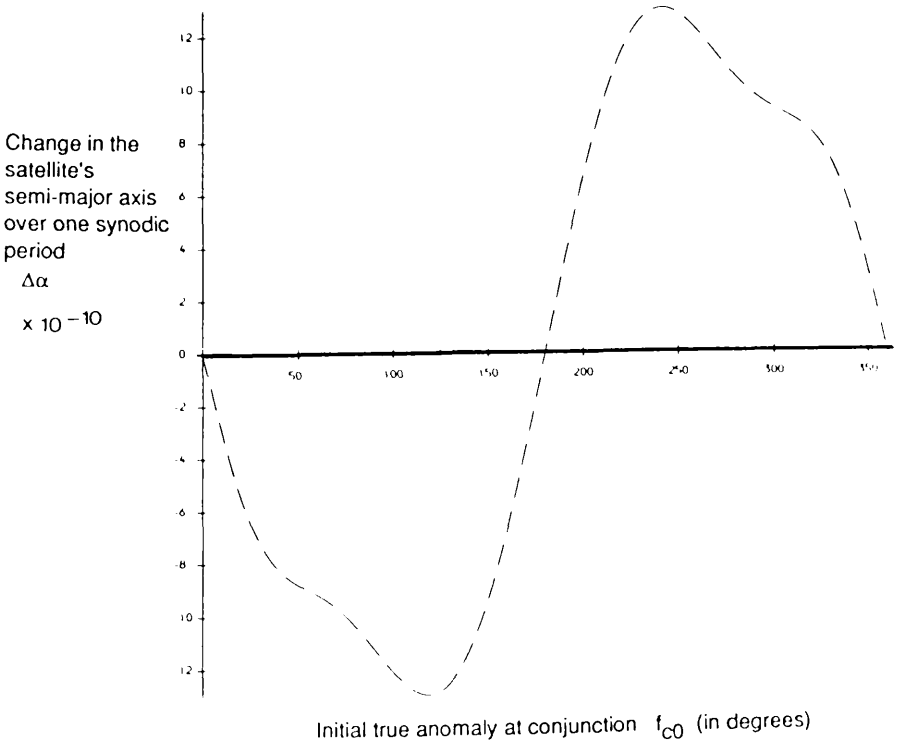
Change in the satellite's semi-major axis over one synodic period
Δα
x 10 −10
12
10
8
6
4
2
0
-2
-4
-6
-8
-10
-12
50
100
150
200
250
300
350
Initial true anomaly at conjunction f_{c0} (in degrees)

(b)

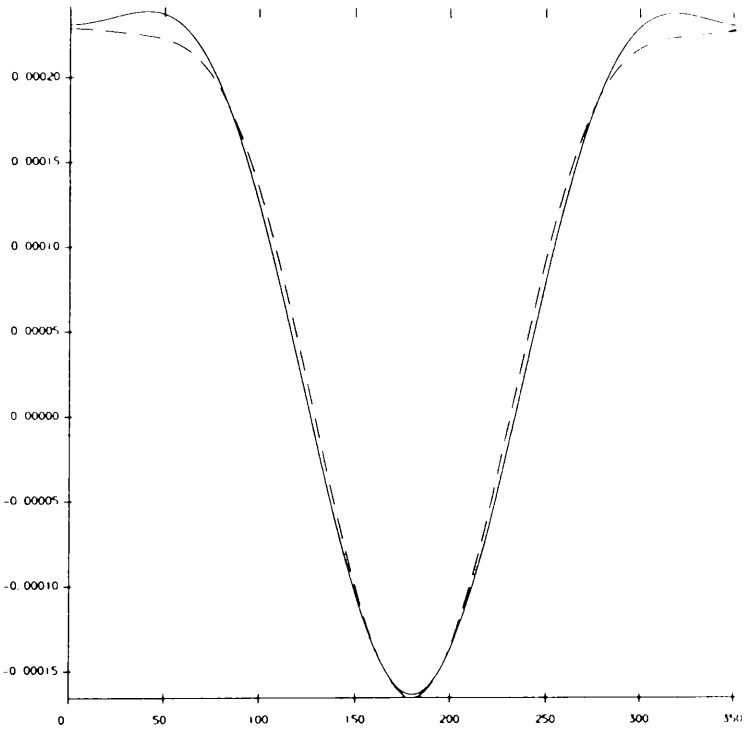

Change in the satellite's mean longitude at epoch over one synodic period
$\Delta\epsilon$
(in radians)

(c)

Initial true anomaly at conjunction f_{c0} (in degrees)

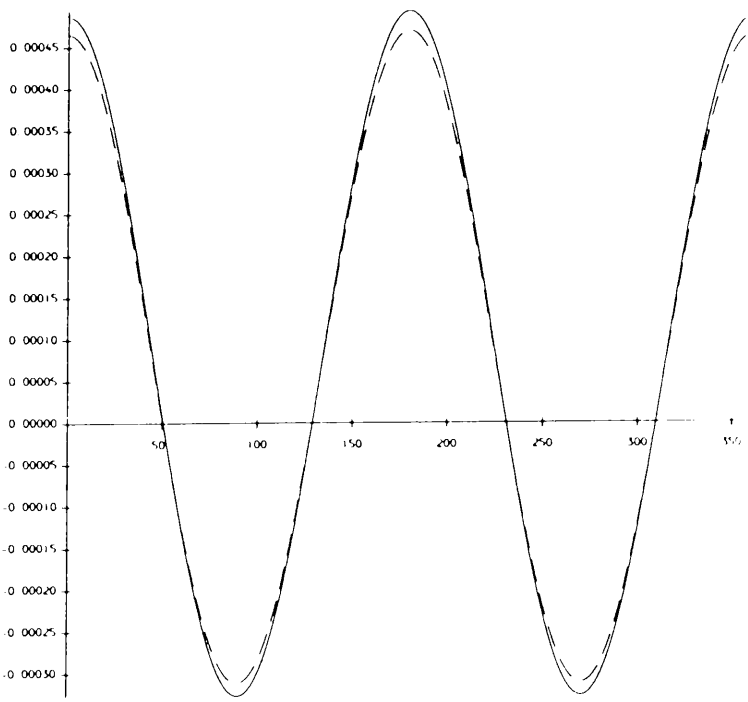

Change in the satellite's longitude of pericentre over one synodic period
$\Delta\varpi$
(in radians)

(d)

Initial true anomaly at conjunction f_{c0} (in degrees)

The occurrence of zeros at $f_{c0} = 0°$ and 180° merely confirms the validity of the mirror theorem described in Chapter 1. For the coplanar case, a conjunction of the bodies lying in the direction of the satellite's apocentre or pericentre is in actual fact a mirror configuration of the type where the masses are arranged collinearly with their velocity vectors perpendicular to the straight line through their masses. Thus, according to the mirror theorem (Roy and Ovenden, 1955), the system's behavior after the epoch at which the mirror configuration occurs is a mirror image of its behavior prior to that epoch. The resulting net change on the size and shape of the orbit due to solar perturbations over a time interval centred on such an epoch is zero. This mirror symmetry about 0° and 180° is not only obvious in the graphs, but can also be proven mathematically to be valid for our second order approximations. Using Equation (34a) it can be shown that

$$\Delta e(-K_0) = -\Delta e(K_0)$$

$$\Delta e(-K_0+180°) = -\Delta e(K_0+180°)$$

The extrema for the Δe curve occur at approximately $f_{c0} = 45°$, 135°, 225° and 315° or a 45° angle to the semi-major axis of the elliptical orbit, if e is much greater than α. As α is increased in size with respect to e, these angles shrink until the extrema occur only at 90° and 270° for the case of α much greater than e. For each particular relationship between α and e, a line drawn through any one of the extrema angles will divide the ellipse into two portions which are the least symmetric to each other. Thus, conjunctions which occur at such f_{c0} angles produce configurations which are the farthest removed possible from mirror configurations. Due to the lack of symmetry, cancellation of the solar perturbations is minimized over any time interval centred on such a configuration and as a result, the Δe are maxima and minima at these values of f_{c0}.

Figures 3.2(c), (d) and 3.3(c), (d) show that the extrema for the $\Delta\varpi$ and $\Delta\epsilon$ curves occur at $f_{c0} = 0°$, 180°, 360°... or at the mirror configurations. During a

synodic period centred on a mirror configuration, the apse line of the orbit is moving its fastest. At this point the changes in the mean longitude at the epoch and the changes in the longitude of pericentre will therefore be at their greatest.

The maximum change in e or Δe_{max} for the Jupiter-Callisto case is seen from Figures 3.2(a) and 3.3(a) to occur near the angle $f_{c0} = 135°$. Its exact value and the exact true anomaly f_{c0} at which it occurs depend on the values of the initial parameters. Δe_{max} can be approximated through a simple optimization of Equation (34a) with respect to the true anomaly f_{c0}.

The derivative of Δe with respect to f_{c0} is

$$\frac{d\,\Delta e}{d\,f_{c0}} = \frac{d\,\Delta e}{d\,K_0}\,\frac{d\,K_0}{d\,f_{c0}}$$

$$= \pi\,\nu^2\,[\,A_1 \cos K_0 - 2\,A_2 \cos 2K_0\,]\,\frac{d\,K_0}{d\,f_{c0}} \qquad (36)$$

where $A_1 = \frac{15}{8}\alpha - \frac{39}{32}\alpha\nu + 4\nu + \frac{40}{3}\nu^2$

$A_2 = \frac{15}{2}e + \frac{33}{2}e\nu$

$K_0 = \frac{1}{1-\nu}\,(f_{c0} - \nu M_0)$

The maxima and minima are given by the values of K_0 which make Equation (36) zero. dK_0/df_{c0} is always greater than zero, for small values of ν and e. Therefore,

$$A_1 \cos K_0 - 2\,A_2 \cos 2K_0 = 0$$

which can be solved to give

$$\cos K_0 = \frac{A_1 \pm \sqrt{A_1^2 + 32\,A_2^2}}{8\,A_2}$$

$$\sin K_0 = \pm \sqrt{\frac{1}{2} - \frac{A_1}{4\,A_2}\cos K_0}$$

$\sin K_0$ is found using the trigonometric identity $\sin^2 K_0 + \cos^2 K_0 = 1$.

There are four extrema corresponding to the four unique pairs of $\sin K_0$ and $\cos K_0$ solutions. This result is confirmed by Figures 3.2(a) and 3.3(a). Solving for the second derivatives of Δe with respect to f_{c0} shows that the maximum Δe occurs when $\cos K_0 \leq 0$ and $\sin K_0 \geq 0$ (ie when K_0 is located in the second quadrant). Thus,

$$\Delta e_{max} = \pi \nu^2 [\, A_1 - 2\,A_2 \cos K_0 \,] \sin K_0 \qquad (37)$$

where

$$\cos K_0 = \frac{A_1 - \sqrt{A_1^2 + 32\,A_2^2}}{8\,A_2}$$

$$\sin K_0 = \sqrt{\frac{1}{2} - \frac{A_1}{4\,A_2}\cos K_0}$$

Note that from Equation (34a) we can see that if $\alpha >> e$, the $A_1 \sin K_0$ term will dominate the equation for Δe, and Δe_{max} will occur nearer $f_{c0} = 90°$. On the other hand if $e >> \alpha$, as is the case in Figures 3.2(a) and 3.3(a), the $-A_2 \sin 2K_0$ term will dominate the equation for Δe, and Δe_{max} will occur nearer $f_{c0} = 135°$.

If we rewrite Equation (34e) into the form $f_{c0} = f(f_{c0}, K_0)$, substitute a form of Equation (19) for M_0 and expand about the small parameters, we get f_{c0} as a function of K_0

$$f_{c0} \approx K_0 - 2e(\nu + \nu^2)\sin K_0 + \frac{3}{4}e^2\nu \sin 2K_0 + \ldots$$

Thus for small e and v, f_{c0} is approximately equal to K_0. Equation (37) for Δe_{max} will become very important in Chapter 6 when we apply the first level of our finite-time stability criteria method, but for now it can be used to study the limitations of our analytical solution.

From Figures 3.2 and 3.3, we can see that as the eccentricity e is increased, our analytical solution begins to deviate from the numerical solution. The deviation is at its worst at the extrema of the graphs for $\Delta\sigma(f_{c0})$. Since Δe has proven to be the parameter of greatest interest for the detectability of dangers to the stability of the system, and since Δe_{max} is the location of the worst approximation of Δe to the numerical solution, we can use Δe_{max} as a measure of how accurately the analytical solution compares with the numerical solution for a range of initial parameters e_0, α_0 and μ.

Figures 3.4 show the contours in α_0 - e_0 space which indicate a 1%, 3% and 5% relative difference between the analytical and numerical solutions for the maximum possible change Δe_{max} in the satellite's eccentricity over one synodic period. The different figures (a) through to (e) depict the error contours for satellites orbiting each of the five planets of varying mass ratios μ. Also plotted on the relevant figures are the positions in α_0 - e_0 space of the known satellites orbiting each planet. The upper limits of α in the Figures 3.4 are chosen to be the approximate values of α which produce a value for Δe greater than 1.

From Figures 3.4, we can see that most of the satellites of the planetary systems are located within the limits of our analytical theory. Only the retrograde satellites of Jupiter fall outside the region where our second order analytical theory is accurate to within a 5% error. This result is not unexpected, since the restricted three-body problem is only marginally applicable to these satellites.

With the exception of Saturn's Phoebe and Jupiter's outer satellite group, the remainder of the satellites are found well within the 1% error contour. Of the satellites found within the 1% error contour, all but the Moon, remain within the 5%

Figures 3.4(a) to (e) Show the contours in α-e space which indicate a 1%, 3% or 5% relative difference between the analytical and numerical solutions for the maximum possible change in the satellite's eccentricity or Δe_{max} over one synodic period.

The figures (a) through to (e) depict the error contours for satellites orbiting each of the following planets:

(a) Jupiter with $\mu = 1.1 \times 10^3$

(b) Saturn with $\mu = 3.5 \times 10^3$

(c) Uranus with $\mu = 2.28 \times 10^4$

(d) Earth with $\mu = 3.33 \times 10^5$

(e) Mars with $\mu = 3.08 \times 10^6$.

The plus signs indicate the locations in α-e space of the major satellites of each planet.

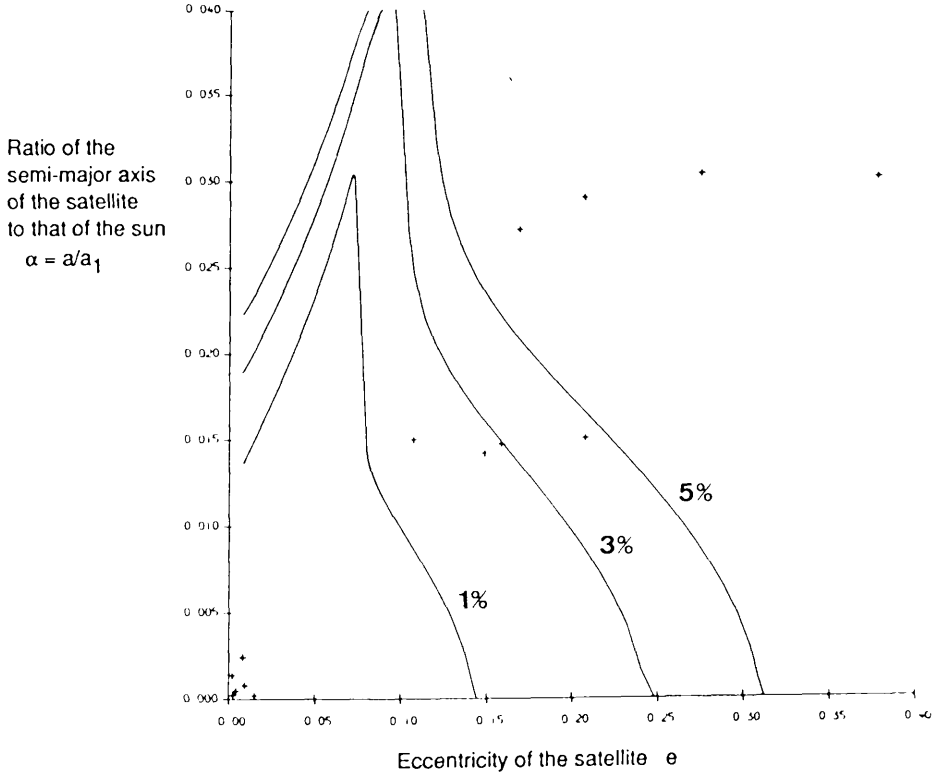

(a)

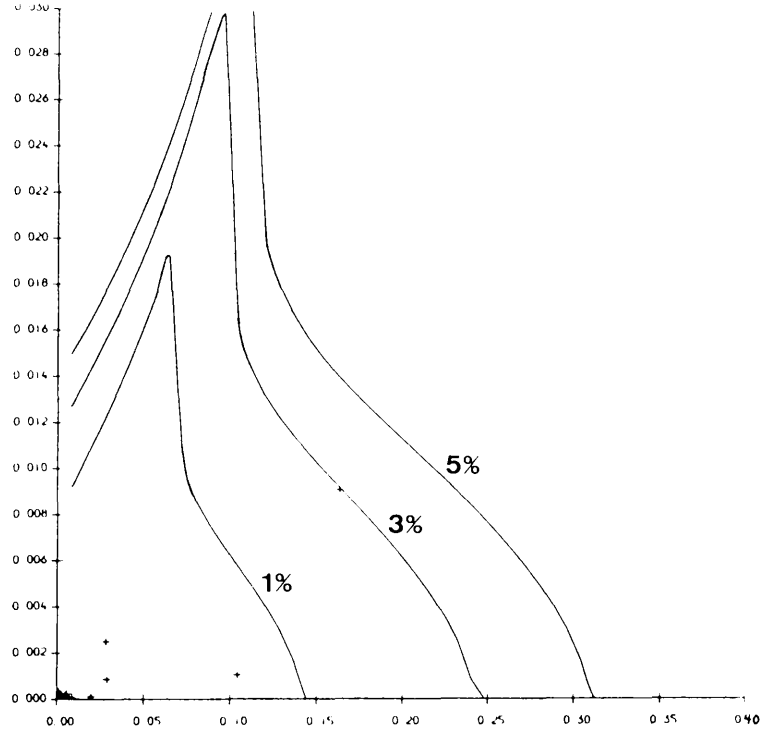
Ratio of the semi-major axis of the satellite to that of the sun
α = a/a1
0.028
0.026
0.024
0.022
0.020
0.018
0.016
0.014
0.012
0.010
0.008
0.006
0.004
0.002
0.000
0.00
0.05
0.10
0.15
0.20
0.25
0.30
0.35
0.40
5%
3%
1%
Eccentricity of the satellite e

(b)

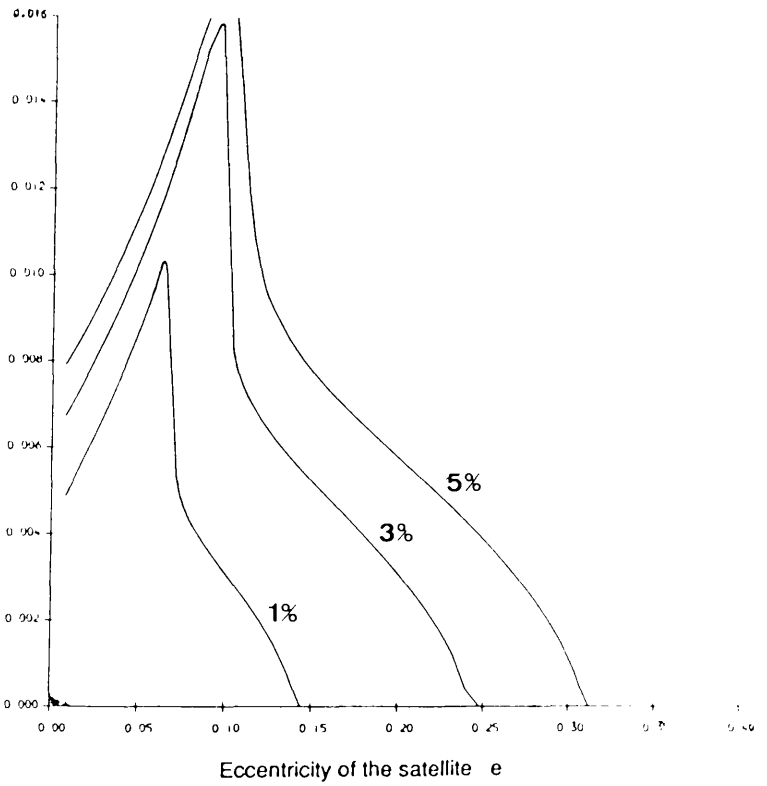
Ratio of the semi-major axis of the satellite to that of the sun
α = a/a1
0.012
0.010
0.008
0.004
0.002
0.000
0.00
0.05
0.10
0.15
0.20
0.25
0.30
5%
3%
1%
Eccentricity of the satellite e

(c)

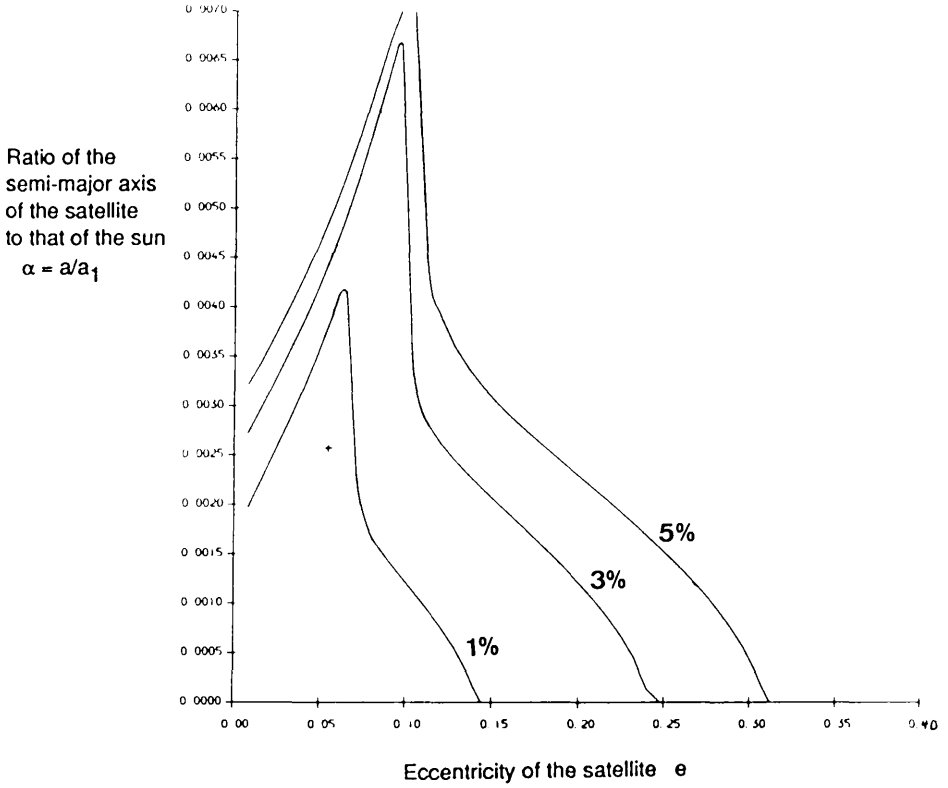
Ratio of the semi-major axis of the satellite to that of the sun
α = a/a1
0 0065
0 0060
0 0055
0 0050
0 0045
0 0040
0 0035
0 0030
0 0025
0 0020
0 0015
0 0010
0 0005
0 0000
0 00
0 05
0 10
0 15
0 20
0 25
0 30
0 35
0 40
5%
3%
1%
Eccentricity of the satellite e

(d)

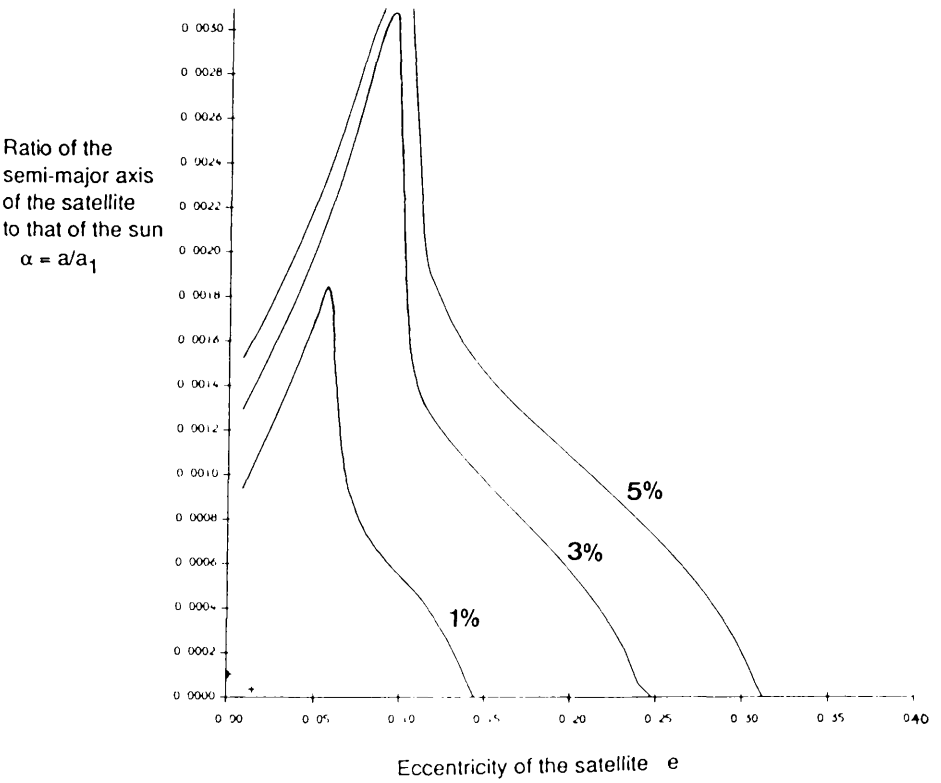
Ratio of the semi-major axis of the satellite to that of the sun
α = a/a1
0 0030
0 0028
0 0026
0 0022
0 0020
0 0018
0 0016
0 0012
0 0010
0 0008
0 0006
0 0002
0 0000
0 00
0 05
0 25
0 30
0 35
040
5%
3%
1%
Eccentricity of the satellite e

(e)

contour line when their eccentricities are increased to e = 0.3. The Moon would be located approximately within the 9% error contour, if its eccentricity were to be increased to e = 0.3.

Note also that as the mass ratio μ is increased, the influence of the Sun's mass becomes stronger and the α-e space within each percentage contour decreases. In other words, the neglected terms are becoming larger as μ increases and hence smaller values of α and e are sufficient to form the same percentage error contours.

When the eccentricity becomes greater than 0.3, our analytical solution begins to deviate noticeably (ie by greater than 5%) from the numerical solution. This is valid for most solar system values of α and μ. We could therefore arbitrarily choose the breakdown point of our analytical solution to be the upper limit e_u to which we allow the eccentricity of each satellite system to grow before we say an unstable situation is developing. The time taken for the system to reach an eccentricity of e_u=0.3 would then be the minimum duration of the system.

An error in the analytical solution of less than 5% is more than sufficient accuracy for our purposes. We are not interested so much in the exact positions of the bodies at any given time, but rather in the minimum time the Sun requires to render the satellite's orbit parabolic.

Reaching an eccentricity of e = 0.3 does not necessarily mean the satellite's orbit becomes unstable. The orbit could endure for much longer, may never reach an eccentricity of 1 and in fact, may have its eccentricity subsequently reduced. The limit of e = 0.3 is merely set by the limits of our analytical theory and is sufficient to provide a minimum time that a system will endure. Even when such a small upper limit as e = 0.3 is used, as compared to the definitely unstable situation of e = 1, the minimum duration times found using the different levels of our finite-time stability method can be substantial and therefore of interest.

These minimum durations will be calculated for the circular case over a range of the initial parameters e_0, α_0 and μ in Chapter 5. We later show in Chapter 4 that a much greater upper limit of e = 0.50 can be achieved by using the more accurate third order analytical solution to the circular problem derived from the third order

analytical solution to the elliptical case. For the present, in Chapter 4 we now repeat the previous analysis, but for the elliptical case, finding both numerically and analytically the changes in the orbital elements $\Delta\sigma$ over one synodic period, and comparing the two solutions.

CHAPTER 4

THE CHANGES IN THE ORBITAL ELEMENTS OVER ONE SYNODIC PERIOD FOR THE ELLIPTICAL COPLANAR RESTRICTED THREE-BODY PROBLEM

4.1 The Elliptical Model

4.2 A Numerical Integration of the Problem

(i) The elongation S as a function of the true anomalies f and f_1

(ii) The variable f_1 as a function of the true anomaly f

(iii) Numerical integration of Lagrange's planetary equations with respect to f

4.3 An Analytical Development of the Problem

(i) Expansion of the components of Lagrange's planetary equations $d\sigma/df$

(ii) The expanded form of Lagrange's planetary equations $d\sigma/df$

(iii) The expanded relationships between f_1, f and S

(iv) $\sin (jf + kf_1 + qS)$ and $\cos (jf + kf_1 + qS)$ expressed as functions of S

(v) Transformation of the derivatives with respect to f to ones with respect to S

(vi) The general form of Lagrange's planetary equations $d\sigma/dS$ as a function of S

(vii) The method used to transform the individual terms of the equations of motion $d\sigma/df$ (f, f_1, S) to $d\sigma/dS$ (S)

(viii) The general integration of Lagrange's planetary equations $d\sigma/dS$

(ix) The transformation of de/df to de/dS and its subsequent integration

4.4 Discussion of the Analytic Theory, its Implications and Limitations

"Sod's Law: Murphy was an optimist!"

4.1 The Elliptical Model

Having developed a method for integrating Lagrange's planetary equations in the circular case, we extend the development to include the elliptic case where the sun is assumed to move in a fixed elliptic planetocentric orbit. The sun's orbital eccentricity and semi-major axis are now taken to be constant values of e_1 and a_1 respectively.

At any point in time, the sun's position can be described by its radius vector $\mathbf{r}_1$ such that

$$r_1 = \frac{a_1 (1 - e_1^2)}{1 + e_1 \cos f_1} \tag{1}$$

where f_1 is the true anomaly of the sun at that time. See Figure 4.1 for a diagram of the three bodies and the parameters describing their orbits.

The above assumptions result in the following simplifications to the general form of Lagrange's planetary equations derived in Chapter 2. The equations of motion are still those given in Equations (35) of Chapter 2, namely:

$$\frac{de}{df} = \nu^2 \left(\frac{\rho}{\alpha}\right)^3 \{ Q(F_e - \rho \sin f) - \sin f \} \tag{2a}$$

$$\frac{d\alpha}{df} = \frac{2\nu^2}{1 - e^2} \alpha \left(\frac{\rho}{\alpha}\right)^3 \{ Q(F_\alpha - e\rho \sin f) - e \sin f \} \tag{2b}$$

$$\frac{d\varpi}{df} = -\frac{\nu^2}{e} \left(\frac{\rho}{\alpha}\right)^3 \{ Q(F_\varpi - \rho \cos f) - \cos f \} \tag{2c}$$

$$\frac{d\epsilon}{df} = -\frac{2\nu^2}{1 - e^2} \left(\frac{\rho}{\alpha}\right)^3 \{ Q(F_\epsilon - \rho K) - K \} + \left(1 - \sqrt{1 - e^2}\right) \frac{d\varpi}{df} \tag{2d}$$

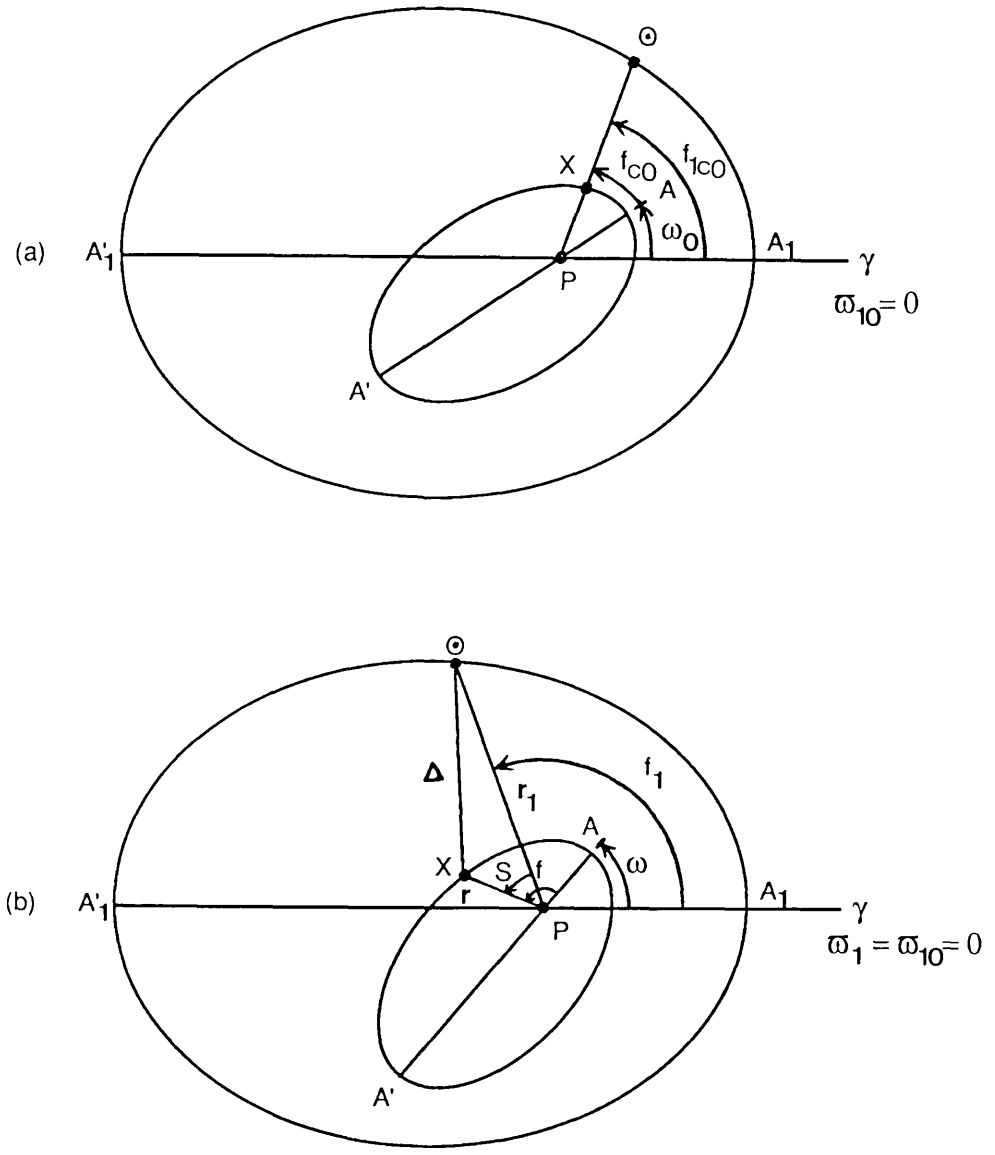

Figure 4.1 The elliptical coplanar restricted three-body problem where the planet P - satellite X system is disturbed by the sun ⊙, which is assumed to be moving in a fixed elliptical orbit of eccentricity e_1 and semi-major axis a_1.

The initial configuration, Figure (a), of the planet-satellite-sun system is chosen to be a conjunction. At this time t=0, the longitude of the sun's pericentre ϖ_{10} is arbitrarily chosen to be zero, so that $\overline{PA_1}$ lies in the reference direction $\overline{P\gamma}$.

Figure (b) describes the configuration some time t later. Note that the sun's orbit does not change with time.

However, the ratio of the magnitudes of the radius vectors $\rho = r/r_1$ can now be rewritten as a function of e, e_1, a, a_1, f and f_1.

$$\rho^n = \left(\frac{r}{r_1}\right)^n = \alpha^n \left[\left(\frac{1-e^2}{1-e_1^2}\right)\left(\frac{1+e_1\cos f_1}{1+e\cos f}\right)\right]^n \tag{2e}$$

The rest of the subsidiary equations remain the same as those given in Equations (33h) to (33 m) and (34) of Chapter 2, viz.

$$Q = 3\cos S + \frac{3}{2}\rho(5\cos^2 S - 1) + \frac{5}{2}\rho^2(7\cos^3 S - 3\cos S) + \frac{15}{8}\rho^3(1 - 14\cos^2 S + 21\cos^4 S) + \ldots \tag{2f}$$

$$F_e = \sin f \cos S - \left(\frac{e(1+\cos^2 f) + 2\cos f}{1 + e\cos f}\right)\sin S \tag{2g}$$

$$F_\alpha = e \sin f \cos S - (1 + e\cos f)\sin S \tag{2h}$$

$$F_\varpi = \cos f \cos S + \left(\frac{2 + e\cos f}{1 + e\cos f}\right)\sin f \sin S \tag{2i}$$

$$N = \frac{3}{2} n t \tag{2j}$$

$$K = \frac{(1-e^2)^{3/2}}{1 + e\cos f} - N e \sin f \tag{2k}$$

$$F_\epsilon = K\cos S + N(1 + e\cos f)\sin S \tag{2l}$$

The expanded versions of the above expressions, ie Equations (16) to (18) and (20) to (22) of Chapter 3, also remain valid for the elliptical case.

With the relevant equations of motion ready for integration, we need only specify the starting conditions. As in the circular case, the satellite's orbit and position within its orbit at any time t are completely described by the orbital elements a, e, ϵ, ϖ and time t. The sun's orbit and position within its orbit at any time t however, are now described by the constant orbital elements a_1, e_1, ϵ_1, ϖ_1 and

time t. The bodies themselves are still solely described by a ratio of their point masses $\mu = m_1/(M_p + m)$, which is still a constant of the three-body problem.

Again, we take the time at which the satellite and the sun pass through a conjunction to be arbitrarily t = 0. We use as an initial orbital parameter the true anomaly of the satellite at conjunction f_c, instead of the equivalent parameter of the satellite's mean longitude at the epoch or ϵ. Likewise, we use the true anomaly of the sun at conjunction f_{1c}, instead of the sun's equivalent parameter of the sun's mean longitude at the epoch or ϵ_1.

At time t = 0, the satellite's orbit is therefore completely described by the four orbital elements a_0, e_0, ϖ_0 and f_{c0}. Similarly at this time, the sun's orbit is completely described by the four orbital elements a_{10}, e_{10}, ϖ_{10} and f_{1c0}. In fact, since the sun's orbit is assumed to remain unchanged, these initial orbital elements describe the sun's orbit for all time.

Because we are studying the perturbing effect of the sun on the satellite's orbit, we are only interested in describing the satellite's orbit relative to the sun's planetocentric orbit. Therefore, the ratio of the semi-major axes $\alpha = a/a_1$ is sufficient to describe the relative sizes of their orbits, and knowledge of the individual values of a or a_1 is unnecessary.

The orientation of the sun's orbit relative to a specific reference point is also irrelevant to the problem. Only the orientation of the satellite's orbit with respect to the sun's orbit is of importance. We therefore arbitrarily choose ϖ_{10} to be zero, so that at time t = 0 and for all time since the sun's orbit is assumed to be fixed, the sun's periapsis lies in the same direction as the reference direction. See Figure 4.1.

From the figure we can see that, if the three-body system begins at a conjunction, then the satellite's initial longitude of pericentre will now be completely specified by the initial true anomalies of the satellite and the sun at conjunction, ie

$$\varpi_0 = f_{1c0} - f_{c0} \qquad (3)$$

In summary, the problem now contains only two additional independent initial parameters to those of the circular problem. These orbital elements describe completely the sun's orbit and its position within its orbit at time t = 0. They are the eccentricity of the sun's orbit at time t = 0 or e_{10} and the true anomaly of the sun in the conjunction which occurs at time t = 0 or f_{1c0}.

As in the circular case, the initial orbit of the satellite and its position relative to the sun's orbit and sun's position is still completely described by: the ratio of the semi-major axes of the satellite and the sun at time t = 0 or α_0; the eccentricity of the satellite's orbit at time t = 0 or e_0; and the true anomaly of the satellite in the conjunction which occurs at time t = 0 or f_{c0}. Again, the bodies themselves are described by the ratio of their masses μ .

We are now ready to integrate the problem in order to find the changes in the orbital elements of the satellite $\Delta\sigma$, where $\sigma = \alpha$, e, ϖ or ϵ, over one synodic period. Like the circular case this is done both analytically and numerically in order to confirm the validity, and to ascertain the limitations, of the analytic theory.

Section 4.2 contains a description of the numerical method used to integrate Equations (2), while Section 4.3 gives the derivation of our analytic expansion and subsequent analytical integration of the same equations. In Section 4.4 we compare the analytical and numerical results for a range of the six initial conditions α_0, e_0, f_{c0}, μ, e_{10} and f_{1c0}, discuss the limitations of the analytic theory, and compare the analytical results for the elliptical case with those of the circular case.

4.2 A Numerical Integration of the Problem

As in the circular case, we integrate Lagrange's planetary equations numerically over one synodic period from $f_{-\pi}$ to $f_{+\pi}$. To do this we use Lagrange's planetary equations written in an exact form with respect to the true anomaly (Equations (2)), so that the only approximations made are, as before, the expansion of the component Q. Thus,

$$\Delta\sigma = \int_{f_{-\pi}}^{f_{+\pi}} \frac{d\sigma}{df}\, df$$

In order to perform the above integration, it is necessary to express each of the components as a function of f. This process involves finding the relationships between the time variables t, f, S and f_1. To get these relationships, we follow the equivalent method developed for the circular case in Section 3.2 , with the inclusion of the time variable f_1 which now describes the sun's elliptical movement. We therefore first find S in terms of f and f_1, and then f_1 in terms of f.

(i) The elongation S as a function of the true anomalies f and f_1

Figure 4.1(b) shows that

$$S = f - f_1 + \varpi - \varpi_1 \qquad (4)$$

At time t = 0, Equation (4) simplifies to

$$0 = f_{c0} - f_{1c0} + \varpi_0 - \varpi_{10} \qquad (5)$$

Equation (4) can therefore be rewritten to include the initial conditions found in Equation (5).

$$S = f - f_{c0} - (f_1 - f_{1c0}) + \varpi - \varpi_0 - (\varpi_1 - \varpi_{10}) \qquad (6)$$

Since the sun's orbit is assumed to be fixed, $\varpi_1 - \varpi_{10} = 0$. Also, over one synodic period we assume that the changes in the orbital elements are very small. Therefore, $\varpi - \varpi_0$ is essentially zero. Hence Equation (6) becomes

$$S = f - f_{c0} - (f_1 - f_{1c0}) \qquad (7)$$

Equation (7) is similar to Equation (8) of Chapter 3 for the circular case. If the orientations of the two orbits with respect to each other do not change very much in one synodic period, then the angle S between the two radius vectors a time t after conjunction is simply the angle between the satellite's original position f_{c0} and its current position f, minus the angle swept out by the sun's radius vector in that time.

(ii) The variable f_1 as a function of the true anomaly f

We now find the true anomaly of the sun f_1 as a function of the true anomaly of the satellite f.

f_1 can be written in terms of the sun's eccentric anomaly E_1 using

$$\tan \frac{f_1}{2} = \left(\frac{1 + e_1}{1 - e_1} \right)^{1/2} \tan \frac{E_1}{2}$$

while the eccentric anomaly of the sun E_1 can be written in terms of the time t using an expression similar to Equation (10) of Chapter 3.

$$n_1 t = E_1 - e_1 \sin E_1 - M_{10}$$

The time t can also be written in terms of the eccentric anomaly E of the satellite using Equation (10) of Chapter 3.

$$n_1 t = v\ (E - e \sin E - M_0)$$

Finally, the eccentric anomaly E of the satellite can be written in terms of the satellite's true anomaly f through the use of

$$\tan \frac{E}{2} = \left(\frac{1 - e}{1 + e} \right)^{1/2} \tan \frac{f}{2}$$

Thus given f, we can find S, t and f_1 by solving the following sequence of equations for the variables listed below:

$$\text{E:} \quad \tan \frac{E}{2} = \left(\frac{1 - e}{1 + e} \right)^{1/2} \tan \frac{f}{2} \tag{8a}$$

$$\text{t:} \quad n_1 t = v\ (E - e \sin E - M_0) \tag{8b}$$

$$E_1\text{:} \quad n_1 t = E_1 - e_1 \sin E_1 - M_{10} \tag{8c}$$

$$f_1\text{:} \quad \tan \frac{f_1}{2} = \left(\frac{1 + e_1}{1 - e_1} \right)^{1/2} \tan \frac{E_1}{2} \tag{8d}$$

$$\text{S:} \quad S = f - f_{c0} - (f_1 - f_{1c0}) \tag{8e}$$

This sequence is identical to that of the circular case (Equations (11) of Chapter 3), with the addition of expressions for finding E_1 and f_1, and the adjustment of expressing S in terms of f and f_1 instead of in terms of f and t.

The initial mean anomaly M_0 is found using Equations (12) of Chapter 3 along with the initial condition f_{c0}, while M_{10} is found using a similar set of equations along with the initial condition f_{1c0}, ie

$$M_{10} = E_{10} - e_1 \sin E_{10}$$

$$\tan \frac{E_{10}}{2} = \left(\frac{1 - e_1}{1 + e_1} \right)^{1/2} \tan \frac{f_{1c0}}{2}$$

The initial mean longitude at the epoch ϵ_0 for the satellite is now a function of f_{c0} and f_{1c0} through M_0 and ϖ_0. For example using Equation (3) of Chapter 4, Equation (13) of Chapter 3 simplifies to

$$\epsilon_0 = M_0 + f_{1c0} - f_{c0}$$

The limits of the integral are found by substituting $S = -\pi$ or $S = +\pi$ into Equation (8e), then writing the equation solely as a function of f using the remaining Equations (8), and solving numerically for f.

Equations (2) can now be easily integrated numerically with respect to f since the limits of the integral and all the components of Lagrange's planetary equations are known as functions of f and the initial conditions α_0, e_0, f_{c0}, μ, e_{10} and f_{1c0}.

(iii) Numerical integration of Lagrange's planetary equations with respect to f

The Equations (2) are integrated numerically using the same NAG integrator as that used in the circular case. The same subroutines are also used. In addition, a subroutine was developed to find the proper quadrant for f_1 given E_1, using Equation (8d) and

$$\cos f_1 = \frac{\cos E_1 - e_1}{1 - e_1 \cos E_1} \tag{9a}$$

$$\sin f_1 = \frac{\sqrt{1 - e_1^2}\sin E_1}{1 - e_1 \cos E_1} \tag{9b}$$

which originate from the development of the two-body problem.

Like the search for the limits of the integration, the solving of Equation (8c) for the sun's eccentric anomaly E_1 requires the use of a Newton-Raphson method. These values are found to an accuracy of six decimal places. The results of the numerical integration are compared with the results of the analytical theory in Section 4.4.

4.3 An Analytical Development of the Problem

The analytical integration of Lagrange's planetary Equations (2) over one synodic period for the elliptical case is done in the same manner as that for the circular case. The equations $d\sigma/df$ are expanded about the small parameters α, e, ν and e_1 to third order. Thus, we retain only those terms containing $\alpha^I e^J \nu^K e_1^L$ where $I+J+K+L \leq 3$ and I, J, K, L are integers. The equations of motion are then transformed to a set of differential equations $d\sigma/dS$, which are functions of S. These are integrated analytically in S over one synodic period centred on a conjunction, ie

$$\Delta\sigma = \int_{S=-\pi}^{S=+\pi} \frac{d\sigma}{dS}\, dS$$

(i) Expansion of the components of Lagrange's planetary equations $d\sigma/df$

Many of the components required for the integration have already been expanded in Chapter 3 to third order in anticipation of their use for the elliptical problem. These expressions are given by Equations (16) to (18) and (20) to (22) of Chapter 3 which are now renumbered as:

$$\begin{aligned} F_e = &-\left(\frac{1}{2}e + \frac{1}{8}e^3\right)\sin S + \left(\frac{3}{2} - \frac{1}{8}e^2\right)\sin \overline{f-S} - \left(\frac{1}{2} - \frac{1}{8}e^2\right)\sin \overline{f+S} \\ &+\frac{1}{4}e\,[\sin \overline{2f+S} - \sin \overline{2f-S}] - \frac{1}{8}e^2\,[\sin \overline{3f+S} - \sin \overline{3f-S}] \\ &+\frac{1}{16}e^3\,[\sin \overline{4f+S} - \sin \overline{4f-S}] \end{aligned} \tag{10a}$$

$$F_\alpha = e\sin \overline{f-S} - \sin S \tag{10b}$$

$$\begin{aligned} F_\varpi = &\left(\frac{3}{2} + \frac{1}{8}e^2\right)\cos \overline{f-S} - \left(\frac{1}{2} + \frac{1}{8}e^2\right)\cos \overline{f+S} \\ &-\left(\frac{1}{4}e + \frac{1}{8}e^3\right)[\cos \overline{2f-S} - \cos \overline{2f+S}] + \frac{1}{8}e^2\,[\cos \overline{3f-S} - \cos \overline{3f+S}] \\ &-\frac{1}{16}e^3\,[\cos \overline{4f-S} - \cos \overline{4f+S}] \end{aligned} \tag{10c}$$

$$K = 1 + \frac{1}{2}e^2 + \left(-e + \frac{3}{16}e^3\right)\cos f - e^2\cos 2f + \frac{5}{16}e^3\cos 3f$$
$$-\frac{3}{2}e(f - M_0)\sin f \qquad (10d)$$

$$F_\epsilon = \left(1 + \frac{1}{2}e^2\right)\cos S + \frac{3}{2}(f - M_0)\sin S - \frac{3}{2}(f - M_0)\,e\sin\overline{f-S}$$
$$+\left(-2e + \frac{3}{8}e^3\right)\cos\overline{f-S} + \left(e - \frac{3}{16}e^3\right)\cos\overline{f+S} - \frac{11}{16}e^2\cos\overline{2f-S}$$
$$-\frac{5}{16}e^2\cos\overline{2f+S} + \frac{3}{16}e^3\cos\overline{3f-S} + \frac{1}{8}e^3\cos\overline{3f+S} \qquad (10e)$$

$$Q = \frac{9}{4}\rho + \frac{225}{64}\rho^3 + \left(3 + \frac{45}{8}\rho^2\right)\cos S + \left(\frac{15}{4}\rho + \frac{105}{16}\rho^3\right)\cos 2S$$
$$+\frac{35}{8}\rho^2\cos 3S + \frac{315}{64}\rho^3\cos 4S \qquad (10f)$$

Note that Q is not completely expanded into the standard form, since ρ is still a complicated non-standard function of e, e_1, cos f and cos f_1. Using the trigonometric identities (15) of Chapter 3 and a binomial series expansion about the small parameters, $(\rho/\alpha)^n$ can be expressed to third order as

$$\left(\frac{\rho}{\alpha}\right)^n = 1 + \frac{n}{4}[(n-3)e^2 + (n+3)e_1^2] - ne\left(1 + \frac{n^2-5n+2}{8}e^2 + \frac{n(n+3)}{4}e_1^2\right)\cos f$$
$$+\frac{n(n+1)}{4}e^2\cos 2f - \frac{n(n+1)(n+2)}{24}e^3\cos 3f$$
$$+ne_1\left(1 + \frac{n^2+5n+2}{8}e_1^2 + \frac{n(n-3)}{4}e^2\right)\cos f_1 + \frac{n(n-1)}{4}e_1^2\cos 2f_1$$
$$+\frac{n(n-1)(n-2)}{24}e_1^3\cos 3f_1 - \frac{n^2 ee_1}{2}(\cos\overline{f-f_1} + \cos\overline{f+f_1})$$
$$+\frac{n^2(n+1)}{8}e^2e_1(\cos\overline{2f-f_1} + \cos\overline{2f+f_1})$$
$$-\frac{n^2(n-1)}{8}ee_1^2(\cos\overline{f-2f_1} + \cos\overline{f+2f_1})$$

Thus, the various powers of ρ/α to third order are:

$$\frac{\rho}{\alpha} = 1 + \frac{1}{4}(4e_1^2 - 2e^2) - e\left(1 - \frac{1}{4}e^2 + e_1^2\right)\cos f + \frac{1}{2}e^2 \cos 2f$$

$$-\frac{1}{4}e^3 \cos 3f + e_1\left(1 + e_1^2 - \frac{1}{2}e^2\right)\cos f_1$$

$$-\frac{ee_1}{2}(\cos \overline{f-f_1} + \cos \overline{f+f_1}) + \frac{e^2e_1}{4}(\cos \overline{2f-f_1} + \cos \overline{2f+f_1})$$

$$\left(\frac{\rho}{\alpha}\right)^2 = 1 + \frac{1}{2}(5e_1^2 - e^2) - 2e\left(1 - \frac{1}{2}e^2 + \frac{5}{2}e_1^2\right)\cos f + \frac{3}{2}e^2 \cos 2f$$

$$-e^3 \cos 3f + 2e_1\left(1 + 2e_1^2 - \frac{1}{2}e^2\right)\cos f + \frac{1}{2}e_1^2 \cos 2f_1$$

$$-2ee_1(\cos \overline{f-f_1} + \cos \overline{f+f_1}) + \frac{3}{2}e^2e_1(\cos \overline{2f-f_1} + \cos \overline{2f+f_1})$$

$$-\frac{1}{2}ee_1^2(\cos \overline{f-2f_1} + \cos \overline{f+2f_1})$$

$$\left(\frac{\rho}{\alpha}\right)^3 = 1 + \frac{9}{2}e_1^2 - 3e\left(1 - \frac{1}{2}e^2 + \frac{9}{2}e_1^2\right)\cos f + 3e^2 \cos 2f$$

$$-\frac{5}{2}e^3 \cos 3f + 3e_1\left(1 + \frac{13}{4}e_1^2\right)\cos f_1 + \frac{3}{2}e_1^2 \cos 2f_1$$

$$+\frac{1}{4}e_1^3 \cos 3f_1 - \frac{9ee_1}{2}(\cos \overline{f-f_1} + \cos \overline{f+f_1})$$

$$+\frac{9}{2}e^2e_1(\cos \overline{2f-f_1} + \cos \overline{2f+f_1})$$

$$-\frac{9}{4}ee_1^2(\cos \overline{f-2f_1} + \cos \overline{f+2f_1})$$

while the various powers of ρ to third order are:

$$\rho = \alpha\left\{1 + e_1^2 - \frac{1}{2}e^2 - e\cos f + \frac{1}{2}e^2 \cos 2f + e_1 \cos f_1\right.$$

$$\left.-\frac{ee_1}{2}(\cos \overline{f-f_1} + \cos \overline{f+f_1})\right\} \qquad (11a)$$

$$\rho^2 = \alpha^2\{1 - 2e\cos f + 2e_1 \cos f_1\} \qquad (11b)$$

$$\rho^3 = \alpha^3 \qquad (11c)$$

The expression for Q (Equation (10f)) can now be written in our standard tabular form by replacing ρ^n with Equations (11) and expanding to third order. The results for the five terms containing cos jS, where j = 0 to 4, found in Equation (10f) are given in Tables 4.1 (a) through to (e) respectively.

Again, using Equations (11) for ρ^n, the remaining unexpanded components of Equations (2) become:

$$\rho\sin f = \alpha\left\{ \left(1 - \frac{3}{4}e^2 + e_1^2\right)\sin f - \frac{e}{2}\sin 2f + \frac{e^2}{4}\sin 3f \right.$$
$$\left. + \frac{e_1}{2}(\sin \overline{f-f_1} + \sin \overline{f+f_1}) - \frac{ee_1}{4}(\sin \overline{2f-f_1} + \sin \overline{2f+f_1}) \right\}$$

$$\rho e\sin f = \alpha e\left\{ \sin f - \frac{e}{2}\sin 2f + \frac{e_1}{2}(\sin \overline{f-f_1} + \sin \overline{f+f_1}) \right\}$$

$$\rho\cos f = \alpha\left\{ -\frac{e}{2} + \left(1 - \frac{1}{4}e^2 + e_1^2\right)\cos f - \frac{e}{2}\cos 2f + \frac{e^2}{4}\cos 3f \right.$$
$$-\frac{ee_1}{2}\cos f_1 + \frac{e_1}{2}(\cos \overline{f-f_1} + \cos \overline{f+f_1})$$
$$\left. -\frac{ee_1}{4}(\cos \overline{2f-f_1} + \cos \overline{2f+f_1}) \right\}$$

$$\rho K = \alpha\left\{ 1 + e_1^2 + \frac{1}{2}e^2 - 2e\cos f + e_1\cos f_1 - ee_1(\cos \overline{f-f_1} + \cos \overline{f+f_1}) \right.$$
$$-\frac{3}{2}e(f - M_0)\sin f + \frac{3}{4}e^2(f - M_0)\sin 2f$$
$$\left. -\frac{3}{4}ee_1(f - M_0)(\sin \overline{f-f_1} + \sin \overline{f+f_1}) \right\}$$

(ii) The expanded form of Lagrange's planetary equations $d\sigma/df$

Similar to the circular case, the series of cosine and sine terms which make up each component of Lagrange's planetary equations can now be substituted into Equations (2) to obtain $d\sigma/df$ in their expanded form. The multiplication of these long strings of sine and cosine terms is again most efficiently done using a tabular form. The resulting expanded equations of motion with respect to f are given in Table 4.2(a) to (d). Note that the symbol -" in the coefficient column means the coefficient is the negative of the coefficient immediately above it. For example, in Table 4.2(a) the coefficients of the seventh and eighth terms are $(-45/8)ee_1$ and $(+45/8)ee_1$ respectively.

$\frac{9}{4}\alpha$

Coeff.	f	f_1	S
$1 + e_1^2 - \frac{1}{2}e^2 + \frac{225}{144}\alpha^2$	0	0	0
$-e$	1	0	0
$\frac{1}{2}e^2$	2	0	0
e_1	0	1	0
$-\frac{1}{2}ee_1$	1	1	0
"	1	-1	0

(a)

Coeff.	f	f_1	S
$3 + \frac{45}{8}\alpha^2$	0	0	1
$-\frac{45}{8}\alpha^2 e$	1	0	1
"	1	0	-1
$\frac{45}{8}\alpha^2 e_1$	0	1	1
"	0	1	-1

(b)

$\frac{15}{8}\alpha$

Coeff.	f	f_1	S
$2 + 2e_1^2 - e^2 + \frac{7}{2}\alpha^2$	0	0	2
$-e$	1	0	2
"	1	0	-2
$\frac{1}{2}e^2$	2	0	2
"	2	0	-2
e_1	0	1	2
"	0	1	-2
$-\frac{1}{2}ee_1$	1	1	2
"	1	1	-2
"	1	-1	2
"	1	-1	-2

(c)

$\frac{35}{16}\alpha^2$

Coeff.	f	f_1	S
2	0	0	3
$-2e$	1	0	3
"	1	0	-3
$2e_1$	0	1	3
"	0	1	-3

(d)

Coeff.	f	f_1	S
$\frac{315}{64}\alpha^3$	0	0	4

(e)

Tables 4.1(a) to (e) A tabular form of an expansion of Q about the small parameters α, e, e_1 and ν. Tables (a) through to (e) contain the expansions for each of the individual terms of Q given in Equation (10f) ie

(a) $\frac{9}{4}\rho + \frac{225}{64}\rho^3$

(b) $\left(3 + \frac{45}{8}\rho^2\right)\cos S$

(c) $\left(\frac{15}{4}\rho + \frac{105}{16}\rho^3\right)\cos 2S$

(d) $\frac{35}{8}\rho^2 \cos 3S$

(e) $\frac{315}{64}\rho^3 \cos 4S$

Tables 4.2(a) to (d) The expanded form of the equations of motion $d\sigma/df$ of the satellite written with respect to the satellite's true anomaly f, where σ is one of the satellite's orbital elements α, e, ϵ or ϖ.

Tables (a) through to (d) display the terms of de/df, $d\alpha/df$, $d\varpi/df$ and $d\epsilon/df$ respectively.

$\frac{de}{df} \times \nu^2$ =

Coeff.	f	f_1	S
$\frac{21}{16}\alpha e$	0	0	1
$\frac{15}{4}e + \frac{45}{16}\alpha^2 e + \frac{135}{8}ee_1^2 \quad \frac{15}{8}e^3$	0	0	2
$\frac{105}{16}\alpha e$	0	0	3
$\frac{315}{32}\alpha^2 e$	0	0	4
$\frac{21}{8}\alpha e e_1$	0	1	1
"	0	1	-1
$\frac{45}{8}ee_1$	0	1	-2
"	0	1	2
$\frac{105}{8}\alpha e e_1$	0	1	-3
"	0	1	3
$\frac{45}{16}ee_1^2$	0	2	2
"	0	2	-2
$\frac{1}{2} + \frac{9}{16}\alpha^2 + \frac{9}{4}e_1^2 - \frac{3}{4}e^2$	1	0	0
$\frac{123}{64}\alpha e^2 + \frac{3}{16}\alpha + \frac{45}{128}\alpha^3 + \frac{21}{16}\alpha e_1^2$	1	0	1
$\frac{15}{64}\alpha e^2 + \frac{15}{16}\alpha + \frac{105}{128}\alpha^3 + \frac{105}{16}\alpha e_1^2$	1	0	-1
$\frac{9}{4} + \frac{5}{4}\alpha^2 + \frac{81}{8}e_1^2 + \frac{3}{8}e^2$	1	0	-2
$\frac{3}{4} \quad \frac{27}{8}e_1^2 - \frac{21}{8}e^2$	1	0	2
$\frac{45}{16}\alpha + \frac{255}{64}\alpha e^2 + \frac{385}{256}\alpha^3 + \frac{315}{16}\alpha e_1^2$	1	0	-3
$\frac{15}{16}\alpha - \frac{435}{64}\alpha e^2 \quad \frac{105}{16}\alpha e_1^2 \quad \frac{35}{256}\alpha^3$	1	0	3
$\frac{35}{32}\alpha^2$	1	0	4
$\frac{105}{32}\alpha^2$	1	0	-4
$-\frac{315}{256}\alpha^3$	1	0	5
$\frac{945}{256}\alpha^3$	1	0	-5
$\frac{3}{4}e_1 + \frac{45}{32}\alpha^2 e_1 + \frac{39}{16}e_1^3 \quad \frac{9}{8}e^2 e_1$	1	1	0
" " " "	1	-1	0
$\frac{15}{8}\alpha e_1$	1	1	-1
"	1	-1	-1
$\frac{3}{8}\alpha e_1$	1	1	1
"	1	-1	1

sin

+ ν^2 =

Coeff.	f	f_1	S
$\frac{27}{8}e_1 + \frac{9}{16}e^2 e_1 + \frac{25}{8}\alpha^2 e_1 + \frac{351}{32}e_1^3$	1	1	-2
" " " "	1	-1	-2
$-\frac{9}{8}e_1 - \frac{63}{16}e^2 e_1 - \frac{117}{32}e_1^3$	1	-1	2
" " "	1	1	2
$-\frac{15}{8}\alpha e_1$	1	1	3
"	1	-1	3
$\frac{45}{8}\alpha e_1$	1	1	-3
"	1	-1	-3
$-\frac{175}{64}\alpha^2 e_1$	1	-1	4
"	1	1	4
$\frac{525}{64}\alpha^2 e_1$	1	1	-4
"	1	-1	-4
$\frac{3}{8}e_1^2$	1	2	0
"	1	-2	0
$\frac{9}{32}\alpha e_1^2$	1	2	1
"	1	-2	1
$\frac{45}{32}\alpha e_1^2$	1	2	-1
"	1	-2	-1
$-\frac{9}{16}e_1^2$	1	2	2
"	1	-2	2
$\frac{27}{16}e_1^2$	1	2	-2
"	1	-2	-2
$-\frac{45}{32}\alpha e_1^2$	1	2	3
"	1	-2	3
$\frac{135}{32}\alpha e_1^2$	1	2	-3
"	1	-2	-3
$\frac{1}{16}e_1^3$	1	3	0
"	1	-3	0
$-\frac{3}{32}e_1^3$	1	3	2
"	1	-3	2
$\frac{9}{32}e_1^3$	1	3	-2
"	1	-3	-2

(a)

over ...

$\frac{de}{df}$ continued ...

+ ν^2 sin

Coeff.	f	f_1	S
$-\frac{3}{4}e - \frac{45}{32}\alpha^2 e + e^3 - \frac{27}{8}ee_1^2$	2	0	0
$\frac{63}{32}\alpha e$	2	0	-1
$\frac{9}{32}\alpha e$	2	0	1
$\frac{3}{2}e + \frac{5}{32}\alpha^2 e + \frac{9}{8}e^3 + \frac{27}{4}ee_1^2$	2	0	2
$-\frac{15}{4}e - \frac{105}{32}\alpha^2 e + \frac{15}{8}e^3 - \frac{135}{8}ee_1^2$	2	0	-2
$\frac{75}{32}\alpha e$	2	0	3
$-\frac{195}{32}\alpha e$	2	0	-3
$\frac{105}{32}\alpha^2 e$	2	0	4
$-\frac{35}{4}\alpha^2 e$	2	0	-4
$\frac{9}{8}ee_1$	2	1	0
"	2	-1	0
$-\frac{9}{16}\alpha ee_1$	2	1	1
"	2	-1	1
$\frac{63}{16}\alpha ee_1$	2	1	-1
"	2	-1	-1
$\frac{9}{4}ee_1$	2	1	2
"	2	-1	2
$\frac{45}{8}ee_1$	2	1	-2
"	2	-1	-2
$\frac{75}{16}\alpha ee_1$	2	1	3
"	2	-1	3
$\frac{195}{16}\alpha ee_1$	2	1	-3
"	2	-1	-3
$\frac{9}{16}ee_1^2$	2	2	0
"	2	-2	0
$\frac{9}{8}ee_1^2$	2	2	2
"	2	-2	2
$\frac{45}{16}ee_1^2$	2	2	-2
"	2	-2	-2

+ ν^2 sin

Coeff.	f	f_1	S
$\frac{3}{4}e^2$	3	0	0
$\frac{15}{64}\alpha e^2$	3	0	1
$\frac{165}{64}\alpha e^2$	3	0	-1
$-\frac{15}{8}e^2$	3	0	2
$\frac{33}{8}e^2$	3	0	-2
$-\frac{225}{64}\alpha e^2$	3	0	3
$\frac{525}{64}\alpha e^2$	3	0	-3
$\frac{9}{8}e^2 e_1$	3	1	0
"	3	-1	0
$-\frac{45}{16}e^2 e_1$	3	1	2
"	3	-1	2
$\frac{99}{16}e^2 e_1$	3	1	-2
"	3	-1	-2
$-\frac{5}{8}e^3$	4	0	0
$\frac{15}{8}e^3$	4	0	2
$-\frac{15}{4}e^3$	4	0	-2

$\frac{d\alpha}{df} = 2v^2$ sin

Coeff.	f	f_1	S
$-\frac{3}{8}\alpha^2$	0	0	1
$-\frac{3}{2}\alpha - \frac{5}{8}\alpha^3 - \frac{27}{4}\alpha e_1^2 + \frac{3}{4}\alpha e^2$	0	0	2
$-\frac{15}{8}\alpha^2$	0	0	3
$-\frac{35}{16}\alpha^3$	0	0	4
$-\frac{3}{4}\alpha^2 e_1$	0	1	1
"	0	1	-1
$-\frac{9}{4}\alpha e_1$	0	1	2
"	0	1	-2
$-\frac{15}{4}\alpha^2 e_1$	0	1	3
"	0	1	-3
$-\frac{9}{8}\alpha e_1^2$	0	2	2
"	0	2	-2
$\frac{1}{2}\alpha e$	1	0	0

+ $2v^2$ sin

Coeff.	f	f_1	S
$\frac{9}{8}\alpha^2 e$	1	0	1
$\frac{9}{4}\alpha e$	1	0	2
$-\frac{3}{4}\alpha e$	1	0	-2
$\frac{15}{4}\alpha^2 e$	1	0	3
$-\frac{15}{8}\alpha^2 e$	1	0	-3
$\frac{3}{4}\alpha e e_1$	1	1	0
"	1	-1	0
$\frac{27}{8}\alpha e e_1$	1	1	2
"	1	-1	2
$-\frac{9}{8}\alpha e e_1$	1	1	-2
"	1	-1	-2
$-\frac{3}{4}\alpha e^2$	2	0	0
$-\frac{9}{4}\alpha e^2$	2	0	2

(b)

$\frac{dm}{df}$ $\frac{v^2}{e}$ cos

Coeff.	f	f_1	S
$\frac{3}{4}e - \frac{45}{32}\alpha^2 e + \frac{3}{8}e^3 - \frac{27}{8}e e_1^2$	0	0	0
$\frac{9}{4}\alpha e$	0	0	1
$-\frac{9}{4}e - \frac{25}{8}\alpha^2 e - \frac{81}{8}e e_1^2 + \frac{9}{8}e^3$	0	0	2
$\frac{15}{4}\alpha e$	0	0	3
$\frac{175}{32}\alpha^2 e$	0	0	4
$-\frac{9}{4}e e_1$	0	1	0
$-\frac{9}{2}\alpha e e_1$	0	1	1
"	0	1	-1
$\frac{27}{8}e e_1$	0	1	2
"	0	1	-2
$-\frac{15}{2}\alpha e e_1$	0	1	3
"	0	1	-3
$-\frac{9}{8}e e_1^2$	0	2	0
$-\frac{27}{16}e e_1^2$	0	2	2
"	0	2	-2
$\frac{1}{2} + \frac{9}{16}\alpha^2 + \frac{9}{4}e_1^2 + \frac{3}{4}e^2$	1	0	0
$\frac{147}{64}\alpha e^2 + \frac{3}{16}\alpha + \frac{45}{128}\alpha^3 + \frac{21}{16}\alpha e_1^2$	1	0	1
$\frac{105}{64}\alpha e^2 + \frac{15}{16}\alpha + \frac{105}{128}\alpha^3 + \frac{105}{16}\alpha e_1^2$	1	0	-1
$\frac{9}{4} + \frac{5}{4}\alpha^2 + \frac{81}{8}e_1^2 - \frac{3}{8}e^2$	1	0	-2
$-\frac{3}{4} - \frac{27}{8}e_1^2 + \frac{21}{8}e^2$	1	0	2

+ $\frac{v^2}{e}$ cos

Coeff.	f	f_1	S
$\frac{45}{16}\alpha + \frac{105}{64}\alpha e^2 + \frac{385}{256}\alpha^3 + \frac{315}{16}\alpha e_1^2$	1	0	-3
$-\frac{15}{16}\alpha + \frac{315}{64}\alpha e^2 - \frac{105}{16}\alpha e_1^2 - \frac{35}{256}\alpha^3$	1	0	3
$-\frac{35}{32}\alpha^2$	1	0	4
$\frac{105}{32}\alpha^2$	1	0	-4
$-\frac{315}{256}\alpha^3$	1	0	5
$\frac{945}{256}\alpha^3$	1	0	-5
$\frac{3}{4}e_1 + \frac{45}{32}\alpha^2 e_1 + \frac{39}{16}e_1^3 + \frac{9}{8}e^2 e_1$	1	1	0
" " " "	1	-1	0
$\frac{15}{8}\alpha e_1$	1	1	-1
"	1	-1	-1
$\frac{3}{8}\alpha e_1$	1	1	1
"	1	-1	1
$\frac{27}{8}e_1 - \frac{9}{16}e^2 e_1 + \frac{25}{8}\alpha^2 e_1 + \frac{351}{32}e_1^3$	1	1	-2
" " " "	1	-1	-2
$-\frac{9}{8}e_1 + \frac{63}{16}e^2 e_1 - \frac{117}{32}e_1^3$	1	1	2
" " "	1	-1	2
$-\frac{15}{8}\alpha e_1$	1	1	3
"	1	-1	3
$\frac{45}{8}\alpha e_1$	1	1	-3
"	1	-1	-3
$\frac{175}{64}\alpha^2 e_1$	1	1	4
"	1	-1	4

(c)

over ...

$\frac{d\varpi}{df}$ continued ...

$\frac{d\varpi}{df} = -\frac{\nu^2}{e}$ cos

Coeff.	f	f_1	S
$\frac{525}{64}\alpha^2 e_1$	1	1	-4
-	1	-1	-4
$\frac{3}{8}e_1^2$	1	2	0
-	1	-2	0
$\frac{9}{32}\alpha e_1^2$	1	2	1
-	1	-2	1
$\frac{45}{32}\alpha e_1^2$	1	2	-1
-	1	-2	-1
$-\frac{9}{16}e_1^2$	1	2	2
-	1	-2	2
$\frac{27}{16}e_1^2$	1	2	-2
-	1	-2	-2
$-\frac{45}{32}\alpha e_1^2$	1	2	3
-	1	-2	3
$\frac{135}{32}\alpha e_1^2$	1	2	-3
-	1	-2	-3
$-\frac{1}{16}e_1^3$	1	3	0
-	1	-3	0
$-\frac{3}{32}e_1^3$	1	3	2
-	1	-3	2
$\frac{9}{32}e_1^3$	1	3	-2
-	1	-3	-2
$\frac{3}{4}e - \frac{45}{32}\alpha^2 e - \frac{1}{4}e^3 - \frac{27}{8}ee_1^2$	2	0	0
$-\frac{63}{32}\alpha e$	2	0	-1
$-\frac{9}{32}\alpha e$	2	0	1
$\frac{3}{2}e + \frac{5}{32}\alpha^2 e - \frac{21}{8}e^3 + \frac{27}{4}ee_1^2$	2	0	2
$-\frac{15}{4}e - \frac{105}{32}\alpha^2 e + \frac{15}{8}e^3 - \frac{135}{8}ee_1^2$	2	0	-2
$\frac{75}{32}\alpha e$	2	0	3
$\frac{195}{32}\alpha e$	2	0	-3
$\frac{105}{32}\alpha^2 e$	2	0	4
$\frac{35}{4}\alpha^2 e$	2	0	-4
$-\frac{9}{8}ee_1$	2	1	0
-	2	-1	0
$\frac{9}{16}\alpha ee_1$	2	1	1
-	2	-1	1
$-\frac{63}{16}\alpha ee_1$	2	1	-1
-	2	-1	-1
$\frac{9}{4}ee_1$	2	1	2
-	2	-1	2

$+ -\frac{\nu^2}{e}$ cos

Coeff.	f	f_1	S
$-\frac{45}{8}ee_1$	2	1	-2
-	2	-1	-2
$\frac{75}{16}\alpha ee_1$	2	1	3
-	2	-1	3
$-\frac{195}{16}\alpha ee_1$	2	1	-3
-	2	-1	-3
$-\frac{9}{16}ee_1^2$	2	2	0
-	2	-2	0
$\frac{9}{8}ee_1^2$	2	2	2
-	2	-2	2
$-\frac{45}{16}ee_1^2$	2	2	-2
-	2	-2	-2
$\frac{3}{4}e^2$	3	0	0
$\frac{15}{64}\alpha e^2$	3	0	1
$\frac{165}{64}\alpha e^2$	3	0	-1
$-\frac{15}{8}e^2$	3	0	2
$\frac{33}{8}e^2$	3	0	-2
$-\frac{225}{64}\alpha e^2$	3	0	3
$\frac{525}{64}\alpha e^2$	3	0	-3
$\frac{9}{8}e^2 e_1$	3	1	0
-	3	-1	0
$-\frac{45}{16}e^2 e_1$	3	1	2
-	3	-1	2
$\frac{99}{16}e^2 e_1$	3	1	-2
-	3	-1	-2
$-\frac{5}{8}e^3$	4	0	0
$\frac{15}{8}e^3$	4	0	2
$-\frac{15}{4}e^3$	4	0	-2

$$\frac{d\epsilon}{dt} = \frac{d\epsilon_1}{dt} + \frac{d\epsilon_2}{dt} + \frac{1}{2}e^2\frac{dm}{dt}$$

(d)

$$\frac{d\epsilon_1}{dt} = -2\nu^2$$ cos

Coeff.	f	f_1	S
$\frac{1}{2} + \frac{9}{16}\alpha^2 + \frac{9}{4}e_1^2 + \frac{3}{2}e^2$	0	0	0
$\frac{9}{8}\alpha + \frac{63}{8}\alpha e_1^2 + \frac{81}{16}\alpha e^2 + \frac{75}{64}\alpha^3$	0	0	1
$\frac{3}{2} + \frac{5}{4}\alpha^2 + \frac{27}{4}e_1^2 + \frac{9}{2}e^2$	0	0	2
$\frac{15}{8}\alpha + \frac{175}{128}\alpha^3 + \frac{105}{8}\alpha e_1^2 + \frac{105}{16}\alpha e^2$	0	0	3
$\frac{35}{16}\alpha^2$	0	0	4
$\frac{315}{128}\alpha^3$	0	0	5
$\frac{3}{2}e_1 + \frac{45}{16}\alpha^2 e_1 + \frac{39}{8}e_1^3 + \frac{9}{2}e^2 e_1$	0	1	0
$\frac{9}{4}\alpha e_1$	0	1	1
"	0	1	-1
$\frac{9}{4}e_1 + \frac{25}{8}\alpha^2 e_1 + \frac{117}{16}e_1^3 + \frac{27}{4}e^2 e_1$	0	1	2
"	0	1	-2
$\frac{15}{4}\alpha e e_1$	0	1	3
"	0	1	-3
$\frac{175}{32}\alpha^2 e_1$	0	1	4
"	0	1	-4
$\frac{3}{4}e_1^2$	0	2	0
$\frac{27}{16}\alpha e_1^2$	0	2	1
"	0	2	-1
$\frac{9}{8}e_1^2$	0	2	2
"	0	2	-2
$\frac{45}{16}\alpha e_1^2$	0	2	3
"	0	2	-3
$\frac{1}{8}e_1^3$	0	3	0
$\frac{3}{16}e_1^3$	0	3	2
"	0	3	-2
$-2e - \frac{27}{8}\alpha^2 e - 9ee_1^2 - \frac{61}{32}e^3$	1	0	0
$-\frac{9}{4}\alpha e$	1	0	1
$-\frac{27}{8}\alpha e$	1	0	-1
$-\frac{3}{4}e - \frac{45}{16}\alpha^2 e - \frac{27}{8}ee_1^2 - \frac{309}{64}e^3$	1	0	2
$-\frac{21}{4}e - \frac{75}{16}\alpha^2 e - \frac{189}{8}ee_1^2 - \frac{57}{64}e^3$	1	0	-2
$-\frac{15}{8}\alpha e$	1	0	3
$-\frac{15}{2}\alpha e$	1	0	-3
$-\frac{105}{32}\alpha^2 e$	1	0	4
$-\frac{315}{32}\alpha^2 e$	1	0	-4

+

$$2\nu^2$$ cos

Coeff.	f	f_1	S
$-3ee_1$	1	1	0
"	1	-1	0
$-\frac{9}{2}\alpha e e_1$	1	1	1
"	1	-1	1
$-\frac{27}{4}\alpha e e_1$	1	1	-1
"	1	-1	-1
$-\frac{9}{8}ee_1$	1	1	2
"	1	-1	2
$-\frac{63}{8}ee_1$	1	1	-2
"	1	-1	-2
$-15\alpha e e_1$	1	1	-3
"	1	-1	-3
$-\frac{15}{4}\alpha e e_1$	1	1	3
"	1	-1	3
$-\frac{3}{2}ee_1^2$	1	2	0
"	1	-2	0
$-\frac{9}{16}ee_1^2$	1	2	2
"	1	-2	2
$-\frac{63}{16}ee_1^2$	1	2	-2
"	1	-2	-2
$\frac{7}{4}e^2$	2	0	0
$\frac{297}{128}\alpha e^2$	2	0	1
$\frac{567}{128}\alpha e^2$	2	0	-1
$-\frac{15}{32}e^2$	2	0	2
$\frac{183}{32}e^2$	2	0	-2
$\frac{1395}{128}\alpha e^2$	2	0	-3
$\frac{45}{128}\alpha e^2$	2	0	3
$\frac{21}{8}e^2 e_1$	2	1	0
"	2	-1	0
$-\frac{45}{64}e^2 e_1$	2	1	2
"	2	-1	2
$\frac{549}{64}e^2 e_1$	2	1	-2
"	2	-1	-2
$-\frac{35}{32}e^3$	3	0	0
$\frac{81}{64}e^3$	3	0	2
$-\frac{291}{64}e^3$	3	0	-2

over ...

$\frac{d\epsilon}{df}$ continued ...

$\frac{d\epsilon_2}{df} = -2v^2(f - M_0)$

Coeff.	f	f_1	sin S
$\frac{9}{16}\alpha + \frac{63}{16}\alpha e_1^2 + \frac{45}{128}\alpha^3$	0	0	1
$\frac{9}{4} + \frac{15}{16}\alpha^2 + \frac{81}{8}e_1^2 - \frac{9}{8}e^2$	0	0	2
$\frac{45}{16}\alpha + \frac{315}{256}\alpha^3 + \frac{315}{16}\alpha e_1^2$	0	0	3
$\frac{105}{32}\alpha^2$	0	0	4
$\frac{945}{256}\alpha^3$	0	0	5
$\frac{9}{8}\alpha e_1$	0	1	1
"	0	1	-1
$\frac{27}{8}e_1 + \frac{75}{32}\alpha^2 e_1 + \frac{351}{32}e_1^3 - \frac{27}{16}e^2 e_1$	0	1	2
"	0	1	-2
$\frac{45}{8}\alpha e_1$	0	1	3
"	0	1	-3
$\frac{525}{64}\alpha^2 e_1$	0	1	4
"	0	1	-4
$\frac{27}{32}\alpha e_1^2$	0	2	1
"	0	2	-1
$\frac{27}{16}e_1^2$	0	2	2
"	0	2	-2
$\frac{135}{32}\alpha e_1^2$	0	2	3
"	0	2	-3
$\frac{9}{32}e_1^3$	0	3	2
"	0	3	-2
$-\frac{3}{4}e - \frac{27}{32}\alpha^2 e + \frac{3}{8}e^3 - \frac{27}{8}ee_1^2$	1	0	0
$-\frac{27}{16}\alpha e$	1	0	1
$-\frac{27}{8}e + \frac{15}{32}\alpha^2 e - \frac{243}{16}ee_1^2 + \frac{27}{16}e^3$	1	0	2
$\frac{9}{8}e + \frac{15}{16}\alpha^2 e + \frac{81}{16}ee_1^2 - \frac{9}{16}e^3$	1	0	-2
$-\frac{45}{8}\alpha e$	1	0	3
$\frac{45}{16}\alpha e$	1	0	-3
$-\frac{525}{64}\alpha^2 e$	1	0	4
$\frac{315}{64}\alpha^2 e$	1	0	-4

+

$-2v^2(f - M_0)$

Coeff.	f	f_1	sin S
$-\frac{9}{8}ee_1$	1	1	0
"	1	-1	0
$-\frac{27}{8}\alpha ee_1$	1	1	1
"	1	-1	1
$-\frac{81}{16}ee_1$	1	1	2
"	1	-1	2
$\frac{27}{16}ee_1$	1	1	-2
"	1	-1	-2
$-\frac{45}{4}\alpha ee_1$	1	1	3
"	1	-1	3
$\frac{45}{8}\alpha ee_1$	1	1	-3
"	1	-1	-3
$-\frac{9}{16}ee_1^2$	1	2	0
"	1	-2	0
$-\frac{81}{32}ee_1^2$	1	2	2
"	1	-2	2
$\frac{27}{32}ee_1^2$	1	2	-2
"	1	-2	-2
$\frac{9}{8}e^2$	2	0	0
$\frac{81}{32}\alpha e^2$	2	0	1
$\frac{27}{32}\alpha e^2$	2	0	-1
$\frac{27}{8}e^2$	2	0	2
$\frac{225}{32}\alpha e^2$	2	0	3
$\frac{45}{32}\alpha e^2$	2	0	-3
$\frac{27}{16}e^2 e_1$	2	1	0
"	2	-1	0
$\frac{81}{16}e^2 e_1$	2	1	2
"	2	-1	2
$-\frac{9}{8}e^3$	3	0	0
$-\frac{45}{16}e^3$	3	0	2
$-\frac{9}{16}e^3$	3	0	-2

(iii) The expanded relationships between f_1, f and S

At this stage of our analysis Lagrange's planetary equations with respect to f are expressed in the following form

$$\frac{d\sigma}{df} = \sum_{i=1}^{n} A_i \sin (j_i f + k_i f_1 + q_i S) + \sum_{l=1}^{m} B_l \cos (j_l f + k_l f_1 + q_l S)$$
$$+(f - M_0) \sum_{p=1}^{w} D_p \sin (j_p f + k_p f_1 + q_p S)$$

where σ is any one of the orbital elements α, e, ϖ, or ϵ; j_i, k_i, q_i, j_l, k_l, q_l, j_p, k_p and q_p are all integers for i = 1 to n, l = 1 to m and p = 1 to w; n, m and w are the number of terms retained in each series expansion; and the coefficients of each term A_i, B_l and D_p are functions of e, e_1, α, and ν.

In order to integrate these series of terms with respect to S, we must express each component of the equations as a function of S and transform the derivatives with respect to f to ones with respect to S. Both of these steps require knowledge of the relationship between f_1, f and S.

f_1 as a function of f can be easily found using a series expansion of the true anomaly f_1 in terms of the mean anomaly M_1 given in Smart (1953, page 120).

$$f_1(M_1) = M_1 + \left(2e_1 - \frac{1}{4}e_1^3\right)\sin M_1 + \frac{5}{4}e_1^2 \sin 2M_1$$
$$+\frac{13}{12}e_1^3 \sin 3M_1 + O(e_1^4) + \ldots \qquad (12)$$

We can write the mean anomaly of the sun M_1 in terms of the mean anomaly of the satellite M using Equation (9) of Chapter 3. Thus, for the satellite and the sun

$$M_1 = \nu M + \delta_0 \qquad \text{where } \delta_0 = M_{10} - \nu M_0 \qquad (13)$$

Note that δ_0 is a constant.

Now recall from the circular case, that the mean anomaly M can be expressed as a function of the true anomaly. For example, using Equation (19) of Chapter 3, we can write

$$M = f + m(f) \tag{14a}$$

$$m(f) = -2e\sin f + \frac{3}{4}e^2 \sin 2f - \frac{1}{3}e^3 \sin 3f + \ldots \tag{14b}$$

There is a similar relation for $M_1(f_1)$.

$$M_1 = f_1 + m_1(f_1)$$

If we substitute Equation (14) for M(f) into Equation (13), the result is

$$M_1(f) = \nu f + \nu m(f) + \delta_0 \tag{15}$$

We can now substitute Equation (15) for $M_1(f)$ into Equation (12) for $f_1(M_1)$ to get $f_1(f)$.

To write the result in a simple form requires the expansion about the small parameters of the trigonometric functions $\sin(nM_1)$, where n=1 to 3. We therefore divide the argument of the trigonometric function or nM_1 into a sum of large terms G_1, small terms g_1 and constants K_{10}, ie

$$M_1 = G_1 + g_1 + K_{10}$$

where $G_1 = \nu f$

$$g_1 = \nu m(f) = -2e\nu \sin f + 3/4e^2\nu \sin 2f$$

$$K_{10} = \delta_0$$

and expand about the small parameter g_1. $\sin(nM_1)$ becomes:

$$\sin(nM_1) = \sin \overline{n(G_1+K_{10})} - ne\nu[\sin \overline{f-n(G_1+K_{10})} + \sin \overline{f+n(G_1+K_{10})}]$$

The above equation is then substituted, along with Equation (15) into $f_1(M_1)$ (ie Equation (12) to give to third order

$$f_1(f) = \nu f + \delta_0 - 2e\nu \sin f + \frac{3}{4}e^2\nu \sin 2f - m_1(f) \qquad (16a)$$

$$m_1(f) = -2e_1 \sin \overline{\nu f+\delta_0} + 2ee_1\nu[\sin \overline{f-(\nu f+\delta_0)} + \sin \overline{f+(\nu f+\delta_0)}]$$
$$+\frac{1}{4}e_1^3 \sin \overline{\nu f+\delta_0} - \frac{5}{4}e_1^2 \sin \overline{2(\nu f+\delta_0)} - \frac{13}{12}e_1^3 \sin \overline{3(\nu f+\delta_0)} \qquad (16b)$$

The derivation of f as a function of S is a much more complicated problem. Recall from Section 4.2 that

$$S = f - f_1 - (f_{c0} - f_{1c0}) \qquad (17)$$

Using Equation (15) and $M_1 = f_1 + m_1$, we can write

$$f_1 = \nu(f + m) - m_1 + \delta_0$$

The above equation can then be substituted into Equation (17) to give

$$S = (1 - \nu)f - \nu m(f) + m_1(f) - (\delta_0 + f_{c0} - f_{1c0})$$

We now have S as a function of f.

To reverse the relationship, we solve for f

$$f = \frac{1}{1-\nu} S + \frac{\nu}{1-\nu} m(f) - \frac{1}{1-\nu} m_1(f) + K_{20}$$

where

$$K_{20} = \frac{1}{1-\nu}(\delta_0 + f_{c0} - f_{1c0})$$

Expanding about small ν then gives

$$f = (1+\nu+\nu^2+\nu^3)\, S + (\nu+\nu^2+\nu^3)\, m(f) - (1+\nu+\nu^2+\nu^3)\, m_1(f) + K_{20} \qquad (18)$$

In order to write the right hand side of this equation solely as a function of S, we substitute Equation (18) for f into itself, expand about the small parameters and repeat the process until the right hand side is no longer a function of f. We first separate f into a sum of large terms G_2, small terms g_2 and constants K_{20} or

$$f = G_2 + g_2 + K_{20} \qquad \text{where} \quad G_2 = S$$

$$g_2 = (\nu+\nu^2+\nu^3)\, S + (\nu+\nu^2+\nu^3)\, m(f) - (1+\nu+\nu^2+\nu^3)\, m_1(f)$$

$$K_{20} = \frac{\delta_0 + f_{c0} - f_{1c0}}{1-\nu} \qquad (19)$$

g_2 can be written as

$$g_2 = (\nu+\nu^2+\nu^3)S + g_{21}(f) - g_{22}(f)$$

where the components of g_2 expanded to third order are:

$$g_{21}(f) = (\nu + \nu^2 + \nu^3)\, m(f)$$
$$= -2e\nu(1 + \nu) \sin f + \frac{3}{4}e^2\nu \sin 2f$$

$$g_{22}(f) = (1 + \nu + \nu^2 + \nu^3)\, m_1(f)$$
$$= m_1(f) - 2e_1\nu(1 + \nu)\sin \overline{\nu f + \delta_0} - \frac{5}{4}e_1^2\nu \sin \overline{2(\nu f + \delta_0)}$$

To express g_2 as a function solely of S, we substitute Equations (19) for f in the above equation $g_2(f)$ to get a transcendental equation involving g_2. The right hand side of the equation is then expanded about the small parameter g_2. This expansion involves writing

$$\sin \overline{n(S + K_{20} + g_2)} = \sin \overline{n(S + K_{20})} + n\nu S \cos \overline{n(S + K_{20})}$$
$$-2ne_1 \cos \overline{n(S + K_{20})} \sin \overline{\nu f + \delta_0}$$

and gives:

$$g_{21}(f) = -2e\nu(1 + \nu) \sin \overline{S + K_{20}} - 2e\nu^2 S \cos \overline{S + K_{20}}$$
$$+4ee_1\nu \cos \overline{S + K_{20}} \sin \overline{\nu f + \delta_0} + \frac{3}{4}e^2\nu \sin \overline{2(S + K_{20})}$$

$g_{22}(f)$ contains new arguments for the trigonometric functions. We therefore divide the new arguments once again into large terms, small terms and constants. The arguments can be rewritten as

$$\nu f + \delta_0 = g_3 + K_{30} \qquad \text{where} \quad g_3 = \nu S + \nu g_2$$
$$K_{30} = \nu K_{20} + \delta_0$$

$$f - \nu f - \delta_0 = S + g_4 + K_{40} \qquad \text{where} \quad g_4 = -\nu S + (1 - \nu) g_2$$
$$K_{40} = (1 - \nu) K_{20} - \delta_0$$

$$f + \nu f + \delta_0 = S + g_5 + K_{50} \qquad \text{where} \quad g_5 = \nu S + (1 + \nu)g_2$$

$$K_{50} = (1 + \nu)K_{20} + \delta_0$$

Substitution of Equation (19) into the equation $g_{22}(f)$ and subsequent expansion about the small parameters g_3, g_4, and g_5 give

$$\begin{aligned} g_{22}(S,f) = & -2e_1(\nu + \nu^2)\, S\cos K_{30} - 4e_1^2\nu\cos K_{30} \sin \overline{\nu f + \delta_0} - 2e_1 \sin K_{30} \\ & + e_1\nu^2 S^2 \sin K_{30} + 2ee_1\nu[\sin \overline{S + K_{40}} + \sin \overline{S + K_{50}}] \\ & + \frac{1}{4}e_1^3 \sin K_{30} - \frac{5}{2}e_1^2\nu S\cos 2K_{30} - \frac{5}{4}e_1^2 \sin 2K_{30} \\ & - \frac{13}{12}e_1^3 \sin 3K_{30} - 2e_1\nu^2 S\cos K_{30} - 2e_1\nu \sin K_{30} \\ & - 2e_1\nu^2 \sin K_{30} - \frac{5}{4}e_1^2\nu \sin 2K_{30} \end{aligned}$$

A few of the terms in g_{12} and g_{22} are still functions of f. If we repeat the substitution of Equation (19) into the terms containing f, using the new equation for g_2 (ie $g_2 = f(g_{12}, g_{22})$, and expand about the small parameters, we get as a final solution:

$$f = S + g_6 + K_{60}$$

$$\begin{aligned} \text{where} \quad g_6 = & \nu[X_0 S - e_1\nu S^2 \sin K_{30} - 2e(1 + \nu)\sin \overline{S + K_{20}} \\ & - 4ee_1 \sin \overline{S + K_{40}} + \frac{3}{4}e^2 \sin \overline{2(S + K_{20})} \\ & - 2e\nu S\cos \overline{S + K_{20}}] \end{aligned}$$

$$\begin{aligned} K_{60} = & K_{20} + \left[2e_1(1 + \nu + \nu^2) - \frac{1}{4}e_1^3 \right] \sin K_{30} \\ & + \frac{5}{4}e_1^2 \sin 2K_{30} + \frac{13}{12}e_1^3 \sin 3K_{30} \\ & + \frac{13}{4}e_1^2\nu \sin 2K_{30} \end{aligned}$$

$$X_0 = 1 + \nu + \nu^2 + 2e_1(1 + 2\nu)\cos K_{30} + \frac{5}{2}e_1^2 \cos 2K_{30} \qquad (20)$$

Note that the expansion of g_2 has produced some small constants which have been added to K_{20} to form a new set of constant terms K_{60} and a new set of small terms g_6.

(iv) sin (jf +kf_1 + qS) and cos (jf +kf_1 + qS) expressed as functions of S

We can now substitute Equation (17) and Equation (20) into the right hand side of the equations of motion (ie Equations (2)) to get $d\sigma/df(S)$. In particular the argument of the trigonometric functions becomes

$$jf + kf_1 + qS = (j + q)S + (j + k)g_6 + Y_{jk} \quad (21a)$$

$$Y_{jk} = (j + k)K_{60} + k(f_{1c0} - f_{c0}) \quad (21b)$$

We have again divided the argument into large terms (j+q)S, small terms $(j+k)g_6$ and constants Y_{jk} ready for expansion to third order about the small terms. After some lengthy algebra, such an expansion gives

$$\sin (jf + kf_1 + qS) = S^0 + S^1 + S^2 + S^3 \quad (22a)$$

$$\cos (jf + kf_1 + qS) = C^0 + C^1 + C^2 + C^3 \quad (22b)$$

where

$$S^0 = \sin \overline{(j+q)S+Y_{jk}} \quad (22c)$$

$$S^1 = (j + k)\nu X_0 S \cos \overline{(j+q)S+Y_{jk}} \quad (22d)$$

$$S^2 = -(j + k)e\nu[\sin \overline{(j+q+1)S+Y_{jk}+K_{20}} - \sin \overline{(j+q-1)S+Y_{jk}-K_{20}}]$$
$$-\frac{1}{2}(j + k)^2\nu^2 X_0^2 S^2 \sin \overline{(j+q)S+Y_{jk}} \quad (22e)$$

$$S^3 = (j+k)\nu\Big\{ -\frac{1}{2}e_1\nu S^2[\sin\overline{(j+q)S+Y_{jk}+K_{30}} - \sin\overline{(j+q)S+Y_{jk}-K_{30}}]$$
$$-ev[\sin\overline{(j+q+1)S+Y_{jk}+K_{20}} - \sin\overline{(j+q-1)S+Y_{jk}-K_{20}}]$$
$$-evS[\cos\overline{(j+q+1)S+Y_{jk}+K_{20}} + \cos\overline{(j+q-1)S+Y_{jk}-K_{20}}]$$
$$+\frac{3}{8}e^2[\sin\overline{(j+q+2)S+Y_{jk}+2K_{20}} - \sin\overline{(j+q-2)S+Y_{jk}-2K_{20}}]$$
$$-2ee_1[\sin\overline{(j+q+1)S+Y_{jk}+K_{40}} - \sin\overline{(j+q-1)S+Y_{jk}-K_{40}}]\Big\}$$
$$+(j+k)^2ev^2X_0S[-\cos\overline{(j+q+1)S+Y_{jk}+K_{20}} + \cos\overline{(j+q-1)S+Y_{jk}-K_{20}}]$$
$$-\frac{1}{6}(j+k)^3\nu^3X_0^3S^3\cos\overline{(j+q)S+Y_{jk}} \qquad (22f)$$

$$C^0 = \cos\overline{(j+q)S+Y_{jk}} \qquad (22g)$$

$$C^1 = -(j+k)\nu X_0S\sin\overline{(j+q)S+Y_{jk}} \qquad (22h)$$

$$C^2 = (j+k)ev[-\cos\overline{(j+q+1)S+Y_{jk}+K_{20}} + \cos\overline{(j+q-1)S+Y_{jk}-K_{20}}]$$
$$-\frac{1}{2}(j+k)^2\nu^2X_0^2S^2\cos\overline{(j+q)S+Y_{jk}} \qquad (22i)$$

$$C^3 = -(j+k)\nu\Big\{ -\frac{1}{2}e_1\nu S^2[-\cos\overline{(j+q)S+Y_{jk}+K_{30}} + \cos\overline{(j+q)S+Y_{jk}-K_{30}}]$$
$$-ev[-\cos\overline{(j+q+1)S+Y_{jk}+K_{20}} + \cos\overline{(j+q-1)S+Y_{jk}-K_{20}}]$$
$$-evS[\sin\overline{(j+q+1)S+Y_{jk}+K_{20}} + \sin\overline{(j+q-1)S+Y_{jk}-K_{20}}]$$
$$+\frac{3}{8}e^2[-\cos\overline{(j+q+2)S+Y_{jk}+2K_{20}} + \cos\overline{(j+q-2)S+Y_{jk}-2K_{20}}]$$
$$-2ee_1[-\cos\overline{(j+q+1)S+Y_{jk}+K_{40}} + \cos\overline{(j+q-1)S+Y_{jk}-K_{40}}]\Big\}$$
$$+(j+k)^2ev^2X_0S[\sin\overline{(j+q+1)S+Y_{jk}+K_{20}} - \sin\overline{(j+q-1)S+Y_{jk}-K_{20}}]$$
$$+\frac{1}{6}(j+k)^3\nu^3X_0^3S^3\sin\overline{(j+q)S+Y_{jk}} \qquad (22j)$$

For easier multiplication of terms by these two expressions in the future, their components have been divided into groups containing terms of the same order. Thus for example, S^0 includes only zero order terms, S^1 includes only first order terms, and so on.

(v) Transformation of the derivative with respect to f to ones with respect to S

We now have the general form of $d\sigma/df$ as a function of S. To complete the conversion from the time variable f to the time variable S, we need to change $d\sigma/df$ to $d\sigma/dS$. This is easily done using the transformation

$$\frac{d\sigma}{dS} = G\frac{d\sigma}{df} \qquad \text{where } G(S) = \left(\frac{dS}{df}\right)^{-1}$$

Differentiation of Equation (7) gives

$$\frac{dS}{df} = 1 - \frac{df_1}{df}$$

The derivative of $f_1(f)$ (ie Equations (16)) with respect to f contains only small terms, ie

$$\frac{df_1}{df} = \nu(1 - 2F)$$

$$F = e\cos f - e_1\cos\overline{\nu f+\delta_0} - \frac{3}{4}e^2\cos 2f - \frac{5}{4}e_1^2\cos\overline{2(\nu f+\delta_0)}$$

$$+ee_1[\cos\overline{f-(\nu f+\delta_0)} + \cos\overline{f+(\nu f+\delta_0)}]$$

And hence, upon expansion about the small parameters of df_1/df, G(f) becomes

$$G(f) = 1 + \nu + \nu^2 + \nu^3 - 2\nu(1 + 2\nu)F$$

This expression for G however, is not a function of S. It also contains arguments which are not in our standard form of $(jf+kf_1+qS+K)$, where K is one of the constants K_{20}, K_{30} or K_{40}. In other words, we have no expression for the sine or cosine of these arguments as a function solely of S. We therefore replace f in the non-standard arguments with Equation (20) and expand about the small parameters to third order. We will express the standard trigonometric functions as functions of S

after we multiply G by dσ/df, which also contains the standard argument.

As before, we divide the non-standard arguments into large terms, small terms and constants. These arguments can then be rewritten as

$$vf + \delta_0 = g_7 + K_{70} \qquad \text{where} \quad g_7 = vS + vg_6, \quad K_{70} = vK_{60} + \delta_0$$

$$f - vf - \delta_0 = S + g_8 + K_{80} \qquad \text{where} \quad g_8 = -vS + (1 - v)g_6, \quad K_{80} = (1 - v)K_{60} - \delta_0$$

$$f + vf + \delta_0 = S + g_9 + K_{90} \qquad \text{where} \quad g_9 = vS + (1 + v)g_6, \quad K_{90} = (1 + v)K_{60} + \delta_0$$

Expansion about the small terms g_7, g_8, and g_9 then gives the following expression for G as a function of $(jf+kf_1+qS)$. We have written it in tabular form for easier manipulation of the terms.

$$G = Q_0 - 2ev \begin{array}{|c|c|c|c|}\hline & & & \cos \\ \text{Coeff.} & f & S & K \\ \hline 1+2v & 1 & 0 & 0 \\ -\frac{3}{4}e & 2 & 0 & 0 \\ e_1 & 0 & 1 & K_{80} \\ " & 0 & 1 & K_{90} \\ \hline \end{array} - 2e_1v^2 S \sin K_{70} \qquad (23)$$

where

$$Q_0 = 1 + v + v^2 + v^3 + 2e_1v(1 + 2v)\cos K_{70} + \frac{5}{2}e_1^2 v \cos 2K_{70}$$

Note that the column headed K contains any constants found within the argument. For example, the third line of the table describes the term $-2ee_1\nu\cos\overline{S+K_{80}}$.

(vi) The general form of Lagrange's planetary equations $d\sigma/dS$ as a function of S

We can now find $d\sigma/dS$ by multiplying G by $d\sigma/df$. $d\sigma/df$ contains $\sin(jf+kf_1+qS)$ and $\cos(jf+kf_1+qS)$, so we therefore need to know $G\sin(jf+kf_1+qS)$ and $G\cos(jf+kf_1+qS)$ as a function solely of S. A simple multiplication of trigonometric functions and the use of the trigonometric identities contained in Equations (15) of Chapter 3 give

$$G\sin(jf + kf_1 + qS) = S_1 + S_2 + S_3 + S_4 + S_5 + S_6 \qquad (24a)$$

$$G\cos(jf + kf_1 + qS) = C_1 + C_2 + C_3 + C_4 + C_5 + C_6 \qquad (24b)$$

where

$$S_1 = (S^0 + S^1 + S^2 + S^3)\,Q_0 \qquad (24c)$$

$$S_2 = -e\nu\left[\sin\overline{(j+q+1)S+Y_{j+1,k}} + \sin\overline{(j+q-1)S+Y_{j-1,k}}\right] \qquad (24d)$$
$$-(j+k+1)e\nu^2 X_0 S\cos\overline{(j+q+1)S+Y_{j+1,k}}$$
$$-(j+k-1)e\nu^2 X_0 S\cos\overline{(j+q-1)S+Y_{j-1,k}}$$

$$S_3 = -2e\nu^2\left[\sin\overline{(j+q+1)S+Y_{j+1,k}} + \sin\overline{(j+q-1)S+Y_{j-1,k}}\right] \qquad (24e)$$

$$S_4 = \frac{3}{4}e^2\nu\left[\sin\overline{(j+q+2)S+Y_{j+2,k}} + \sin\overline{(j+q-2)S+Y_{j-2,k}}\right] \qquad (24f)$$

$$S_5 = -ee_1\nu\left[\sin\overline{(j+q+1)S+Y_{jk}+K_{80}} + \sin\overline{(j+q-1)S+Y_{jk}-K_{80}}\right. \qquad (24g)$$
$$\left. + \sin\overline{(j+q+1)S+Y_{jk}+K_{90}} + \sin\overline{(j+q-1)S+Y_{jk}-K_{90}}\right]$$

$$S_6 = -e_1\nu^2 S\left[-\cos\overline{(j+q)S+Y_{jk}+K_{70}} + \cos\overline{(j+q)S+Y_{jk}-K_{70}}\right] \qquad (24h)$$

$$C_1 = (C^0 + C^1 + C^2 + C^3)\, Q_0 \qquad (24i)$$

$$C_2 = -ev[\cos\overline{(j+q+1)S+Y_{j+1,k}} + \cos\overline{(j+q-1)S+Y_{j-1,k}}] \qquad (24j)$$
$$+ (j+k+1)ev^2 X_0 S\sin\overline{(j+q+1)S+Y_{j+1,k}}$$
$$+ (j+k-1)ev^2 X_0 S\sin\overline{(j+q-1)S+Y_{j-1,k}}$$

$$C_3 = -2ev^2[\cos\overline{(j+q+1)S+Y_{j+1,k}} + \cos\overline{(j+q-1)S+Y_{j-1,k}}] \qquad (24k)$$

$$C_4 = \frac{3}{4}e^2 v[\cos\overline{(j+q+2)S+Y_{j+2,k}} + \cos\overline{(j+q-2)S+Y_{j-2,k}}] \qquad (24l)$$

$$C_5 = -ee_1 v[\cos\overline{(j+q+1)S+Y_{jk}+K_{80}} + \cos\overline{(j+q-1)S+Y_{jk}-K_{80}} \qquad (24m)$$
$$+ \cos\overline{(j+q+1)S+Y_{jk}+K_{90}} + \cos\overline{(j+q-1)S+Y_{jk}-K_{90}}]$$

$$C_6 = -e_1 v^2 S[\sin\overline{(j+q)S+Y_{jk}+K_{70}} - \sin\overline{(j+q)S+Y_{jk}-K_{70}}] \qquad (24n)$$

Note that S^0, S^1, S^2, S^3, C^0, C^1, C^2 and C^3 are given by Equations (22c) to (22j).

(vii) The method used to transform the individual terms of the equations of motion $d\sigma/df(f, f_1, S)$ to $d\sigma/dS(S)$

The individual terms of $d\sigma/dS$ are simply found by multiplying the coefficients of each term in $d\sigma/df$ by the expansion for $G\sin(jf+kf_1+qS)$ or the expansion for $G\cos(jf+kf_1+qS)$, depending on which trigonometric functions are included with the coefficients of $d\sigma/df$. Because the orders of the components of $G\sin(jf+kf_1+qS)$ and $G\cos(jf+kf_1+qS)$ vary, the most efficient method of expressing $d\sigma/dS$ as a function of S to third order is therefore to multiply the specified component only by those coefficients of $d\sigma/df$ whose orders add to the order of the component to form a maximum order of three. Thus, such components as S_3, S_4, S_5, S_6 etc., which are of order three, need only be multiplied by coefficients of $d\sigma/df$ terms whose orders are zero. S_2 and C_2 can each be split into two terms of order two (ie S_2^2 and C_2^2) and

order three (ie S_2^3 and C_2^3). Thus

$$S_2 = S_2^2 + S_2^3 \tag{25a}$$

$$C_2 = C_2^2 + C_2^3 \tag{25b}$$

where

$$S_2^2 = -ev[\sin\overline{(j+q+1)S+Y_{j+1,k}} + \sin\overline{(j+q-1)S+Y_{j-1,k}}] \tag{25c}$$

$$S_2^3 = -(j+k+1)ev^2 X_0 S\cos\overline{(j+q+1)S+Y_{j+1,k}} - (j+k-1)ev^2 X_0 S\cos\overline{(j+q-1)S+Y_{j-1,k}} \tag{25d}$$

$$C_2^2 = -ev[\cos\overline{(j+q+1)S+Y_{j+1,k}} + \cos\overline{(j+q-1)S+Y_{j-1,k}}] \tag{25e}$$

$$C_2^3 = +(j+k+1)ev^2 X_0 S\sin\overline{(j+q+1)S+Y_{j+1,k}} + (j+k-1)ev^2 X_0 S\sin\overline{(j+q-1)S+Y_{j-1,k}} \tag{25f}$$

The superscript denotes the order of the terms in each group. Likewise, the components S_1 and C_1 can also be broken into groups of similar order, ie

$$S_1 = (S^0 + S^1 + S^2 + S^3)Q_0$$

$$C_1 = (C^0 + C^1 + C^2 + C^3)Q_0$$

Note that Q_0 is a constant of minimum order zero and therefore is not involved in calculating the order of the expansion.

Considerable effort can be saved if each table of $d\sigma/df$ is divided into four separate tables containing terms of similar order. For example, Table 4.2(a) listing the terms of de/df can be divided into the four groups of different orders listed in Tables 4.3(a) to (d). Thus, in the subsequent conversion of $d\sigma/df$ to $d\sigma/dS$: the components S_3, S_4, S_5, S_6, S_2^3, Q_0S^3, C_3, C_4, C_5, C_6, C_2^3 and Q_0C^3 need only be multiplied by the coefficients of zero order (eg by Table 4.3(a) for de/df); the components S_2^2, Q_0S^2, C_2^2 and Q_0C^2 by the coefficients of zero and first order

(eg by Tables 4.3(a) and (b) for de/df); the components Q_0S^1 and Q_0C^1 by the coefficients of zero, first and second order (eg by Tables 4.3(a), (b) and (c) for de/df); and the components Q_0S^0 and Q_0C^0 by all the coefficients (eg by the original Table 4.2(a) for de/df).

At this point we could easily find $d\sigma/dS$ as a function of S for every single term of $d\sigma/df(f, f_1, S)$ found in Tables 4.2(a) to (d). However, since many of the terms disappear when integrated over an interval of 2π, it is more efficient to find the general form of each of the integrals, note the conditions which make these integrals non-zero, and then search for the terms $d\sigma/df(f, f_1, S)$ which will fulfill these conditions. The relevant $d\sigma/df$ terms can then be converted to $d\sigma/dS(S)$ terms and integrated to give the terms for σ.

Tables 4.3(a) to (d) These tables group the terms found in the expanded equation of motion de/df by the order of their coefficients. Table (a) involves only the zero order terms, Table (b) the first order terms, Table (c) the second order terms and Table (d) the third order terms.

v^2 sin

Coeff.	f	f_1	S
$\frac{1}{2}$	1	0	0
$\frac{9}{4}$	1	0	-2
$-\frac{3}{4}$	1	0	2

(a)

v^2 sin

Coeff.	f	f_1	S
$\frac{15}{4}e$	0	0	2
$\frac{3}{16}\alpha$	1	0	1
$\frac{15}{16}\alpha$	1	0	-1
$\frac{45}{16}\alpha$	1	0	-3
$-\frac{15}{16}\alpha$	1	0	3
$\frac{3}{4}e_1$	1	1	0
-	1	-1	0
$\frac{27}{8}e_1$	1	1	-2
-	1	-1	-2
$-\frac{9}{8}e_1$	1	1	2
-	1	-1	2
$-\frac{3}{4}e$	2	0	0
$\frac{3}{2}e$	2	0	2
$-\frac{15}{4}e$	2	0	-2

(b)

v^2 sin

Coeff.	f	f_1	S
$\frac{21}{16}\alpha e$	0	0	1
$\frac{105}{16}\alpha e$	0	0	3
$\frac{45}{8}ee_1$	0	1	2
-	0	1	-2
$\frac{9}{16}\alpha^2 + \frac{9}{4}e_1^2 - \frac{3}{4}e^2$	1	0	0
$\frac{5}{4}\alpha^2 + \frac{81}{8}e_1^2 + \frac{3}{8}e^2$	1	0	-2
$-\frac{27}{8}e_1^2 - \frac{21}{8}e^2$	1	0	2
$-\frac{35}{32}\alpha^2$	1	0	4
$\frac{105}{32}\alpha^2$	1	0	-4
$\frac{15}{8}\alpha e_1$	1	1	-1
-	1	-1	-1
$\frac{3}{8}\alpha e_1$	1	1	1
-	1	-1	1
$-\frac{15}{8}\alpha e_1$	1	1	3
-	1	-1	3
$\frac{45}{8}\alpha e_1$	1	1	-3
-	1	-1	-3
$\frac{3}{8}e_1^2$	1	2	0
-	1	-2	0
$-\frac{9}{16}e_1^2$	1	2	2
-	1	-2	2
$\frac{27}{16}e_1^2$	1	2	-2
-	1	-2	-2
$-\frac{63}{32}\alpha e$	2	0	-1
$-\frac{9}{32}\alpha e$	2	0	1
$\frac{75}{32}\alpha e$	2	0	3
$-\frac{195}{32}\alpha e$	2	0	-3

+

v^2 sin

Coeff.	f	f_1	S
$-\frac{9}{8}ee_1$	2	1	0
-	2	-1	0
$\frac{9}{4}ee_1$	2	1	2
-	2	-1	2
$-\frac{45}{8}ee_1$	2	1	-2
-	2	-1	-2
$\frac{3}{4}e^2$	3	0	0
$-\frac{15}{8}e^2$	3	0	2
$\frac{33}{8}e^2$	3	0	-2

(c)

ν^2	Coeff.	f	f_1	sin S
	$\frac{45}{16}\alpha^2 e + \frac{135}{8} e e_1^2 - \frac{15}{8} e^3$	0	0	2
	$\frac{315}{32}\alpha^2 e$	0	0	4
	$\frac{21}{8}\alpha e e_1$	0	1	1
	-	0	1	-1
	$\frac{105}{8}\alpha e e_1$	0	1	3
	-	0	1	-3
	$\frac{45}{16} e e_1^2$	0	2	2
	-	0	2	-2
	$-\frac{123}{64}\alpha e^2 + \frac{45}{128}\alpha^3 + \frac{21}{16}\alpha e_1^2$	1	0	1
	$\frac{15}{64}\alpha e^2 + \frac{105}{128}\alpha^3 + \frac{105}{16}\alpha e_1^2$	1	0	-1
	$\frac{255}{64}\alpha e^2 + \frac{385}{256}\alpha^3 + \frac{315}{16}\alpha e_1^2$	1	0	-3
	$-\frac{435}{64}\alpha e^2 - \frac{105}{16}\alpha e_1^2 - \frac{35}{256}\alpha^3$	1	0	3
	$\frac{315}{256}\alpha^3$	1	0	5
	$\frac{945}{256}\alpha^3$	1	0	-5
	$\frac{45}{32}\alpha^2 e_1 + \frac{39}{16} e_1^3 - \frac{9}{8} e^2 e_1$	1	1	0
	- - -	1	-1	0
	$\frac{9}{16} e^2 e_1 + \frac{25}{8}\alpha^2 e_1 + \frac{351}{32} e_1^3$	1	1	-2
	- - -	1	-1	-2
	$-\frac{63}{16} e^2 e_1 - \frac{117}{32} e_1^3$	1	1	2
	- -	1	-1	2
	$-\frac{175}{64}\alpha^2 e_1$	1	1	4
	-	1	-1	4
	$\frac{525}{64}\alpha^2 e_1$	1	1	-4
	-	1	-1	-4
	$\frac{9}{32}\alpha e_1^2$	1	2	1
	-	1	-2	1
	$\frac{45}{32}\alpha e_1^2$	1	2	-1
	-	1	-2	-1
	$-\frac{45}{32}\alpha e_1^2$	1	2	3
	-	1	-2	3
	$\frac{135}{32}\alpha e_1^2$	1	2	-3
	-	1	-2	-3
	$\frac{1}{16} e_1^3$	1	3	0
	-	1	-3	0
	$\frac{3}{32} e_1^3$	1	3	2
	-	1	-3	2
	$\frac{9}{32} e_1^3$	1	3	-2
	-	1	-3	-2

+

ν^2	Coeff.	f	f_1	sin S
	$-\frac{45}{32}\alpha^2 e + e^3 - \frac{27}{8} e e_1^2$	2	0	0
	$\frac{5}{32}\alpha^2 e + \frac{9}{8} e^3 + \frac{27}{4} e e_1^2$	2	0	2
	$-\frac{105}{32}\alpha^2 e + \frac{15}{8} e^3 - \frac{135}{8} e e_1^2$	2	0	-2
	$\frac{105}{32}\alpha^2 e$	2	0	4
	$-\frac{35}{4}\alpha^2 e$	2	0	-4
	$-\frac{9}{16}\alpha e e_1$	2	1	1
	-	2	-1	1
	$-\frac{63}{16}\alpha e e_1$	2	1	-1
	-	2	-1	-1
	$\frac{75}{16}\alpha e e_1$	2	1	3
	-	2	-1	3
	$-\frac{195}{16}\alpha e e_1$	2	1	-3
	-	2	-1	-3
	$-\frac{9}{16} e e_1^2$	2	2	0
	-	2	-2	0
	$\frac{9}{8} e e_1^2$	2	2	2
	-	2	-2	2
	$-\frac{45}{16} e e_1^2$	2	2	-2
	-	2	-2	-2
	$\frac{15}{64}\alpha e^2$	3	0	1
	$\frac{165}{64}\alpha e^2$	3	0	-1
	$-\frac{225}{64}\alpha e^2$	3	0	3
	$\frac{525}{64}\alpha e^2$	3	0	-3
	$\frac{9}{8} e^2 e_1$	3	1	0
	-	3	-1	0
	$-\frac{45}{16} e^2 e_1$	3	1	2
	-	3	-1	2
	$\frac{99}{16} e^2 e_1$	3	1	-2
	-	3	-1	-2
	$-\frac{5}{8} e^3$	4	0	0
	$\frac{15}{8} e^3$	4	0	2
	$-\frac{15}{4} e^3$	4	0	-2

(d)

(viii) The general integration of Lagrange's planetary equations $d\sigma/dS$

The terms $d\sigma/dS(S)$, which we will be integrating from $S = -\pi$ to $S = +\pi$, are of the form

$$\frac{d\sigma}{dS} = G\frac{d\sigma}{df} = \sum_{i=1}^{n} A_i \sum_{q=1}^{6} S_q(i) + \sum_{l=1}^{m} B_l \sum_{q=1}^{6} C_q(l) + (S + K_{60} + g_6 - M_0) \sum_{p=1}^{W} D_p \sum_{q=1}^{6} S_q(p)$$

where the general forms of S_q and C_q for q = 1 to 6 are given in Equations (24), and the constants A_i, B_l, and D_p are the coefficients found in Tables 4.2 for $d\sigma/df$. Note that the specific forms of S_q and C_q depend on the values of j and k in the sine or cosine argument $(jf+kf_1+kS)$ for each individual term found in Tables 4.2. Integration of the above sum of terms involves the same integrals whose general solutions are given in Table 3.1. The only difference is that now the constant kK_0 is taken to be whichever constant is found in the argument of the trigonometric function and the integer j is taken to be the integer sum which multiplies the variable S in the argument of the term being integrated.

The following properties of the function Y_{jk} are also useful for collation purposes

$$Y_{00} = 0$$

$$Y_{0k} = -Y_{0,-k}$$

$$Y_{jk} = -Y_{-j,-k}$$

Note that the transformation of $d\epsilon/df$ to $d\epsilon/dS$ requires the use of the trigonometric identities listed as Equations (15) of Chapter 3 to change the $d\epsilon/dS$ terms into the standard form ready for integration, since both the function g_6 and the sum of the S_q terms from q = 1 to 6 contain trigonometric functions of S.

(ix) The transformation of de/df to de/dS and its subsequent integration

The method of transforming $d\sigma/df$ to $d\sigma/dS$ and then integrating $d\sigma/dS$ to get $\Delta\sigma$ has so far been described only in a very abstract sense. We now illustrate the method by applying it to the integration of the equation of motion de/df or Table 4.2(a).

de/df is of the form

$$\frac{de}{df} = \sum_{i=1}^{n} A_i \sin (j_i f + k_i f_1 + q_i S)$$

Therefore, in order to transform de/df into de/dS, we multiply each of the coefficients A_i of the terms found in de/df by the sum of the expressions for S_q given by Equations (24).

$$\frac{d\sigma}{dS} = \sum_{i=1}^{n} A_i \sum_{q=1}^{6} S_q(i)$$

We do this only for those terms of de/dS which will produce non-zero results when integrated from $S = -\pi$ to $S = +\pi$.

For example, from Equation (24e) we can see that S_3 terms produce type (a) integrals of Table 3.1 and are therefore non-zero if j+q+1=0 or j+q-1=0. Since S_3 terms are of order three, we look only at the coefficients of order zero or in other words, at Table 4.3(a) for de/df. The following de/df terms produce non-zero integrals

$\frac{de}{df}$: v^2

		sin			
	Coeff.	f	f_1	S	
	$\frac{1}{2}$	1	0	0	j+q-1=0
	$\frac{9}{4}$	1	0	-2	j+q+1=0

Using Equation (24e) for S_3, the above terms are transformed into

$\frac{de}{dS}$: ν^2

Coeff.	S	Y_{jk}
$-e\nu^2$	0	Y_{00}
$-\frac{9}{2}e\nu^2$	0	Y_{20}

sin

and using Tables 3.1, are integrated to give

Δe: $\nu^2\pi$

Coeff.	Y_{jk}
$-9e\nu^2$	Y_{20}

sin

S_4 terms require j+q-2=0 or j+q+2=0 in order for a non-zero integral to occur. There are no non-zero terms to be found in Table 4.3(a).

From Equation (24g) we can see that S_5 terms lead to type (a) integrals, which are non-zero if j+q+1=0 or j+q-1=0. Looking at Table 4.3(a), the following give non-zero results:

$\frac{de}{df}$: ν^2

Coeff.	f	f_1	S	
$\frac{1}{2}$	1	0	0	j+q-1=0
$\frac{9}{4}$	1	0	-2	j+q+1=0

sin

Transformation to de/dS, using Equation (24g) gives

$\frac{de}{dS}$: ν^2

sin

Coeff.	S	Y_{jk}	K
$-\frac{1}{2}ee_1\nu$	0	Y_{10}	$-K_{80}$
"	0	Y_{10}	$-K_{90}$
$-\frac{9}{4}ee_1\nu$	0	Y_{10}	K_{80}
"	0	Y_{10}	K_{90}

which integrates to form

Δe: $\nu^2\pi$

sin

Coeff.	Y_{jk}	K
$-ee_1\nu$	Y_{10}	$-K_{80}$
"	Y_{10}	$-K_{90}$
$-\frac{9}{2}ee_1\nu$	Y_{10}	K_{80}
"	Y_{10}	K_{90}

S_6 terms produce type (b) integrals which are non-zero if $j+q\neq 0$. Looking at Table 4.2(a) all the de/df terms are relevant. Applying Equation (24h) gives

$\frac{de}{dS}$: $\nu^2 S\{$

cos

Coeff.	S	Y_{jk}	K
$-\frac{1}{2}e_1\nu^2$	1	Y_{10}	$-K_{70}$
$-$"	1	Y_{10}	K_{70}
$-\frac{9}{4}e_1\nu^2$	-1	Y_{10}	$-K_{70}$
$-$"	-1	Y_{10}	K_{70}

$+$

cos

Coeff.	S	Y_{jk}	K
$\frac{3}{4}e_1\nu^2$	3	Y_{10}	$-K_{70}$
$-$"	3	Y_{10}	K_{70}

$\}$

and using the general solution of type (b) integrals found in Table 3.1, we get

sin

Δe: $\nu^2\pi$	Coeff.	Y_{jk}	K
	$4e_1\nu^2$	Y_{10}	K_{70}
	$-$"	Y_{10}	$-K_{70}$

$S_2{}^3$ terms contain type (b) integrals and are non-zero when $j+q+1\neq 0$ or $j+q-1\neq 0$. One of these conditions occur for each of the following de/df terms

sin

$\frac{de}{df}$: ν^2	Coeff.	f	f_1	S	
	$\frac{9}{4}$	1	0	-2	$j+q-1\neq 0$
	$-\frac{3}{4}$	1	0	2	$j+q-1\neq 0$, $j+q+1\neq 0$
	$\frac{1}{2}$	1	0	0	$j+q-1\neq 0$

Transformation of these terms by Equation (25d) for $S_2{}^3$ gives

cos

$\frac{de}{dS}$: $\nu^2 S$	Coeff.	S	Y_{jk}
	$-e\nu^2 X_0$	2	Y_{20}
	$\frac{3}{2}e\nu^2 X_0$	4	Y_{20}

or upon integration

sin

Δe: $\nu^2\pi$	Coeff.	Y_{jk}
	$-\frac{1}{4}e\nu^2 X_0$	Y_{20}

The component $S_2{}^2$ is of order two and therefore requires a search through both Tables 4.3(a) and (b) for non-zero integrals. $S_2{}^2$ terms form type (a)

integrals, which are non-zero for j+q+1=0 or j+q-1=0. Studying Tables 4.3(a) and (b), the following de/df terms produce non-zero results.

$\frac{de}{df}$: ν^2 {

Coeff.	f	f_1	S (sin)	
$\frac{9}{4}$	1	0	-2	j+q+1=0
$\frac{27}{8}e_1$	1	-1	-2	"
"	1	1	-2	"

+

Coeff.	f	f_1	S (sin)	
$\frac{1}{2}$	1	0	0	j+q-1=0
$\frac{3}{4}e_1$	1	1	0	"
"	1	-1	0	"

}

Using Equation (25c), these are transformed to

$\frac{de}{dS}$: ν^2

Coeff.	S	Y_{jk} (sin)
$-\frac{9}{4}e\nu$	0	Y_{20}
$-\frac{27}{8}ee_1\nu$	0	$Y_{2,-1}$
"	0	Y_{21}

+ ν^2

Coeff.	S	Y_{jk} (sin)
$-\frac{1}{2}e\nu$	0	Y_{00}
$-\frac{3}{4}ee_1\nu$	0	Y_{01}
-"	0	Y_{01}

and integrated, using Table 3.1 to get

Δe: $\nu^2\pi$

Coeff.	Y_{jk} (sin)
$-\frac{9}{2}e\nu$	Y_{20}
$-\frac{27}{4}ee_1\nu$	$Y_{2,-1}$
"	Y_{21}

The S_1 terms contain four components of different orders Q_0S^0, Q_0S^1, Q_0S^2 and Q_0S^3 where the superscript denotes the order. Equation (22c) giving S^0 shows that a non-zero integral will result only if j+q=0. Since S^0 is of order zero, we must search through the whole of the original Table 4.2(a) of de/df in order to obtain all

the final terms to a maximum order of three. The following de/df terms produce non-zero results

$\frac{de}{df} : \nu^2$

Coeff.	f	f_1	S
$\frac{15}{16}\alpha e^2 + \frac{15}{16}\alpha + \frac{105}{128}\alpha^3 + \frac{105}{16}\alpha e_1^2$	1	0	-1
$-\frac{15}{4}e - \frac{105}{32}\alpha^2 e + \frac{15}{8}e^3 - \frac{135}{8}ee_1^2$	2	0	-2
$\frac{15}{8}\alpha e_1$	1	1	-1
"	1	-1	-1
$\frac{45}{32}\alpha e_1^2$	1	2	-1
"	1	-2	-1

sin

+ ν^2

Coeff.	f	f_1	S
$\frac{525}{64}\alpha e^2$	3	0	-3
$-\frac{45}{8}ee_1$	2	1	-2
"	2	-1	-2
$-\frac{45}{16}ee_1^2$	2	2	-2
"	2	-2	-2

sin

Equation (22c) is used to transform these to de/dS

$\frac{de}{dS} : \nu^2 Q_0$

Coeff.	S	Y_{jk}
Same	0	Y_{10}
as	0	Y_{20}
above	0	Y_{11}
	0	$Y_{1,-1}$
	0	Y_{12}
	0	$Y_{1,-2}$

sin

+ $\nu^2 Q_0$

Coeff.	S	Y_{jk}
Same	0	Y_{30}
as	0	Y_{21}
above	0	$Y_{2,-1}$
	0	Y_{22}
	0	$Y_{2,-2}$

sin

The terms are type (a) integrals and therefore integrate to form

Δe: $\nu^2\pi Q_0$

Coeff.	Y_{jk} (sin)
$\frac{15}{32}\alpha e^2+\frac{15}{8}\alpha+\frac{105}{64}\alpha^3+\frac{105}{8}\alpha e_1^2$	Y_{10}
$-\frac{15}{2}e-\frac{105}{16}\alpha^2 e+\frac{15}{4}e^3-\frac{135}{4}ee_1^2$	Y_{20}
$\frac{15}{4}\alpha e_1$	Y_{11}
"	$Y_{1,-1}$
$\frac{45}{16}\alpha e_1^2$	Y_{12}
"	$Y_{1,-2}$

$+\ \nu^2\pi Q_0$

Coeff.	Y_{jk} (sin)
$\frac{525}{32}\alpha e^2$	Y_{30}
$-\frac{45}{4}ee_1$	Y_{21}
"	$Y_{2,-1}$
$-\frac{45}{8}ee_1^2$	Y_{22}
"	$Y_{2,-2}$

S^1 terms lead to type (b) integrals which are non-zero if $j+q\neq 0$. Searching through Tables 4.3(a),(b) and (c) gives the following results

$\frac{de}{df}$: ν^2

Coeff.	f	f_1	S (sin)
$\frac{1}{2}+\frac{9}{16}\alpha^2+\frac{9}{4}e_1^2-\frac{3}{4}e^2$	1	0	0
$\frac{9}{4}+\frac{5}{4}\alpha^2+\frac{81}{8}e_1^2+\frac{3}{8}e^2$	1	0	-2
$-\frac{3}{4}-\frac{27}{8}e_1^2-\frac{21}{8}e^2$	1	0	2

$+\ \nu^2$

Coeff.	f	f_1	S (sin)
$\frac{3}{2}e$	2	0	2
$-\frac{3}{4}e$	2	0	0
$\frac{21}{16}\alpha e$	0	0	1

$\frac{de}{df}$: ν^2 sin

Coeff.	f	f_1	S
$\frac{3}{16}\alpha$	1	0	1
$\frac{15}{4}e$	0	0	2
$\frac{45}{16}\alpha$	1	0	-3
$-\frac{15}{16}\alpha$	1	0	3
$\frac{27}{8}e_1$	1	-1	-2
"	1	1	-2
$-\frac{45}{8}ee_1$	0	1	-2
–"	0	1	2
$\frac{105}{16}\alpha e$	0	0	3
$-\frac{63}{32}\alpha e$	2	0	-1
$-\frac{9}{32}\alpha e$	2	0	1
$\frac{3}{8}\alpha e_1$	1	1	1
"	1	-1	1
$\frac{75}{32}\alpha e$	2	0	3
$-\frac{15}{8}\alpha e_1$	1	1	3
"	1	-1	3
$-\frac{35}{32}\alpha^2$	1	0	4
$-\frac{15}{8}e^2$	3	0	2
$\frac{3}{4}e^2$	3	0	0

+ ν^2 sin

Coeff.	f	f_1	S
$\frac{3}{4}e_1$	1	1	0
"	1	-1	0
$-\frac{9}{8}e_1$	1	-1	2
"	1	1	2
$\frac{9}{4}ee_1$	2	1	2
"	2	-1	2
$-\frac{9}{8}ee_1$	2	1	0
"	2	-1	0
$-\frac{9}{16}e_1^2$	1	2	2
"	1	-2	2
$\frac{3}{8}e_1^2$	1	-2	0
"	1	2	0
$-\frac{195}{32}\alpha e$	2	0	-3
$\frac{45}{8}\alpha e_1$	1	1	-3
"	1	-1	-3
$\frac{105}{32}\alpha^2$	1	0	-4
$\frac{33}{8}e^2$	3	0	-2
$\frac{27}{16}e_1^2$	1	-2	-2
"	1	2	-2

These are transformed to de/dS using Equation (22d) to give

$$\frac{de}{dS} : \nu^2 Q_0 \nu X_0 S\{$$

cos

Coeff.	S	Y_{jk}
$\frac{1}{2}+\frac{9}{16}\alpha^2+\frac{9}{4}e_1^2-\frac{3}{4}e^2$	1	Y_{10}
$\frac{9}{4}+\frac{5}{4}\alpha^2+\frac{81}{8}e_1^2+\frac{3}{8}e^2$	-1	Y_{10}
$-\frac{3}{4}-\frac{27}{8}e_1^2-\frac{21}{8}e^2$	3	Y_{10}
$\frac{3}{16}\alpha$	2	Y_{10}
$\frac{45}{16}\alpha$	-2	Y_{10}
$-\frac{15}{16}\alpha$	4	Y_{10}
$3e$	4	Y_{20}
$-\frac{3}{2}e$	2	Y_{20}
$\frac{3}{2}e_1$	1	Y_{11}
$-\frac{9}{4}e_1$	3	Y_{11}
$\frac{27}{4}e_1$	-1	Y_{11}
$-\frac{45}{8}ee_1$	-2	Y_{01}
$-"$	2	Y_{01}
$-\frac{63}{16}\alpha e$	1	Y_{20}
$-\frac{9}{16}\alpha e$	3	Y_{20}
$\frac{3}{4}\alpha e_1$	2	Y_{11}
$\frac{75}{16}\alpha e$	5	Y_{20}
$-\frac{15}{4}\alpha e_1$	4	Y_{11}

$+$

cos

Coeff.	S	Y_{jk}
$-\frac{35}{32}\alpha^2$	5	Y_{10}
$-\frac{45}{8}e^2$	5	Y_{30}
$\frac{9}{4}e^2$	3	Y_{30}
$\frac{27}{4}ee_1$	4	Y_{21}
$\frac{9}{4}ee_1$	4	$Y_{2,-1}$
$-\frac{27}{8}ee_1$	2	Y_{21}
$-\frac{9}{8}ee_1$	2	$Y_{2,-1}$
$-\frac{27}{16}e_1^2$	3	Y_{12}
$\frac{9}{16}e_1^2$	3	$Y_{1,-2}$
$-\frac{3}{8}e_1^2$	1	$Y_{1,-2}$
$\frac{9}{8}e_1^2$	1	Y_{12}
$-\frac{195}{16}\alpha e$	-1	Y_{20}
$\frac{45}{4}\alpha e_1$	-2	Y_{11}
$\frac{105}{32}\alpha^2$	-3	Y_{10}
$\frac{99}{8}e^2$	1	Y_{30}
$-\frac{27}{16}e_1^2$	-1	$Y_{1,-2}$
$\frac{81}{16}e_1^2$	-1	Y_{12}

$\}$

Integration then gives

$\Delta e: \nu^2 \pi \nu X_0 Q_0 \{$

Coeff.	Y_{jk} (sin)
$4+4\alpha^2+18e_1^2+4e^2-\frac{99}{32}\alpha$	Y_{10}
$-18\alpha e$	Y_{20}
$12e_1-\frac{99}{8}\alpha e_1$	Y_{11}
$\frac{45}{4}ee_1$	Y_{01}

$+$

Coeff.	Y_{jk} (sin)
$-24e^2$	Y_{30}
$9e_1^2$	Y_{12}
$-3e_1^2$	$Y_{1,-2}$

$\}$

S^2 terms contain two different types of integrals, types (a) and (c). The type (a) integrals require that j+q+1=0 or j+q-1=0 in order for non-zero results to be produced. Looking at Tables 4.3(a) and (b), we get the following de/df terms which obey these conditions:

$\frac{de}{df}: \nu^2$ (sin)

Coeff.	f	f_1	S	
$\frac{9}{4}$	1	0	-2	j+q+1=0
$\frac{27}{8}e_1$	1	-1	-2	"
"	1	1	-2	"

$+ \nu^2$ (sin)

Coeff.	f	f_1	S	
$\frac{1}{2}$	1	0	0	j+q-1=0
$\frac{3}{4}e_1$	1	1	0	"
"	1	-1	0	"

Applying the transformation of the appropriate part of Equation (22e) gives

$\frac{de}{dS}: \nu^2 e \nu Q_0$ (sin)

Coeff.	S	Y_{jk}	K
$-\frac{9}{4}$	0	Y_{10}	K_{20}
$-\frac{27}{4}e_1$	0	$-Y_{11}$	K_{20}
$\frac{1}{2}$	0	Y_{10}	$-K_{20}$
$\frac{3}{2}e_1$	0	Y_{11}	$-K_{20}$

and integration from $S = -\pi$ to $S = +\pi$ produces

$\Delta e: \quad \nu^2 \pi e \nu Q_0$

sin

Coeff.	Y_{jk}	K
$-\frac{9}{2}$	Y_{10}	K_{20}
$-\frac{27}{2}e_1$	Y_{11}	K_{20}
1	Y_{10}	$-K_{20}$
$3e_1$	Y_{11}	$-K_{20}$

The type (c) integrals have two different answers depending on whether j+q=0 or j+q≠0. Searching through Tables 4.3(a) and (b), the following have j+q=0

$\frac{de}{df}: \nu^2$

sin

Coeff.	f	f_1	S
$\frac{15}{16}\alpha$	1	0	-1
$-\frac{15}{4}e$	2	0	-2

while the rest have j+q≠0. Using the relevant part of Equation (22e), de/dS becomes

$\frac{de}{dS}: \nu^2 Q_0 \nu^2 X_0^2 S^2 \{$

sin

Coeff.	S	Y_{jk}
$-\frac{15}{32}\alpha$	0	Y_{10}
$\frac{15}{2}e$	0	Y_{20}
$-\frac{1}{4}$	1	Y_{10}
$-\frac{9}{8}$	-1	Y_{10}
$\frac{3}{8}$	3	Y_{10}
$-\frac{3}{32}\alpha$	2	Y_{10}
$-\frac{45}{32}\alpha$	-2	Y_{10}

+

sin

Coeff.	S	Y_{jk}
$\frac{15}{32}\alpha$	4	Y_{10}
$-3e$	4	Y_{20}
$\frac{3}{2}e$	2	Y_{20}
$-\frac{3}{2}e_1$	1	Y_{11}
$\frac{9}{4}e_1$	3	Y_{11}
$-\frac{27}{4}e_1$	-1	Y_{11}

$\}$

Then applying the general solution for type (c) integrals from Table 3.1, we get

$$\Delta e: \quad \nu^2\pi\, Q_0\nu^2 X_0^2 \{$$

Coeff.	sin Y_{jk}
$-\frac{15}{16}\pi^2\alpha$	Y_{10}
$5\pi^2 e$	Y_{20}
$\frac{16}{3} - \frac{177}{128}\alpha$	Y_{10}

$+$

Coeff.	sin Y_{jk}
$\frac{3}{4}e$	Y_{20}
$32e_1$	Y_{11}

$\}$

The final term S^3 includes all four types of integrals found in Table 3.1. Type (a) integrals produce non-zero results if $j+q+1=0$, $j+q-1=0$, $j+q+2=0$ or $j+q-2=0$. Since S^3 terms are of order three, we need only search through Table 4.3(a) for the de/df terms which adhere to one of the above conditions. We obtain

$\frac{de}{df}: \nu^2$

Coeff.	f	f_1	S	sin
$\frac{9}{4}$	1	0	-2	$j+q+1=0$
$\frac{1}{2}$	1	0	0	$j+q-1=0$

Using the components of S^3 which form type (a) integrals, the above table is transformed to

$\frac{de}{dS}: \nu^2 Q_0$

Coeff.	S	sin Y_{jk}	K
$-\frac{9}{4}e\nu^2$	0	Y_{10}	K_{20}
$\frac{1}{2}e\nu^2$	0	Y_{10}	$-K_{20}$
$-\frac{9}{2}ee_1\nu$	0	Y_{10}	K_{40}
$ee_1\nu$	0	Y_{10}	$-K_{40}$

Integrated the table becomes

Δe: $\nu^2 \pi Q_0$

sin

Coeff.	Y_{jk}	K
$-\frac{9}{2}e\nu^2$	Y_{10}	K_{20}
$e\nu^2$	Y_{10}	$-K_{20}$
$-9ee_1\nu$	Y_{10}	K_{40}
$2ee_1\nu$	Y_{10}	$-K_{40}$

The type (b) integrals give non-zero results if $j+q+1\neq 0$ or $j+q-1\neq 0$. From Table 4.3(a), the following transform into non-zero integrals:

$\frac{de}{df}$: ν^2

sin

Coeff.	f	f_1	S	
$\frac{9}{4}$	1	0	-2	$j+q-1\neq 0$
$-\frac{3}{4}$	1	0	2	$j+q-1\neq 0$, $j+q+1\neq 0$
$\frac{1}{2}$	1	0	0	$j+q+1\neq 0$

Transforming these terms by the parts of S^3 which form type (b) integrals we get

$\frac{de}{dS}$: $\nu^2 Q_0 e\nu^2 S$ {

cos

Coeff.	S	Y_{jk}	K
$-\frac{9}{4}$	-2	Y_{10}	$-K_{20}$
$\frac{3}{4}$	2	Y_{10}	$-K_{20}$
$-\frac{1}{2}$	2	Y_{10}	K_{20}
$\frac{3}{4}$	4	Y_{10}	K_{20}

+

cos

Coeff	S	Y_{jk}	K
$\frac{9}{4}X_0$	-2	Y_{10}	$-K_{20}$
$-\frac{3}{4}X_0$	2	Y_{10}	$-K_{20}$
$-\frac{1}{2}X_0$	2	Y_{10}	K_{20}
$\frac{3}{4}X_0$	4	Y_{10}	K_{20}

}

Integration then gives

$\Delta e: \quad \nu^2 \pi e \nu^2 Q_0$

Coeff.	Y_{jk} sin	K
$-\frac{1}{8}(1+X_0)$	Y_{10}	K_{20}
$3(1-X_0)$	Y_{10}	$-K_{20}$

Type (c) integrals have two different answers depending on whether j+q=0 or j+q≠0. Looking at Table 4.3(a) there are no j+q=0 terms, therefore using the relevant portion of S^3, all of the Table 4.3(a) terms transform to

$\frac{de}{dS}: \nu^2 Q_0 e_1 \nu^2 S^2 \{$

Coeff.	S	Y_{jk} sin	K
$-\frac{1}{4}$	1	Y_{10}	K_{30}
"	1	Y_{10}	$-K_{30}$
$-\frac{9}{8}$	-1	Y_{10}	K_{30}
"	-1	Y_{10}	$-K_{30}$

+

Coeff	S	Y_{jk} sin	K
$\frac{3}{8}$	3	Y_{10}	K_{30}
"	3	Y_{10}	$-K_{30}$

$\}$

Integration then gives

$\Delta e: \quad \nu^2 \pi e_1 \nu^2 Q_0$

Coeff.	Y_{jk} sin	K
$\frac{16}{3}$	Y_{10}	K_{30}
$-\frac{16}{3}$	Y_{10}	$-K_{30}$

The type (d) integral requires j+q≠0 in order for the results to be non-zero. In Table 4.3(a), this condition occurs for all the terms. Multiplying the coefficients by the applicable portion of Equation (22f) gives

$\frac{de}{dS}$: $\nu^2 S^3 Q_0 \nu^3 X_0^3$

		cos
Coeff.	S	Y_{jk}
$-\frac{1}{12}$	1	Y_{10}
$-\frac{3}{8}$	-1	Y_{10}
$\frac{1}{8}$	3	Y_{10}

Using Table 3.1 to integrate, the above table becomes

Δe: $\nu^2\pi$

Coeff.	sin Y_{jk}
$\nu^3 Q_0 X_0^3 \left(\frac{32}{9} - \frac{2}{3}\pi^2\right)$	Y_{10}

The final collated version of the set of terms forming Δe is found in Table 4.4(a), where the constants are as follows

$$\delta_0 = M_{10} - \nu M_0 \tag{26a}$$

$$K_{20} = \frac{1}{1-\nu}(\delta_0 + f_{c0} - f_{1c0}) \tag{26b}$$

$$K_{30} = \nu K_{20} + \delta_0 \tag{26c}$$

$$K_{40} = (1-\nu)K_{20} - \delta_0 \tag{26d}$$

$$K_{60} = K_{20} + \left[2e_1(1+\nu+\nu^2) - \frac{1}{4}e_1^3\right]\sin K_{30} + \frac{5}{4}e_1^2 \sin 2K_{30} + \frac{13}{12}e_1^3 \sin 3K_{30} + \frac{13}{4}e_1^2\nu \sin 2K_{30} \tag{26e}$$

$$Y_{jk} = (j+k)K_{60} + k(f_{1c0} - f_{c0}) \tag{26f}$$

$$X_0 = 1 + \nu + \nu^2 + 2e_1(1+2\nu)\cos K_{30} + \frac{5}{2}e_1^2 \cos 2K_{30} \tag{26g}$$

$$K_{70} = \nu K_{60} + \delta_0 \tag{26h}$$

$$K_{80} = (1-\nu)K_{60} - \delta_0 \tag{26i}$$

$$K_{90} = (1+\nu)K_{60} + \delta_0 \tag{26j}$$

$$Q_0 = 1 + \nu + \nu^2 + \nu^3 + 2e_1\nu(1+2\nu)\cos K_{70} + \frac{5}{2}e_1^2\nu \cos 2K_{70} \tag{26k}$$

$\Delta e = \nu^2\pi$

Coeff.	sin Y_{jk}	K
$\left(-\frac{17}{2}+5\pi^2\right)e\nu^2 - \frac{9}{2}e\nu - \frac{105}{16}\alpha^2 e + \frac{15}{4}e^3 - \frac{135}{4}ee_1^2 - 18\alpha e\nu - \frac{15}{2}eQ_0$	Y_{20}	0
$-ee_1\nu$	Y_{10}	$-K_{80}$
"	"	$-K_{90}$
$-\frac{9}{2}ee_1\nu$	Y_{10}	K_{80}
"	"	K_{90}
$4e_1\nu^2$	Y_{10}	K_{70}
$-$"	"	$-K_{70}$
$-\frac{27}{4}ee_1\nu - \frac{45}{4}ee_1Q_0$	$Y_{2,1}$	0
" "	Y_{21}	0
$\frac{15}{32}\alpha e^2 + \frac{105}{64}\alpha^3 + \frac{105}{8}\alpha e_1^2 + 4\alpha^2\nu + 18e_1^2\nu + 4e^2\nu - \left(\frac{15}{16}\pi^2+\frac{177}{128}\right)\alpha\nu^2$	Y_{10}	0
$+\left(\frac{32}{9}-\frac{2}{3}\pi^2\right)\nu^3 + Q_0\left(\frac{15}{8}\alpha + 4\nu X_0 - \frac{99}{32}\alpha\nu X_0 + \frac{16}{3}\nu^2 X_0^2\right)$	"	-
$32e_1\nu^2 - \frac{99}{8}\alpha e_1\nu + Q_0\left(\frac{15}{4}\alpha e_1 + 12e_1\nu X_0\right)$	Y_{11}	0
$\frac{15}{4}\alpha e_1 Q_0$	$Y_{1,-1}$	0
$\frac{45}{16}\alpha e_1^2 + 9e_1^2\nu$	Y_{12}	0
$\frac{45}{16}\alpha e_1^2 - 3e_1^2\nu$	$Y_{1,-2}$	0
$\frac{525}{32}\alpha e^2 - 24e^2\nu$	Y_{30}	0
$-\frac{45}{8}ee_1^2$	Y_{22}	0
"	$Y_{2,-2}$	0
$\frac{45}{4}ee_1\nu$	Y_{01}	0
$-\frac{19}{4}e\nu^2 - \frac{9}{2}e\nu Q_0$	Y_{10}	K_{20}
$e\nu^2 + e\nu Q_0$	Y_{10}	$-K_{20}$
$-\frac{27}{2}ee_1\nu$	Y_{11}	K_{20}
$3ee_1\nu$	Y_{11}	$-K_{20}$
$-9ee_1\nu$	Y_{10}	K_{40}
$2ee_1\nu$	Y_{10}	$-K_{40}$
$\frac{16}{3}e_1\nu^2$	Y_{10}	K_{30}
$-$"	"	$-K_{30}$

Table 4.4(b)

$\Delta\alpha = -\nu^2\pi(\alpha\nu)$

Coeff.	sin Y_{jk}
$9e_1$	Y_{01}
$8e$	Y_{10}

Table 4.4(c)

$\Delta\varpi = -\frac{\nu^2}{e}\pi$

Coeff.	Y_{jk}	K
$-ev(1+2\nu)+\frac{3}{4}e^3-\frac{45}{16}\alpha^2 e-\frac{27}{4}ee_1^2-\frac{3}{2}eQ_0$	0	0
$\left(-\frac{17}{2}+5\pi^2\right)ev^2-\frac{9}{2}ev-\frac{105}{16}\alpha^2 e+\frac{15}{4}e^3-\frac{135}{4}ee_1^2-18\alpha ev-\frac{15}{2}eQ_0$	Y_{20}	0
$-ee_1\nu$	Y_{10}	$-K_{80}$
"	"	$-K_{90}$
$-\frac{9}{2}ee_1\nu$	Y_{10}	K_{80}
"	"	K_{90}
$4e_1\nu^2$	Y_{10}	K_{70}
"	"	$-K_{70}$
$-\frac{27}{4}ee_1\nu-\frac{45}{4}ee_1Q_0$	$Y_{2,1}$	0
" "	Y_{21}	0
$\frac{105}{32}\alpha e^2+\frac{105}{64}\alpha^3+\frac{105}{8}\alpha e_1^2+4\alpha^2\nu+18e_1^2\nu-4e^2\nu-\left(\frac{5}{16}\pi^2+\frac{177}{128}\right)\alpha\nu^2$	Y_{10}	0
$+\left(\frac{32}{9}-\frac{2}{3}\pi^2\right)\nu^3+Q_0\left(\frac{15}{8}\alpha+4\nu X_0-\frac{99}{32}\alpha\nu X_0+\frac{16}{3}\nu^2X_0^2\right)$	"	"
$32e_1\nu^2-\frac{99}{8}\alpha e_1\nu+Q_0\left(\frac{15}{4}\alpha e_1+12e_1\nu X_0\right)$	Y_{11}	0
$\frac{15}{4}\alpha e_1Q_0$	$Y_{1,1}$	0
$\frac{45}{16}\alpha e_1^2+9e_1^2\nu$	Y_{12}	0
$\frac{45}{16}\alpha e_1^2-3e_1^2\nu$	$Y_{1,2}$	0
$\frac{525}{32}\alpha e^2-24e^2\nu$	Y_{30}	0
$-\frac{45}{8}ee_1^2$	Y_{22}	0
"	$Y_{2,2}$	0
$-\frac{9}{2}ee_1Q_0-3ee_1\nu$	Y_{01}	0
$-\frac{19}{4}ev^2-\frac{9}{2}evQ_0$	Y_{10}	K_{20}
ev^2+evQ_0	Y_{10}	$-K_{20}$
$-\frac{27}{2}ee_1\nu$	Y_{11}	K_{20}
$3ee_1\nu$	Y_{11}	$-K_{20}$
$-9ee_1\nu$	Y_{10}	K_{40}
$2ee_1\nu$	Y_{10}	$-K_{40}$
$\frac{16}{3}e_1\nu^2$	Y_{10}	K_{30}
"	"	$-K_{30}$
$-\frac{9}{4}ee_1^2$	Y_{02}	0

Table 4.4(d)

$\Delta\epsilon = -2\nu^2\pi$

Coeff.	Y_{jk} cos	K
$\frac{5}{8}e^2\nu - \frac{165}{64}\alpha^2\nu - \frac{81}{8}e_1^2\nu + 21\alpha e_1^2 + 3\alpha^3$	0	0
$+ Q_0\left(-\frac{93}{64}\alpha^2 - \frac{45}{8}e_1^2 + \frac{33}{8}e^2 - \frac{5}{4} + 3\alpha - \frac{9}{4}\nu X_0 + 3\alpha\nu X_0\right)$	"	"
$\frac{111}{8}\alpha e\nu - 6e\nu + e\nu^2\left(-\frac{158}{3}+3\pi^2\right) - \frac{157}{16}\alpha^2 e - 27ee_1^2 + 3e^3$	Y_{10}	0
$+ Q_0\left(\frac{9}{16}\alpha e - 12e\nu X_0 - 6e\right)$	"	"
$\frac{15}{16}\alpha^2 e_1 - \frac{195}{16}e_1^3 + \frac{99}{8}e^2 e_1 + e_1\nu^2\left(\frac{23}{8}\pi^2 - \frac{117}{16}\right)$	Y_{01}	0
$- \frac{525}{64}\alpha^2 e_1 + 12\alpha e_1\nu + Q_0\left(-\frac{15}{4}e_1 - \frac{27}{4}e_1\nu X_0 + 12\alpha e_1\right)$	"	"
$\frac{9}{8}\alpha e e_1 - 36 e e_1\nu - 9 e e_1 Q_0$	Y_{11}	0
$\frac{9}{8}\alpha e e_1 - 18 e e_1\nu - 9 e e_1 Q_0$	$Y_{1,-1}$	0
$\frac{109}{8}e^2\nu + 9\alpha e^2 + \frac{69}{8}e^2 Q_0$	Y_{20}	0
$\frac{207}{16}e^2 e_1$	Y_{21}	0
"	$Y_{2,-1}$	0
$-\frac{9}{8}\alpha e\nu - 6e\nu^2$	0	K_{20}
$\frac{27}{16}e^2\nu$	0	$2K_{20}$
$2e^2\nu$	Y_{10}	$+K_{20}$
$\frac{165}{16}e^2\nu$	Y_{10}	K_{20}
$3 e e_1\nu$	0	K_{80}
"	"	K_{90}
$-\frac{27}{8}e_1^2(\nu + Q_0) + 9\alpha e_1^2$	Y_{02}	0
$-3e^3$	Y_{30}	0
$-\frac{9}{2}e e_1^2$	Y_{12}	0
"	$Y_{1,-2}$	0
$-\frac{9}{16}e_1^3$	Y_{03}	0
$-9 e e_1\nu$	Y_{01}	K_{20}
$-$"	"	$+K_{20}$

over . . .

$\Delta\epsilon$ continued ...

$-2\nu^2\pi(K_{60} - M_0)$

Coeff.	Y_{jk} sin	K
$\frac{9}{2}e_1\nu^2$	0	K_{70}
$-\frac{99}{16}\alpha e\nu - 3e\nu^2 + 6e\nu X_0Q_0$	Y_{10}	0
$\frac{27}{4}e_1\nu X_0Q_0 - 12\alpha e_1\nu$	Y_{01}	0
$18ee_1\nu$	Y_{11}	0
$\frac{27}{4}e_1^2\nu$	Y_{02}	0
$-\frac{9}{4}e^2\nu$	Y_{10}	K_{20}
$-\frac{3}{2}e^2\nu$	Y_{10}	$-K_{20}$

$+ \frac{1}{2}e^2\Delta\varpi$

Tables 4.4(a) to (d) A listing of the terms which add up to give the change in the specified orbital element over one synodic period centred on a conjunction for a sun-perturbed satellite. Tables (a) through to (d) list the terms for Δe, $\Delta\alpha$, $\Delta\varpi$ and $\Delta\epsilon$, respectively.

The planet-satellite system is assumed to adhere to the quidelines of the restricted elliptical coplanar three-body model. Note that the expressions for the constants are given in Equations (26).

$d\alpha/df$, $d\varpi/df$ and $d\epsilon/df$ are transformed into $d\alpha/dS$, $d\varpi/dS$ and $d\epsilon/dS$, and then integrated using the same method as that described for de/df. We will not go into the details of these calculations in this thesis, as the calculations are lengthy and are generally a repetition of the procedure already described for de/df. Tables 4.4(a) to (d) contain the final results, that is the changes in the orbital elements over one synodic period centred on a conjunction, of a satellite moving in a sun-perturbed orbit obeying the restrictions of the restricted elliptical coplanar three-body problem. Table 4.4(a) lists the terms of Δe, Table 4.4(b) the terms of $\Delta\alpha$, Table 4.4(c) the terms of $\Delta\varpi$ and Table 4.4(d) the terms of $\Delta\epsilon$.

As a check that our elliptical and circular analytical solutions are consistent with each other, we can easily derive the circular third order analytical solution from the third order elliptical solution and compare it with the circular second order analytical solution derived in Chapter 3. The circular solution to the problem described in Chapter 3 is a special case of the elliptical solution, where e_1 and ϖ are zero and therefore, by Equation (3), f_{1c0} equals f_{c0}. Equations (26) for the required constants simplify to:

$$\delta_0 = f_{c0} - \nu M_0$$
$$K_{20} = K_0$$
$$K_{60} = K_0$$
$$Y_{jk} = (j+k)K_0$$
$$X_0 = 1 + \nu + \nu^2$$
$$Q_0 = 1 + \nu + \nu^2 + \nu^3$$

The third order circular analytical solution for the changes in the orbital elements over one synodic period centred on a conjunction then becomes:

$\Delta e = \nu^2\pi$ (sin)

Coeff.	K_0
$\frac{15}{8}\alpha + 4\nu - \frac{39}{32}\alpha\nu + \frac{40}{3}\nu^2 + \frac{15}{32}\alpha e^2 + \frac{105}{64}\alpha^3 + 4\alpha^2\nu + 4e^2\nu$ $-\left(\frac{15}{16}\pi^2 + \frac{729}{128}\right)\alpha\nu^2 + \left(\frac{284}{9} - \frac{2}{3}\pi^2\right)\nu^3$	1
$-\frac{15}{2}e - \frac{33}{2}e\nu + \left(-\frac{101}{4} + 5\pi^2\right)e\nu^2 - \frac{105}{16}\alpha^2 e + \frac{15}{4}e^3 - 18\alpha e\nu$	2
$\frac{525}{32}\alpha e^2 - 24e^2\nu$	3

(27a)

$$\Delta\alpha = \nu^2\pi[-8\alpha e\nu \sin K_0] \tag{27b}$$

$\Delta\varpi = \frac{\nu^2\pi}{e}$ (cos)

Coeff.	K_0
$\frac{3}{2}e + \frac{3}{2}e\nu + \frac{3}{2}e\nu^2 + \frac{45}{16}\alpha^2 e - \frac{3}{4}e^3$	0
$-\frac{15}{8}\alpha - 4\nu + \frac{39}{32}\alpha\nu - \frac{40}{3}\nu^2 - \frac{105}{32}\alpha e^2 - \frac{105}{64}\alpha^3 - 4\alpha^2\nu + 4e^2\nu$ $+\left(\frac{5}{16}\pi^2 + \frac{729}{128}\right)\alpha\nu^2 - \left(\frac{284}{9} - \frac{2}{3}\pi^2\right)\nu^3$	1
$\frac{15}{2}e + \frac{33}{2}e\nu - \left(-\frac{101}{4} + 5\pi^2\right)e\nu^2 + \frac{105}{16}\alpha^2 e - \frac{15}{4}e^3 + 18\alpha e\nu$	2
$-\frac{525}{32}\alpha e^2 + 24e^2\nu$	3

(27c)

$\Delta\epsilon = \nu^2\pi$

cos

Coeff.	K_0
$\frac{5}{2} + 7\nu - 6\alpha - 12\alpha\nu + \frac{23}{2}\nu^2 + \frac{93}{32}\alpha^2 - \frac{15}{2}e^2 - \frac{51}{4}e^2\nu$ $+\frac{129}{16}\alpha^2\nu - 6\alpha^3 + 16\nu^3 - 18\alpha\nu^2$	0
$12e - \frac{33}{16}\alpha e + 46e\nu - \frac{1665}{64}\alpha e\nu - e\nu^2(-184 + 6\pi^2)$ $+\frac{157}{8}\alpha^2 e - 6e^3$	1
$-\frac{27}{2}e^2 - 18\alpha e^2 - \frac{241}{4}e^2\nu$	2
$6e^3$	3

(27d)

+ $(K_0 - M_0)$

sin

Coeff.	K_0
$-12e\nu - 18e\nu^2 + \frac{99}{8}\alpha e\nu$	1
$\frac{9}{2}e^2\nu$	2

The second order circular analytical solution given by Equations (34) of Chapter 3 is consistent with the above set of equations.

4.4 Discussions of the Analytic Theory, Its Implications and Limitations

Like the circular case, the elliptical analytical solution for the changes in the orbital elements over one synodic period can also provide us with much valuable information on the factors which affect the stability of a planet-satellite system against solar perturbations.

Generally, the inclusion of the eccentricity of the Sun's planetocentric orbit into the restricted three-body problem does not change the overall conclusions found for the circular case in Section 3.4. The elliptical analytical solutions displayed in Tables 4.4 still show $\Delta\alpha$ to be esentially zero (ie of the order of 10^{-11} to 10^{-10}) for typical solar system values of the initial parameters. Again $\Delta\alpha$ contains no secular terms, thus concurring with Poisson's theorem that no secular terms exist in the first order perturbation expansion for α.

Changes in the longitude of the pericentre and the mean longitude at the epoch still cannot directly indicate any approaching instability in the planet-satellite system. Thus, as in the circular case, we must observe the changes in the satellite's eccentricity in order to get any indication of possible impending unstable situations.

To this end we study the relationships between the changes $\Delta\sigma$ in the orbital elements and the satellite's true anomaly f_{c0} at the initial conjunction. The only difference between the above study and the equivalent circular study is that, the elliptical case now involves two new initial parameters: the eccentricity e_1 of the Sun in its planetocentric orbit and the true anomaly f_{1c0} of the Sun at the initial conjunction.

Because of the complexity of studying the effects of six parameters on $\Delta\sigma$, we simplify the problem by studying for the rest of our elliptical analysis satellites orbiting the five planets Jupiter, Saturn, Uranus, Earth and Mars. In other words, we fix the mass ratio μ and the eccentricity of the Sun e_1 to agree with those values currently observed today for the five planets (See Table 1.1).

Since e_1 can vary considerably due to the mutual perturbations of the other

planets over time scales greater than 10^6 years, we also include a variation on the above data range where the theoretical maximum eccentricity of the planet is used instead of its current eccentricity. These approximate maximum eccentricities are taken from the Cohen, Hubbard and Oesterwinter (1973) numerical integrations of the equations of motion of the five outer planets of the solar system from -500,000 years to +500,000 years. From their graphs, we find that Jupiter's eccentricity can vary in a cyclic curve from approximately 0.027 to 0.06, Saturn's eccentricity from 0.012 to 0.085 and Uranus' eccentricity from 0.008 to 0.07. Thus, we also study a Jupiter-like satellite system with $e_1 = 0.06$ and $\mu = 1100$, a Saturn-like satellite system with $e_1 = 0.085$ and $\mu = 3500$ and a Uranus-like system with $e_1 = 0.07$ and $\mu=2.28\times10^4$.

We have now reduced the number of initial parmeters to be studied to four: α_0, e_0, f_{c0} and f_{1c0}. The satellite's initial parameters e_0, α_0 and f_{c0} are taken to vary over the same ranges as in the circular case, while f_{1c0} is taken to vary from 0° to 360°. The changes in the orbital elements as functions of the satellite's and the Sun's initial true anomaly at conjunction are found both numerically and anlytically for a variety of initial parameters.

The general shapes of each of the curves Δe, $\Delta\varpi$ and $\Delta\epsilon$ as a function of f_{c0} remain unchanged from those of the circular case for the complete range of values studied for the initial parameters. The curve for $\Delta\alpha$ is not the same, since $\Delta\alpha$ is no longer always zero. All the curves remain cyclic over the range of $f_{c0} = 0°$ to 360°.

Δe and $\Delta\alpha$ are still zero or approximately zero depending on the value of f_{1c0} at the mirror configurations or near mirror configurations found at $f_{c0} = 0°$ and $f_{c0}=180°$. Note that because the Sun's orbit is now elliptical, the three bodies will only be collinear with their velocity vectors perpendicular to the line drawn through the three bodies, when both the satellite and the Sun are located at their respective pericentres or apocentres. In other words, a perfect mirror configuration will only occur when either $f_{c0} = 0°$ or $f_{c0} = 180°$ and either $f_{1c0} = 0°$ or $f_{1c0} = 180°$.

Substitution of f_{1c0} = 0° or 180° and f_{c0} = 0° or 180° into Table 4.4(a), confirms that Δe is always zero at these points. Because we study only cases where e_1 is relatively small, near-mirror configurations occur whenever f_{c0} = 0° or f_{c0}=180° regardless of the value of f_{1c0}. Hence the graphs of $\Delta\sigma$ vs. f_{c0} show that Δe and $\Delta\alpha$ are approximately zero for all values of f_{1c0} as long as f_{c0} = 0° or f_{c0} = 180°.

The Δe and $\Delta\alpha$ graphs still have extrema located at a value for f_{c0} close to the location of the extrema of the circular case. Obviously, the further e_1 is removed from zero, the further removed the extrema are from the circular case. But again we are dealing with small values of e_1, so the differences between the elliptical and circular cases are small.

Similarly $\Delta\varpi$ and $\Delta\epsilon$ still have their extrema occurring at the mirror-configurations or near mirror configurations found at f_{c0} = 0°, 180°, 360°,... etc. Δe and $\Delta\alpha$ no longer display an exact odd symmetry about f_{c0} = 180°, but they are still very close to being symmetric. Likewise, $\Delta\epsilon$ and $\Delta\varpi$ are almost evenly symmetric about f_{c0} = 180°.

Figures 4.2(a) to (d) The variations in the changes of the satellite's orbital elements, ie (a) Δe, (b) $\Delta\alpha$, (c) $\Delta\epsilon$ and (d) $\Delta\varpi$, over one synodic period with the satellite's true anomaly f_{c0} at the initial conjunction for nine values of the Sun's true anomaly f_{1c0} at the initial conjunction.

The data used here is that of a typical Jupiter-Gallilean satellite system where e=0.01, α = 0.0025, μ = 1100 and e_1= 0.048. The dashed lines represent those curves whose values of f_{1c0} are greater than 180°.

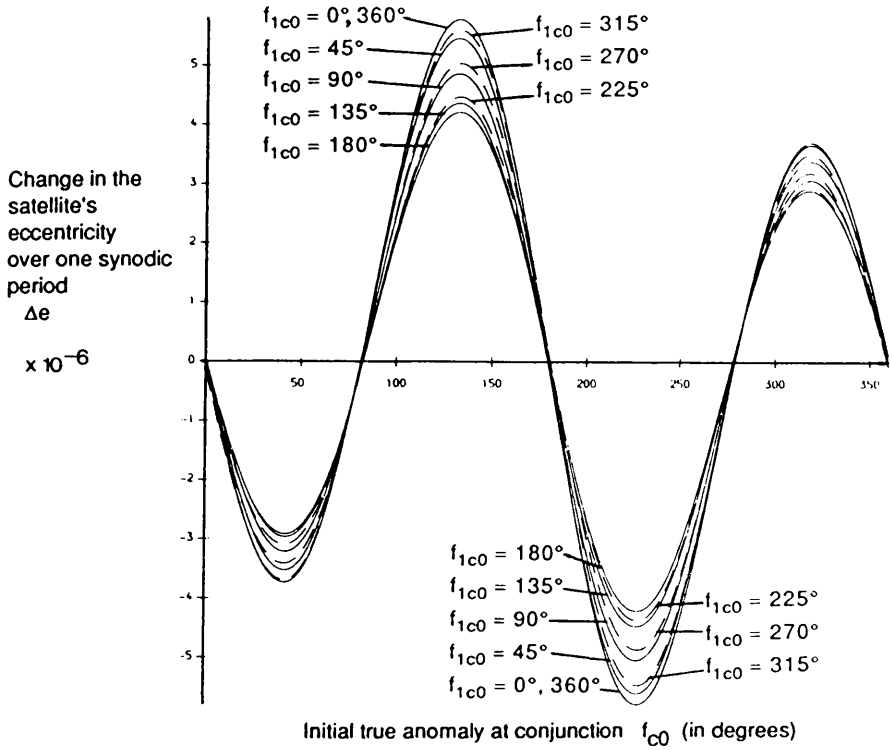
Change in the satellite's eccentricity over one synodic period
Δe
x 10⁻⁶
f1c0 = 0°, 360°
f1c0 = 45°
f1c0 = 90°
f1c0 = 135°
f1c0 = 180°
f1c0 = 315°
f1c0 = 270°
f1c0 = 225°
f1c0 = 180°
f1c0 = 135°
f1c0 = 90°
f1c0 = 45°
f1c0 = 0°, 360°
f1c0 = 225°
f1c0 = 270°
f1c0 = 315°
Initial true anomaly at conjunction fc0 (in degrees)

(a)

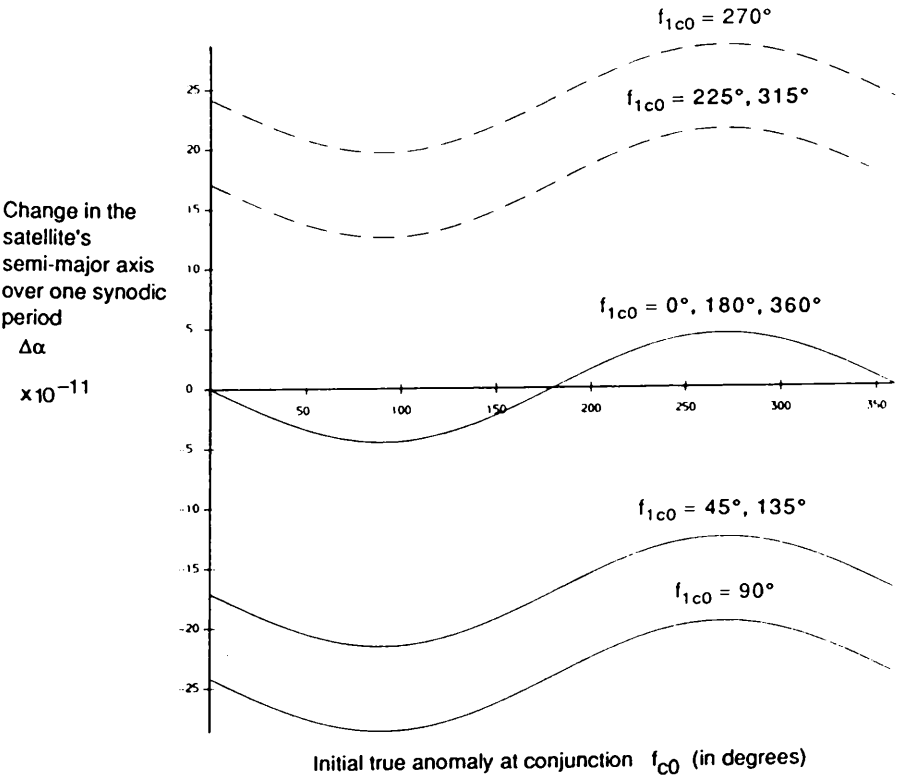
Change in the satellite's semi-major axis over one synodic period
Δα
x10⁻¹¹
f1c0 = 270°
f1c0 = 225°, 315°
f1c0 = 0°, 180°, 360°
f1c0 = 45°, 135°
f1c0 = 90°
Initial true anomaly at conjunction fc0 (in degrees)

(b)

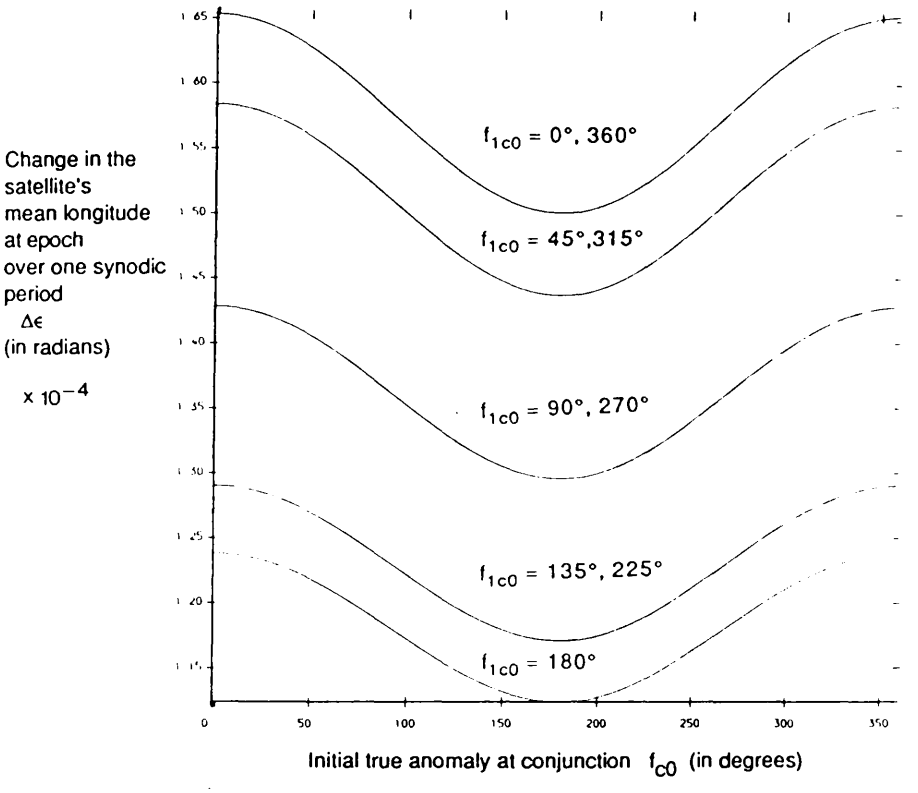
Change in the satellite's mean longitude at epoch over one synodic period
Δϵ
(in radians)
x 10⁻⁴
f1c0 = 0°, 360°
f1c0 = 45°,315°
f1c0 = 90°, 270°
f1c0 = 135°, 225°
f1c0 = 180°
0
50
100
150
200
250
300
350
Initial true anomaly at conjunction fc0 (in degrees)

(c)

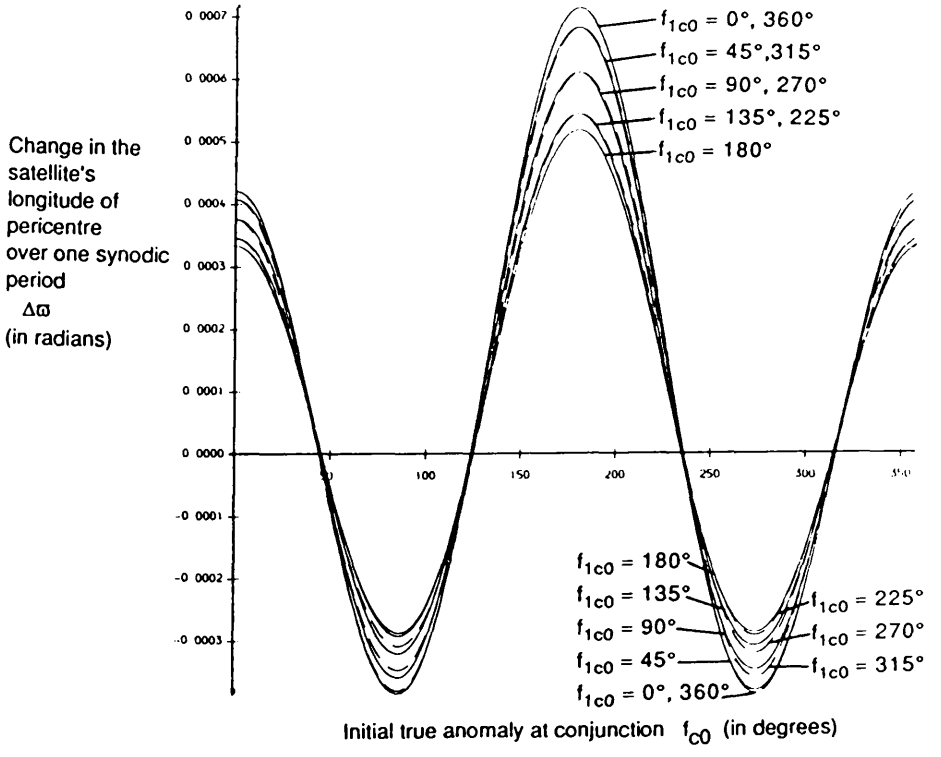
Change in the satellite's longitude of pericentre over one synodic period
Δϖ
(in radians)
0 0007
0 0006
0 0005
0 0004
0 0003
0 0002
0 0001
0 0000
-0 0001
-0 0002
-0 0003
f1c0 = 0°, 360°
f1c0 = 45°,315°
f1c0 = 90°, 270°
f1c0 = 135°, 225°
f1c0 = 180°
100
150
200
250
300
f1c0 = 180°
f1c0 = 135°
f1c0 = 90°
f1c0 = 45°
f1c0 = 0°, 360°
f1c0 = 225°
f1c0 = 270°
f1c0 = 315°
Initial true anomaly at conjunction fc0 (in degrees)

(d)

All these similarities to the circular case can be easily seen in Figures 4.2 and 4.3, which give fairly typical examples of the relationship between $\Delta\sigma$ and f_{c0} for a range of values of f_{1c0} varying from 0° to 360°. Both figures show the results for an approximation to the same Jupiter-Callisto system portrayed in Chapter 3 where e_0, α_0 and μ are taken to be 0.01, 0.0025 and 1100 respectively and the new initial parameter e_1 is chosen to be Jupiter's current eccentricity of 0.048.

Figures 4.2 show the variations of $\Delta\sigma$ as a function of f_{c0} for nine values of f_{1c0} ranging from 0° to 360° at intervals of 45°. The dashed lines indicate those curves whose values of f_{1c0} are greater than 180°.

Figures 4.3 indicate the location of the circular case's equivalent curve relative to the spread of the curves found in Figures 4.2 for the elliptical case. For greater clarity, only those curves corresponding to f_{1c0} = 0°, 45°, 90°, 135° and 180° are included. The dashed line now represents the curve for the circular case. Both Figures 4.2 and 4.3 are derived from the analytical solution.

Figures 4.3(a) to (d) The same graphs as in Figures 4.2, except that the locations of the equivalent curves for the circular case (dashed lines) are shown within the spread of the elliptical curves.

For greater clarity, only the elliptical curves whose values of f_{1c0} are less than or equal to 180° are included.

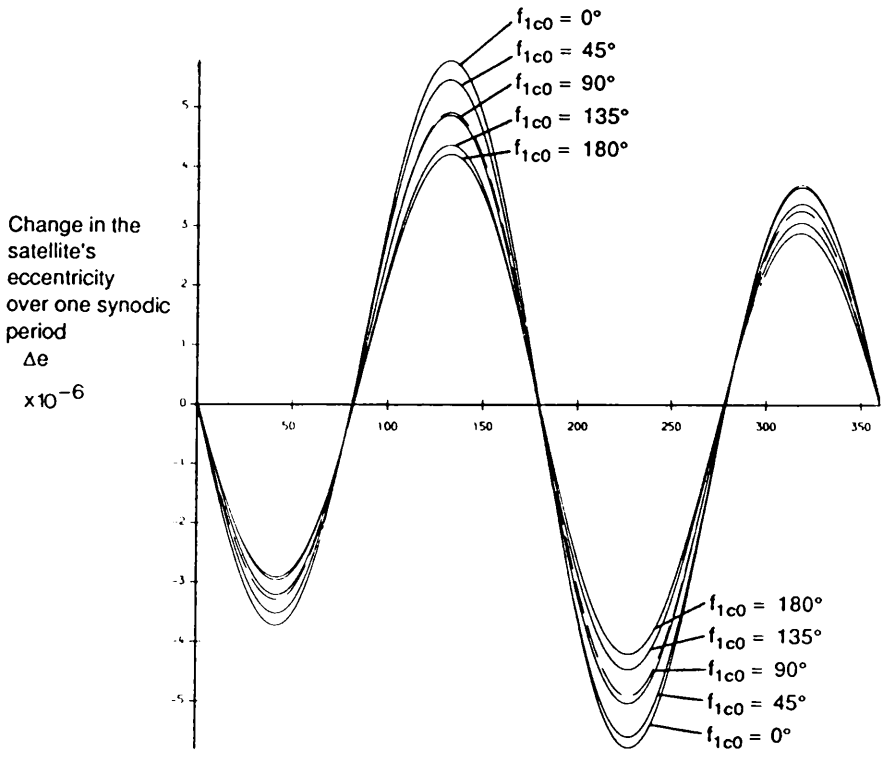
Change in the satellite's eccentricity over one synodic period
Δe
x10⁻⁶
f1c0 = 0°
f1c0 = 45°
f1c0 = 90°
f1c0 = 135°
f1c0 = 180°
f1c0 = 180°
f1c0 = 135°
f1c0 = 90°
f1c0 = 45°
f1c0 = 0°
Initial true anomaly at conjunction fc0 (in degrees)

(a)

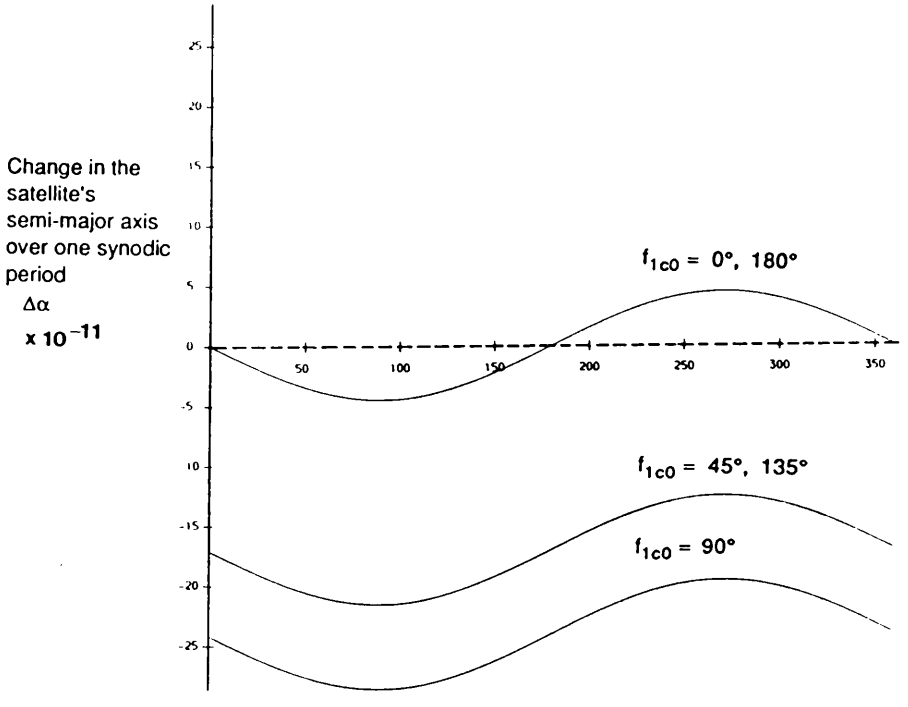
Change in the satellite's semi-major axis over one synodic period
Δα
x 10⁻¹¹
f1c0 = 0°, 180°
f1c0 = 45°, 135°
f1c0 = 90°
Initial true anomaly at conjunction fc0 (in degrees)

(b)

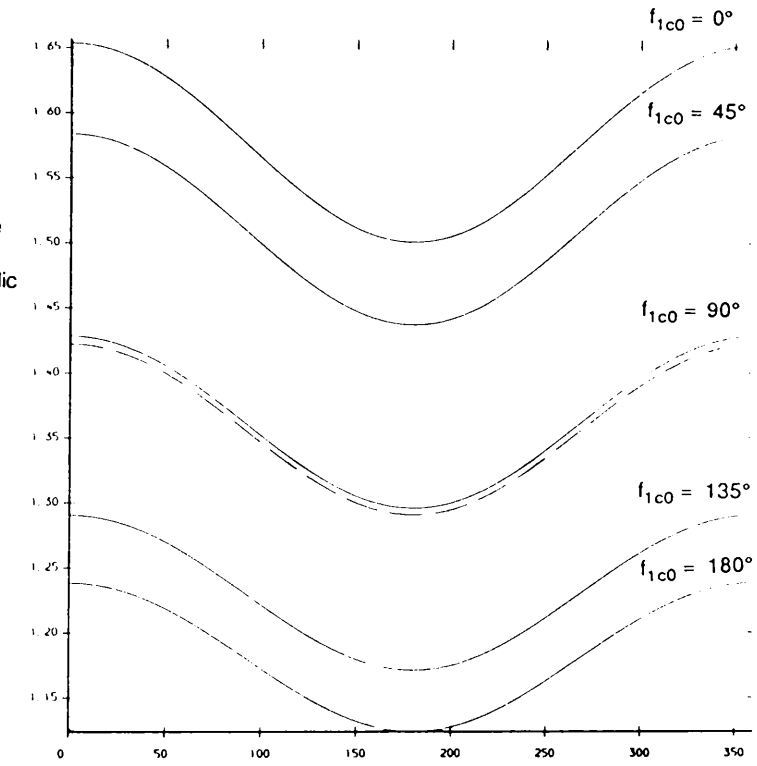

Change in the satellite's mean longitude at epoch over one synodic period
$\Delta\epsilon$
(in radians)
$\times 10^{-4}$

(c)

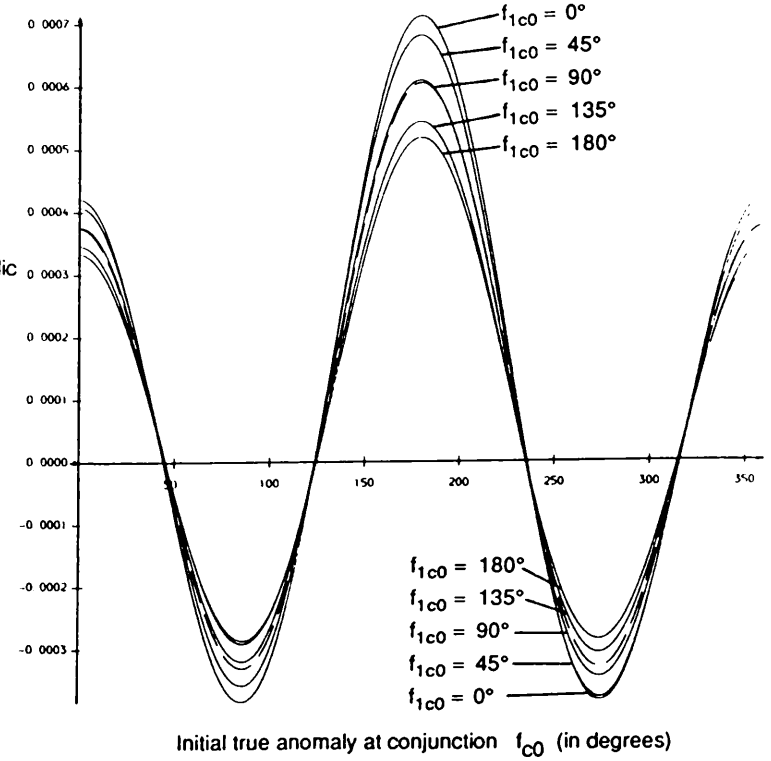

Change in the satellite's longitude of pericentre over one synodic period
$\Delta\varpi$
(in radians)

(d)

Figures 4.4 and 4.5 depict the same relationships as shown in Figures 4.2 and 4.3 for the same Jupiter-Callisto system, with the exception that the satellite eccentricity has now been increased to e = 0.3.

Figures 4.2 to 4.5 show that the only marked effect of adding the eccentricity of the Sun, is to spread the values of $\Delta\sigma$ at a particular f_{c0} about the corresponding circular value for $\Delta\sigma$. The range of $\Delta\sigma$'s at each f_{c0} correspond to the different values of the Sun's intitial true anomaly at conjunction f_{1c0}. For the Δe and $\Delta\varpi$ curves, the spread of values at a particluar f_{c0} is largest at the extrema and virtually nothing at the zeros.

The maxima have their largest values at $f_{1c0} = 0°$, decrease to their smallest values at $f_{1c0} = 180°$ and then increase back to their largest values at $f_{1c0} = 360°$. Likewise, the minima have their smallest values at $f_{1c0} = 0°$, increase to their largest values at $f_{1c0} = 180°$ and then decrease back to their smallest values at $f_{1c0}=360°$.

Figures 4.4(a) to (d) The variation of $\Delta\sigma$ as a function of f_{c0} and f_{1c0} for the same Jupiter-Gallilean satellite system as found in Figures 4.2, with the exception that the satellite's eccentricity is now taken to be e=0.3. σ is alternatively e, α, ϵ and ϖ for Figures (a) through to (d) respectively.

The dashed lines representing those curves with f_{1c0} greater than 180° are now virtually indistinguishable from the related curves whose f_{1c0} are less than 180° for Δe, $\Delta\varpi$ and $\Delta\epsilon$.

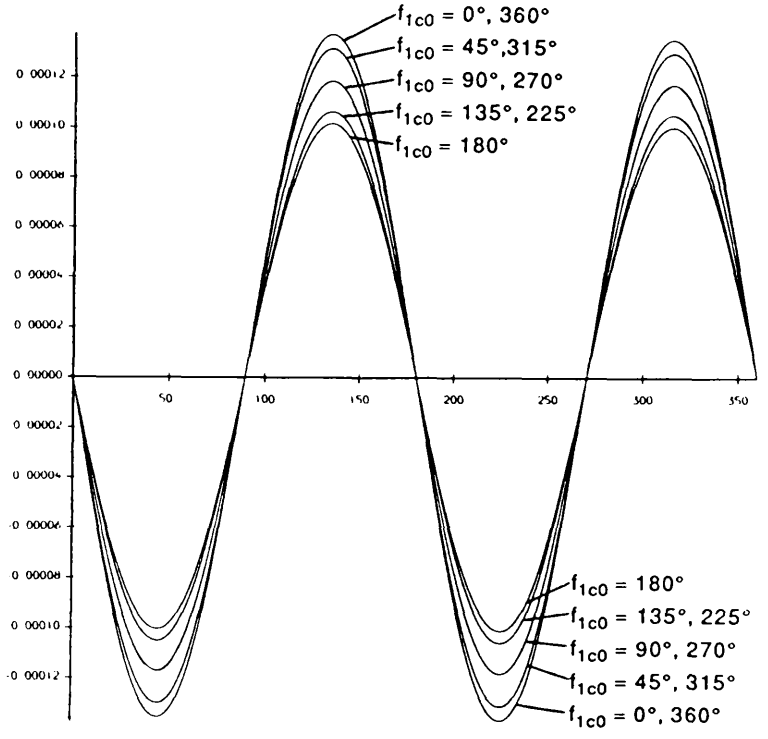

Change in the satellite's eccentricity over one synodic period
Δe

(a)

Initial true anomaly at conjunction f_{c0} (in degrees)

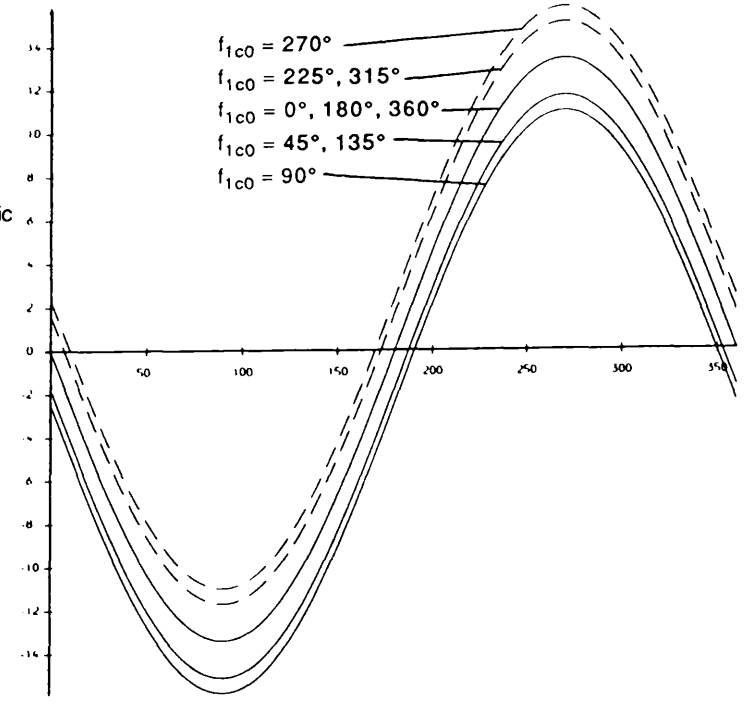

Change in the satellite's semi-major axis over one synodic period
$\Delta\alpha$
$\times 10^{-10}$

(b)

Initial true anomaly at conjunction f_{c0} (in degrees)

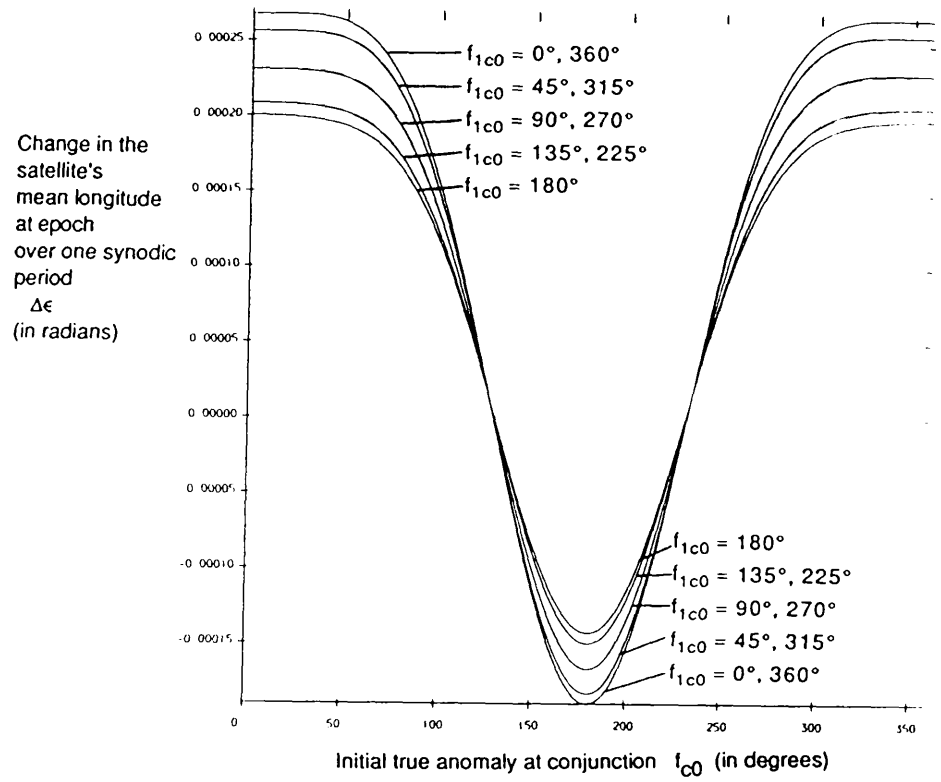
Change in the satellite's mean longitude at epoch over one synodic period
Δϵ
(in radians)
0 00025
0 00020
0 00015
0 00010
0 00005
0 00000
-0 00010
-0 00015
f_{1c0} = 0°, 360°
f_{1c0} = 45°, 315°
f_{1c0} = 90°, 270°
f_{1c0} = 135°, 225°
f_{1c0} = 180°
f_{1c0} = 180°
f_{1c0} = 135°, 225°
f_{1c0} = 90°, 270°
f_{1c0} = 45°, 315°
f_{1c0} = 0°, 360°
0
50
100
150
200
250
300
350
Initial true anomaly at conjunction f_{c0} (in degrees)

(c)

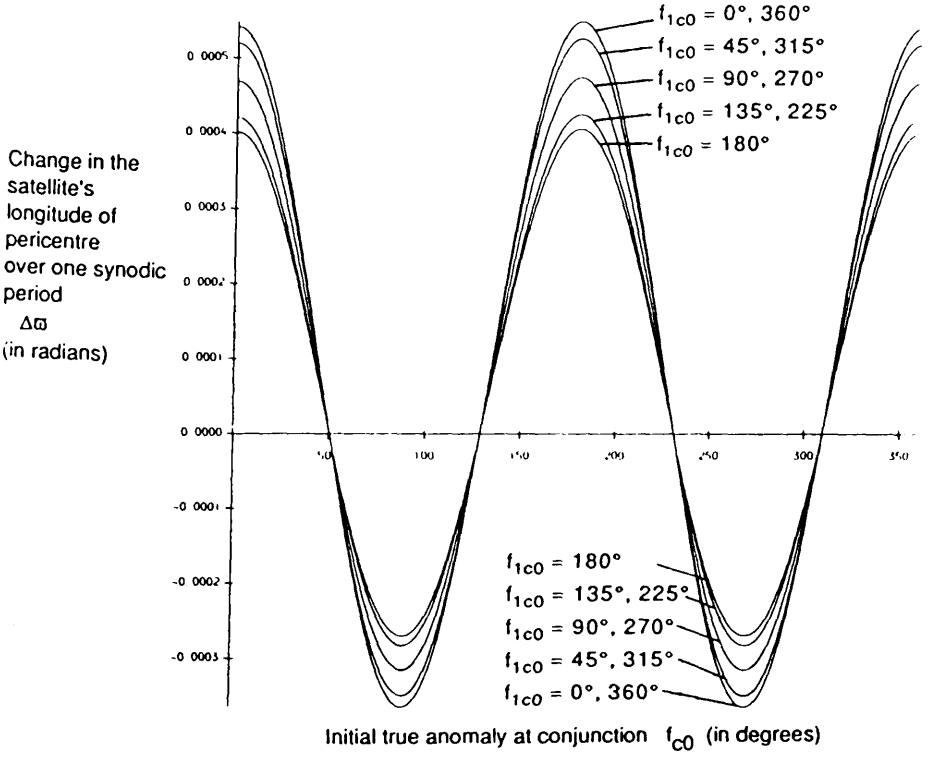
Change in the satellite's longitude of pericentre over one synodic period
Δϖ
(in radians)
0 0005
0 0004
0 0003
0 0002
0 0001
0 0000
-0 0001
-0 0002
-0 0003
f_{1c0} = 0°, 360°
f_{1c0} = 45°, 315°
f_{1c0} = 90°, 270°
f_{1c0} = 135°, 225°
f_{1c0} = 180°
100
300
f_{1c0} = 180°
f_{1c0} = 135°, 225°
f_{1c0} = 90°, 270°
f_{1c0} = 45°, 315°
f_{1c0} = 0°, 360°
Initial true anomaly at conjunction f_{c0} (in degrees)

(d)

Figures 4.2 to 4.5 (c) and (d) are approximately evenly symmetric about $f_{1c0} = 180°$, while Figure 4.4(a) shows that Δe is also approximately evenly symmetric about $f_{1c0} = 180°$, if e_0 is large enough. Thus,

$$\Delta\sigma\ (f_{1c0} + 180°) \approx \Delta\sigma\ (f_{1c0}) \qquad \text{for } \sigma = \epsilon, \varpi \text{ and } e, \text{ if } e_0 \text{ is large.}$$

The $\Delta\alpha$ curve is approximately oddly symmetric about $f_{1c0} = 180°$. The values of $\Delta\alpha$ for a specific f_{c0} first decrease to a minima at $f_{1c0} = 90°$, then increase to a maxima at $f_{1c0} = 270°$ and then return to their original values at $f_{1c0} = 360°$. Thus

$$\Delta\alpha(f_{1c0} + 180°) \approx -\Delta\alpha(f_{1c0}) + 2\Delta\alpha(f_{1c0} = 0)$$

Figures 4.3 and 4.5 show that the appropriate curve for the circular case consistently falls at the centre of the spread due to varying f_{1c0}. The closest elliptical curve to the circular case is that corresponding to $f_{1c0} = 90°$ or 270°. Obviously within an elliptical orbit, the Sun will be moving at its most circular-like motion when it is located on its semi-minor axis (ie when its true anomaly is 90° or 270°).

Figures 4.5(a) to (d) The same graphs as in Figures 4.4, except that the locations of the equivalent curves for the circular case (dashed line) are shown within the spread of the elliptical curves.

Only the elliptical curves whose values of f_{1c0} are less than or equal to180° are plotted here.

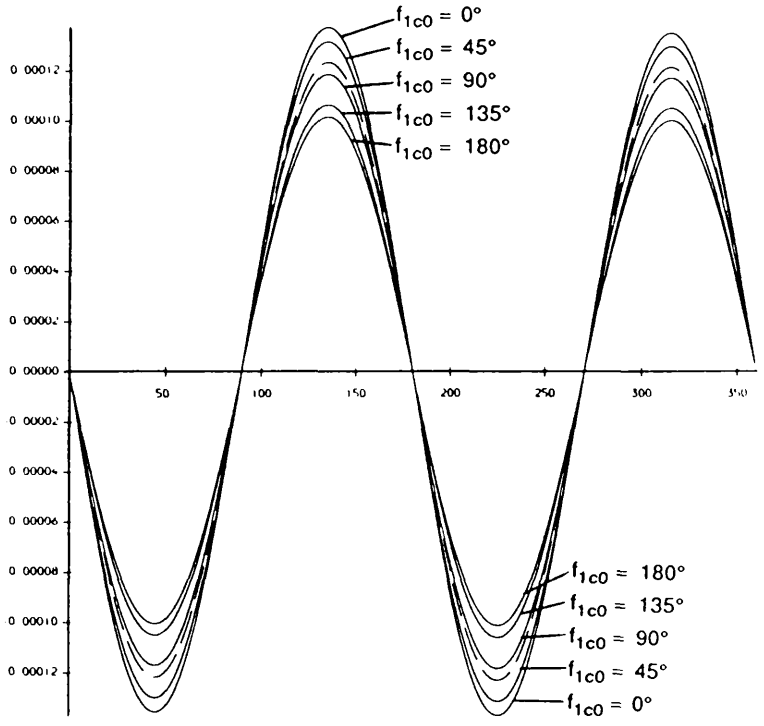

Change in the satellite's eccentricity over one synodic period Δe

(a)

Initial true anomaly at conjunction f_{c0} (in degrees)

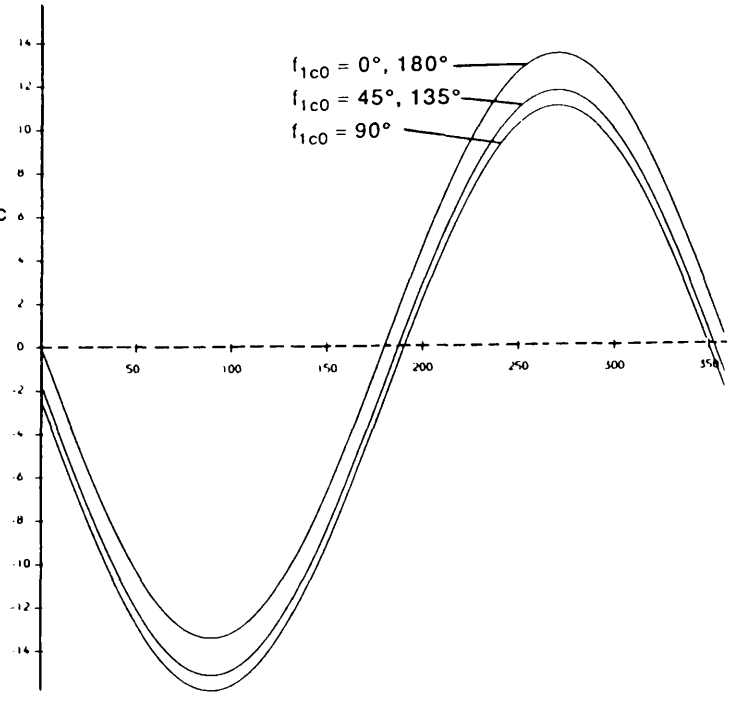

Change in the satellite's semi-major axis over one synodic period $\Delta\alpha$ $\times 10^{-10}$

(b)

Initial true anomaly at conjunction f_{c0} (in degrees)

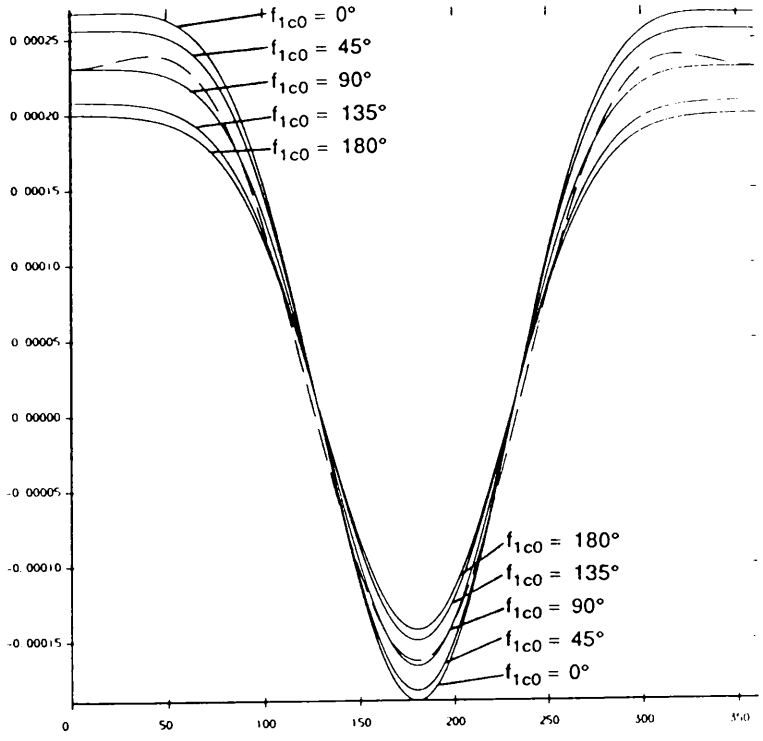
f_{1c0} = 0°
f_{1c0} = 45°
f_{1c0} = 90°
f_{1c0} = 135°
f_{1c0} = 180°
f_{1c0} = 180°
f_{1c0} = 135°
f_{1c0} = 90°
f_{1c0} = 45°
f_{1c0} = 0°
0 00025
0 00020
0 00015
0 00010
0 00005
0 00000
-0 00005
-0 00010
-0 00015
0
50
100
150
200
250
300
Change in the satellite's mean longitude at epoch over one synodic period
$\Delta\epsilon$
(in radians)
Initial true anomaly at conjunction f_{c0} (in degrees)

(c)

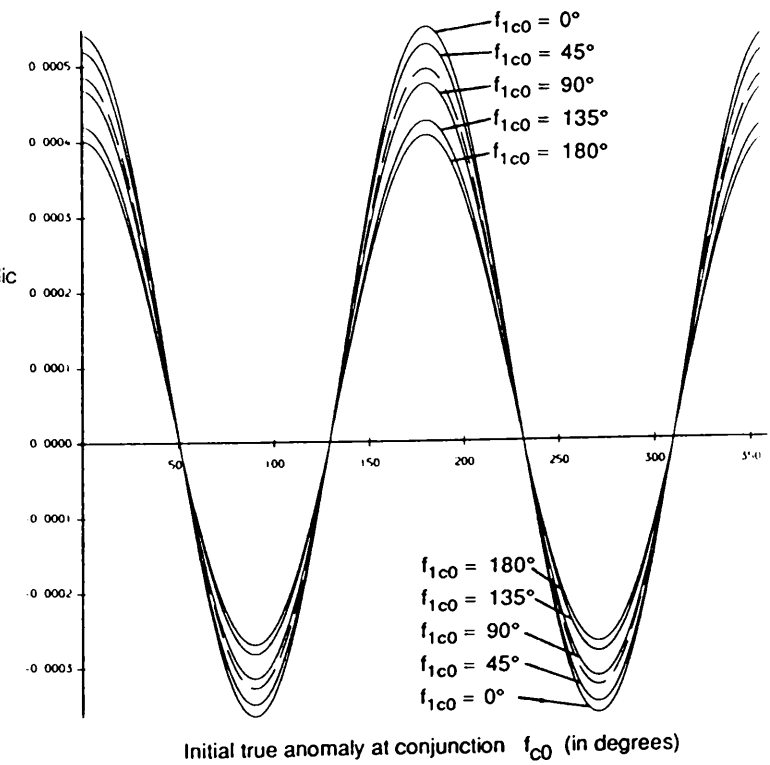
f_{1c0} = 0°
f_{1c0} = 45°
f_{1c0} = 90°
f_{1c0} = 135°
f_{1c0} = 180°
f_{1c0} = 180°
f_{1c0} = 135°
f_{1c0} = 90°
f_{1c0} = 45°
f_{1c0} = 0°
0 0005
0 0004
0 0003
0 0002
0 0001
0 0000
0 0001
-0 0002
-0 0003
50
100
150
200
250
300
Change in the satellite's longitude of pericentre over one synodic period
$\Delta\varpi$
(in radians)
Initial true anomaly at conjunction f_{c0} (in degrees)

(d)

The effect of increasing e_1 to its likely maximum for each planetary system is very small. The spread in the change of an orbital element for a specific value of f_{c0} caused by varying f_{1c0} is increased slightly, but that is all.

Generally we can conclude that for the small values of the planet's eccentricities e_1 which we are interested in studying, the changes in the orbital elements as a function of f_{c0} are really not that much different from the equivalent changes in the orbital elements for the circular case.

Figures 4.6 and 4.7 compare the analytical and numerical solutions for a few of the cases depicted in Figures 4.2 through to 4.5. The dashed lines represent the numerical solutions, while the solid lines represent the analytical solutions. In the interests of brevity we display only those curves where f_{1c0} is either 0° or 180°, since the analytical solutions for Δe and also $\Delta\varpi$ are closest to the numerical solutions at f_{1c0}=180° and furtherest removed from the numerical solutions at f_{1c0}=0°.

Clearly, when the Sun is in conjunction at its pericentre (ie f_{1c0} = 0°), it will be at its closest approach to the satellite, and therefore the solar perturbations which cause Δe will be at their greatest. Conversely, the Sun will have its weakest effect on the satellite's orbit when it is located at its apocentre during the conjunction (ie f_{1c0}=180°). As the solar perturbations become larger, the value of the biggest neglected term in the analytical solution increases, causing the difference between the numerical and analytical solutions to also increase. Hence the difference between the two solutions is greatest at f_{1c0}=0°.

Figures 4.6(a) to (d) A comparison between the numerical and analytical solutions for (a) Δe, (b) $\Delta\alpha$, (c) $\Delta\epsilon$ and (d)$\Delta\varpi$. For each change in the orbital element $\Delta\sigma$, two cases (i) f_{1c0} = 0° and (ii) f_{1c0} = 180° are shown.

The dashed lines represent the numerical solution and the solid, the analytical solution. The data used here is the same Jupiter-Gallilean satellite system found in Figures 4.2 and 4.3.

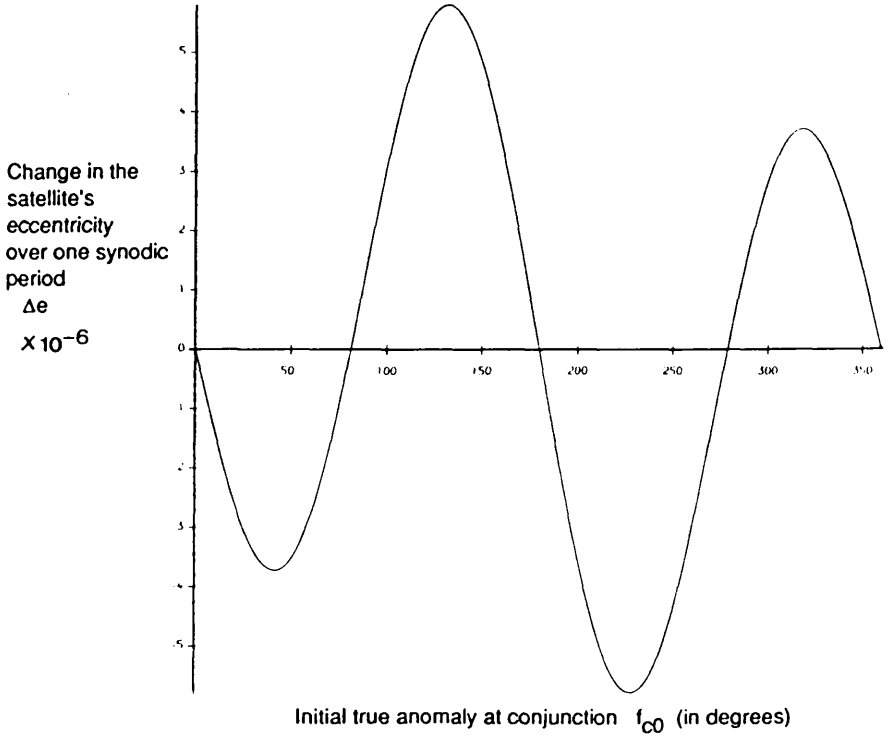
Change in the satellite's eccentricity over one synodic period
Δe
x 10⁻⁶
5
4
3
2
1
0
-1
-2
-3
-4
-5
50
100
150
200
250
300
350
Initial true anomaly at conjunction f_{c0} (in degrees)

(a) i

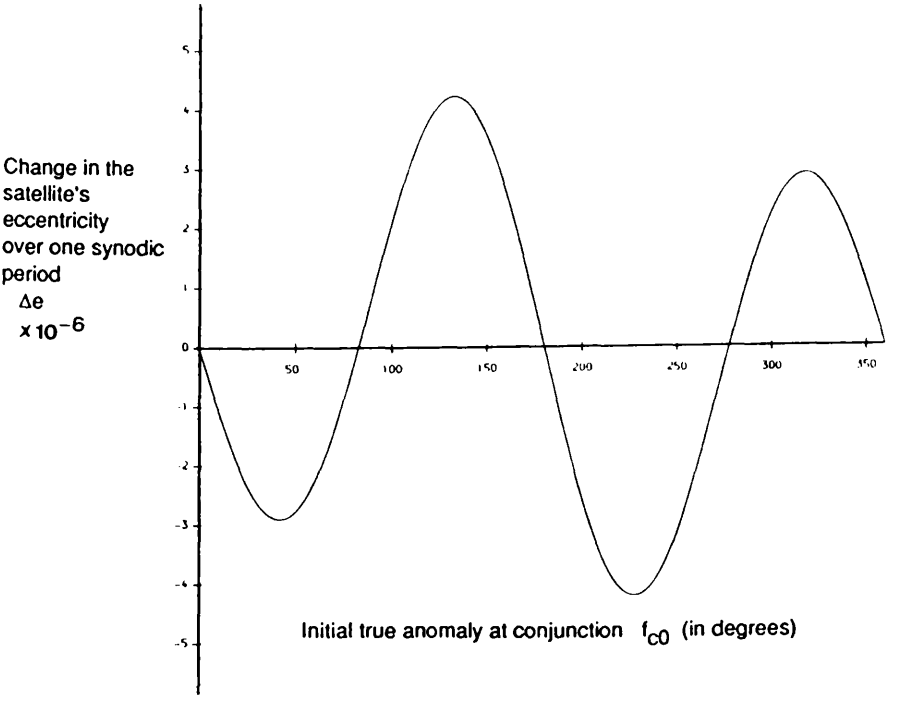
Change in the satellite's eccentricity over one synodic period
Δe
x 10⁻⁶
5
4
3
2
1
0
-1
-2
-3
-4
-5
50
100
150
200
250
300
350
Initial true anomaly at conjunction f_{c0} (in degrees)

(a) ii

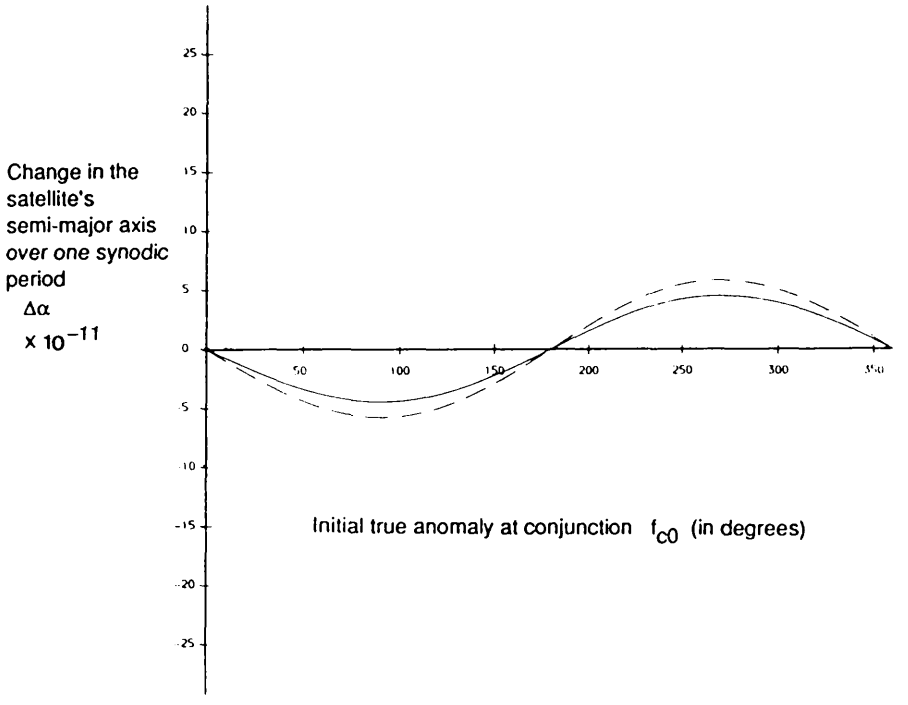
Change in the satellite's semi-major axis over one synodic period
Δα
x 10⁻¹¹
25
20
15
10
5
0
-5
-10
-15
-20
-25
50
100
150
200
250
300
Initial true anomaly at conjunction f_{c0} (in degrees)

(b) i

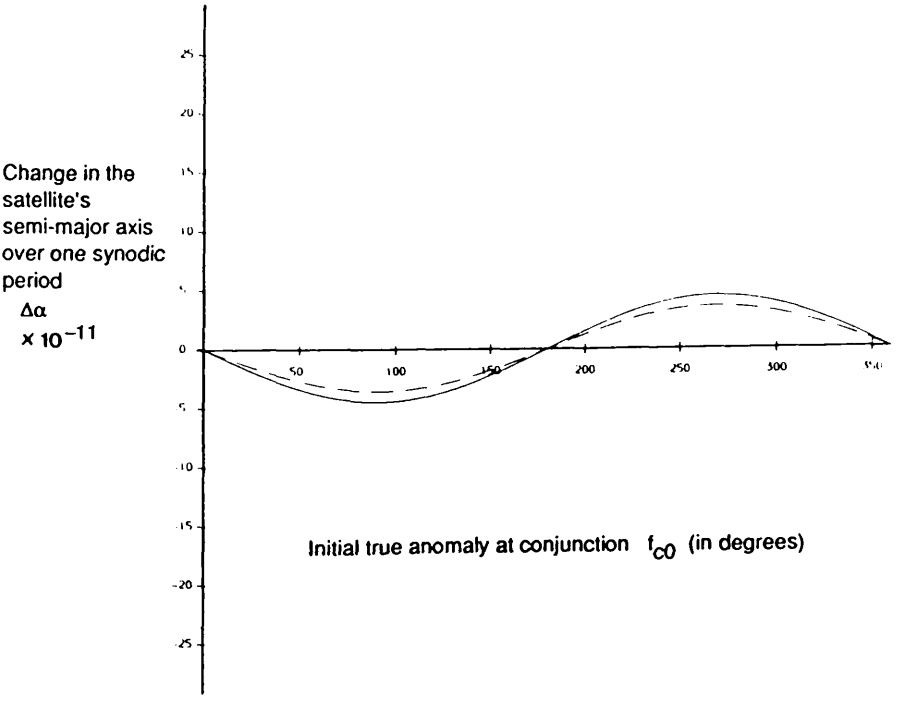
Change in the satellite's semi-major axis over one synodic period
Δα
x 10⁻¹¹
0
50
100
150
200
250
300
Initial true anomaly at conjunction f_{c0} (in degrees)

(b) ii

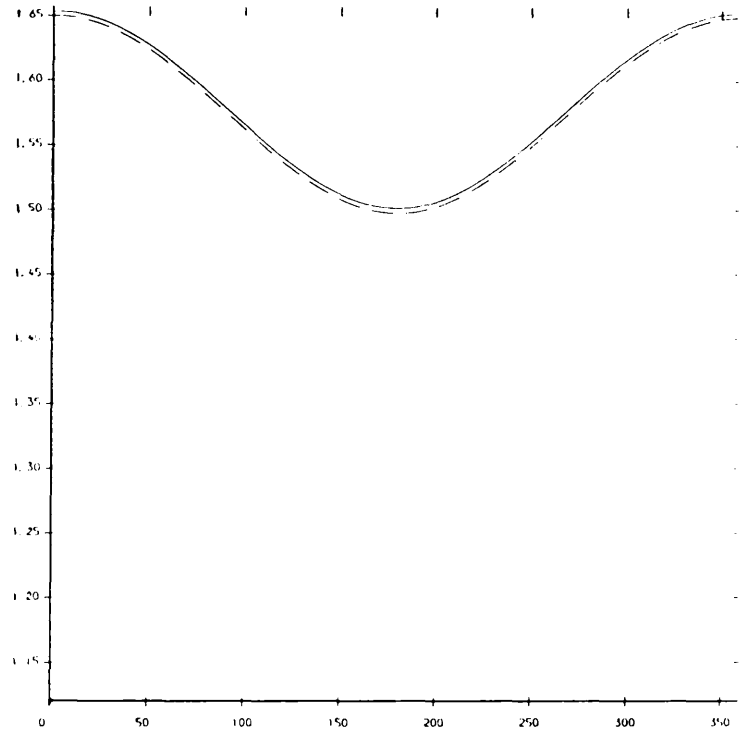
Change in the satellite's mean longitude at epoch over one synodic period
Δϵ
(in radians)
x 10⁻⁴
1.65
1.60
1.55
1.50
1.45
1.40
1.35
1.30
1.25
1.20
1.15
0
50
100
150
200
250
300
350
Initial true anomaly at conjunction f_c0 (in degrees)

(c) i

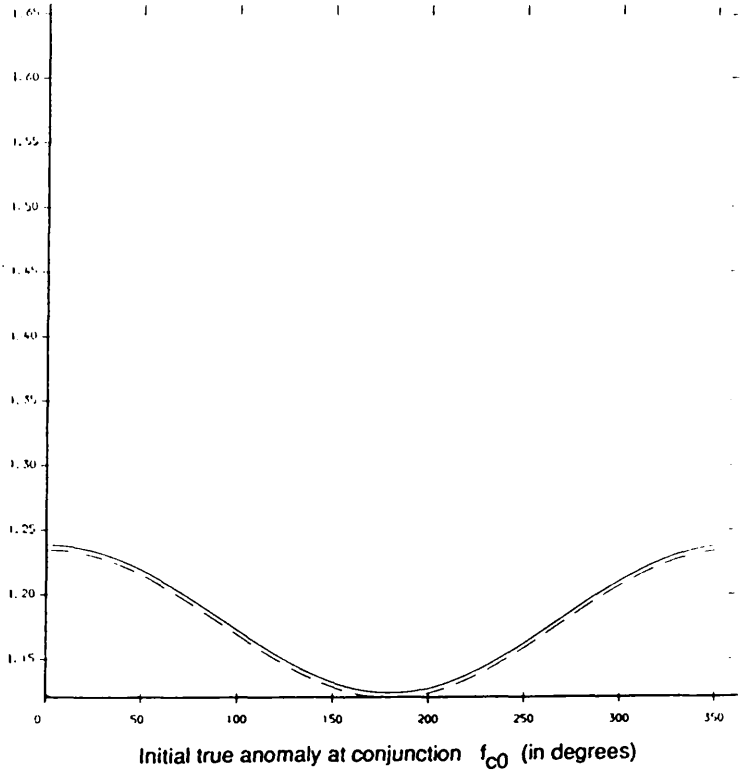
Change in the satellite's mean longitude at epoch over one synodic period
Δϵ
(in radians)
x 10⁻⁴
1.65
1.60
1.55
1.50
1.45
1.40
1.35
1.30
1.25
1.20
1.15
0
50
100
150
200
250
300
350
Initial true anomaly at conjunction f_c0 (in degrees)

(c) ii

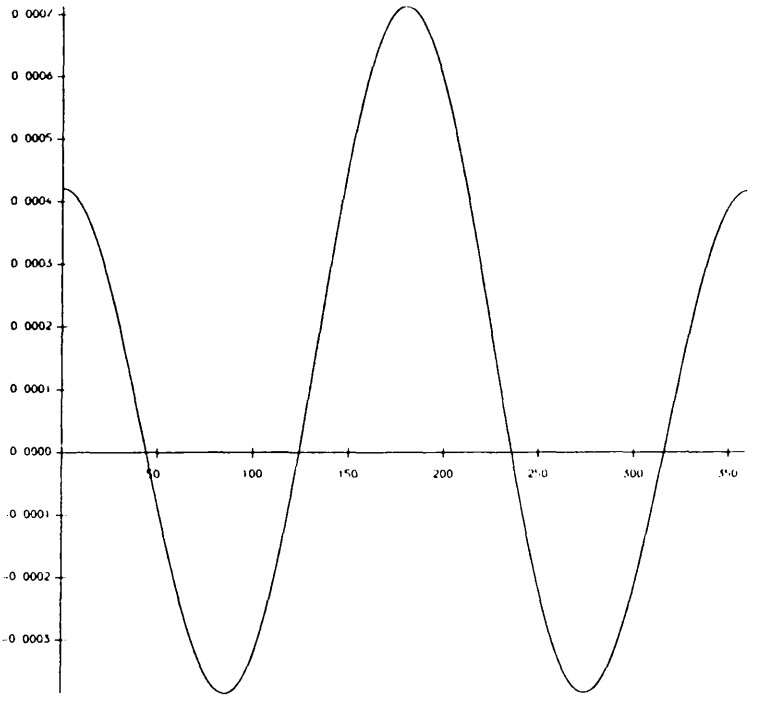
Change in the satellite's longitude of pericentre over one synodic period
Δϖ
(in radians)
0 0007
0 0006
0 0005
0 0004
0 0003
0 0002
0 0001
0 0000
-0 0001
-0 0002
-0 0003
100
150
200
250
300
350
Initial true anomaly at conjunction f_{c0} (in degrees)

(d)i

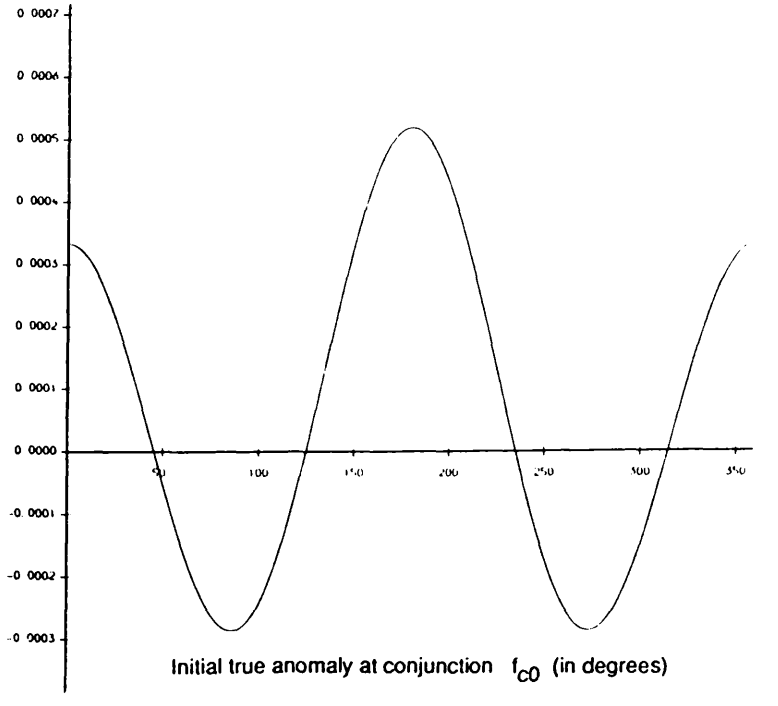
Change in the satellite's longitude of pericentre over one synodic period
Δϖ
(in radians)
0 0007
0 0006
0 0005
0 0004
0 0003
0 0002
0 0001
0 0000
-0 0001
-0 0002
-0 0003
100
150
200
250
300
350
Initial true anomaly at conjunction f_{c0} (in degrees)

(d)ii

Figures 4.6 show the changes in the orbital elements as a function of f_{c0} for the Jupiter-Callisto system, where the initial parameters are taken to be α_0=0.0025, μ = 1100, e_1 = 0.048 and e_0 = 0.01. Note that the analytical solutions for Δe and $\Delta\varpi$ are virtually indistinguishable from the numerical solution.

Figures 4.7 depict the same type of comparisons of the numerical and analytical solutions as in Figures 4.6, with the exception that the initial eccentricity e_0 is now increased to e_0=0.5. The differences between the analytical solution and the numerical solutions are now apparent. The average relative difference between the two solutions of Δe at f_{1c0} = 0° is about 0.1% for e=0.01 (Figure 4.6(a)i) and about 1.0% for e = 0.5 (Figure 4.7(a)i). These results are a great improvement on the accuracy of the second order circular analytical solution which can generally only allow the eccentricity to be increased to 0.3 before a relative error between the numerical and analytical solutions of 5.0% is reached.

Again, like the circular case, the worst approximations to the numerical solution occur at the extrema of the graphs. Therefore, we can again use the maximum change in the eccentricity or Δe_{max} as a measure of how accurately the analytical solution compares with the numerical solution for a range of initial parameters e_0, α_0 and μ.

The equations for Δe in the elliptical case are far more complicated than in the circular case and therefore cannot be easily optimized analytically with respect to f_{c0} and f_{1c0}, in order to find Δe_{max}. However from the graphs we already know that Δe is a maximum at f_{1c0} = 0°. Then since e_1 is small, we can easily use the circular

Figures 4.7(a) to (d) A comparison between the numerical and analytical solutions for $\Delta\sigma$ exactly the same as in Figures 4.6, with the exception that the satellite's eccentricity is now taken to be e=0.5.

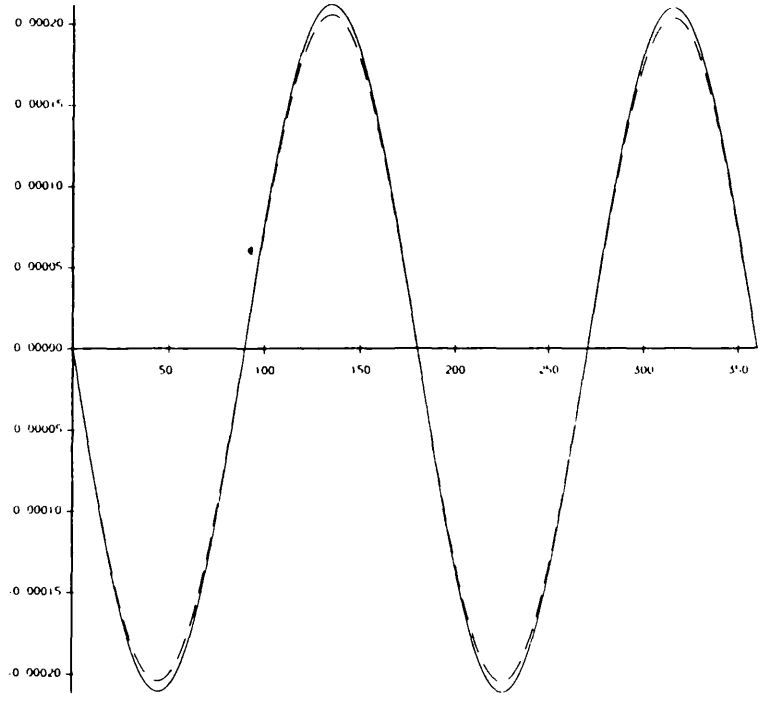
Change in the satellite's eccentricity over one synodic period Δe
0 00020
0 00015
0 00010
0 00005
0 00000
-0 00005
-0 00010
-0 00015
-0 00020
50
100
150
200
250
300
350
Initial true anomaly at conjunction f_{c0} (in degrees)

(a) i

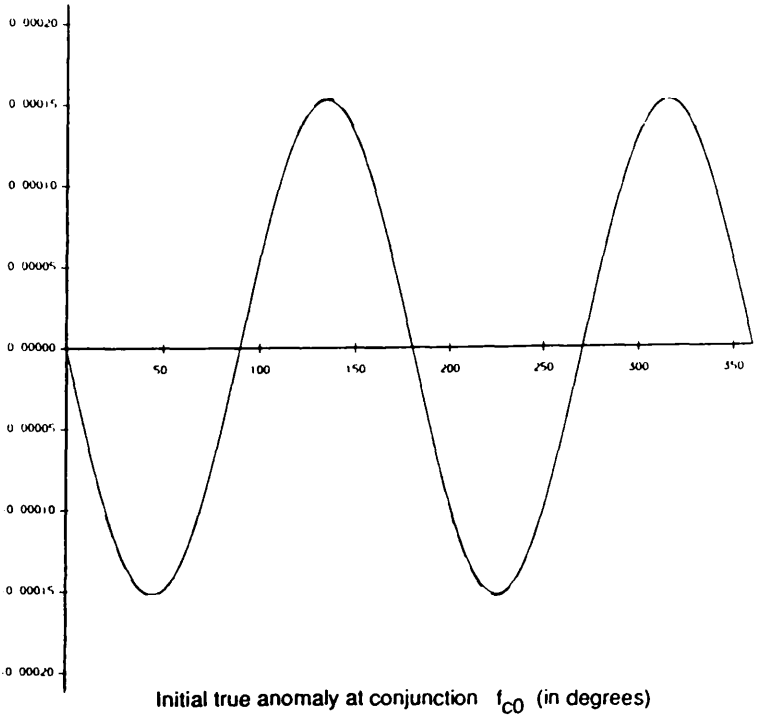
Change in the satellite's eccentricity over one synodic period Δe
0 00020
0 00015
0 00010
0 00005
0 00000
-0 00005
-0 00010
-0 00015
-0 00020
50
100
150
200
250
300
350
Initial true anomaly at conjunction f_{c0} (in degrees)

(a) ii

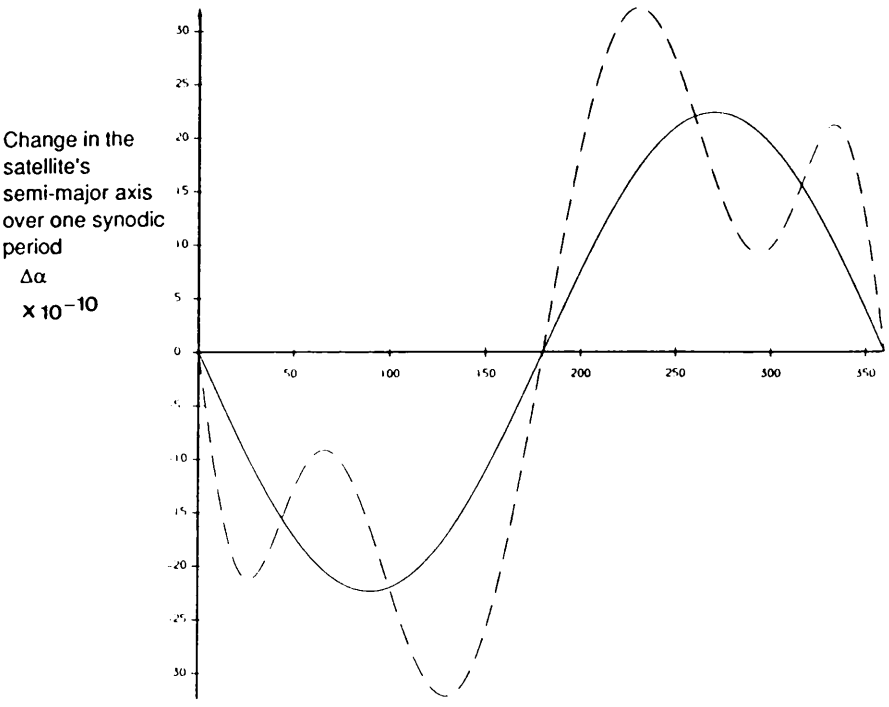
Change in the satellite's semi-major axis over one synodic period
Δα
x 10⁻¹⁰
50
100
150
200
250
300
350
Initial true anomaly at conjunction f_{c0} (in degrees)

(b) i

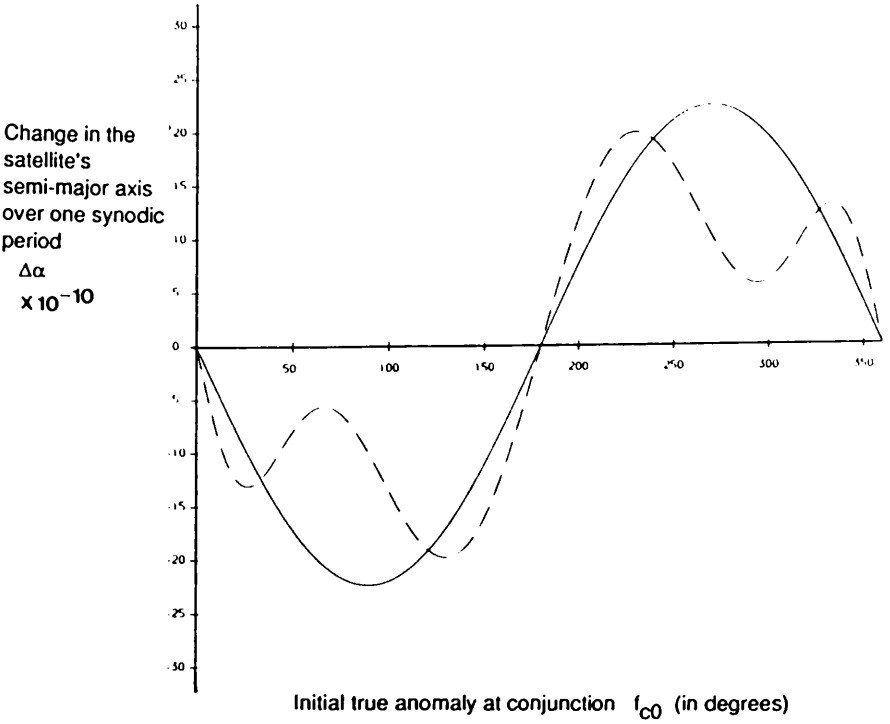
Change in the satellite's semi-major axis over one synodic period
Δα
x 10⁻¹⁰
50
100
150
200
300
Initial true anomaly at conjunction f_{c0} (in degrees)

(b) ii

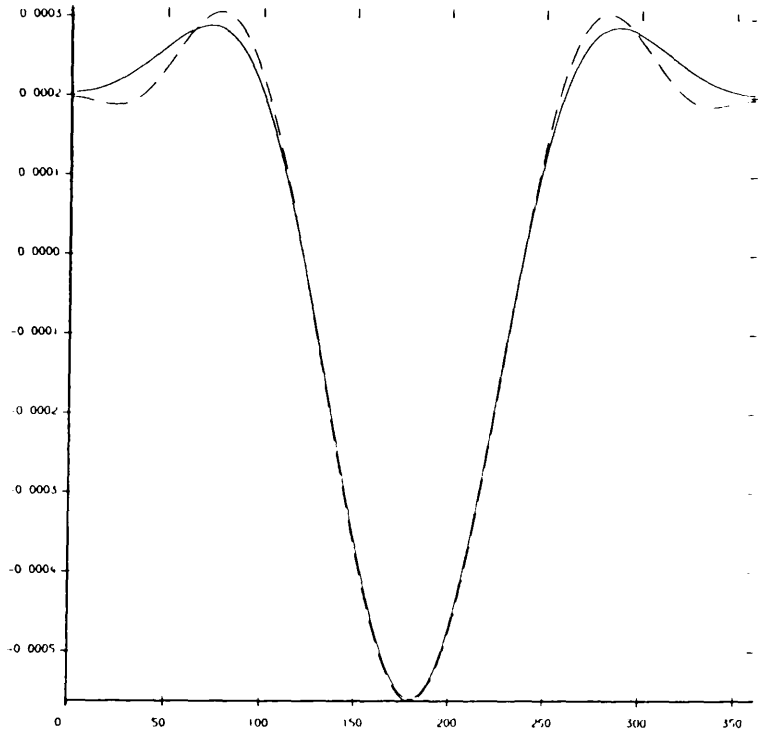
Change in the satellite's mean longitude at epoch over one synodic period Δϵ (in radians)
0 0003
0 0002
0 0001
0 0000
-0 0001
-0 0002
-0 0003
-0 0004
-0 0005
0
50
100
150
200
250
300
Initial true anomaly at conjunction f_{c0} (in degrees)

(c)i

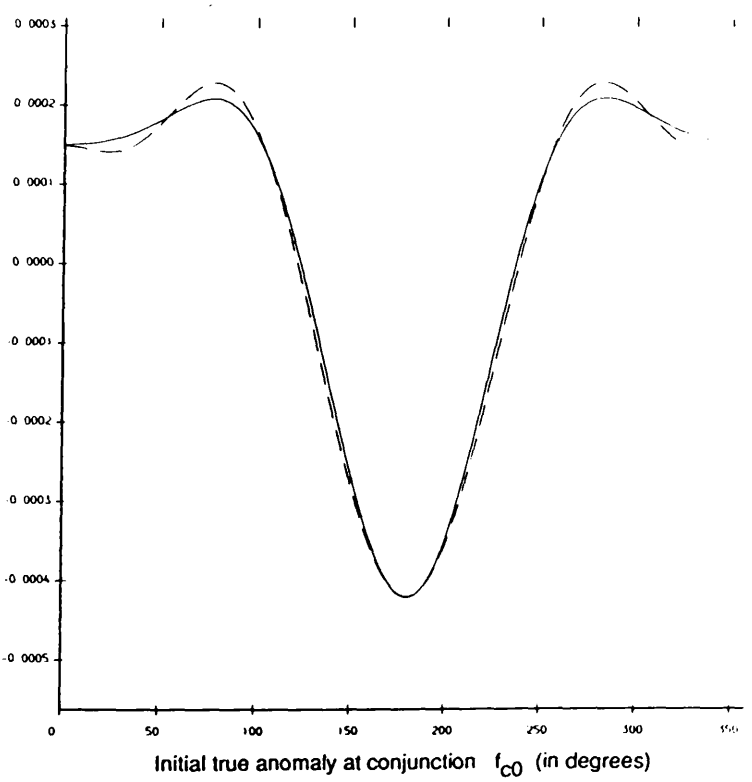
Change in the satellite's mean longitude at epoch over one synodic period Δϵ (in radians)
0 0003
0 0002
0 0001
0 0000
-0 0001
-0 0002
-0 0003
-0 0004
-0 0005
0
50
100
150
200
250
300
Initial true anomaly at conjunction f_{c0} (in degrees)

(c)ii

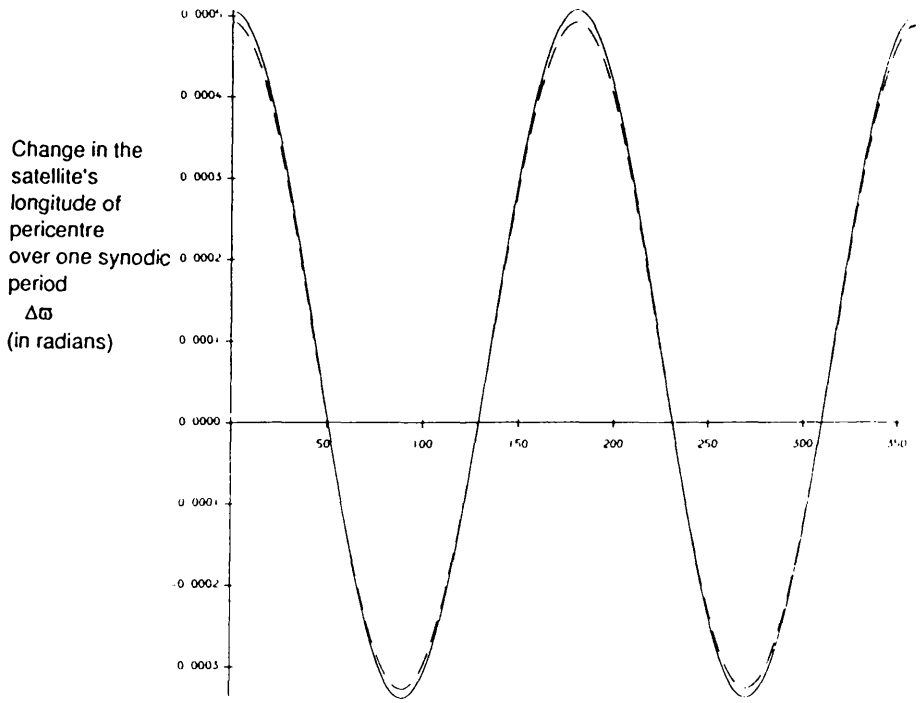
Change in the satellite's longitude of pericentre over one synodic period
Δϖ
(in radians)
0 0004
0 0003
0 0002
0 0001
0 0000
-0 0002
-0 0003
50
100
150
200
250
300
Initial true anomaly at conjunction f_{c0} (in degrees)

(d) i

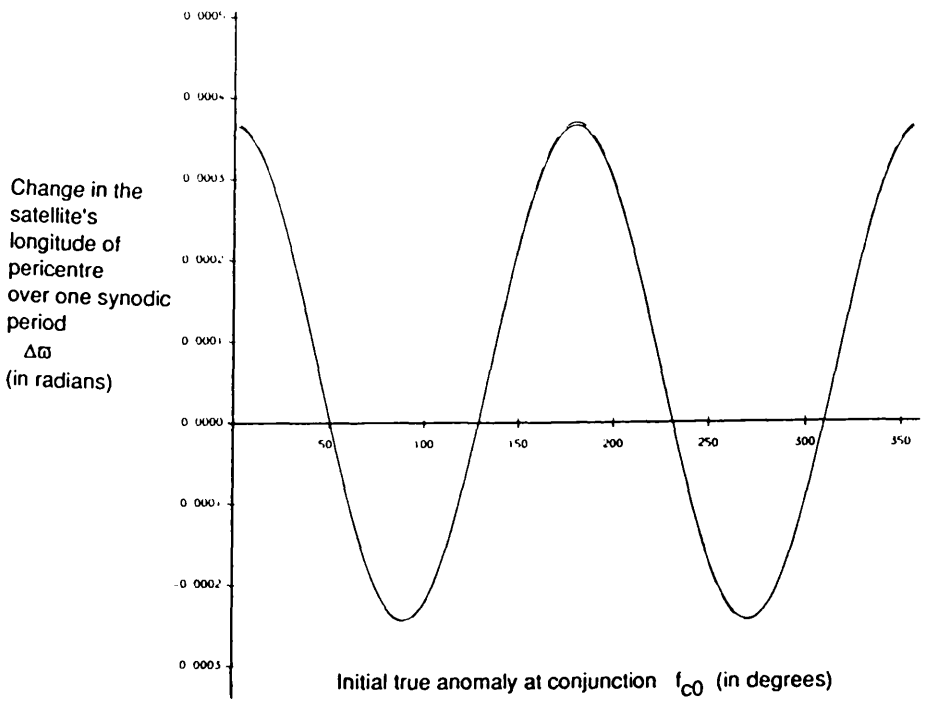
Change in the satellite's longitude of pericentre over one synodic period
Δϖ
(in radians)
0 0004
0 0003
0 0002
0 0001
0 0000
-0 0002
-0 0003
50
100
150
200
250
300
350
Initial true anomaly at conjunction f_{c0} (in degrees)

(d) ii

solution for Δe_{max} as a first approximation to the elliptical problem. Thus, we optimize the elliptical equation for Δe found in Table 4.4(a) numerically with respect to f_{c0}, keeping $f_{1c0} = 0°$ until the correct Δe_{max} as a function of f_{c0} and f_{1c0} is found, to the required accuracy of say 0.1%.

The three contours in Figures 4.8 indicate the points of 1%, 3% and 5% relative difference between the elliptical case's analytical and numerical solutions for the maximum possible change in the eccentricity (Δe_{max}) over one synodic period. The different figures (a) to (h) depict the error contours for each of the five planetary systems with various mass ratios μ and eccentricities e_1. Also plotted on the relevant figures are the major satellites of each satellite system. The upper regions of α in Figures 4.8 give theoretical values for Δe greater than 1; however, we are chiefly concerned with the lower regions of α and can therefore avoid the problem of dealing with Δe's or resulting eccentricities greater than 1.

Figures 4.8 (a) to (h) The contours in α_0 - e_0 space which indicate a 1%, 3% and 5% relative difference between the elliptical analytical and numerical solutions for the maximum possible change in the eccentricity or Δe_{max} over one synodic period.

The figures (a) through to (h) depict the error contours for satellites orbiting each of the following planets:

(a) Jupiter: $\mu = 1100$ and $e_1 = 0.048$

(b) " " $e_1 = 0.06$

(c) Saturn: $\mu = 3500$ and $e_1 = 0.056$

(d) " " $e_1 = 0.085$

(e) Uranus: $\mu = 2.28 \times 10^4$ and $e_1 = 0.047$

(f) " " $e_1 = 0.07$

(g) Earth: $\mu = 3.33 \times 10^5$ and $e_1 = 0.017$

(h) Mars: $\mu = 3.08 \times 10^6$ and $e_1 = 0.093$

The plus signs indicate the locations in α_0-e_0 space of the major satellites of each planet.

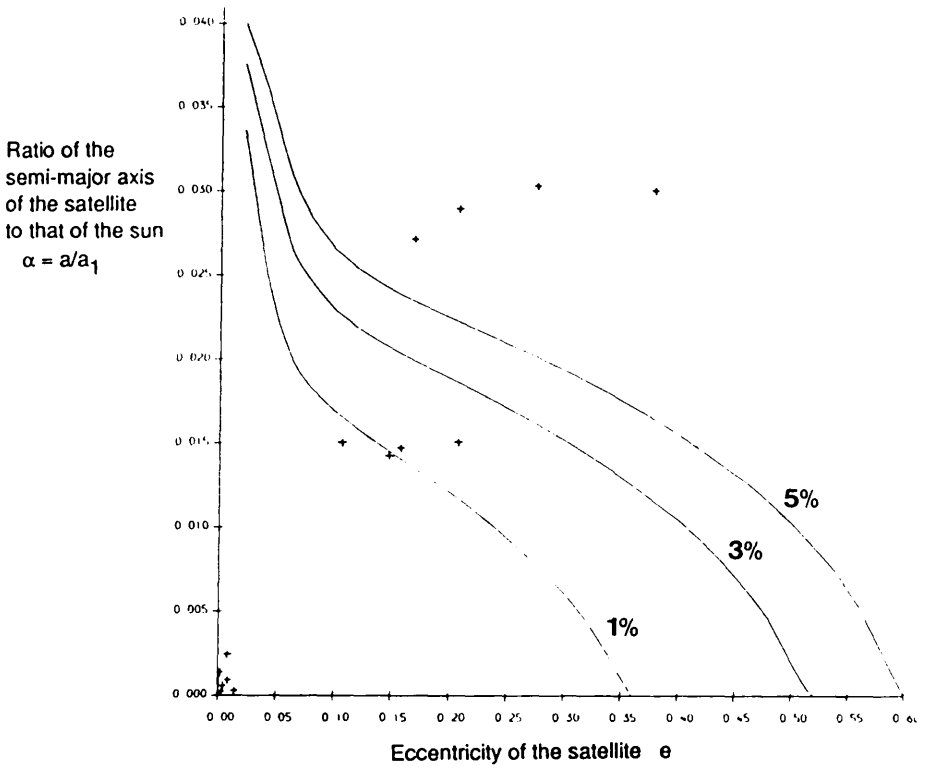
Ratio of the semi-major axis of the satellite to that of the sun
α = a/a1
5%
3%
1%
Eccentricity of the satellite e

(a)

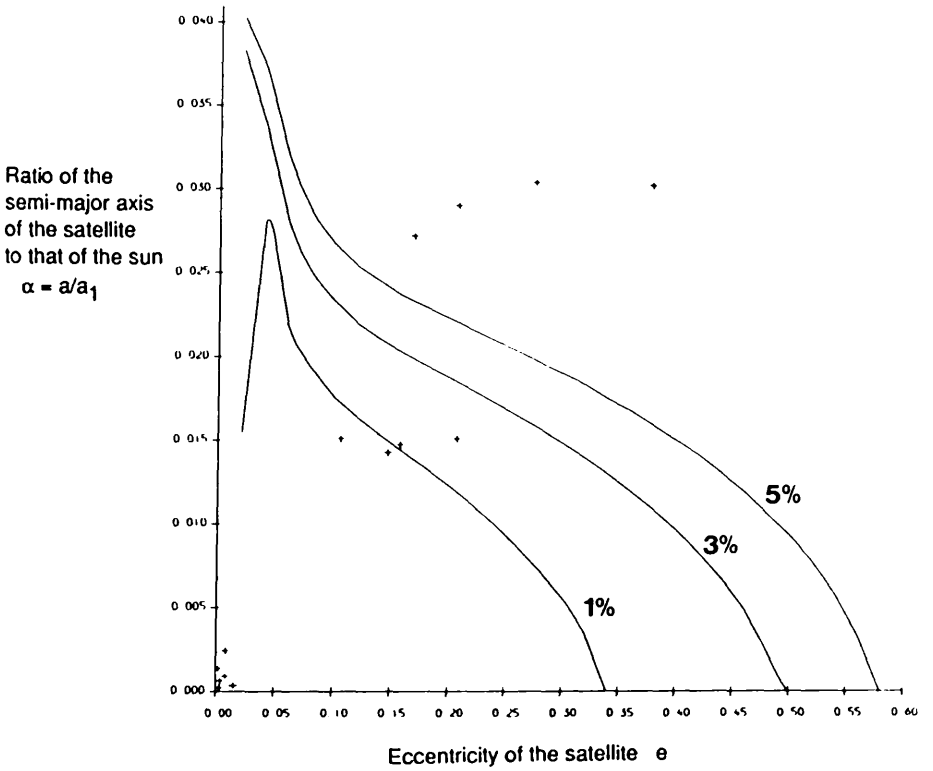
Ratio of the semi-major axis of the satellite to that of the sun
α = a/a1
5%
3%
1%
Eccentricity of the satellite e

(b)

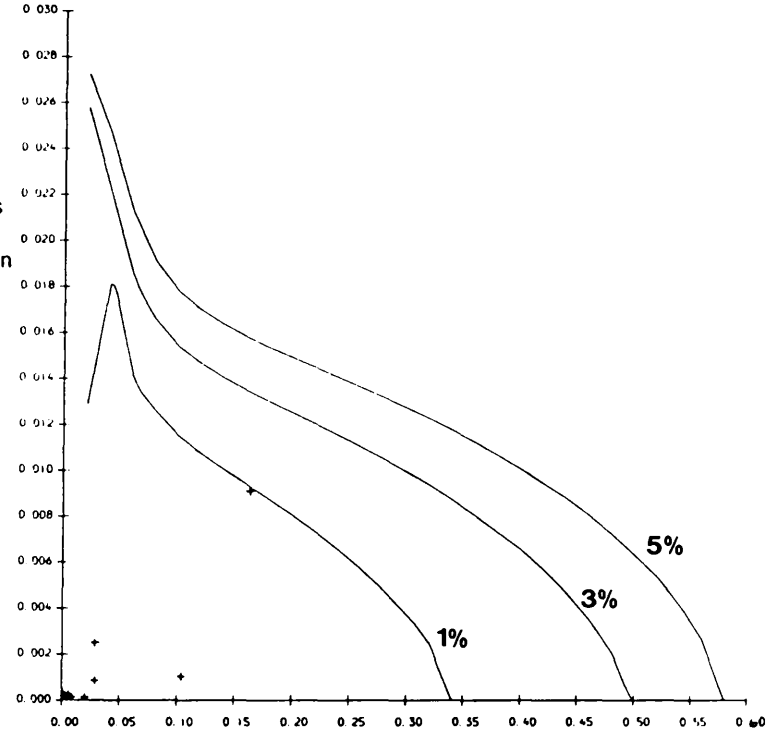
Ratio of the semi-major axis of the satellite to that of the sun
α = a/a1
5%
3%
1%
Eccentricity of the satellite e

(c)

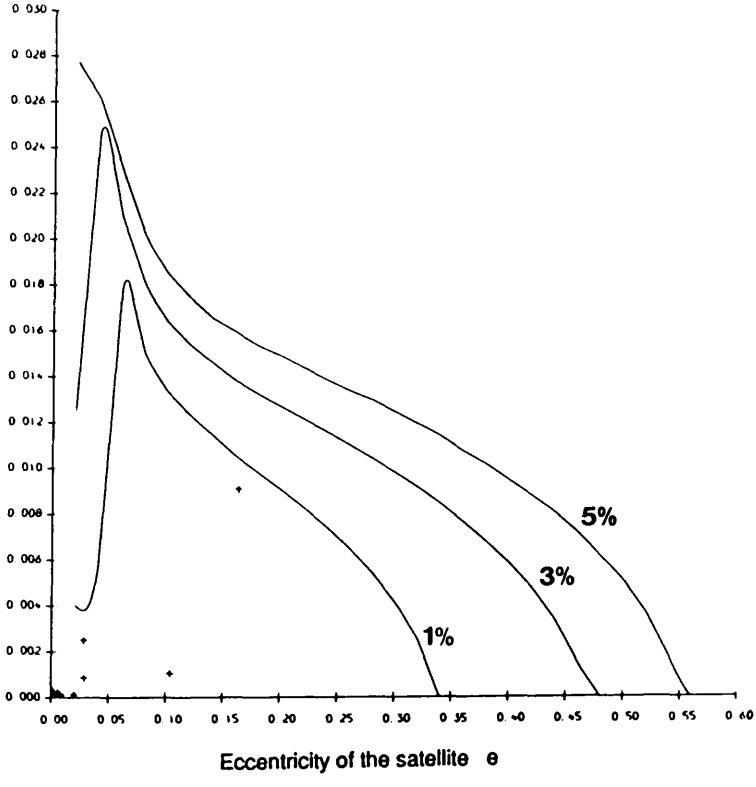
Ratio of the semi-major axis of the satellite to that of the sun
α = a/a1
5%
3%
1%
Eccentricity of the satellite e

(d)

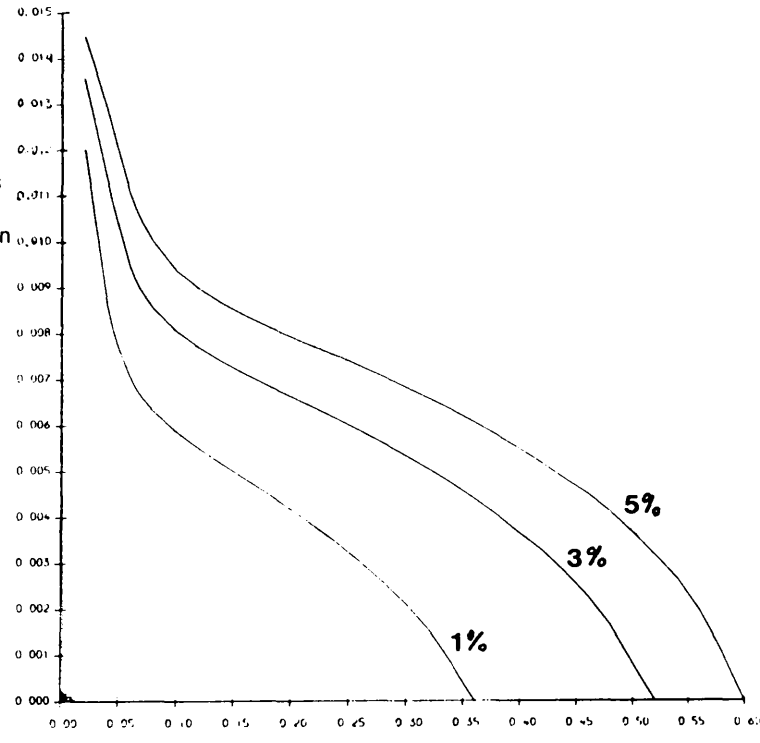
Ratio of the semi-major axis of the satellite to that of the sun
α = a/a1
5%
3%
1%
Eccentricity of the satellite e

(e)

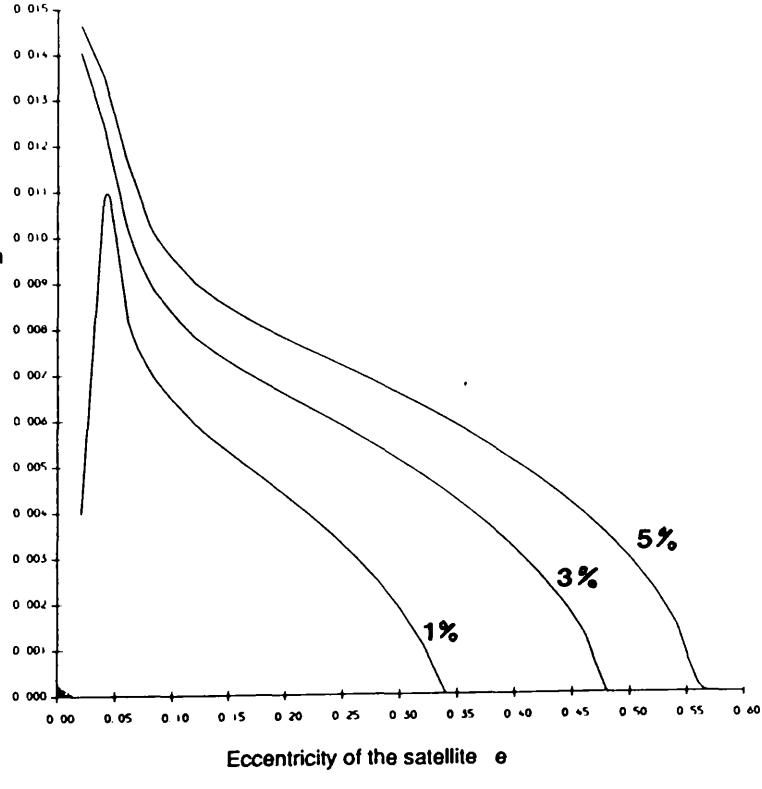
Ratio of the semi-major axis of the satellite to that of the sun
α = a/a1
5%
3%
1%
0.00 0.05 0.10 0.15 0.20 0.25 0.30 0.35 0.40 0.45 0.50 0.55 0.60
Eccentricity of the satellite e

(f)

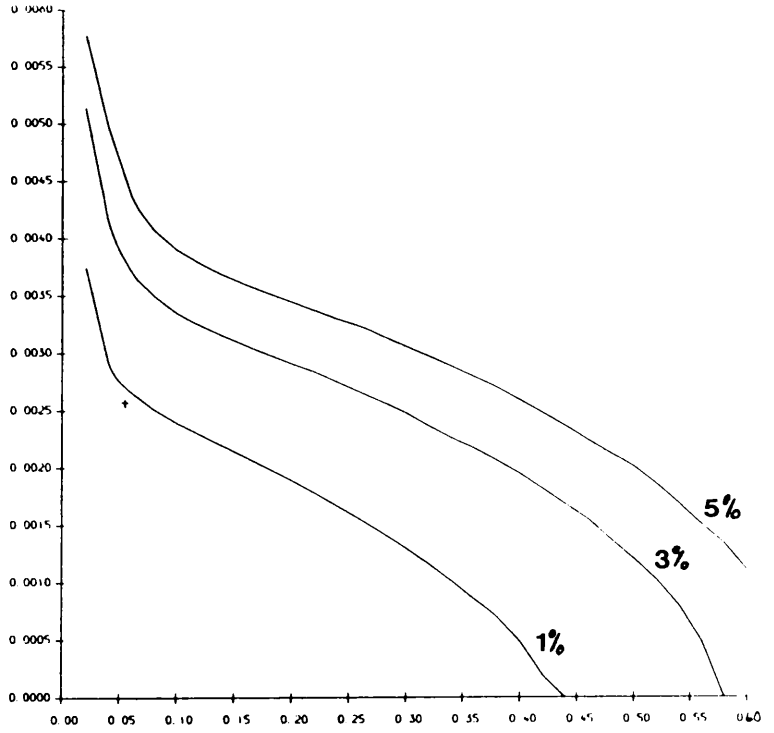
Ratio of the semi-major axis of the satellite to that of the sun
α = a/a1
0.0055
0.0050
0.0045
0.0040
0.0035
0.0030
0.0025
0.0020
0.0015
0.0010
0.0005
0.0000
0.00
0.05
0.10
0.15
0.20
0.25
0.30
0.35
0.40
0.45
0.50
0.55
0.60
5%
3%
1%
Eccentricity of the satellite e

(g)

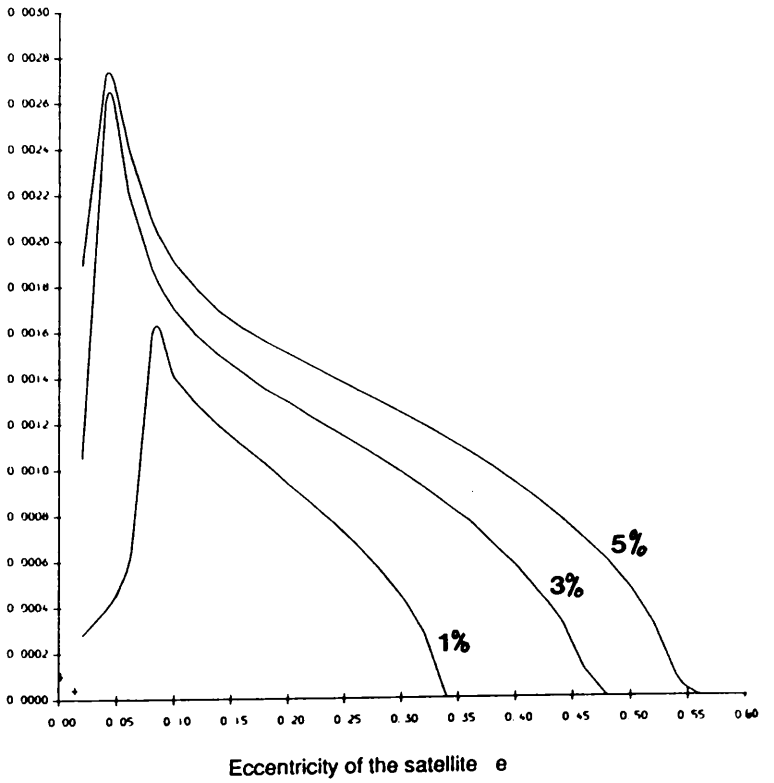
Ratio of the semi-major axis of the satellite to that of the sun
α = a/a1
0.0030
0.0028
0.0026
0.0024
0.0022
0.0020
0.0018
0.0016
0.0014
0.0012
0.0010
0.0008
0.0006
0.0004
0.0002
0.0000
0.00
0.05
0.10
0.15
0.20
0.25
0.30
0.35
0.40
0.45
0.50
0.55
0.60
5%
3%
1%
Eccentricity of the satellite e

(h)

Figures 4.8 show similar error contours in α_0-e_0 space to those found in Figures 3.4 for the circular case. From Figures 4.8 we see that like the circular case, only the retrograde satellites of Jupiter fall outside the region where the analytical theory is accurate to within a 5% relative error. However, Figures 4.8 show that the third order elliptical solutions for $\Delta\sigma$ accurately fit the numerical elliptical solutions for a wider range of the initial parameters α_0 and e_0, than is found in the circular case. This is not surprising since the elliptical analytical solution has been expanded to include more higher order terms and is therefore more accurate.

Of the remaining satellites only Jupiter's outer satellite group is not found within the 1% error contour line, a definite improvement on the circular second order analytical solution. An even greater improvement on the circular case is the fact that all the satellites (with the exception of Jupiter's outer satellite group, Saturn's Phoebe and the Earth's Moon) can now have their eccentricities increased to e=0.5 instead of the e = 0.3 found in the circular case, before the differences between the analytical and numerical solutions become greater than 5%. Even the three exceptions mentioned above can have their eccentricities increased to e = 0.4 and still remain within the 5% error contour. An increase in their eccentricities to e = 0.5 would only result in an error of about 7%.

We can now choose a much higher upper limit of e_u = 0.5 to which the eccentricity of each satellite system can grow before we say that an unstable situation is developing. The time taken for the system to reach this upper limit would then be the minimum duration of the system. Of course the retrograde satellites of Jupiter cannot be included in this analysis since their semi-major axes and eccentricities are too large for our analytical solution to be accurate to within 5%, but all the other major satellites of the five planets studied can be included.

Note that the differences between using the maximum likely eccentricities and the current eccentricities of the planets are very small. The error contours show that when a larger e_1 is used, our analytical solution tends to be more accurate for large α and small e, and less accurate for small α and large e. Since results using the planets' maximum eccentricities are similar to results using the planets' current

eccentricities, we use only the planets' current eccentricities for the rest of this thesis.

Because the third order circular analytical solution (ie Equations (27)) derived from the third order elliptical solution is so much more accurate than the second order circular analytical solution derived in Chapter 3, we will continue to use the third order solution. To gain a clearer idea of the improvements that can be achieved by using the third order circular analytical solution, we repeat the calculations which produced Figures 3.4 using the third order solution instead of the second order circular solution.

Again the major satellites of each planetary system are plotted in the relevant α_0-e_0 space and as before the upper limits of α are chosen to be the approximate values of α which produce a value for Δe greater than one. Thus Figures 4.9 show the 1%, 3% and 5% error contours in α_0-e_0 space for the third order circular analytical solution relative to the same circular numerical solution used in Figures 3.4.

Comparing Figures 3.4 and 4.9, we can see that the range of α_0 and e_0, for which the relative error between the analytical and numerical solutions is less than 5%, has increased dramatically when the third order circular solution is used. The range is now even greater than that found for the third order elliptical solution, which is not surprising since the circular solution is simply a special case of the elliptical solution where e_1 is zero. The circular solution will be more accurate than the elliptical solution expanded to the same order because the errors caused by neglecting any terms containing e_1 are zero in the circular case.

Figure 4.9(a) shows that at least one of Jupiter's retrograde satellites falls within the 5% error contour, while the rest of the satellites excepting the retrograde ones fall within the 1% error contour. This result is an improvement on the second order circular solution where none of Jupiter's retrograde satellites lie within the 5% contour and Jupiter's outer satellite group, Saturn's Phoebe and the Earth's Moon do not lie within the 1% contour line.

Figures 4.9(a) to (e) The error contours in α_0- e_0 space for the same cases as found in Figures 3.4, except that the third order circular analytical solution, instead of the second order solution, is now compared with the circular numerical solution.

The figures (a) through to (e) depict the error contours for satellites orbiting each of the following planets:

(a) Jupiter with $\mu = 1.1 \times 10^3$

(b) Saturn with $\mu = 3.5 \times 10^3$

(c) Uranus with $\mu = 2.28 \times 10^4$

(d) Earth with $\mu = 3.33 \times 10^5$

(e) Mars with $\mu = 3.08 \times 10^6$.

The plus signs indicate the locations in α_0-e_0 space of the major satellites of each planet.

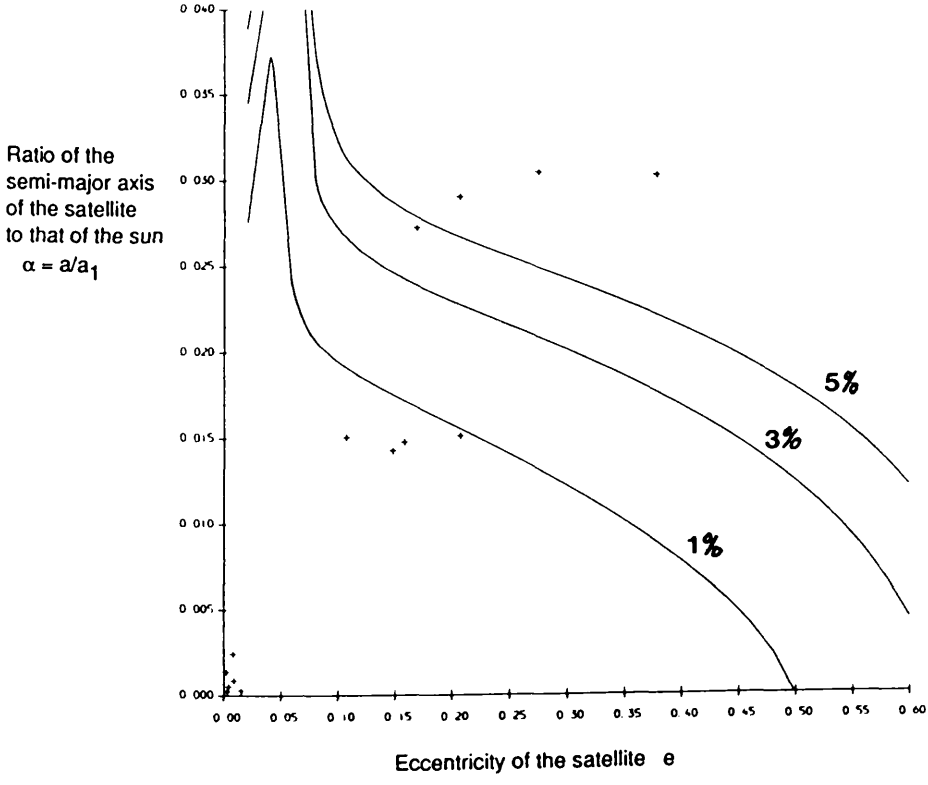

(a)

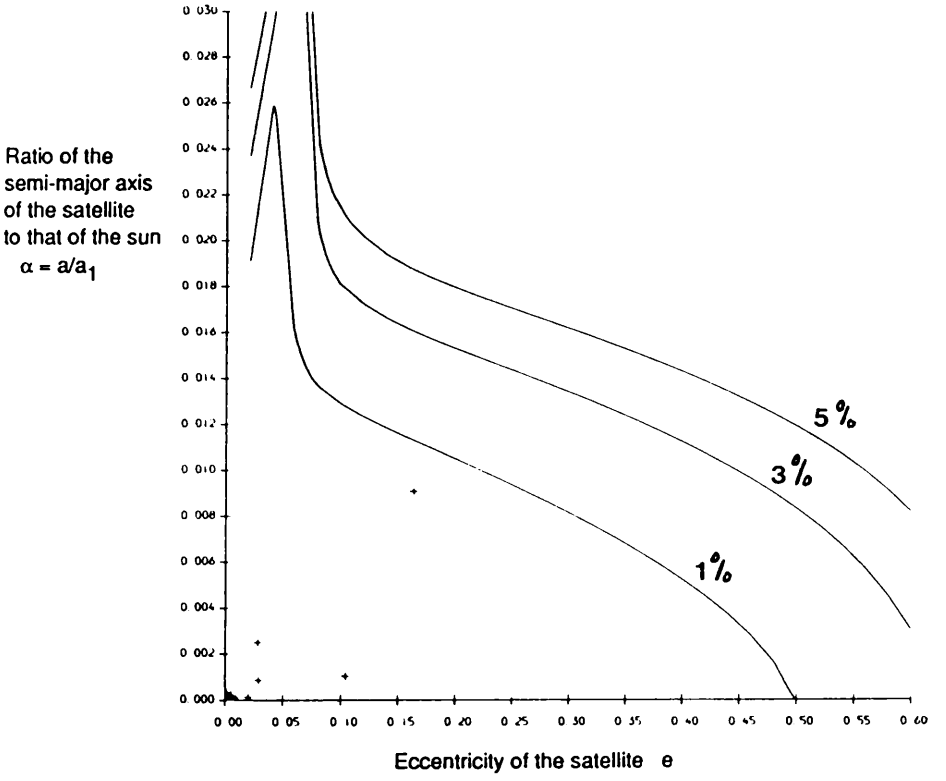
Ratio of the semi-major axis of the satellite to that of the sun
α = a/a1
0.030
0.028
0.026
0.024
0.022
0.020
0.018
0.016
0.014
0.012
0.010
0.008
0.006
0.004
0.002
0.000
0.00 0.05 0.10 0.15 0.20 0.25 0.30 0.35 0.40 0.45 0.50 0.55 0.60
5%
3%
1%
Eccentricity of the satellite e

(b)

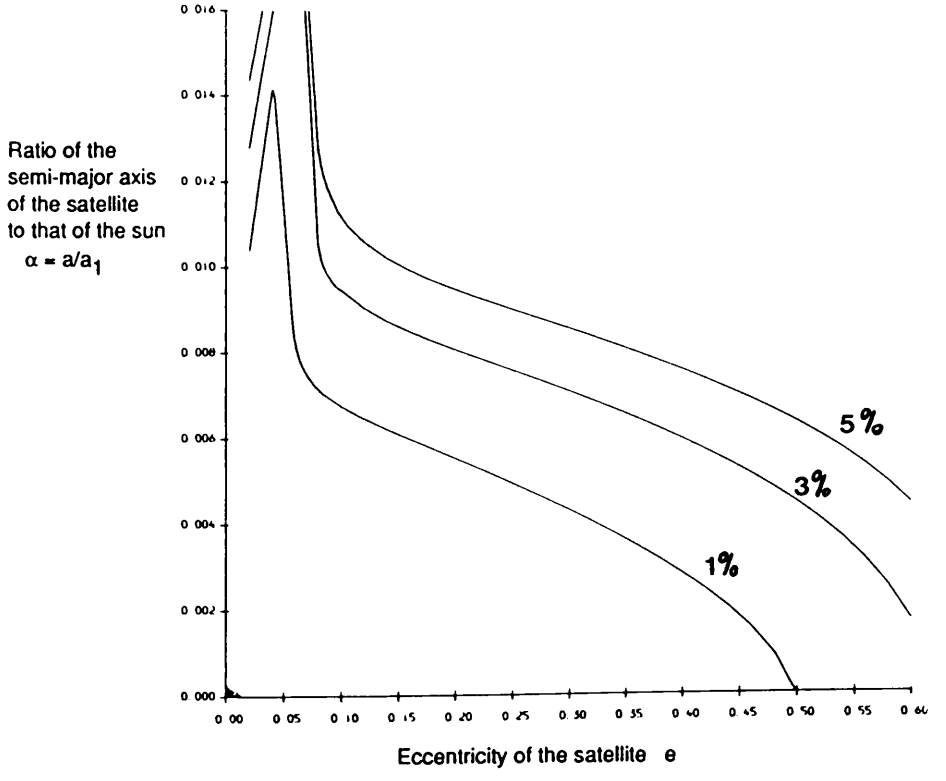
Ratio of the semi-major axis of the satellite to that of the sun
α = a/a1
0.016
0.014
0.012
0.010
0.008
0.006
0.004
0.002
0.000
0.00 0.05 0.10 0.15 0.20 0.25 0.30 0.35 0.40 0.45 0.50 0.55 0.60
5%
3%
1%
Eccentricity of the satellite e

(c)

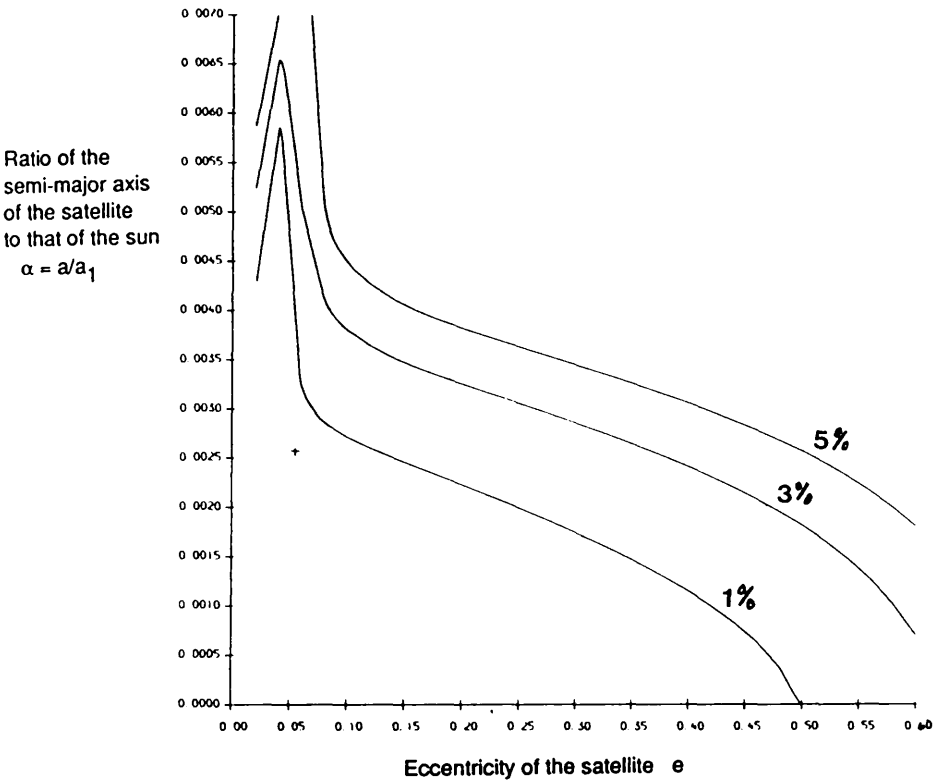
Ratio of the semi-major axis of the satellite to that of the sun
α = a/a1
0 0070
0 0065
0 0060
0 0055
0 0050
0 0045
0 0040
0 0035
0 0030
0 0025
0 0020
0 0015
0 0010
0 0005
0 0000
0 00
0 05
0 10
0 15
0 20
0 25
0 30
0 35
0 40
0 45
0 50
0 55
0 60
5%
3%
1%
Eccentricity of the satellite e

(d)

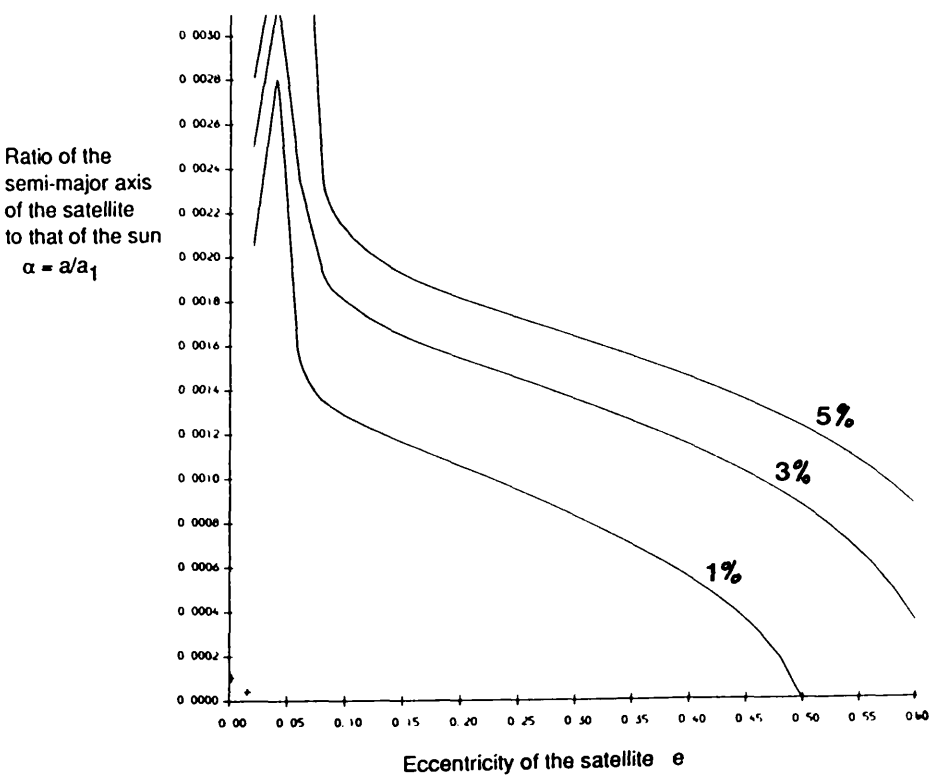
Ratio of the semi-major axis of the satellite to that of the sun
α = a/a1
0 0030
0 0028
0 0026
0 0024
0 0022
0 0020
0 0018
0 0016
0 0014
0 0012
0 0010
0 0008
0 0006
0 0004
0 0002
0 0000
0 00
0 05
0 10
0 15
0 20
0 25
0 30
0 35
0 40
0 45
0 50
0 55
0 60
5%
3%
1%
Eccentricity of the satellite e

(e)

In addition, with the exception of Jupiter's retrograde satellites, all the satellites using the third order circular solution can now have their eccentricities increased to $e_u = 0.5$ and still lie well within the 5% error contour. This result includes Jupiter's outer satellite group, Saturn's Phoebe and the Earth's Moon, all of which were located slightly outside the 5% error contour at an eccentricity of $e = 0.5$ for the third order elliptical solution.

Thus, if we use the third order circular analytical solution and the third order elliptical analytical solution, we can safely allow the eccentricities of most of the satellites found in the solar system to increase to a value of 0.5 before our analytical solutions start to deviate noticeably from their corresponding numerical solutions. We arbitrarily choose this breakdown point to be the upper limit e_u up to which we allow the eccentricity of each satellite system to grow before we say that an unstable situation is developing.

The duration of the satellite system will then be at least the time taken for the system to attain this upper limit e_u. The actual lifetime of the satellite system may be considerably longer than this minimum duration, but this method can provide minimum durations which are still long enough to be interesting. We find these minimum durations for various levels of our finite-time stability criteria in the next chapter.

CHAPTER 5

THE FINITE-TIME STABILITY CRITERIA APPLIED TO THE CIRCULAR AND ELLIPTICAL COPLANAR RESTRICTED THREE-BODY PROBLEMS

5.1 Introduction

5.2 The First Level, Using the Maximum Possible Change in the Eccentricity Over One Synodic Period

5.3 The Second Level, Using the Maximum Possible Change in the Eccentricity Over One Conjunction Cycle

- (i) A theoretical method for calculating the changes in the orbital elements over one cycle of conjunctions
- (ii) A numerical method for calculating the changes in the orbital elements over one cycle of conjunctions
- (iii) A study of the cyclic nature of the orbital elements over one conjunction cycle
- (iv) The minimum durations of various satellite systems

5.4 The Third Level, Using the Maximum Possible Change in the Eccentricity Over One Mirror Configuration Cycle

- (i) A theoretical and numerical method for calculating the changes in the orbital elements over one mirror configuration cycle for the circular case
- (ii) A study of the cyclic nature of the orbital elements over one mirror configuration cycle for the circular case
- (iii) The minimum durations of various satellite systems for the circular case
- (iv) Modification of the mirror configuration cycle method for the case of non-zero solar eccentricity
- (v) A comparison of the minimum durations of various satellite systems for both the circular and elliptical cases

5.5 Conclusions

" They told him it couldn't be done.
He laughed and went right to it.
He tackled the thing that couldn't be done -
And couldn't do it!"

5.1 Introduction

The analytical theories developed in Chapters 3 and 4 can now be used to find the minimum lifetimes of a variety of circular and elliptical coplanar restricted three-body systems. To each three-body system, we apply progressively less pessimistic levels of the finite-time stability method, based on the successively larger natural cycles found in the orbital dynamics of the planet-satellite-Sun system. These cycles: the synodic cycle, the conjunction cycle, and the mirror configuration cycle and the levels of the finite-time stability method which incorporate them are described in Sections 5.2, 5.3, and 5.4 respectively.

Section 5.2 includes a quick method of approximating the minimum lifetimes of the systems, while Section 5.3 developes both an analytical and a numerical procedure for mapping one synodic period to the next synodic period of the system. These mapping procedures are then used in Sections 5.3 and 5.4 to study the cyclic behavior of the orbital elements of the planet-satellite system, as the system moves through enough synodic cycles to complete either a conjunction cycle or a mirror-configuration cycle.

The three Sections 5.2, 5.3 and 5.4 each finish with an evaluation of the minimum durations of the given planet-satellite systems using the natural cycle discussed in each section. The final results of all three levels of the finite-time stability method are compared and summarized in Section 5.5.

5.2 The First Level, Using the Maximum Possible Change in the Eccentricity Over One Synodic Period

In the most pessimistic case for calculating the minimum duration of a Sun-perturbed planetary satellite system, we assume that the maximum possible change in the satellite's eccentricity over one synodic period Δe_{max} is added onto the satellite's current eccentricity every synodic period. We next find the number of synodic periods N_1 that will occur before the eccentricity accumulates to the arbitrarily chosen upper limit of $e_u = 0.5$, where the analytical solutions for both the circular and the elliptical cases begin to deviate noticeably from the equivalent numerical solutions.

The minimum duration T'_{min} of the planetary satellite system for the first level of our finite-time stability criteria then becomes

$$T'_{min} = N_1 T_S \tag{1}$$

where T_S is the synodic period of the Sun-planet-satellite system.

Of course, the maximum change in the satellite's eccentricity Δe_{max} over one synodic period varies with the eccentricity of the satellite. We therefore must ensure that Δe_{max} is evaluated for each synodic period using the current value of the eccentricity for that synodic period. Thus

$$\begin{aligned}
e_1 &= e_0 + \Delta e_{max}(e_0) \\
e_2 &= e_1 + \Delta e_{max}(e_1) \\
e_3 &= e_2 + \Delta e_{max}(e_2) \\
&\vdots \\
e_{i+1} &= e_i + \Delta e_{max}(e_i) \\
&\vdots \\
e_u = e_{N_1} &= e_{N_1-1} + \Delta e_{max}(e_{N_1-1})
\end{aligned} \tag{2}$$

where i is the number of synodic periods that have occurred; e_i is the satellite's eccentricity during the i^{th} synodic period; and $\Delta e_{max}(e_i)$ is the maximum possible change in the satellite's eccentricity over the i^{th} synodic period evaluated at e_i. N_1 is thus simply the number of $\Delta e_{max}(e_i)$'s that can accumulate before an eccentricity of e_u is reached.

In order to find a quick estimate of the size of N_1 and subsequently T'_{min}, we can assume that Δe_{max} remains constant as the eccentricity is increased every synodic period until $e_u = 0.5$ is reached. If we take Δe_{max} to be always evaluated at $e = e_0$, we get an upper limit for N_1 of

$$N_{1up} = \frac{e_u - e_0}{\Delta e_{max}(e_0)}$$

If we assume Δe_{max} to be always evaluated at $e = e_u$, we get a lower limit for N_1 of

$$N_{1low} = \frac{e_u - e_0}{\Delta e_{max}(e_u)}$$

The actual number of synodic periods lies somewhere between the two values.

$$N_{1low} < N_1 < N_{1up}$$

Figure 5.1 compares the relationships between the three values of N (the upper limit of N_1, the lower limit of N_1 and the actual value of N_1) with the eccentricity e as the eccentricity is increased to e_u by either adding a constant Δe_{max} or a varying $\Delta e_{max}(e_i)$ onto the eccentricity each synodic period. The graph is formed for a typical circular coplanar Jupiter-Gallilean satellite system with $e = 0.01$, α=0.0025 and $\mu = 1100$, but the results are much the same for any of the systems we

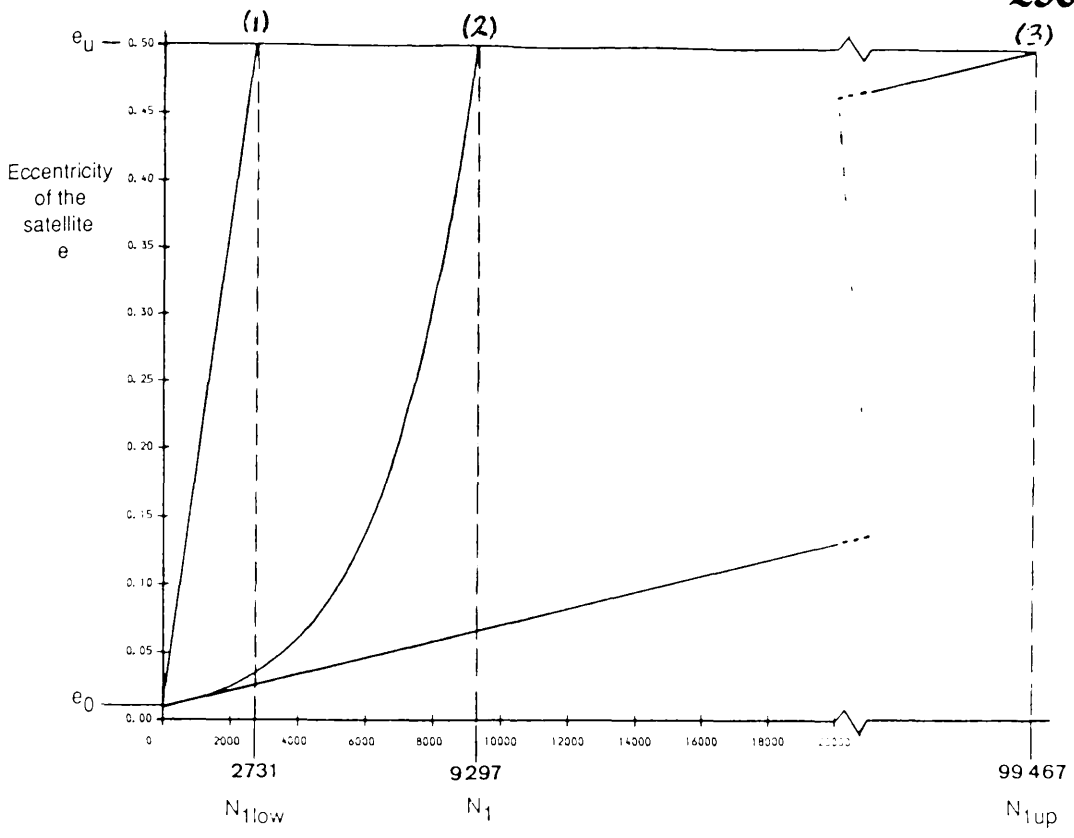

Figure 5.1 Shows the growth in the satellite's eccentricity e with the number of synodic periods N which have occurred for the following three cases where:

(1) the maximum possible change in the eccentricity for $e=e_u$ (ie $\Delta e_{max}(e_u)$) is added on to the eccentricity every synodic period

(2) the maximum possible change in the eccentricity for the current synodic period (ie $\Delta e_{max}(e_i)$) is added onto the eccentricity every synodic period

(3) the maximum possible change in the eccentricity for $e=e_o$ (ie $\Delta e_{max}(e_o)$) is added on to the eccentricity every synodic period.

N_{1low}, N_1 and N_{1up} represent the number of synodic periods that have occurred for each of the above cases respectively, by the time the satellite's eccentricity reaches an upper limit of $e_u = 0.5$.

The initial parameters of the satellite are taken to be those of a circular coplanar Jupiter-Callisto system with $e = 0.01$, $\alpha = 0.0025$ and $\mu = 1100$.

have been studying. These calculations of N_{1low} and N_{1up} are useful for gaining a rough idea of the size of N_1 and therefore, an idea of the time required by the computer to complete the iterative calculations described in Equations (2).

If e_0 and $\Delta e_{max}(e_i)$ are small, the time required to calculate N_1 and T'_{min} may be far beyond reasonable time limitations on the computer. In such a case, we use an approximation for N_1 that is similar to the trapezoidal rule, except that slopes are analyzed instead of areas.

In a first approximation for N_1, we take the maximum possible Δe over the synodic period where $e = e_u$ to be a constant added on to the eccentricity every synodic period. Thus, our first approximation to N_1 becomes N_{T1} (ie the lower limit N_{1low} mentioned previously)

$$N_{T1} = N_{1low} = \frac{e_u - e_0}{\Delta e_{max}(e_u)} \tag{3}$$

The value of N_{T1} relative to the actual value of N_1 for the Jupiter-Callisto system where $\alpha = 0.0025$, $e = 0.01$ and $\mu = 1100$, is given in Figure 5.2. The figure shows pictorially how each of the successive approximations to N_1 are calculated.

A second better approximation to N_1 is found by dividing the interval e_0 to e_u into two substeps. The maximum possible Δe over one synodic period is then assumed to be a constant for each substep and is evaluated using the eccentricity at the endpoint of each interval. Thus, the eccentricity at the end of the first substep is given by

$$e_1^2 = \frac{e_u + e_0}{2}$$

where the subscript of a variable containing both a subscript and a superscript refers to the number of the substep being examined and the superscript refers to the total number of substeps which divide the interval e_0 to e_u. N_1^2, the number of synodic

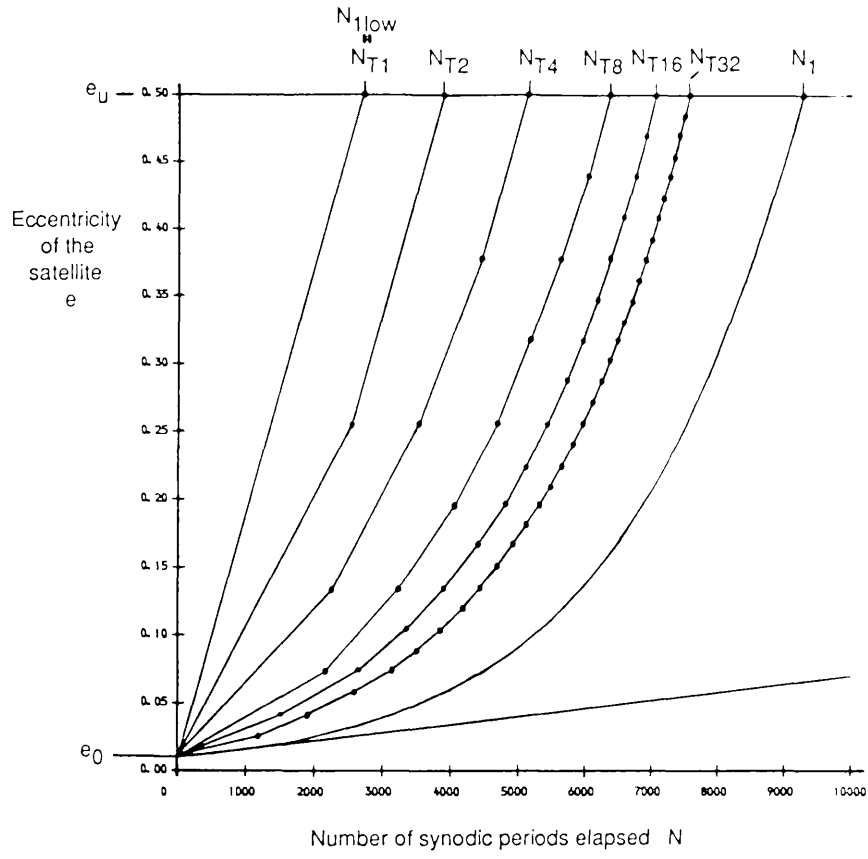

Figure 5.2 Shows the improvement in the approximations N_{Tn} to the actual number of synodic periods N_1, as n is doubled repeatedly.

In the evaluation of N_1 Δe_{max} is assumed to change as a function of the eccentricity every synodic period. In the evaluation of N_{Tn} the interval e_0 to e_u is divided into n substeps, Δe_{max} is assumed to change only every substep and Δe_{max} is evaluated using the eccentricity at the end of each substep.

The same satellite initial conditions used in Figure 5.1 are also applied here.

periods which occur over this first substep, is

$$N_1^2 = \frac{e_1^2 - e_0}{\Delta e_{max}(e_1^2)} = \frac{N_{T1}}{2} \frac{\Delta e_{max}(e_u)}{\Delta e_{max}(e_1^2)}$$

while N_2^2, the number of synodic periods which occur over the second substep, is

$$N_2^2 = \frac{e_u - e_1^2}{\Delta e_{max}(e_u)} = \frac{N_{T1}}{2}$$

The second approximation to N_1 then becomes

$$N_{T2} = N_1^2 + N_2^2 = \frac{N_{T1}}{2}\left[1 + \frac{\Delta e_{max}(e_u)}{\Delta e_{max}(e_1^2)}\right] \qquad (4)$$

A better approximation to N_1 can be found by doubling the number of substeps between e_0 and e_u to four. The endpoints of each substep now become:

$$e_1^4 = \frac{1}{4}(e_u + 3e_0)$$

$$e_2^4 = \frac{1}{4}(2e_u + 2e_0)$$

$$e_3^4 = \frac{1}{4}(3e_u + e_0)$$

$$e_4^4 = e_u$$

The numbers of synodic periods which occur over the substeps are then given by:

$$N_1^4 = \frac{e_1^4 - e_0}{\Delta e_{max}(e_1^4)} = \frac{N_{T1}}{4} \frac{\Delta e_{max}(e_u)}{\Delta e_{max}(e_1^4)}$$

$$N_2^4 = \frac{e_2^4 - e_1^4}{\Delta e_{max}(e_2^4)} = \frac{N_{T1}}{4} \frac{\Delta e_{max}(e_u)}{\Delta e_{max}(e_2^4)}$$

$$N_3^4 = \frac{e_3^4 - e_2^4}{\Delta e_{max}(e_3^4)} = \frac{N_{T1}}{4} \frac{\Delta e_{max}(e_u)}{\Delta e_{max}(e_3^4)}$$

$$N_4^4 = \frac{e_u - e_3^4}{\Delta e_{max}(e_u)} = \frac{N_{T1}}{4}$$

This latest approximation to N_1 becomes

$$N_{T4} = \frac{N_{T1}}{4} \left[1 + \Delta e_{max}(e_u) \left(\frac{1}{\Delta e_{max}(e_1^4)} + \frac{1}{\Delta e_{max}(e_2^4)} + \frac{1}{\Delta e_{max}(e_3^4)} \right) \right] \quad (5)$$

If we now generalize Equations (3), (4) and (5), and divide the interval e_0 to e_u into n substeps, we get the following approximation to N_1:

$$N_{Tn} = \frac{N_{T1}}{n} [1 + \Delta e_{max}(e_u)\, S_n]$$

where $$N_{T1} = \frac{e_u - e_0}{\Delta e_{max}(e_u)}$$

$$e_i = \frac{1}{n} [\, i e_u + (n - i)\, e_0 \,]$$

$$S_n = \sum_{i=1}^{n-1} \frac{1}{\Delta e_{max}(e_i)}$$

The number of substeps n can be continually doubled until the required accuracy is met, in other words, until

$$\frac{N_{T2n} - N_{Tn}}{N_{Tn}} \leq \text{given error}$$

where N_{T2n} is an approximation for N_1 which uses twice the number of substeps 2n as that of the previous approximation for N_1 or N_{Tn}. The process of finding N_{T2n} is made easier by the fact that the terms in the new sum S_{2n}, which are functions of the eccentricities at the endpoints of the even numbered substeps, are identical to those terms previously calculated for the old sum S_n. For example, note that $e_2^4 = e_1^2$. Therefore, only the eccentricities with the odd numbered subscripts need to be evaluated for each new approximation to N_1. Thus,

$$N_{T2n} = \frac{N_{T1}}{2n}\left[1 + \Delta e_{max}(e_u)\left(\sum_{j=1}^{n} \frac{1}{\Delta e_{max}(e_{2j-1})} + S_n\right)\right]$$

where

$$e_{2j-1} = \frac{1}{2n}\left[(2j - 1)\, e_u + (2n - 2j + 1)\, e_0\right]$$

The above method of approximating N_1 proves to be very efficient for the Jupiter-Callisto example given in Figures 5.1 and 5.2 as long as a relative percentage error of greater than 0.05% is required. As can be seen from Figure 5.2, the initial convergence of successive approximations to N_1 is very fast, but becomes much slower as N_{Tn} approaches N_1. Thus, the number of successive doubling of substeps, which must be made in order to achieve the same level of improvement in accuracy, increases as N_{Tn} approaches N_1. Eventually as the given accuracy is improved, the number of substeps required in order to achieve the specified accuracy becomes far greater than the number of steps required to calculate the value of N_1 exactly. At this point, an exact calculation of N_1 using a Δe_{max} which varies with each synodic period, is the most efficient method of finding N_1.

Since we require only an order of magnitude accuracy in our values for N_1, the approximation method of obtaining a value for N_1 will always be the fastest method. For example, the approximation method generally requires only about 200 substeps (ie evaluations of $\Delta e_{max}(e_i)$) in order to reach an accuracy of 1%, while the exact method of calculating N_1 requires N_1 evaluations of $\Delta e_{max}(e_i)$, which can be a very large value of the order of greater than 10^6.

Besides being fast, the approximation method of computing N_1 also has the advantage of producing an approximation to N_1 which is always less than the actual value of N_1. This is caused by consistently choosing to evaluate the constant Δe_{max} for a particular substep at the endpoint of that substep. As a result, T'_{min} derived from the approximation to N_1 is less than the minimum time found when using the exact value of N_1 and hence is still a valid minimum lifetime for the satellite system.

Having found an efficient method of calculating N_1, we need only derive an expression for T_S in order to calculate the minimum duration of the planetary system. If both the satellite and the Sun move in circular orbits at constant speeds of n and n_1 respectively, their synodic period would simply be given by the familiar formula

$$T_S = \frac{2\pi}{n - n_1} \tag{6}$$

Even when the two orbits are elliptical, the synodic period should, on average, still be given by Equation (6). The exact time between particular successive conjunctions however, depends on the eccentricities of the two orbits e and e_1, and the true anomalies of the satellite and the Sun at the first conjunction f_{c0} and f_{1c0}, as we shall see later in Section 5.2.

The differences in our evaluations of T'_{min} as a result of using the average time between successive conjunctions as opposed to the actual value of the time between conjunctions are minimal, and are certainly much less than the differences caused by

using the approximation method of finding N_1 instead of the exact calculation of N_1. We therefore use the average synodic period for the variable T_S in Equation (1).

Equation (6) can be rewritten in terms of the sidereal period of the planet to become

$$T_S = \frac{T_1 \nu}{1 - \nu} \qquad \text{where} \quad \nu = \frac{n_1}{n}$$

Having derived a quick method of approximating N_1 and calculating T_S to within a given accuracy, we can now find minimum lifetimes for any three-body system in which the elliptical or circular coplanar restricted three-body problem is applicable. Minimum durations are found for a variety of imaginary satellites orbiting each of the planets Jupiter, Saturn, Uranus, Earth and Mars.

The satellites studied have initial orbital parameters ranging from $e_0 \approx 0$ to $e_0 = 0.2$, and $\alpha_0 \approx 0$ to the largest value of α_0 for each planet which still produces less than a 5% relative error between the analytical and numerical solutions for Δe_{max}, when the eccentricity is increased to e=0.5. These maximum allowable values for α_0 are listed in Table 5.1 and are measured from the percentage relative error contours of Figures 4.8 and 4.9. For easier comparison of the minimum lifetimes found for the circular and elliptical cases, we choose the maximum allowable α_0's for the elliptical case to be the upper limit of the range of α_0's for both cases.

Out of interest, we also calculate the minimum lifetimes for some of the real satellites whose α_0, e_0 parameters fall just outside of the 5% relative error contour line for the elliptical case if the eccenticity is increased to e = 0.5. These satellites include Jupiter's outer satellites at approximately $\alpha_0 = 0.015$, Saturn's Phoebe at α_0=0.009, and the Earth's Moon at $\alpha_0 = 0.0026$. Since the relative error for these satellites, if the eccentricity is allowed to increase to 0.5, is only about 7 to 8%, the resulting minimum durations should not be too inaccurate.

Planet	Maximum Allowable α_0	
	Circular Case	Elliptical Case
Jupiter	0.018	0.010
Saturn	0.012	0.0065
Uranus	0.0066	0.0037
Earth	0.0026	0.0020
Mars	0.00125	0.00045

Table 5.1 The largest possible values of α_0, for each planet and each of the cases circular or elliptical, which produce analytical values of Δe_{max} that are still within a 5% relative error of the equivalent numerical solutions.

The results are measured from Figures 4.8 and 4.9.

The minimum lifetimes of satellites orbiting each planet are plotted in the form of contours in α_0-e_0 space. Figures 5.3, 5.4, and 5.5 show the T'_{min} contours for the Jupiter, Saturn and Uranus satellite systems respectively. The solid lines describe the cases where the Sun is assumed to be moving in a fixed circular orbit, while the dashed lines describe the cases where the Sun is assumed to be moving in a fixed elliptical orbit. For reference, the positions of the major satellites of each planet are also plotted in α_0-e_0 space.

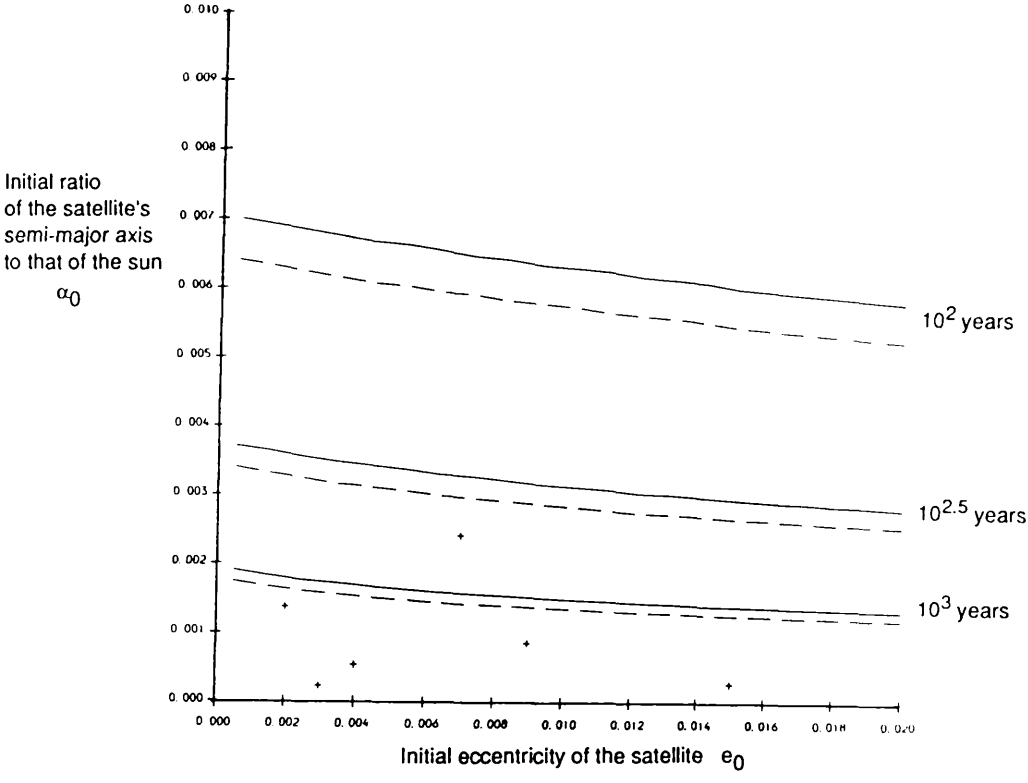

Figure 5.3 The contours for the first level minimum durations T^{I}_{min} of a coplanar Jupiter-satellite system, where the initial orbital parameters of the satellite are α_0 and e_0. The solid lines represent the cases where the Sun is assumed to move in a fixed circular orbit, while the dashed lines represent the cases where the Sun is assumed to move in a fixed elliptical orbit of $e_1 = 0.048$.

The mass ratio μ is taken to be 1100. The plus signs represent the positions in α_0-e_0 space of the known satellites of Jupiter existing in this region.

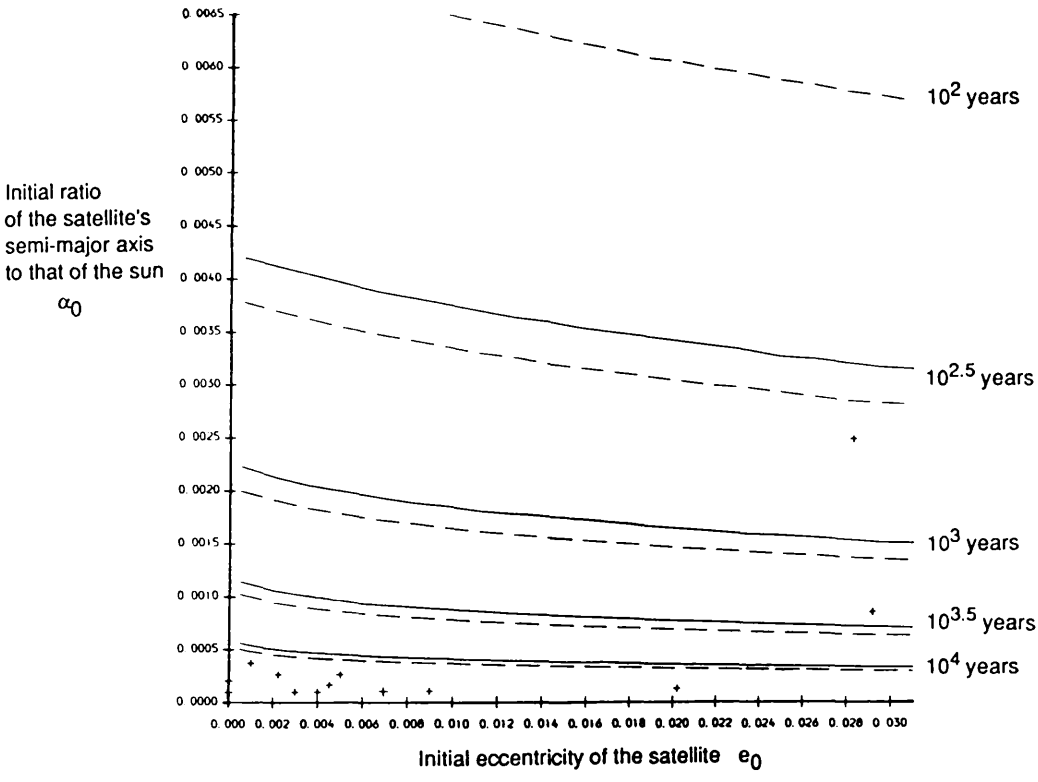

Figure 5.4 The T'_{min} contours in α_0-e_0 space for Saturn-satellite systems. μ is taken to be 3500, while e_1 is 0.056 for the elliptical case.

The plus signs represent the positions in α_0-e_0 space of the known satellites of Saturn existing in this region.

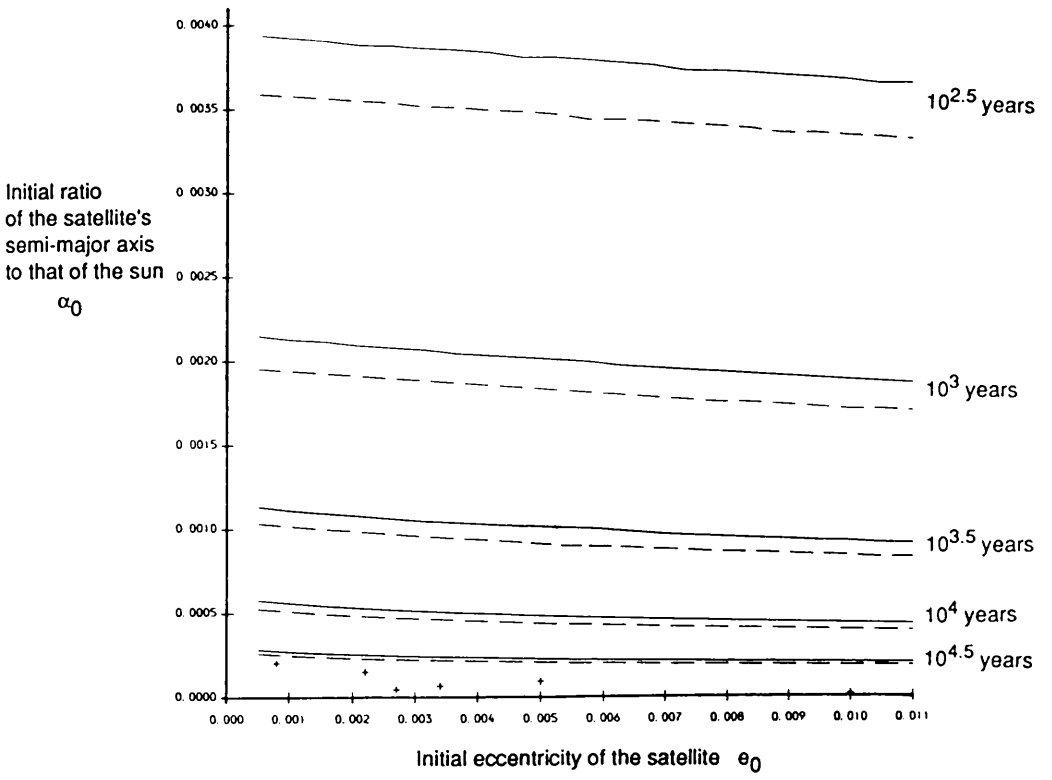

Figure 5.5 The T'_{min} contours in α_0-e_0 space for Uranus-satellite systems. μ is taken to be 2.28×10^4, while e_1 is 0.047 for the elliptical case.

The plus signs represent the positions in α_0-e_0 space of the known satellites of Uranus existing in this region.

The computing time required to calculate each T'_{min} contour for the Earth and Mars satellite systems is greater than one hour. For these systems, we therefore evaluate the lifetimes of satellites whose initial orbital parameters cover the required region of α_0-e_0 space at equal intervals. The minimum durations for each α_0-e_0 pair are sorted into intervals of time on a logarithmic scale. Each time interval is assigned a unique symbol specified in the figure captions. The symbols are then plotted in α_0-e_0 space.

Figures 5.6(a) and (b) display the binned values of T'_{min} over α_0-e_0 space for the circular and elliptical cases involving the Earth. Figures 5.7(a) and (b) show the equivalent graphs for Mars. The regions where the symbols change provide a rough outline of the T'_{min} contours similar to those displayed in Figures 5.3 to 5.5.

Figures 5.6(a) and (b) The intervals of the first level minimum durations for a variety of Earth satellites whose initial orbital elements are α_0 and e_0.

The symbols represent the following intervals of time, where $T=\log_{10} T'_{min}$.

$T \leq 1.0$	Δ
$1.0 < T \leq 1.5$	X
$1.5 < T \leq 2.0$	$\square$
$2.0 < T \leq 2.5$	*
$2.5 < T \leq 3.0$	O

μ and e_1 are taken to be 3.33×10^5 and 0.017 respectively. The dashed lines show where the actual T'_{min} contours like those displayed in Figures 5.3 to 5.5, might occur.

Part (a) gives the case where the Sun is assumed to be moving in a fixed circular orbit, while part (b) gives the case where the Sun is assumed to be moving in a fixed elliptical orbit.

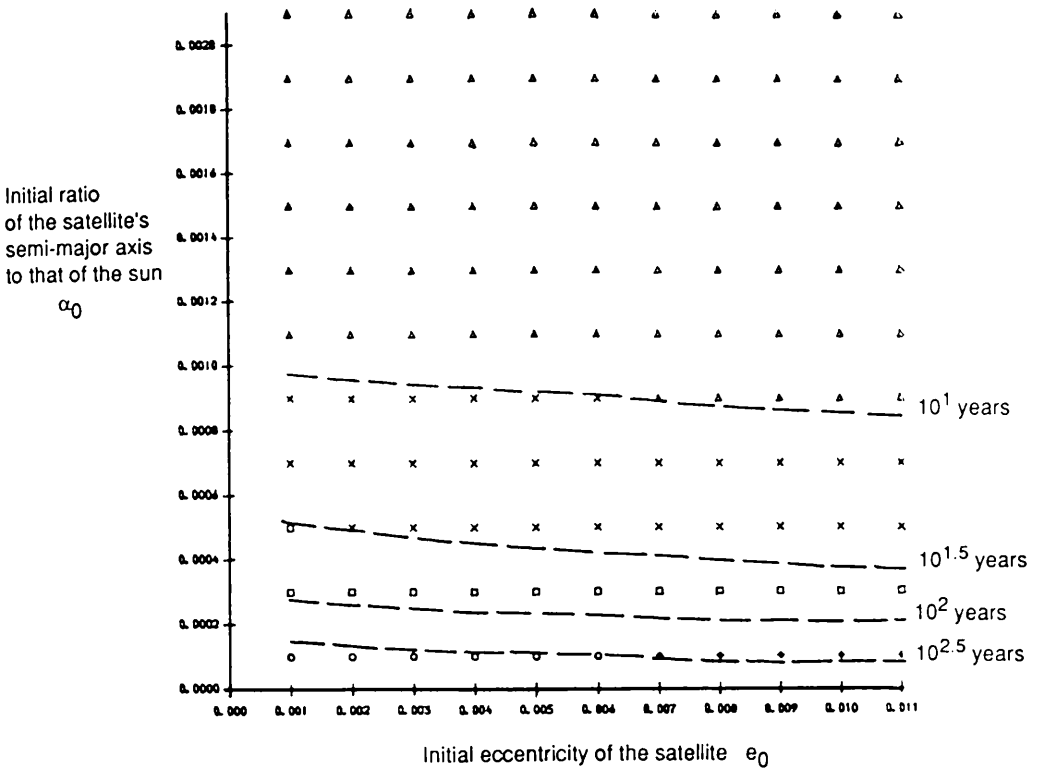
Initial ratio
of the satellite's
semi-major axis
to that of the sun
α_0
(a)
10^1 years
$10^{1.5}$ years
10^2 years
$10^{2.5}$ years
Initial eccentricity of the satellite e_0

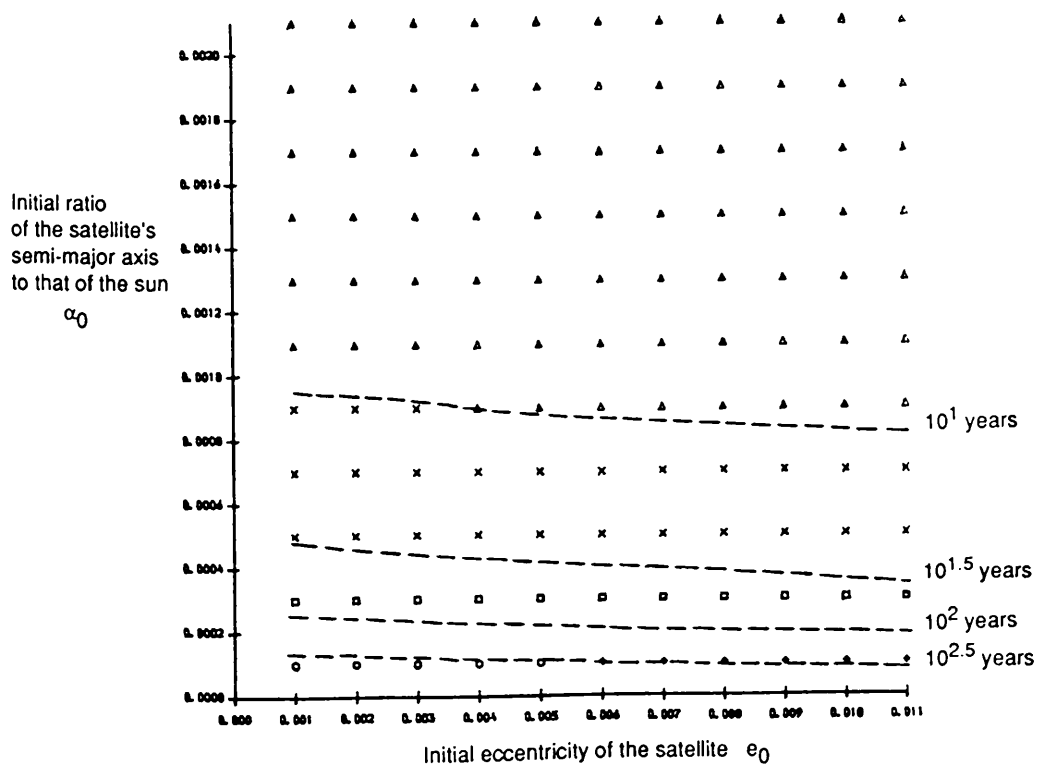
Initial ratio
of the satellite's
semi-major axis
to that of the sun
α_0
(b)
10^1 years
$10^{1.5}$ years
10^2 years
$10^{2.5}$ years
Initial eccentricity of the satellite e_0

Figures 5.7 (a) and (b) The equivalent graphs to Figures 5.6 for the satellites of Mars. μ and e_1 are taken to be 3.08×10^6 and 0.093 respectively. The symbols represent the following intervals of time, where $T = \log_{10} T'_{min}$:

$1.0 < T \leq 1.5$ X
$1.5 < T \leq 2.0$ □
$2.0 < T \leq 2.5$ *
$2.5 < T \leq 3.0$ O
$3.0 < T \leq 3.5$ ✠
$3.5 < T \leq 4.0$ ◊

The plus signs represent the positions in α_0-e_0 space of the known satellites of Mars existing in this region.

Part (a) gives the case where the Sun is assumed to be moving in a fixed circular orbit, while part (b) gives the case where the Sun is assumed to be moving in a fixed elliptical orbit.

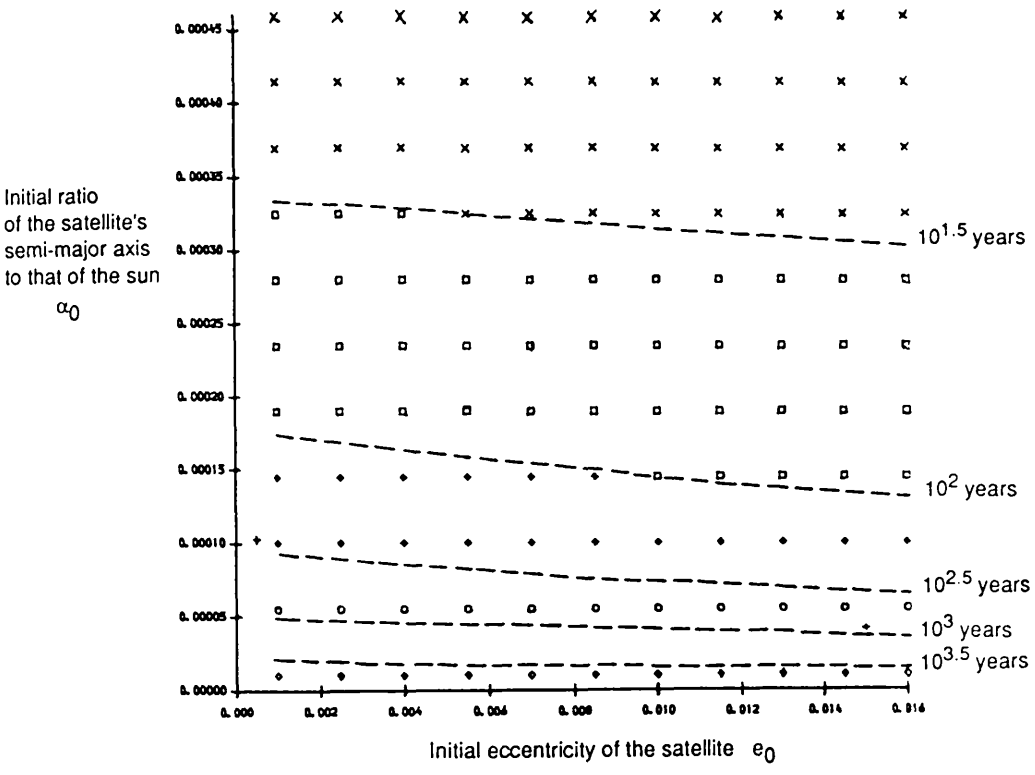
Initial ratio
of the satellite's
semi-major axis
to that of the sun
α_0
$10^{1.5}$ years
10^2 years
$10^{2.5}$ years
10^3 years
$10^{3.5}$ years
(a)
Initial eccentricity of the satellite e_0

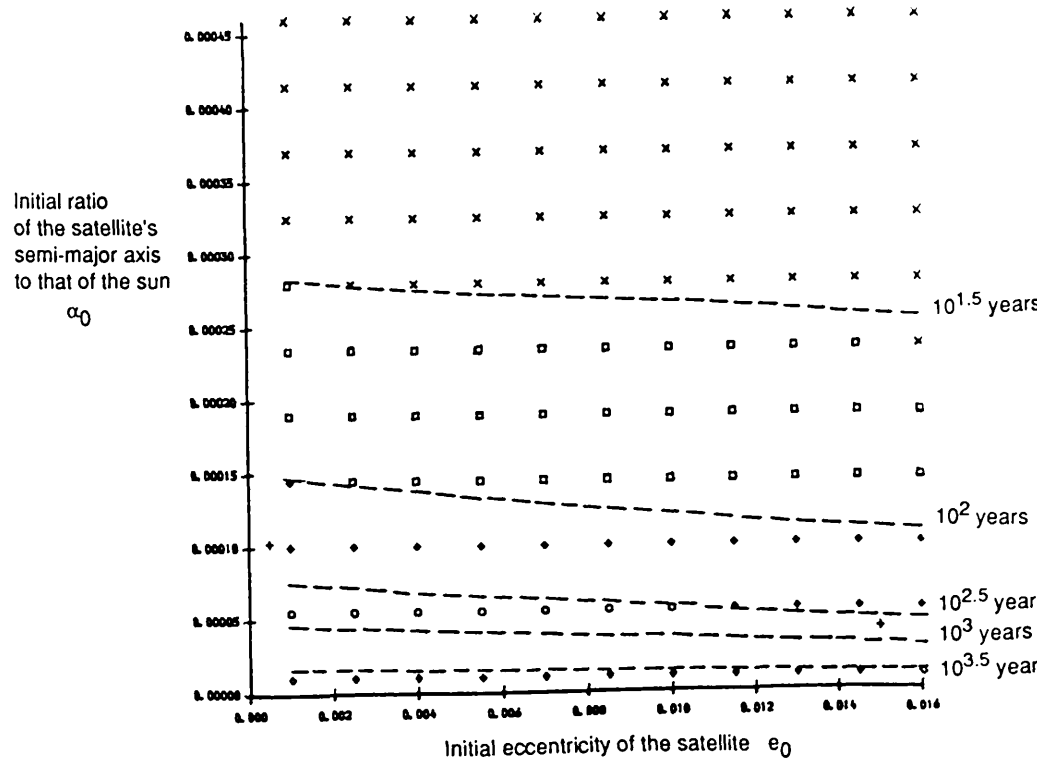
Initial ratio
of the satellite's
semi-major axis
to that of the sun
α_0
$10^{1.5}$ years
10^2 years
$10^{2.5}$ years
10^3 years
$10^{3.5}$ years
(b)
Initial eccentricity of the satellite e_0

We have also calculated the first level minimum durations for all the existing satellites of Jupiter, Saturn, Uranus, Earth and Mars whose $e_0 \neq 0$, and whose α_0 and e_0 are known. These calculations were done for both cases, firstly where the Sun is assumed to be moving in a circular planetocentric orbit and secondly where it is assumed to be moving in an elliptical planetocentric orbit. The results are listed in Tables 5.2 to 5.6. The first level minimum durations are found to within 1% accuracy using the trapezoidal type approximation to N_1. They are therefore accurate to at least two digits.

Satellite	T'_{min} (years)	
	Circular	Elliptical
Amalthea	2.2×10^4	1.9×10^4
Thebe	1.1×10^4	9.6×10^3
Io	5.8×10^3	5.0×10^3
Europa	2.4×10^3	2.1×10^3
Ganymede	1.5×10^3	1.3×10^3
Callisto	5.2×10^2	4.4×10^2
Leda	9.9	8.3
Himalia	8.9	7.4
Lysithea	1.1×10^1	9.3
Elara	6.7	5.6

Table 5.2 The first level minimum lifetimes for the known satellites of Jupiter, if the Sun is assumed to be moving in a fixed circular or elliptical orbit. Jupiter's sidereal period is taken to be 11.86198 years.

Satellite	T'_{min} (years)	
	Circular	Elliptical
Prometheus	1.1×10^5	9.4×10^4
Pandora	1.0×10^5	8.7×10^4
Janus	8.3×10^4	7.0×10^4
Epimetheus	7.8×10^4	6.6×10^4
Mimas	4.6×10^4	3.9×10^4
Enceladus	4.6×10^4	3.9×10^4
Dione	2.6×10^4	2.2×10^4
1980S6	2.3×10^4	1.9×10^4
Rhea	1.8×10^4	1.5×10^4
Titan	2.4×10^3	2.0×10^3
Hyperion	1.0×10^3	8.5×10^2
Iapetus	4.7×10^2	3.9×10^2
Phoebe	2.6×10^1	2.1×10^1

Table 5.3 The first level minimum lifetimes for the known satellites of Saturn, if the Sun is assumed to be moving in a fixed circular or elliptical orbit. Saturn's sidereal period is taken to be 29.45709 years.

Satellite	T'_{min} (years)	
	Circular	Elliptical
1986U8	1.1×10^6	9.9×10^5
Miranda	4.1×10^5	3.5×10^5
Ariel	2.2×10^5	1.9×10^5
Umbriel	1.2×10^5	1.1×10^5
Titania	6.8×10^4	5.9×10^4
Oberon	5.1×10^4	4.4×10^4

Table 5.4 The first level minimum lifetimes for the known satellites of Uranus, if the Sun is assumed to be moving in a fixed circular or elliptical orbit. Uranus' sidereal period is taken to be 84.01151 years.

Satellite	T'_{min} (years)	
	Circular	Elliptical
Moon	9.9×10^{-1}	9.3×10^{-1}

Table 5.5 The first level minimum lifetimes for the known satellites of Earth, if the Sun is assumed to be moving in a fixed circular or elliptical orbit. Earth's sidereal period is taken to be 1.00002 years.

Satellite	T'_{min} (years)	
	Circular	Elliptical
Phobos	6.1×10^{2}	4.5×10^{2}
Deimos	2.6×10^{2}	1.9×10^{2}

Table 5.6 The first level minimum lifetimes for the known satellites of Mars, if the Sun is assumed to be moving in a fixed circular or elliptical orbit. Mars' sidereal period is taken to be 1.88085 years.

Figures 5.3 to 5.7 and Tables 5.2 to 5.6 show that the minimum duration of a planet-satellite system is much the same whether the Sun is assumed to be moving in a fixed circular orbit or a fixed elliptical orbit, the circular case values being only slightly larger than the elliptical case values. This result is not unexpected since Figures 4.3 and 4.5 show that the elliptical case produces graphs of Δe plotted against f_{c0} which are very similar in shape to those of the circular case, but which are spread equally on either side of the equivalent circular graph for the different values of f_{1c0}. Obviously the similar shapes of the graphs indicate that the values of T'_{min} for both cases will also be similar, while the spread around the circular graph

implies that the largest possible Δe for the elliptical case will always be slightly larger than that of the circular case. Hence, the resulting minimum lifetimes of the satellite systems for the ellipical case will always be slightly smaller than that of the circular case.

In Figures 5.3 to 5.7 the minimum durations of the satellite systems for both elliptical and circular cases are shown to increase as either α_0 or e_0 are decreased. Obviously as α_0 decreases, the planet's gravitational hold on the satellite becomes larger relative to the perturbative effects of the Sun, and therefore the system will take longer to reach an unstable situation caused by the Sun. Likewise, a decrease in the initial eccentricity e_0 of the satellite system means the maximum solar perturbations acting on the satellite's orbit become smaller and as a result, the system can persevere through a greater number of synodic periods before an eccentricity of e_u is accumulated. Also, the system will take that much longer to reach e_u, if it begins at a smaller initial eccentricity.

Table 5.2 lists, for the known satellites of Jupiter applicable to our theory, minimum durations which range from as low as 4.4×10^2 years to as high as 2.2×10^4 years. The outer satellites of Jupiter, which were included in the calculations despite being outside the 5% relative error limitation of the analytical theory, produced minimum times of slightly less than 10 years.

The satellites of Saturn have first level minimum lifetimes which range from 3.9×10^2 to 1.1×10^5 years, with Phoebe, also outside the 5% error limitation, persevering for at least 20 years.

The satellites of Uranus, with their small eccentricities and small ratios of the semi-major axes, remain orbiting Uranus for at least 4.4×10^4 years to 1.1×10^6 years.

The first level of the finite-time stability criteria for the Earth's Moon, also just barely outside the 5% error limitation of the analytical theory, gives a disappointing minimum lifetime of about 1 year, while the two satellites of Mars have more reasonable first level minimum durations of 1.9×10^2 years and 4.5×10^2 years for the elliptical case.

The minimum durations found for the solar system satellites using this first level criteria are generally quite low compared to the known lifetime of the solar system of approximately 5×10^9 years. Clearly the finite-time stability method, as it stands so far, is of no use for studying our own Earth-Moon system with its large mass ratio and the Moon's large eccentricity. Nor is the theory likely to be useful in studying the stability of the outer satellites of Jupiter or Saturn's Phoebe. The first level of the theory cannot even guarantee that these satellites will remain in orbit about their respective planets for at least one revolution of their planet's orbit about the Sun.

The minimum lifetimes found for the majority of Jupiter's and Saturn's satellites and all of Uranus' satellites at 10^4 to 10^5 years are, however, quite promising and show that even when using the crudest of approximations, the finite-time stability method can produce fairly large minimum lifetimes.

The most important point to note about the minimum durations found for this first level of our method, is that for almost all of the satellites of the solar system, the minimum durations are sufficiently large enough to allow us to proceed to the next level of the finite-time stability method and thereby to increase their minimum durations to even higher values. The second level of the finite-time stability method and the requirements needed to achieve it are discussed in the next section.

5.3 The Second Level, Using the Maximum Possible Change in the Eccentricity Over One Conjunction Cycle

It is of course, very pessimistic to assume that the maximum possible change in the satellite's eccentricty over one synodic period is added on to the satellite's eccentricity every synodic period. Figures 3.2 or 4.3 show that as the true anomaly f_{c0} of the conjunction at the centre of the synodic period is chosen to range from 0° to 360°, the change in the eccentricity is essentially cyclic. As the system passes from one conjunction to the next, in other words from one synodic period to the next, the true anomaly of the conjunction at the centre of each successive synodic period, will also range between 0° to 360°. The resulting changes in eccentricity over each synodic period will therefore also vary in a cyclic fashion as a function of time.

The accumulation of these changes in eccentricity to the satellite's initial eccentricity would then result in, not a steadily growing eccentricity as used in the first level, but in an oscillating eccentricity where the current changes in the eccentricity can cancel the effects of previous changes in the eccentricity. Thus, to add the maximum possible change in the eccentricity over one synodic period on to the satellite's eccentricity every synodic period, when Δe_{max} occurs only once over the range f_{c0} = 0° to 360°, can only give the crudest approximations for the minimum duration of the system.

It makes sense therefore, to allow the satellite system to pass from one synodic period to the next, until the next largest natural cycle of the planet-satellite-Sun system is attained. If the system can be guaranteed to remain in a stable situation until the larger cycle is reached, then the maximum possible change in the satellite's eccentricity over this larger cycle can be used as a means of deriving a minimum lifetime for the satellite system, in much the same manner as the maximum possible change in eccentricity over a synodic period was used in the first level to find minimum lifetimes. Because this new change in the satellite's eccentricity is found over a longer time span, the resulting minimum duration of the satellite system against solar perturbations should be a less pessimistic and more realistic estimate of the minimum time taken for the eccentricity to increase to e_u.

After the synodic period, the next largest natural cycle of the planet-satellite-Sun system is the conjunction cycle. A conjunction cycle is defined to be the revolution of the conjunction line through approximately an angle of 2π with respect to a fixed reference point, to end at the conjunction falling closest to the location of the initial conjunction.

By assuming that the ratio ν of the mean motions of the satellite and the Sun is small, we are assuming that the satellite moves much faster than the Sun around the planet. This means each successive conjunction of the satellite and Sun will occur only a small angle θ further on from the previous conjunction. In other words, while the Sun has only moved through a small angle θ between conjunctions, the satellite has moved through an angle of $2\pi + \theta$. In this manner, the conjunction line moves by an angle θ every synodic period. The conjunction cycle is completed when the conjunction located nearest to the position of the original conjunction is reached. A conjunction cycle will not end at its beginning position unless the angles θ between successive conjunctions divide the interval of 2π exactly. Figure 5.8 displays the successive conjunctions of the satellite and Sun which form a conjunction cycle.

The conjunction cycle period is approximately the sidereal period T_1 of the Sun in its revolution about the planet. It cannot be exactly equal to the Sun's sidereal period because the final conjunction rarely occurs in exactly the same position as the initial conjunction; however, on average, the conjunction cycle period should be equal to the Sun's sidereal period, since the final conjunction line can fall equally on either side of the original conjunction line to within a small angle $\theta/2$.

We shall see later that the angle between successive conjunctions θ depends on the values of the orbital elements. Since these values are changing as the system passes from one synodic period to the next, θ is not a constant throughout the conjunction cycle. However, because the changes in the orbital elements over one conjunction cycle are small, the changes in the angle between successive conjunctions are also small. Figure 5.8, therefore, shows the angles between successive conjunctions to be almost constant.

Note that the apsidal line of the satellite's orbit should be taken to be moving;

however, since the changes in the longitude of pericentre over a conjunction cycle are very small, the diagram is essentially correct. The fact that the satellite's apse line moves and that the angle between consecutive conjunction lines varies with changing values of the orbital elements should be included in the actual problem.

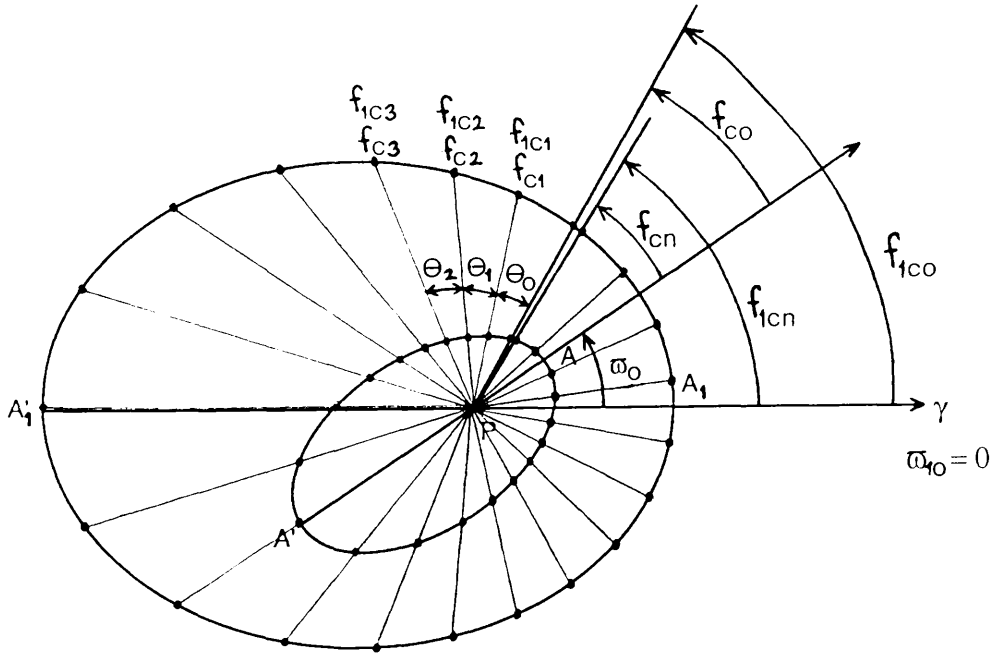

Figure 5.8 Shows the movement of the Sun-satellite-planet conjunction line through a complete conjunction cycle. The conjunction cycle begins at the conjunction located at f_{c0} and f_{1c0} and ends at the conjunction falling nearest to a true anomaly of $(f_{1c0} + 2\pi)$ or f_{1cn}.

Having defined the next largest natural cycle (ie the conjunction cycle) which can be used in the finite-time stability method, we now need to find a method of mapping one synodic period to the next, in order to allow the planet-satellite system to pass through one conjunction cycle. If the minimum duration of the satellite system

found for the first level is much greater than the time taken for the system to pass through one conjunction cycle, ie

$$T^{1}_{min} >> T_1$$

then the satellite will have time to pass through many conjunction cycles, and the net change in the eccentricity over each conjunction cycle will be very much smaller than if we allowed the eccentricity to grow by Δe_{max} every synodic period.

The second level of the finite-time stability method can then be applied to the satellite system. The second level follows the same procedure as that of the first level. We need to:

(1) find the changes $\Delta\sigma_c$ in the orbital elements over one conjunction cycle

(2) calculate the maximum possible change $\Delta e_{max\text{-}c}$ in the eccentricity over one conjunction cycle

(3) count the number of conjunction cycles N_2 needed to increase the satellite's eccentricity to the chosen upper limit of e_u, where $\Delta e_{max\text{-}c}$ is assumed to be added onto the current eccentricity every conjunction cycle, and where $\Delta e_{max\text{-}c}$ is re-evaluated every conjunction cycle using the current values for the orbital elements

(4) and finally, evaluate the minimum duration T^{2}_{min} of the planet-satellite system for the second level of the finite-time stability method using the following equation

$$T^{2}_{min} = N_2 T_1 \qquad (7)$$

The only added restriction to those of the first level, is that the accumulated

eccentricity within a conjunction cycle cannot become greater than e_u. If it does, then the system will have reached a potentially unstable situation by our definition, even though the total change in the eccentricity over the conjunction cycle may not increase the satellite's eccentricity to a value greater than or equal to e_u.

Note that if the criteria for attaining the second level is not met, in other words if T'_{min} is approximately equal to T_1 or is less than T_1, it does not mean that hierarchical instability will eventually result. The finite-time stability method is simply unable to provide any meaningful results for this particular case. In this thesis, we therefore confine our attention to the cases where $T'_{min} >> T_1$.

(i) A theoretical method for calculating the changes in the orbital elements over one cycle of conjunctions

We now use the analytical theory to map synodic period to synodic period in order to obtain, for an initial value f_{c0} of the true anomaly at the first conjunction, the changes in the orbital elements $\Delta\sigma_c$ over a complete conjunction line cycle where the revolution is taken with respect to a fixed reference point.

Let θ_i be the angular distance between the i^{th} conjunction and the $(i+1)^{th}$ conjunction with respect to a fixed reference point γ and let T_{Si} be the time interval between these two conjunctions. During this time interval of one synodic period, as in Chapter 2, we take the orbital elements to be constants equalling e_i, α_i, ϖ_i and ϵ_i. The i^{th} conjunction is taken to occur at true anomalies of f_{ci} and f_{1ci}, while the $(i+1)^{th}$ conjunction is taken to occur at true anomalies of $f_{c(i+1)}$ and $f_{1c(i+1)}$.

See Figures 5.9 and 5.10 for a diagram of these parameters. Figure 5.9 describes the orbital parameters for the satellite and the Sun at the centre of the i^{th} and $(i+1)^{th}$ synodic periods for the circular case and Figure 5.10 represents the equivalent diagram for the elliptical case.

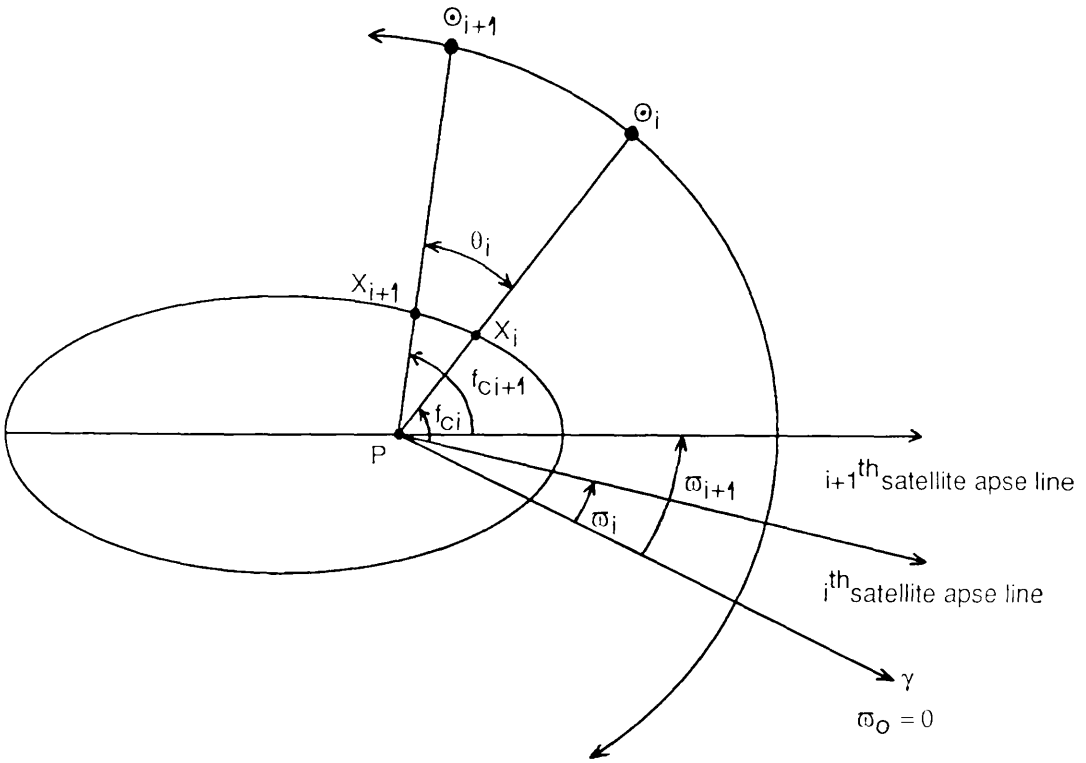

Figure 5.9 The orbital parameters which describe the positions of the satellite X and the Sun ⊙ at the centre of the i^{th} synodic period (denoted by the i subscript), and at the centre of the $(i+1)^{th}$ synodic period (denoted by the (i+1) subscript). At both these times, the planet-satellite-Sun system is taken to be at a conjunction.

In the above diagram the Sun is assumed to be moving in a fixed circular orbit.

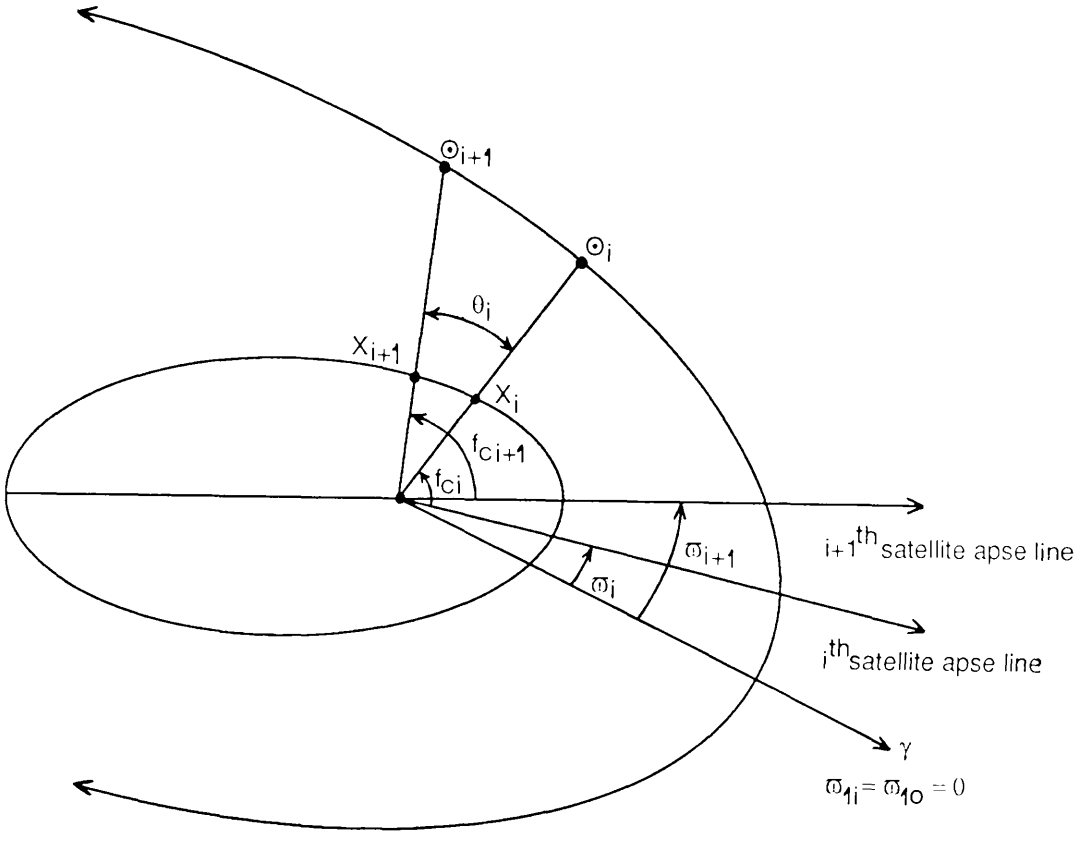

Figure 5.10 The equivalent diagram to Figure 5.9, except that the Sun is assumed to be moving in a fixed elliptical orbit.

Using Tables 4.4 or Equations (27) of Chapter 4, the changes in the orbital elements over the i^{th} synodic period centred on the i^{th} conjunction can be found. Let these values be denoted by Δe_i, $\Delta \alpha_i$, $\Delta \varpi_i$ and $\Delta \epsilon_i$. We update the current values of the orbital elements only at the midpoint of the time interval over which the changes occur or in other words, at a conjunction of the satellite and the Sun. Thus at the $(i+1)^{th}$ conjunction, the orbital elements become

$$\sigma_{i+1} = \sigma_i + \Delta\sigma_i$$

where: σ is any one of the four orbital parameters; $\Delta\sigma_i$ is the change in the specified orbital parameter which occurs over one synodic period centred on the i^{th}

conjunction; i represents the i^{th} conjunction; and i+1 represents the $(i+1)^{th}$ conjunction.

Thus from Figures 5.9 and 5.10, we find that the angle θ_i between the location of the i^{th} and $(i+1)^{th}$ conjunctions is given by

$$f_{c(i+1)} = f_{ci} + \theta_i - (\varpi_{i+1} - \varpi_i) \qquad (8)$$

using the satellite's true anomalies at the two conjunctions, or by

$$f_{1c(i+1)} = f_{1ci} + \theta_i \qquad (9)$$

using the Sun's true anomalies at the conjunctions.

Note that in Equation (8), the angle θ_i is measured in terms of the difference of the satellite's true anomalies, which are measured with respect to the satellite's line of apses. The formula must therefore include an adjustment to allow for the change which occurs in the position of the apsidal line with respect to a fixed reference point γ over the time interval between the two conjunctions. Note also that Equation (9) does not include this adjustment, because in both the circular and elliptical cases the Sun's orbit is assumed to be fixed in space and therefore the Sun's apsidal line does not move.

As in previous chapters, we now assume that any changes in ϖ are very small over one synodic period. Thus, $\Delta\varpi_i$ is taken to be zero. Equation (8) can be rewritten as

$$f_{c(i+1)} \cong f_{ci} + \theta_i \qquad (10)$$

For the satellite, which moves much faster than the Sun around the planet, the time between successive conjunctions T_{Si} will be the time the satellite takes to complete one orbit about its planet (ie its sidereal period T) plus a small time t needed for the satellite to catch up to the new position of the Sun with respect to a fixed reference point. This time t is approximately the time taken by the satellite to

move through an angle θ_i, beginning at a true anomaly of f_{ci}. Thus,

$$T_{Si} = T + t \qquad \text{where} \qquad t = \int_{f = f_{ci}}^{f = f_{ci} + \theta_i} \left(\frac{dt}{df} \right) df \tag{11}$$

For the Sun on the other hand, the time between succesive conjunctions T_{Si} is the time taken by the Sun to move through an angle θ_i, beginning at a true anomaly of f_{1ci}, ie

$$T_{Si} = \int_{f_1 = f_{1ci}}^{f_1 = f_{1ci} + \theta_i} \left(\frac{dt}{df_1} \right) df_1 \tag{12}$$

The derivative dt/df can be written in terms of the radius of the orbit r and the body's angular momentum h using Kepler's second law.

$$\frac{dt}{df} = \frac{r^2}{h} \tag{13}$$

Substituting the elliptical orbit expressions for r and h, ie

$$r = \frac{a(1 - e^2)}{1 + e\cos f}$$

$$h = a^2 n \sqrt{1 - e^2}$$

into Equation (13) produces:

$$\frac{dt}{df} = \frac{(1 - e^2)^{3/2}}{n} (1 + e\cos f)^{-2}$$

Equation (11) and (12) can then be expressed totally in terms of known parameters and the two unknown parameters θ_i and T_{Si}. Equation (11) becomes

$$T_{Si} = \frac{2\pi}{n} + \frac{(1 - e_i^2)^{3/2}}{n} I(\theta_i)$$

$$\text{where} \qquad I(\theta_i) = \int_{f = f_{ci}}^{f = f_{ci} + \theta_i} (1 + e_i \cos f)^{-2} \, df \qquad (14)$$

while Equation (12) becomes

$$T_{Si} = \frac{(1 - e_{1i}^2)^{3/2}}{n_1} I_1(\theta_i)$$

$$\text{where} \qquad I_1(\theta_i) = \int_{f_1 = f_{1ci}}^{f_1 = f_{1ci} + \theta_i} (1 + e_{1i} \cos f_1)^{-2} \, df_1 \qquad (15)$$

We now have two equations (14) and (15) and two unknowns θ_i and T_{Si}. In the circular case, Equation (15) is simply

$$T_{Si} = \frac{\theta_i}{n_1} \qquad (16)$$

since the Sun is assumed to move in a fixed circular orbit at a constant speed of n_1. To avoid repetition, we shall not, however, solve the elliptical and circular problems separately. Instead, we first solve Equations (14) and (15) describing the complete elliptical problem for θ_i and T_{Si}, and then derive the circular solution from the elliptical solution by setting e_{1i} to zero.

Equating Equations (14) and (15), in order to eliminate T_{Si}, produces a complicated transcendental function of θ_i. viz.

$$2\pi v + (1 - e_i^2)^{3/2} \, v \, I(\theta_i) = (1 - e_{1i}^2)^{3/2} \, I_1(\theta_i) \qquad (17)$$

Equation (17) can be solved for θ_i by expanding the equation about the small parameters and solving for θ_i as a function of the non-linear functions of θ_i. Then by repeatedly substituting $\theta_i = f(\theta_i)$ into the right hand side of the equation for θ_i and expanding about the small parameters, θ_i can be completely eliminated from the right hand side of the equation to the required order. In other words, we use the same procedure already applied previously in Chapters 3 and 4 for solving transcendental equations to a specified order.

Expansion of $I(\theta_i)$ to third order about the small parameter e_i gives

$$I = \left(1 + \frac{3}{2}e_i^2\right)\theta_i - 2e_i\left(1 + \frac{3}{2}e_i^2\right)[\sin \overline{f_{ci} + \theta_i} - \sin f_{ci}]$$
$$+\frac{3}{4}e_i^2\,[\sin \overline{2(f_{ci} + \theta_i)} - \sin 2f_{ci}] - \frac{1}{3}e_i^3\,[\sin \overline{3(f_{ci} + \theta_i)} - \sin 3f_{ci}]$$

We then isolate the angle θ_i within the trigonometric arguments using Equations (15) of Chapter 3. $I(\theta_i)$ then becomes:

$$I(\theta_i) = \left(1 + \frac{3}{2}e_i^2\right)\theta_i + W(\theta_i)$$

where $W(\theta_i) = -2e_i\,[\sin f_{ci}\,(\cos\theta_i - 1) + \cos f_{ci} \sin\theta_i]$

$$+\frac{3}{4}e_i^2\,[\sin 2f_{ci}\,(\cos 2\theta_i - 1) + \cos 2f_{ci} \sin 2\theta_i]$$
$$-\frac{1}{3}e_i^3\,[\sin 3f_{ci}\,(\cos 3\theta_i - 1) + \cos 3f_{ci} \sin 3\theta_i]$$
$$-3e_i^3\,[\sin f_{ci}\,(\cos\theta_i - 1) + \cos f_{ci} \sin\theta_i] \qquad (18)$$

Similarly, $I_1(\theta_i)$ becomes:

$$I_1(\theta_i) = \left(1 + \frac{3}{2}e_{1i}^2\right)\theta_i + W_1(\theta_i)$$

where $W_1(\theta_i) = -2e_{1i}[\sin f_{1ci}\ (\cos\theta_i - 1) + \cos f_{1ci} \sin\theta_i]$

$$+\frac{3}{4}e_{1i}^2[\sin 2f_{1ci}\ (\cos 2\theta_i - 1) + \cos 2f_{1ci} \sin 2\theta_i]$$

$$-\frac{1}{3}e_{1i}^2[\sin 3f_{1ci}\ (\cos 3\theta_i - 1) + \cos 3f_{1ci} \sin 3\theta_i]$$

$$-3e_{1i}^2[\sin f_{1ci}\ (\cos\theta_i - 1) + \cos f_{1ci} \sin\theta_i] \qquad (19)$$

Substitution of Equations (18) and (19) into (17) and further expansion about the small parameters e_{1i} and e_i and ν gives

$$\theta_i = 2\pi\nu(1 + \nu + \nu^2) + (\nu + \nu^2)\, W(\theta_i) - (1 + \nu + \nu^2)\, W_1(\theta_i)$$

$$+\frac{3}{2}e_{1i}^2\, W_1(\theta_i) \qquad (20)$$

We now have θ_i written as a complicated function of itself, involving $W(\theta_i)$ and $W_1(\theta_i)$. Substitution of the above expression for θ_i into its right-hand side involves the expansion of the trigonometric functions $\cos n\theta_i$ and $\sin n\theta_i$ about the small parameters of θ_i. Since θ_i has a minimum order of one due to the multiple $2\pi\nu$, we can in fact expand about small θ_i. Thus, to third order, $W(\theta_i)$ becomes

$$W(\theta_i) = e_i(\theta_i^2 \sin f_{ci} - 2\theta_i \cos f_{ci}) + \frac{3}{2}e_i^2\theta_i \cos 2f_{ci}$$

Likewise, $W_1(\theta_i)$ to third order is

$$W_1(\theta_i) = e_{1i}(\theta_i^2 \sin f_{1ci} - 2\theta_i \cos f_{1ci}) + \frac{3}{2}e_{1i}^2\theta_i \cos 2f_{1ci}$$

Hence, θ_i as a function of itself is:

$$\theta_i = 2\pi\nu(1 + \nu + \nu^2) + \nu(-2e_i \cos f_{ci})\,\theta_i - e_{1i}(\theta_i^2 \sin f_{ci} - 2\theta_i \cos f_{1ci})$$
$$-\frac{3}{2}e_{1i}^2\,\theta_i \cos 2f_{1ci} + 2e_{1i}\,\nu\theta_i \cos f_{1ci} \qquad (21)$$

Successive substitutions of θ_i into the right-hand side of Equation (21) and expansions about the small parameters θ_i eventually produce the following series approximation to θ_i:

$$\theta_i = 2\pi\nu\,[1 + \nu + \nu^2 - 2e_i\,\nu\cos f_{ci} - 2\pi e_{1i}\,\nu\sin f_{1ci}$$
$$+(2e_{1i} + 4e_{1i}\,\nu)\cos f_{1ci} - \frac{3}{2}e_{1i}^2 \cos 2f_{1ci} + 4e_{1i}^2 \cos^2 f_{1ci}] \qquad (22)$$

The synodic period T_{Si} is found by substituting Equation (19) into an expansion of Equation (15) about the small parameter e_{1i} and replacing θ_i with our new expression for θ_i (ie Equation (22)). Thus, firstly

$$T_{Si} = \frac{T_1}{2\pi}\left(1 - \frac{3}{2}e_{1i}^2\right)\left[\left(1 + \frac{3}{2}e_{1i}^2\right)\theta_i + W_1(\theta_i)\right]$$

where T_1 is the Sun's sidereal period. After substitution of Equation (22) and a little reduction, the synodic period becomes

$$T_{Si} = T_1\nu(1 + \nu + \nu^2 - 2e_i\,\nu\cos f_{ci} + 2e_{1i}\,\nu\cos f_{1ci}) \qquad (23)$$

Setting $e_{1i} = 0$, produces the following solution for the circular problem.

$$\theta_i = 2\pi\nu\,[1 + \nu + \nu^2 - 2e_i\,\nu\cos f_{ci}) \qquad (24)$$

$$T_{Si} = T_1\nu(1 + \nu + \nu^2 - 2e_i\,\nu\cos f_{ci}) \qquad (25)$$

The changes in the orbital elements over a conjunction cycle can be found by: beginning with the inital orbital elements e_0, α_0, ϖ_0, ϵ_0 and the initial true anomalies f_{c0} and f_{1c0} at the first conjunction; using Equation (27) of Chapter 4 or Tables 4.4 to calculate the changes $\Delta\sigma_0$ in the orbital elements over a synodic period; and adding the changes to the initial orbital elements to get the new orbital elements, viz

$$\sigma_1 = \Delta\sigma_0 + \sigma_0$$

The new values for the true anomalies of the satellite and the Sun at the conjunction centred in this new synodic period then become

$$f_{c1} \cong f_{c0} + \theta_0 \qquad \text{and} \qquad f_{1c1} = f_{1c0} + \theta_0$$

using Equation (24) for the circular case or Equation (22) for the elliptical case.

The orbital elements σ_1 and the true anomalies f_{c1} and f_{1c1} for the new synodic period are then used to calculate the changes in the orbital elements over this new synodic period, and so on. This process is continued until the conjunction line has swept through approximately an angle of 2π with respect to a fixed reference point. For example, since the Sun's apse is assumed to be fixed, we allow the process to continue until the true anomaly of the Sun at conjunction has moved from f_{1c0} to the next closest value to $f_{1c0} + 2\pi$. The total changes in the orbital elements $\Delta\sigma_c$ over this conjunction cycle are then evaluated for use in the second level of the finite-time stability method.

It is interesting to note the effectiveness of using the average value of the synodic period given by Equation (6), instead of using the actual synodic period as given by Equation (25) for the circular case or Equation (23) for the elliptical case.

Equation (6) can be rewritten in terms of the Sun's sidereal period T_1 and expanded about the small parameter ν in order to compare it with Equation (23) or (25). The result

$$T_{Si} = \frac{T_1 \nu}{1 - \nu} \cong T_1 \nu (1 + \nu + \nu^2 \ldots)$$

shows that the average synodic period is a good approximation to the actual synodic period between any two successive conjunctions, for both circular and elliptical cases to second order.

It is also interesting to note that a special solution to the elliptical case of T_{Si} where the two elliptical orbits have: collinear semi-major axes ($\varpi_i = \varpi_{10}$); identical eccentricities ($e_i = e_{1i}$); and a fixed orbital orientation with respect to each other (ie $\Delta\varpi_i = 0$); results in a constant synodic period which is equal to the average synodic period given by Equation (6), no matter where the first conjunction begins. This fact can be easily shown by studying Equations (14) and (15).

Assuming $\Delta\varpi_i = 0$, the two equations become

$$T_{Si} = T\left[1 + \frac{(1 - e_i^2)^{3/2}}{2\pi} I(\theta_i)\right] \tag{26}$$

$$T_{Si} = \frac{T_1}{2\pi} (1 - e_{1i}^2)^{3/2} I(\theta_i) \tag{27}$$

Solving for 2π in Equation (27) and substituting the result into Equation (26) gives the following expression involving T_{Si}, T and T_1:

$$T_{Si} = T\left[1 + \left(\frac{1 - e_i^2}{1 - e_{1i}^2}\right)^{3/2} \frac{I}{I_1} \frac{T_{Si}}{T_1}\right] \tag{28}$$

If we now rearrange Equation (28) into a form similar to the equation for the average synodic period, we obtain:

$$\frac{1}{T_{Si}} = \frac{1}{T} - \frac{Q}{T_1}$$

$$Q = \left(\frac{1 - e_i^2}{1 - e_{1i}^2} \right)^{3/2} \frac{I}{I_1} = \left(\frac{1 - e_i^2}{1 - e_{1i}^2} \right)^{3/2} \frac{\int_{f_{ci}}^{f_{ci} + \theta_i} (1 + e_i \cos f)^{-2} \, df}{\int_{f_{1ci}}^{f_{1ci} + \theta_i} (1 + e_{1i} \cos f_1)^{-2} \, df_1}$$

Q becomes 1 when $e_i = e_{1i}$ and $f_{ci} = f_{1ci}$. In other words, the synodic period for two bodies moving in fixed elliptical orbits about the same focus is the same as that for the case where the two bodies move in fixed circular orbits about the same centre, if the two elliptical orbits have collinear semi-major axes and are identical in shape, but not necessarily in size.

(ii) A numerical method for calculating the changes in the orbital elements over one cycle of conjunctions

The numerical integration method used to find the changes in the orbital elements over one synodic period can also be used to map one synodic period to the next in order to obtain the changes in the orbital elements over a conjunction cycle.

Let the orbital elements of a satellite for the i^{th} synodic period centred on the i^{th} conjunction be σ_i, where $\sigma_i = e_i, \alpha_i, \varpi_i$ or ϵ_i. Let the true anomaly of the central conjunction for the satellite be f_{ci}, and for the Sun be f_{1ci}. Let the true anomalies of the satellite at the opposition occurring at the beginning and end of the i^{th} synodic period be $f_i(s=-\pi)$ and $f_i(s=+\pi)$ respectively.

The changes in the orbital elements $\Delta\sigma_i$ over the i^{th} synodic period centred on the i^{th} conjunction can then easily be found by integrating numerically Equations (2) of Chapter 3 for the circular case or Equations (2) of Chapter 4 for the elliptical case, ie

$$\Delta\sigma_i = \int_{f_i(S=-\pi)}^{f_i(S=+\pi)} \frac{d\sigma_i}{df}\, df \qquad (29)$$

The new orbital elements σ_{i+1} for the $(i+1)^{th}$ synodic period centred on the $(i+1)^{th}$ conjunction then become

$$\sigma_{i+1} = \sigma_i + \Delta\sigma_i \qquad (30)$$

Using the above procedure we can then map synodic period to synodic period and follow the changes in the orbital elements over longer periods than the synodic period. However, in order to find the orbital elements σ_{i+1} of the next $(i+1)^{th}$ synodic period, we must first know the following parameters of the i^{th} synodic period: σ_i, f_{ci}, f_{1ci}, $f_i(S=-\pi)$ and $f_i(S=+\pi)$. These are calculated using the parameters of the $(i-1)^{th}$ synodic period which in turn are calculated using the corresponding parameters of the $(i-2)^{th}$ synodic period, and so on back to the parameters of the

zeroth synodic period which are given.

The relationship between the parameters of one synodic period and the parameters of the next synodic period are derived as follows. The true anomaly of the satellite at the beginning of the i^{th} synodic period must be identical to the satellite's true anomaly at the end of the $(i-1)^{th}$ synodic period in order for the orbit to be continuous. Therefore,

$$f_i\,(S=-\pi) = f_{i\,-1}\,(S=+\pi) - 2\pi \tag{31}$$

Because our numerical integration procedure requires that the angle S between the radius vector of the satellite and the radius vector of the Sun remains between the angles $-\pi$ and $+\pi$, we must subtract 2π.

For the elliptical case, the true anomaly of the Sun at the beginning of the i^{th} synodic period can be found from the true anomaly of the satellite at the beginning of the i^{th} synodic period using the relation $S=f-f_1+\varpi$ (See Figure 4.1(b)) and the fact that at this point in time the system is in oppostion, with $S = -\pi$. Thus,

$$f_{1i}\,(S=-\pi) = f_i\,(S=-\pi) + \varpi_i + \pi \tag{32}$$

For the circular case, given $f_i(S=-\pi)$ and σ_i, we can find the true anomaly f_{ci} of the satellite at the central conjunction of the i^{th} synodic period, by solving the following equations for the variables indicated below:

$$\begin{aligned}
E_i: &\qquad \tan\frac{E_i}{2} = \left(\frac{1-e_i}{1+e_i}\right)^{1/2} \tan\frac{f_i}{2} \\
n_1 t: &\qquad n_1 t = \nu_i\,(E_i - e_i \sin E_i - (\epsilon_i - \varpi_\iota)\,) \\
f_{ci}: &\qquad f_{ci} = f_i + \pi - n_1 t
\end{aligned} \tag{33}$$

Note that the variables f_i, E_i and t are evaluated at $S = -\pi$, while the variable f_{ci} is evaluated at $S = 0$. See Section 3.2 for the origin of these equations.

For the elliptical case, given $f_i(S=-\pi)$, $f_{1i}(S=-\pi)$ and σ_i, the true anomalies of the satellite f_{ci} and the Sun f_{1ci} at the central conjunction for the i^{th} synodic period are found by solving the following set of equations for the listed variables.

$$
\begin{aligned}
E_i: \quad & \tan\frac{E_i}{2} = \left(\frac{1-e_i}{1+e_i}\right)^{1/2} \tan\frac{f_i}{2} \\
n_1 t: \quad & n_1 t = \nu_i \left(E_i - e_i \sin E_i - (\epsilon_i - \varpi_\upsilon)\right) \\
E_{1i}: \quad & \tan\frac{E_{1i}}{2} = \left(\frac{1-e_{1i}}{1+e_{1i}}\right)^{1/2} \tan\frac{f_{1i}}{2} \\
E_{1ci}: \quad & n_1 t = E_{1i} - e_1 \sin E_{1i} + e_1 \sin E_{1ci} - E_{1ci} \\
f_{1ci}: \quad & \tan\frac{f_{1ci}}{2} = \left(\frac{1+e_1}{1-e_1}\right)^{1/2} \tan\frac{E_{1ci}}{2} \\
f_{ci}: \quad & f_{ci} = f_i - f_{1i} + f_{1ci} + \pi
\end{aligned}
\tag{34}
$$

Note that the variables f_i, E_i, t, E_{1i} and f_{1i} are evaluated at $S = -\pi$, while the variables E_{1ci}, f_{ci} and f_{1ci} are evaluated at $S = 0$ or at the conjunction. See Section 4.2 for the origin of these equations.

The upper limit of the integration (ie the true anomaly $f_i(S=+\pi)$ of the satellite at the end of the i^{th} synodic period) is found, given f_{ci} and f_{1ci}, using the same methods used in Section 3.2 for the circular case or Section 4.2 for the elliptical case.

In summary, we begin with the initial orbital elements σ_0 of the satellite and the true anomalies f_{c0} and f_{1c0} of the satellite and the Sun at the initial conjunction located at the centre of the zeroth synodic period. The true anomalies of the satellite at the beginning $f_0(S=-\pi)$ and end $f_0(S=+\pi)$ of the zeroth synodic period, given f_{c0} and f_{1c0}, are found using the same method described in Section 3.2 for the circular case or Section 4.2 for the elliptical case. Note, that in these chapters $f_0(S=-\pi)$ and

$f_0(S=+\pi)$ are referred to as $f_{-\pi}$ and $f_{+\pi}$ respectively.

We then use Equation (29) to find the change $\Delta\sigma_1$ in the orbital elements over the first synodic period. Equation (30) gives the orbital elements σ_1 of the first synodic period, while Equations (31) and (32) can be used to calculate the true anomalies of the satellite $f_1(S=-\pi)$ and the Sun $f_{11}(S=-\pi)$ at the beginning of the first synodic period. From Equations (33) or (34) we then can evaluate the true anomalies of the satellite f_{c1} and the Sun f_{1c1} at the first conjunction. Finally Equations (11) of Chapter 3 or Equations (8) of Chapter 4 can be used to obtain the true anomaly $f_1(S=+\pi)$ of the satellite at the end of the first synodic period.

The same procedure is then repeated to find the values of the parameters for the second synodic period, and so on. In this manner, the orbital elements of the planet-satellite system during any particular synodic period can be found. The changes in the orbital elements over one cycle of conjunctions are then simply the differences between the orbital elements in the final synodic period and the initial synodic period of the conjunction cycle.

Because large amounts of computing time are necessary to calculate numerically the orbital elements over intervals greater than one conjunction cycle period, we use the numerical procedure only to check the accuracy of the analytical procedure. Due to time limitations on the computer, error contours like those found in Chapters 3 and 4 are not a feasible means of displaying the accuracy of the analytical solution. Instead, we check the accuracy of the analytical solution for the worst examples that we plan to study at this second level.

These worst cases involve those planet-satellite systems whose initial parameters are the largest of the cases to be investigated. As before, we study the accuracy of the eccentricity, the most important orbital element for questions of the stability of the system. Once again, the greatest difference between the numerical and the analytical solutions occurs at the maximum possible change in the eccentricity over the cycle being studied. We therefore compare the analytical and numerical values of the maximum possible change in the eccentricity for satellites with an eccentricity equal to the upper limit of 0.5 and a semi-major axes ratio equal to the

largest value of α_0 found amongst the satellites orbiting each planet. The remainder of the cases studied should have percentage relative errors which are less than those of the worst cases, when the eccentricity is allowed to grow to e_u.

The relative percentage differences between the numerical changes in the eccentricity over a conjunction cycle and the equivalent analytical values for both the circular and elliptical cases are listed in Table 5.7. Only the worst cases of each planet are included. The errors are no greater than 2.2% for the circular case and 7.3% for the elliptical case.

Planet	Satellite	Percentage Error of Worst Case	
		Circular Case	Elliptical Case
Jupiter	Callisto	0.2%	1.5%
Saturn	Iapetus	2.2	7.3
Uranus	Oberon	0.9	4.6
Mars	Deimos	0.6	5.3

Table 5.7 The percentage relative differences between the analytical and the numerical values of the maximum possible change in the satellite's orbital eccentricity over one conjunction cycle for both the circular and elliptical cases.

Only the results for the satellite with the worst difference between the analytical and numerical solutions from each of the planets are listed here.

The analytical mapping procedure is therefore sufficiently accurate for our purposes since we desire only one significant figure in the final values of the minimum lifetimes of the planet-satellite systems. In particular, it appears that the relative errors between the analytical and numerical solutions for the changes in the

eccentricity over one synodic period are not cumulative as the system passes through many synodic periods, just as the eccentricity itself does not steadily increase with time.

For all future analysis, we use the analytical procedure described in Section 5.2(i) to calculate the changes in the orbital elements over a cycle of conjunctions.

(iii) A study of the cyclic nature of the orbital elements over one conjunction cycle

If we now map synodic period to synodic period using the analytical theory, we can calculate the values of the orbital elements σ_i for each synodic period and the changes in the orbital elements which occur over each synodic period, as the satellite system moves through one conjunction cycle.

Figures 5.11 parts (i) show the relationships between the changes (Δe_i, $\Delta \alpha_i$, $\Delta \epsilon_i$ and $\Delta \varpi_i$) in the orbital elements over each successive synodic period in a conjunction cycle, and the true anomalies f_{ci} of the conjunctions located at the centre of each successive synodic period in a conjunction cycle. Parts (ii) of the figures give the relationships between the accumulated orbital elements (e_i, α_i, ϵ_i and ϖ_i) over successive synodic periods in a conjunction cycle, and the true anomalies f_{ci} of the conjunctions in a conjunction cycle.

Initial conditions similar to those of the Jupiter-Callisto system are used, where $\alpha_0 = 0.0025$, $e_0 = 0.01$ and $\mu = 1{,}100$, but the results apply to any planet-satellite-Sun system in the solar system. The initial conjunction of the satellite, planet and Sun is assumed to be located in the direction of the satellite's semi-major axis (ie at a true anomaly of $f_{c0} = 0°$). The Sun is assumed to be moving in a fixed circular orbit for Figures 5.11.

Figures 5.11 (a) to (d) The variations in (i) the changes $\Delta\sigma$ in the satellite's orbital elements over one synodic period and (ii) the satellite's accumulated orbital elements σ as the satellite passes through successive i^{th} synodic periods to complete one conjunction cycle.

$\Delta\sigma$ and σ are evaluated only at discrete positions (ie at true anomalies f_{ci} where the planet-satellite-Sun system is in conjunction). σ is taken to be e, α, ϵ or ϖ for parts (a) through to (d) respectively.

The data used here is that of a circular coplanar Jupiter-Callisto system with α=0.0025, e = 0.01 and μ = 1100.

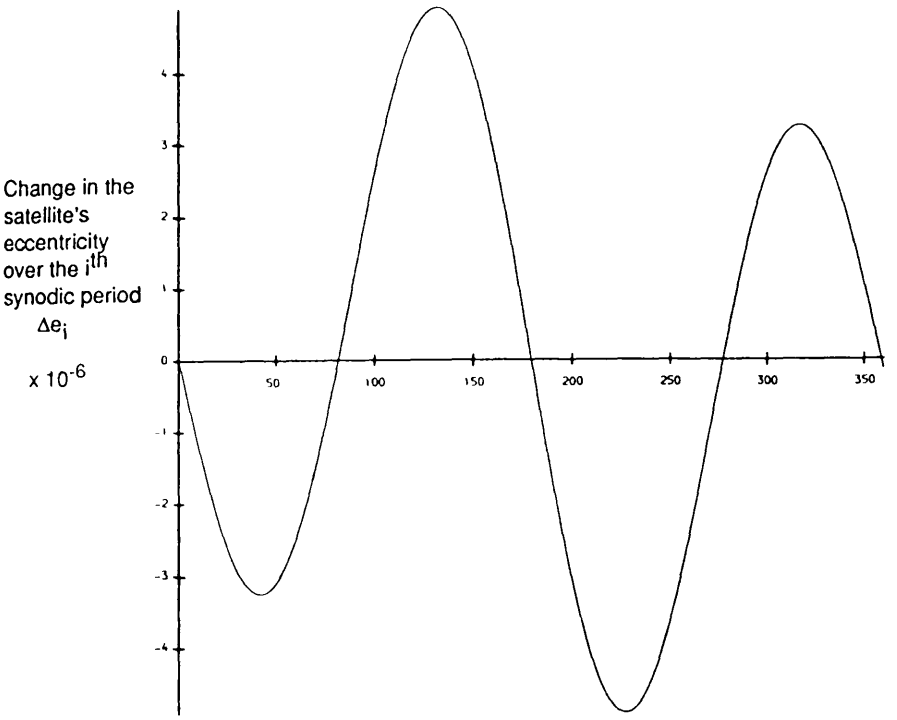
Change in the satellite's eccentricity over the i^th synodic period
Δe_i
x 10^-6
4
3
2
1
0
-1
-2
-3
-4
50
100
150
200
250
300
350
True anomaly of the i^th conjunction f_ci (in degrees)

(a)i

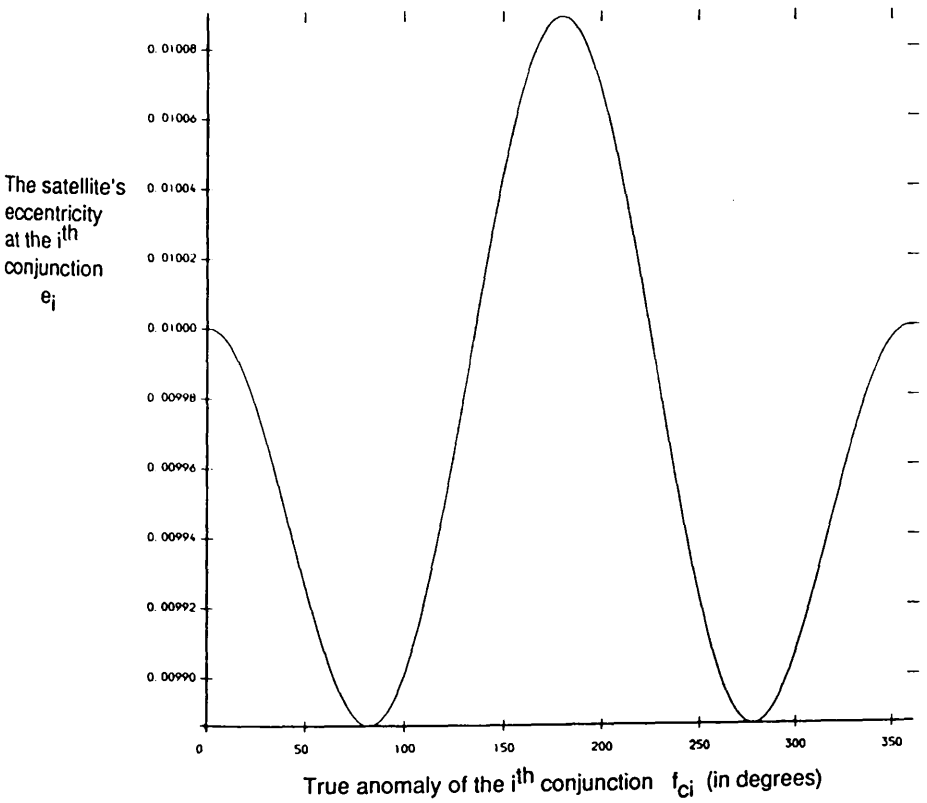
The satellite's eccentricity at the i^th conjunction
e_i
0.01008
0.01006
0.01004
0.01002
0.01000
0.00998
0.00996
0.00994
0.00992
0.00990
0
50
100
150
200
250
300
350
True anomaly of the i^th conjunction f_ci (in degrees)

(a)ii

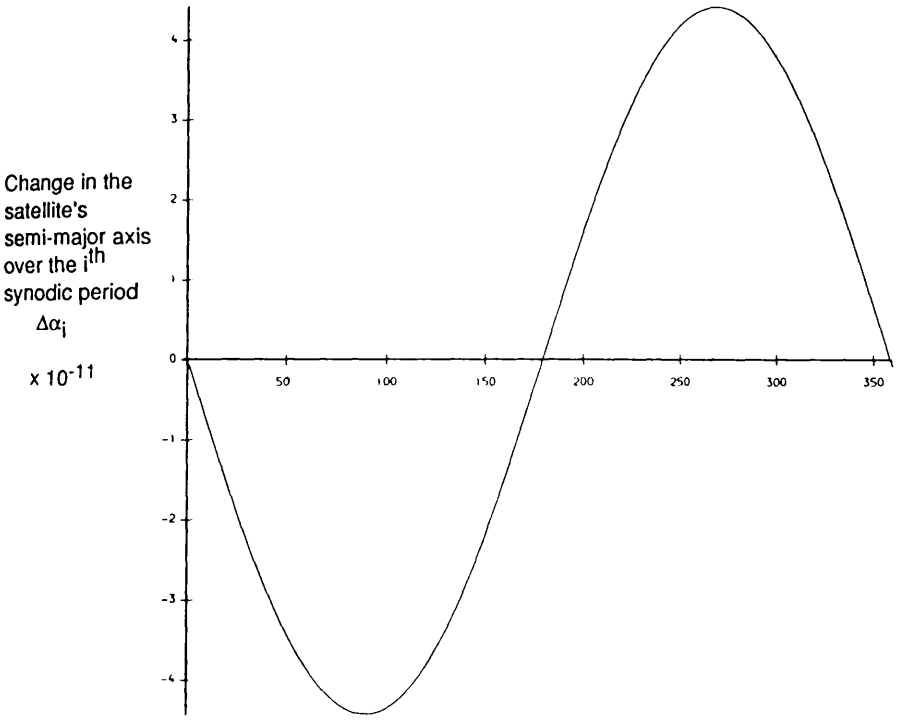
Change in the satellite's semi-major axis over the i^th synodic period
Δα_i
x 10^-11
4
3
2
1
0
-1
-2
-3
-4
50
100
150
200
250
300
350
True anomaly of the i^th conjunction f_ci (in degrees)

(b) i

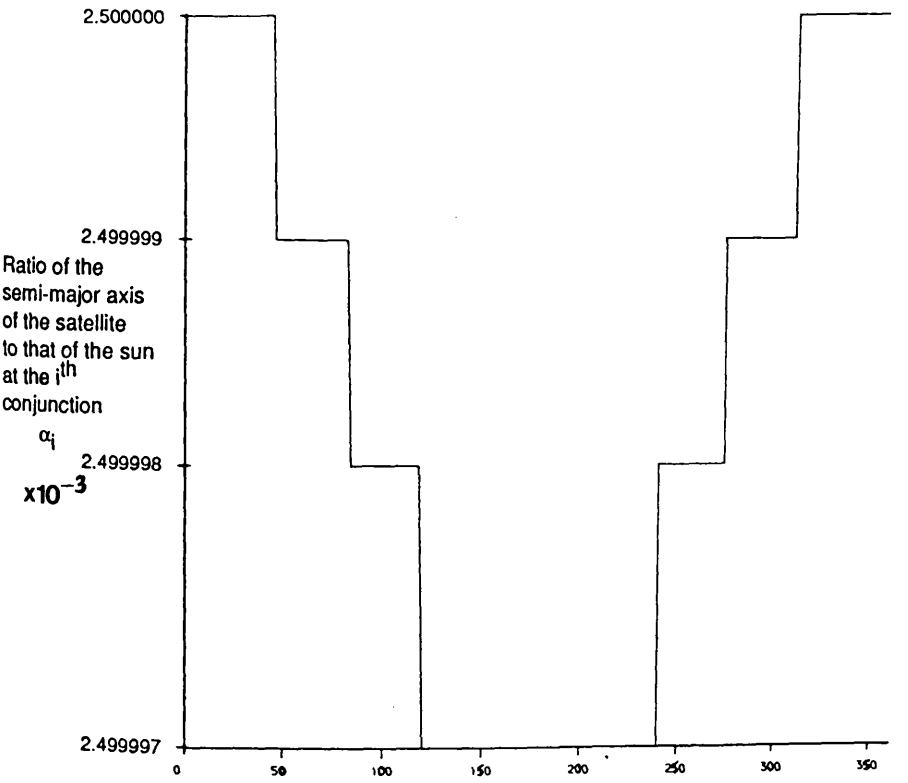
2.500000
2.499999
Ratio of the semi-major axis of the satellite to that of the sun at the i^th conjunction
α_i
2.499998
x10^-3
2.499997
0
50
100
150
200
250
300
350
True anomaly of the i^th conjunction f_ci (in degrees)

(b) i i

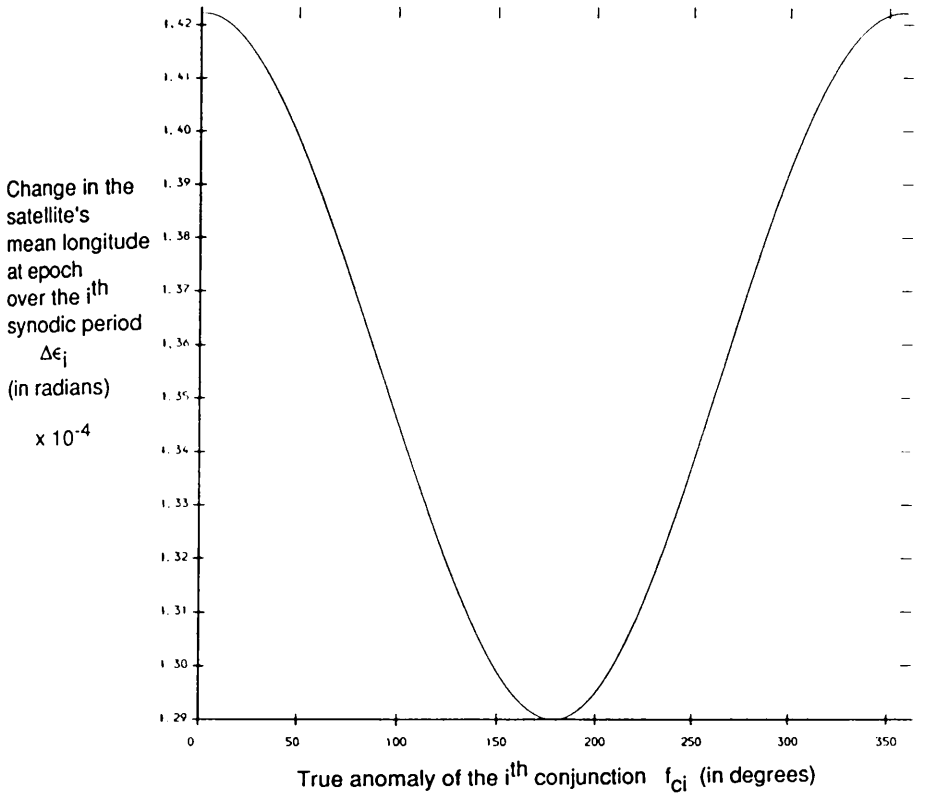
Change in the satellite's mean longitude at epoch over the i^th synodic period Δε_i (in radians) x 10^-4
1.42
1.41
1.40
1.39
1.38
1.37
1.36
1.35
1.34
1.33
1.32
1.31
1.30
1.29
0
50
100
150
200
250
300
350
True anomaly of the i^th conjunction f_ci (in degrees)

(c) i

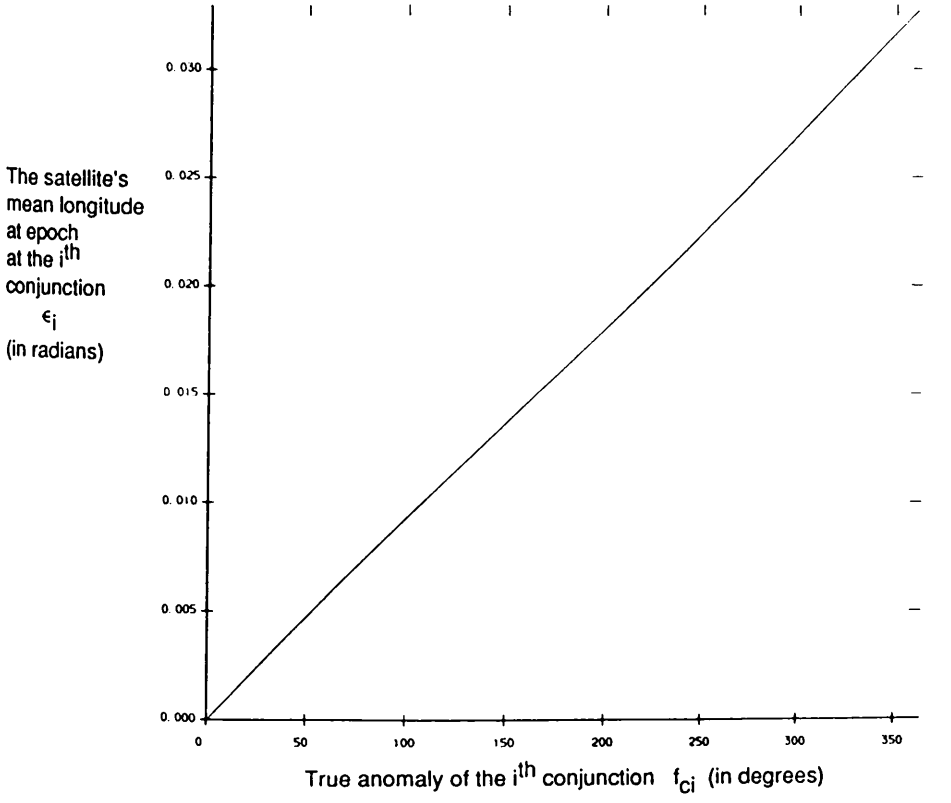
The satellite's mean longitude at epoch at the i^th conjunction ε_i (in radians)
0.030
0.025
0.020
0.015
0.010
0.005
0.000
0
50
100
150
200
250
300
350
True anomaly of the i^th conjunction f_ci (in degrees)

(c) i i

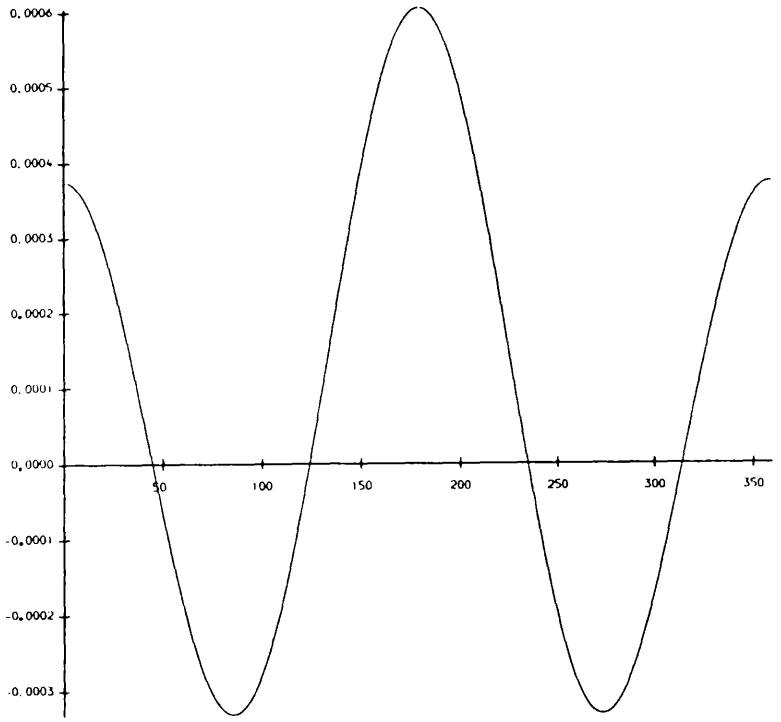

Change in the satellite's longitude of pericentre over the i^{th} synodic period $\Delta\varpi_i$ (in radians)

(d) i

True anomaly of the i^{th} conjunction f_{ci} (in degrees)

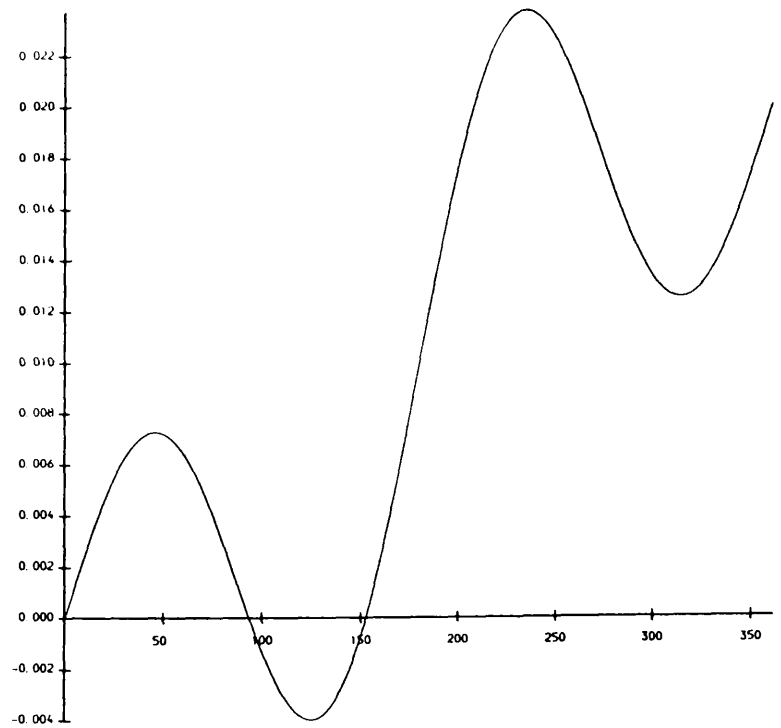

The satellite's longitude of pericentre at the i^{th} conjunction ϖ_i (in radians)

(d) i i

True anomaly of the i^{th} conjunction f_{ci} (in degrees)

Figures 5.11(a) to (d), parts (i) are very similar to the graphs displayed in Figures 3.2(a) to (d). The major difference between the two sets of graphs is that Figures 3.2(a) to (d) plot the changes in the orbital elements over one synodic period $\Delta\sigma$ for a sampling of different true anomalies of the central conjunction f_{c0} ranging from 0° to 360°, while Figures 5.11(a) to (d), parts (i) display the actual changes in the orbital elements $\Delta\sigma_i$ over each successive synodic period. In Figures 3.2, the orbital elements σ are kept constant throughout the graphs, while in Figures 5.11(a) to (d), parts (i), the orbital elements σ_i change every synodic period as the satellite system moves through successive conjunctions f_{ci} beginning with the initial one at $f_{c0}=0°$.

The two sets of graphs are very similar in size and shape because the changes in the orbital elements over one conjunction cycle are very small relative to the maximum sizes of $\Delta\sigma_i$. For this reason also, the choice of the initial true anomaly f_{c0} in Figures 5.11(a) to (d),parts (i) is irrelevant to the graphs. The size and shape of the figures remain the same relative to the scales of the graphs regardless of our choice of f_{c0}, except that the graph begins at the true anomaly f_{c0} chosen. When calculating the change in the orbital elements over one conjunction cycle the choice of f_{c0}, of course, becomes important.

Figure 5.11(a)ii shows that the accumulation of the eccentricity e as the satellite system passes through successive synodic periods is indeed nearly cyclic and not growing steadily as was pessimistically assumed in Section 5.2. The accumulation in the semi-major axis ratio α is also nearly cyclic (See Figure 5.11(b)ii); however, the changes in α are so small that the graphics package, which can only handle eight digit accuracy, plots the points in the form of a step function.

Figure 5.11(c)ii displays an almost linear relationship between the mean longitude at the epoch ϵ_i and the true anomaly at conjunction f_{ci} because the oscillations caused by adding a value of $\Delta\epsilon_i$ which varies between $1.29\text{x}10^{-4}$ and $1.42\text{x}10^{-4}$ to ϵ every synodic period , cannot be seen on the 10^{-2} scale used in Figure

5.11(c)ii. The longitude of the pericentre ϖ is shown in Figure 5.11(d)ii to oscillate about an apparent linearly increasing average as time increases.

The equivalent graphs to Figures 5.11(a) to (d) for the case where the Sun is assumed to be moving in a fixed elliptical orbit, exhibit similar shapes to those found in Figures 5.11(a) to (d). However, the scale of the graphs and the locations of the extrema vary about the circular cases depending on the choice of the Sun's true anomaly f_{1c0} at the initial conjunction.

Having confirmed that the eccentricity does indeed change in a cyclic fashion and that it would certainly be very pessimistic to add the maximum possible change in the eccentricity over one synodic period onto the eccentricity every synodic period, we go on to the second level of the finite-time stability method and study the changes in the orbital elements $\Delta\sigma_c$ over one conjunction cycle.

Like the first level, we now sample the size of $\Delta\sigma_c$, where σ = e, α, ϵ or ϖ, for different starting values of the true anomaly of the initial conjunction f_{c0}. This sampling is done for a range of values for the initial parameters typical of the satellites found in the solar system. All the cases studied produced similar results.

Figures 5.12(a) through to (d) give the relationships between the changes in the orbital elements over one conjunction cycle $\Delta\sigma_c$ and the true anomaly f_{c0} of the first conjunction. This is done for a coplanar Jupiter-Callisto system, where the Sun is assumed to move in a fixed circular orbit. Thus, e_0, α_0 and μ are taken to be 0.01, 0.0025 and 1100 respectively. The dashed lines, also plotted on these graphs, are the relationships between the change in the orbital elements over one synodic period and f_{c0}, which have already been displayed in Figures 3.2(a) to (d).

The two sets of curves $\Delta\sigma$ and $\Delta\sigma_c$ as functions of f_{c0} are similar in shape, with their extrema occurring at the same values for f_{c0}. Figures 5.12(c) and (d) show that although $\Delta\varpi_c$ and $\Delta\epsilon_c$ are similar in shape to $\Delta\varpi$ and $\Delta\epsilon$, they are separated by what appears to be a constant value of ϖ and ϵ. This separation is the result of the average linear relation of both ϖ and ϵ with time. Because a conjunction cycle lasts

longer than a synodic period, the change in the satellite's longitude at epoch and the change in the satellite's longitude of pericentre is greater over one conjunction cycle than over one synodic period. On the scale of 10^{-2} used in Figure 5.12(c), the oscillations of order 10^{-5} in $\Delta\epsilon_c$ and $\Delta\epsilon$ cannot be seen. Thus, the curves appear to be horizontal lines.

The Δe_c and $\Delta\alpha_c$ relationships shown in Figures 5.12(a) and (b) are not only similar in shape to the Δe and $\Delta\alpha$ curves, but also have their zeros located at the same true anomalies f_{c0}. In other words, the Roy-Ovenden mirror theorem is still valid over this next largest cycle. For the circular case, the changes in the satellite's eccentricity and the ratio of the semi-major axes are always zero when the cycle is centred on one of the mirror configurations found at $f_{c0} = 0°$ or 180°.

Figures 5.12 (a to d) The variation in the changes of the satellite's orbital elements (a)Δe_c, (b)$\Delta\alpha_c$, (c)$\Delta\epsilon_c$ and (d)$\Delta\varpi_c$ over one conjunction cycle for different starting values of the true anomaly at the initial conjunction f_{c0}.

The data used here is that of a circular coplanar Jupiter-Callisto system with $e = 0.01$, $\alpha = 0.0025$ and $\mu = 1100$. The solid lines represent $\Delta\sigma_c$, while the dashed lines depict the changes in the orbital elements $\Delta\sigma$ over one synodic period as a function of the different starting values of f_{c0}.

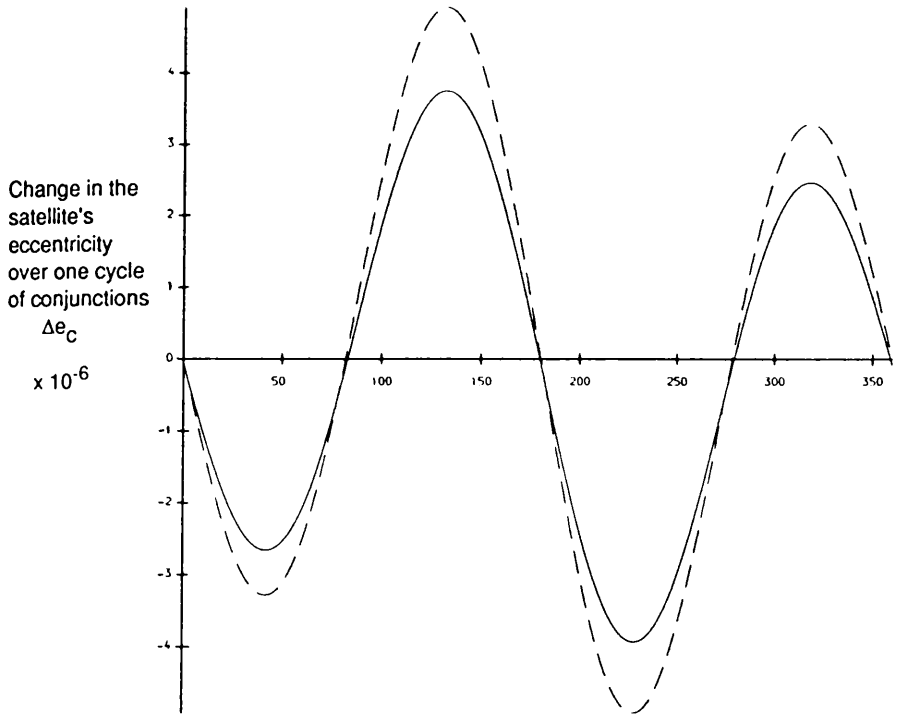
Change in the satellite's eccentricity over one cycle of conjunctions
Δe_c
x 10^{-6}
4
3
2
1
0
-1
-2
-3
-4
50
100
150
200
250
300
350
Initial true anomaly at conjunction f_{c0} (in degrees)

(a)

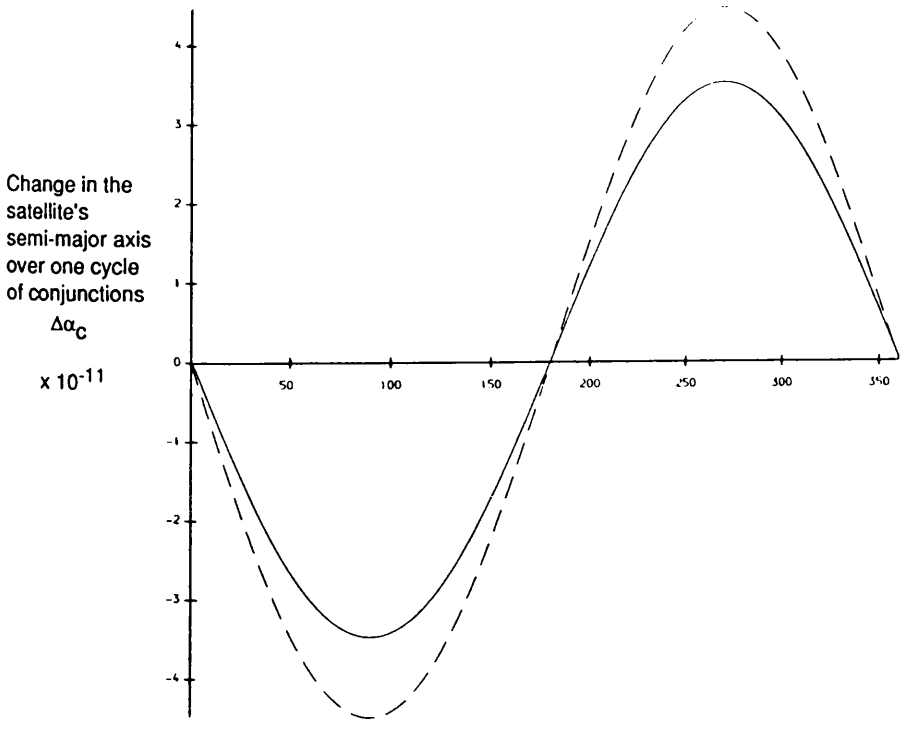
Change in the satellite's semi-major axis over one cycle of conjunctions
Δa_c
x 10^{-11}
4
3
2
1
0
-1
-2
-3
-4
50
100
150
200
250
300
350
Initial true anomaly at conjunction f_{c0} (in degrees)

(b)

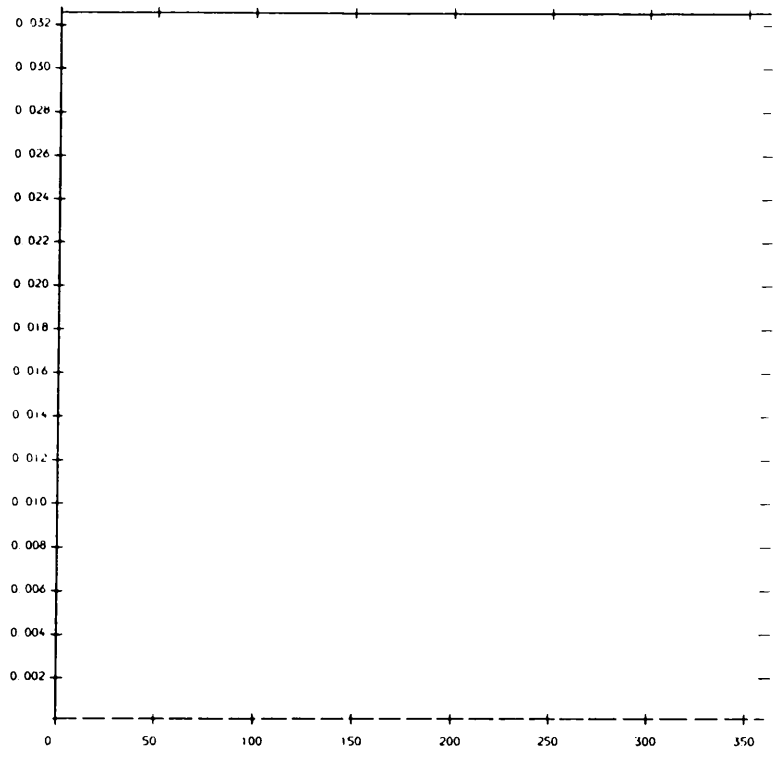

Change in the satellite's mean longitude at epoch over one cycle of conjunctions $\Delta\epsilon_c$ (in radians)

(c)

Initial true anomaly at conjunction f_{c0} (in degrees)

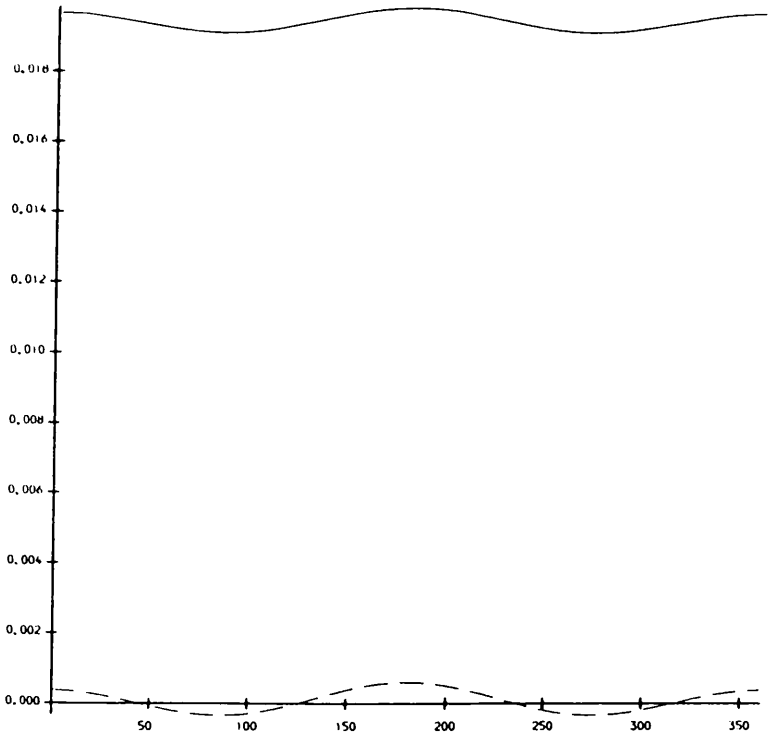

Change in the satellite's longitude of pericentre over one cycle of conjunctions $\Delta\varpi_c$ (in radians)

(d)

Initial true anomaly at conjunction f_{c0} (in degrees)

More importantly, Figures 5.12(a) and (b) show that the maximum changes in the orbital elements e and α over one conjunction cycle are less than the maximum changes in the orbital elements e and α over one synodic period. This means that a minimum duration incorporating the maximum possible change in the eccentricity over one conjunction cycle $\Delta e_{max\text{-}c}$ will be much longer than a minimum duration using Δe_{max}. Not only has the period of the cycle increased, but so too has the number of cycles required to reach an eccentricity of e_u, since $\Delta e_{max\text{-}c}$ is smaller than Δe_{max}. Thus, if the satellite system for the circular case can last through several conjunction cycles, the minimum lifetime of the system can easily be extended to beyond the times calculated in the first level of the finite-time stability method.

When the problem is extended to include the Sun moving in a fixed elliptical orbit, the resulting graphs are very similar to those found for the circular case. Figures 5.13(a) to (d) show the relationships between the changes in the orbital elements over one cycle of conjunctions $\Delta\sigma_c$ and the true anomaly of the satellite at the first conjunction f_{c0}, for a sampling of the true anomalies f_{1c0} of the Sun at the first conjunction ranging from 0° to 360° in 12° intervals. Again the initial satellite data are the same as that used in Figures 5.12, with the addition that the Sun is now assumed to be moving in a fixed elliptical orbit with an eccentricity of $e_1 = 0.048$.

Figures 5.13 (a to d) Variations in the changes of the satellite's orbital elements (a)Δe_c, (b)$\Delta\alpha_c$, (c)$\Delta\epsilon_c$ and (d)$\Delta\varpi_c$ over one conjunction cycle with the satellite's true anomaly f_{c0} at the initial conjunction, for different starting values of the Sun's true anomaly at the initial conjunction f_{1c0} ranging from 0° to 360° in 12° intervals.

The data used here is that of an elliptical coplanar Jupiter-Callisto system with $e = 0.01$, $\alpha = 0.0025$, $\mu = 1100$ and $e_1 = 0.048$. The thickest solid line describes the curve for $f_{1c0} = 0°$. The dashed lines represent those curves whose values of f_{1c0} are greater than 180°.

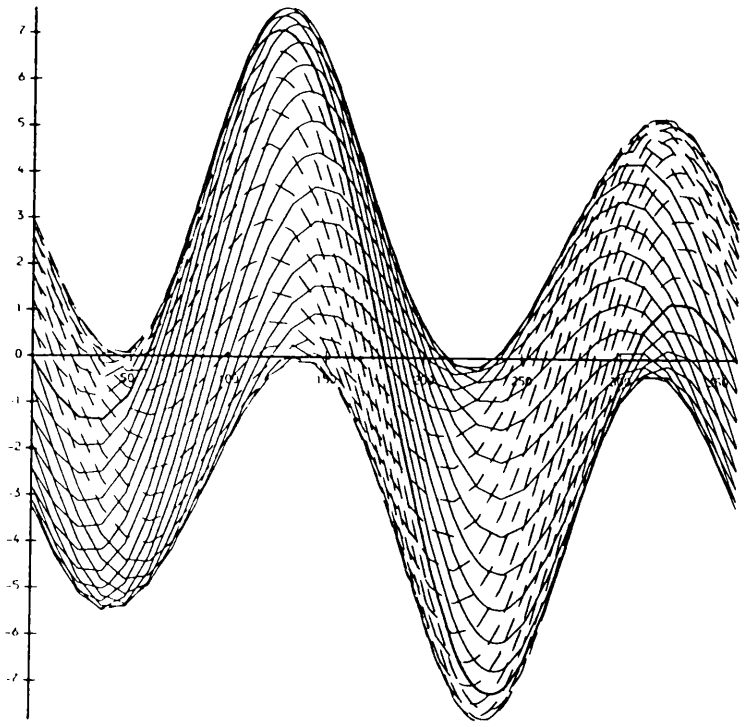
Change in the satellite's eccentricity over one cycle of conjunctions
Δe_c
x 10^{-6}
Initial true anomaly at conjunction f_{c0} (in degrees)

(a)

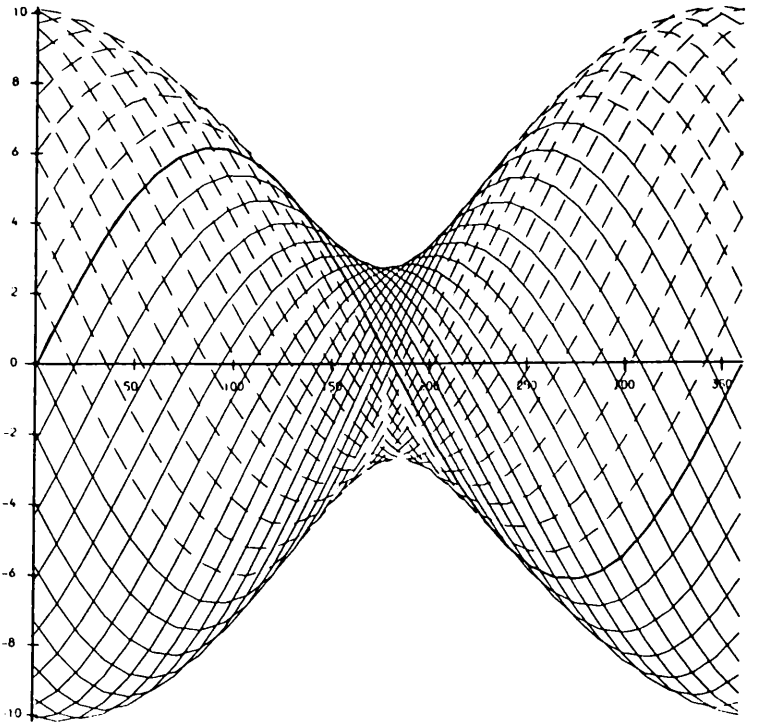
Change in the satellite's semi-major axis over one cycle of conjunctions
$\Delta \alpha_c$
x 10^{-10}
Initial true anomaly at conjunction f_{c0} (in degrees)

(b)

Change in the satellite's mean longitude at epoch over one cycle of conjunctions $\Delta\epsilon_c$ (in radians)

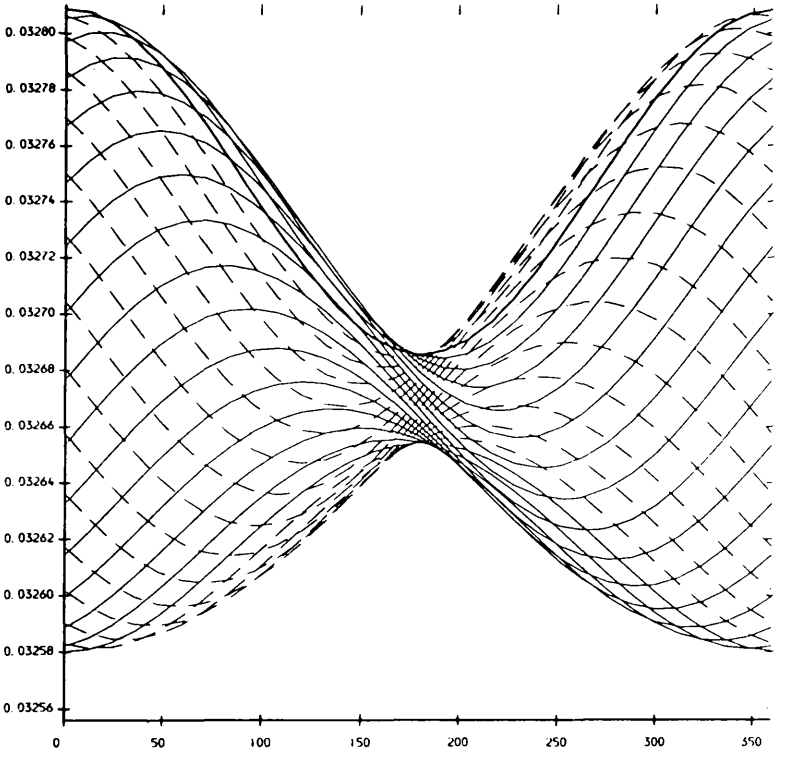

(c)

Change in the satellite's longitude of pericentre over one cycle of conjunctions $\Delta\varpi_c$ (in radians)

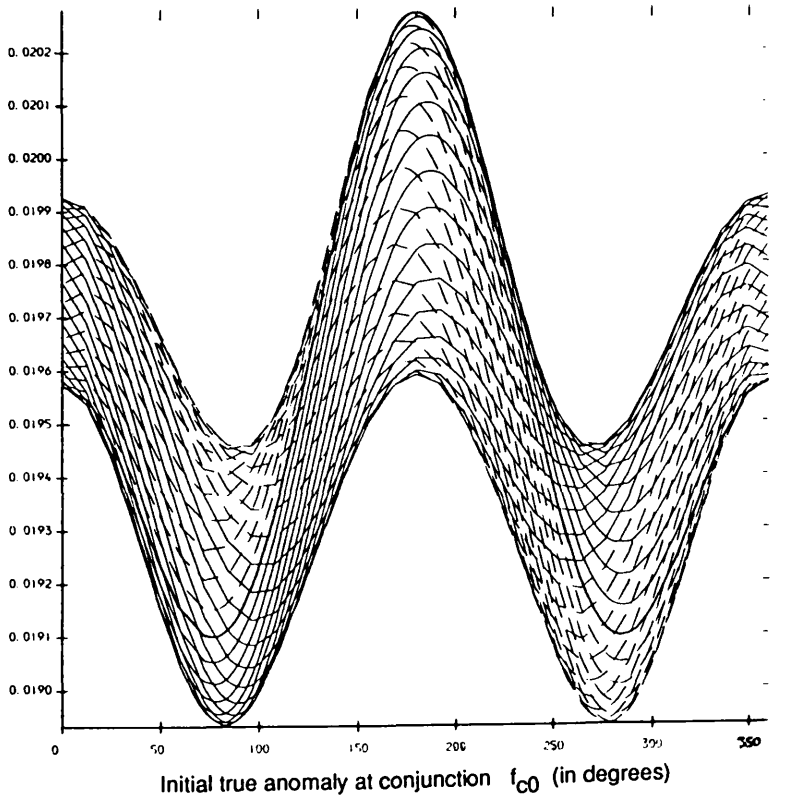

(d)

Note that the locations of the extrema and the sizes of the extrema vary considerably as f_{1c0} is varied; however, the general shapes of the curves remain the same. The locations of the zeros also vary considerably depending on the choice of the true anomaly of the Sun at the central conjunction. However, again confirming the Roy-Ovenden mirror theorem for the elliptical case, the changes in the satellite's eccentricity and the ratio of the semi-major axes over a conjunction cycle are always zero, when the cycle is centred on a mirror configuration located at the satellite's true anomaly of $f_{c0} = 0°$ or 180°, and the sun's true anomaly of $f_{1c0} = 0°$ or 180°. For example, the thickest solid line in each of the Figures 5.13(a to d) depict the curves where $f_{1c0} = 0°$. Figures 5.13 (a) and (b) show that these curves have zeros at $f_{c0}=0°$ and 180°.

Graphs similar to Figures 5.13 were completed for a range of initial parameters typical of the satellites found in the solar system. The results were much the same as those depicted in Figures 5.13, even when the eccentricity of the satellite was increased to e = 0.5.

Figures 5.14(a) to (d) indicate the boundaries (solid lines) of the $\Delta\sigma_c$-f_{c0} space covered by the elliptical case in Figures 5.13(a) to (d) and show that the equivalent graph of $\Delta\sigma_c$ vs. f_{c0} for the circular case (dashed lines) lies at the centre of this region for Δe_c, $\Delta\alpha_c$ and $\Delta\varpi_c$. This result is remarkable given that the extrema of the $\Delta\sigma_c$ versus f_{c0} curves for the elliptical case can shift over a range of 90° or more as f_{1c0} is varied.

Figures 5.14(a to d) A comparison of the $\Delta\sigma_c$ - f_{c0} region covered by the curves in Figures 5.13 (between the solid lines), with the equivalent curves, Figures 5.12, for the circular case (dashed lines).

$\Delta\sigma_c$ is Δe_c, $\Delta\alpha_c$, $\Delta\epsilon_c$ and $\Delta\varpi_c$ for the figures (a) through to (d) respectively.

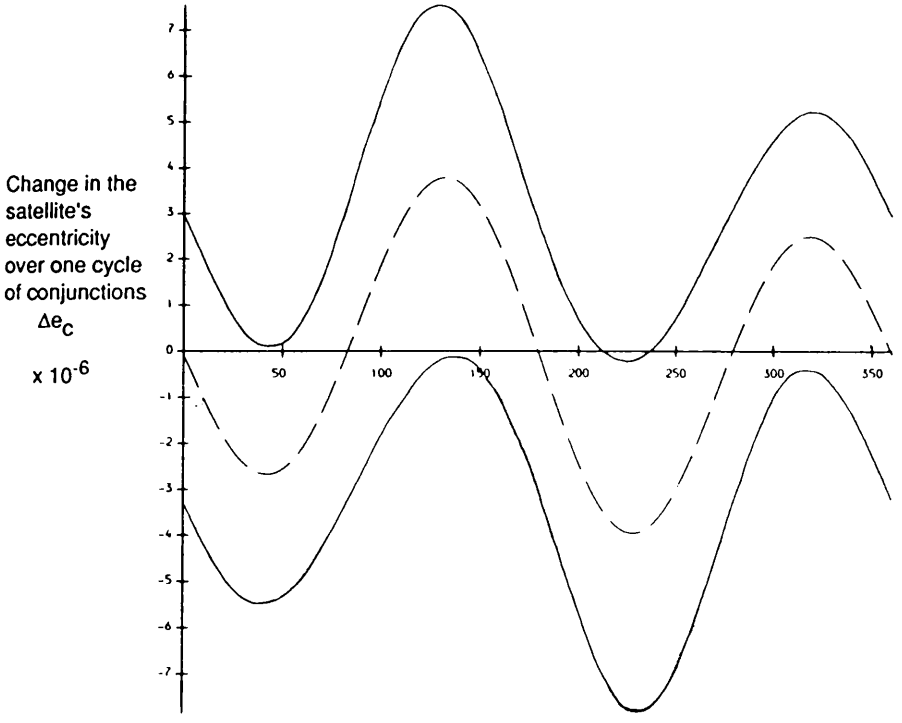
Change in the satellite's eccentricity over one cycle of conjunctions
Δe_c
x 10^{-6}
7
6
5
4
3
2
1
0
-1
-2
-3
-4
-5
-6
-7
50
100
150
200
250
300
350
Initial true anomaly at conjunction f_{c0} (in degrees)

(a)

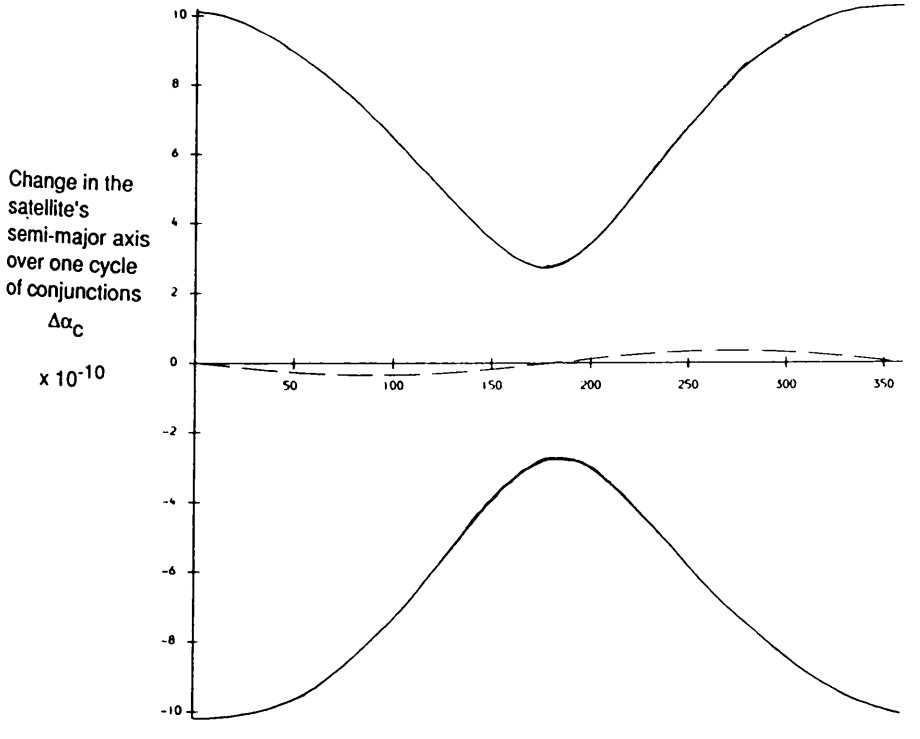
Change in the satellite's semi-major axis over one cycle of conjunctions
$\Delta \alpha_c$
x 10^{-10}
10
8
6
4
2
0
-2
-4
-6
-8
-10
50
100
150
200
250
300
350
Initial true anomaly at conjunction f_{c0} (in degrees)

(b)

Change in the satellite's mean longitude at epoch over one cycle of conjunctions $\Delta\epsilon_c$ (in radians)

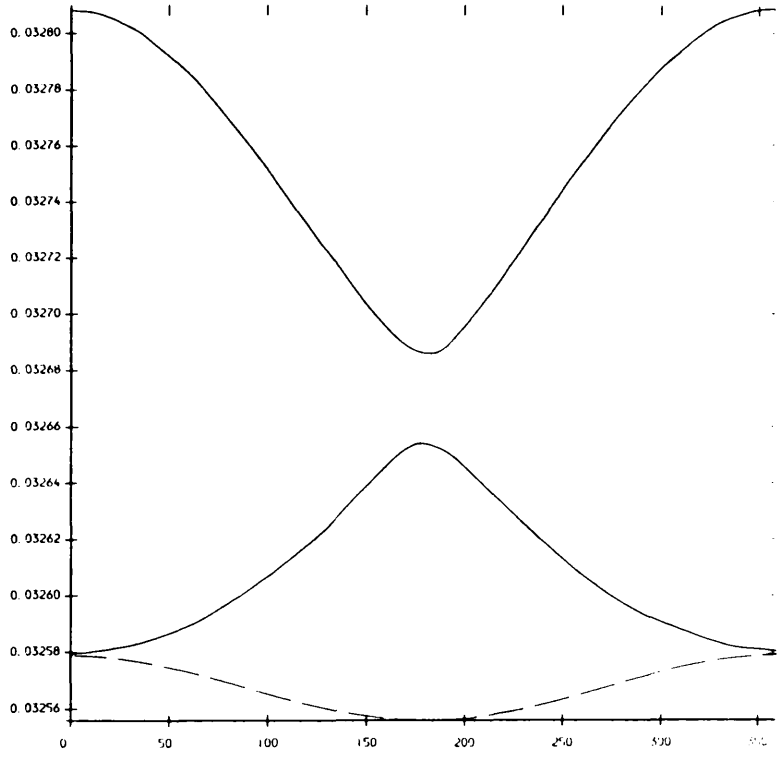

Initial true anomaly at conjunction f_{c0} (in degrees)

(c)

Change in the satellite's longitude of pericentre over one cycle of conjunctions $\Delta\varpi_c$ (in radians)

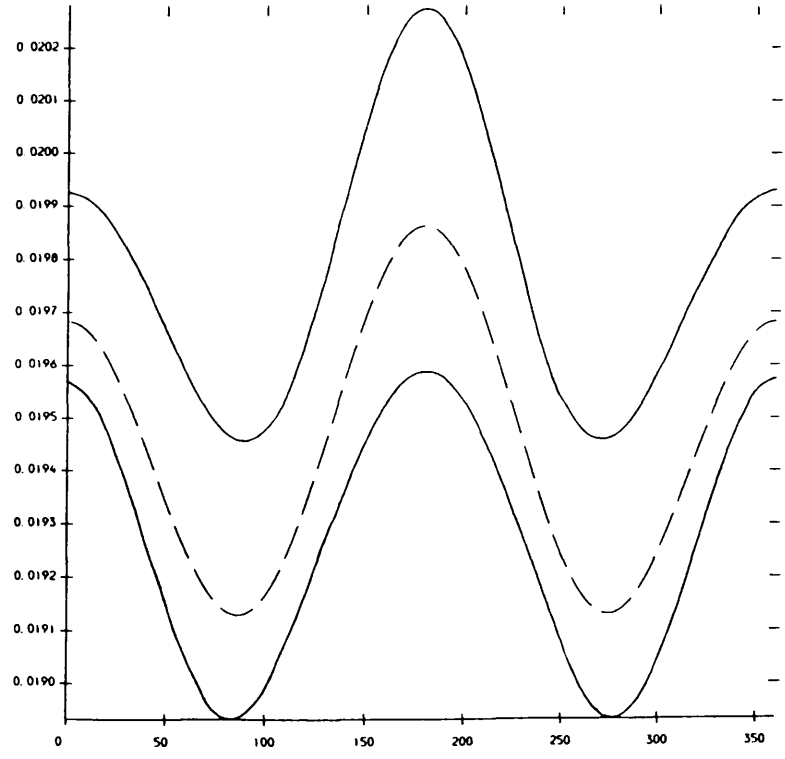

Initial true anomaly at conjunction f_{c0} (in degrees)

(d)

Like the results for the first level, the changes in the orbital elements for the elliptical case over one conjunction cycle as a function of f_{c0} are similar in size to, and are still spread equally on either side of, the equivalent function for the circular case. Again, the elliptical case is seen to be merely an extension of the circular case. Thus, minimum durations derived for the elliptical cases using the maximum possible change in the eccentricity over one conjunction cycle should be of similar, but smaller values to those of the equivalent circular case.

Note that $\Delta\epsilon_c$ for the circular case, while not located at the centre of the boundaries for the elliptical $\Delta\epsilon_c$ curves in $\Delta\epsilon_c$- f_{c0} space, is the correct shape to fit at the centre of the bounded region if it was shifted upward by a constant value of ϵ.

(iv) The minimum durations of various satellite systems

The maximum possible change in the eccentricity over one cycle of conjunctions is seen from Figure 5.12(a) to occur at approximately the same value of the true anomaly of the satellite at the initial conjunction as the maximum change in the eccentricity over one synodic period does. This is true for both the circular and elliptical cases. For the elliptical case, $\Delta e_{max\text{-}c}$ occurs for a value of f_{1c0} somewhere between 0° and 90°.

Thus, to find the maximum possible eccentricity over one cycle of conjunctions for either the elliptical or circular cases, we begin with the above starting points for f_{c0} and f_{1c0} and optimize the function Δe_c (f_{c0}, f_{1c0}) numerically until $\Delta e_{max\text{-}c}$ is obtained to within a 0.1% error. We then follow the same procedure as in the first level and calculate the number of conjunction cycles N_2 needed to increase the eccentricity from e_0 to e_u=0.5.

The minimum durations of the systems are then found using Equation (7). Again, the method of approximating the minimum duration by dividing the interval e_0 to e_u into substeps and assuming that the change in the eccentricity over a cycle of conjunctions is a constant within each substep, is necessary to evaluate quickly an

estimate to within an order of magnitude of the minimum durations. As before, Δe_c for each substep is evaluated using the final endpoint eccentricity of each substep.

Minimum duration contours for the range of imaginary satellites orbiting each of the planets Jupiter, Saturn, Uranus, Earth and Mars studied in Figures 5.3 to 5.6 could not be found easily due to time restrictions on the computer. These graphs are possible to compute but would take up large amounts of CPU time and as a result, are kept at the bottom of any queue for the use of the computer. They were therefore left to be completed for a future more extensive study of the finite-time stability method when greater computing and man-hour time may be available.

Table 5.8 provides a list of the various computing times in CPU seconds required by the different studies of the minimum lifetimes for each of the circular and elliptical cases and for each of the levels of the finite-time stability method. Note that Table 5.8 gives the computing times only for the Jupiter-Callisto example used throughout this thesis. Because of its relatively large eccentricity and semi-major axis, Callisto's minimum durations are smaller than those found for many of the satellites in the solar system and for a large part of the imaginary satellites studied in Figures 5.3 to 5.6. Its minimum durations are therefore quicker to evaluate than the minimum durations of these other satellites. Hence, computing times for other satellites are generally longer than those given in Table 5.8.

As we can see from the table, the minimum lifetimes for the elliptical case take much longer to find than those for the circular case. The calculation of the maximum possible change in the orbital eccentricity over each cycle for the elliptical case is much more complex than the equivalent calculation for the circular case. Δe_{max} over the cycles for the elliptical case can only be found through a numerical optimization procedure which requires the evaluation of at least three changes in the eccentricity over the specified cycle, while Δe_{max} for the circular case can be found almost immediately analytically.

Each successive level of the finite-time stability method requires more time to compute the minimum lifetime of the system because the maximum possible changes in the eccentricity are being calculated over longer periods of time.

Calculation	First Level		Second Level		Third Level	
	Circular	Elliptical	Circular	Elliptical	Circular	Elliptical
$\Delta\sigma$, $\Delta\sigma_c$, $\Delta\sigma_m$ for $f_{c0}=1°$, $f_{1c0}=2°$						
Analytical:	0.685	0.762	0.869	1.214	0.983	1.331
Numerical:	1.010	1.157	24.278	46.468	49.237	91.112
Individual Minimum Durations	0.962	1.501	44.921	837.107	92.266	1667.716
Grid Minimum Durations	20.380	100.425	——	——	——	——
Contour Minimum Durations	40.718	216.826	——	——	——	——

Table 5.8 The computing times (in CPU seconds) required to calculate:

(1) the changes in the orbital elements $\Delta\sigma$, $\Delta\sigma_c$, or $\Delta\sigma_m$ analytically and numerically;

(2) the minimum durations of individual satellites;

(3) the minimum durations of 100 satellites in a grid pattern over α_0-e_0 space;

(4) the minimum duration contours in α_0-e_0 space,

for each level of the finite-time stability method and for each of the cases, circular or elliptical.

The data used are that of a coplanar Jupiter-Callisto system with $\alpha_0 = 0.0025$, $e_0 = 0.01$, $\mu = 1100$, T_1=11.86198 years, $e_1 = 0.048$ and $e_u = 0.5$. The table is left blank where the required computing times are greater than 3600 CPU seconds.

Calculation of minimum lifetime contours over α_0-e_0 space for satellites orbiting each of the planets requires more than 40 CPU seconds for the circular case and more than 220 CPU seconds for the elliptical case at the first level, while the same calculations at the second level require greater than 3600 CPU seconds. Calculations of the minimum lifetimes of individual satellites orbiting each of the planets, on the other hand, require reasonable times of approximately 1, 45, and 92 CPU seconds for the first, second and third levels of the circular case respectively and 1.5, 840, 1670 CPU seconds for the first, second and third levels of the elliptical case respectively. Therefore, calculations of individual minimum durations can easily be completed, while evaluation of contours requires an unreasonably large amount of computer time.

A study of the minimum durations of the known satellites of Jupiter, Saturn, Uranus, Earth and Mars for the different levels can still provide valuable information on the use of the finite-time stability method as a means of testing the stability of satellites perturbed by the Sun. The minimum durations for the second level of the finite-time stability method for these individual satellites are given in Tables 5.9 to 5.13. The calculations were completed for both the circular and elliptical cases to within a 1% accuracy where computing time limitations permitted and to within a 10% accuracy otherwise. Where N_2 has been approximated to within 1%, T^2_{min} values should be accurate to at least two digits. Where N_2 has been approximated to within 10%, T^2_{min} values should be accurate to at least one digit. The second level minimum durations listed in Tables 5.9 to 5.13 have been rounded off accordingly.

Note that the outer satellites of Jupiter: Leda, Himalia, Lysithea and Elara, Saturn's furthermost satellite Phoebe and the Earth's Moon, all fail to achieve a first level minimum lifetime greater than the length of the natural cycle used in the second finite-time stability level. As a result, a second level minimum lifetime cannot be found for these satellites and their minimum lifetimes must remain at the first level, even though these satellites have obviously persisted in their orbits about their planets for much longer than the approximate ten years given by the first level criteria. The finite-time stability method as it stands is therefore not much use in studying the stability of these satellites. In Chapter 6, we look at the

Earth-Moon-Sun system and suggest a larger natural cycle found within the system, which might be used to find a more reasonable minimum lifetime for the Moon.

Tables 5.9 to 5.13 show that the second level minimum durations of a planet-satellite system are not much different whether the Sun is assumed to be moving in a fixed circular orbit or a fixed elliptical orbit. The minimum lifetimes for the elliptical case are still always slightly less but usually of the same order of magnitude as those of the circular case. Second level minimum lifetimes for both elliptical and circular cases still increase as either α_0 or e_0 is decreased.

Satellite	T'_{min} (years)		T^2_{min} (years)	
	Circular	Elliptical	Circular	Elliptical
Amalthea	2.2×10^4	1.9×10^4	3×10^8	1×10^8
Thebe	1.1×10^4	9.6×10^3	5×10^7	3×10^7
Io	5.8×10^3	5.0×10^3	3×10^7	9×10^6
Europa	2.4×10^3	2.1×10^3	4.3×10^6	2.5×10^6
Ganymede	1.5×10^3	1.3×10^3	1.3×10^6	7.9×10^5
Callisto	5.2×10^2	4.4×10^2	1.7×10^5	1.2×10^5
Leda	9.9	8.3	——	——
Himalia	8.9	7.4	——	——
Lysithea	1.1×10^1	9.3	——	——
Elara	6.7	5.6	——	——

Table 5.9 The first and second level minimum lifetimes for the known satellites of Jupiter, if the Sun is assumed to be moving in a fixed circular or elliptical orbit. Jupiter's sidereal period is taken to be 11.86198 years.

Satellite	T^1_{min} (years)		T^2_{min} (years)	
	Circular	Elliptical	Circular	Elliptical
Prometheus	1.1×10^5	9.4×10^4	2×10^9	2×10^9
Pandora	1.0×10^5	8.7×10^4	2×10^9	2×10^9
Janus	8.3×10^4	7.0×10^4	9×10^8	8×10^8
Epimetheus	7.8×10^4	6.6×10^4	9×10^8	8×10^8
Mimas	4.6×10^4	3.9×10^4	5×10^8	4×10^8
Enceladus	4.6×10^4	3.9×10^4	5×10^8	2×10^8
Dione	2.6×10^4	2.2×10^4	9×10^7	5×10^7
1980S6	2.3×10^4	1.9×10^4	8×10^7	4×10^7
Rhea	1.8×10^4	1.5×10^4	3.4×10^7	1.8×10^7
Titan	2.4×10^3	2.0×10^3	1.6×10^6	1.2×10^6
Hyperion	1.0×10^3	8.5×10^2	4.0×10^5	3.0×10^5
Iapetus	4.7×10^2	3.9×10^2	1.3×10^5	9.4×10^4
Phoebe	2.6×10^1	2.1×10^1	———	———

Table 5.10 The first and second level minimum lifetimes for the known satellites of Saturn, if the Sun is assumed to be moving in a fixed circular or elliptical orbit. Saturn's sidereal period is taken to be 29.45709 years.

Satellite	T^1_{min} (years)		T^2_{min} (years)	
	Circular	Elliptical	Circular	Elliptical
1986U8	1.1×10^6	9.9×10^5	1×10^{11}	7×10^{10}
Miranda	4.1×10^5	3.5×10^5	1×10^{10}	5×10^9
Ariel	2.2×10^5	1.9×10^5	2×10^9	1×10^9
Umbriel	1.2×10^5	1.1×10^5	1×10^9	6×10^8
Titania	6.8×10^4	5.9×10^4	2×10^8	1×10^8
Oberon	5.1×10^4	4.4×10^4	1.5×10^8	8.8×10^7

Table 5.11 The first and second level minimum lifetimes for the known satellites of Uranus, if the Sun is assumed to be moving in a fixed circular or elliptical orbit. Uranus' sidereal period is taken to be 84.01151 years.

Satellite	T^{1}_{min} (years)		T^{2}_{min} (years)	
	Circular	Elliptical	Circular	Elliptical
Moon	9.9×10^{-1}	9.3×10^{-1}	——	——

Table 5.12 The first and second level minimum lifetimes for the known satellites of Earth, if the Sun is assumed to be moving in a fixed circular or elliptical orbit. Earth's sidereal period is taken to be 1.00002 years.

Satellite	T^{1}_{min} (years)		T^{2}_{min} (years)	
	Circular	Elliptical	Circular	Elliptical
Phobos	6.1×10^{2}	4.5×10^{2}	1×10^{6}	1×10^{6}
Deimos	2.6×10^{2}	1.9×10^{2}	1×10^{5}	1×10^{5}

Table 5.13 The first and second level minimum lifetimes for the known satellites of Mars, if the Sun is assumed to be moving in a fixed circular or elliptical orbit. Mars' sidereal period is taken to be 1.88085 years.

The second level minimum durations T^{2}_{min} are typically 10^{2} to 10^{4} times as large as the first level minimum lifetimes T^{1}_{min} depending on the size of T^{1}_{min}. A satellite with a larger value of T^{1}_{min} will also have a much greater ratio between the two minimum durations, ie T^{2}_{min}: T^{1}_{min}. Thus, for example, the second level minimum duration for Callisto is only about 10^{2} times as big as its first level minimum duration of 5×10^{2} years, while Amalthea's second level minimum duration is approximately 10^{4} times as big as its first level minimum duration of 2×10^{4} years.

The minimum durations for the second level are much closer to the known lifetime of the solar system of $5x10^9$ years than the first level minimum durations. Some of the lifetimes are even one hundred times greater than the lifetime of the solar system. The second level minimum durations for Jupiter's satellites range from $1x10^5$ to $3x10^8$ years, for Saturn's satellites from $9x10^4$ to $2x10^9$ years, for Uranus' satellites from $9x10^7$ to $1x10^{11}$ years and for Mars' satellites from $1x10^5$ to $1x10^6$ years.

Even though these minimum lifetimes are very good in themselves, they can still be increased further by using the next largest natural cycle of a planet-satellite-Sun system, the mirror configuration cycle, and applying the third level of the finite-time stability method. All the satellites studied in Tables 5.9 to 5.13 for the second level have second level minimum durations which are large enough to allow many mirror configuration cycles to occur. The third level can therefore be applied to all of them. The third level of the finite-time stability method and the requirements needed to achieve it are discussed in the next section.

5.4 The Third Level, Using the Maximum Possible Change in the Eccentricity Over One Mirror Configuration Cycle

By this stage, the short periodic behavior of the satellite's motion of a size similar to the planet-satellite-Sun's synodic period and the much longer periodic behavior of a size similar to a conjunction cycle period or the planet's sidereal period have been effectively removed from the problem. However, the minimum time necessary for the Sun to tear the satellite away from its primary can still be increased by applying yet another larger natural cycle involving approximate mirror configurations.

In the coplanar three-body model, the only type of mirror configuration that can occur is one where the masses are collinear and the velocity vectors are perpendicular to that line. In the case where the Sun is assumed to be moving in a fixed circular orbit, a mirror configuration is formed whenever a conjunction or opposition of the three bodies falls along the satellite's orbital semi-major axis. In terms of the satellite's and the Sun's orbital elements, a mirror configuration therefore occurs when $f_{c0} = 0°$ or $180°$.

Where the Sun is assumed to be moving in a fixed elliptical orbit, a mirror configuration is formed whenever a conjunction or opposition of the three bodies falls along an alignment of the semi-major axes of both the satellite's and the Sun's orbits. In terms of the satellite's and Sun's orbital elements, a mirror configuration occurs when $f_{c0} = 0°$ or $180°$ and $f_{1c0} = 0°$ or $180°$.

The likelihood that a conjunction or opposition will occur exactly along the satellite's semi-major axis for the circular case or along an alignment of the satellite's and the Sun's semi-major axes for the elliptical case is very small. However, because the angle θ_i between successive conjunctions (or the angle $\theta_i/2$ between successive conjunction and opposition) is very small, a close approximation to a Roy-Ovenden mirror configuration occurs each time the conjunction line falls near the satellite's apse line for the circular case, or near an approximate alignment of the satellite's and the Sun's lines of apses for the elliptical case.

How can this mirror symmetry be used in the finite-time stability method? A

cycle which is always centred on a close approximation to a mirror configuration will, by the mirror theorem, produce very small changes in the orbital elements over that cycle.

We first discuss the case where the Sun is assumed to move in a fixed circular orbit about the planet. Let a mirror configuration cycle be a cycle centred on a conjunction which occurs nearest to the satellite's pericentre. Then let the cycle extend forward through an approximate revolution of the conjunction line to the next closest conjunction to the satellite's pericentre. Also let the cycle extend backward through an approximate revolution of the conjunction line to the previous closest conjunction to the satellite's pericentre.

Whereas a conjunction cycle begins and ends with conjunctions nearest the same fixed reference direction, the mirror configuration cycle begins, is centred and ends, with those conjunctions which lie nearest the moving apse line of the satellite's orbit. Because the satellite's apse line moves very little over one conjunction cycle, there is practically no difference between the lengths of one mirror configuration cycle and two consecutive conjunction cycles.

In order to find the minimum lifetimes using the mirror configuration cycle, we must first find the largest possible change in the orbital eccentricity of the satellite over one mirror cycle.

The conjunction falling nearest the apse line at the centre of a mirror cycle will vary in its angular distance from the apse line by at most $\theta_i/2$ (ie half the distance between any two consecutive conjunctions). The angle θ_i depends on the values of the orbital elements and the true anomalies of the satellite and the Sun at one of the conjunctions. The further the closest conjunction to the apse line at the centre of the cycle is from the apse line, the greater the changes in the orbital elements over the cycle become. Therefore, the maximum possible change in the eccentricity over such a cycle will occur when the central conjunction is the farthest from the satellite's apse line. In other words, it occurs when the central conjunction lies at a true anomaly of $f_{c0} = \theta_{max}/2$, where θ_{max} is the largest possible value for the angle between any two consecutive conjunctions. The two particular consecutive conjunctions which form θ_{max} may not necessarily be anywhere near the apse line or

a true anomaly of $f_{c0} = 0°$, but consistent with the philosophy used in previous levels of the finite-time stability method, we choose the worst possible case.

The resulting maximum possible change in the eccentricity over a mirror cycle $\Delta e_{max\text{-}m}$ is then assumed to be added onto the current eccentricity of the satellite every mirror cycle until the arbitrary limit to the eccentricity of $e_u = 0.5$ is reached, when the planet-satellite-Sun system is taken to be in danger of becoming unstable. The time taken for the eccentricity to grow to this value is then the minimum time T^3_{min} that the system will last if changes in the orbital elements over one mirror cycle can be used.

On average, similar to the period of the conjunction cycle $T_1 = 2\pi/n_1$, the period of the mirror configuration cycle is equal to

$$2\left(\frac{2\pi}{n_1 - \dot{\varpi}}\right)$$

The rate of change of the satellite's apse line $\dot{\varpi}$ is generally very much smaller than the mean motion of the Sun. For example in the Jupiter-Callisto case, the largest change in the satellite's longitude of pericentre over a cycle of conjunctions is of the order $2\text{x}10^{-2}$ radians, while in that time the Sun moves through approximately 2π radians. We therefore neglect $\dot{\varpi}$ to obtain an average period for a mirror configuration cycle of $2T_1$.

As before, when moving on to a higher level of the finite-time stability method, we must first confirm that the three-body system can persevere in its current state until at least several periods of the next largest natural cycle have elapsed. Therefore, the minimum lifetime of the satellite's orbit about the planet for the second level must be much greater than the period of a mirror configuration cycle, ie

$$T^2_{min} >> 2T_1$$

All the satellites listed in Tables 5.9 to 5.13 for the second level easily meet this restriction.

Application of the third level of the finite-time stability method follows the same procedure described for applying the first and second levels of the method. We need to:

(1) find the changes $\Delta\sigma_m$ in the orbital elements over one mirror configuration cycle

(2) calculate the maximum possible change $\Delta e_{max\text{-}m}$ in the eccentricity over one mirror configuration cycle

(3) count the number of mirror configuration cycles N_3 needed to increase the satellite's eccentricity to the chosen upper limit of e_u, if $\Delta e_{max\text{-}m}$ is assumed to be added onto the current eccentricity every mirror configuration cycle, and if $\Delta e_{max\text{-}m}$ is re-evaluated every mirror configuration cycle using the current values for the orbital elements

(4) and finally, we need to evaluate the minimum duration T^3_{min} of the planet-satellite system for the third level of the finite-time stability method using the following equation

$$T^3_{min} = N_3 \, (2T_1) \qquad (35)$$

Again, a check must be made that the accumulated eccentricity within any particular mirror configuration cycle does not become greater than e_u. Otherwise, by definition, the system will have become potentially unstable even though the total change in eccentricity may subsequently decrease to values below e_u.

(i) A theoretical and numerical method for calculating the changes in the orbital elements over one mirror configuration cycle for the circular case

Using the analytical theory developed in Section 5.3(i), we can map synodic period to synodic period, both forward and backward from the initial value of the true anomaly at the first conjunction f_{c0}. From this we can obtain the changes in the satellite's orbital elements $\Delta\sigma_m$ over one mirror configuration cycle.

Beginning with the initial orbital elements σ_0 and an initial true anomaly at the first conjunction lying close to the satellite's apse line (ie $f_{c0} = \varepsilon$, where ε is a small angle), we map forward, synodic period to synodic period, until the true anomaly of the next conjunction falling closest to 2π is reached. This procedure involves calculating for each $(i+1)^{th}$ synodic period

$$\sigma_{i+1} = \sigma_i + \Delta\sigma_i$$
$$f_{c(i+1)} = f_{ci} + \theta_i$$

where, for the circular case, the changes in the orbital parameters over one synodic period $\Delta\sigma_i$ are given by Equations (27) of Chapter 4, and the angle between the i^{th} and the $(i+1)^{th}$ conjunctions is given by Equation (24). The orbital elements σ_n at the final conjunction are found.

We then repeat the same process mapping backwards, synodic period to synodic period, until the true anomaly of the next conjunction falling closest to -2π is reached. This procedure involves calculating for each $(i-1)^{th}$ synodic period

$$\sigma_{i-1} = \sigma_i - \Delta\sigma_i$$
$$f_{c(i-1)} = f_{ci} - \theta_i$$

The orbital elements σ_{-n} at this final conjunction are found.

In the above procedures, we are indirectly assuming that the orbital elements σ_i don't change very much over two synodic periods. We assume that the changes in

the orbital elements moving forward one synodic period are the same as the changes in the orbital elements moving backward one synodic period. We also assume that the angle between the i^{th} and the $(i+1)^{th}$ conjunctions is approximately the same as the angle between the i^{th} and the $(i-1)^{th}$ conjunctions. These assumptions were checked by comparing the orbital elements σ_i found at each synodic period mapped forward from the initial conditions σ_0 and f_{c0} to the final derived conditions σ_n and f_{cn}, with the orbital elements σ_i found at each synodic period mapped backward from the conditions σ_n and f_{cn} to the original conditions σ_0 and f_{c0}. The two sets of σ_i were virtually indistinguishable.

The changes in the orbital elements over a mirror configuration cycle then become the differences between the final orbital elements of the forward mapping σ_n and backward mapping σ_{-n}. ie

$$\Delta\sigma_m = \sigma_n - \sigma_{-n}$$

The results were checked numerically for the worst cases described in Section 5.2(ii) by using the values of the orbital elements at the end of the backwards analytical mapping σ_{-n} as the initial orbital elements, and mapping forward using the numerical procedure described in Section 5.2(ii). This procedure is carried out until the second conjunction to fall closest to the satellite's pericentre is reached (ie until the conjunction with a true anomaly closest to 4π is found). The final orbital elements σ_n are then subtracted from the initial orbital elements σ_{-n} to get the numerical changes in the orbital elements over one mirror configuration cycle.

The same "worst case" planet-satellite systems tested in Section 5.2(ii) are tested here, using the same initial satellite parameters of $e_0 = 0.5$ and α_0 equal to the largest value of α found amongst the satellites orbiting each planet. However, the greatest difference between the numerical and analytical solutions now occurs when

the central conjunction falls at $\theta_{max}/2$. θ_{max} is found using Equation (42) and the above initial values for e_0 and α_0. The relative errors between the analytical and numerical solutions for the circular case of $\Delta\sigma_m$ are no greater than 4%. See Table 5.14.

Planet	Satellite	Percentage Error of Worst Case	
		Circular Case	Elliptical Case
Jupiter	Callisto	0.4%	3.2%
Saturn	Iapetus	3.9	11.1
Uranus	Oberon	1.6	6.1
Mars	Deimos	1.4	7.4

Table 5.14 The percentage relative differences between the analytical and the numerical values of the maximum possible change in the satellite's orbital eccentricity over one mirror configuration cycle, for both the circular and elliptical cases.

Only the results for the satellites which give the worst difference between the analytical and numerical solutions for each of the planets are listed here.

(ii) A study of the cyclic nature of the orbital elements over one mirror configuration cycle for the circular case

If we now map synodic period to synodic period using the analytical theory, we can calculate the values of the orbital elements σ_i for each synodic period and find the changes in the orbital elements which occur over each synodic period. These calculations can be done for a satellite which moves forward and backward from a

close approximation to a mirror configuration occurring at some small value of f_{c0}.

Figures 5.15(a) to (d), parts (i) show the relationships between the changes (Δe_i, $\Delta\alpha_i$, $\Delta\epsilon_i$, $\Delta\varpi_i$) in the orbital elements over each successive synodic period and the true anomalies f_{ci} of the conjunctions located at the centre of each successive synodic period for a complete mirror cycle centred on a perfect mirror configuration. Parts (ii) of the figures give the relationships between the accumulated orbital elements (e_i, α_i, ϵ_i, ϖ_i) over successive forward and backward synodic periods and the true anomalies f_{ci} of the conjunctions for the same mirror cycle. The solid lines describe the $\Delta\sigma_i$ or σ_i as the satellite moves forward from the central conjunction located at $f_{c0} = 0°$ (ie the perfect mirror configuration), while the dashed lines describe the $\Delta\sigma_i$ or σ_i as the satellite moves backward from the central conjunction.

Figures 5.15 (a) to (d) The variations in (i) the changes $\Delta\sigma$ in the satellite's orbital element over one synodic period and (ii) the satellite's accumulated orbital element σ as the satellite passes through successive i^{th} synodic periods to complete one mirror cycle.

The solid line depicts the orbital element or the change in the orbital element as the satellite moves forward from a central conjunction of $f_{c0}=0°$, while the dashed line shows the orbital element or the change in the orbital element as the satellite moves backward from the central conjunction.

Graphs (a) to (d) portray the above relationships for the orbital elements σ = e, α, ϵ and ϖ respectively.

The data used here are those of a circular coplanar Jupiter-Callisto system with α_0=0.0025, e_0 = 0.01 and μ = 1100.

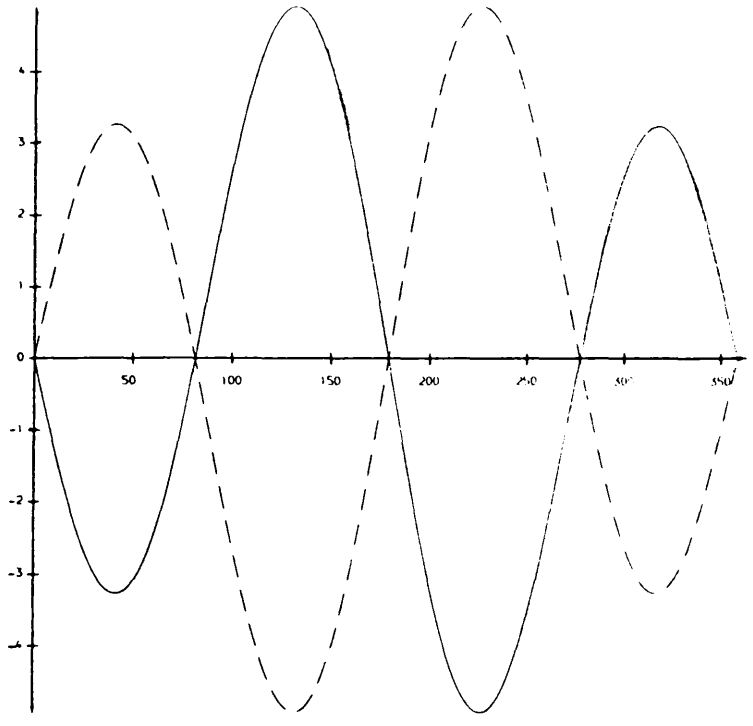

(a)i

The absolute difference between the true anomalies of the $+i^{th}$ conjunction or the $-i^{th}$ conjunction and the central conjunction. ($f_{c+i} - f_{c0}$) or $-(f_{c-i} - f_{c0})$ (in degrees)

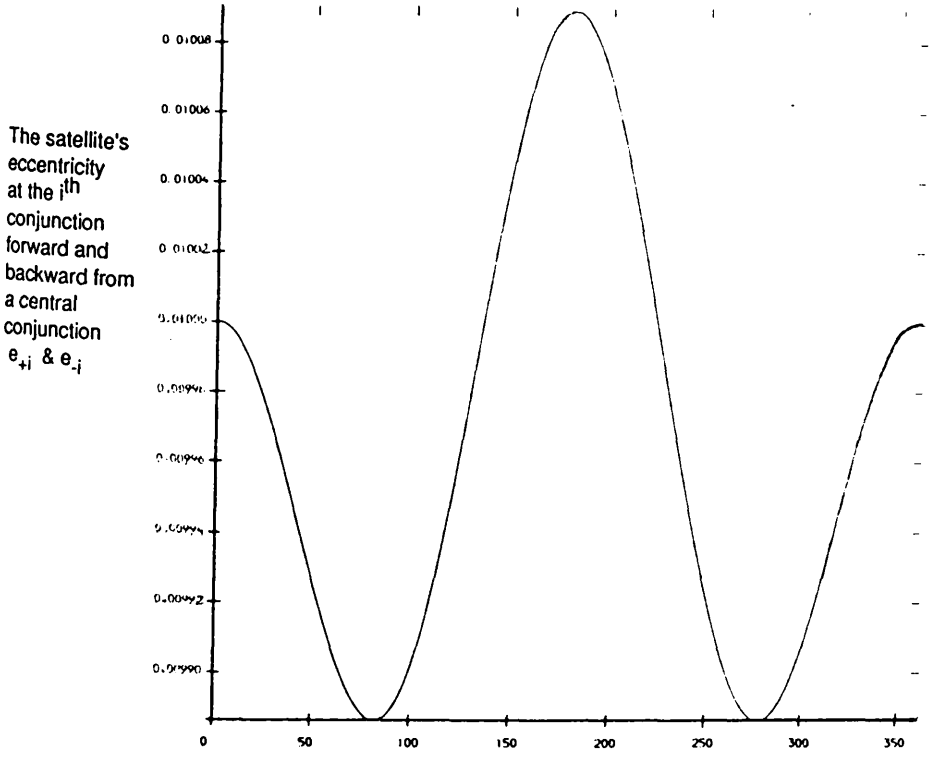

(a)ii

The absolute difference between the true anomalies of the $+i^{th}$ conjunction or the $-i^{th}$ conjunction and the central conjunction. ($f_{c+i} - f_{c0}$) or $-(f_{c-i} - f_{c0})$ (in degrees)

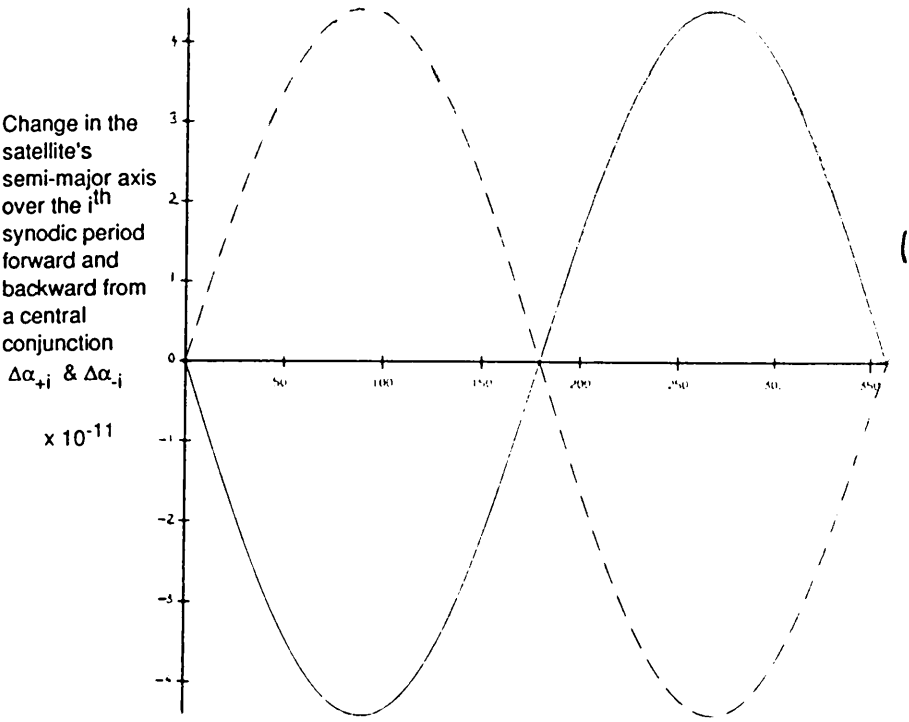

(b) i

The absolute difference between the true anomalies of the $+i^{th}$ conjunction or the $-i^{th}$ conjunction and the central conjunction. $(f_{c+i} - f_{c0})$ or $-(f_{c-i} - f_{c0})$ (in degrees)

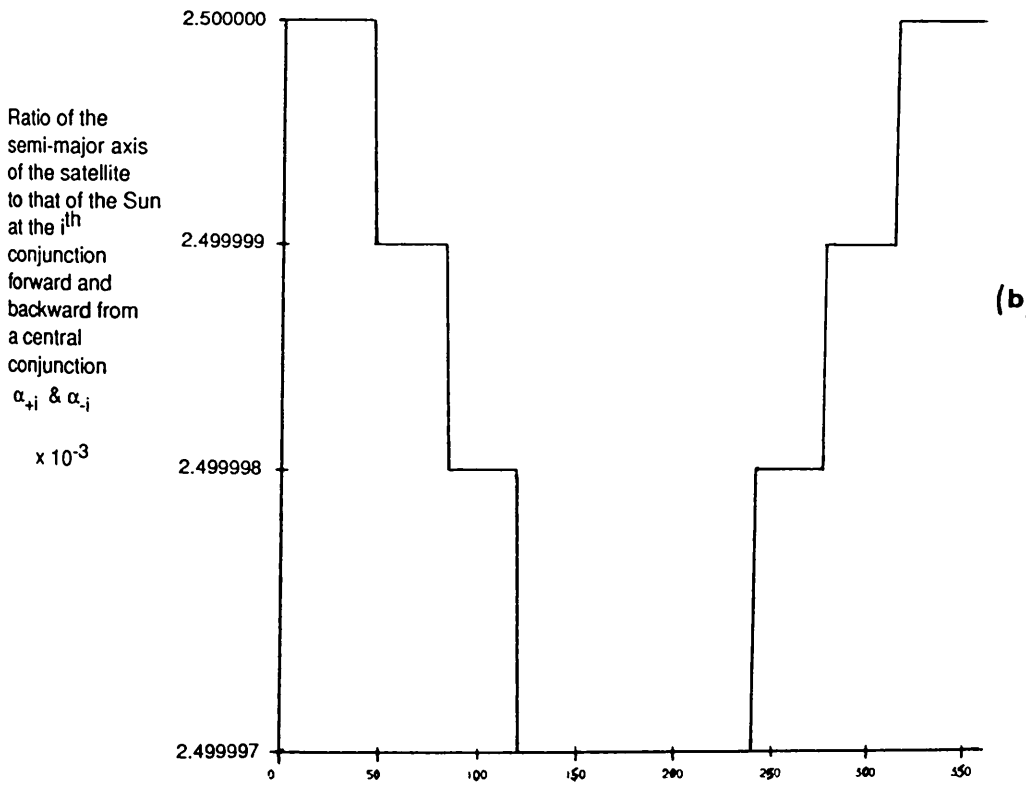

(b) i i

The absolute difference between the true anomalies of the $+i^{th}$ conjunction or the $-i^{th}$ conjunction and the central conjunction. $(f_{c+i} - f_{c0})$ or $-(f_{c-i} - f_{c0})$ (in degrees)

Change in the satellite's mean longitude at epoch over the i^{th} synodic period forward and backward from a central conjunction $\Delta\epsilon_{+i}$ & $\Delta\epsilon_{-i}$ (in radians)

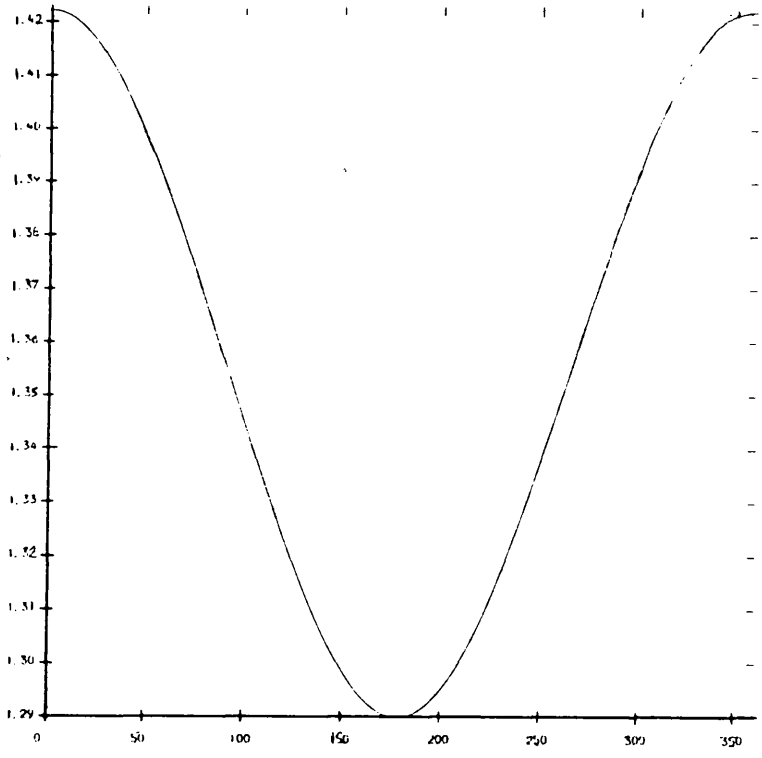

(c) i

The absolute difference between the true anomalies of the $+i^{th}$ conjunction or the $-i^{th}$ conjunction and the central conjunction. $(f_{c+i} - f_{c0})$ or $-(f_{c-i} - f_{c0})$ (in degrees)

The satellite's mean longitude at epoch at the i^{th} conjunction forward and backward from a central conjunction ϵ_{+i} & ϵ_{-i} (in radians)

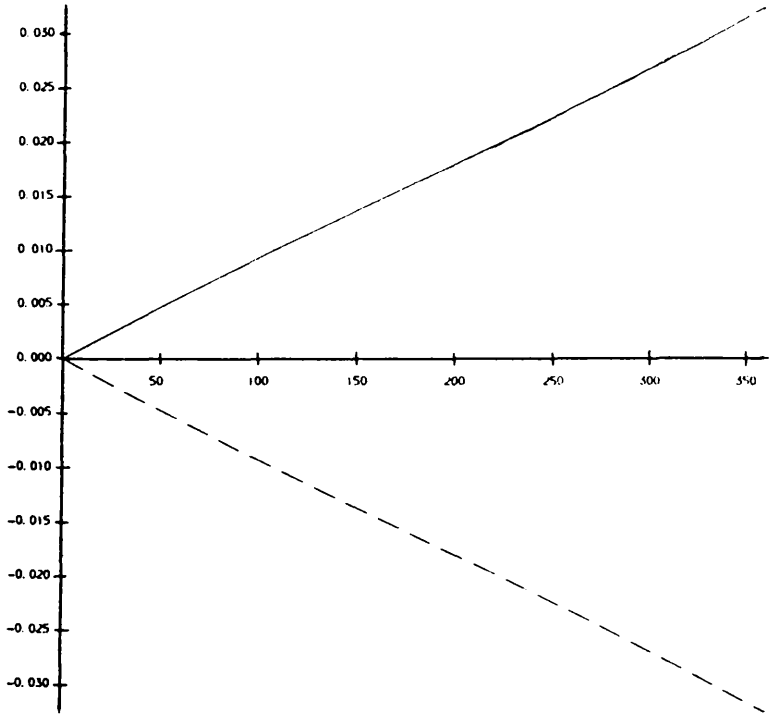

(c) ii

The absolute difference between the true anomalies of the $+i^{th}$ conjunction or the $-i^{th}$ conjunction and the central conjunction. $(f_{c+i} - f_{c0})$ or $-(f_{c-i} - f_{c0})$ (in degrees)

Change in the satellite's longitude of pericentre over the i^{th} synodic period forward and backward from a central conjunction $\Delta\varpi_{+i}$ & $\Delta\varpi_{-i}$ (in radians)

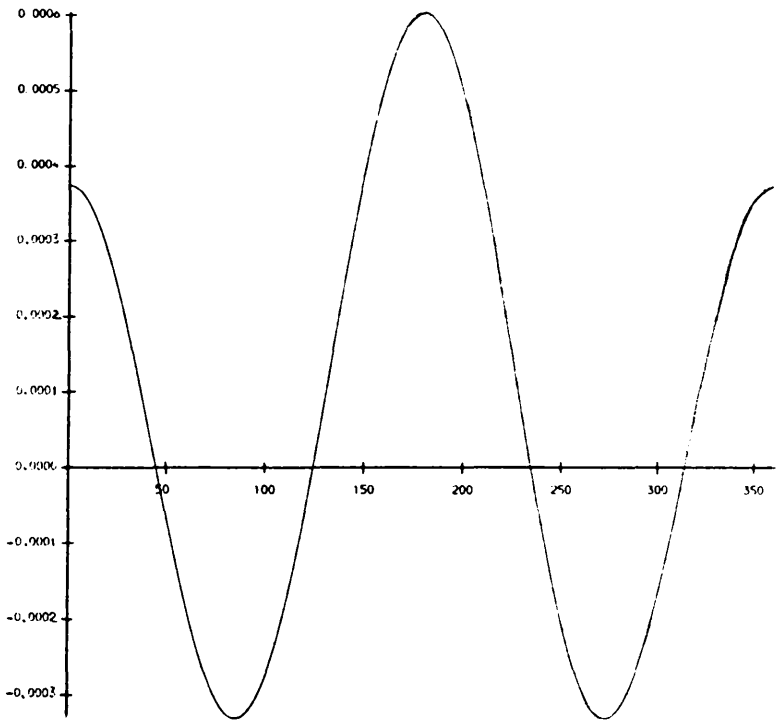

(d) i

The absolute difference between the true anomalies of the $+i^{th}$ conjunction or the $-i^{th}$ conjunction and the central conjunction. $(f_{c+i} - f_{c0})$ or $-(f_{c-i} - f_{c0})$. (in degrees)

The satellite's longitude of pericentre at the i^{th} conjunction forward and backward from a central conjunction ϖ_{+i} & ϖ_{-i} (in radians)

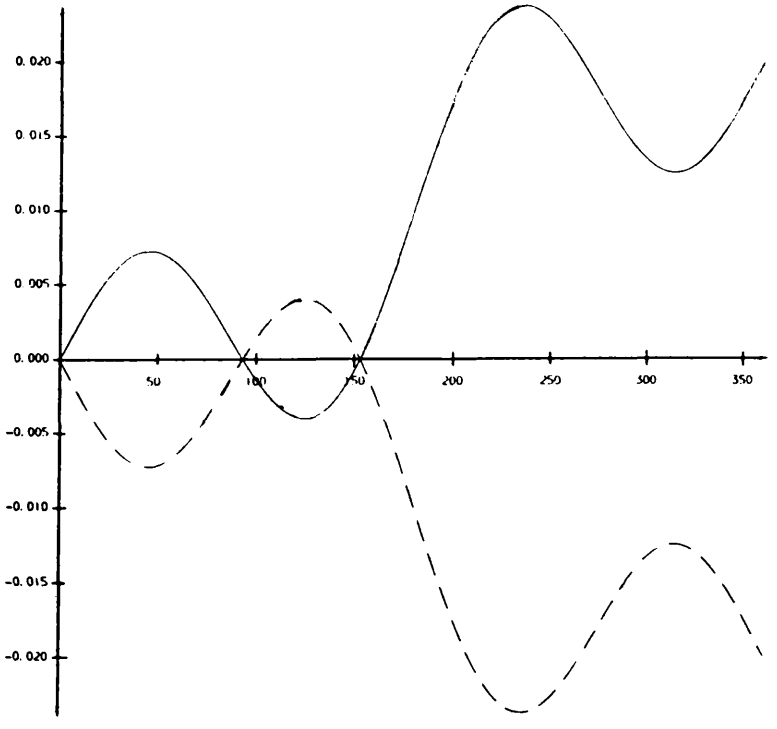

(d) ii

The absolute difference between the true anomalies of the $+i^{th}$ conjunction or the $-i^{th}$ conjunction and the central conjunction. $(f_{c+i} - f_{c0})$ or $-(f_{c-i} - f_{c0})$ (in degrees)

A +i subscript denotes those elements $\Delta\sigma_{+i}$ or σ_{+i} which are found in the forward part of the mirror cycle, while a -i subscript denotes those elements $\Delta\sigma_{-i}$ or σ_{-i} which are found in the backward part of the mirror cycle.

For easy comparison of the orbital elements forwards and backwards from the central conjunction located at f_{c0}, the graphs have been centred on the true anomaly f_{c0}, where the forward orbital elements are plotted against $(f_{ci} - f_{c0})$ and the backward orbital elements are plotted on the same scale against $-(f_{ci} - f_{c0})$. The initial conditions used are those of the Jupiter-Callisto example studied throughout the thesis (ie $\alpha_0 = 0.0025$, $e_0 = 0.01$ and $\mu = 1100$), where the Sun is assumed to be moving in a fixed circular orbit. The step function found in Figure 5.15(b)ii is caused by the inability of the graphics package to handle numbers to greater than eight digit accuracy.

Figures 5.15 are beautiful examples of the mirror theorem at work. Figures 5.15(a)i and (b)i confirm that the changes in the size $\Delta\alpha_i$ and shape Δe_i of the satellite's orbit after the three-body system reaches a perfect mirror configuration are the exact opposite of the changes which occur in the satellite's orbital size and shape before the mirror configuration is attained. ie

$$\Delta e_{+i} = -\Delta e_{-i} \qquad (36)$$

$$\Delta\alpha_{+i} = -\Delta\alpha_{-i} \qquad (37)$$

The net change in the satellite's eccentricity or the ratio of the semi-major axes over any period centred on a mirror configuration is therefore always zero, with the result that the shape and size of the satellite's orbit a time t before the mirror configuration are identical to the shape and size of the satellite's orbit a time t after the mirror configuration. Hence, the curves in Figures 5.15(a)ii and (b)ii representing the accumulated values of the satellite's eccentricity and the ratio of the semi-major axes forwards in time from $f_{c0} = 0°$ are indistinguishable from the

curves representing the same variables backwards in time from $f_{c0} = 0°$. ie

$$e_{+i} = e_{-i} \tag{38}$$

$$\alpha_{+i} = \alpha_{-i} \tag{39}$$

The mirror theorem states that not only the positional behavior, but also the dynamical behavior of the three-body system before a mirror configuration is mirrored after the mirror configuration. This means that not only the size and shape of the satellite's orbit, but also the motion of the satellite's orbital orientation (ie the rate of change of its apse-line) and the motion of the satellite within its orbit (ie the rate of change of the satellite's expected time of arrival at its pericentre) will be the same at a time t before and after the mirror configuration.

These last two characteristics are displayed in Figures 5.15(c)i and (d)i. The curve depicting the change $\Delta\varpi_{+i}$ in the mean longitude of the satellite's apse line forward a time t from a mirror configuration is identical to the curve depicting the change $\Delta\varpi_{-i}$ in the mean longitude of the satellite's pericentre backward a time t from the mirror configuration. Likewise, the curves showing the changes in the satellite's mean longitude at epoch forward and backward ($\Delta\epsilon_{+i}$ and $\Delta\epsilon_{-i}$) are also indistinguishable from each other.

In other words,

$$\Delta\varpi_{+i} = \Delta\varpi_{-i} \tag{40}$$

$$\Delta\epsilon_{+i} = \Delta\epsilon_{-i} \tag{41}$$

The resulting accumulated mean longitude of pericentre forwards ϖ_{+i} and backwards ϖ_{-i} from the central mirror configuration are therefore symmetric about the value of the mean longitude of pericentre ϖ_0 at the mirror configuration. The symmetry is similar for the mean longitudes at the epoch forwards ϵ_{+i} and backwards

ϵ_{-i} from the central mirror configuration. See Figures 5.15(c)ii and (d)ii.

Note that the curves found in Figures 5.15 representing the forward motion of the satellite from a mirror configuration are almost the same as Figures 5.11 to 5.14 which describe the changes in the same variables forward from $f_{c0} = 0°$ one cycle of conjunctions. This confirms that one mirror cycle is very similar to two cycles of conjunctions, where the first conjunction cycle ends, and the second one begins at a conjunction falling very close to the satellite's line of apses.

We now study the cyclic behavior of the orbital elements over one mirror cycle which is centred only on a close approximation to a mirror configuration (ie $f_{c0} = \varepsilon$, where ε is small). We again look at the Jupiter-Callisto case where $\alpha_0 = 0.0025$, $e_0 = 0.01$ and $\mu = 1100$, but the results are similar for any of the typical values of the initial orbital elements found in the solar system.

We take the worst possible case and assume that the central conjunction falls the farthest possible angular distance from the satellite's apse line, given the initial conditions. The true anomaly of the conjunction is therefore equal to half the maximum possible angle between any two consecutive conjunction lines. For the Jupiter-Callisto example this angle is $f_{c0} = 0.7494°$. We shall show later in Section 5.4(iii) how this value is derived.

For now, Figures 5.16 display the same relationships shown in Figures 5.15, except that each variable is depicted forward (solid line) and backward (dashed line) from a central conjunction located at the farthest distance possible from the satellite's apse line (ie $f_{c0} = 0.7494°$).

Figures 5.16 (a) to (d) The same graphs as in Figures 5.15, except that the central conjunction is now located at its farthest possible angular distance from a perfect mirror condition (ie for the Jupiter-Callisto circular case, at $f_{c0} = 0.7494°$).

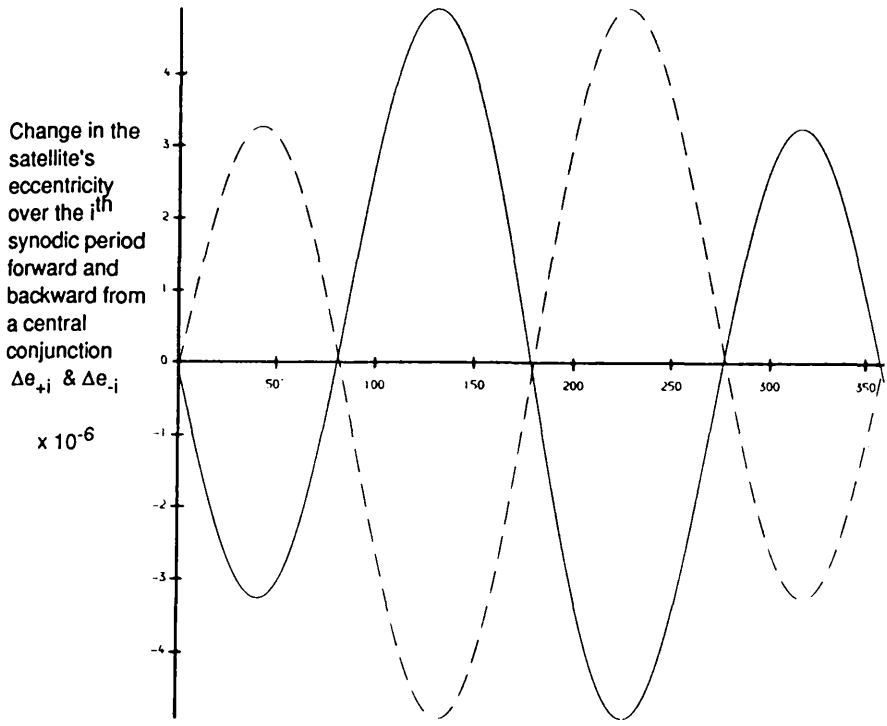

(a)i

The absolute difference between the true anomalies of the $+i^{th}$ conjunction or the $-i^{th}$ conjunction and the central conjunction. $(f_{c+i} - f_{c0})$ or $-(f_{c-i} - f_{c0})$ (in degrees)

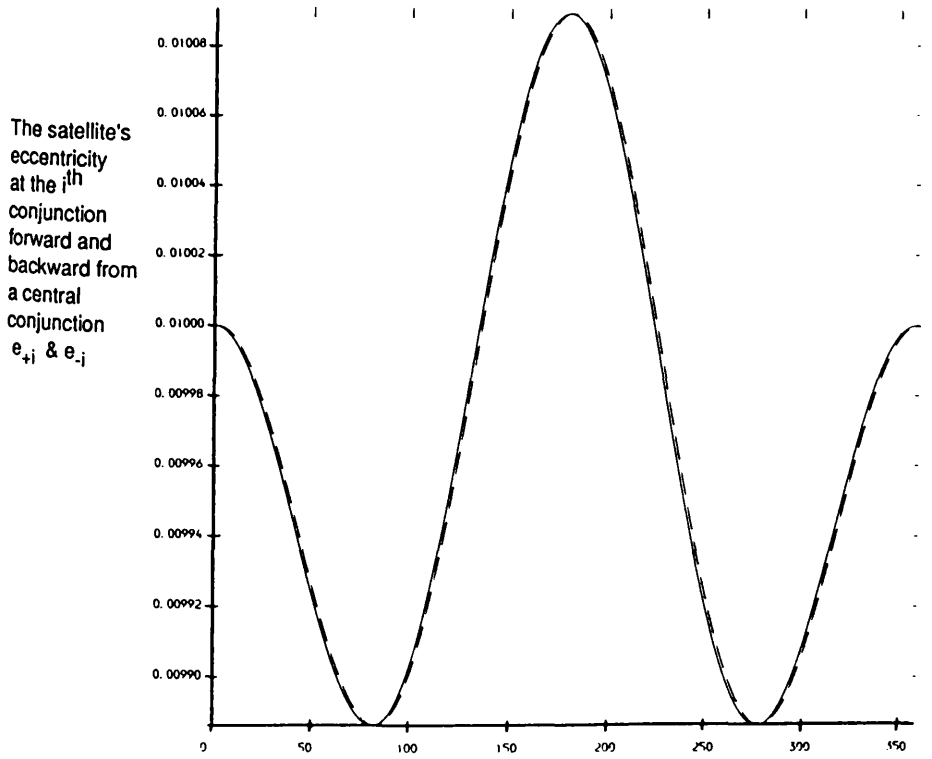

(a)ii

The absolute difference between the true anomalies of the $+i^{th}$ conjunction or the $-i^{th}$ conjunction and the central conjunction. $(f_{c+i} - f_{c0})$ or $-(f_{c-i} - f_{c0})$ (in degrees)

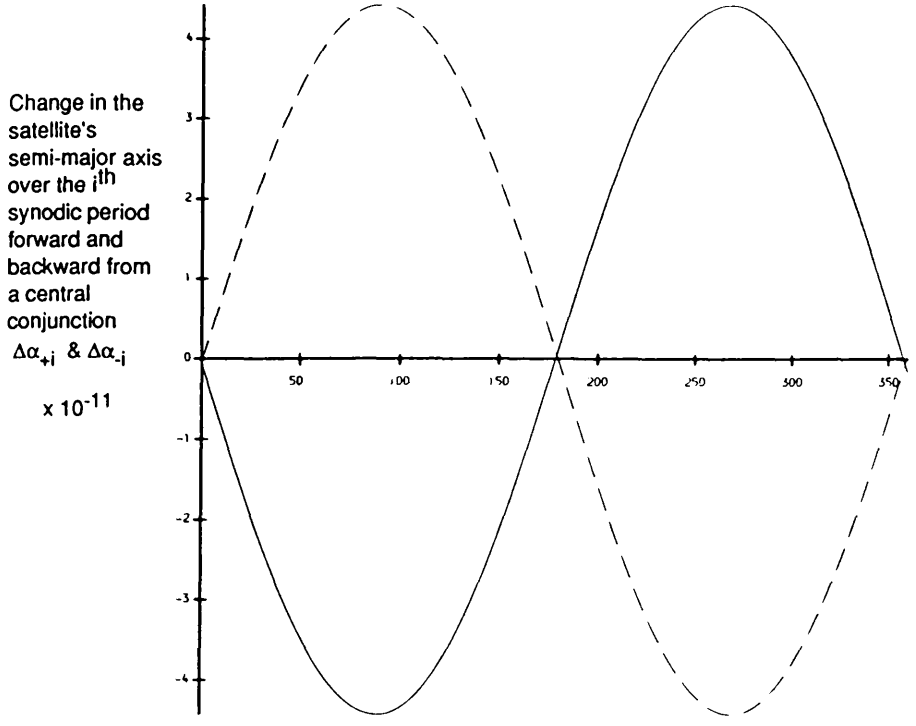

(b) i

The absolute difference between the true anomalies of the $+i^{th}$ conjunction or the $-i^{th}$ conjunction and the central conjunction. ($f_{c+i} - f_{c0}$) or $-(f_{c-i} - f_{c0})$ (in degrees)

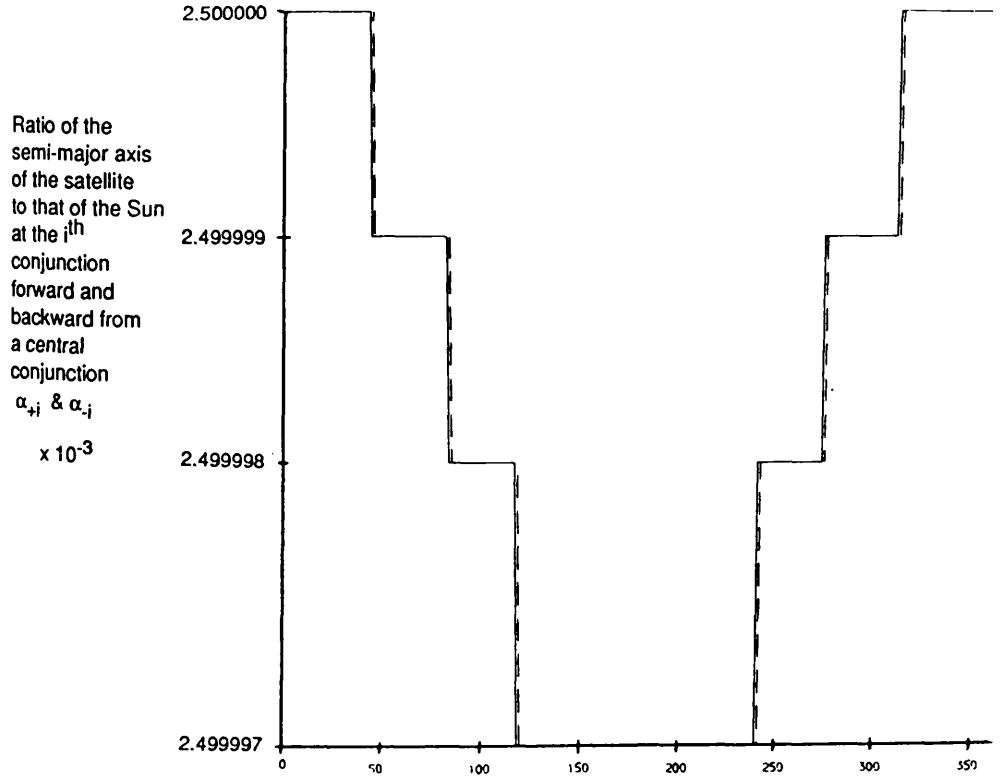

(b) i i

The absolute difference between the true anomalies of the $+i^{th}$ conjunction or the $-i^{th}$ conjunction and the central conjunction. ($f_{c+i} - f_{c0}$) or $-(f_{c-i} - f_{c0})$ (in degrees)

Change in the satellite's mean longitude at epoch over the i^{th} synodic period forward and backward from a central conjunction $\Delta\epsilon_{+i}$ & $\Delta\epsilon_{-i}$ (in radians)

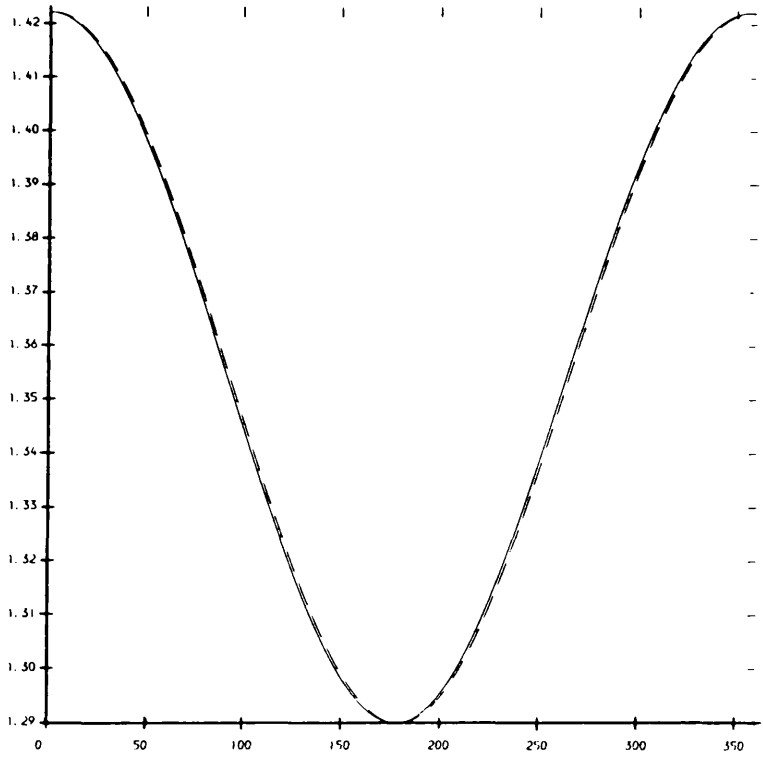

(c) i

The absolute difference between the true anomalies of the $+i^{th}$ conjunction or the $-i^{th}$ conjunction and the central conjunction. $(f_{c+i} - f_{c0})$ or $-(f_{c-i} - f_{c0})$ (in degrees)

The satellite's mean longitude at epoch at the i^{th} conjunction forward and backward from a central conjunction ϵ_{+i} & ϵ_{-i} (in radians)

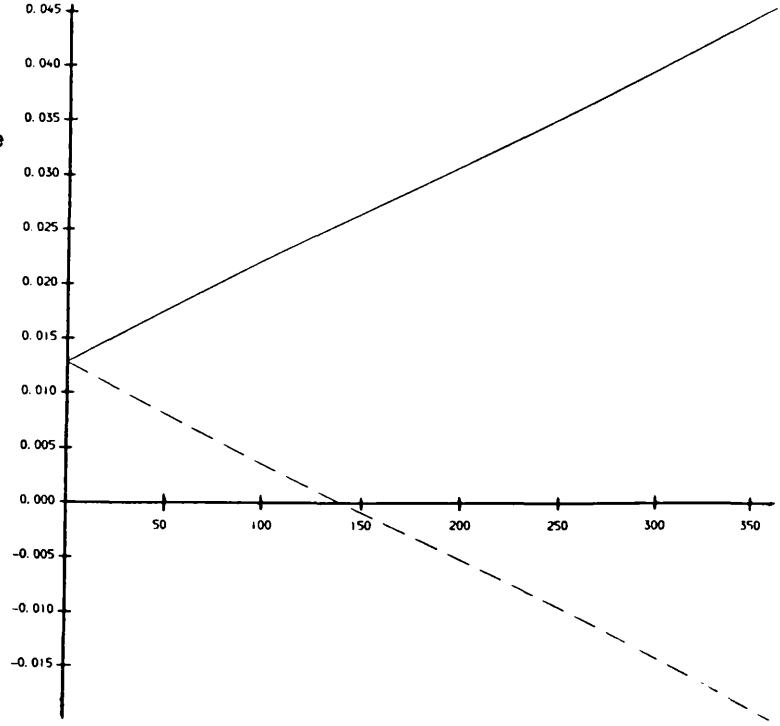

(c) ii

The absolute difference between the true anomalies of the $+i^{th}$ conjunction or the $-i^{th}$ conjunction and the central conjunction. $(f_{c+i} - f_{c0})$ or $-(f_{c-i} - f_{c0})$ (in degrees)

Change in the satellite's longitude of pericentre over the i^{th} synodic period forward and backward from a central conjunction $\Delta\varpi_{+i}$ & $\Delta\varpi_{-i}$ (in radians)

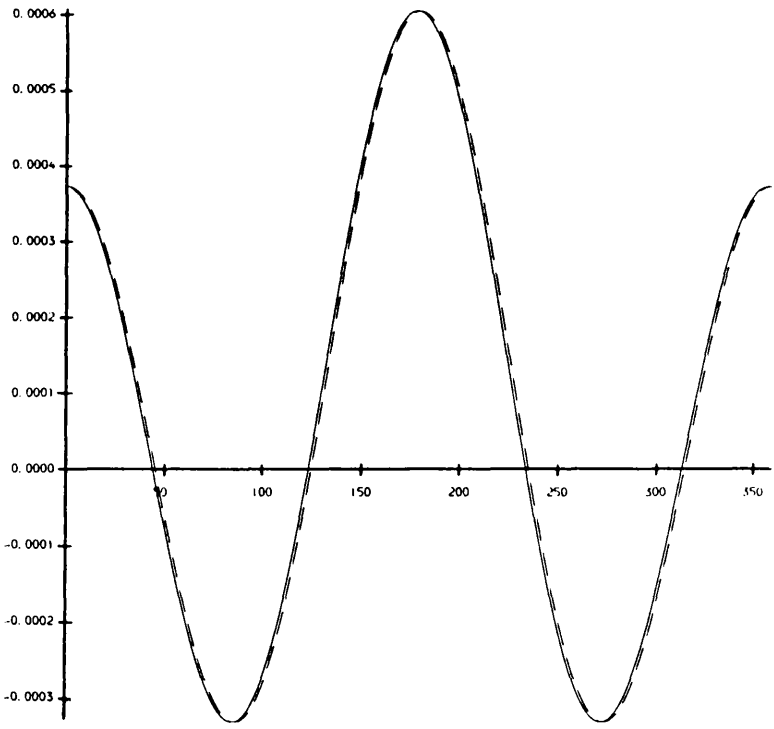

(d) i

The absolute difference between the true anomalies of the $+i^{th}$ conjunction or the $-i^{th}$ conjunction and the central conjunction. $(f_{c+i} - f_{c0})$ or $-(f_{c-i} - f_{c0})$ (in degrees)

The satellite's longitude of pericentre at the i^{th} conjunction forward and backward from a central conjunction ϖ_{+i} & ϖ_{-i} (in radians)

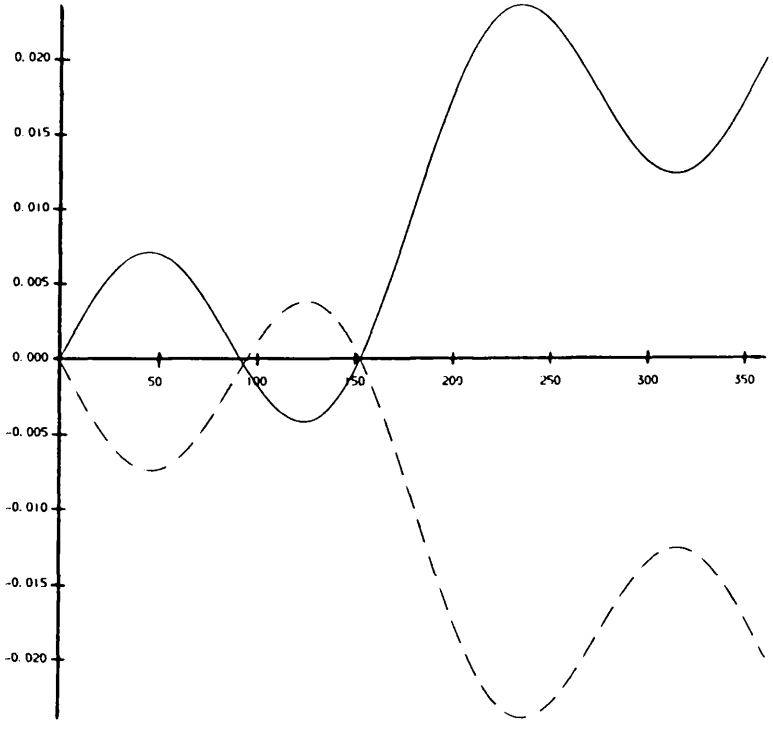

(d) i i

The absolute difference between the true anomalies of the $+i^{th}$ conjunction or the $-i^{th}$ conjunction and the central conjunction. $(f_{c+i} - f_{c0})$ or $-(f_{c-i} - f_{c0})$ (in degrees)

Figures 5.16 are much the same as Figures 5.15 except that, because the central conjunction no longer forms a perfect mirror configuration, the following curves in Figures 5.16 are no longer exactly aligned:

(1) the accumulated eccentricity forwards e_{+i} and backwards e_{-i} from the central conjunction (Figure 5.16(a)ii);

(2) the accumulated ratio of the semi-major axes forwards α_{+i} and backwards α_{-i} from the central conjunction (Figure 5.16(b)ii);

(3) the change in the mean longitude at the epoch forwards $\Delta\epsilon_{+i}$ and backwards $\Delta\epsilon_{-i}$ from the central conjunction (Figure 5.16(c)i);

(4) the change in the mean longitude of the pericentre forwards $\Delta\varpi_{+i}$ and backwards $\Delta\varpi_{-i}$ from the central conjunction (Figure 5.16(d)i)

Equations (38) to (41) are now only approximately true.

Figures 5.17 to 5.20 show the differences between the forward and backward values in the above curves. The differences oscillate about zero and are approximately cyclic over one mirror cycle. But most importantly, even when the worst case is chosen, the differences are still very small and still therefore, exhibit the characteristics of a close mirror reversal.

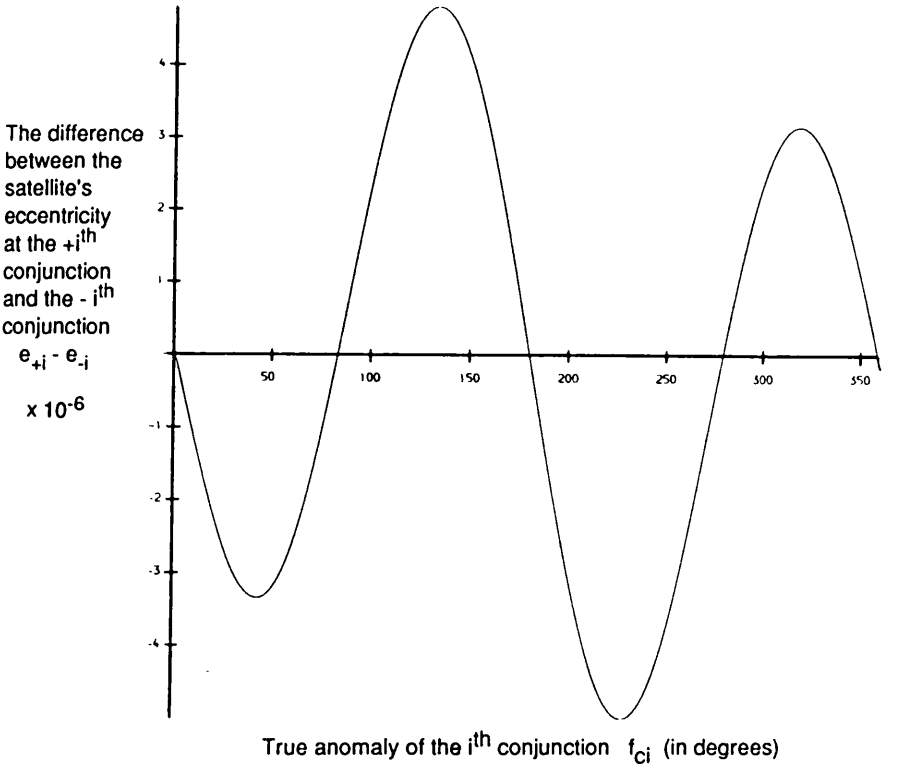

Figure 5.20 The difference between the satellite's accumulated eccentricity forward e_{+i} from a central conjunction located at $f_{c0} = 0.7494°$ and the satellite's accumulated eccentricity backward e_{-i} from the same conjunction as a function of the true anomaly of the i^{th} conjunction.

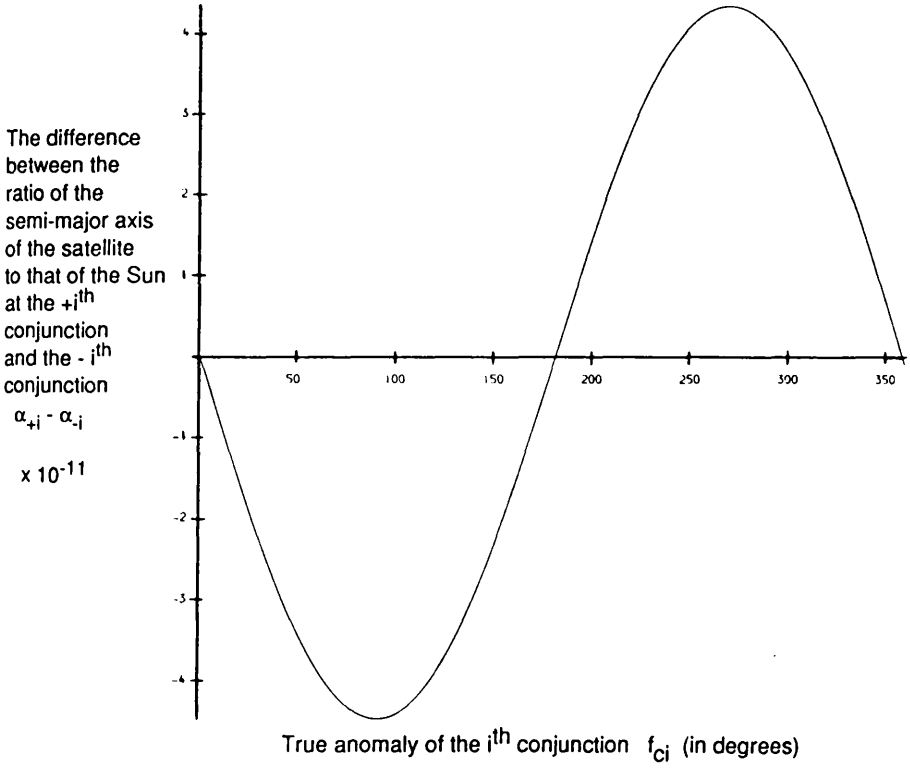

Figure 5.21 The difference between the satellite's accumulated ratio of the semi-major axes forward α_{+i} from a central conjunction located at $f_{c0} = 0.7494°$ and the satellite's accumulated ratio of the semi-major axes backward α_{-i} from the same conjunction as a function of the true anomaly of the i^{th} conjunction.

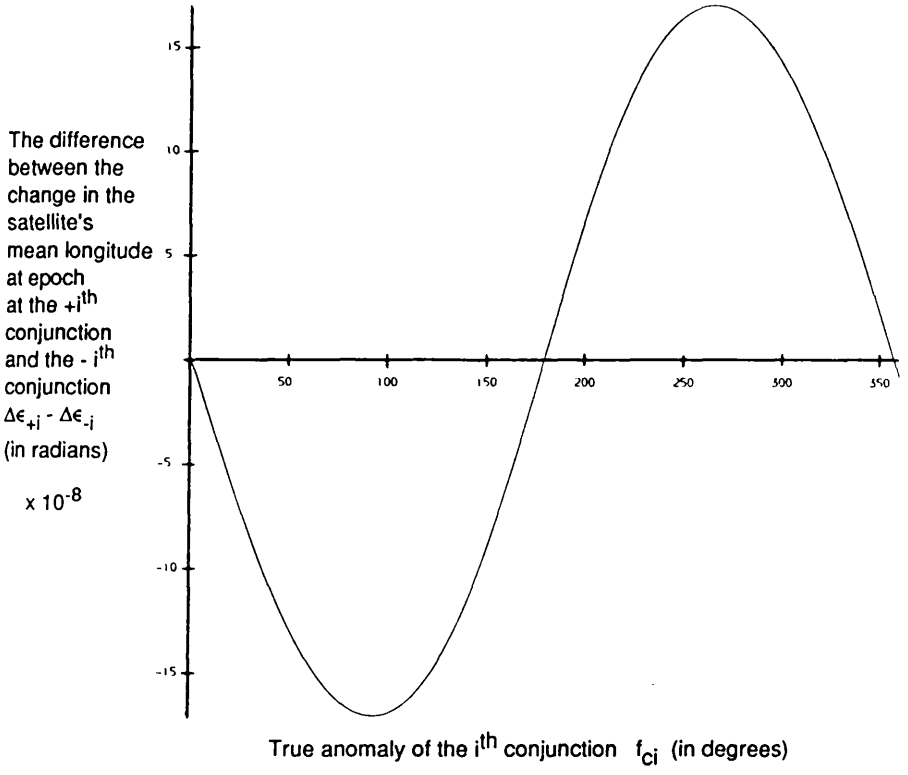

Figure 5.22 The difference between the satellite's change in the mean longitude at epoch forward $\Delta\epsilon_{+i}$ from a central conjunction located at $f_{c0} = 0.7494°$ and the satellite's change in the mean longitude at epoch backward $\Delta\epsilon_{-i}$ from the same conjunction as a function of the true anomaly of the i^{th} conjunction.

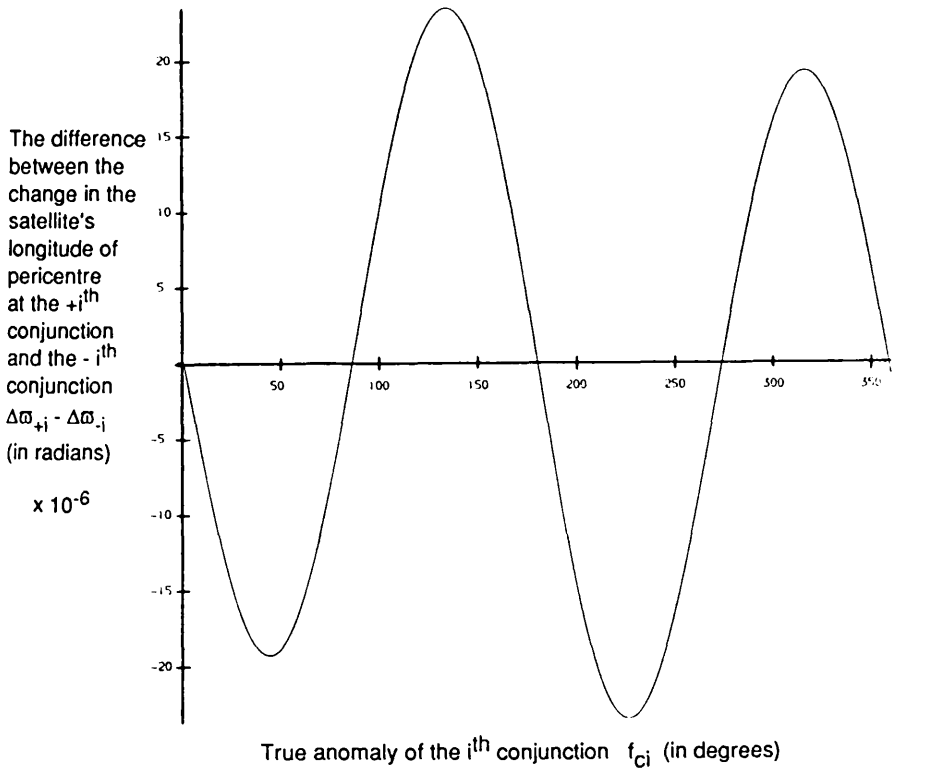

Figure 5.23 The difference between the satellite's change in the longitude of the pericentre forward $\Delta\varpi_{+i}$ from a central conjunction located at $f_{c0} = 0.7494°$ and the satellite's change in the longitude of pericentre backward $\Delta\varpi_{-i}$ from the same conjunction as a function of the true anomaly of the i^{th} conjunction.

As in the first two levels of the finite-time stability method, we now study the changes in the orbital elements $\Delta\sigma_m$ over one mirror cycle. Figures 5.21(a) to (d) show the sizes of $\Delta\sigma_m$, where σ = e, α, ϵ, or ϖ respectively, for different starting values of the true anomaly of the central conjunction f_{c0}. The example given in Figure 5.21 is that of the Jupiter-Callisto system where e_0 = 0.01, α_0 = 0.0025, μ = 1100 and the Sun is assumed to move in a fixed circular orbit, but the results are similar for most typical satellites found in the solar system. Since the largest possible deviation of the central conjunction from the satellite's apse line is no bigger than half the maximum possible angle between any two consecutive conjunctions, an angle which is generally very small for typical solar system examples, the range of f_{c0} is taken to be no greater than 10°.

The changes in the satellite's orbital elements over one mirror cycle, for central conjunctions falling only small angles away from the satellite's apse line, increase negatively from zero as the true anomaly of the central conjunction is increased.

Figures 5.21 (a) to (d) The relationships between the changes in the orbital elements over one mirror cycle $\Delta\sigma_m$ and the true anomaly of the central conjunction f_{c0} nearest the satellite's apse line. Graphs (a) through to (d) depict $\Delta\sigma_m = \Delta e_m$, $\Delta\alpha_m$, $\Delta\epsilon_m$ and $\Delta\varpi_m$ respectively.

The initial conditions used here are those of a Jupiter-Callisto system α_0 = 0.0025, e_0=0.01 and μ = 1100. The Sun is assumed to be moving in a fixed ciruclar orbit.

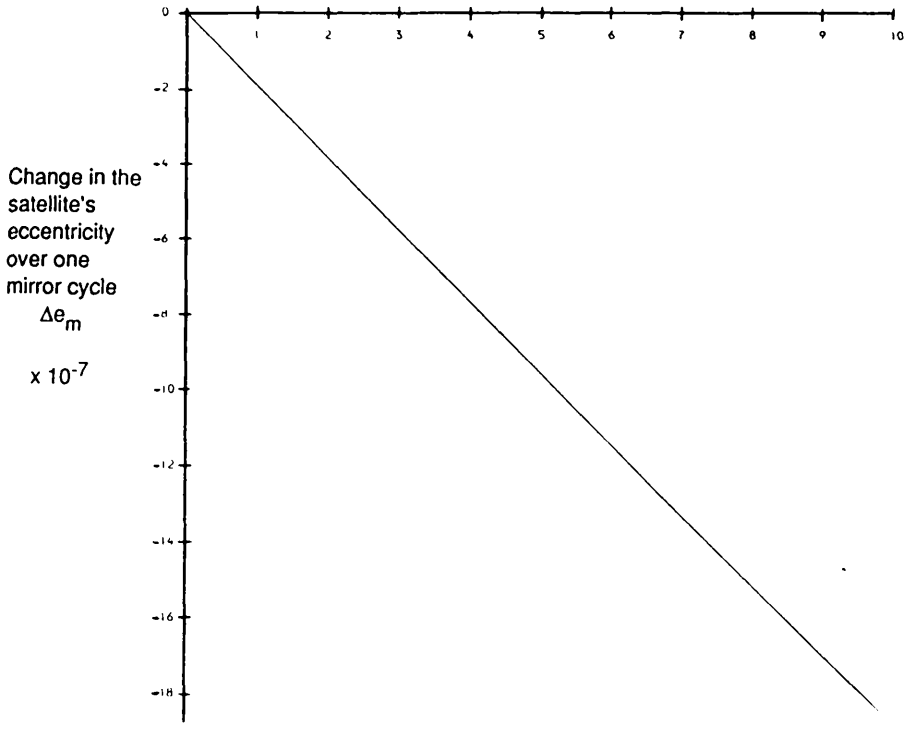
Change in the satellite's eccentricity over one mirror cycle
Δe_m
x 10^{-7}
0
-2
-4
-6
-8
-10
-12
-14
-16
-18
1
2
3
4
5
6
7
8
9
10
The satellite's true anomaly at the central conjunction f_{c0}
(in degrees)

(a)

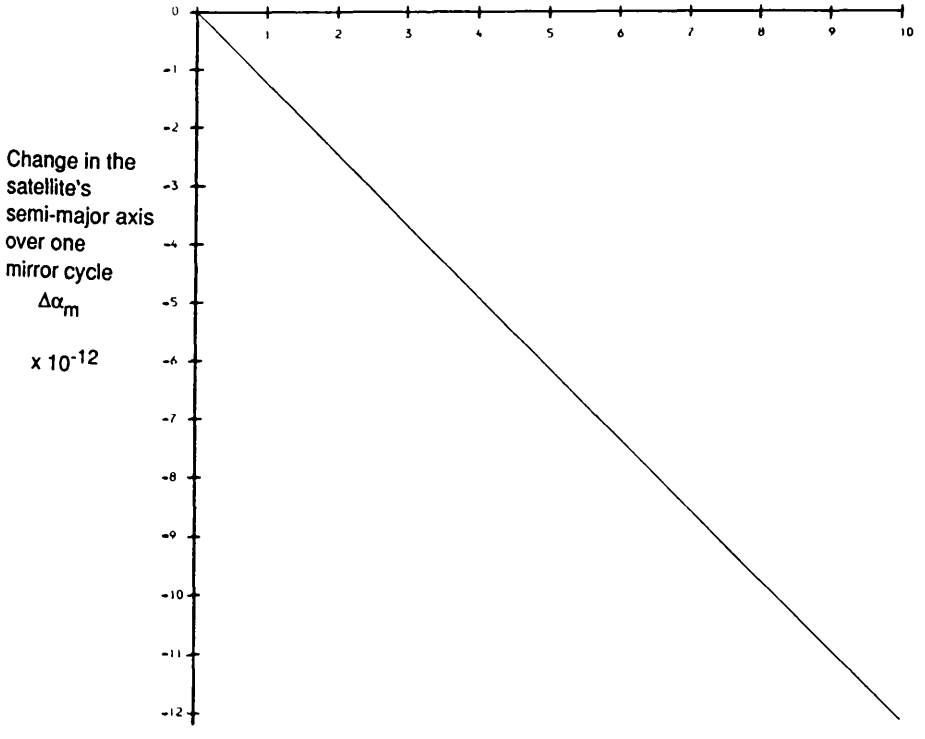
Change in the satellite's semi-major axis over one mirror cycle
$\Delta \alpha_m$
x 10^{-12}
0
-1
-2
-3
-4
-5
-6
-7
-8
-9
-10
-11
-12
1
2
3
4
5
6
7
8
9
10
The satellite's true anomaly at the central conjunction f_{c0}
(in degrees)

(b)

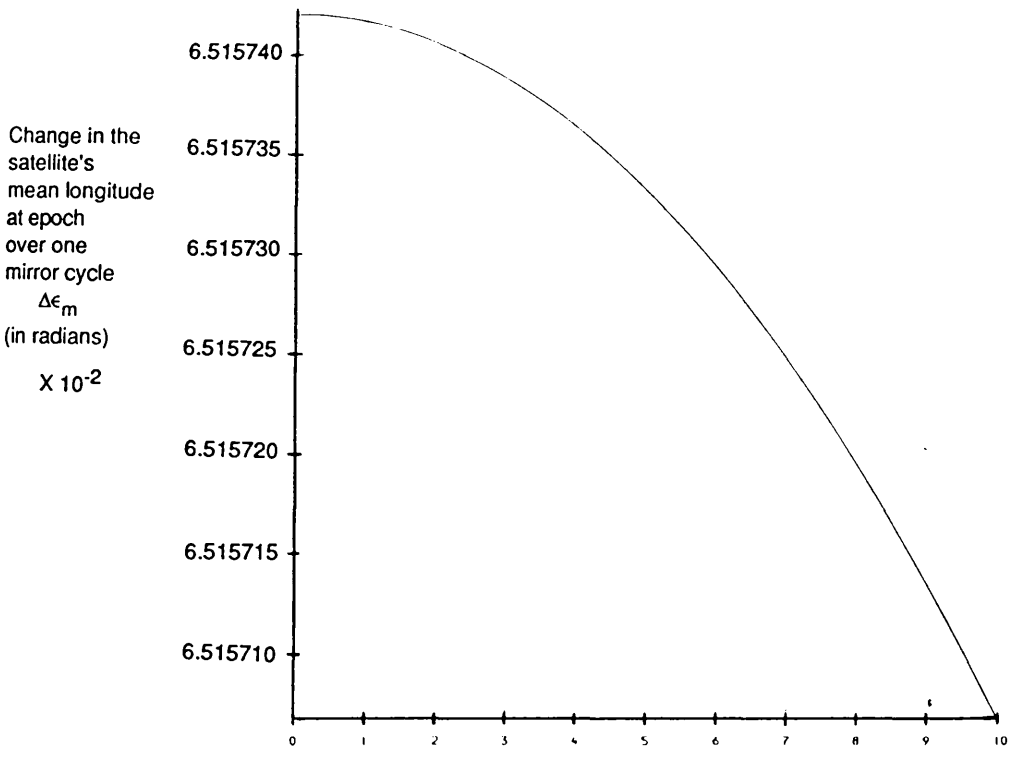
Change in the satellite's mean longitude at epoch over one mirror cycle $\Delta\epsilon_m$ (in radians) X 10^{-2}
6.515740
6.515735
6.515730
6.515725
6.515720
6.515715
6.515710
0
1
2
3
4
5
6
7
8
9
10
The satellite's true anomaly at the central conjunction f_{c0} (in degrees)

(c)

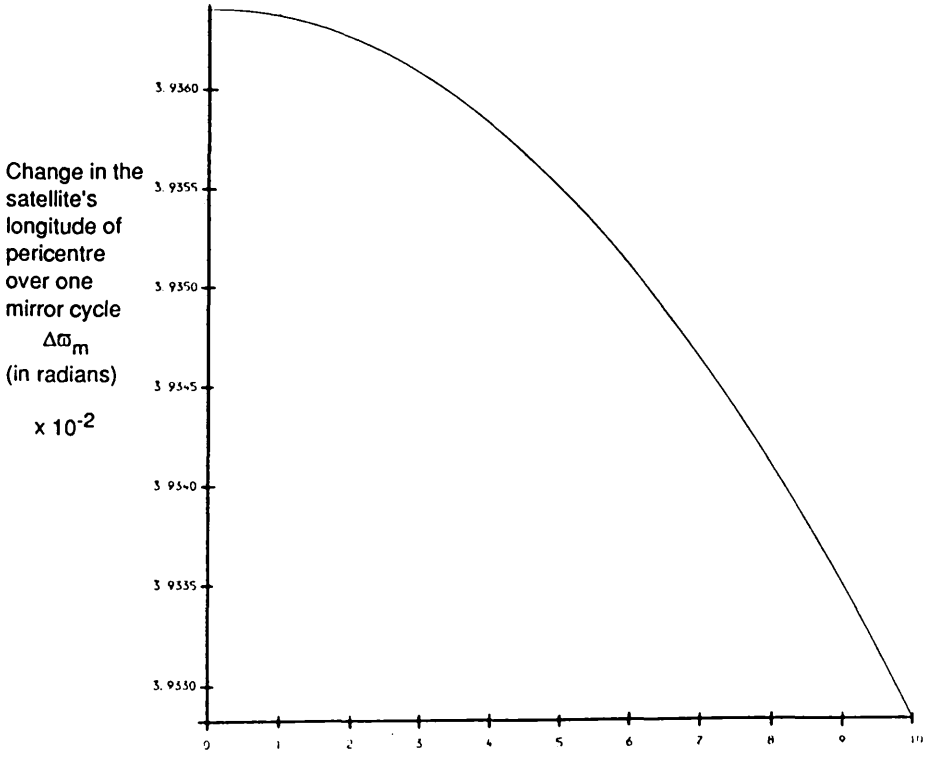
Change in the satellite's longitude of pericentre over one mirror cycle $\Delta\varpi_m$ (in radians) x 10^{-2}
3.9360
3.9355
3.9350
3.9345
3.9340
3.9335
3.9330
0
1
2
3
4
5
6
7
8
9
10
The satellite's true anomaly at the central conjunction f_{c0} (in degrees)

(d)

The most important thing to note about Figures 5.21 is that for small ranges of f_{c0}, the absolute value of the maximum possible change in the satellite's eccentricity occurs at the largest possible true anomaly of the central conjunction.

Also, the size of these maximum changes in the satellite's eccentricity over one mirror cycle (eg in the Jupiter-Callisto case of the order of 10^{-7}) are much smaller than the size of the maximum possible changes in the satellite's eccentricity over one cycle of conjunctions (eg in the Jupiter-Callisto case of the order of 10^{-5}). In addition, the period of the mirror cycle is twice that of the conjunction cycle. Thus, if the satellite for the circular case can persevere through several mirror cycles, the minimum lifetime of the system can easily be extended to beyond the times calculated for the second level of the finite-time stability method.

(iii) The minimum durations of various satellite systems using the third level of the finite-time stability method for the circular case

We have seen from Figures 5.21 that the largest possible change in the eccentricity over a mirror cycle for the circular case occurs at the largest deviation of the central conjunction from the apse line. In other words, it occurs at the largest possible value of f_{c0}. This value can be no larger than half the maximum possible angular distance θ_{max} between any two consecutive conjunctions. The angle θ_i found between two consecutive conjunctions located at true anomalies of f_{ci} and f_{1ci} for the circular case is given by Equation (24). It is a function of the values of the orbital elements and the true anomaly of the satellite at the conjunction found at the centre of the i^{th} synodic period.

From Equation (24) we can see that the largest possible angle between two consecutive conjunctions θ_{max} would occur when one of the conjunctions is located at a true anomaly of $f_{ci} = 180°$. ie

$$\theta_{max} = 2\pi\nu(1 + \nu + \nu^2 + 2e_i\nu) \qquad (42)$$

The largest possible change in the eccentricity over one mirror cycle would then

occur when the central conjunction is located at a true anomaly of

$$f_{c0} = \pi\nu(1 + \nu + \nu^2 + 2e_i\nu) \qquad (43)$$

Choosing the above value for the central conjunction's true anomaly is of course overly pessimistic since by the definition of a mirror cycle the central conjunction is closest to pericentre with a true anomaly of approximately 0° and not 180°. However, in order to find the minimum possible lifetime of the planet-satellite-Sun system we continue to study the worst possible scenario.

To find the minimum lifetimes of planet-satellite-Sun systems T^3_{min}, we next find the number of mirror cycles N_3 needed to increase the eccentricity from e_0 to e_u=0.5 and substitute this value into Equation (35) to get T^3_{min}. The procedure to obtain T^3_{min} is exactly the same as that used to obtain T^1_{min} and T^2_{min} (See Section 5.2 and 5.3(iv)), except that the change Δe_m in the eccentricity over one mirror cycle centred on $f_{c0} = \theta_{max}/2$, is negative. We therefore take the largest possible change in the eccentricity over one mirror configuration cycle to be the absolute value of the above Δe_m.

The minimum durations for the circular case of the third level for the known satellites of Jupiter, Saturn, Uranus, Earth and Mars are listed in Tables 5.15 to 5.19 respectively. See Section 5.4(iv) for the tables. The level of accuracy for the minimum lifetime values is comparable with the accuracy achieved at the previous stage of the finite-time stability method.

Before discussing in detail the minimum lifetimes obtained for the circular case by application of the mirror configuration cycle, we first consider the introduction of the sun's orbital eccentricity (ie the elliptical case) to the problem.

(iv) Modification of the mirror configuration cycle method for the case of non-zero solar eccentricity

In this case, a mirror configuration occurs whenever a conjunction or opposition of the three bodies falls along an alignment of the semi-major axes of both the satellite's and the Sun's orbits. In terms of the satellite's and Sun's orbital elements, a mirror configuration occurs when a conjunction is located at $f_{c0} = 0°$ or 180°, and $f_{1c0} = 0°$ or 180°.

As in the circular case we begin, centre and end a mirror configuration cycle with approximate mirror configurations. Since the Sun's apse line is stationary and conjunctions occur far more frequently than alignments of the two apse lines, the above cycle would on average be of length equal to the time taken for the satellite's orbital apse line to rotate through 2π.

During the cycle, alignment of the two apses would occur when the satellite's longitude of pericentre ϖ equals 0° or 180°, since the longitude of pericentre for the Sun is taken to be always 0°. Because the apse line of the satellite's orbit changes so slowly compared to the movement of the bodies themselves, a conjunction of the bodies will occur near every approximate alignment of the apse lines to produce, in each case, a close approximation to a mirror configuration.

In order to compare the elliptic case with the circular case at this third level, we choose to modify the above mirror configuration cycle, making it more similar in definition to the one in the circular case. Instead of insisting that a near mirror configuration occurs only when a conjunction falls near an alignment of the apses, we broaden the definition and state that a near mirror configuration occurs everytime a conjunction occurs near the satellite's apse line, regardless of the position of the sun's apse line. These near mirror configurations are not as good as ones which also include an alignment with both apses, but they still approximate mirror conditions.

Then, to be consistently pessimistic, we assume that the Sun's apse is always situated in the worst location for close mirror configurations to occur in the elliptical case. In other words, the Sun's apse is placed at 90° to the satellite's apse, so that a conjunction of the bodies occurring near the satellite's apse produces the largest deviation of the Sun's velocity vector from perpendicularity to the Sun's radius

vector.

Note that during the above type of mirror configuration cycle, the angle between the two apse lines will change very little, since the synodic period of the apses is so much greater than the length of the mirror configuration cycle of $2T_1$.

With the above modification, the mirror configuration cycle for the elliptical case is, as for the circular case, a cycle centred on a conjunction which occurs nearest to the satellite's pericentre; it extends forward through an approximate revolution of the conjunction line to the next closest conjunction to the satellite's pericentre; and it extends backward through an approximate revolution of the conjunction line to the previous closest conjunction to the satellite's pericentre. The only difference from the mirror configuration cycle of the circular case, is that the Sun's apse is taken to lie at 90° to the satellite's apse and thus ϖ_0 is assumed to be ~90°.

The minimum lifetimes in the third level for the elliptic case are calculated using the same procedure as that used for the circular case, except that Tables 4.4 and Equations (22) are used to calculated $\Delta\sigma_i$ and θ_i respectively. See Section 5.4(i).

The angle θ_i now becomes a maximum for a given set of orbital elements e_1 and ν, when $f_{ci} = 180°$ and $f_{1ci} \approx 0°$. ie

$$\theta_{max} = 2\pi\nu\left(1 + \nu + \nu^2 + 2e_i\nu + 2e_1 + 4e_1\nu + \frac{5}{2}e_1^2\right) \qquad (44)$$

The largest possible change in the eccentricity over one mirror cycle would then occur when the true anomaly of the central conjunction falling nearest the satellite's apse line is

$$f_{c0} = \pi\nu\left(1 + \nu + \nu^2 + 2e_i\nu + 2e_1 + 4e_1\nu + \frac{5}{2}e_1^2\right) \qquad (45)$$

Again, choosing f_{c0} to occur at $\theta_{max}/2$ is overly pessimistic because by the definition of a mirror cycle for the elliptical case, the central conjunction we are interested in studying occurs at $f_{c0} \approx 0°$ and $f_{1c0} \approx 90°$, and not at the pair of angles

$f_{c0} = 180°$ and $f_{1c0} \approx 0°$ required to give the maximum possible angular difference between two consecutive conjunctions.

The relative percentage errors between the analytical and numerical solutions for $\Delta\sigma_m$ are calculated in the same manner as for the circular case at the third level (See Section 5.4(i)). The worst cases are listed in Table 5.14 and are no greater than 11.1%.

A study of the cyclic behavior of the orbital elements over one mirror configuration cycle for the elliptical case produces similar results to that of the circular case. The graphs for the elliptical case that are equivalent to Figures 5.15 to 5.20 for the circular case have similar shapes; however, the scale of the graphs and the locations of the extrema vary about the circular case depending on the value of the Sun's true anomaly f_{1c0} at the initial conjunction.

It has been stated that the worst approximation to a mirror configuration should occur approximately when the two semi-major axes lie perpendicular to each other (ie when $\varpi_0 = 90°$). The exact worst value for ϖ_0 depends on the position of the central conjunction f_{c0}, since the worst approximation to a mirror configuration is one where the velocity vectors of the satellite and the Sun are farthest from being perpendicular to their respective radius vectors.

The relationships between the changes (Δe_m, $\Delta\alpha_m$, $\Delta\epsilon_m$ and ϖ_m) in the orbital elements over one mirror cycle as a function of the mean longitude of the pericentre of the satellite's orbit at the central conjunction are give in Figures 5.22 (a) to (d) respectively. The true anomaly of the satellite at the central conjunction f_{c0} is kept constant at the worst case where $f_{c0} = \theta_{max}/2$ (ie at 0.8259° for the Jupiter-Callisto example), while the true anomaly of the Sun at the central conjunction is allowed to change through the variation of ϖ_0 (ie $f_{1c0} - f_{c0} = \varpi_0$).

The data used in Figures 5.22 is that of a Jupiter-Callisto system where e_0=0.01, $\alpha_0 = 0.0025$, $\mu = 1100$, $e_1 = 0.048$ and the Sun is assumed to move in a fixed elliptical orbit. Figures 5.22 confirm that the largest possible change in the

eccentricity, and indeed also the largest change in the ratio of the semi-major axes over one mirror cycle, occur at essentially $\varpi_0 = 90°$, when the central conjunction approximately aligned with the satellite's apse falls at the farthest possible angular distance from the Sun's apse line.

Again, like the second level of the finite-time stability method, the largest possible change in the satellite's eccentricity over one mirror cycle for the elliptical case is greater than the equivalent change in the satellite's eccentricity for the circular case. But more importantly, even when using a mirror cycle based on a conjunction occurring near the satellite's apse line regardless of the position of the Sun's apse line, the worst possible changes in the eccentricity are still much smaller than the maximum possible changes in the eccentricity measured over one conjunction cycle for both the circular and elliptical cases. Thus minimum durations for the third level can still be extended beyond the minimum lifetimes found in Section 5.3 for the second level of the finite-time stability method.

Figures 5.22 (a) to (d) The variation of the changes in the orbital elements (a) Δe_m, (b) $\Delta \alpha_m$, (c) $\Delta \epsilon_m$ and (d) $\Delta \varpi_m$ over one mirror cycle with different values of the satellite's longitude of the pericentre at the central conjunction ϖ_0, given a true anomaly of the satellite at the central conjunction of $f_{c0} = \theta_{max}/2 = 0.8259°$.

The initial conditions are those of an elliptical coplanar Jupiter-Callisto system with $\alpha_0 = 0.0025$, $e_0 = 0.01$, $\mu = 1100$ and $e_1 = 0.048$.

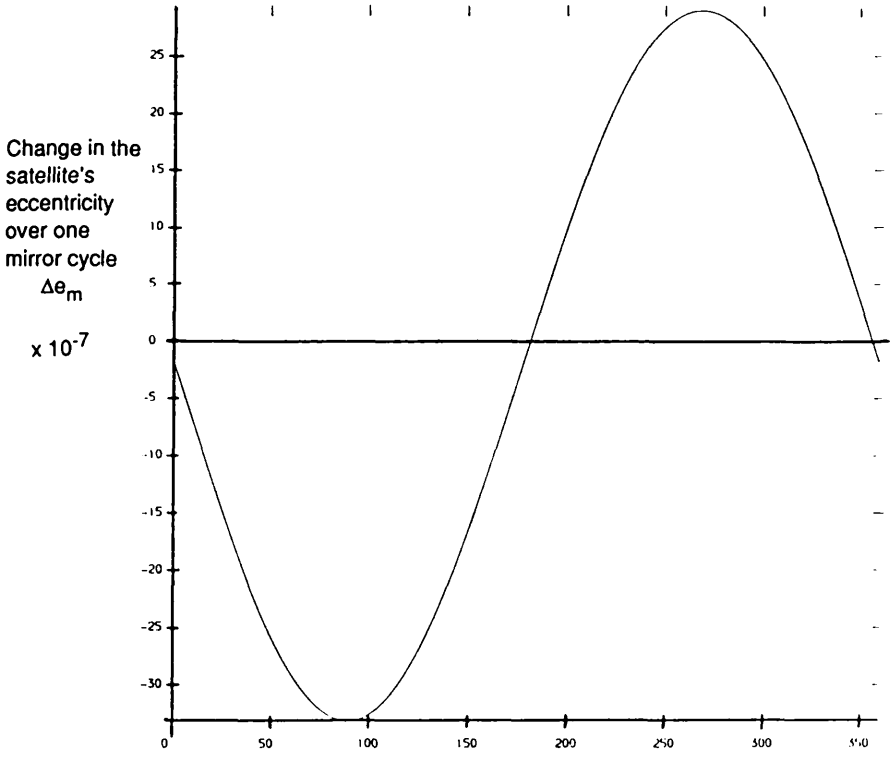
Change in the satellite's eccentricity over one mirror cycle
Δe_m
x 10^{-7}
25
20
15
10
5
0
-5
-10
-15
-20
-25
-30
0
50
100
150
200
250
300
The satellite's longitude of pericentre at the central conjunction ϖ_0
(in degrees)

(a)

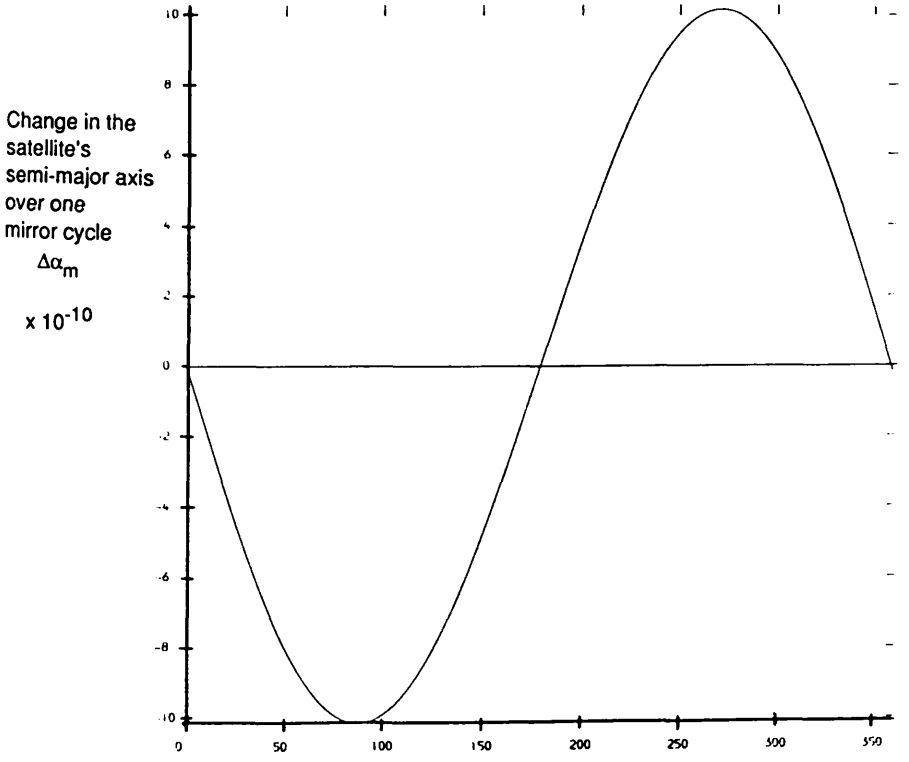
Change in the satellite's semi-major axis over one mirror cycle
$\Delta \alpha_m$
x 10^{-10}
10
8
6
0
-6
-8
-10
0
50
100
150
200
250
300
The satellite's longitude of pericentre at the central conjunction ϖ_0
(in degrees)

(b)

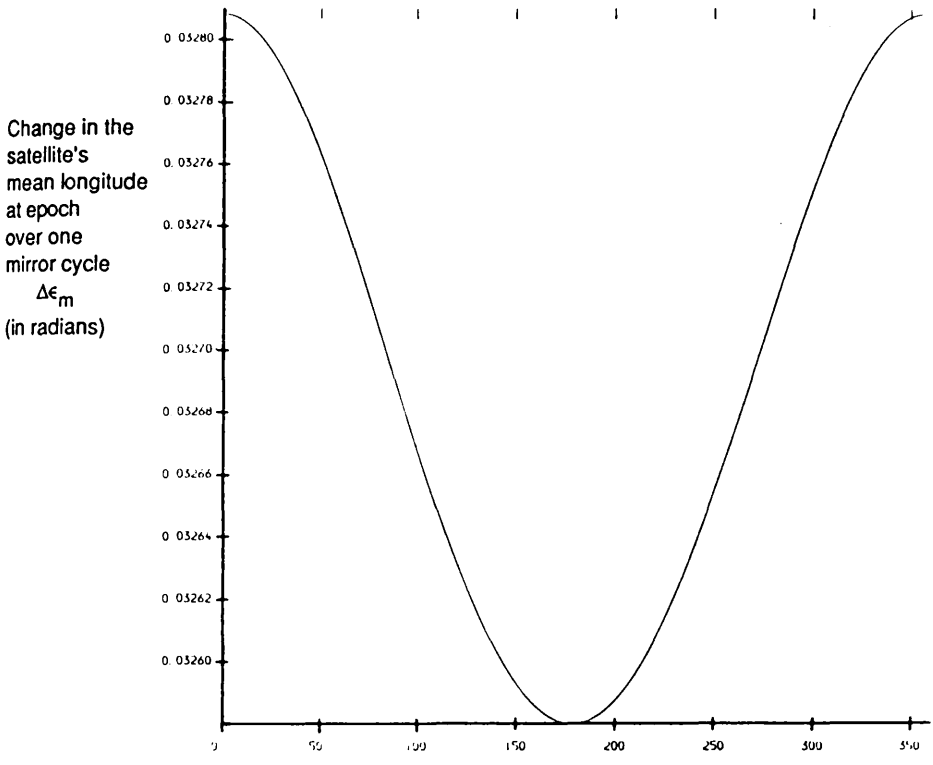
Change in the satellite's mean longitude at epoch over one mirror cycle $\Delta\epsilon_m$ (in radians)
0.03280
0.03278
0.03276
0.03274
0.03272
0.03270
0.03268
0.03266
0.03264
0.03262
0.03260
0
50
100
150
200
250
300
350
The satellite's longitude of pericentre at the central conjunction ϖ_0 (in degrees)

(c)

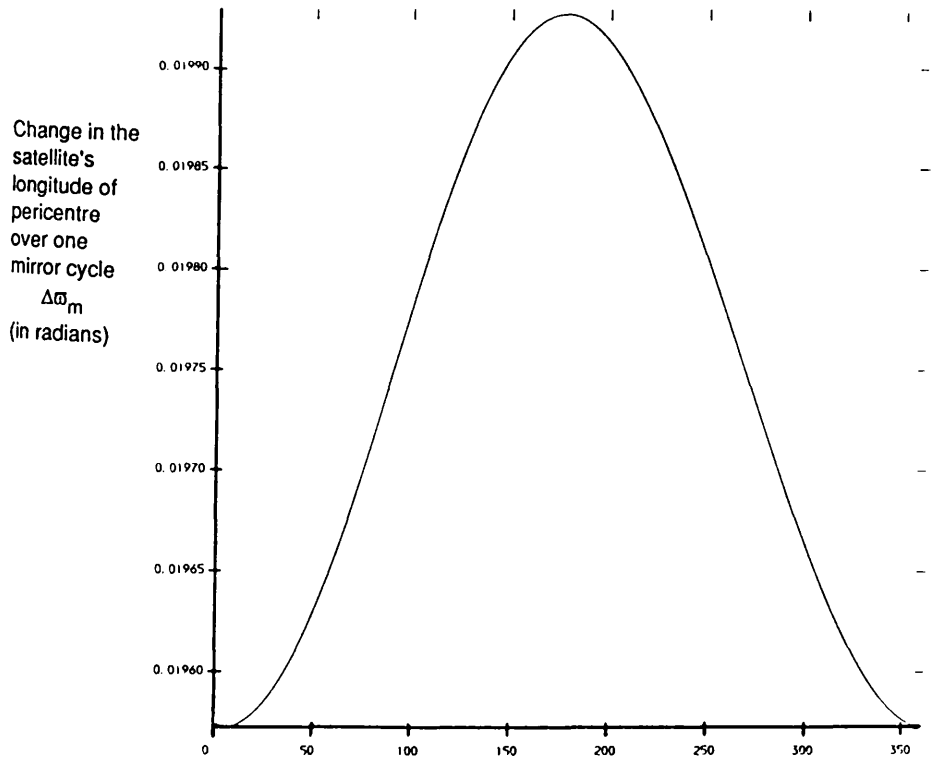
Change in the satellite's longitude of pericentre over one mirror cycle $\Delta\varpi_m$ (in radians)
0.01990
0.01985
0.01980
0.01975
0.01970
0.01965
0.01960
0
50
100
150
200
250
300
350
The satellite's longitude of pericentre at the central conjunction ϖ_0 (in degrees)

(d)

As in the second level of the finite-time stability method, computer time limitations make it only possible to compute minimum lifetimes for individual satellites against solar perturbations. Table 5.8 shows the computing time required to find the minimum lifetime of the Jupiter-Callisto example for the circular and elliptical cases at the third level. While calculations of the second level minimum durations require about fifty times more computing time than calculations of the first level minimum durations, the calculations of the third level minimum durations require only approximately twice the computing time that calculations for the second level require.

The third level minimum lifetimes for the known satellites of Jupiter, Saturn, Uranus and Mars are given in Tables 5.15 to 5.19 respectively. The error in the minimum durations for the elliptical case is generally less than 10%.

Satellite	T^1_{min} (years)		T^2_{min} (years)		T^3_{min} (years)	
	Circular	Elliptical	Circular	Elliptical	Circular	Elliptical
Amalthea	2.2×10^4	1.9×10^4	3×10^8	1×10^8	4×10^{11}	1×10^9
Thebe	1.1×10^4	9.6×10^3	5×10^7	3×10^7	5×10^{10}	7×10^8
Io	5.8×10^3	5.0×10^3	3×10^7	9×10^6	4×10^9	1×10^8
Europa	2.4×10^3	2.1×10^3	4.3×10^6	2.5×10^6	7.5×10^8	3.4×10^7
Ganymede	1.5×10^3	1.3×10^3	1.3×10^6	7.9×10^5	1.2×10^8	9.3×10^6
Callisto	5.2×10^2	4.4×10^2	1.7×10^5	1.2×10^5	7.2×10^6	1.6×10^6
Leda	9.9	8.3	——	——	——	——
Himalia	8.9	7.4	——	——	——	——
Lysithea	1.1×10^1	9.3	——	——	——	——
Elara	6.7	5.6	——	——	——	——

Table 5.15 The first, second and third level minimum lifetimes for the known satellites of Jupiter, if the Sun is assumed to be moving in a fixed circular or elliptical orbit. Jupiter's sidereal period is taken to be 11.86198 years.

Satellite	T^1_{min} (years)		T^2_{min} (years)		T^3_{min} (years)	
	Circular	Elliptical	Circular	Elliptical	Circular	Elliptical
Prometheus	1.1×10^5	9.4×10^4	2×10^9	2×10^9	6×10^{12}	1×10^{10}
Pandora	1.0×10^5	8.7×10^4	2×10^9	2×10^9	5×10^{12}	1×10^{10}
Janus	8.3×10^4	7.0×10^4	9×10^8	8×10^8	2×10^{12}	9×10^9
Epimetheus	7.8×10^4	6.6×10^4	9×10^8	8×10^8	2×10^{12}	9×10^9
Mimas	4.6×10^4	3.9×10^4	5×10^8	4×10^8	7×10^{11}	5×10^9
Enceladus	4.6×10^4	3.9×10^4	5×10^8	2×10^8	7×10^{11}	3×10^9
Dione	2.6×10^4	2.2×10^4	9×10^7	5×10^7	6×10^{10}	8×10^8
1980S6	2.3×10^4	1.9×10^4	8×10^7	4×10^7	5.0×10^{10}	8.2×10^8
Rhea	1.8×10^4	1.5×10^4	3.4×10^7	1.8×10^7	1.4×10^{10}	3.3×10^8
Titan	2.4×10^3	2.0×10^3	1.6×10^6	1.2×10^6	1.8×10^8	2.7×10^7
Hyperion	1.0×10^3	8.5×10^2	4.0×10^5	3.0×10^5	3.3×10^7	9.7×10^6
Iapetus	4.7×10^2	3.9×10^2	1.3×10^5	9.4×10^4	2.5×10^6	7.2×10^5
Phoebe	2.6×10^1	2.1×10^1	———	———	———	———

Table 5.16 The first, second and third level minimum lifetimes for the known satellites of Saturn, if the Sun is assumed to be moving in a fixed circular or elliptical orbit. Saturn's sidereal period is taken to be 29.45709 years.

Satellite	T^1_{min} (years)		T^2_{min} (years)		T^3_{min} (years)	
	Circular	Elliptical	Circular	Elliptical	Circular	Elliptical
1986U8	1.1×10^6	9.9×10^5	1×10^{11}	7×10^{10}	1×10^{14}	9×10^{11}
Miranda	4.1×10^5	3.5×10^5	1×10^{10}	5×10^9	4×10^{13}	9×10^{10}
Ariel	2.2×10^5	1.9×10^5	2×10^9	1×10^9	4×10^{12}	3×10^{10}
Umbriel	1.2×10^5	1.1×10^5	1×10^9	6×10^8	1×10^{12}	1×10^{10}
Titania	6.8×10^4	5.9×10^4	2×10^8	1×10^8	1×10^{11}	3×10^9
Oberon	5.1×10^4	4.4×10^4	1.5×10^8	8.8×10^7	5.6×10^{10}	1.5×10^9

Table 5.17 The first, second and third level minimum lifetimes for the known satellites of Uranus, if the Sun is assumed to be moving in a fixed circular or elliptical orbit. Uranus' sidereal period is taken to be 84.01151 years.

Satellite	T^{1}_{min} (years)		T^{2}_{min} (years)		T^{3}_{min} (years)	
	Circular	Elliptical	Circular	Elliptical	Circular	Elliptical
Moon	9.9×10^{-1}	9.3×10^{-1}	—	—	—	—

Table 5.18 The first, second and third level minimum lifetimes for the known satellites of Earth, if the Sun is assumed to be moving in a fixed circular or elliptical orbit. Earth's sidereal period is taken to be 1.00002 years.

Satellite	T^{1}_{min} (years)		T^{2}_{min} (years)		T^{3}_{min} (years)	
	Circular	Elliptical	Circular	Elliptical	Circular	Elliptical
Phobos	6.1×10^{2}	4.5×10^{2}	1×10^{6}	1×10^{6}	4×10^{8}	2×10^{7}
Deimos	2.6×10^{2}	1.9×10^{2}	1×10^{5}	1×10^{5}	2×10^{7}	2×10^{6}

Table 5.19 The first, second and third level minimum lifetimes for the known satellites of Mars, if the Sun is assumed to be moving in a fixed circular or elliptical orbit. Mars' sidereal period is taken to be 1.88085 years.

(v) A comparison of the minimum durations of various satellite systems for both the circular and elliptical cases

More than two thirds of the satellites tested now have minimum lifetimes of the same order of magnitude or greater than the known lifetime of the solar system. The third level minimum durations for Jupiter 's satellites range from 2×10^{6} to 1×10^{9} years for the elliptical case and 7×10^{6} to 4×10^{11} years in the circular case; for Saturn's satellites from 3×10^{6} to 6×10^{12} years for the circular case and 7×10^{5} to 1×10^{10} years in the elliptical case; for Uranus' satellites from 6×10^{10} to 1×10^{14} years in the circular case and 2×10^{9} to 9×10^{11} years in the elliptical case; and for

Mars' satellites from $2x10^7$ to $4x10^8$ in the circular case and $2x10^6$ to $2x10^7$ years in the elliptical case.

Tables 5.15 to 5.19 show that like the first and second level minimum durations, the third level minimum durations for the elliptical case are less than those found for the circular case. However, unlike the first two levels, the minimum durations found for the elliptical case are not always very close to the values found for the circular case. For the larger lifetimes, the circular case can produce minimum lifetimes as much as two orders of magnitude greater than those of the elliptical case.

This does not mean that the behavior of the orbital elements over one mirror configuration cycle for the elliptical case is not similar to the equivalent behavior for the circular case. The marked difference between the minimum lifetimes for the two cases is simply caused by the necessity of choosing different starting values for f_{c0} in order to obtain the maximum possible change in the eccentricity for each case. For example, in the Jupiter-Callisto system, the worst possible central mirror configuration occurred at a satellite's true anomaly of $f_{c0} = 0.7494°$ for the circular case and at $f_{c0} = 0.8259°$ for the elliptical case.

In fact, it should be emphasized that in all three levels of the finite-time stability method, the cyclic behavior of the elliptical case was found to be merely an expansion about the cyclic behavior of the corresponding circular case.

If we were to centre the mirror cycle on a near mirror configuration which included a near alignment of the apse lines of the satellite and the Sun, the differences between the circular and the elliptical cases for the third level would be considerably reduced. However, this has not been attempted in the present work because the computing time required for such a calculation would be more than an order of magnitude greater than the computing time required for the equivalent calculation in the second level.

It should be noted that although the present investigation of the third level uses only conjunction and pericentre alignments as occasions for reversal of solar perturbations, there are in reality four times as many such occasions since conjunctions or oppositions at both apocentre and pericentre are equally good as mirror configurations.

Aside from the full mirror cycle involving a synodic period of the apses, there seems to be no further natural cycles in the coplanar case, that are not simply multiples of the synodic, conjunction or mirror configuration cycles, to which we could apply further levels of the finite-time stability method.

5.5 Conclusions

In this chapter we have shown that even with the crudest approximations, we can extend the majority of the minimum lifetimes of the satellites in the solar system to beyond the known lifetime of the solar system, and beyond the lifetimes predicted by any previous studies of the coplanar three-body problem incorporating the eccentricity of the Sun's orbit.

For the case where the Sun is assumed to be moving in a fixed circular orbit, we have derived minimum lifetimes for Jupiter's inner satellites which range from $7x10^6$ to $4x10^{11}$ years. For the case where the Sun is assumed to be moving in a fixed elliptical orbit, the range is still impressive at $2x10^6$ to $1x10^9$ years.

Results from the finite-time stability analysis suggest that the satellites of Uranus cannot be detached from Uranus by the Sun within the lifetime of the solar system, even when the eccentricity of Uranus' orbit is taken into consideration. The minimum lifetimes for the satellites of Uranus range from $6x10^{10}$ to $1x10^{14}$ years, when the Sun is assumed to be moving in a fixed circular orbit and from $2x10^9$ to $9x10^{11}$ years, when the Sun is assumed to be moving in a fixed elliptical orbit.

Saturn's satellites are stable against solar perturbations for a range of at least $3x10^6$ to $6x10^{12}$ years in the circular case and a range of at least $7x10^5$ to $1x10^{10}$ years in the elliptical case.

Generally, satellites which have smaller initial ratios of the semi-major axes α_0 or smaller initial eccentricities e_0 will have larger minimum durations.

The most important conclusion is that extension of the finite-time stability method to the case where the Sun is assumed to be moving in a fixed elliptical orbit, produces results that are similar to the results of the circular case, only slightly smaller. In fact, for the first two levels of the finite-time stability method, the minimum durations found for both the circular and elliptical cases are of the same order of magnitude.

The similarity between the circular and elliptical cases is particularly striking when changes in the orbital elements over the appropriate cycle are graphed as a function of the satellite's true anomaly of the initial or central conjunction. For all three levels, the curves describing the circular case are located almost exactly at

the centre of the region bounded by the equivalent curves describing the elliptical case where the Sun's true anomaly of the initial or central conjunction is varied. The elliptical case appears to be merely an extension of the circular case.

The large minimum durations found for the case where the Sun is assumed to be moving in a fixed circular orbit are in agreement with the results of Walker and Roy (1980), which indicate that all the satellites in the solar system are guaranteed hierarchical stability according to the c^2H criterion for all time.

The failure of the c^2H criterion in the general three-body problem to guarantee the stability of any of the satellites found in the solar system when the eccentricity of the Sun's planetocentric orbit is included in the problem (Valsecchi, Carusi and Roy, 1984), suggests that the c^2H criterion is far too stringent a test for most of the real cases of interest in the solar system. A more modest search for a simple finite-time stability criterion can produce estimates closer to our beliefs in the long orbital lifetimes of the satellites of the solar system, as supported by planetological studies of their surface histories.

The real beauty of the finite-time stability method is in its simplicity. Given the crudest approximations, we can still find minimum durations for the solar system satellites which are surprisingly large, regardless of whether the Sun is assumed to be moving in a fixed circular or elliptical orbit. The method uses very little computing time and works for a range of initial conditions. In addition, although we have assumed a coplanar three-body system throughout this thesis, the method can easily be extended to include inclined systems. With plenty of computer time the method can also be used to find regions of α_0-e_0 space which will produce large minimum lifetimes for imaginary satellites orbiting a particular planet.

The application of the finite-time stability method failed to provide useful results in the cases of the Earth's Moon, Jupiter's outer satellites and Saturn's Phoebe. Solar perturbations on these bodies are high. If the finite-time stability method is to be applicable, a starting point other than the simple synodic period must be found. In the following chapters, the Moon's case is considered further and a possible approach is suggested.

CHAPTER 6

THE SAROS CYCLE AND ITS USE IN THE FINITE-TIME STABILITY METHOD FOR THE LUNAR PROBLEM

"If you can keep your head, when all about you are losing theirs, then it may be you just haven't assessed the situation correctly."

6.1 Introduction

In our conclusions to Chaper 5 we suggested that in order to apply our finite-time stability criteria to the question of the stability of the Earth-Moon Sun-perturbed system, we would require a larger base periodic cycle than the synodic cycle. One such possible near periodicity in the lunar problem is a cycle called the Saros, known to the ancient Chaldeans.

In Section 6.2, we describe the Saros cycle and its properties. Through the use of eclipse records, the relative dynamical geometry of the Earth-Moon-Sun system during eclipses is shown to repeat itself very closely over one Saros period. We go on, in Section 6.3, to look at the historical importance of the Saros cycle and other similar quasi-periodic cycles.

We then consider, in Section 6.4, the implications of the fact that although the Saros is a relationship involving mean quantities and therefore "fictitious" bodies, eclipses which are formed by the real Earth-Moon-Sun system, are still repeated. Using the refined lunar ephemeris computed at JPL (Newhall, 1989), which includes all solar system perturbations, we show that the 'real' dynamical configuration of the Earth-Moon-Sun system at any time, and not just at times of eclipses, is very nearly repeated after one Saros period.

In Section 6.5, we discuss a possible mechanism involving mirror configurations, by which solar perturbations acting on the Earth-Moon system can be effectively reversed over one Saros period in order to produce the nearly periodic behavior observed.

Section 6.6 describes how the Saros period can be used in the finite-time stability method to find a minimum lifetime for the Earth-Moon system acting under solar perturbations. Finally, Section 6.7 involves a discussion of the possible relevance of the quasi-periodic behavior of the Earth-Moon-Sun relative orbital dynamics over one Saros cycle to the stability of the Earth-Moon-Sun system.

6.2 The Saros Cycle and Its Properties

The Saros is a period of 6,585.32 days (ie approximately 18 years and 10 or 11 days depending on the number of leap years in the interval). It is the time that elapses between successive repetitions of a particular sequence or "family" of solar and lunar eclipses. 'Saros', in fact, is the Greek word for 'repetition'. At the end of a Saros period, the Earth, the Sun, the Moon, the nodes of the Moon's orbit and the pericentre and apocentre of the Moon's orbit have returned to approximately the same relative positions that they held at the beginning of the Saros period.

This repetition of the relative geometry of the Earth-Moon-Sun system is so close that after one Saros period, a sequence of eclipses will recur with approximately the same order of type of eclipses, the same duration of the eclipses and the same time intervals between the eclipses, as the previous sequence of eclipses. In other words, after one Saros period a large partial lunar eclipse will be followed by a large partial lunar eclipse; a total solar eclipse of short duration will be followed by a total solar eclipse of short duration; an annular solar eclipse will be followed by an annular solar eclipse and so on. Thus, the solar and lunar eclipse pattern which occurred in the previous Saros period can be used to predict the solar and lunar eclipses in the next Saros period.

A solar or lunar eclipse occurs whenever the Earth, the Moon and the Sun lie in approximately a straight line. If the Moon's orbital plane were exactly the same as the ecliptic plane, a solar eclipse would occur at every new moon when the Moon is at conjunction, and a lunar eclipse would occur at every full moon when the Moon is at opposition. See Figure 6.1.

However, since the two planes are inclined at an angle of about 5° to each other, eclipses can only be possible when the Sun is also near a node and is therefore located in approximately the same plane as the Earth-Moon system. Figure 6.2 shows that, if the Moon is near the same node as the Sun, a solar eclipse will occur, while, if the Moon is near the opposite node, a lunar eclipse will occur.

The ecliptic limit, ie the maximum angular distance that the new or full moon can be from the nodes in order for an eclipse to occur, is about 10° to 12° for a partial eclipse and 5° to 6° for a total eclipse.

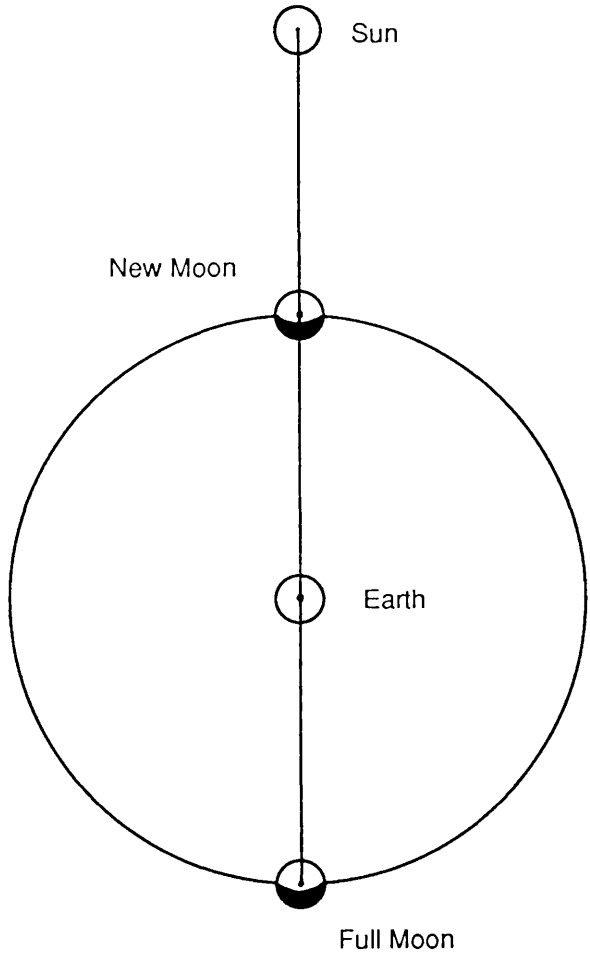

Figure 6.1 If the Earth-Moon-Sun system were coplanar, a solar eclipse would occur at every new moon and a lunar eclipse would occur at every full moon.

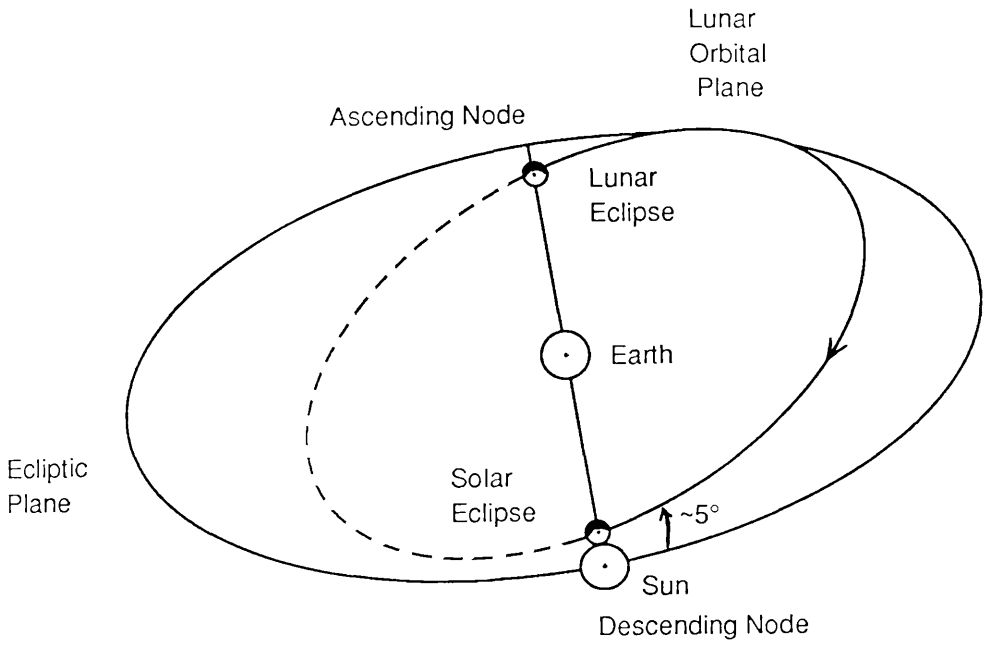

Figure 6.2 Because the lunar orbital plane is inclined about 5° to the ecliptic plane, lunar and solar eclipses will only occur when the Sun is near one of the Moon's orbital nodes.

Consecutive lunar eclipses occur approximately six months apart, when the Sun returns to a position near one of the Moon's nodes. After six synodic months (ie 177.18 days), the Sun and hence the positions of the full or new moon have moved, on average, by about (177.18 days/365.24 days)x360°=174.64° in longitude. However, in this time, because the nodes of the lunar orbit are moving at a rate of $d\Omega/dt$=-0.052954°/day, the nodes have receded by about 177.18days x -0.052954°/day = 9.38°. The opposite node is located at a longitude of 180°-9.38°=170.62°. Therefore, the full moon has moved relative to the node by about 174.64°-170.62°=4.02° (Pannekoek, 1961).

We have seen that an eclipse will occur as long as the Moon is located within approximately ±12° of a node. If the Moon progresses about 4° relative to the node every time it comes back to a position where both it and the Sun are near a node, then approximately 5 or 6 consecutive lunar eclipses separated by about six months are possible before the Moon moves beyond the ecliptic limits. Figure 6.3 portrays a possible series of eclipses. Note that the type of eclipse depends on the angular distance from the Moon to its node.

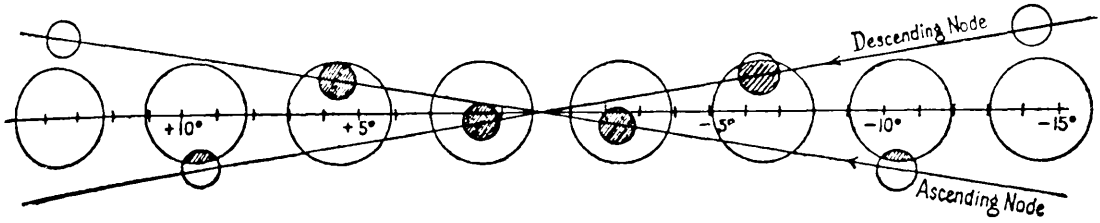

Figure 6.3 Shows a possible series of eclipses. The large circles denote the Earth's shadow, while the small circles describe the Moon's shadow. The scale indicates the angular separation between the Moon's position and the Moon's orbital nodes.

The diagram describes, from right to left, the following eclipses occurring about every 6 months:

Angular separation between the Moon and its nodal line.	Lunar eclipse type
-14.50°	no eclipse
-10.48	partial?
-6.45	partial
-2.43	total
1.59	total
5.62	total?
9.65	partial
13.67	no eclipse

This diagram and data were taken from Pannekoek (1961), pg. 46.

A new series of eclipses then begins when the positions of the Sun, the full moon and the nodes coincide again. This occurs about 47 months after the first series began. The new series, like the old, contains 5 or 6 lunar eclipses each approximately six months apart; however, the characteristics of the new series, namely the eclipse type and duration, are not the same as that of the old series.

The type of the eclipse which occurs not only depends on the angular separation between the Moon and its node, but also on the distance between the Earth and the Moon, and on the position of the Earth observer. Although the Moon is almost four hundred times smaller than the Sun, it is also approximately four hundred times closer to the Earth than the Sun. Thus, having almost the same apparent angular size as the Sun, the Moon can totally obscure the Sun.

If the Moon is far enough away, it appears to be smaller than the Sun. In this case, a ring of light encircles the Moon as the Moon eclipses the Sun. This type of eclipse is called an annular eclipse.

If the Moon is close enough to the Earth, the Moon's apparent diameter is greater than that of the Sun and the umbra or dark cone-shaped inner region of the Moon's shadow just barely reaches the Earth's surface. Any observer on Earth positioned along the path taken by the umbra will experience a total solar eclipse. Any Earth observer located in the outer lighter region or penumbra of the Moon's shadow will see a partial solar eclipse. The extent of the penumbra and umbra shadow regions, and therefore likewise the types of both lunar and solar eclipses observed, depend on the distance between the Moon and the Earth.

The Earth-Moon separation also affects the duration of an eclipse. The length of time that the Moon and the Sun remain in an eclipse configuration is governed by the Moon's velocity, which varies according to its position in its elliptical orbit, and hence varies according to the distance between the Earth and the Moon.

Therefore, because the eclipse characteristics such as duration and type depend on the Earth-Moon distance, the first repetition of an eclipse series where the eclipse characteristics are also repeated, occurs when not only the position of the Sun, the new or full moon and the nodes lie in approximately a straight line again, but also when this event coincides with the Moon and the Sun lying in the same positions relative to their pericentres. This occurs approximately after one Saros period or

about five series of eclipses.

The ease with which people can use records of eclipses that occurred in the previous Saros period to predict future solar and lunar eclipses suggests how closely the geometry of the Earth-Moon-Sun system must be repeated every Saros period. Table 6.1, for example, shows the values of the semi-diameters of the Moon and the Sun during four eclipses, each of which occurred approximately every Saros period in the years 1898, 1916, 1934, 1952, and 1970. The data is taken from the relevant Astronomical Ephemeris.

Even without allowing for the fact that over a span of seventy-two years, methods for calculating the ephemerides have changed (ie orbital constants of the Earth, Moon and Sun have been improved, and more accurate and constant time reference frames have been implemented), the semi-diameters of the Moon and the Sun vary only slightly from eclipse to eclipse over a single Saros period. Because the Saros cycle is not exactly periodic, in other words the relative geometry of the Earth-Moon-Sun system is not repeated exactly over one Saros period, a comparison of the relative geometry over many Saros periods will start to show discrepancies. However, a comparison of even five Saros periods still shows a close agreement between the lunar and the solar semi-diameters at the beginning and the end of the five Saros periods.

This is particularly remarkable, given that the total range within which the semi-diameters of the Sun and the Moon can vary over time is considerably larger than the small differences in their semi-diameters over one Saros period. For example, Table 6.2 compares the sizes of the average absolute differences in semi-diameters for the Sun and the Moon over one Saros period with the total possible range in semi-diameters for the Sun and the Moon. The Sun's semi-diameter can range from 15.75 to 16.30 arcminutes, while the Moon's semi-diameter ranges from 14.70 to 16.73 arcminutes. The lunar differences over one Saros period are about 1% of the total differences possible, while the solar differences are about 3 to 6 % of the total.

The solar semi-diameter and hence the Sun's geocentric distance will not be as closely repeated as the lunar semi-diameter because, after one Saros period, the Sun has not returned to exactly the same position relative to its apse line. Instead of

Eclipse		Years				
		1898	1916	1934	1952	1970
(1)	Date	Jan. 7	Jan. 19	Jan. 30	Feb.10-11	Feb. 21
	Moon	14.8667'	14.830'	14.808'	14.788'	14.780'
	Sun	16.2645'	16.255'	16.235'	16.207'	16.172'
(2)	Date	Jan.21	Feb.3	Feb.13-14	Feb. 25	Mar. 7
	Moon	16.4050	16.423	16.455	16.487	16.527
	Sun	16.2472	16.225	16.193	16.157	16.113
(3)	date	Jul. 3	Jul.14	Jul.26	Aug. 5	Aug. 17
	Moon	16.7220	16.715	16.718	16.720	16.732
	Sun	15.7310	15.735	15.748	15.770	15.798
(4)	Date	Jul. 18	Jul.29	Aug. 10	Aug. 20	Aug. 31-Sept. 1
	Moon	14.7645	14.733	14.720	14.708	14.710
	Sun	15.7393	15.755	15.780	15.810	15.847

Table 6.1 The semi-diameters (in arc-minutes) of the Sun and the Moon during eclipses which occurred approximately every Saros period of 18 years and 10 or 11 days.

The above information, taken from the appropriate Nautical Almanac and Astronomical Ephemeris is tabulated for the following four different eclipses:

(1) a partial lunar eclipse (Feb. 21, 1970)

(2) a total solar eclipse (Mar. 7, 1970)

(3) a partial lunar eclipse (Aug. 17, 1970)

(4) an annular solar eclipse (Aug. 31 - Sept. 1, 1970).

This table is taken from A. E. Roy (1988).

Eclipse		Average absolute differences in semi-diameter over		% differences in semi-diameter relative to total possible differences for	
		1 Saros	5 Saros'	1 Saros	5 Saros'
(1)	Moon	0.022'	0.087'	1.08 %	4.29 %
	Sun	0.023	0.093	4.18	16.91
(2)	Moon	0.031	0.122	1.53	6.01
	Sun	0.034	0.134	6.18	24.36
(3)	Moon	0.006	0.010	0.30	0.49
	Sun	0.017	0.067	3.09	12.18
(4)	Moon	0.015	0.055	0.74	2.71
	Sun	0.027	0.108	4.91	19.64

Table 6.2 A comparison of the differences in the lunar and the solar semi-diameters over 1 and 5 Saros periods with the total differences that are possible in the lunar and solar semi-diameters. The Sun's semi-diameter can range from 15.75 to 16.30 arcminutes, while the Moon's semi-diameter ranges from 14.70 to 16.73 arcminutes. The data found in Table 6.1 is used here.

revolving through 18 complete cycles of its orbit, the Sun has gone through 18.03 cycles. Of course, the apse line of the Sun has also moved in those 18 years and 10 or 11 days. However since these changes in the Sun's orbital geometry are small over one Saros period, the Sun's semi-diameters are still very closely repeated.

A repetition of the configuration and characteristics of an eclipse must include a repetition of the relative velocity vectors, as well as the relative radius vectors of the Moon and the Sun. In other words, the complete relative dyamical geometry of the Earth-Moon-Sun system must be repeated. If we now look at the full set of relative position and velocity coordinates for the Earth-Moon-Sun system at a particular eclipse epoch and compare these quantities with the same eclipse event one Saros

period later, we find that, in general, all of them are closely repeated.

Eclipse Date	Positional coordinates			
	$\lambda_s - \lambda_m$	$\beta_s - \beta_m$	σ_m	σ_s
Feb. 10-11, 1952	179.915°	-0.8473°	14.788'	16.207'
Feb. 21, 1970	179.912	-0.8615	14.780	16.172

Eclipse Date	Velocity coordinates			
	$\dot{\lambda}_s - \dot{\lambda}_m$	$\dot{\beta}_s - \dot{\beta}_m$	$\dot{\sigma}_m$	$\dot{\sigma}_s$
Feb. 10-11, 1952	-10.944 °/day	65.348 '/day	3.84 "/day	-0.18 "/day
Feb. 21, 1970	-10.915	65.305	3.49	-0.22

Table 6.3 A comparison of the relative position and velocity coordinates for the Moon and the Sun during a partial lunar eclipse which occurred on Feb. 11, 1952 and then recurred one Saros period later on Feb. 21, 1970. This table is taken from A. E. Roy (1988).

In Table 6.3 we see that the semi-diameters of the Sun σ_s and the Moon σ_m, the differences between the Sun and the Moon's geocentric ecliptic longitudes (λ_s-λ_m) and latitudes (β_s-β_m), and the daily rates of change of these coordinates $\dot{\sigma}_s$, $\dot{\sigma}_m$, ($\dot{\lambda}_s$-$\dot{\lambda}_m$), ($\dot{\beta}_s$-$\dot{\beta}_m$), all return to much the same values after one Saros period. The data in Table 6.3 describe a partial eclipse of the Moon which occurred on February 10-11, 1952 and recurred one Saros period later on February 21, 1970. The suffixes m and s denote a parameter of the Moon and Sun respectively, while the dot refers to a derivative with respect to time. The data are taken from the appropriate Astronomical Ephemeris, and are interpolated using a simple algorithm involving Taylor expansions to obtain the rates of change of the coordinates.

The near repetition of eclipses is a consequence of the set of high-integer near

commensurabilities which exist between the Moon's synodic period, its anomalistic period and its nodical period. The lunar synodic period is the time taken for the Earth-Moon-Sun system to move from one conjunction to the next, ie for the Moon to pass from full moon to full moon. The lunar anomalistic period is the time taken for the Moon to move through one complete cycle of its orbit relative to its line of apse. Finally, the lunar draconic or nodical period is the time taken for the Moon to move through one complete cycle of its orbit relative to its line of nodes.

The mean values of these periods are listed in the 1988 Nautical Almanac as:

Synodic period	T_S = 29.530 589 days
Anomalistic period	T_A = 27.554 550 days
Nodical period	T_N = 27.212 221 days

Although the actual values of these different lunar months can vary quite extensively from one revolution of the Moon to another because of solar perturbations on the Moon's orbit, these mean values remain constant to within one second over many centuries.

The commensurable set of integers which makes up the Saros period is then:

$$223\ T_S = 6585.3213 \text{ days}$$

$$239\ T_A = 6585.5375 \text{ days}$$

$$242\ T_N = 6585.3575 \text{ days}$$

Recall that in order for an eclipse to occur, the Earth, the Sun and the Moon must lie in approximately a straight line. This configuration can only occur when the Moon is at conjunction or opposition, and the Moon and the Sun are located near the Moon's orbital nodes. At this point, a series of 5 or 6 lunar eclipses will occur about every six months before the required configuration is disrupted once again. A conjunction of the Moon and Sun occurs every lunar synodic period, while the Moon passes its ascending node every lunar nodical month. Therefore, conditions for the

occurrence of an eclipse series must result whenever an integer multiple of the synodic month is approximately equal to an integer multiple of the nodical month. The lowest integer multiple set which meets these requirements is:

$$47\ T_S = 1387.937\ 683 \text{ days}$$

$$51\ T_N = 1387.823\ 271 \text{ days}$$

Hence, we have the reason why a new eclipse series was observed to begin approximately every 47 lunar months.

To obtain a repetition of the characteristics of the eclipse series as well, we need to ensure that both the Earth-Moon and the Earth-Sun distances are repeated. A repetition of the Earth-Moon distance occurs once every lunar anomalistic month. A repetition of eclipse series characteristics would therefore occur over a period which equalled integer multiples of the synodic, nodical and the anomalistic months. The first set of integers to meet these requirements approximately, is the set which makes up the Saros period.

Normally, a repetition of the characteristics of an eclipse series would also require a commensurability with the Sun's anomalistic period. This does not occur within the Saros cycle. However, because the Saros period is only ~10 days longer than 18 solar years and because the Sun's orbit is almost circular with an eccentricity of 0.017, the Sun's geocentric radius vector is still repeated approximately over one Saros period, despite its lack of a commensurability with the solar anomalistic period. After one Saros period, the Sun's geocentric radius vector is only about (10days/365days)x360° ≈ 10° from its former positon. Using familiar elementary properties of elliptical orbital motion (see Roy (1983)), a displacement of 10° in the true anomaly changes the Sun's radius vector, velocity vector and the angle between them by at most 0.3%. A commensurability with the Sun's anomalistic period does not therefore seem to be so crucial for a repetition of the relative geometry of the Earth-Moon-Sun system.

The near commensurabilities between T_S, T_A, and T_N, suffice to ensure that the mean relative geometry of the Earth-Moon-Sun system at the beginning of a Saros

cycle is almost exactly repeated at the end of a Saros cycle. The whole system is simply rotated about 10° from its previous position.

Let us now look at what was known about the Saros cycle in the past and the uses that were made of the Saros and other cycles like it.

6.3 The Historical Importance of the Saros Cycle and Other Similar Cycles

The Saros cycle was probably first discovered by the Babylonians from their records of eclipses extending back over many centuries. A. Pannekoek (1961) gives an excellent, well documented history of the development of Babylonian astronomy in his book A History of Astronomy. A summary of his history follows.

The Babylonians lived on the plains between the Euphrates and the Tigris rivers from some time before 3000 B.C. The whole of Mesopotamia was first united around 2500 B.C. Babylon became the capital and grew into a great commercial and cultural centre circa 2000 B.C. under the reign of Hammurabi.

The Babylonians began making regular observations of the Moon in order to be able to predict when the different seasons were approaching and therefore to know when to start planting and harvesting crops. This led to a belief that the heavenly bodies were related to the Gods and Goddesses, and that the movements of these bodies held great significance to changes in the lives of people on Earth.

The Assyrians, a military people living on the northern part of the Tigris river, rose to become the most powerful state in near-Asia around 800 B.C, and eventually destroyed Babylon in 689 B.C. When the Assyrians conquered the Babylonians, they adopted much of their culture and it became very important for the Assyrians to know what was happening in the sky in order to interpret its meaning and relate it to the success of any large-scale military enterprise or the well-being of the country.

Eclipses were, in particular, very important omens. The exact month, day, time of day, and place in the sky for every eclipse observed was recorded. A different interpretation of the eclipse was made, depending on the exact time it occurred. Thus, for example, we find recorded such predictions as:

> "An eclipse in the morning-watch means disease . . . The morning-watch is Elam, the 14th day is Elam, Simannu is Amurru, the second side is Akkad . . . When an eclipse happens in the morning-watch and it completes the watch, a north wind blowing, the sick in Akkad will recover. When an eclipse begins on the first side and stands on the second side, there will be slaughter of Elam; Guti

> will not approach Akkad . . . When an eclipse happens and stands on the second side, the gods will have mercy on the land. When the Moon is dark in Simannu, after a year Ramanu [the storm-god] will inundate. When the Moon is eclipsed in Simannu, there will be flood and the produce of the waters of the land will be abundant . . ."

taken from Pannekoek (1961), but originally published in R. C. Thompson's (1900) The Reports of the Magicians and Astrologers of Nineveh and Babylon, page 271.

From these accurate observations of eclipses, the Babylonian-Assyrians were able to identify regular patterns. Their reports then began to show that they expected eclipses to occur, by announcing the consequences of such events before they occurred. For example, Thompson (1900, pages 273 - 274) records the following prophecies made by court astrologers:

> "On the 14th an eclipse will take place; it is evil for Elam and Amurru, lucky for the king, my lord; let the king, my lord, rest happy. It will be seen without Venus. To the king, my lord, I say: there will be an eclipse. From Irasshi-ilu, the king's servant."

> "To the king of countries, my lord thy servant Bil-usur. May Bel, Nebo, and Shamash be gracious to the king, my lord. An eclipse has happened but it was not visible in the capital. As that eclipse approached, at the capital where the king dwells, behold, the clouds were everywhere, and whether the eclipse took place or did not take place we don't know. Let the lord of kings send to Ashur, to all cities, to Babylon, Nippur, Uruk and Borsippa; whatever has been seen in those cities the king will hear for certain ... The great gods who dwell in the city of the king, my lord, overcast the sky and did not permit to see the eclipse. So let the king know that this eclipse is not directed against the king, my lord, nor his land. Let the king rejoice ..."

They were probably using, at this point in time, the simple regularity that once an eclipse series began, there would be 5 or 6 lunar eclipses each separated by approximately six months. Thus, when a new series of eclipses began 1 or 2 years later, they could predict eclipses again.

The Assyrian empire weakened by wars against barbarian tribes from Europe, eventually crumbled under the combined attack of the Babylonians and the Medes. In 606 B.C., Ninevah, the Assyrian capital, was ruined and Babylon became the capital once again. The new Babylonian empire was extended by Nebuchadnezar

(604-561B.C.) to include all of near-Asia. During this time, the Babylonian priesthood held great power arising from their ability to predict the fortunes of people and countries by reading the signs laid out in the sky. In 539 B.C., the Persians conquered Babylon and eventually Babylon was reduced to the status of other Persian capitals.

The Persian kings had no use for omens of good luck or evil from foreign gods; however, the priests maintained their power by changing their role from that of court astrologer to that of the elite group of people who knew the ways of the gods by knowing their movements in the heavens. In order to prove this knowledge, their observations of the sky became more accurate and detailed. It was probably during this interval that they discovered the Saros period.

The famous 'Saros-Canon' tablet studied by J. N. Strassmaier and J. Epping is a fragment of a list of eclipse months which extend from 373 to 277 B.C. Because each column consists of 38 lines spanning 223 months, and each eclipse series is clearly demarcated by horizontal lines and a total eclipse month is located in the centre of each series, it is believed that this list of eclipse months was used as a means of predicting future eclipse months by applying the repetitive properties of the Saros cycle. Certainly, the Babylonians knew of and used the Saros period in later centuries because Babylonian 'Auxillary Tables' have been discovered where it is obvious that eclipse times have been calculated from data taken 18 years earlier.

The Greeks also studied the heavens, but their main purpose for observing the sky was to help with the navigation of their ships and to enable accurate calendar time-keeping. Thales of Miletus (624-547 B.C.) was accorded by Herodotus with having predicted a solar eclipse. However, Herodotus only states that Thales foretold that an eclipse would occur within the year. Because of the vagueness of Thales' prediction, Pannekoek (1961, page **99**) feels Thales was probably unaware of the use of the Saros cycle as a means of predicting eclipses.

Another Greek, Meton (c.433 B.C.) discovered the 19 year cycle within which an integer multiple of lunar months approximately equals an integer multiple of solar tropical years. A tropical year is the time interval between two successive passages of the Sun through the vernal equinox, in other words, the solar nodical period. Since the seasons recur every tropical year, the tropical year is the ideal average length for

the calendar year.

Given that the mean solar tropical year is T_γ = 365.24220 days, the metonic cycle consists of:

$$235\ T_S = 6939.69 \text{ days}$$

$$19\ T_\gamma = 6939.60 \text{ days}$$

and allows time-keeping by the lunar month to be incorporated into a solar calendar which keeps a measure of the changing seasons. In other words, for twelve calendar years out of the nineteen, the year would consist of twelve lunar months, while for seven calendar years a thirteenth month would be intercalculated to make up for the fact that twelve lunar months are only 354.37 days and not the 365.24 days of the solar year. The Babylonians also knew of this cycle and it is not known whether Meton discovered it independently or borrowed it from them.

Hipparchus made careful observations of eclipses between 146 and 135 B.C. and compared these results with earlier Babylonian eclipse records, not to predict future eclipses, but in order to get more accurate values of the mean synodic and nodical lunar months. According to Delambre (1817, page 144), Hipparchus not only used the Saros cycle, but he also used a 345 year cycle of:

$$4267\ T_S = 126\ 007.02 \text{ days}$$

$$4573\ T_A = 126\ 006.96 \text{ days}$$

$$4612\ T_{si} = 126\ 007.51 \text{ days}$$

$$345\ T_\gamma = 126\ 008.56 \text{ days}$$

where T_{si} = 27.321 662 days is the mean lunar sidereal period. In addition, Hipparchus used a cycle of about 441 years and 103 days

$$5458\ T_S = 161\ 177.95 \text{ days}$$

$$5923\ T_N = 161\ 177.99 \text{ days;}$$

and a cycle of 20 years and approximately 107 days given by:

$$251\ T_S = 7412.1778 \text{ days}$$

$$269\ T_A = 7412.1740 \text{ days.}$$

In recent history, various commentators on the Saros cycle have taken it to refer principally to the commensurability existing between the lunar synodic period and the lunar nodical period because a good commensurability between these two values is the minimum requirement for eclipse prediction. Consequently, they have often ignored that the Saros cycle also contains a commensurability with the lunar anomalistic period and have searched, instead, for more accurate metonic-like cycles (ie cycles produced by commensurabilities between only two periods) which consist of integer multiples of the synodic period approximately equalling integer mutliples of the nodical period.

The use of one such period of 29 years minus 20 days where,

$$358\ T_S = 10\ 571.951 \text{ days}$$

$$388.5\ T_N = 10\ 571.948 \text{ days}$$

$$\text{but}\quad 383.673\ T_A = 10\ 571.95 \text{ days}$$

was advocated by John Stockwell (1901). He felt that the 29 year cycle was a vast improvement on the Saros cycle traditionally used for eclipse prediction because it was more accurate, and therefore slower to change from cycle to cycle. It was also longer than the Saros cycle and therefore contained a larger series of eclipses for prediction. At the same time, it was not too long that use of it for eclipse predictions became cumbersome.

A.C.D. Crommelin (1901) and S. Newcomb (1882) point out that cycles like

Stockwell's cycle, while they may have very close commensurabilities between the synodic and nodical periods, and therefore can be used to predict with great accuracy when eclipses will occur, are of no use for predicting the type of successive eclipses or the location of these eclipses. Without the added commensurability with the anomalistic period which the Saros cycle contains, the characteristics of an eclipse cannot be repeated every cycle because the Moon's true anomaly has not returned to its original value at the beginning of the cycle. In addition, the Saros cycle brings the Sun's position back to within 10° of its former true anomaly. This means that, unlike the other cycles so far described, the Saros cycle enables the circumstances of an eclipse at its beginning to be almost totally duplicated at its end or in other words, the relative geometry of the Earth-Moon-Sun system to be almost exactly repeated.

Crommelin(1901) mentions a few other cycles of interest which do maintain some of the important characteristics of the Saros cycle. He describes the triple Saros of 54 years and 33 days

$$3 \times (223)\, T_S = 19\ 755.964 \text{ days}$$

$$3 \times (239)\, T_A = 19\ 756.612 \text{ days}$$

$$3 \times (242)\, T_N = 19\ 756.072 \text{ days}$$

which was known to the Greeks as the 'Exelignos' cycle. It has the advantage of having a period almost equal to a whole number of days. This means that after one 'Exelignos' cycle, the Earth has revolved back to its original position and that therefore the eclipse track on the Earth will also be found in almost the same position. This is helpful for predicting the locations on Earth where the solar eclipses can be seen. However after one Exelignos cycle, the Sun has moved about 30° from its former position and the Sun's geocentric distance is not quite repeated.

He also looks at a cycle of about 1805 years minus 6 days first discovered by M. Oppert, which Crommelin calls the Megalosaros

22 325 T_S = 659 270.40 days

23 926 T_A = 659 270.16 days

24 227 T_N = 659 270.48 days

The Megalosaros is just slightly greater than 100 times the Saros cycle. The commensurabilities over one Megalosaros cycle are closer to being exact than the commensurabilites for the Saros cycle are over the same time span. However, the relative geometry of the Earth-Moon-Sun system is still repeated more accurately over one Saros period than over one Megalosaros period.

Finally, Crommelin mentions a 521 year cycle which is 18 Stockwell cycles:

$$18\times(358)\ T_S = 6444\ T_S = 190\ 295.12 \text{ days}$$

$$18\times(388.5)\ T_N = 6993\ T_N = 190\ 295.06 \text{ days}$$

$$6906\ T_A = 190\ 291.72 \text{ days}$$

$$521\ T_\gamma = 190\ 291.19 \text{ days}$$

Again it is not as accurate as the Saros cycle.

All of these cycles show close commensurablities between T_S, T_N, and T_A, but because their large sizes make them a bit unmanageable for eclipse prediction and because they are less accurate, the use of the Saros cycle has remained the most popular method of predicting eclipses.

We are not, however, primarily concerned with the uses made of such metonic-type or saros-type cycles for calendar and eclipse predictions. Our interest instead lies with the property that some of these cycles have, of almost repeating exactly the relative geometry of the Earth-Moon-Sun system, and the implications that this property has for the stability of the Earth-Moon system perturbed by the Sun.

Crommelin (1901) states that it is well-known that the Saros cycle "reproduces the distances, diameters and rates of motion of Sun and Moon with very considerable accuracy". Yet no one seems to have considered that the existence of the

Saros cycle for at least 2,300 years, ie more than 130 Saros cycles, implies that the Earth-Moon system perturbed by the Sun is moving in a nearly periodic orbit of one Saros period. We study this nearly periodic behavior more closely in Section 6.4.

6.4 The Near Periodicity of the Earth-Moon-Sun Dynamical System

Until now, we have been discussing only the mean motions of the Moon and the Sun through the use of the mean periods T_S, T_N, and T_A. This implies that we have only been studying a fictitious dynamical system. Yet, despite the fact that the Saros cycle is a relationship involving these mean motions, the closeness with which eclipses can be predicted in the real Earth-Moon-Sun system suggests that not only is the mean relative geometry repeated over one Saros period, but so is the real relative geometry.

This result is surprising, given that the eccentricities of the solar and lunar orbits may cause the Sun and the Moon to be up to ±2° or ±5° respectively from their mean positions. Their relative positions can, as a result, vary by as much as 7° from their mean relative positions at any time. Newcomb (1882) mentions that such a large variation could change the eclipse time by half a day, and the distance of the Sun and the Moon from the nodes by about 2°. The combination of the above two effects could cause a recurring eclipse to be almost a day late or early. The character of the eclipse could change from a total to a partial eclipse, or a partial eclipse to one that fails to occur at all, or the reverse. Because none of these possible scenarios actually occur, the real relative geometry of the Earth-Moon-Sun system, as well as the mean relative geometry, must be nearly repeated every Saros period.

More importantly, this repetition of the relative geometry over one Saros period does not just occur at eclipse times, but at any time. After all, there is nothing special about the geometry of an eclipse except that its occurrence is visible from the Earth. If the relative geometry of an eclipse is nearly repeated every Saros period, then so must the relative geometry of the Earth-Moon-Sun system in general also be repeated.

In order to test this hypothesis the following procedure was adopted. An epoch t_1 was chosen randomly, but avoiding the time of a solar or lunar eclipse. Then, using the JPL high-precision numerically integrated planetary and lunar ephemerides (Newhall, 1989), the relative position and velocity coordinates of the Moon and the Sun are found at this epoch t_1. Similar to Table 6.3, we find: the geocentric distances

of the Moon r_m: the differences between the Sun and the Moon's geocentric ecliptic longitudes ($\lambda_s - \lambda_m$) and latitudes ($\beta_s - \beta_m$); and the daily rates of change of these coordinates $\dot{r}_m$, ($\dot{\lambda}_s - \dot{\lambda}_m$), ($\dot{\beta}_s - \dot{\beta}_m$). The subscripts s and m denote parameters of the Sun and the Moon respectively.

Note that we do not consider the Sun's geocentric distance r_s and rate of change $\dot{r}_s$, as these parameters would introduce a long-term libration with a period of the order 18 years x 360°/10° ≈ 650 years. See Section 6.2 for a description of the closeness with which the Sun repeats its relative dynamical geometry over one Saros period.

The JPL Ephemeris is used here because it is a completely computerized database which allows easy access to the data. It also incorporates interpolation packages which allow the position and the velocity coordinates of the Moon and the Sun to be found very easily at any time within the time range covered by the specific JPL Ephemeris. Unlike the Nautical Ephemeris, it is also consistent, using the same time reference and constants throughout.

We take the value of the Saros period to be approximately $\overline{T}_{saros}$ = 6585.3 days and search through the ephemeris within the interval ($t_1 + \overline{T}_{saros} \pm 0.5$ days) for the time t_2 at which the differences between the relative position and velocity coordinates of the two epochs t_1 and t_2 are minimized. If the relative dynamical geometry of the Earth-Moon-Sun system is repeated after one Saros period, the results should show that a minimum of the differences in the coordinates at epochs t_1 and t_2, occurs at a time approximately equal to the Saros period and that these differences are very small.

In order to minimize the differences between the six coordinates simultaneously, we choose a goodness of fit expression Q, which consists of:

$$Q = \sqrt{\sum_{i=1}^{6} \left(\frac{x_{2i} - x_{1i}}{\Delta x_{max\, i}} \right)^2}$$

where x_{1i} and x_{2i} are the values for one of the relative coordinates at epochs t_1 and t_2 respectively. i=1 to 6 represent the six relative coordinates r_m, $(\lambda_s-\lambda_m)$, $(\beta_s-\beta_m)$, $\dot{r}_m$, $(\dot{\lambda}_s-\dot{\lambda}_m)$, $(\dot{\beta}_s-\dot{\beta}_m)$ specifying the relative dynamical geometry of the Earth-Moon-Sun system at any given time.

We find the relative discrepancy between the coordinates of epoch t_1 and t_2 (ie we divide each difference by the maximum possible difference between any two values for each coordinate) instead of the absolute discrepancy, in order to remove the problem of giving more weight in the summation to the larger valued coordinates. Thus, $\Delta x_{max\ i}$ is the maximum possible difference between any two values of a particular relative coordinate.

For example, the maximum possible difference between two values of r_m is the radial distance at apocentre minus the radial distance at pericentre, ie $\Delta r_{max} = 2ae$.

The maximum difference between any two angles which range from 0 to 2π is π. Therefore, $\Delta(\lambda_s - \lambda_m)_{max} = \pi$.

The latitude of the Sun β_s relative to the size of the latitude of the Moon β_m is essentially zero. Therefore, we can assume that $\beta_s - \beta_m \approx - \beta_m$. The largest value of the Moon's latitude is equal to the inclination i of the Moon's orbit relative to the equatorial plane. The maximum difference between any two values of $\beta_s - \beta_m$ is therefore $\Delta(\beta_s - \beta_m)_{max} = 2i$.

The two-body problem gives

$$\dot{r} = \frac{he\sin f}{a(1-e^2)} \qquad \text{where} \quad h = na^2 (1 - e^2)^{1/2}$$

sin f varies from -1 to +1. Therefore, the maximum difference between any two values of $\dot{r}_m$ is

$$\dot{\lambda}_{s} - \dot{\lambda}_{m} = \frac{2\pi ae}{\sqrt{1-e^2}}$$

The maximum possible differences between the rates of change of the Sun's and Moon's longitudes $\Delta\dot{\lambda}_s - \dot{\lambda}_m\ _{max}$ and latitudes $\Delta\dot{\beta}_s - \dot{\beta}_m\ _{max}$ are slightly more complicated to derive. In both parameters we assume that the rates of change of the Sun's latitude and longitude are small compared to the equivalent values of the Moon, and may, can therefore be neglected.

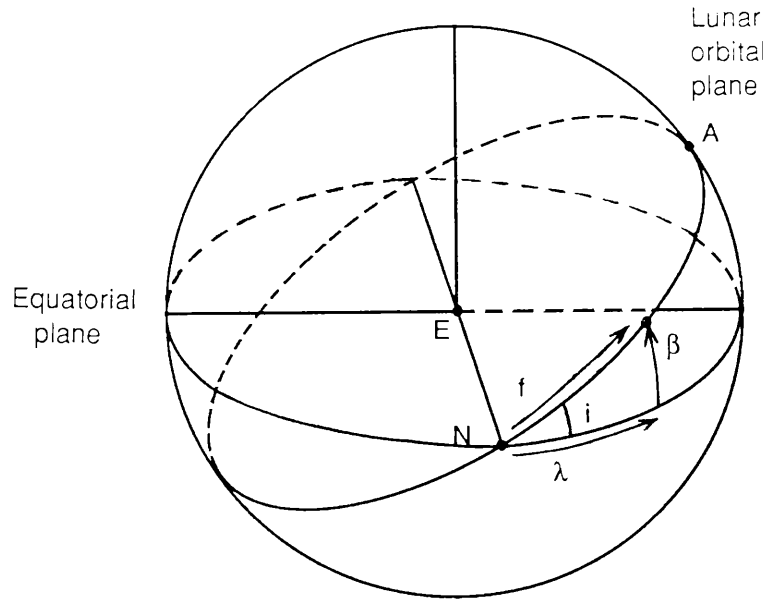

Figure 6.4 A description of the parameters which can be used to find the minimum and maximum values of the six positional and velocity coordinates that define the Moon's orbit.

f describes the Moon's true anomaly. i is the Moon's orbital inclination with respect to the equatorial plane. β depicts the Moon's latitude and λ denotes the Moon's longitude.

Figure 6.4 shows the Moon's orbit inclined at angle i with respect to the equatorial plane. The Moon's true anomaly f, latitude β, longitude λ and orbital inclination i are all described in the figure. 'A' marks the lunar orbit's point of largest latitude, while 'N' marks its ascending node where the latitude is zero.

The rate of change of the Moon's longitude $\dot{\lambda}_m$ is a maximum at 'A', where the vector $\dot{f}$ is acting parallel to the equatorial plane. $\dot{\lambda}_m$ is a minimum at 'N', where the vector $\dot{f}$ has its largest component acting in the direction of the latitude vector β.

Using simple spherical trigonometry, the value of $\dot{\lambda}_m$ at point 'A' is given by

$$\dot{f} = \dot{\lambda}_m \cos i \qquad \text{or} \quad \dot{\lambda}_m = \frac{h}{r^2 \cos i} \tag{1}$$

Equation (1) will be at its maximum when r is equal to its smallest value, ie when 'A' is the pericentre of the Moon's orbit. This gives a maximum possible value of $\dot{\lambda}_m$ of

$$\dot{\lambda}_{m\,max} = \frac{h}{a^2 (1 - e)^2 \cos i}$$

$\dot{\lambda}_m$ at point N is found using simple trigonometric relations to be

$$\dot{\lambda}_m = \dot{f} \cos i = \frac{h}{r^2} \cos i \tag{2}$$

Equation (2) will be at its minimum when r is equal to its largest value, ie when 'N' is the apocentre of the Moon's orbit. Hence

$$\dot{\lambda}_{m\,min} = \frac{h}{a^2 (1 + e)^2} \cos i$$

The maximum difference between any two values of $(\dot{\lambda}_s - \dot{\lambda}_m)$ is therefore

$$\Delta(\dot{\lambda}_s - \dot{\lambda}_m)_{max} \approx \Delta\dot{\lambda}_{m\,max} = n\sqrt{1-e^2}\left[\frac{1}{(1-e)^2\cos i} - \frac{\cos i}{(1+e)^2}\right]$$

The maximum and minimum rates of change in the Moon's latitude occur at the lunar nodes, where the minimum value of $\dot{\beta}_m$ is equal to the negative of the maximum value of $\dot{\beta}_m$. At point 'N'

$$\dot{\beta}_m = \dot{f}\sin i = \frac{h}{r^2}\sin i \qquad (3)$$

The largest value for Equation (3) occurs when the Moon is at pericentre, ie

$$\dot{\beta}_{m\,max} = \frac{n\sqrt{1-e^2}}{(1-e)^2}\sin i$$

The maximum difference between any two values of $(\dot{\beta}_s - \dot{\beta}_m)$ is therefore

$$\Delta(\dot{\beta}_s - \dot{\beta}_m)_{max} \approx \Delta\dot{\beta}_{m\,max} = \frac{2n\sqrt{1+e}}{(1-e)^{3/2}}\sin i$$

Having derived values for $\Delta x_{max\ i}$, we then search through the ephemeris for the time t_2 near $t_1 + \overline{T}_{saros}$, which minimizes Q. $T_{saros} = t_2 - t_1$ is then equal to the real value of the Saros period for that particular epoch t_1. This procedure was repeated for values t_1 which span approximately two Saros periods from t_1 = 1952, February 11.02729 to t_1 = 1990, May 6.96329.

In total, 106 values of t_1 were tested. The results are so similar to each other that we give only a sample set of six in Table 6.4. From it, we can see that regardless of the time chosen, the relative positions and velocities of the Moon and the Sun are repeated approximately one Saros period later. The expression Q can also give an indication of the average percentage relative discrepancy between the values of a

Saros period (days)	Beginning t_1 End t_2	r_m (km)	$\dot{r}_m$ (km/day)	$\lambda_s - \lambda_m$ (deg)	$\dot{\lambda}_s - \dot{\lambda}_m$ (deg/day)	$\beta_s - \beta_m$ (deg)	$\dot{\beta}_s - \dot{\beta}_m$ (deg/day)	Q	% Discrepancy
6585.32696	1952.02110272900	403 657.9	-1749.7	179.925	-10.942	-0.848	1.091	0.01486	0.19
	1970.02213542489	404 162.9	-1591.9	179.924	-10.916	-0.864	1.087		
6585.327508	1958.10208910900	392 136.2	4829.7	254.564	-11.633	-4.980	0.401	0.02336	0.29
	1976.10312185982	391 372.4	4877.1	254.561	-11.677	-4.990	0.397		
6585.279115	1964.07156314900	390 917.8	5398.4	279.984	-11.755	-5.163	0.227	0.03177	0.40
	1982.07269106050	389 942.7	5522.6	279.978	-11.817	-5.184	0.210		
6585.365007	1974.02048654900	359 560.4	-2023.8	209.769	-13.991	1.620	1.281	0.00402	0.05
	1992.02162304967	359 473.7	-2206.4	209.769	-14.001	1.611	1.282		
6585.362895	1979.10316058900	364 882.5	-1481.2	229.510	-13.543	1.011	1.272	0.00866	0.11
	1997.11109687853	364 603.2	-1727.4	229.510	-13.559	0.992	1.276		
6585.323579	1988.06077164900	370 856.4	1595.6	84.094	-13.086	-0.380	-1.234	0.01361	0.17
	2006.06190400691	370 542.8	1308.2	84.093	-13.112	-0.305	-1.237		

Table 6.4 Examples of the "osculating" Saros periods or the time intervals which minimize Q.

The times t_1 and t_2 are given in the form of the year (the first four digits), the month (the next two digits), the day (the next two digits) and the fraction of the day beginning at midnight (the remaining digits). The Q given is the value which minimizes the differences between coordinates.

single coordinate at epochs t_1 and t_2 by dividing Q by the total number of coordinates in the sum. Some of these percentage discrepancies are tabulated in the final column of Table 6.4 and show that on average, the relative coordinates of the Earth-Moon-Sun system are repeated approximately one Saros period later, to within at least 0.5%.

Figure 6.5 plots the values of the osculating Saros period found for each choice of the starting epoch t_1 against t_1. The three horizontal lines indicate the three different values of the Saros period found by multiplying each lunar month: synodic, anomalistic or nodical, by the corresponding integer multiple which forms the Saros cycle.

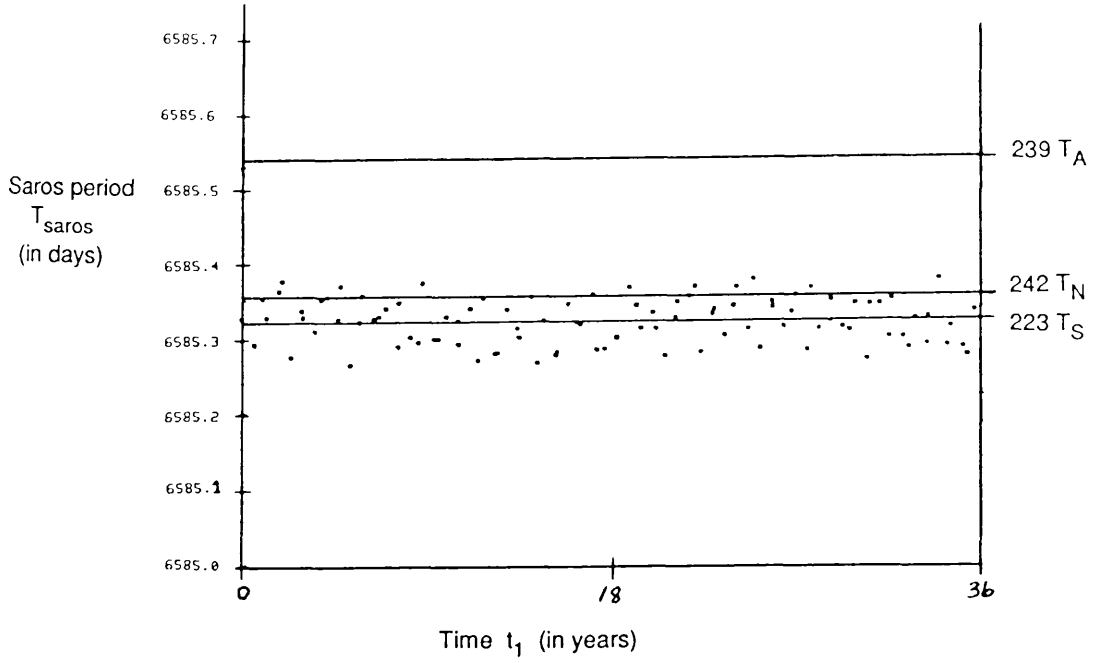

Figure 6.5 The Saros periods found through the numerical minimization of Q plotted as a function of the starting date t_1 of each Saros cycle.

The time interval spans two Saros periods. Zero time refers to the date 1952, February 11.02729 and the horizontal lines mark the Saros periods computed using the specified mean lunar period.

Figure 6.5 shows clearly that no significant difference is found in the value of the osculating Saros period, regardless of when the Saros cycle is started. The average osculating Saros period from the total range of t_1 values tested is 6585.320 days with a standard deviation of 0.03 days.

Traditionally the Saros period is taken to be $223T_S$ = 6585.321 days, which involves only the synodic period. By adopting the idea of a goodness of fit expression Q to find the Saros period numerically, we have changed its definition from that commonly accepted, to one which involves all the relative positional and velocity coordinates of the Earth-Moon-Sun system. However, the average Saros period found in this manner is still remarkably close to the traditional result. This suggests that the synodic period plays the dominant role in driving the system towards the repetition of any particular configuration.

It should also be noted that this confirmation of the value for the Saros period to this accuracy is obtained using only the criterion that the relative geometry of the Earth-Moon-Sun system is repeated after one Saros period. The Saros period is therefore evident in the JPL Ephemeris despite the fact that the JPL Ephemeris, in its calculations of the positions of the Earth, Moon and the Sun at any time, incorporates not only the effects of the gravitational interaction between the three bodies, but also the effects of the figures of the Earth and the Moon, the effects of the tides raised on the Earth by the Moon, and the effects of the point mass gravitational interactions of the other planets and the five largest asteroids. This underlines the fact that at any given time, these other perturbations on the Moon's orbit are very small compared to the gravitational perturbations of the Sun.

Generally, we can conclude that the relative dynamical geometry of the Earth-Moon-Sun system over one Saros period is repeated at any "osculating" phase of the period, and not just in the mean geometry reference frame or simply at the occurrence of certain particular events. In other words the perturbations of the Sun on the Earth-Moon system, particularly the large disturbances in the Moon's semi-major axis, eccentricity and inclination, are almost completely cancelled out by each other over any Saros period started at any time. This suggests that the Saros period could have relevance to any question of the stability of the Earth-Moon system

against solar perturbations. We shall expand further on the utilization of the Saros cycle as a stabilizing mechanism in Section 6.7.

In the following section we discuss a possible mechanism, involving mirror configurations, for producing the Saros quasi-periodicity in the Earth-Moon-Sun system.

6.5 Mirror Configurations in the Saros Cycle

How is it that the solar perturbations acting on the Earth-Moon system are nearly cancelled over one Saros period to such an extent that no matter when the Saros begins, the dynamical geometry of the system is very nearly repeated at its end?

Recall that, if at a certain epoch a system of n point masses affected by their mutual gravitational interaction is aligned in such a way that all the bodies' radius vectors relative to the system's centre of mass are perpendicular to every mutual velocity vector, the behavior of the system after that epoch is a mirror image of its behavior before that epoch (Roy and Ovenden, 1955). There exist only two "mirror configurations", one where the bodies are collinear with their velocity vectors perpendicular to the line and one where the bodies are coplanar with their velocity vectors lying perpendicular to that plane. Most importantly, recall that if the system passes through two exact mirror configurations, it is periodic (Roy and Ovenden, 1955).

However, even near mirror configurations can be used to make a system periodic for a finite length of time. As long as the intervals between successive near mirror configurations remain small, the perturbations in the orbital elements do not have time to accumulate before a second mirror configuration is attained and the reversal of perturbative effects begins. The system will then lie close to a nearly periodic orbit of a period approximately equal to the time between consecutive near mirror configurations of the same type. The duration of such a nearly periodic system is a function of the discrepancy between the bodies' actual configuration and a perfect mirror configuration.

The Saros cycle has been known to exist for at least 2,300 years. Also, the calculations of Section 6.4 show that the repetition of the relative geometry of the Earth-Moon-Sun system after one Saros period is very accurate no matter when the beginning of the Saros period is chosen. It would seem therefore, that the Earth-Moon-Sun must pass through a minimum of two near mirror configurations every Saros period.

This can be easily proven in the case of a hypothetical perfect Saros cycle where the Sun's geocentric orbit is assumed to be essentially circular. Let the Saros

period be T_{saros} = 6585.3 days and the Saros cycle be perfect with:

$$223\ T_S = 239\ T_A = 242\ T_N = T_{saros}$$

If we now take the Earth, Moon and Sun to be collinear, the Moon to be located at its pericentre, and the Moon's line of nodes to be collinear with the line formed by the Earth, Moon and Sun, then at that epoch the mutual velocities of the three bodies are perpendicular to their radius vectors and a perfect mirror configuration exists.

Suppose the Earth-Moon-Sun system is also in conjunction and that the Sun is located in the direction of the descending node ☊. See Figure 6.6 (a). Then one half Saros period later, when $T_{saros}/2 = 115.5\ T_S = 119.5\ T_A = 121\ T_N$ months have elapsed, the Earth, Moon and Sun are once again collinear but in opposition. The Moon is now at its apocentre and the Sun is located in the direction of the ascending node Ω. See Figure 6.6 (b). Hence, a second mirror configuration is formed which will reverse the solar perturbations built up in the first half of the Saros period to return the system to its original mirror configuration, by the end of the Saros period.

The Saros cycle is, however, not perfect and the Sun's geocentric orbit is not circular. If we now study the observed mean motions of the Moon, the Sun, the Moon's pericentre and the Moon's ascending node, we can still show that even in the actual Earth-Moon-Sun mean dynamical system, any mean near mirror configuration of the Earth, Moon, and Sun is followed one half Saros period later by a second near mirror configuration.

The observed mean longitudes of the Moon λ_m, the Moon's pericentre ϖ, the Moon's ascending node Ω and the Sun λ_s are given by the following formulae taken from The Explanatory Supplement to the Astronomical Ephemeris (1961, pp 98 and 107)

$$\lambda_m = 270.434\ 164 + 13.176\ 396\ 5268\ d \quad \text{degrees}$$

$$\varpi = 334.329\ 556 + 0.111\ 404\ 0803\ d \quad \text{degrees}$$

$$\Omega = 259.183\ 275 - 0.052\ 953\ 9222\ d \quad \text{degrees}$$

$$\lambda_s = 279.696\ 678 + 0.985\ 647\ 3354\ d \quad \text{degrees}$$

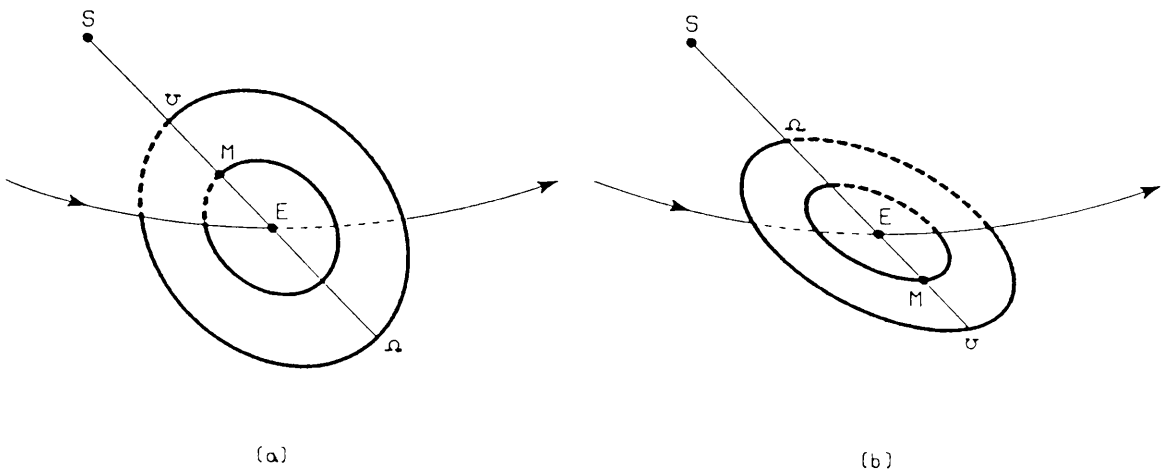

Figure 6.6 The two mirror configurations that the Earth-Moon-Sun system will pass through in one Saros period, if the present Saros cycle is taken to be perfect with

$T_{saros} = 6585.3$ days $= 223T_S = 239T_A = 242T_N$

and the Sun is assumed to be moving in a circular geocentric orbit.

Ω = the direction of the lunar ascending node

$\mathfrak{V}$ = the direction of the lunar descending node

Figure (a) shows a possible first mirror configuration, while Figure (b) shows the next mirror configuration occurring one-half Saros period later.

d is the number of Julian days that have elapsed from the epoch 241 5020.0 JD or 1900 January 0.5 ephemeris time. Higher order terms of d are neglected since they are very small for times of the order of one Saros period.

The Moon's mean position with respect to the Sun, with respect to the lunar pericentre and with respect to the lunar ascending node are therefore given by Equations (4) to (6) respectively.

$$\Delta\lambda = \lambda_m - \lambda_s = 350.737\ 486 + 12.190\ 749\ 1914\ d \quad \text{degrees} \qquad (4)$$

$$\Delta\varpi = \lambda_m - \varpi = 296.104\ 608 + 13.064\ 992\ 4465\ d \quad \text{degrees} \qquad (5)$$

$$\Delta\Omega = \lambda_m - \Omega = 11.250\ 889 + 13.229\ 350\ 4490\ d \quad \text{degrees} \qquad (6)$$

Let us study the values of $\Delta\lambda$, $\Delta\varpi$ and $\Delta\Omega$ at a time d and at a time $d+t_1$ later, where t_1 is 6585.3/2 days = 3292.65 days or 1/2 Saros period. If we take the differences between the values of $\Delta\lambda$, $\Delta\varpi$ and $\Delta\Omega$ at these two times, we obtain:

$$\Delta\lambda(d + t_1) - \Delta\lambda(d) = 40\ 140.479^\circ = 180.479^\circ$$

$$\Delta\varpi\ (d + t_1) - \Delta\varpi(d) = 179.101^\circ$$

$$\Delta\Omega\ (d + t_1) - \Delta\Omega(d) = 0.282^\circ$$

Thus the results show that if the Earth-Moon-Sun's mean dynamical system is at, or near, a mirror configuration at time d, a similar configuration will occur at time $d+t_1$, one half Saros period later.

We now show that the first near mirror configuration must occur within an interval of time equal to one half Saros period. Let us first assume that in the Earth-Moon-Sun system the eccentricity of the Moon's orbit is more important than the lunar inclination in the formation of mirror configurations and that, as a first approximation, we can therefore neglect the Moon's inclination and study the occurrence of mirror configurations in the simpler coplanar case. Using the

elementary properties of elliptical orbits discussed in Roy (1983), we can show that this assumption is not unreasonable for the Earth-Moon-Sun system.

In an elliptic orbit, the angle γ between the radius vector **r** and the velocity vector **v** (See Figure 6.7) is given by Roy(1983) to be

$$\sin\gamma = \frac{1 + e\cos f}{\sqrt{1 + e^2 + 2e\cos f}}$$

$$\cos\gamma = \frac{-e\sin f}{\sqrt{1 + e^2 + 2e\cos f}}$$

where e and f are the eccentricity and the true anomaly respectively, of the body in its orbit. The deviation of the angle γ from 90° is then q, where $\gamma = 90° + q$ and

$$\sin q = \frac{e\sin f}{\sqrt{1 + e^2 + 2e\cos f}} \tag{7a}$$

$$\cos q = \frac{1 + e\cos f}{\sqrt{1 + e^2 + 2e\cos f}} \tag{7b}$$

Note that as f tends to zero or π, q tends to zero and that for small e

$$\sin q \approx e\sin f$$

q is maximized when $f \approx \pi/2$ or $3\pi/2$ or

$$\sin q_{max} \cong \frac{e}{\sqrt{1 + e^2}}$$

$$\cos q_{max} \cong \frac{1}{\sqrt{1 + e^2}}$$

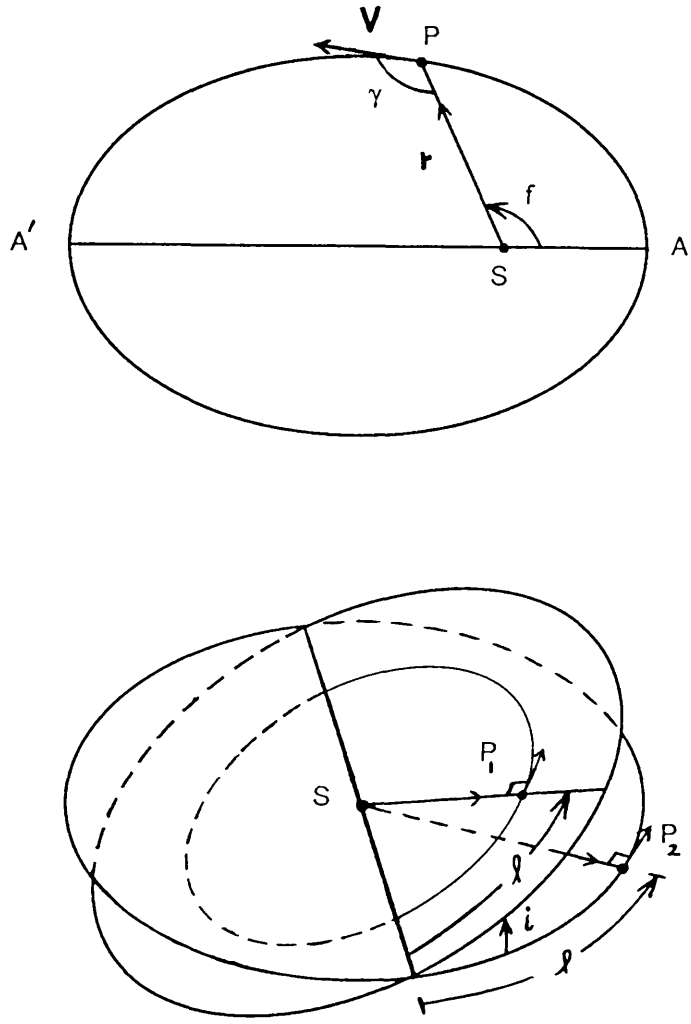

Figure 6.7 Depicts the possible deviations from a perfect mirror configuration:

(a) in the eccentric coplanar case, where q is the deviation of γ from 90°

(b) in the circular inclined case, where p is the deviation from 90° of the angle between P_1's radius vector and P_2's velocity vector when P_1 and P_2 are each located at an angle ℓ along their respective orbital planes from their mutual line of nodes.

In the Earth-Moon-Sun eccentric coplanar system, the largest possible deviation q_{max} from a mirror configuration is approximately equal to 3.15° and is caused by the eccentricity of the Moon's orbit (ie e = 0.055). For a value of f as small as 1.0°, q ≈ 3.1 arcminutes.

Let us now examine a circular inclined system where two bodies orbit a third in circular orbits with a mutual inclination i. Roy (1983) shows that the deviation p from 90° of the angle between the velocity vector of one body and the radius vector of the other is given by

$$\sin p = \frac{1}{2}(1 - \cos i) \sin 2\ell \qquad (8)$$

when they are each located at an angle ℓ measured along their respective orbital planes from their mutual line of nodes. See Figure 6.7(b).

For a given inclination, p is maximized when $\ell = \pi/4, 3\pi/4, 5\pi/4$, or $7\pi/4$ with

$$\sin p_{max} = \frac{1}{2}(1 - \cos i)$$

Therefore, using the Moon's mean orbital inclination value of 5.15°, p_{max} becomes 0.1156° or 6.94 arcminutes, a value which is almost thirty times smaller than the maximum deviation q_{max} possible in the eccentric coplanar case. For a value of ℓ as small as 1.0°, p ≈ 0.24 arcminutes.

Thus, it is clear that the Moon's orbital eccentricity is more effective at producing deviations from perfect mirror configurations at conjunctions and oppositions than the Moon's orbital inclination. We therefore assume, to a first approximation, that the Earth-Moon-Sun system is coplanar.

Approximately every six months or every seven synodic periods, a pair of alignments, one opposition and one conjunction, occur consecutively so as to straddle the Moon's orbital major axis. The opposition or conjunction nearer to the axis is the more effective one at reversing perturbations, and would be completely effective if it

occurred exactly on the axis (neglecting the inclination). The worst possible approximation to a mirror configuration would therefore be one where both the conjunction and the opposition in the straddling pair occur equidistant from the apse. We now show that the time interval between this 'worst' case and one where an opposition or conjunction occurs very close to the major axis, is less than one half Saros period.

The mean angle ϕ between a consecutive opposition and conjunction of the Sun and the Moon has a value given by

$$\phi = n_1 \frac{T_S}{2}$$

At first, it might be thought that the consecutive mean opposition and conjunction straddling the Moon's major axis can at most both be

$$\frac{\phi}{2} = n_1 \frac{T_S}{4}$$

from the apse; however, this is not the case. Because the Moon's line of apses is also moving at a mean rate of $\dot{\varpi} = 0.11140360$ °/day, in one half synodic period the following conjunction would occur closer to the apse than the preceeding opposition by an angle $\dot{\varpi}\, T_S/4 = 0.82245°$. Hence, the 'worst' possible case will be one where the opposition occurs at an angle

$$-\phi_A = -(n_1 - \dot{\varpi}) \frac{T_S}{4} = -6.454233°$$

behind the apse, while the following conjunction occurs at an angle ϕ_A ahead of the moving apse line. n_1 is taken from the 1988 Astronomical Almanac to be 0.98564736°/day.

Every seven synodic periods thereafter, the opposition-conjunction pair straddling the apse line moves at a constant rate in such a way that the opposition

occurs nearer and nearer to the apse line while the conjunction departs further and further from it. This movement continues until the conjunction which occurs previous to the opposition is now occurring closer to the apse line than the original conjunction. This new conjunction and the old opposition become the new pair which straddle the apse. The same slippage process continues with the new pair. The pair slip at a rate of $\theta_s = 7T_S\,(n_1 - \dot{\varpi}) - \pi = 0.7185°$ per seven synodic months. See Table 6.5 for an illustration of this process.

Note that the appearance of multiples of π in the slippage formula is a consequence of the fact that the relevant end of the major axis, from which longitude differences between the opposition-conjunction pair and the apse line are measured, is the one lying between the opposition-conjunction pair.

Note also that the equation giving the slippage rate is quantized in the sense that the formula is only relevant to the opposition-conjunction pair straddling the apse, in other words only valid every seven synodic periods.

The time interval necessary for the opposition in the 'worst' case to reach the apse line is of the order of

$$\frac{\phi_A}{\theta_s}\,7T_S = 5.084 \text{ years}$$

which is less than one half Saros period. After ~5 years, the opposition will, at best, be exactly aligned with the apse or, at worst, the opposition on one side of the moving apse and the succeeding one on the other side of the moving apse will be equidistant from it at an angle of $\theta_s/2 = 0.35922°$. Even in the 'worst' case, the final near mirror configuration deviates from a perfect mirror by a q value of only 1.185 arcminutes. Thus, not only will a near mirror configuration occur within any half Saros interval, but it will also be a very good one.

By the arguments given at the beginning of this section, once the first good near mirror occurs, a second near mirror configuration will follow one half Saros period later. The occurrence of two good near mirror configurations in any Saros period implies that the Earth-Moon-Sun dynamical system is moving in a nearly periodic orbit of period equal to one Saros period.

Epoch	Longitude of the Sun at		Longitude of the apse	Difference in longitude between the conj./oppos. line and the apse line
	Conjunction	Opposition		
0	——	$-\frac{1}{4}n_1 T_S$	$-\frac{1}{4}\dot{\varpi} T_S$	$-\frac{1}{4}(n_1 - \dot{\varpi}) T_S$
$\frac{T_S}{2}$	$\frac{1}{4}n_1 T_S$	——	$\frac{1}{4}\dot{\varpi} T_S$	$\frac{1}{4}(n_1 - \dot{\varpi}) T_S$
$7T_S$	——	$\frac{27}{4}n_1 T_S$	$\frac{27}{4}\dot{\varpi} T_S$	$\frac{27}{4}(n_1 - \dot{\varpi}) T_S - \pi$
$\frac{15}{2}T_S$	$\frac{29}{4}n_1 T_S$	——	$\frac{29}{4}\dot{\varpi} T_S$	$\frac{29}{4}(n_1 - \dot{\varpi}) T_S - \pi$
$14T_S$	——	$\frac{55}{4}n_1 T_S$	$\frac{55}{4}\dot{\varpi} T_S$	$\frac{55}{4}(n_1 - \dot{\varpi}) T_S - 2\pi$
$\frac{29}{2}T_S$	$\frac{57}{4}n_1 T_S$	——	$\frac{57}{4}\dot{\varpi} T_S$	$\frac{57}{4}(n_1 - \dot{\varpi}) T_S - 2\pi$
∴ 'Slippage' per seven synodic periods: $\theta_s = 7T_S (n_1 - \dot{\varpi}) - \pi$				

(a)

Epoch	Longitude of the Sun at		Longitude of the apse	Difference in longitude between the conj./oppos. line and the apse line
	Conjunction	Opposition		
0	——	−7.277°	− 0.822°	− 6.455°
$\frac{T_S}{2}$	7.277°	——	0.822°	6.455°
$7T_S$	——	196.471°	22.206°	− 5.735°
$\frac{15}{2}T_S$	211.024°	——	23.851°	7.173°
$14T_S$	——	400.218°	45.235°	−5.017°
$\frac{29}{2}T_S$	414.771°	——	46.880°	7.891°
∴ 'Slippage' per seven synodic periods: $\theta_s = 0.71843°$				

(b)

Table 6.5 Calculation of the quantized rate at which the opposition-conjunction pair straddling the apse moves with respect to the apse. Part (a) shows the theoretical analysis, while part (b) gives the equivalent numerical values for the formulae found in part (a).

It is interesting to note that the time derived for the coplanar system to move from the worst approximation to the best approximation of a mirror configuration is in fact one quarter of the Hipparchus cycle of $251T_S$ = 20.29 years. If 5.084 years is the time needed to change from the worst approximation to the best approximation of a mirror configuration, then 10.168 years must be the time interval between consecutive best mirror conditions for the coplanar case. If a near mirror configuration is formed by a conjunction occurring at the apse, then the next good mirror will be formed when an opposition occurs at the apse. Therefore, the complete cycle from opposition at the apse to the next opposition at the apse lasts 20.33 years or approximately 251 T_S.

The Hipparchus cycle is also evident in Table 7.2, which lists all the integer mulitples of T_S that equal integer multiples of T_A to within a 1.7% error and whose integer multiples are less than 1000. From the table, we can see that a near mirror configuration of the same alignment occurs every 14 synodic periods for about the first 4 such intervals and then is not repeated again for 139 synodic periods. During this gap, the Earth-Moon-Sun system is farthest removed from a perfect mirror configuration. The time interval between the two best consecutive mirror configurations (ie where the minimum residual ε_{12} is the smallest), is then obviously the Hipparchus cycle of $251T_S$.

Hipparchus' cycle is so good at repeating nearly perfect mirror configurations, that if a conjunction or opposition occurs on the apse line, then after one Hipparchus cycle of 251 synodic periods, the conjunction or opposition occurs only 0.0463° or 2.779 arcminutes from the apse. This angle is equivalent to a deviation angle q of only 9.17 arcseconds. However, this seemingly very good cycle fails to take into account the fact that the Moon's orbital inclination is not zero and so it excels only in the coplanar case.

In actual fact, the angle between the apse and the conjunction-opposition alignment grows slowly enough that, if a very good near mirror configuration occurs in the coplanar case at an angle $\ell = \pi/4, 3\pi/4, 5\pi/4$, or $7\pi/4$, which all produce the largest deviations p in the inclined case, then the system will still evolve into a better

near mirror configuration in the inclined case before the near mirror configuration in the coplanar case deteriorates. Hence, a good near mirror configuration in three dimensions can always be found within one half Saros period.

For example, consider the worst possible case with the line of nodes located at an angle $\ell = \pi/4$ from an alignment of the apse and conjunction-opposition pair. Then the total deviation from a perfect mirror in the inclined case is ~6.94 arcminutes. Seven synodic periods later, the conjunction-opposition pair straddling the aspe has drifted only by the slippage angle $\theta_s = 0.7185°$. At the same time, the line of nodes has now moved to an angle $\ell = (\dot{\varpi} - \dot{\Omega})\ 7T_S + \pi/4 = 78.9748°$ with respect to the apse line. Equation (8) now gives p = 2.61 arcminutes, while Equation (7), with f taken to be the slippage angle, gives q = 2.37 arcminutes only. Such small deviations describe a good near mirror configuration.

The Moon's inclination i can only be neglected in the previous calculations because its value is small. Indeed it is known (Lidov, 1963) that if the Moon's orbital plane were rotated to an inclination i of 90° while all the other lunar elements were kept the same, solar perturbations would increase the Moon's orbital eccentricity to such an extent that a collision of the Moon with the Earth would occur within ten years!

6.6 Use of the Saros Cycle in the Finite-Time Stability Method

Having shown that the Earth-Moon-Sun dynamical system is at present moving in a nearly periodic orbit of period equal to one Saros period, it becomes obvious that the Saros cycle is the natural averaging period of time by which solar perturbations can be most effectively removed in any search into the long term evolution of the lunar orbit. Likewise the Saros period is also the logical base period to use, instead of the synodic period, in the application of the finite-time stability method to the lunar problem.

In this thesis we do not attempt to solve the lunar problem using the above procedure, but the following scenario may be a possible approach to the problem. The analytical series developed in this thesis for evaluating the changes in the orbital elements of the satellite over one synodic period were found to be just barely applicable to the lunar problem with its large mass ratio and ratio of the semi-major axes. In fact, the truncation errors in these series were probably the main cause of the failure of the finite-time stability method to produce a minimum lifetime for the Moon beyond one year. In the lunar problem, a similar analytical expansion evaluating the changes in the orbital elements over the longer period of the Saros, would be even more inaccurate. It would therefore probably be a more reasonable approach to attempt to modify one of the existing analytical lunar theories, one which is already proven to accurately model the behavior of the Moon's orbit under solar perturbations for short time intervals.

If one of these theories such as Delaunay's or the Hill-Brown lunar theory, could be rewritten in order to provide the changes in the lunar orbital elements over one Saros period or 223 synodic periods, the same procedure applied at each level of the finite-time stability method could also be applied to the lunar problem over one Saros period. In other words, the maximum change in the eccentricity over one Saros period could be crudely assumed to be added on to the satellite's eccentricity every Saros period. The minimum lifetime of the Moon's orbit would then be the time required for the eccentricity to increase from its present value to an arbitrarily chosen upper limit like $e_u = 0.5$. As before, the upper limit could be taken to be the largest eccentricity for which the series expansions of the changes in the orbital

elements over one Saros period still provide reasonably accurate results.

Since the Saros period is much longer than the synodic period and since the perturbations in the eccentricity over one Saros period are much smaller than those over one synodic period, use of the Saros cycle as the base period in the finite-time stability method stands a much better chance of producing a minimum lifetime for the Moon's orbit which is more in keeping with the results expected through planetological studies of the age of the solar system. In any case, the new approach should certainly improve on the Moon's minimum lifetime of less than one year, obtained when applying the finite-time stability method using the synodic period as the base period.

6.7 The Saros Cycle as a Possible Stabilizing Mechanism

In the previous sections, we have shown that the Earth-Moon-Sun system is moving in a nearly periodic orbit for a finite time because the system passes through two near mirror configurations every Saros period. Knowing this, can we say anything about the stability of such a system? Periodicity, in itself, does not guarantee the stability of the system against perturbations by external forces. A system can be periodic and still be unstable, in the sense that a slight disturbance by a small external force could send the system into a non-periodic orbit which could result in a marked irreversible change from the original orbit.

This can easily be seen in the case of the collinear equilibrium solutions to the circular restricted three-body problem. See Roy (1988, page **121**). The solutions, placing the mass-less particle at one of the Lagrange points L_1, L_2, or L_3 along the line joining the finite masses m_1 and m_2, are all highly unstable. The bodies are collinear with their velocity vectors perpendicular to that line and hence they form a mirror configuration at some epoch t_0. However, if the mass-less particle were to be displaced slightly from one of the Lagrange points by an external force, the result would be a rapid departure of the particle from that position, even though its displaced position and velocity would still be very close to a mirror configuration of the system.

A second near mirror configuration might occur before the particle escaped to infinity or collided with one of the finite masses, but there is no way of predicting this event and therefore stability cannot be guaranteed. If, however, a second mirror configuration did occur soon after the first, then by the mirror theorem, the system would return to the neighbourhood of the first and the system would be stable for that interval of time.

Roy and Ovenden (1955) argue that although periodicity does not guarantee stability, periodic orbits which pass through mirror configurations are more stable, if the time intervals between successive mirror configurations are shorter. As long as a second mirror configuration is able to occur before disturbances have enough time to accumulate to the point of causing irreversible change to the orbit, the system will return to the neighbourhood of its original orbit, with the second mirror

configuration reversing the perturbations caused by the small external force.

While Roy and Ovenden (1955) state that they do not treat the question of stability in an exhaustive and rigorous manner, they do show that their hypothesis is confirmed by observations made in the solar system. They prove that two orbiting masses having nearly commensurable mean motions, and certain values for either of the orbital parameters $\dot{\varpi}$ or $\dot{\Omega}$, depending on whether eccentricities or inclinations dominate the system, will produce frequent occurrences of mirror configurations. They then study the nearly commensurable systems of low integer values in the solar system and verify that these systems are indeed arranged in such a way as to allow the most frequent occurrences of mirror configurations. The greater stability of systems passing through frequent mirror configurations is then suggested to be the reason why more commensurable systems exist in the solar system than are expected by mere chance (Roy and Ovenden, 1954).

In actual fact, the orbital mean motions do not necessarily have to be nearly commensurable in order for frequent mirror configurations to occur. That they are generally commensurable for most of the three-body systems in the solar system exhibiting frequent occurrence of mirror configurations is simply the result of the fact that most of the systems have values of $\dot{\varpi}$ and $\dot{\Omega}$ which are much smaller than their mean motions.

For the collinear-type mirror configurations, the shortest time between successive perfect mirror configurations in a three-dimensional system occurs when the bodies are in conjunction or opposition every time the bodies are positioned along their mutual line of nodes and their orbital apsidal lines. For example, if we take a case similar to the Earth-Moon-Sun system where the Sun's orbit is taken to be circular, frequent occurrences of mirror configurations will occur if the satellite, the Sun, the satellite's line of nodes, and the satellite's pericentre or apocentre are alligned as often as possible, ie

$$A_1 T_S = A_2 T_A = A_3 T_N \qquad (9)$$

where A_i for i = 1,2,3 are small integers. In other words frequent occurrence of

mirror configurations occurs when the system contains a perfect saros cycle.

Equation (9) can be rewritten in terms of the mean motions of the satellite n, the Sun n_1, the satellite's pericentre $\dot{\varpi}$ and the satellite's line of nodes $\dot{\Omega}$, ie

$$2\pi \frac{A_1}{n - n_1} = 2\pi \frac{A_2}{n - \dot{\varpi}} = 2\pi \frac{A_3}{n - \dot{\Omega}}$$

If we then take the reciprocal of these equalities and multiply by the factor $A_1A_2A_3/2\pi$, we get

$$B_1(n - n_1) = B_2(n - \dot{\varpi}) = B_3(n - \dot{\Omega}) \qquad (10)$$

where B_i for i = 1,2,3 are again integers but much larger than A_i.

For those systems where $\dot{\varpi}$ and $\dot{\Omega}$ are small relative to their mean motions n, frequent occurrences of mirror configurations would therefore result when the mean motions are nearly commensurable, viz.

$$B_1(n - n_1) \cong B_2\, n \cong B_3\, n$$

or

$$\frac{n}{n_1} \cong \frac{B_1}{B_1 - B_2} \cong \frac{B_1}{B_1 - B_3}$$

In general, however, frequent occurrences of mirror configurations in the circular three-body problem still result when the dynamical system contains a set of commensurabilities like those of Equation (9) or in other words, when the system contains a saros cycle. Extension of the solution to that of the general three-body problem simply requires the addition of commensurabilities with the Sun's anomalistic and nodical periods, to enable the frequent alignments of the Sun's line of nodes and apse with a conjunction or opposition, as well as with the Moon's line of nodes and apse. Then for example,

$$B_1(n - n_1) = B_2(n - \dot{\varpi}) = B_3(n - \dot{\Omega}) = B_4(n_1 - \dot{\varpi}_1) = B_5(n_1 - \dot{\Omega}_1) \qquad (11)$$

In the simpler case, where the Sun is taken to move in an elliptical orbit with small rates of change of pericentre and node relative to its mean motion, the following set of commensurabilities is sufficient for frequent occurrences of mirror configurations:

$$B_1(n - n_1) \cong B_2(n - \dot{\varpi}) \cong B_3(n - \dot{\Omega}) \cong B_4(n_1) \cong B_5(n_1)$$

or in terms of the mean periods

$$A_1 T_S \cong A_2 T_A \cong A_3 T_N \cong A_4 T_\odot$$

where B_i and A_i are integers and $T_\odot$ is the Sun's sidereal period.

Note that Equations (10) and (11) are the same as Equations (**7**) and (**8**) of Chapter 1 which describe the conditions that will produce resonances in the circular three body problem and the general three body problem respectively. Thus, it becomes obvious that the statement that a three-body system moves through two mirror configurations which form a periodic orbit, is equivalent to the statement that the system is moving in a particular resonance. In particular, if a three body system where the outer body moves in a fixed circular orbit perturbing the inner body contains a perfect saros cycle, it also must pass through two mirror configurations, be periodic and be moving in an e-i resonance.

We have already seen in Chapter 1 that the existance of resonances within a planetary system appears to be closely related to the stability of that system. Perhaps, the mirror theorem can be used as a simple way of understanding physically how certain resonances between the mean motions of the bodies, their apsidal lines and their nodal lines can act to stabilize a system.

If the hypothesis, that "periodic orbits are more stable against external perturbations, the shorter the time interval between successive mirror configurations" is true, then circular three-body dynamical systems containing

perfect saros cycles, which we have already seen move through two mirror configurations, will be more stable the smaller the saros period. Saros cycles whose periods are too large may not have enough time to return the dynamic system to its original geometry before solar perturbations grow to the point where the system's orbital elements are changed irreversibly.

If the saros cycle is not perfect, as in the case of the Earth-Moon-Sun system, its duration will also depend on how closely the near saros cycle approaches a perfect saros cycle. Saros cycles which are too inaccurate can not successfully cancel solar perturbations and therefore will not last very long.

Also, if a near saros cycle can help the system to endure long enough to reach a saros cycle that is closer to a perfect saros cycle but of much longer period, then the system will again last longer than if it was only able to use the solar perturbation cancelling properties of the first saros cycle.

In summary, it seems that a circular three-body system will be more stable:

(1) the shorter the saros period
(2) the closer the near saros cycle is to a perfect saros cycle
(3) the greater the number of near saros cycles operating at any given time.

Again it should be stressed that we are not saying circular three-body systems containing saros cycles will be guaranteed stability for all time. Certainly a circular three-body system which contains a perfect saros cycle will remain stable for all time as long as there are no external perturbations, simply because it is periodic. However, we cannot say anything about the stability for all time of a perturbed system containing a perfect saros cycle. What we can say, is that a perturbed circular three-body system containing a perfect saros cycle, or a circular three-body system containing a near saros cycle, is likely to endure longer than a system without a saros cycle.

If the Saros cycle does act as a stabilizing mechanism, then of next importance is the question of how probable it is that such cycles comprised of commensurabilities between the synodic, anomalistic and nodical periods should exist, especially given the

knowledge that tidal evolution has changed these periods in the Moon's past and is continuing to change them today.

Authors such as Mitchell (1951) and Crommelin (1901) merely note that the anomalistic period plays a very convenient role in helping to predict eclipse characteristics. Newcomb (1882), in his paper on "The Recurrence of Solar Eclipses", talks of "two remarkable chance relations connected with the Saros ... without which the period would not have served the purpose of forseeing eclipses so well as it actually does". He is referring to the fact that after one Saros period, the mean anomalies of the Moon and the Sun have returned to within less than 3° and 12° respectively of their original positions. He goes on to say, "There is no a priori reason that this should be the case: it arises only from the fact that 18 years is a close multiple, not only of the times of revolution of the Sun and Moon, but also of the times of revolution of the Moon's node and perigee".

Many people have remarked on the fortuitous existence of the near commensurabilities forming the Saros cycle, but to our knowledge no one has asked the question, "Just how much of a coincidence is the existence of a saros-type cycle within the orbital dynamics of the Earth-Moon-Sun system?" If the existence of a saros-type cycle is improbable, what implications does this have for the Moon's orbital evolution when in the past or the future, the Moon may not have had, or may not have, a saros-type cycle to use as a stability mechanism against solar perturbations? We address these problems in Chapter 7.

CHAPTER 7

THE OCCURRENCE OF SAROS CYCLES IN THE MOON'S ORBITAL EVOLUTION

" 'Tis all a Chequer-board of Nights and Days
Where Destiny with Men for Pieces Plays:
Hither and thither moves, and mates, and slays,
And one by one back in the Closet lays. "

The Rubaiyat of Omar Khayyam

7.1 Introduction

Until now, we have been discussing primarily the properties of the present-day saros cycle and its role as a stabilizing mechanism for the Moon against solar perturbations. But what effect does the evolution of the Moon's orbit have on the Saros cycle?

The Moon's orbital evolution is largely controlled by the tidal interaction between the Moon and the Earth. Tides are raised on the Earth resulting in a transfer of energy and angular momentum from the rotating Earth to the orbiting Moon. This causes changes in the lunar orbital semi-major axis and the Moon's mean motion, with the final result that the Moon is slowly spiralling outward away from the Earth. According to lunar theory such changes, even if no changes occur in the orbital eccentricities of the Moon and the Earth, can also affect the mean rates of motion of the lunar apse $\dot{\varpi}$ and node $\dot{\Omega}$ and consequently the three periods which form the Saros cycle.

Since the Saros cycle seems to be relevant to studies of the stability of the Earth-Moon system against solar perturbations, it becomes important to know what effect tidal evolution has on the Saros cycle. Will tidal evolution eventually destroy the Saros cycle? Is tidal friction pushing the Moon nearer to, or further away from a perfect saros cycle? If the Moon can be removed from its present-day saros cycle, are commensurabilities among the three changing periods T_S, T_N and T_A so common that another close approximation to a perfect saros cycle can be found for the new period set of $T_A(t)$, $T_N(t)$, $T_S(t)$? On the other hand, is the present-day saros cycle a unique coincidence?

If a near saros cycle can always be found, then the Moon's stability is under no

threat from the destruction of the present-day saros cycle. But, if the present saros cycle is a rare occurrence, then it is possible that the loss of the stabilizing mechanism of the Saros cycle through tidal evolution could have drastic effects on the future stability of the Earth-Moon system.

There is also the question of the past evolution of the Moon. If it turned out that the Earth-Moon-Sun system has often been without a saros cycle to cancel solar perturbations, then the Moon's orbital evolutionary history may contain previously unsuspected episodes where the Sun has had a greater effect on the lunar orbit than it does today. Such episodes of unpredictable behaviour on the part of the lunar orbit would have serious consequences for any attempts to estimate the time-scale of the Moon's orbital development through the use of tidal evolution alone.

Most of the questions posed so far contain such vague phrases as "the Saros cycle", "a saros cycle", "a near saros cycle", and "a perfect saros cycle". Before attempting to answer any of the questions asked, we must be very clear as to what is meant by such phrases.

"The Saros cycle" refers to the currently existing saros cycle which is formed from the commensurability between the present-day values of T_S, T_A, and T_N. For the purposes of this discussion we will define, in general, "a saros cycle" to be any cycle formed from a simultaneous near commensurability between the three satellite periods: the synodical T_S, the nodical T_N and the anomalistic T_A months. "A saros period" $T_{Saros(i)}$ is then taken to be one of the three periods T_i (for i=1,2,3) multiplied by its integer multiple A_i (for i=1,2,3). ie

$$T_{Saros\,(i)} = A_i\, T_i$$

"A perfect saros cycle" is one where there exists a unique saros period which is exactly equal to integer multiples of each of the three satellite periods.

$$T_{Saros} = A_1 T_1 = A_2 T_2 = A_3 T_3 \qquad \text{where } A_i \text{ are integers}$$

$$A_i \leq A_{max} \quad \forall \quad i = 1,2,3$$

"A near saros cycle" is one where the three combinations of the satellite periods and their corresponding integer multiples are approximately equal to each other to within a given accuracy q. This may be described mathematically as a triplet of periods (A_1T_1, A_2T_2, A_3T_3) where:

$$\varepsilon_{12} = A_1 T_1 - A_2 T_2 \qquad \text{and} \qquad |\varepsilon_{ij}| \le q$$
$$\varepsilon_{13} = A_1 T_1 - A_3 T_3 \qquad A_i \text{ are integers}$$
$$\varepsilon_{23} = A_2 T_2 - A_3 T_3 \qquad A_i \le A_{max}$$
$$\forall \; i, j = 1,2,3 \quad i < j \qquad (1)$$

ε_{12}, ε_{13} and ε_{23} are the discrepancies between the relevant saros periods. Note that $\varepsilon_{23} = \varepsilon_{13} - \varepsilon_{12}$. Therefore, there are only two independent discrepancies to study.

In both the definitions of a perfect saros cycle and a near saros cycle, we have added the restriction that the integer multiples A_i (for i=1,2,3) must be smaller than some given maximum integer A_{max}. Integers which are larger than this upper limit are assumed to form saros periods so long, that solar perturbations could have time to accumulate to beyond the point where the system becomes unstable before the two mirror configurations can act to reverse the effects of the perturbations.

For near saros cycles, we take the best approximation to the saros period to be an average of the three possible saros periods.
Thus,

$$T_{Saros} = \frac{1}{3} \sum_{i=1}^{3} A_i T_i$$

According to our definitions, the present-day saros cycle is therefore a near saros cycle with an average saros period of 6,585.405 days.

In order to develop a model for describing a saros cycle which consists of near commensurablities between any <u>three</u> periods, it is instructive to first look at the simpler case of a cycle formed from a near commensurability between any <u>two</u>

periods. We call such a cycle, a "metonic cycle" after Meton's cycle (See Section 6.3) because both cycles are formed by a commensurability between a pair of periods.

"A perfect metonic cycle" is defined to be one where the combinations of the integer multiples and their respective periods are exactly equal, and "a near metonic cycle" is one where the combinations differ by at most a small given error q. Thus, a perfect metonic cycle is described by the following statement:

$$A_1 T_1 = A_2 T_2 \qquad \text{where} \quad A_i \text{ are integers}, \quad A_i \le A_{max} \ \forall \ i = 1,2$$

while a near metonic cycle is one where:

$$\varepsilon_{12} = A_1 T_1 - A_2 T_2 \qquad \text{where} \quad |\varepsilon_{12}| \le q, \quad A_i \text{ are integers}, \quad A_i \le A_{max} \ \forall \ i=1,2 \qquad (2)$$

ε_{12} is the discrepancy between the two metonic periods $A_1 T_1$ and $A_2 T_2$.

The average metonic period T_{met} is given by:

$$T_{met} = \frac{1}{2} \sum_{i=1}^{2} A_i \ T_i \qquad \text{with an uncertainty of } \pm \frac{\varepsilon_{12}}{2}.$$

Sections 7.2 to 7.5 are primarily concerned with discovering the likelihood that the Moon's orbit will contain a saros cycle, given that tidal evolution is changing the period set which forms the present saros cycle. Section 7.2 looks at several methods of predicting the expected number of metonic cycles for a given pair of periods. These methods are confirmed in Section 7.3 through the use of extensive numerical random testing and statistical inferences. In Section 7.4, the formula for predicting the number of metonic cycles is expanded in order to predict the expected number of saros cycles for a given triplet of periods. The results of the numerical testing of this formula are then given in Section 7.5.

The effect of tidal evolution on the Saros cycle is discussed in Section 7.6 and if only tidal interaction is taken into account, a possible sequence of saros cycles that the Moon's orbit might evolve through is found. Finally, Section 7.7 summarizes our results.

7.2 Prediction of the Frequency of Occurrence of Metonic Cycles

How frequently do metonic cycles occur given a pair of periods? In other words, how many integer pairs A_1 and A_2 exist for a given set of periods T_1 and T_2 such that:

$$\varepsilon_{12} = A_1 T_1 - A_2 T_2 \qquad (3)$$

where $|\varepsilon_{12}| \leq q$ is a given accuracy criterion, and A_1 and A_2 are integers less than a given upper limit integer of A_{max}?

To answer the above question a search can be made for fractions that will approximate the rational number T_2/T_1. Therefore taking $T_1 > T_2$, we divide Equation (3) by T_1 to give

$$\varepsilon_{12}' = A_1 - A_2 T_2' \qquad \text{where} \quad |\varepsilon_{12}'| \leq q'$$

$$A_i \text{ are integers}$$

$$A_i \leq A_{max} \quad \forall \; i=1,2 \qquad (4)$$

A prime superscript denotes a division of the original parameter by T_1. Normalization of the system by T_1 avoids any problems that might develop later when different scales are used.

(i) Use of a numerical algorithm and the computer

The first and easiest solution to the problem is to use the computer to search for the number of metonic cycles that occur for a given pair of periods and for the stipulated restrictions.

This is done most efficiently by calculating for every integer A_2 from 1 to A_{max}, the two residuals of the rational number A_2T_2' from the nearest upper and lower integers. The absolute minimum of the two residuals is then equal to $|\varepsilon_{12}'|$. If $|\varepsilon_{12}'| \leq q'$, then the integer which produced the chosen ε_{12}' becomes A_1 and the integer set (A_1,A_2) forms a metonic cycle for the period set (T_1,T_2).

Table 7.1 gives an example of such a calculation for $T_2' = T_A/T_S = 0.933085$ where q is chosen to be 0.5 days, a value slightly larger than the largest discrepancy between the three saros periods. q' is then equal to 0.5 days/T_S or 0.016932. Those rows which are highlighted form metonic cycles for the period set (T_S, T_A).

Table 7.2 gives the complete list of metonic cycles for the same example if A_{max} is taken to be 1000. The minimum residual ε_{12}' indicates the closeness of the near metonic cycle to a perfect one since a perfect metonic cycle would have a zero residual.

While a computer algorithm can tell us the number of metonic cycles which exist for a given set of periods, it would be better if we could find a general formula giving the same result, but for any values of T_1, T_2, A_{max} and q'. This problem however, is complicated by the fact that the number of metonic cycles is strongly influenced by the proximity of T_2' to a high or low number commensurability.

A_2	A_2T_2'	Lower residual	Upper residual	Minimum absolute residual $\lvert\varepsilon_1'\rvert$	A_1
1	0.933085	-0.933085	0.066915	0.066915	
2	1.866170	-0.866170	0.133830	0.133830	
3	2.799254	-0.799254	0.200746	0.200746	
4	3.732340	-0.732340	0.267660	0.267660	
5	4.665424	-0.665424	0.334576	0.334576	
6	5.598510	-0.598510	0.401490	0.401490	
7	6.531594	-0.531594	0.468406	0.468406	
8	7.464680	-0.464680	0.535320	0.464680	
9	8.397765	-0.387765	0.602235	0.387765	
10	9.330850	-0.330850	0.669150	0.330850	
11	10.263935	-0.263935	0.736065	0.263935	
12	11.197020	-0.197020	0.802980	0.197020	
13	12.130105	-0.130105	0.869895	0.130105	
14	13.063190	-0.063190	0.936810	0.063190	
15	13.996275	-0.996275	0.003725	0.003725	14
16	14.929360	-0.929360	0.070640	0.070640	
17	15.862445	-0.862445	0.137555	0.137555	
18	16.795517	-0.795517	0.204483	0.204483	
19	17.728607	-0.728607	0.271393	0.271393	
20	18.661697	-0.661697	0.338303	0.338303	
21	19.594772	-0.594772	0.405228	0.405228	
22	20.527863	-0.527863	0.472137	0.472137	
23	21.460953	-0.460953	0.539047	0.460953	
24	22.394028	-0.394028	0.605972	0.394028	
25	23.327118	-0.327118	0.672882	0.327118	

Table 7.1 Calculation of the residuals of the rational number A_2T_2' from the two closest upper and lower integers, for a range of integers A_2 and a given value of $T_2'=T_A/T_S=0.933085$.

T_A and T_S are the anomalistic and synodic lunar months. The highlighted rows indicate those integer pairs (A_1,A_2) which form metonic cycles for T_2', within a given accuracy of $q'=0.016932$.

A_1	A_2	$A_2 T_2'$	Minimum residual ε_{12}'
14	15	13.99672	0.00373
28	30	27.99255	0.00745
42	45	41.98882	0.01118
56	60	55.98510	0.01490
195	209	195.01476	-0.01476
209	224	209.01104	-0.01104
223	239	223.00731	-0.00731
237	254	237.00359	-0.00359
251	269	250.99986	0.00014
265	284	264.99614	0.00386
279	299	278.99241	0.00759
293	314	292.98869	0.01131
307	329	306.98496	0.01504
446	478	446.01463	-0.01463
460	493	460.01090	-0.01090
474	508	474.00718	-0.00718
488	523	488.00345	-0.00345
502	538	501.99973	0.00027
516	553	515.99600	0.00400
530	568	529.99228	0.00772
544	583	543.98855	0.01145
558	598	557.98483	0.01517
697	747	697.01449	-0.01449
711	762	711.01077	-0.01077
725	777	725.00704	-0.00704
739	792	739.00332	-0.00332
753	807	752.99959	0.00041
767	822	766.99587	0.00413
781	837	780.99214	0.00786
795	852	794.98842	0.01158
809	867	808.98469	0.01531

Total Number of Metonic cycles = 31

Table 7.2 The complete list of metonic cycles which exist for the period set (T_S, T_A), where $T_2' = T_A/T_S = 0.933085$, $q' = 0.01693$ and $A_{max} = 1000$.

The residuals ε_{12}' indicate how close the near metonic cycles are to exact metonic cycles. A perfect metonic cycle would have a zero residual.

(ii) A graphical look at the problem

We can study the problem using a graphical method where the equation $A_1=T_2'A_2$ is plotted for various values of A_1 and A_2. T_2' then becomes the slope of the resulting line. Metonic cycles will exist wherever the line passes through a point in which both A_1 and A_2 are very close to integer values. See Figure 7.1, where these points or metonic cycles are denoted by circles. The discrepancy ε_{12}' then becomes the distance from the point $T_2'A_2$ on the y-axis to the nearest integer A_1 on the y-axis.

If T_2' is close to a high number commensurability with integers of order A_{max}, the number of metonic cycles would include only those ratios A_1/A_2 which are each proper fractions that happen to fall within the accuracy q'. $T_2'=0.835792$, 0.697026 and 0.216734 shown in Figure 7.1 are all examples of such a case.

If T_2' forms an exact low number commensurability such as 11/21 or 35/94 (see Figure 7.1), then the only possible metonic cycles are multiples of the first proper fraction that equals T_2'. The number of metonic cycles in this case depends on the size of the denominator in the proper fraction relative to A_{max}. For example,

$$T_2' = \frac{11}{21} = \frac{22}{42} = \frac{33}{63} = \ldots = \frac{517}{987}$$

produces [1000/21] = 47 different metonic cycles, while

$$T_2' = \frac{35}{94} = \frac{70}{188} = \frac{105}{282} = \ldots = \frac{350}{940}$$

produces [1000/94] = 10 different metonic cycles for A_{max} = 1,000.

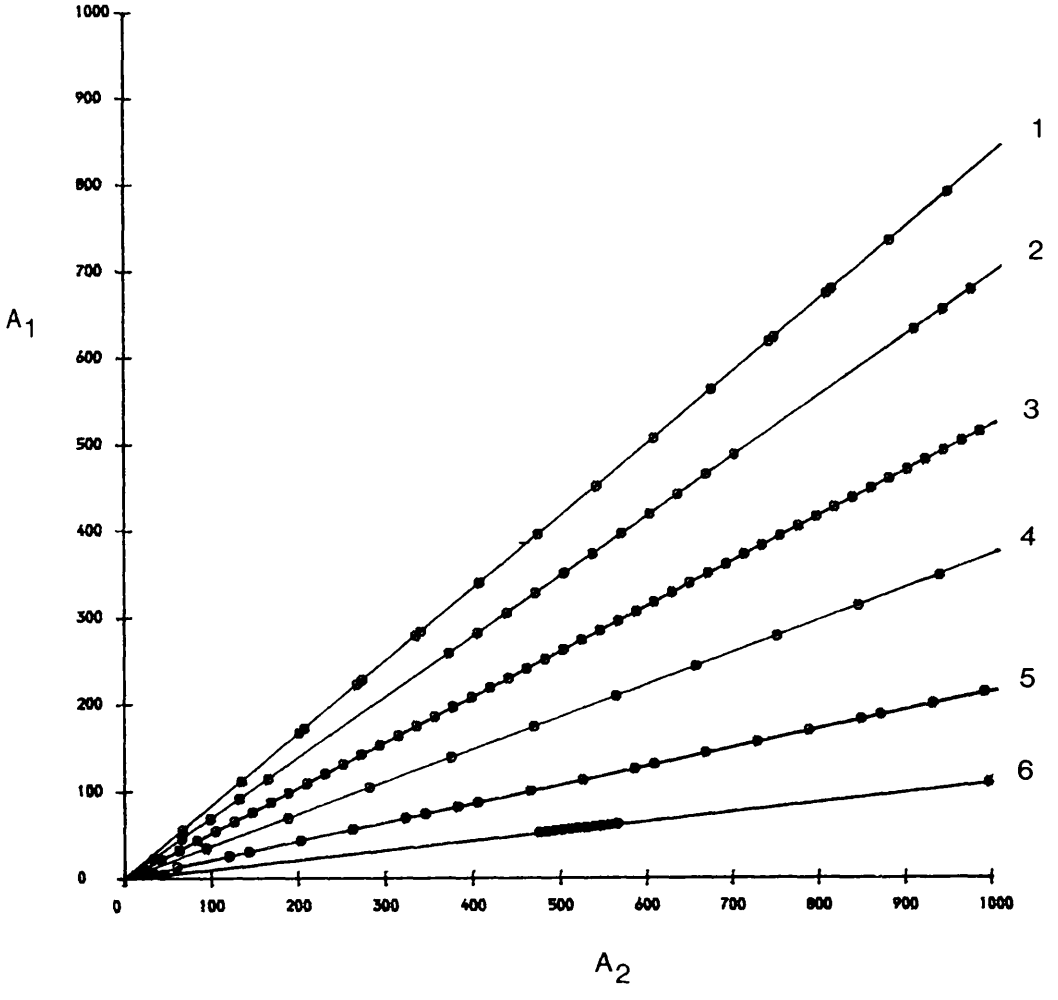

Figure 7.1 A graphical method of describing the location and number N of metonic cycles for a given period set (T_1, T_2) where $T_2'=T_2/T_1$. The lines are plots of the equation $A_1 = T_2'A_2$ and the circles denote metonic cycles (ie the positions along the line where A_1 and A_2 are both equal to integers to within a given error of q' = 0.01).

No.	T_2'	Type	N
1	0.835792	random	19
2	0.697026	random	19
3	0.523800	perfect commens.(=11/21)	47
4	0.372340	perfect commens.(=35/94)	10
5	0.216734	random	20
6	0.111324	near commens. (~1/9)	17

If T_2' happens to be only near a low number commensurability, the number of metonic cycles would include all the proper fractions which form a near commensurability with T_2', plus any multiples of these proper fractions. $T_2'=0.111324\approx 1/9\approx 58/521$ in Figure 7.1 is such a period. Table 7.3 lists the metonic cycles for $T_2'=0.111324$, if q' is taken to be 0.01 and $A_{max}=1{,}000$. Here T_2' produces 17 metonic cycles.

A_1	A_2	$A_2 T_2'$	Minimum residual ε_{12}'
1	9	1.00192	-0.00192
2	18	2.00383	-0.00383
3	27	3.00575	-0.00575
4	36	4.00766	-0.00766
5	45	5.00958	-0.00958
53	476	52.99022	0.00978
54	485	53.99214	0.00786
55	494	54.99406	0.00594
56	503	55.99597	0.00403
57	512	56.99789	0.00211
58	521	57.99980	0.00020
59	530	59.00172	-0.00172
60	539	60.00364	-0.00364
61	548	61.00555	-0.00555
62	557	62.00747	-0.00747
63	566	63.00938	-0.00938
111	997	110.99003	0.00997

Total number of metonic cycles = 17

Table 7.3 List of the metonic cycles which exist for the near low number commensurability of $T_2'=0.111324$ or approximately $1/9 \approx 58/521$, where q'=0.01 and $A_{max}=1000$.

Note that the values of T_2' near high number commensurabilities appear to produce approximately the same number of metonic cycles, while T_2' values near low number commensurabilities appear to produce widely varying counts of metonic cycles.

In general as T_2' decreases, the number of proper fractions which approximate T_2' to within an error q' appear to increase because there are a greater number of integers A_2 which, when divided into the same integer A_1, come close to the value T_2'. Therefore, the number of metonic cycles seems to be inversely proportional to the size of T_2' in some manner. However the opposite effect also appears to be occuring because as T_2' decreases, the possible values for A_2 rapidly approach the upper limit A_{max} before the first proper fraction can be found to approximate T_2'. We shall take a further look at these two opposing trends in Section 7.2 (iv).

While the graphical method helps us to understand the relationship between the period set and the number of metonic cycles that exist for $A_i \leq A_{max}$ and $|\varepsilon_{12}'| \leq q'$, it does not give us an expression for that relationship.

(iii) The use of continuous fractions

Continuous fractions have been used for centuries to obtain rational approximations to real numbers. It therefore might be possible to use them to find the fractions A_1/A_2 that approximate the value T_2' to within the restrictions given by Equation (4).

The definition of a continued fraction can be found in any book on basic numerical analysis. Churchhouse's (1981) Numerical Methods Handbook of Applicable Mathematics, Vol III (pp 225 - 232) gives the following mathematical description of how to approximate any real number θ with a continued fraction.

Let θ be any positive real number and let [x] denote the integer part of x. The continued fraction of θ is:

$$\theta = a_0 + \cfrac{1}{a_1 + \cfrac{1}{a_2 + \cfrac{1}{a_3 + \ldots}}}$$

where

$$\begin{aligned} a_0 &= [\theta], & \theta_0 &= (\theta - a_0)^{-1} \\ a_1 &= [\theta_0], & \theta_1 &= (\theta_0 - a_1)^{-1} \\ a_2 &= [\theta_1], & \theta_2 &= (\theta_1 - a_2)^{-1} \\ &\vdots & &\vdots \\ a_i &= [\theta_{i-1}], & \theta_i &= (\theta_{i-1} - a_i)^{-1} \\ &\vdots & &\vdots \\ a_n &= [\theta_{n-1}], & \theta_n &= (\theta_{n-1} - a_n)^{-1} \end{aligned}$$

The recursive method is repeated until θ is approximated by a fraction to within the required accuracy. The continued fraction of θ is often expressed more conveniently in the form:

$$\theta \approx \theta_n = (a_0, a_1, a_2, a_3, \ldots, a_n)$$

Note also that the numerator and denominator of the i^{th} continued fraction approximating θ (ie $\theta_i = (a_0, a_1, a_2, a_3, \ldots, a_i)$) are given by the following equations:

Numerator of $\theta_i = a_i$ (numerator of θ_{i-1}) + numerator of θ_{i-2}

Denominator of $\theta_i = a_i$ (denominator of θ_{i-1}) + denominator of θ_{i-2}

Thus, for example, Table 7.4 shows how the value $\theta = T_N/T_S = 0.921492626$ can be approximated by successively more accurate continued fractions. Note that the continued fraction $\theta_6 = 223/242$ is one of the commensurabilities found in the Saros

cycle.

i	a_i	θ_i	Continued fraction	Accuracy of the continued fraction ($\lvert fraction_i - \theta_i \rvert$)
0	0	$(0.921492626)^{-1}$	0	0.921492626
1	1	$(0.085195879)^{-1}$	1	0.078507374
2	11	$(0.737656940)^{-1}$	11/12	0.004825959
3	1	$(0.355643722)^{-1}$	12/13	0.001584297
4	2	$(0.811802763)^{-1}$	35/38	0.000439994
5	1	$(0.231826308)^{-1}$	47/51	0.000076002
6	4	$(0.313574282)^{-1}$	223/242	0.000005023
7	3	$(0.189037040)^{-1}$	716/777	0.000000296
8	5	$(0.289968569)^{-1}$	3803/4127	0.000000016
9	3	$(0.448649636)^{-1}$	12125/13158	2×10^{-9}

Table 7.4 The continued fractions of $\theta = T_N/T_S = 0.921492626$

The problem with using continued fractions to count the number of metonic cycles that exist for a given period is that each successive continued fraction is, by the very nature of continued fractions, a closer approximation to θ than the previous one. This means that all of the proper fractions, which are located between these successively more accurate continued fractions and which should be considered near metonic cycles by our criteria of $|\varepsilon_{12}'| \leq q'$, will not be included in the final count.

In addition, when we attempt to extend the use of continued fractions to three periods, we run into the problem of how to find a simultaneous set of two continued fractions where the numerator of one is equal to the denominator or numerator of the other. For example, if the basic criteria for a near saros cycle is:

$$A_1 \approx A_2T_2' \approx A_3T_3' ,$$

we would need to search for a minimum of two of the following simple fractions:

$$A_1/A_2 \approx T_2' \quad \text{and/or} \quad A_1/A_3 \approx T_3' \quad \text{and/or} \quad A_2/A_3 \approx T_3'/T_2'$$

Thus, though the study of continuous fractions is very relevant for discovering which fractions accurately approximate T_2', it is not very helpful for predicting the expected number of near metonic cycles or near saros cycles for a given period set.

(iv) The use of the psuedo-random nature of the residuals

A random number is defined by Koopmans (1981) in his book An Introduction to Contemporary Statistics to be a number which is:

(1) Independently generated (ie the selection of previous numbers does not affect in any manner the present selection of a number).

(2) Selected at random (ie each number has an equal chance of being selected).

A pseudo-random number is a number generated by a computer whose properties closely approximate those of a random number. These numbers are given the name pseudo-random because by the very nature of computers any number generated by a computer is already pre-determined once the computer programme has begun. Therefore, no computer can produce genuinely random numbers. Computers can be programmed, however, to produce numbers which to all appearances exhibit the properties of random numbers. In other words, although pseudo-random numbers are generated through a sequence of established steps, the systematic process which links these numbers together is not obvious in the final table of random numbers. Pseudo-random number generators are used regularly in scientific research to produce random samples for statistical purposes.

When Table 7.1 is examined more closely, the minimum absolute residuals seem to be uniformly distributed between 0.0 and 0.5. If we extend Table 7.1 to include integers A_2 up to 1000 and plot the frequency distribution of the minimum absolute residuals for a bin size of 0.05, the frequency of occurrence of the minimum absolute residual values $|\varepsilon_{12}'|$ is indeed approximately a constant over the range of 0.0 to 0.5. See Figure 7.2(a). In other words, for $T_2'=0.933085$ any residual has an equal probability of occurring. The residuals therefore exhibit one of the two

properties necessary for a variable to be random.

Unfortunately, not all values of T_2' produce residuals which display a uniform frequency distribution. If T_2' is very close to a low number commensurability, then the residuals are locked into an obvious systematic pattern pre-determined by the low number commensurability. For example, Table 7.5 gives the minimum absolute residuals for $T_2'=0.666677\approx 2/3$. Figure 7.3 illustrates the corresponding frequency distribution of the minimum absolute residuals for $T_2'=0.66677\approx 2/3$. It is decidedly not a uniform distribution.

In actual fact, all values of T_2' give rise to residuals which exhibit to varying degrees a repeated pattern, simply because the residuals are always generated by a systematic procedure. Figure 7.2(b) displays the relationship between the minimum absolute residual $|\varepsilon_{12}'|$ and the integer value A_2 which created it, for the case $T_2'=0.933085$ listed in Table 7.1. Here, although each residual has an equal chance of being selected they are not truely random numbers because they are not independent of each other. However, the further removed T_2' is from a low number commensurabilily, the more obscured this cyclic nature becomes in the resulting tables for the residuals.

Figures 7.4 compare the plots of the minimum absolute residuals versus their corresponding integers A_2 for four values of T_2' which are progressively further removed from the low number commensurability of $T_2'=2/3$. As T_2' moves further away from a low number commensurability, the residual values become less rigidly locked into values that are closely repeated. For a value of T_2' very close to a low number commensurability, any residual can be predicted easily from the previous residual. For those T_2' values far removed from a low number commensurability, however, it may only be possible to predict whether the next residual will be greater than or less than the previous one. Figures 7.4 also show that as T_2' deviates further from a low number commensurability, the frequency distribution of the minimum absolute residuals becomes more uniform.

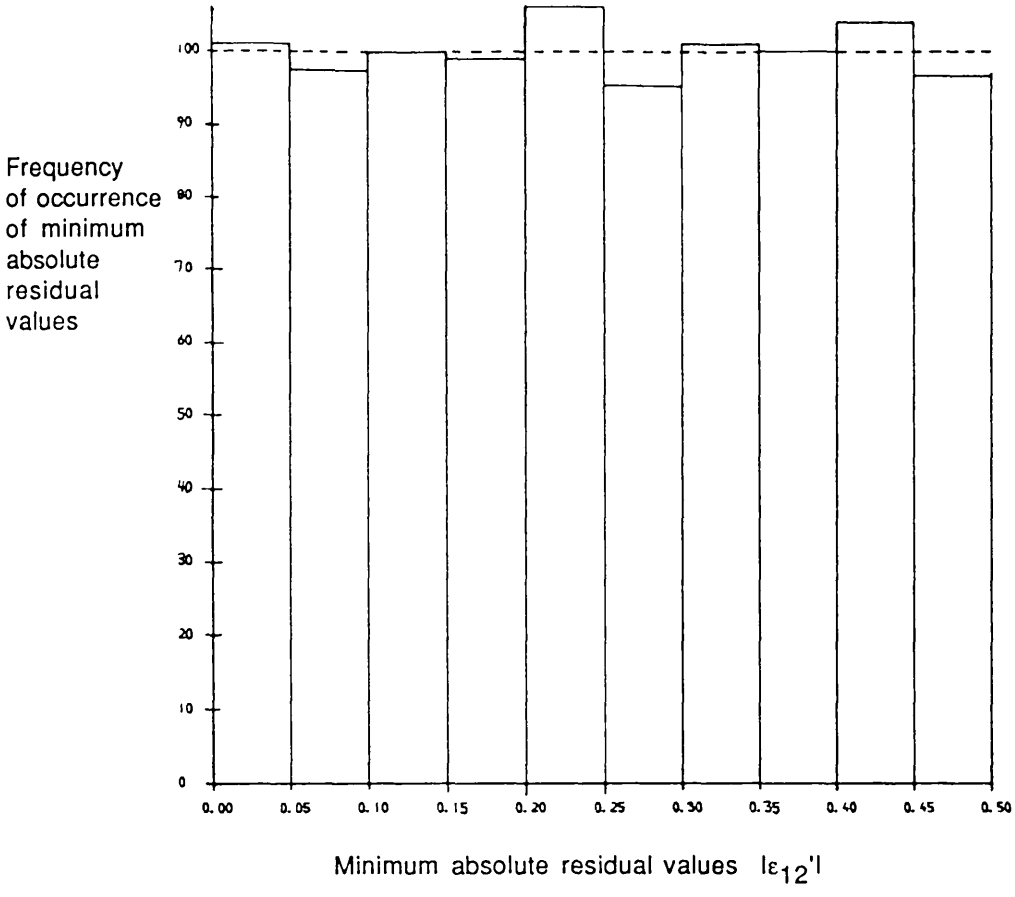

Figure 7.2 (a) The frequency distribution of the minimum absolute residuals for $T_2' = 0.933085$, where the data is taken from a version of Table 7.1 that is extended to $A_2=1000$. Note that the distribution is almost uniform.

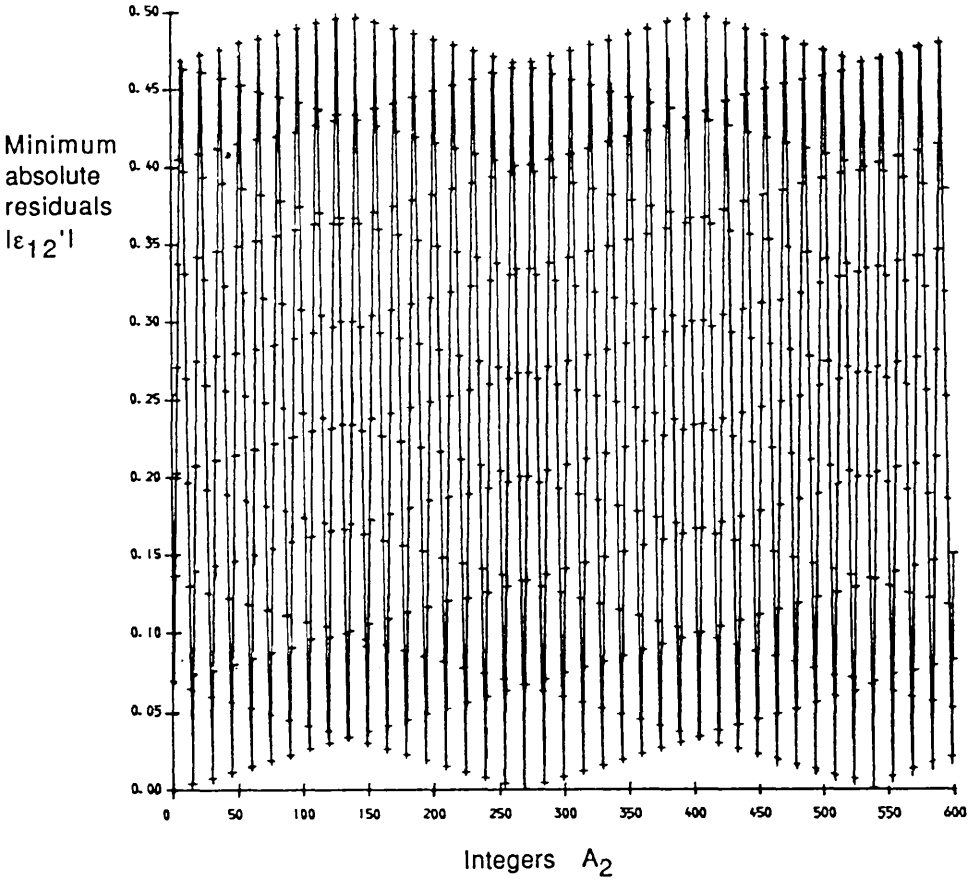

Figure 7.2 (b) The cyclic nature of the minimum absolute residuals $|\varepsilon_{12}'|$ as a function of the integer value of A_2 for the same case. The crosses denote the discrete points of the function.

A_2	A_2T_2'	Lower residual	Upper residual	Minimum absolute residual $\lvert\varepsilon_{12}'\rvert$	A_1
1	0.666670	-0.666670	0.333330	0.333330	
2	1.333340	-0.333340	0.666660	0.333340	
3	2.000010	-0.000010	0.999990	0.000010	2
4	2.666679	-0.666679	0.333321	0.333321	
5	3.333349	-0.333349	0.666651	0.333349	
6	4.000020	-0.000020	0.999980	0.000020	4
7	4.666690	-0.666690	0.333310	0.333310	
8	5.333360	-0.333360	0.666640	0.333360	
9	6.000030	-0.000030	0.999970	0.000030	6
10	6.666699	-0.666699	0.333301	0.333301	
11	7.333370	-0.333370	0.666630	0.333370	
12	8.000040	-0.000040	0.999960	0.000040	8
13	8.666710	-0.666710	0.333290	0.333290	
14	9.333380	-0.333380	0.666620	0.333380	
15	10.000050	-0.000050	0.999950	0.000050	10

Table 7.5 The minimum absolute residual values for T_2' close to a low number commensurability where $T_2'=0.666677\approx 2/3$.

The underlined rows indicate those integer pairs (A_1,A_2) which form metonic cycles for T_2', within a given accuracy of $q'=0.016932$. Note the very obvious systematic sequence for the minimum absolute residuals.

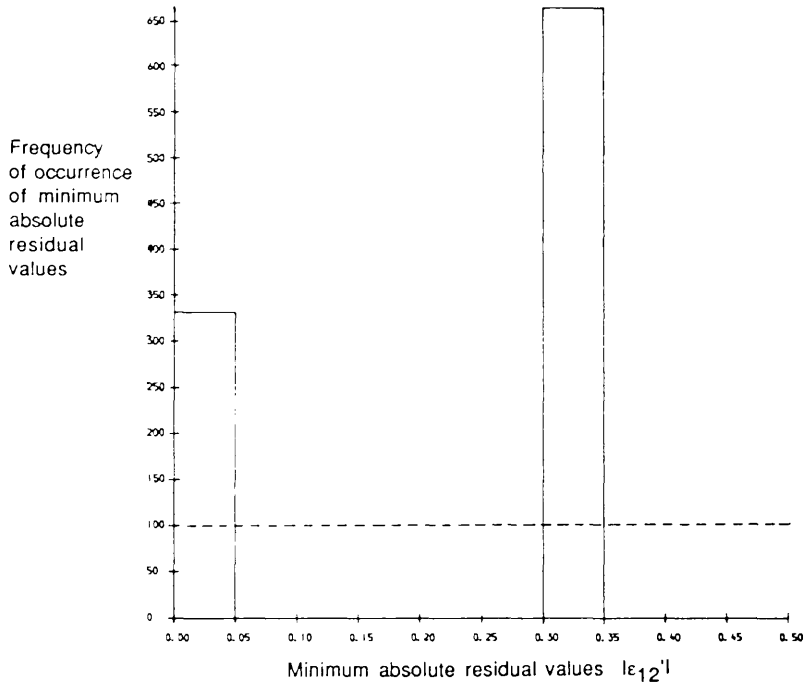

Figure 7.3 The frequency distribution of the minimum absolute residuals for $T_2' = 0.666677 \cong 2/3$. Note it is not a uniform distribution.

The residuals for T_2' far removed from a low number commensurability would therefore appear to act very much like random numbers. Can we use the pseudo-randomness property of the residuals to predict the expected number of metonic cycles for a given T_2' that is not close to a low number commensurability?

Figures 7.4(a) to (d)

The following graphs are:

(i) The frequency distributions of the minimum absolute residuals $|\varepsilon_{12}'|$ and

(ii) the corresponding cyclic relationship between $|\varepsilon_{12}'|$ and the integer A_2. The crosses denote the discrete points of the function.

for four values of T_2' which deviate progressively to a greater extent from a low number commensurability of 2/3.

(a) $T_2' = 0.66673$

(b) $T_2' = 0.6673$

(c) $T_2' = 0.6733$

(d) $T_2' = 0.7333$

Note that as T_2' moves further away from a low number commensurability, $|\varepsilon_{12}'|$ begins to act more like a random variable.

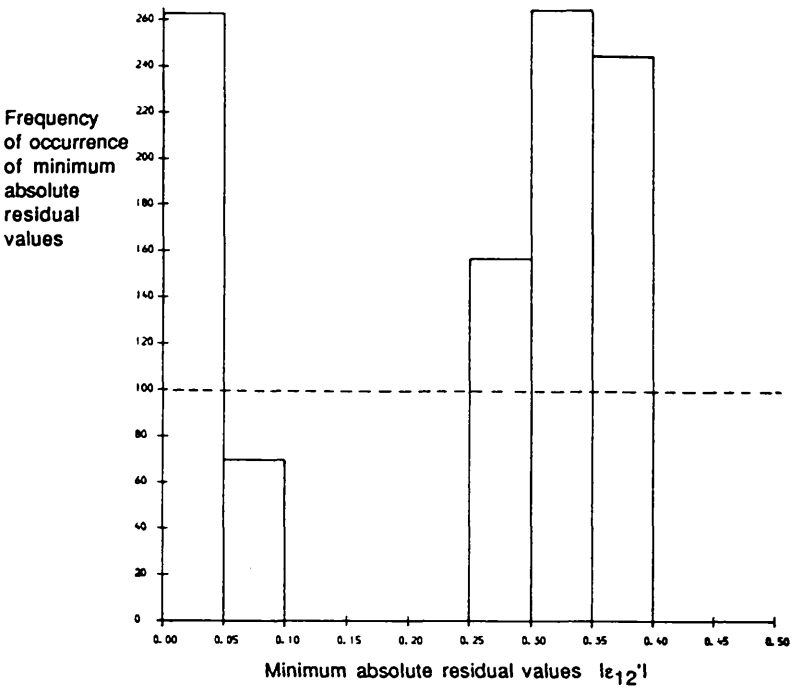
Frequency of occurrence of minimum absolute residual values
260
240
220
200
180
160
140
120
100
80
60
40
20
0
0.00
0.05
0.10
0.15
0.20
0.25
0.30
0.35
0.40
0.45
0.50
Minimum absolute residual values $|\varepsilon_{12}'|$

(a) i

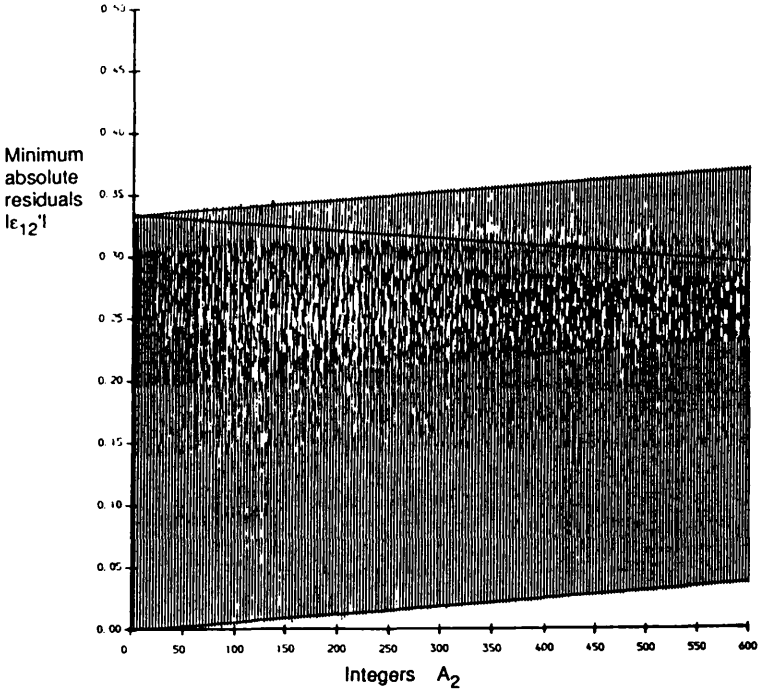
Minimum absolute residuals $|\varepsilon_{12}'|$
0.35
0.20
0.15
0.10
0.05
0.00
0
50
100
150
200
250
300
350
400
450
500
550
600
Integers A_2

(a) ii

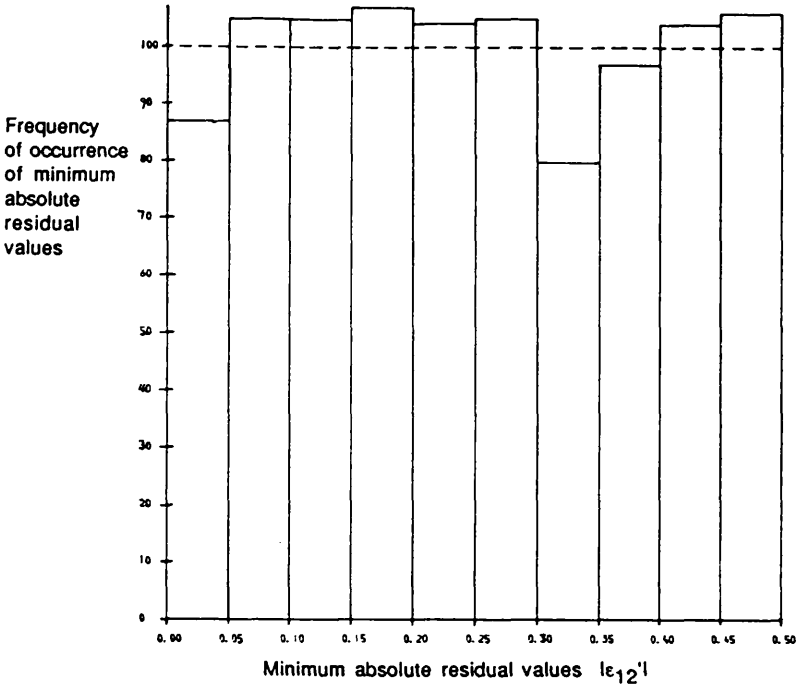
Frequency of occurrence of minimum absolute residual values
100
90
80
70
60
50
40
30
20
10
0
0.00
0.05
0.10
0.15
0.20
0.25
0.30
0.35
0.40
0.45
0.50
Minimum absolute residual values $|\varepsilon_{12}'|$

(b)i

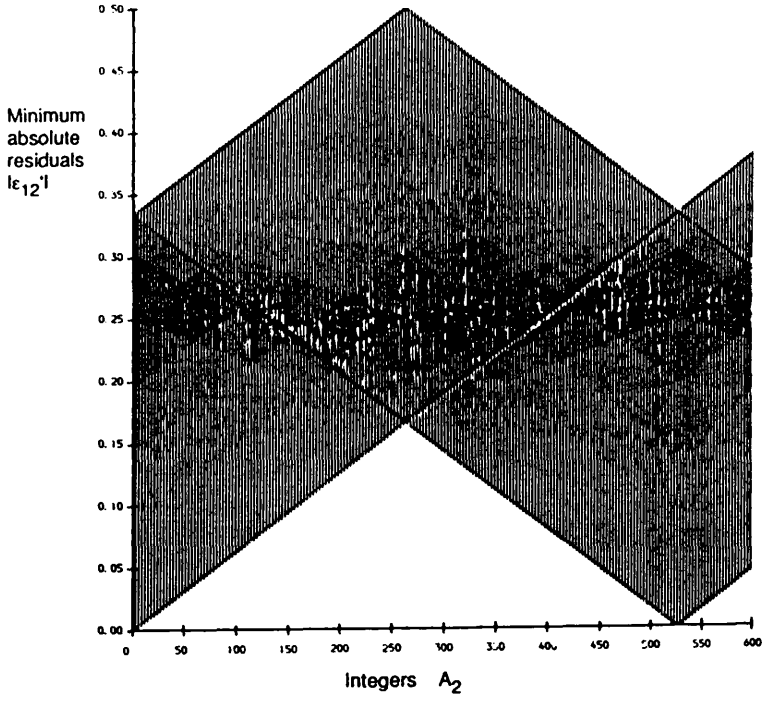
Minimum absolute residuals $|\varepsilon_{12}'|$
0.50
0.45
0.40
0.35
0.30
0.25
0.20
0.15
0.10
0.05
0.00
0
50
100
150
200
250
300
350
400
450
500
550
600
Integers A_2

(b)ii

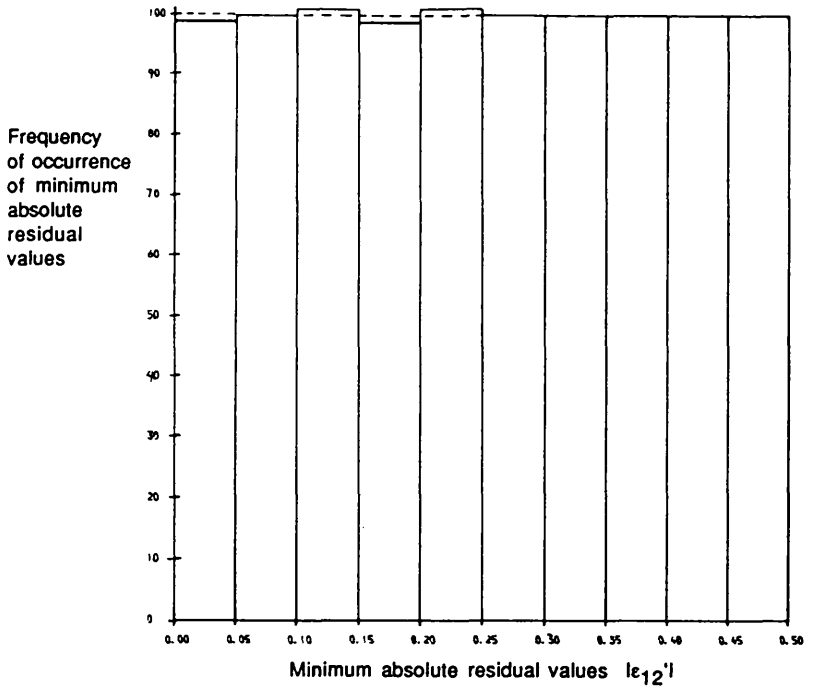
Frequency of occurrence of minimum absolute residual values
100
90
80
70
60
50
40
30
20
10
0
0.00
0.05
0.10
0.15
0.20
0.25
0.30
0.35
0.40
0.45
0.50
Minimum absolute residual values $|\varepsilon_{12}'|$

(c) i

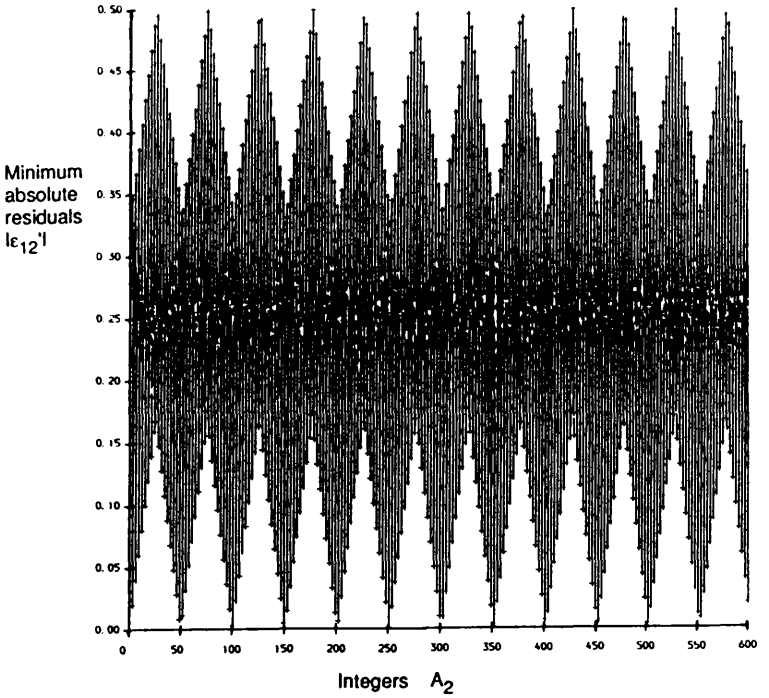
Minimum absolute residuals $|\varepsilon_{12}'|$
0.50
0.45
0.40
0.35
0.30
0.25
0.20
0.15
0.10
0.05
0.00
0
50
100
150
200
250
300
350
400
450
500
550
600
Integers A_2

(c) ii

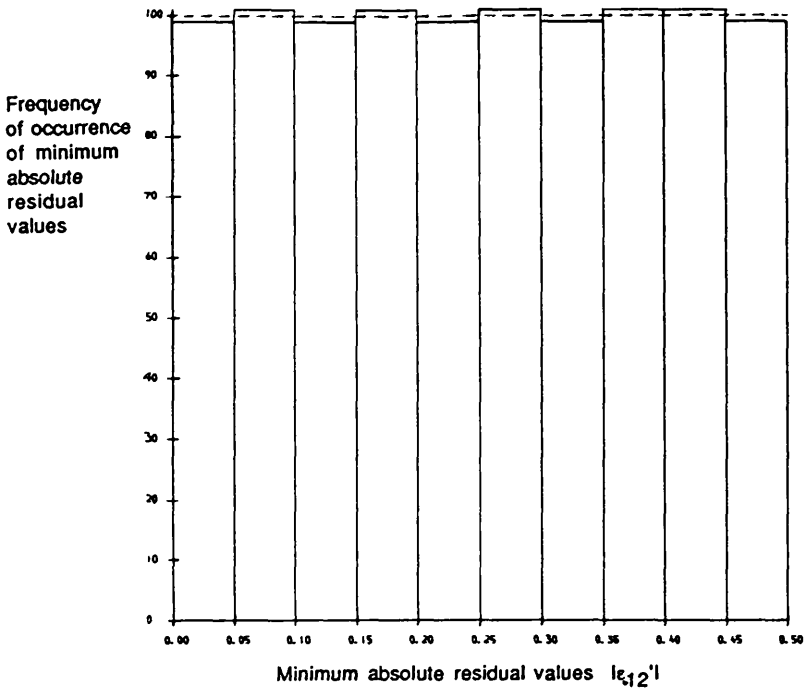
Frequency of occurrence of minimum absolute residual values
100
90
80
70
60
50
40
30
20
10
0
0.00
0.05
0.10
0.15
0.20
0.25
0.30
0.35
0.40
0.45
0.50
Minimum absolute residual values $|\varepsilon_{12}'|$

(d)i

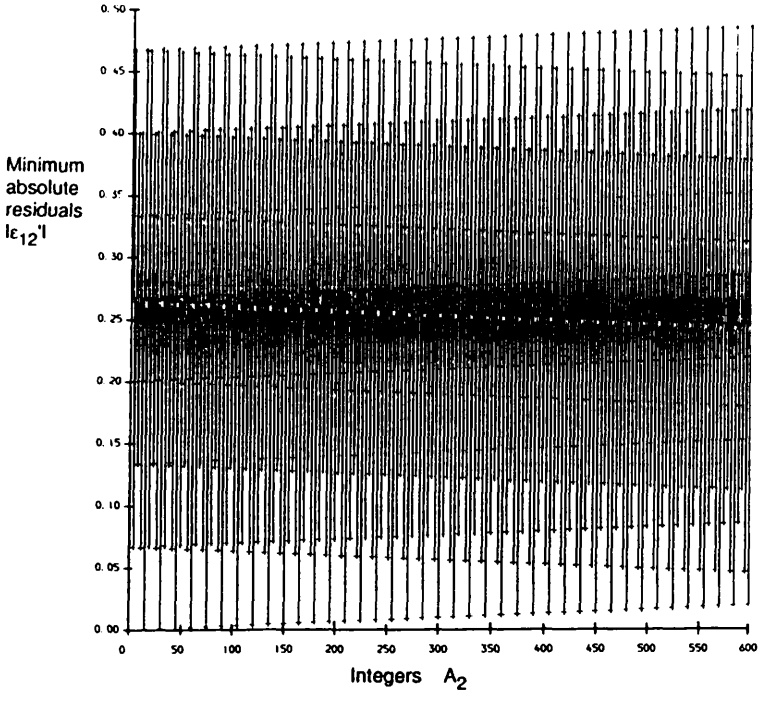
Minimum absolute residuals $|\varepsilon_{12}'|$
0.50
0.45
0.40
0.35
0.30
0.25
0.20
0.15
0.10
0.05
0.00
0
50
100
150
200
250
300
350
400
450
500
550
600
Integers A_2

(d)ii

Let us assume that the residuals for any value of T_2' have a pseudo-random nature. On average this assumption should be valid because T_2' values close to a low number commensurability are much less common than T_2' values far removed from low number commensurabilities.

The problem can then be reworded to ask the following two questions:

(1) What is the probability P that the real value A_2T_2' falls within q' of an integer A_1, where the values A_2T_2' are assumed to fall randomly about the integer A_1 between $-0.5+A_1$ and $0.5+A_1$?

(2) Having found the probability P that a metonic cycle exists near a particular integer A_1, what is the expected total number of metonic cycles, if A_1 and A_2 can be any integers in the range of integers between 0 and A_{max}?

The probability that an event will occur is approximately equal to the relative frequency of occurrence of that event, if a large enough number of trials are made. The probability that a metonic cycle exists near A_1 is therefore given by the following fraction:

$$P = \frac{R_1}{R_2}$$

where R_1 = The size of the region about an integer in which ε_{12}' must be found in order for a metonic cycle to exist.

R_2 = The size of the region about an integer in which ε_{12}' can be located.

Figure 7.5 illustrates the regions R_1 and R_2. The diagram has been centred at the position of an integer A_1.

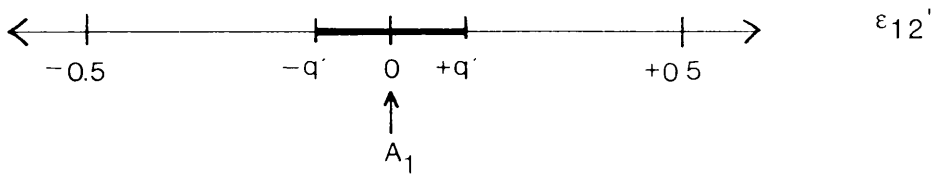

Figure 7.5 The solid line indicates the region, where the residuals ε_{12}' must be located in order for a metonic cycle to exist near the integer A_1. -0.5 and +0.5 indicate the outer boundaries within which the residuals are always found.

The probability P that a metonic cycle exists near an integer A_1 is therefore given by:

$$P = 2q'$$

The expected number of events is the probability that one of the events will occur multiplied by the number of attempts at making the event occur. Thus the expected number of metonic cycles N is given by:

$$N = PN_1N_2$$

where N_1 = the number of times the real value A_2T_2' falls within 0.5 range of a specific integer A_1.

N_2 = the number of integers A_1 that are accessible to the real values A_2T_2'.

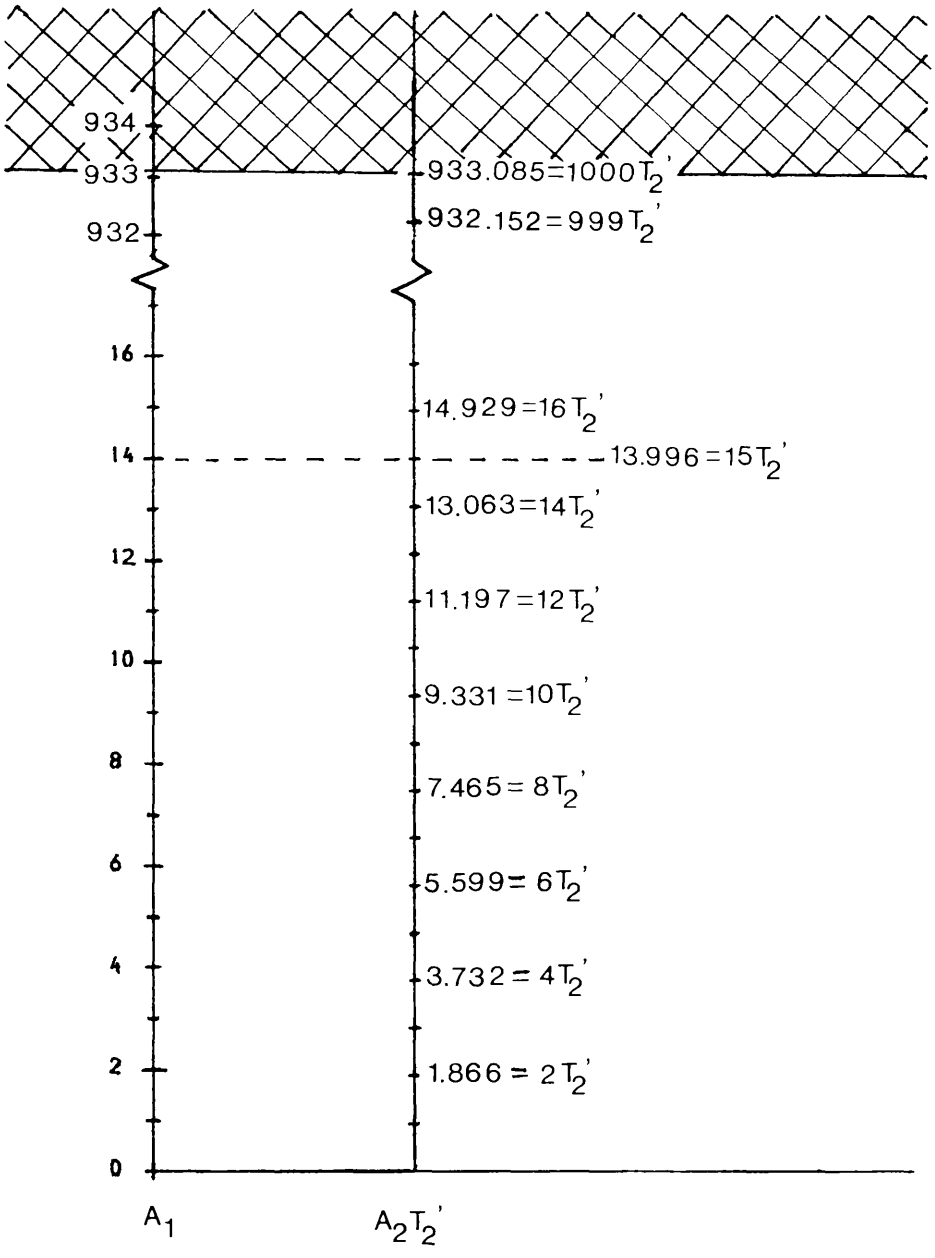

Figure 7.6 Another graphical look at Table 7.1. Column 1 contains the possible integers A_1, while column 2 contains the real values A_2T_2' graphed to the same scale as in column 1.

A metonic cycle occurs whenever A_1 and A_2T_2' equal each other to within an accuracy of q' = 0.016932. The dashed regions indicate the metonic cycles. No metonic cycle can exist in the cross-hatched region because A_1 and A_2 must be less than A_{max}.

We can describe what is occurring using another graphical method shown in Figure 7.6. The integers A_1 from zero to A_{max} are marked in the first column, while the real values A_2T_2' are marked in the second column to the same scale. Wherever a real value A_2T_2' comes within q' of an integer A_1, a metonic cycle occurs. These points are highlighted. In a sense, we can think of the second column of marks as attempts at 'hitting' an integer A_1 in the first column (ie coming to within q' of the integer).

Each integer A_1 may have more than one attempt made by the marks in the second column at hitting it, depending on the size of T_2' relative to 1.0 Thus,

$$N_1 = \frac{1}{T_2}$$

The number N_2 of integers A_1 that are accessible to the values A_2T_2' is constrained by the restriction $A_1<A_2<A_{max}$ arising from the ordering of the periods. Given that $A_1 \approx A_2T_2'$, the largest possible integer A_1 that A_2T_2' can approach is approximately $A_{max}T_2'$. Figure 7.6 shows this cut-off point more clearly. Thus

$$N_2 = T_2' A_{max}$$

Hence N becomes

$$N = 2q' A_{max} \qquad (5)$$

It is interesting to note that N does not ultimately depend on the value of T_2'. In Section 7.2 (ii) we remarked that there seemed to be two opposing effects involving T_2' where:

(1) As T_2' decreases the number of metonic cycles increases, because there are a larger number of integers A_2 which when divided into the same integer A_1 come close to the value T_2'. This is equivalent to our statement $N_1 = 1/T_2'$.

(2) As T_2' decreases the number of metonic cycles also decreases, because the possible values for A_2 rapidly approach the upper limit A_{max} before a set of simple fractions A_1/A_2 can be found to approximate T_2'. This is equivalent to our statement $N_2 = T_2' A_{max}$.

It is obvious that the expected number of metonic cycles should be proportional to q' and A_{max} because at least one metonic cycle can always be found for any given period set (T_1, T_2), if A_{max} is allowed to become large enough, or if conditions on the accuracy q' of a near metonic cycle are relaxed enough.

Equation (5) gives the expected number of near metonic cycles given an upper integer limit of A_{max}, an accuracy criterion q' and a period set (T_1,T_2) which is not close to a low number commensurability. The actual number of metonic cycles for a given T_2' may vary considerably from that predicted by Equation (5) if T_2' is close to a low number commensurability, and the assumption that the residuals ε_{12}' are pseudo-random numbers is no longer valid. The occurrence of low number commensurabilities is, however, highly improbable. The number of metonic cycles should therefore, on average, agree with that predicted by Equation (5).

In the next section we look at the dispersion of the actual values from the predicted value of the number of metonic cycles, and discuss whether or not there is any statistical evidence for the validity of Equation (5).

7.3 Numerical Experiments for the Frequency of Occurrence of Metonic Cycles

The theory for the frequency of occurrence of metonic cycles has been tested against many numerical experiments where the actual numbers of metonic cycles have been found for a random sampling of period sets (T_1,T_2), a range of accuracies q' and a range of integer upper limits A_{max}. For each set of experiments the accuracy q' and the integer upper limit A_{max} are pre-arranged. Real numbers between 0 and 1 are chosen randomly to be the ratio T_2' of the two periods T_1 and T_2. In this manner, the random numbers T_2' represent the full range of ratios of T_S, T_A or T_N possible for any satellite that might be found in the solar system's present, past or future.

The computer then performs calculations of the type described in Section 7.2(i), finding the number of metonic cycles that occur for each ratio T_2'. The frequency distribution of the numbers of metonic cycles occurring for the random sampling of T_2' is plotted in the form of a relative frequency histogram, where the relative frequency is defined to be the number of samplings which have a metonic cycle count in the specified interval, divided by the total number of random samples taken. The use of relative frequencies removes from the resulting frequency distribution any dependence on the sample size and therefore facilitates comparisons between different frequency distributions.

The relative frequency distributions of metonic cycle counts for a range of accuracies q' and integer upper limits A_{max} are shown in Figures 7.7. The predicted number of metonic cycles varies with each histogram in Figure 7.7 depending on the values chosen for q' and A_{max}.

Figures 7.7 (a) to (o)

Show the relative frequency distributions of metonic cycle counts occurring for a range of accuracies q' and integer upper limits A_{max}. Each histogram consists of a random sampling of 100 values of T_2'. μ is the expected number of metonic cycles for the given q' and A_{max}, where $\mu = 2\,q'\,A_{max}$. $\bar{X}_T$ is the 10% trimmed mean number of metonic cycles and $\bar{X}_{Tb}$ is the same trimmed mean adjusted for bias.

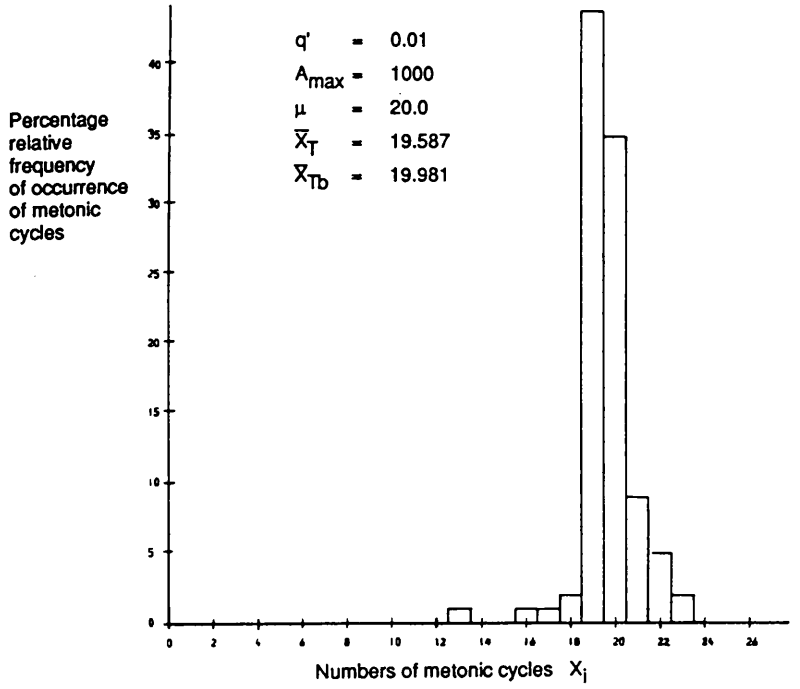

(a)

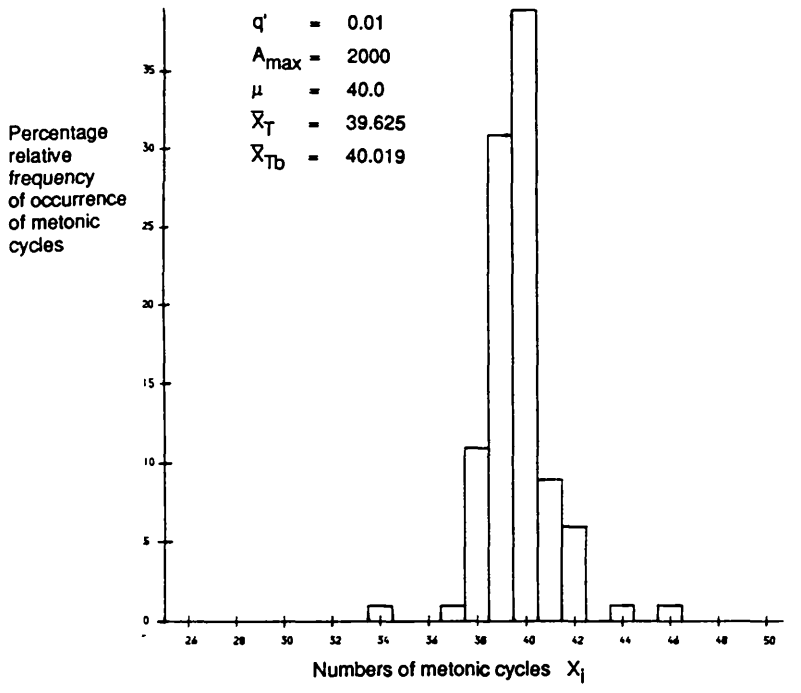
q' = 0.01
A_{max} = 2000
μ = 40.0
$\bar{X}_T$ = 39.625
$\bar{X}_{Tb}$ = 40.019
Percentage relative frequency of occurrence of metonic cycles
Numbers of metonic cycles X_i

(b)

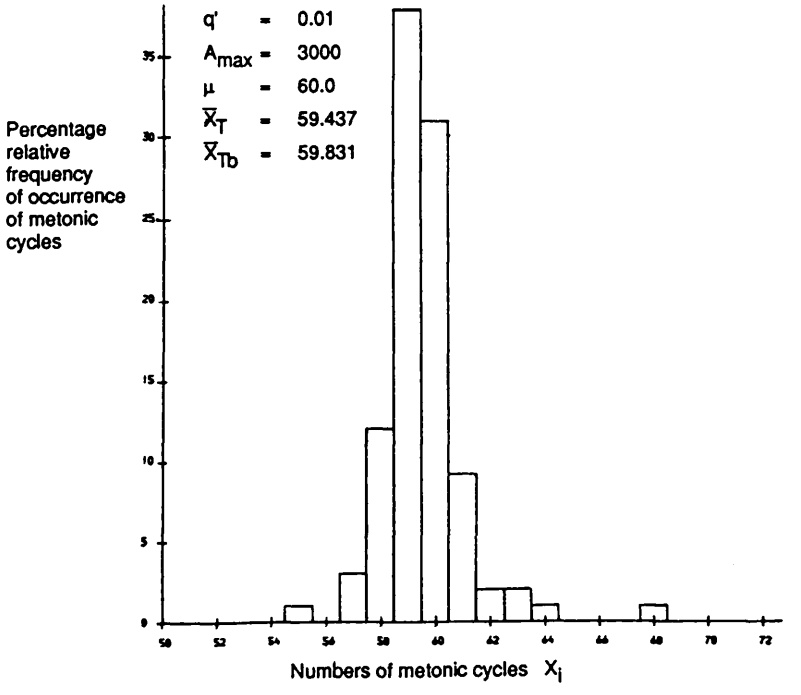
q' = 0.01
A_{max} = 3000
μ = 60.0
$\bar{X}_T$ = 59.437
$\bar{X}_{Tb}$ = 59.831
Percentage relative frequency of occurrence of metonic cycles
Numbers of metonic cycles X_i

(c)

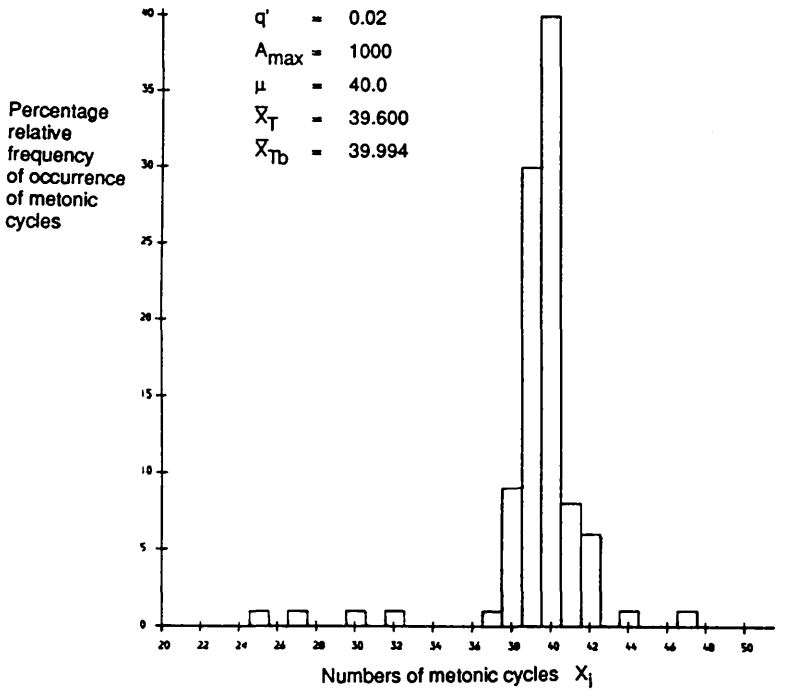
q' = 0.02
A_{max} = 1000
μ = 40.0
$\bar{X}_T$ = 39.600
$\bar{X}_{Tb}$ = 39.994
Percentage relative frequency of occurrence of metonic cycles
Numbers of metonic cycles X_i

(d)

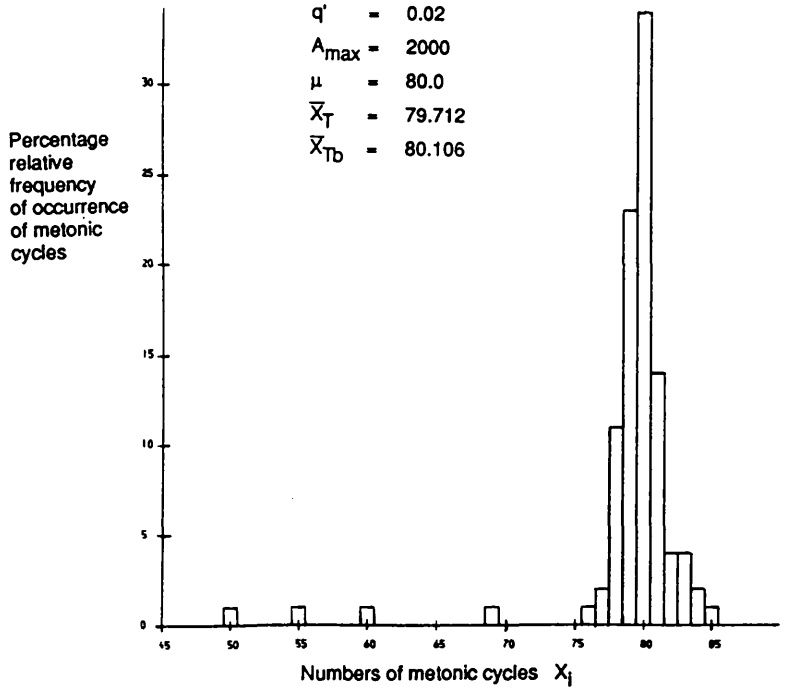
q' = 0.02
A_{max} = 2000
μ = 80.0
$\bar{X}_T$ = 79.712
$\bar{X}_{Tb}$ = 80.106
Percentage relative frequency of occurrence of metonic cycles
Numbers of metonic cycles X_i

(e)

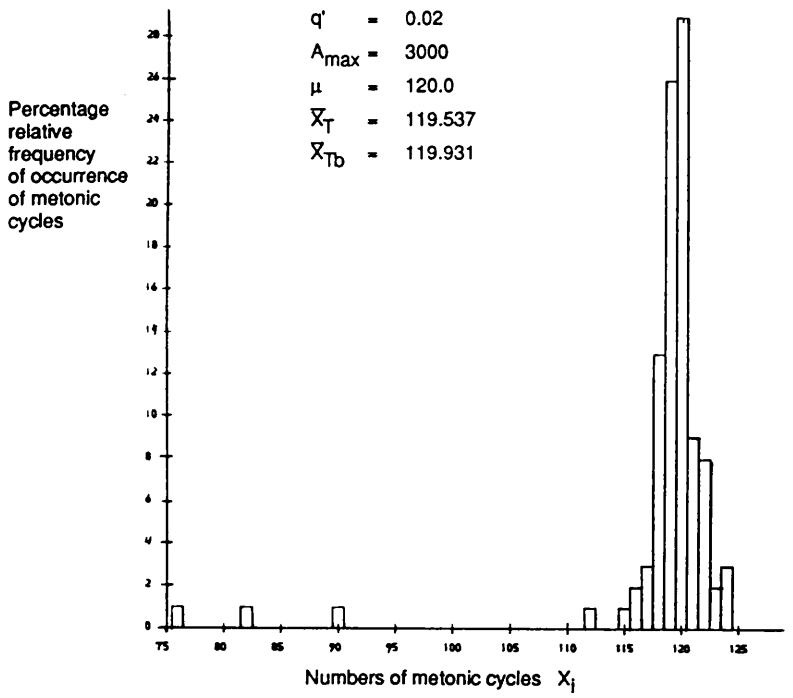
q' = 0.02
A_{max} = 3000
μ = 120.0
$\bar{X}_T$ = 119.537
$\bar{X}_{Tb}$ = 119.931
Percentage relative frequency of occurrence of metonic cycles
Numbers of metonic cycles X_i

(f)

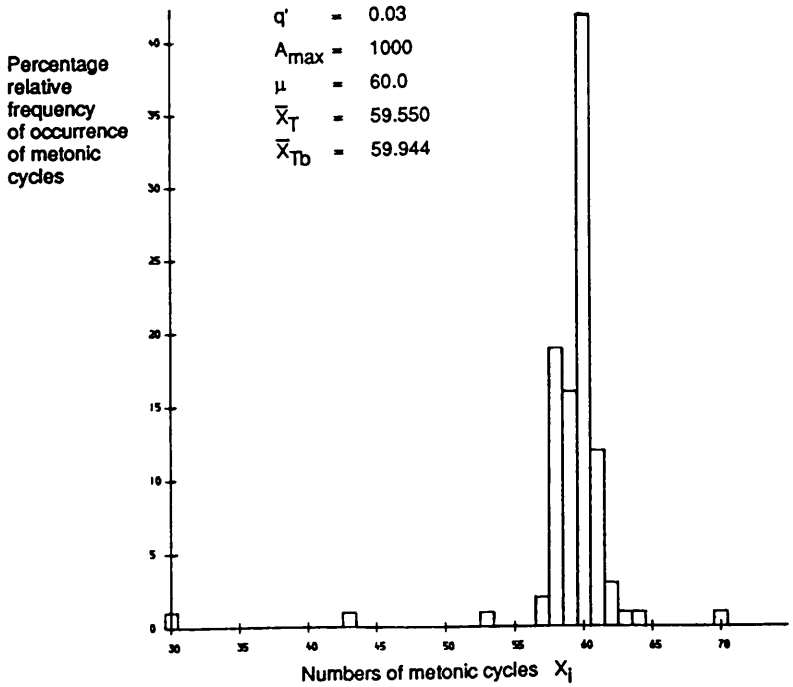
q' = 0.03
A_{max} = 1000
μ = 60.0
$\bar{X}_T$ = 59.550
$\bar{X}_{Tb}$ = 59.944
Percentage relative frequency of occurrence of metonic cycles
Numbers of metonic cycles X_i

(g)

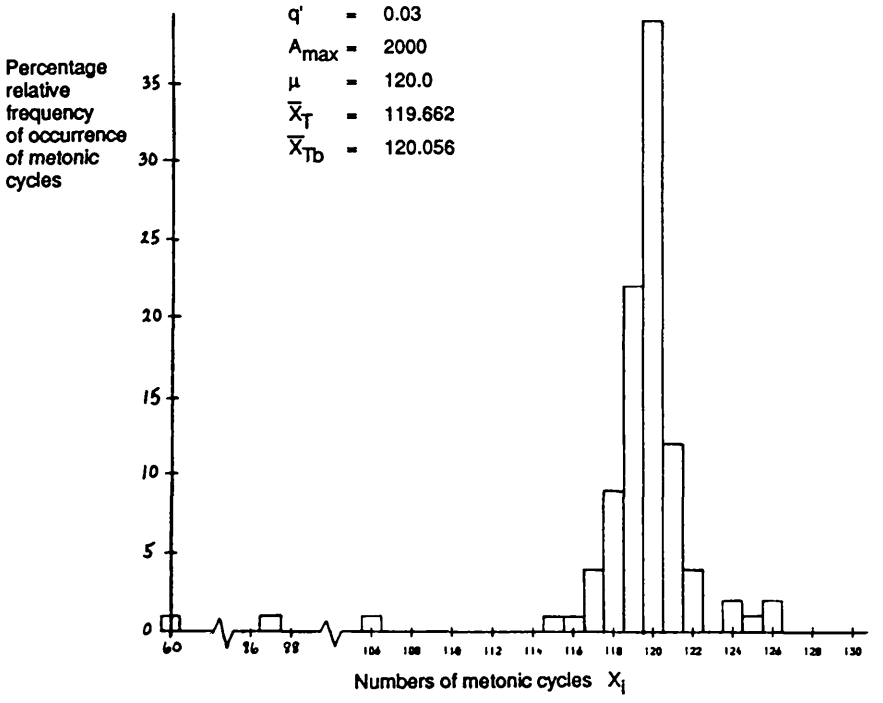
q' = 0.03
A_{max} = 2000
μ = 120.0
$\bar{X}_T$ = 119.662
$\bar{X}_{Tb}$ = 120.056
Percentage relative frequency of occurrence of metonic cycles
Numbers of metonic cycles X_i

(h)

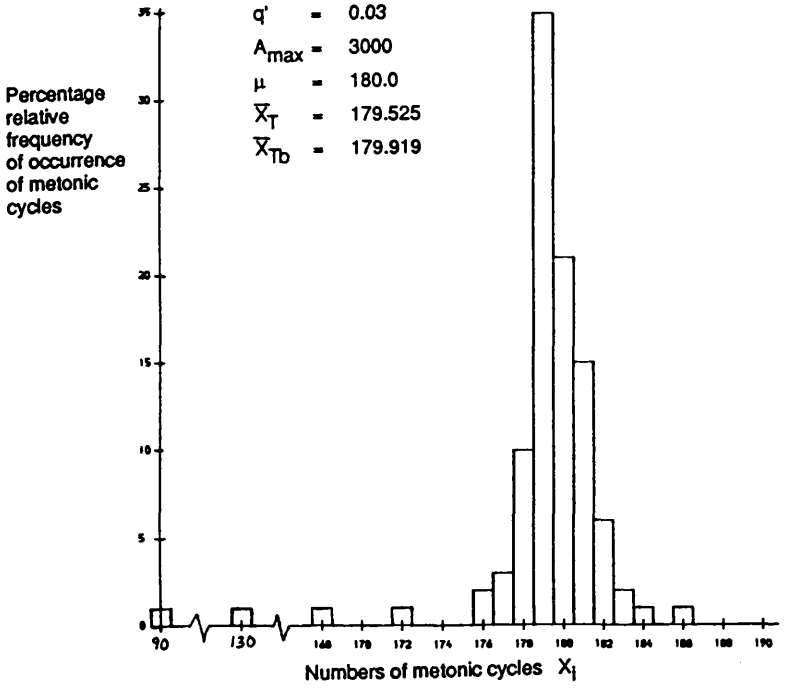
q' = 0.03
A_{max} = 3000
μ = 180.0
$\bar{X}_T$ = 179.525
$\bar{X}_{Tb}$ = 179.919
Percentage relative frequency of occurrence of metonic cycles
Numbers of metonic cycles X_i

(i)

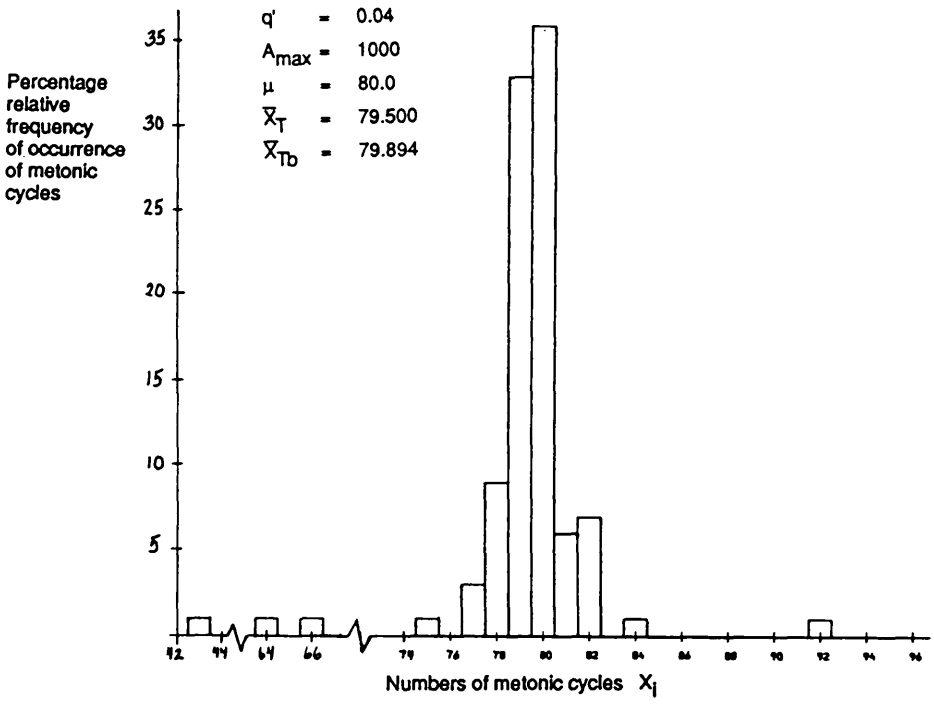
q' = 0.04
A_{max} = 1000
μ = 80.0
$\bar{X}_T$ = 79.500
$\bar{X}_{Tb}$ = 79.894
Percentage relative frequency of occurrence of metonic cycles
35
30
25
20
15
10
5
Numbers of metonic cycles X_i

(j)

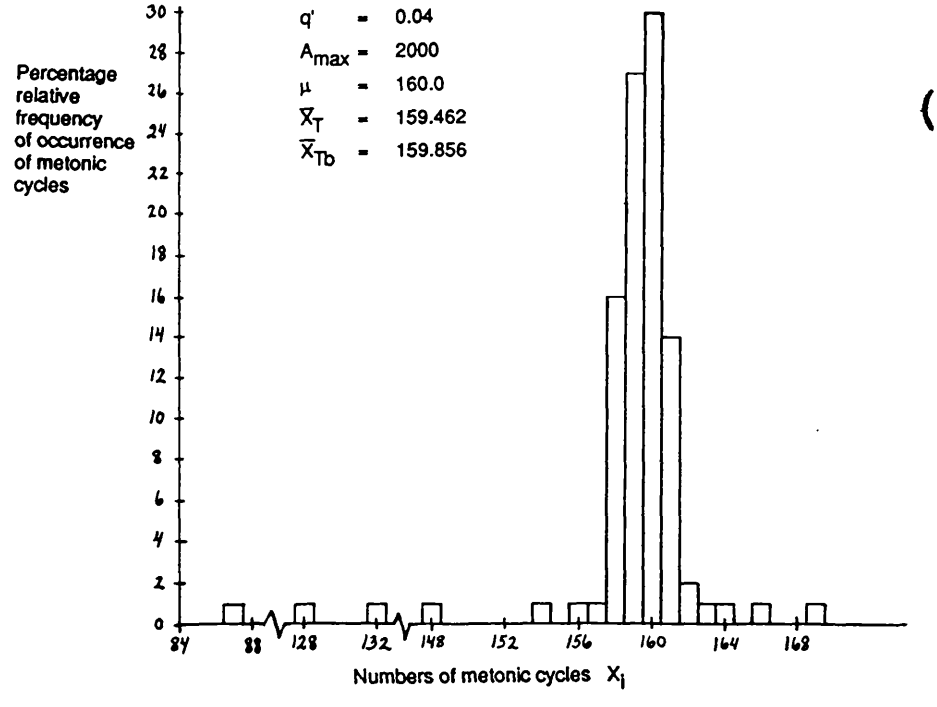
q' = 0.04
A_{max} = 2000
μ = 160.0
$\bar{X}_T$ = 159.462
$\bar{X}_{Tb}$ = 159.856
Percentage relative frequency of occurrence of metonic cycles
30
28
26
24
22
20
18
16
14
12
10
8
6
4
2
0
84
88
128
132
148
152
156
160
164
168
Numbers of metonic cycles X_i

(k)

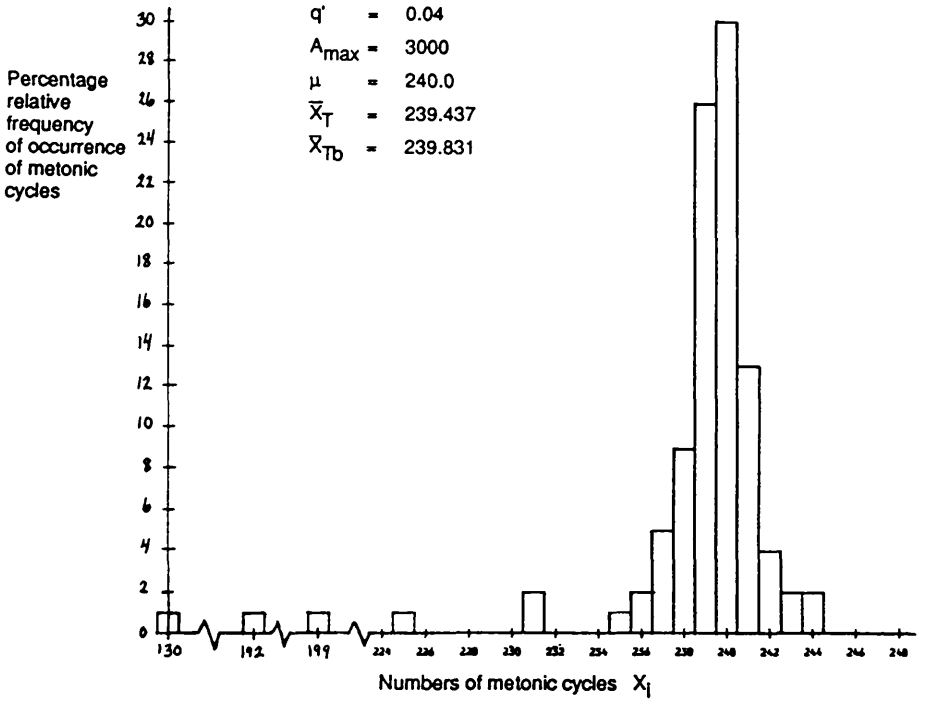
q' = 0.04
A_{max} = 3000
μ = 240.0
$\bar{X}_T$ = 239.437
$\bar{X}_{Tb}$ = 239.831
Percentage relative frequency of occurrence of metonic cycles
Numbers of metonic cycles X_i

(l)

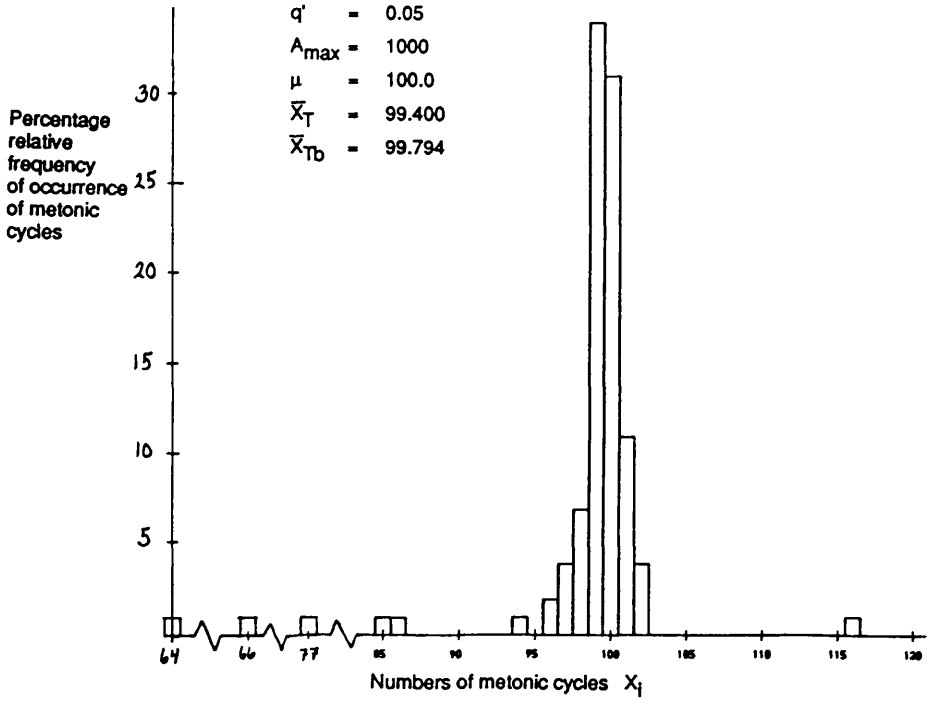
q' = 0.05
A_{max} = 1000
μ = 100.0
$\bar{X}_T$ = 99.400
$\bar{X}_{Tb}$ = 99.794
Percentage relative frequency of occurrence of metonic cycles
Numbers of metonic cycles X_i

(m)

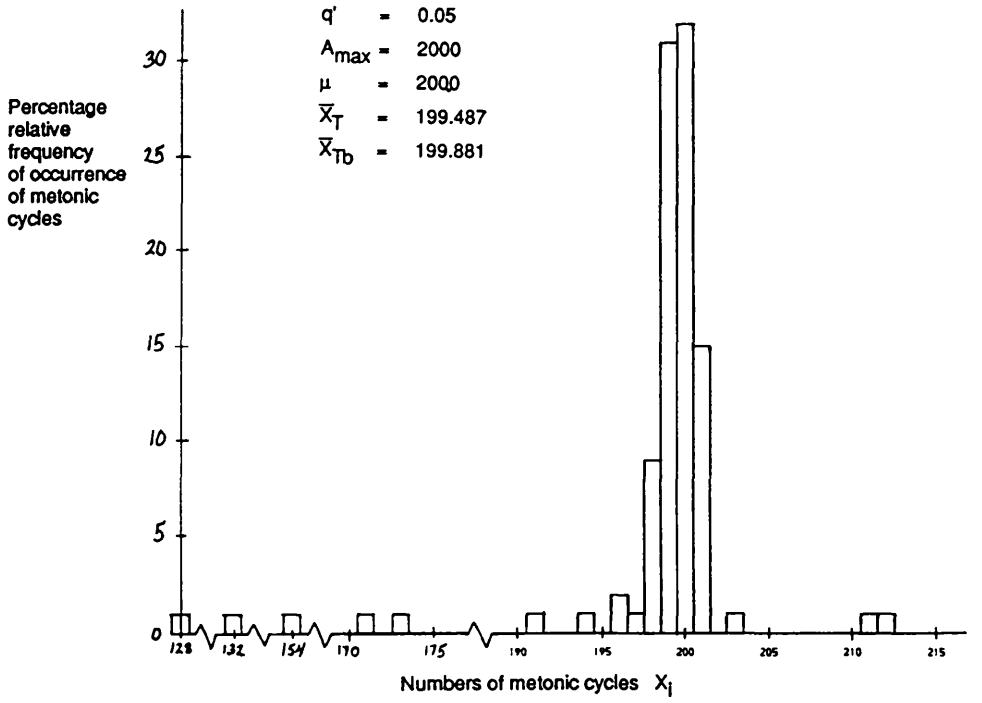
q' = 0.05
A_{max} = 2000
μ = 2000
$\bar{X}_T$ = 199.487
$\bar{X}_{Tb}$ = 199.881
Percentage relative frequency of occurrence of metonic cycles
30
25
20
15
10
5
0
128
132
154
170
175
190
195
200
205
210
215
Numbers of metonic cycles X_i

(n)

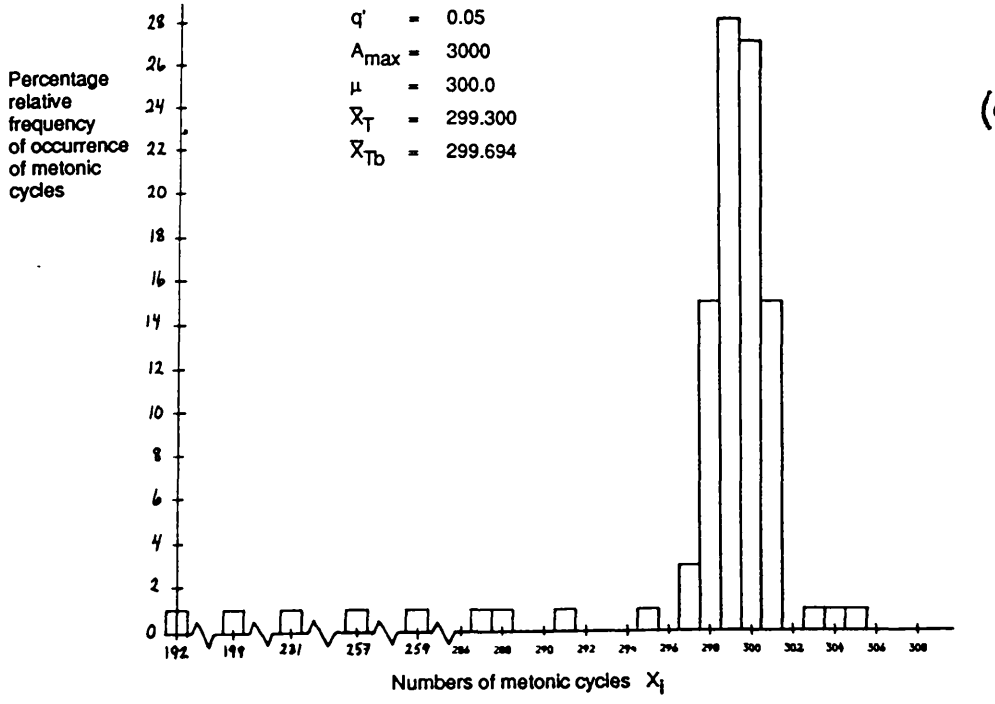
q' = 0.05
A_{max} = 3000
μ = 300.0
$\bar{X}_T$ = 299.300
$\bar{X}_{Tb}$ = 299.694
Percentage relative frequency of occurrence of metonic cycles
28
26
24
22
20
18
16
14
12
10
8
6
4
2
0
192
199
231
257
259
286
288
290
292
294
296
298
300
302
304
306
308
Numbers of metonic cycles X_i

(o)

We can see that the relative frequency distributions are nearly normal; however, they appear to be slightly skewed and display much longer and thicker tails than would be expected if the distribution were truely normal. These deviations from the norm are caused by randomly choosing a period set T_2' near a low number commensurability and thus producing a count far higher or lower than expected. In a sense, our data is contaminated by these low number commensurabilities which are not taken into consideration in our predicted value for the number of metonic cycles. Skewness and long-tailedness are common features of real data that theoretically should exhibit normal distributions.

The best estimators of location and scale for normal data are unquestionably the mean and the standard deviation respectively. One can then use normal statistical methods to find confidence intervals for any data value and student t statistics to test the accuracy of any predicted value. Here we take the sample mean $\bar{X}$ and the sample standard deviation s for a data sample of size n and values X_i to be:

$$\bar{x} = \frac{1}{n} \sum_{i=1}^{n} x_i$$

$$s^2 = \frac{1}{n-1} \sum_{i=1}^{n} (x_i - \bar{x})^2$$

The student t statistic is defined as:

$$t = \frac{\bar{x} - \mu}{SE_{\bar{x}}} \qquad \text{and} \qquad SE_{\bar{x}} = \frac{s}{\sqrt{n}}$$

where μ is the expected or predicted value of $\bar{X}$ and $SE_{\bar{X}}$ is the estimated standard error of the sample mean.

Applying normal statistics to near normal data can however, cause serious errors in the final conclusions about the location and scale of the data, especially for those non-normal distributions which are long-tailed. One can see from the formulae that the sample mean $\bar{X}$ and the sample standard deviation s are both very sensitive to outliers in the data sample. If there are an unexpectedly high proportion of points

lying in the tails of the distribution or if the distribution is assymetric, the sample mean and sample standard deviation may be poor estimators of the location and scale of the data.

The problem of the outliers can be avoided by trimming the outliers from each side of the sample before calculating the sample mean and sample variance. This procedure of forming a trimmed mean has actually been in use for approximately the last two centuries of scientific analysis. One can also use many of the other more complicated estimators developed by statisticians which have the common property of attempting to assign less weight to the extreme observations and more weight to the middle observations so as to safeguard against the effect of long and heavy-tailedness.

In recent years statisticians have made several studies of the robustness of the many different estimators of location and scale that exist. In other words, they have been searching for estimators whose properties remain reasonably constant for a variety of non-normal distribution types that differ from the normal distribution only by the small amounts commonly found in practice.

Tukey (1960) in "A Survey of Sampling From Contaminated Distributions" studied the behaviour of estimators of location and scale for those distributions that were just barely detectable as non-normal distributions. He discovered that the effects could be rather large. To mirror the possible long-tailedness of real data, he used one computer generated normal distribution to contaminate to varying degrees another computer generated normal distribution of the same mean, but different variance. Andrews D F, Biekel P J, et al (1972) expanded on Tukey's studies to complete a comprehensive survey analysing the robustness of over 65 robust estimators.

Using a different approach, Stigler (1977) asked the question: "Which robust estimators work best for <u>real</u> data?", as opposed to the 'phoney' real data generated pseudo-randomly by computers. On the premise that the properties of pseudo-randomly generated samples may not necessarily be characteristic of real data, he evaluated the performance of several robust estimators using data sets recorded by 18^{th} and 19^{th} century scientists who were measuring physical quantities which may not have been well determined at the time of the experiments, but which are assumed to be known today to within the accuracy of the original measurements.

In particular, Stigler (1977) based his study on data taken from James Short's 18th century attempt at measuring the distance from the Earth to the Sun, Michelson and Newcomb's investigations into the speed of light performed in the years 1879-82, and Cavendish's 1798 experiment searching for the mean density of the Earth.

In all of these studies it was discovered that the trimmed mean, despite its simplicity and its arbitrary use for 200 years, was one of the best robust estimators in statistics for slightly contaminated, long-tailed distributions. Tukey and McLaughlin (1963) developed a set of rigorous statistical procedures for the treatment of long-tailed distributions using the trimmed mean and a technique first introduced by C. P. Winsor called Winsorization. We shall use their approach to analyse our contaminated metonic cycle count data.

The treatment begins with the assumption that, although the probability distribution does not necessarily have to be normal, it should be symmetric. Tukey and McLaughlin go on to add that small assymetries will not, however, affect the results too adversely. If the probability distribution is symmetric, the p% trimmed mean $\bar{X}_T$ should coincide with the actual mean μ.

The p% trimmed mean is found by eliminating the outermost p% of the observations from each side of the data set. If p% of the total data sample of size n is not a whole number, the number to be trimmed off is traditionally rounded up to the next integer. The remaining data values make up a trimmed sample of size h.
The trimmed mean then becomes the mean of the trimmed sample:

$$\bar{x}_T = \frac{1}{h} \sum_{i=1}^{h} x_i$$

Tukey and McLaughlin show that for large samples, the p% trimmed data has approximately a normal distribution. Thus, as with normal distributions, we can use the Student t-statistic to gauge the accuracy of a predicted location value μ.

But first we must determine what form the standard error $SE_{\bar{X}_T}$ of the trimmed mean takes. Instinctively, one would suggest finding the standard deviation of the trimmed sample and dividing by h, but Tukey and McLaughlin have developed a version

of the standard error which utilises the near normalness of the p% trimmed data to better advantage.

Their method is based on a winsorized standard deviation s_w which is found by replacing the eliminated outlying data values with the value of the next point from each side, in line for trimming. The winsorized standard deviation is simply the standard deviation of the newly winsorized data sample of size n.

The standard deviation of the trimmed sample s_T based on the winsorized standard deviation is then calculated using the expression:

$$s_T = \sqrt{\frac{(n-1)}{(h-1)} s_W{}^2}$$

and the standard error of X_T becomes:

$$SE_{\bar{x}_T} = \frac{s_T}{\sqrt{h}}$$

The Tukey and McLaughlin method of finding a trimmed standard deviation is better than one using only a truncated sample because it reduces the possible errors caused by over-trimming the data sample.

In summary, the theory involving the trimmed mean $\overline{X}_T$ is the same as that of the ordinary mean $\overline{X}$ except the quantities n, $\overline{X}$, and s are replaced with their trimmed mean counterparts h, $\overline{X}_T$ and s_T. Hence the trimmed mean t-statistic t_T becomes:

$$t_T = \frac{\bar{x}_T - \mu}{SE_{\bar{x}_T}}$$

For large samples of size $n \geq 30$ the student's t-distribution approaches that of the normal distribution. A 95% confidence interval for a two-tailed hypothesis test can then be constructed to test whether or not it is probable that μ is the mean of the data sample. Table 1 in Appendix A gives the critical values z for the standard normal

distribution.

From Table 1, we see that Z=t for large samples will lie outside the interval $|Z| \geq z = 1.96$ with a probability of 5%. Therefore in the unlikely event that the value t does fall outside the range (-1.96,1.96), we can say that there is sufficient evidence, to a significance level of 0.05, against the hypothesis that the mean of the data sample equals μ. The trimmed mean t statistic can be used in a similar manner as the standard t statistic in order to construct confidence intervals or hypothesis tests.

For samples of size $n \leq 30$, Table 2 of Appendix A gives the critical values for confidence intervals and hypothesis tests based on Student's t-distribution where the degrees of freedom ν and the sample size n are related by the expression:

$$\nu = n-1$$

The following example clarifies the use of trimmed means in the forming of confidence intervals and hypothesis tests.

Question:

The mean of a particular data set is predicted to be $\mu = 0.54$. Does the following data sample support this hypothesis? Find a 95% confidence interval for the 10% trimmed mean of the data sample in order to answer this question.

Data Sample

0.10
0.31
0.43 0.43
0.51 0.53 0.53 0.57 0.58 0.59
0.62 0.67 0.69
0.73 **0.74**
0.92

Answer:

Ten percent of the sample size is 0.10 x 16 = 1.6 which is rounded up to 2.0. Therefore, the two smallest and two largest values (ie those highlighted in bold in the data sample) are trimmed from the sample. This leaves a trimmed sample of size h=12. The 10% trimmed mean is then the sample mean of the remaining values

$$\overline{X}_T = 0.57333$$

The sample is winsorized by replacing each of the highlighted outliers with the next value that would be trimmed (ie the boxed numbers) on either side. Thus the data sample becomes:

Data Sample

0.43
0.43
0.43 0.43
0.51 0.53 0.53 0.57 0.58 0.59
0.62 0.67 0.69
0.73 0.73
0.73

The standard deviation of the winsorized sample is:

$$s_w = 0.01122$$

Then the standard deviation of the trimmed sample becomes:

$$s_T = \sqrt{\frac{(16-1)}{(12-1)}(0.1122)^2} = 0.1311$$

The standard error of the trimmed mean is

$$SE_{\bar{x}_T} = \frac{0.1311}{\sqrt{12}} = 0.03784$$

and the t-statistic for the trimmed data sample is

$$t = \frac{0.57333 - 0.54}{0.03784} = 0.8808$$

For a sample of size h = 12, the Student t distribution has $\nu = 12 - 1 = 11$ degrees of freedom and the 95% critical value read from Table 2, Appendix A is z=2.201. Therefore since $|t = 0.8808| < 2.201$, we can say that there is sufficient evidence to within a 0.05 significance level to support the hypothesis that $\mu = 0.54$ is the mean of the data sample.

There is no general rule about choosing a value for the trimming fraction p. Statisticians have recommended anything from 5% to 25% depending on the extent of the contamination found in the data. The best choice for p is one which just removes all the outliers. A trimming fraction of about 10% seems to produce good results for most data sets and indeed works well with our metonic cycle count distributions.

The results of our numerical experiments for a range of accuracies q' and upper integer limits A_{max} are summarized in Table 7.6. The first three columns (the 10% trimmed mean, standard deviation, and t statistic) are the statistics that describe the 10% trimmed frequency distributions of the number of metonic cycles, while the final two columns (the skewness and the curtosis) describe how closely the 10% trimmed frequency distribution approaches 'normality'.

The skewness of a distribution measures the distribution's symmetry, while the curtosis of a distribution measures the thickness of its centre relative to the thickness of its tails. Skewness S_K and curtosis K are defined mathematically to be:

$$S_k = \frac{m_3}{m_2^{3/2}}$$

$$K = \frac{m_4}{m_2^{2}}$$

where $$m_r = \frac{1}{n}\sum_{i=1}^{n}(x_i - \bar{x})^r$$

$$r = 2,3,4$$

If the distribution is normal, the limits within which S_K and K have a 95% chance of being found are given in Table 3 of Appendix A. For a sample size of 80. which is the size of all our trimmed data sets, these limits are

$$-0.5223 \leq S_K \leq +0.5208$$

$$+2.2078 \leq K \leq +4.1358$$

Those values of skewness and curtosis which fail the normality test are underlined in Table 7.6.

From Table 7.6, we can see that for most of the data sets, a 10% trimming has resulted in frequency distributions closely resembling those of the normal distribution. This allows us to apply the p% trimmed normal statistical methods of Tukey and McLauglin (1963) to find the 10% trimmed mean number of metonic cycles $\overline{X}_T$, its corresponding 10% trimmed standard deviation s_T and the 10% t-statistic t_T which measures how likely our predicted number of metonic cycles represents the 10% trimmed mean of the sample.

Relative accuracy q'	Integer upper limit A_{max}	Expected mean no. of metonic cycles $\mu = 2q' A_{max}$	10 % trimmed statistics				
			$\bar{X}_T$	s_T	t_T	S_k	K
0.005	1000	10	9.475	1.012	-4.638	−0.407	2.716
	3000	30	29.500	1.061	-4.213	0.184	2.586
0.01	500	10	9.587	0.802	-4.601	0.406	2.289
	1000	20	19.587	0.833	-4.430	0.583	2.399
	1500	30	29.625	1.019	-3.291	0.143	2.651
	2000	40	39.625	1.032	-3.252	0.007	2.741
	2500	50	49.650	1.065	-2.939	0.117	2.526
	3000	60	59.437	1.048	-4.801	0.119	2.758
0.015	500	15	14.812	0.818	-2.050	0.178	2.381
	1000	30	29.662	1.322	-2.283	0.442	2.604
	1500	45	44.575	1.269	-2.996	0.674	3.418
	2000	60	59.650	1.325	-2.363	0.094	2.880
	2500	75	74.762	1.152	-1.844	0.115	1.974
	3000	90	89.475	1.174	-3.998	0.075	2.253
0.02	500	20	19.525	1.061	-4.004	0.282	2.647
	1000	40	39.600	1.034	-3.461	−0.140	2.820
	1500	60	59.687	1.141	-2.449	−0.102	2.362
	2000	80	79.712	1.369	-1.878	−0.097	2.556
	2500	100	99.787	1.125	-1.689	−0.142	2.389
	3000	120	119.537	1.450	-2.852	0.296	2.716
0.025	1000	50	49.600	0.996	-3.591	0.325	2.556
0.03	500	30	29.525	1.061	-4.004	0.098	2.672
	1000	60	59.550	1.174	-3.429	−0.467	2.346
	1500	90	89.437	1.084	-4.643	−0.116	2.561
	2000	120	119.662	1.133	-2.664	−0.328	2.588
	2500	150	149.750	1.304	-1.715	0.070	2.871
	3000	180	179.525	1.196	-3.553	0.214	2.138

continued ...

Relative accuracy q'	Integer upper limit A_{max}	Expected mean no. of metonic cycles $\mu = 2q' A_{max}$	10 % trimmed statistics				
			$\bar{X}_T$	s_T	t_T	S_k	K
0.035	1000	70	69.550	1.084	-3.713	-0.167	2.644
0.04	500	40	39.525	1.389	-3.058	0.022	2.575
	1000	80	79.500	1.049	-4.262	-0.099	2.721
	1500	120	119.287	1.350	-4.720	-0.376	2.740
	2000	160	159.462	1.185	-4.057	-0.039	2.195
	2500	200	199.625	1.390	-2.414	-0.428	2.869
	3000	240	239.437	1.456	-3.455	-0.462	2.846
0.045	1000	90	89.475	1.119	-4.195	0.012	2.470
0.05	500	50	49.437	1.036	-4.857	0.008	2.749
	1000	100	99.400	1.333	-4.026	-0.367	3.361
	1500	150	149.350	1.315	-4.420	-0.725	3.819
	2000	200	199.487	1.119	-4.095	-0.028	2.467
	2500	250	249.600	1.193	-2.999	-0.199	2.230
	3000	300	299.300	1.408	-4.447	-0.131	2.464

Table 7.6 The results of numerical experiments for randomly chosen values of T_2', testing the validity of the theory predicting the number of metonic cycles expected for a given accuracy q' and an upper integer limit of A_{max}.

Highlighted values of skewness S_k or curtosis K indicate a lack of normality in the distribution, while a highlighted t-statistic t_T suggests a lack of agreement between the predicted mean μ and the observed mean $\bar{X}_T$ at a 95% confidence level. Note, however, that $\bar{X}_T$ is consistently less than μ by a bias of about 0.5.

s_T is the standard deviation of the observed mean $\bar{X}_T$.

According to Student t-statistics, t_T should lie within the interval (-1.99,+1.99) for a 95% confidence interval if the predicted μ is correct. Unfortunately, Table 7.6 clearly shows that, although the observed mean is always fractionally close to the value expected from Equation (5), it does not generally pass the Student t-test at a 95% confidence level. However, a closer look at the 10% trimmed mean number of metonic cycles $\overline{X}_T$ reveals that it is consistently about 0.5 points lower than our predicted number of metonic cycles μ. In other words the mean value of the residuals $(\overline{X}_T - \mu)$ is non-zero and therefore our method of data analysis contains a small bias, which causes our predicted mean to consistently overestimate the observed mean.

A statistical bias in the analysis of frequency distributions arises when what you think you are measuring is not in reality what you are measuring. Throughout our derivation of Equation (5), we have assumed that the period set (T_1,T_2) is not close to a low-number commensurability. This assumption led us to believe that, on average, the metonic cycle count for a randomly chosen period T_2' should agree with our Equation (5). There does exist however, a small probability that a randomly chosen T_2' will be close to a low-number commensurability. If these T_2' values produce anomalous metonic cycle counts that fall symmetrically about the expected metonic cycle count, then the average count of the distribution would still agree with that predicted because the numbers of such T_2' values are very small.

Unfortunately, most T_2' values close to a low-number commensurability are more likely to produce metonic cycle counts that are much lower than the expected count. Suppose the largest integer A_{20} in the proper fraction which forms the low-number commensurability is of comparable size to an integer whose number of multiples within the range A_{max} would produce the predicted number of metonic cycles, ie

$$A_{20} \approx \frac{A_{max}}{N} = \frac{1}{2q'}$$

Then, not including any randomly appearing fractions, the numbers of metonic cycles found would be approximately the same as that predictied. Since a few random high-numbered fractions can appear as well, depending on how close the discrepancy ε_{12}' is to zero, the numbers of metonic cycles counted could actually be slightly greater than the number predicted.

If, however, A_{20} is much greater than 1/(2q'), but still small enough to have the effect of forcing the resulting fractions approximating T_2' into an obvious pattern, then the numbers of metonic cycles, even when the random appearing fractions are included, would be less than that expected.

Since we have chosen values of q' that range from 0.01 to 0.05, the integer A_{20} simply has to be much greater than 50 at the most and 10 at the least, in order for the resulting counts to be less than expected. Clearly, if A_{20} has an equal probability of being any integer between 2 and A_{max}, the majority of the integers randomly chosen will be greater than 1/(2q'). Therefore, a near low-number commensurability T_2' value is most likely to produce smaller counts than expected.

Even though such T_2' values are rare, if most of those which do occur produce counts lower than expected, the distribution which included these anomalous points could be affected enough to cause the average of the distribution to be consistently fractionally smaller than expected. This would then give rise to the small negative biases seen in Table 7.6. Note also that as q' is increased, the chance that A_{20} is greater than 1/2q' becomes greater. Thus, the negative biases should increase negatively as q' is increased.

We can find a good approximation of the bias for each value of q' by performing a linear regression between the variables μ and $\bar{X}_T$. If μ is in fact the expected value of the mean $\bar{X}_T$ and if there were no bias in the data analysis, the best straight line fit would be a line of slope +1 and y-intercept zero; however, if the data analysis which produced $\bar{X}_T$ contains a bias, the relationship between μ

and $\overline{X}_T$ would then be a straight line of slope +1 and y-intercept equal to the bias.

The best least squares line fits to our data for each value of q' give the following relationships:

accuracy q'	least squares line fit	r
0.01	$\overline{X}_T = 0.9984\ \mu - 0.3587$	1.0000
0.015	$\overline{X}_T = 0.9975\ \mu - 0.2130$	1.0000
0.02	$\overline{X}_T = 1.0009\ \mu - 0.4233$	1.0000
0.03	$\overline{X}_T = 1.0008\ \mu - 0.5077$	1.0000
0.04	$\overline{X}_T = 1.0001\mu - 0.5383$	1.0000
0.05	$\overline{X}_T = 1.0000\mu - 0.5762$	1.0000

The correlation coefficient r is a measure of how closely the data 'fits' a straight line. r can lie anywhere between -1 and +1, where:

(1) r = +1 indicates that the data falls exactly on a straight line of positive slope;

(2) r = -1 indicates that the data falls exactly on a straight line of negative slope;

(3) r = 0 indicates that the data cannot be approximated at all by a straight line.

Our values for the correlation coefficients show very clearly that μ and $\overline{X}_T$ are related by a linear function. This fact and the fact that the slopes of the lines are very close to +1 suggest that μ is very likely to be the expected value of the mean when the bias is removed. That the bias also appears to be a function of q' and seems to generally increase negatively as q' increases, tends to corroborate the idea that the bias is caused by low-number commensurabilities which are not included in the formation of Equation (5). However, the differences between the biases may not be

statistically significant.

If we now subtract the appropriate bias from every value of $\overline{X}_T$ to get a new bias-corrected value for the 10% trimmed mean $\overline{X}_{Tb}$, and if we then recompute the t-statistic using this new mean,

$$t_{Tb} = \frac{\bar{x}_{Tb} - \mu}{s_T / \sqrt{h}}$$

we get the results given in Table 7.7. Almost all the bias corrected values of the t-test now fall within the limits set by a 95% confidence level.

Note that subtracting the bias from the distribution has no effect on the distribution's standard deviation. In other words, the general shape of the distribution is unaffected since the distribution is merely shifted right or left by an amount equal to the bias.

With the bias removed, our expected value of the number of metonic cycles given in Equation (5) agrees very well with the numerical experiments over a wide range of accuracies q' and upper integer limits A_{max}. Since the bias for small q' is less than one, Equation (5) is for our purposes a sufficiently accurate method of predicting the most likely number of metonic cycles that will occur for a given accuracy q' and integer upper limit A_{max}.

If we take reasonable values for the accuracy q' and upper integer limit A_{max} to be 0.01 and 1000 respectively, we find that the number of expected metonic cycles from Equation (5) for any ratio of periods T_2' is on average equal to 20. Minus the bias corresponding to q'=0.01, the number is still approximately 20.

Accuracy q'	Integer upper limit A_{max}	Expected mean no. of metonic cycles $\mu = 2q'A_{max}$	Bias	Bias corrected 10% trimmed statistics	
				mean $\bar{X}_{Tb}$	t-statistic t_{Tb}
0.01	500	10	-0.3587	9.946	−0.602
	1000	20		19.946	−0.580
	1500	30		29.984	−0.140
	2000	40		39.984	−0.139
	2500	50		50.009	0.076
	3000	60		59.796	−1.741
0.015	500	15	-0.2130	15.025	0.273
	1000	30		29.875	−0.846
	1500	45		44.788	−1.494
	2000	60		59.863	−0.925
	2500	75		74.975	−0.194
	3000	90		89.688	−2.377
0.02	500	20	-0.4233	19.948	−0.438
	1000	40		40.023	0.199
	1500	60		60.110	0.862
	2000	80		80.135	0.882
	2500	100		100.210	1.670
	3000	120		119.960	−0.247
0.03	500	30	-0.5077	30.033	0.278
	1000	60		60.058	0.442
	1500	90		89.945	−0.454
	2000	120		120.170	1.342
	2500	150		150.258	1.770
	3000	180		180.033	0.247
0.04	500	40	-0.5383	40.063	0.406
	1000	80		80.038	0.324
	1500	120		119.825	−1.159
	2000	160		160.000	0.000
	2500	200		200.163	1.049
	3000	240		239.975	−0.154
0.05	500	50	-0.5762	50.013	0.112
	1000	100		99.976	−0.161
	1500	150		149.926	−0.503
	2000	200		200.063	0.504
	2500	250		250.176	1.320
	3000	300		299.876	−0.788

Table 7.7 The bias corrected 10% trimmed statistics for the frequency distribution of the number of metonic cycles. The appropriate bias has been removed from the results of Table 7.6. Those values of t_{Tb} which are highlighted fail at the 95% confidence level to show agreement between the observed and predicted means.

Such frequency distributions as those depicted in Figures 7.7 can also provide information on the anomalous points. If the frequency distributions were purely normal, less than 1% of the metonic cycle counts would lie beyond three standard deviations from the distribution mean. Therefore, those values of T_2' which produce counts far greater or smaller than the expected count will show up in the frequency distributions as obvious outliers. If it is true that these anomalous points are in fact caused by T_2' values close to low-number commensurabilities, we should be able to use the theory of continuous fractions to identify some of the more extreme points.

Table 7.8 gives a list of some of the obvious outliers found in the frequency distributions of Figures 7.7. Upon studying the complete random set of one hundred values of T_2', we found that all the T_2' values, which formed a metonic cycle with a discrepancy ε_{12}' smaller than about 0.00015, exhibited anomalous behavior for some range of q' in the frequency distributions of Figures 7.7.

Not all the outlying points are caused by T_2' values existing close to low-number commensurablities. Some T_2' values such as $T_2'=0.1108715454\approx 1/9$ produce anomalous counts because they are reasonably close to a low-number commensurability consisting of very small integers. The residuals are locked into a set pattern in this situation just as much as they are in the situation where T_2' is much closer to a low-number commensurability but formed of larger integers.

Anomalous counts are also produced when T_2' is approximately equal to the accuracy q'. In this case, Equation (5) no longer applies becaue the probability that a metonic cycle will occur about a particular integer A_1 is no longer simply 2q'. Theoretically, if the allowed discrepancy between a perfect and a near metonic cycle is of similar value to the period T_2', then every integer multiple of T_2' would produce a metonic cycle to within the error q'. An error which is of the same order as one of the periods is clearly not very useful realistically. Therefore, that Equation (5) fails to hold near $T_2' = q'$ is not very important.

Group number	T_2'	Commensurabilities (A_{10}/A_{20})	Discrepancies ε_1
1	0.1108715454	1/9	0.00216
2	0.3723395365	35/94	0.00008
3	0.9831467632	175/178	0.00012
4	0.3009256677	65/216	0.00006
5	0.7041563575	288/409	0.00005
6	0.6659526062	311/467	0.00013
7	0.2224529442	107/481	0.00014

(a)

Group number	T_2'	q' for which T_2' values are outliers
1	0.0253501000	>0.02
2	0.0275530294	"
3	0.0302595584	"
4	0.0436548692	>0.03
5	0.0642344620	>0.04
6	0.0664753179	"
7	0.0772043397	>0.05
8	0.0858486144	"
9	0.0866216766	"

(b)

Table 7.8 The values of T_2' in the frequency distributions of Figures 7.7, which produce numbers of metonic cycles that deviate greatly from the expected number of metonic cycles for some value of q'.

All the T_2' values in Table (a), can be approximated by a low number commensurability, while those in Table (b) are all approximately equal to q'.

In this section, we have developed a means of analysing the frequency of occurrence of metonic cycles, and a means of discovering which period pairs are very close to low number commensurabilities. These results are very useful if we want to study the likelihood of a metonic cycle occurring between the lunar synodic period T_S and the Sun's sidereal period $T_\odot$ which could then be used for calender time-keeping; however, these results are not very useful in themselves for the study of stability mechanisms for the Earth-Moon-Sun system.

It is the well-known Saros cycle of today and the possibility of the existence of other saros cycles in the past or future of the Earth-Moon-Sun system which is of greatest interest to the stability of that system. In the next section, we expand our analysis of the occurrence of metonic cycles to include the more complicated case of saros cycles and search for a means of predicting the expected number of saros cycles for a given triplet of periods.

7.4 Prediction of the Frequency of Occurrence of Saros Cycles

We follow the same logic as that used in Section 7.2. Without loss of generality we again, order the periods such that:

$$T_i \geq T_{i+1} \qquad \forall \; i = 1,2,3$$

and divide the system parameters throughout by the largest period T_1. Equations (1) then become:

$$\varepsilon_{12}' = A_1 - A_2 T_2' \qquad \text{where} \qquad |\varepsilon_{ij}'| \leq q'$$

$$\varepsilon_{13}' = A_1 - A_3 T_3' \qquad A_i \text{ are integers}$$

$$\varepsilon_{23}' = \varepsilon_{13}' - \varepsilon_{12}' = A_2 T_2' - A_3 T_3' \qquad A_i \leq A_{max}$$

$$\forall \; i,j=1,2,3 \quad i<j \qquad (6)$$

The question of the frequency of the occurrence of saros cycles then becomes: How many integer triplets (A_1,A_2,A_3) exist for a given set of periods (T_1,T_2,T_3) such that Equations (6) hold true? In the metonic cycle case, we discovered two methods by which the equivalent problem could be solved satisfactorily. One method used a numerical algorithm and computer, while the other used the pseudo-randomness of the discrepancy values. The following are an adaption of these two solutions to the saros cycle case.

(i) The use of a numerical algorithm and the computer

The first and easiest solution to the problem of the frequency of occurrence of saros cycles is to write a numerical algorithm which uses the computer to find the number of saros cycles for a given triplet of periods and the stipulated restrictions.

The solution begins with the same algorithm used to find a metonic cycle. Once a metonic cycle is found, a search is made for an integer $A_3 \leq A_{max}$ which will extend the particular metonic cycle set (A_1,A_2) into a saros cycle. In other words, the two possible integer values for A_3 that produce the nearest values A_3T_3' above and below

A_1 are found. The two corresponding residuals between A_3T_3' and A_1 are then computed. The absolute minimum of the two residuals is then equal to $|\varepsilon_{13}'|$ and the integer value producing it becomes A_3. If $|\varepsilon_{13}'| \leq q'$ and if $|\varepsilon_{23}'| = |\varepsilon_{13}'-\varepsilon_{12}'| \leq q'$, then the integer set (A_1,A_2,A_3) forms a saros cycle for the period set (T_1,T_2,T_3).

If we take, for example, the period set (T_S,T_A,T_N) and order and normalize them according to the method described above, we get:

$$T_S > T_A > T_N$$

$$T_2' = \frac{T_A}{T_S} = 0.933085$$

$$T_3' = \frac{T_N}{T_S} = 0.921493$$

Applying our numerical algorithm to find all the integer combinations of the periods (T_2', T_3') which produce a saros cycle to within an accuracy $q'=0.5$ days$/T_S=0.016932$, we discover that $(A_1,A_2,A_3) = (223,239,242)$ is the only integer set less than $A_{max}=1000$ which forms a saros cycle for the given period set. These integer multiples are easily recognized as those which make up the well-known Saros cycle of today. Thus, for the present-day periods T_S, T_A, and T_N, the Saros cycle is unique, given the stipulated restrictions of q' and A_{max}.

But tidal interaction between the Earth and the Moon has changed these three periods, and will continue to change them. Can we predict what the number of saros cycles will be in general for any triplet of periods? Again we have the problem that the total number of saros cycles possible per period set depends on whether or not the period set contains low or high number commensurabilities.

(ii) The use of the pseudo-random nature of the residuals

As before, we use the pseudo-randomness of the residuals to calculate the most probable number of saros cycles for any given period set. From equation (6), we can

see that the formula for the additional independent minimum absolute residual $|\varepsilon_{13}'|$ has the same form as that of $|\varepsilon_{12}'|$. It should therefore exhibit the same properties of pseudo-randomness. Because the minimum absolute residual $|\varepsilon_{23}'|$ is a combination of the other two residuals, we can ignore it until we come to discuss the restrictions placed on all the residuals by q'.

If we now take a large enough range of integers A_{max} to make every residual about an integer possible, we can assume that any residual between 0.0 and 0.5 about an integer A_1 is equally likely. The problem of the frequency of saros cycles can now be reworded to ask the following two questions:

(1) What is the probability P that both real values A_2T_2' and A_3T_3' fall within q' of the same integer A_1 and that the absolute residual $|\varepsilon_{23}'|$ between A_2T_2' and A_3T_3' is also less than or equal to q', where A_2T_2' and A_3T_3' are assumed to fall randomly about the integer A_1 between $-0.5+A_1$ and $0.5+A_1$?

(2) Having found P, what is the expected total number of saros cycles, if A_1, A_2 and A_3 are restricted to the range 0 to A_{max}?

The probability P is given by the following ratio of regions:

$$P = \frac{R_1}{R_2}$$

where R_1 = The area of the region about an integer where ε_{12}' and ε_{13}' must be found in order for a saros cycle to exist.

R_2 = The area of the region about an integer where ε_{12}' and ε_{13}' can be located.

Note that because we are assuming any residual values for ε_{12}' and ε_{13}' between -0.5 and +0.5 are equally likely, the regions are now two dimensional.

Figure 7.8 depicts the regions R_1 and R_2. The diagram is centred on the position of an integer A_1. The shaded region is the region where the restrictions for the existence of a saros,

$$|\varepsilon_{12}'| \leq q'$$
$$|\varepsilon_{13}'| \leq q'$$
$$|\varepsilon_{23}'| = |\varepsilon_{13}' - \varepsilon_{12}'| \leq q'$$

hold true and the square region formed by $-0.5 \leq \varepsilon_{12}' \leq +0.5$ and $-0.5 \leq \varepsilon_{13}' \leq +0.5$ is the total region where the residuals ε_{12}' and ε_{13}' may fall about A_1.

Therefore, the probability P that a saros cycle exists near an integer A_1 is given by:

$$P = \frac{3q'^2}{1} = 3q'^2$$

The expected number N of saros cycles is then simply:

$$N = P\, N_1 N_2$$

where N_1 = The number of times a pair of real values A_2T_2' and A_3T_3' fall within 0.5 range of a particular integer A_1

N_2 = The number of integers A_1 that are available for the real values A_2T_2' and A_3T_3' to fall near

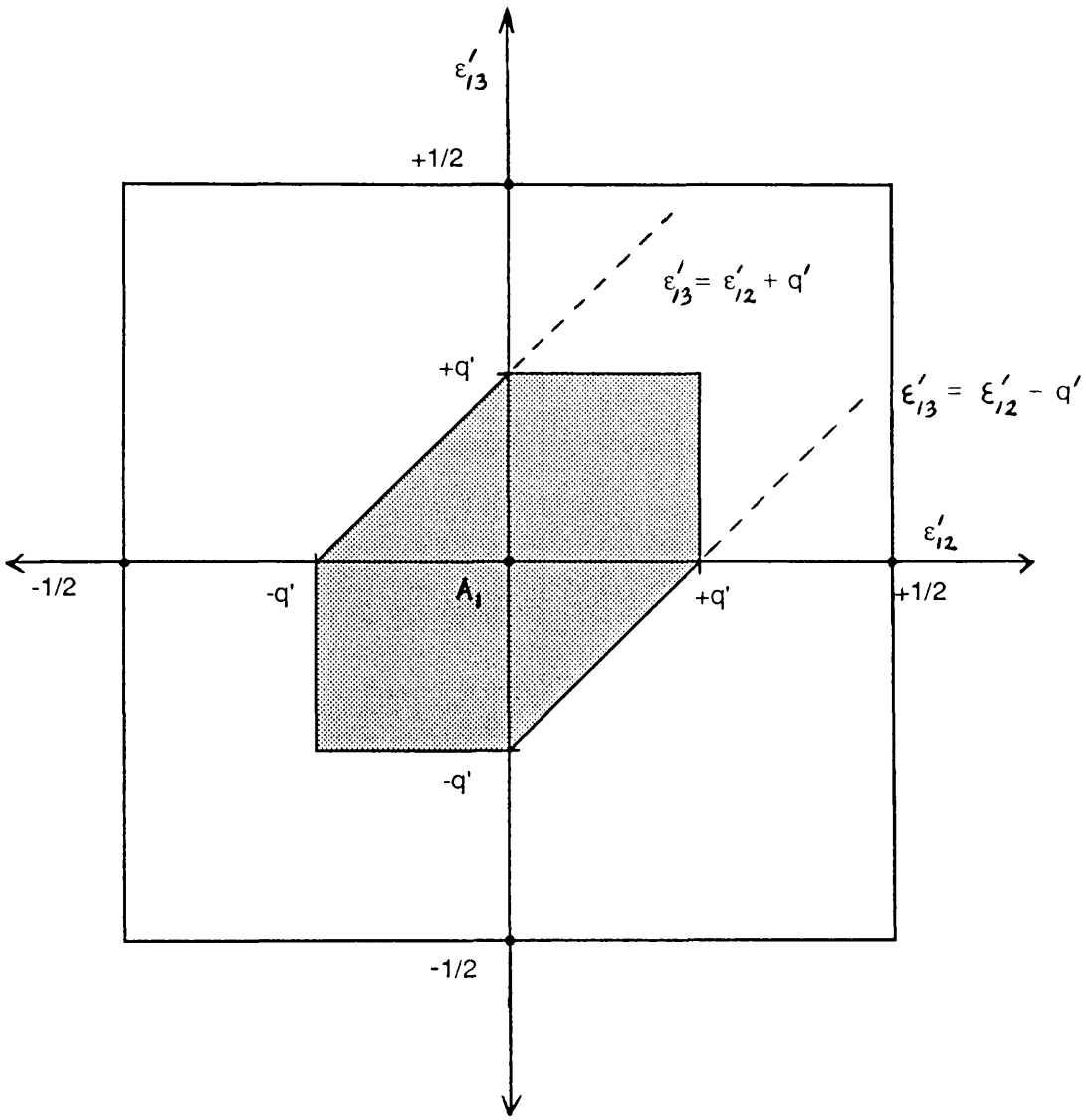

Figure 7.8 Region of acceptable saros cycles.

The shaded region is the area in which the residuals ε_{12}' and ε_{13}' must be found in order for a saros cycle to exist near the integer A_1, while the square region denotes the boundaries within which the residuals are always located.

Like the metonic cycle case, each integer has on average $1/T_2'$ attempts at having A_2T_2' fall within q' of its position. Similarly, each integer A_1 has on average $1/T_3'$ attempts at having A_3T_3' fall within q' of its position. Therefore, the number N_1 of attempts at having distinct pairs of A_2T_2' and A_3T_3' fall within q' of each integer A_1 is a combination of the two numbers of attempts:

$$N_1 = \frac{1}{T_2'}\,\frac{1}{T_3'}$$

The number N_2 of integers A_1 that are accessible to the pairs (A_2T_2', A_3T_3') is restricted by the upper integer limit A_{max}. Because the periods are ordered $T_1>T_2>T_3$, then $A_1<A_2<A_3< A_{max}$, and the largest integer A_1 that a pair A_2T_2' and A_3T_3' can approach is $A_{max}T_3'$. Hence:

$$N_2 = T_3'\,A_{max}$$

Finally, the expected number N of saros cycles becomes:

$$N = \frac{3q'^2}{T_2'}\,A_{max} \qquad (7)$$

Note that, although our formula for the expected number of saros cycles does not ultimately depend on the value of T_3', it does depend on the value of T_2'. In fact, if we were to extend the given period set to include n periods $(T_2', T_3', \ldots, T_n')$, the previous pattern would suggest the following general formula for the expected number of n-period cycles.

$$N = P\,\frac{1}{T_2'}\,\frac{1}{T_3'}\,\frac{1}{T_4'}\cdots\frac{1}{T_n'}\,A_{max}\,T_n' \qquad \text{and } P = k\,q'^{n-1}$$

The probability P that an n-period cycle exists near a particular integer A_1 is governed by some ratio of regions in ε_{ij} phase space of dimension n-1, where i,j=1,2, ... n i<j. Figure 7.8 is an example of these regions for the two-dimensional phase space in ε_{12}' and ε_{13}'.

It would be interesting to generalize our solution to include n number of period sets. Period sets of four would be particularly useful for studying cycles which include a commensurability with the solar anomalistic period. In this manner, we could ensure that the Sun was back in the same position with respect to its apse line and that therefore the Sun's geocentric distance was repeated. This addition would produce an even better stabilizing cycle than the Saros cycle.

This work is, however, beyond the scope of this thesis. We are primarily concerned with the use of these cycles as a stabilizing mechanisms for the Earth-Moon-system and Saros-type cycles are sufficient for this purpose. Also any benefits derived from increasing the number of periods in a commensurable set may be counteracted by the decrease in accuracy that this addition causes. Each additional period increases the chances that one of the periods will be close to a low number commensurability and that the final cycle count will be distorted.

Equation (7) does give a reliable value for the expected number of near saros cycles, given: a period set (T_1,T_2,T_3) which does not have any period ratios close to low number commensurabilities; an integer upper limit of A_{max}; and an allowed discrepancy from a perfect saros of q'. As with the number of metonic cycles, the actual number of saros cycles for a given triplet of periods can vary considerably from the predicted value depending on the nearness of T_2' or T_3' to a low number commensurability, and therefore on the validity of the assumption that the residuals ε_{12}' and ε_{13}' are pseudo-random variables. In section 7.5, we study the dispersion of the actual numbers of saros cycles from the predicted value and give statistical evidence for the validity of equation (7).

7.5 Numerical Experiments for the Frequency of Occurrence of Saros Cycles

Much the same statistical methods as described in Section 7.3 are applied in this section for the study of the frequency of occurrence of saros cycles. As before, the theoretically expected number of saros cycles is compared statistically with the mean of the frequency distribution for the actual number of saros cycles. However, because the actual numbers of saros cycles for the relevant ranges of q' and A_{max} are generally too close to zero to produce a symmetric frequency distribution about a mean count, we use a different method to construct our random sample test of the predicted number of saros cycles. Frequency distributions whose average count values are near zero display an irregularly high proportion of zero counts since counts of saros cycles cannot be negative.

We could choose q' and A_{max} large enough to produce an average count much greater than zero, but a larger A_{max} than previously used would require an extended computer run-time in order to search through the increased number of integers for saros cycles and a larger q' is not realistic. Instead, for each set of random experiments, the accuracy q' and the number of saros cycles to be counted are prearranged. Real numbers between 0 and 1 are randomly chosen to be the ratios T_2' and T_3'. If T_3' is greater than T_2', they are interchanged. Theoretically the ordering of the periods should have no adverse effect on our solution since together the two periods form a uniformly distributed set.

A value for the upper limit A_{max} is then chosen for each period T_2' such that the number of saros cycles predicted by Equation (7) is a constant.

$$A_{max} = \frac{N T_2'}{3 q'^2}$$

where N and q' are given constants.

Calculations of the type described in Section 7.4(i) for finding the number of

saros cycles for given values of q' and A_{max} are performed for a random sample of 100 period sets (T_2',T_3'). The resulting frequency distributions of saros cycle counts for a range of accuracies q' and predicted counts N are shown in Figures 7.9(a) to (k). In order to verify Equation (7), we then compare the average number of saros cycles for the random set of (T_2',T_3') values with the value of N expected from the equation.

Again the frequency distributions are near normal, but exhibit a slight skewness and thicker, longer tails than those of a normal distribution. These distortions from the 'norm' arise from the random choosing of a period T_2' or T_3' near a low-number commensurability; however, because we now have two periods which could be close to a perfect low-number commensurability, the chances of finding anomalies in the normal-like distribution are greater.

In order to avoid most of the problem caused by the anomalous points, we apply the same p% trimming statistics described in Section 7.3 and remove 10% of the outlying points from either side of each of the relative frequency distributions. The resulting 10% trimmed mean, standard deviations, t-statistics, skewness and curtosis for the frequency distributions of the number of saros cycles are given in Table 7.9. For most of the data sets a 10% trimming has resulted in normal distributions. Those values of skewness and curtosis, which fail the normality test are underlined.

Figure 7.9 (a) to (k) The relative frequency distributions of saros cycle counts occurring for a range of accuracies q' and expected numbers of saros cycles N. Each histogram contains counts from 100 pairs of T_2' and T_3' values. $\bar{X}_T$ is the 10% trimmed mean number of saros cycles and $\bar{X}_{Tb}$ is the same trimmed mean corrected for bias.

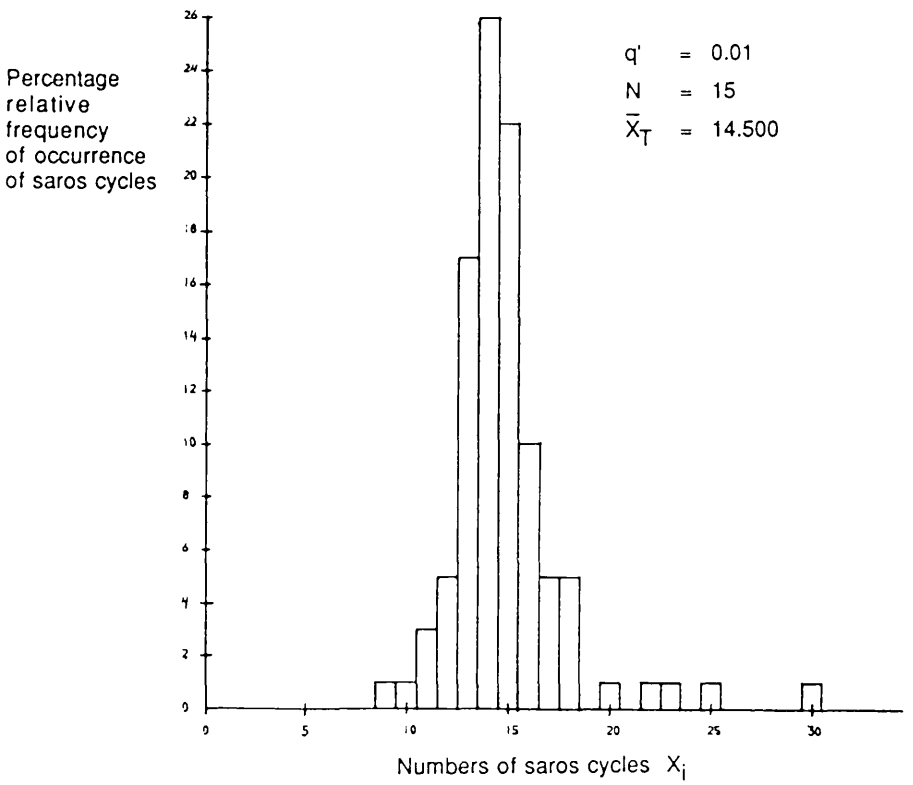

(a)

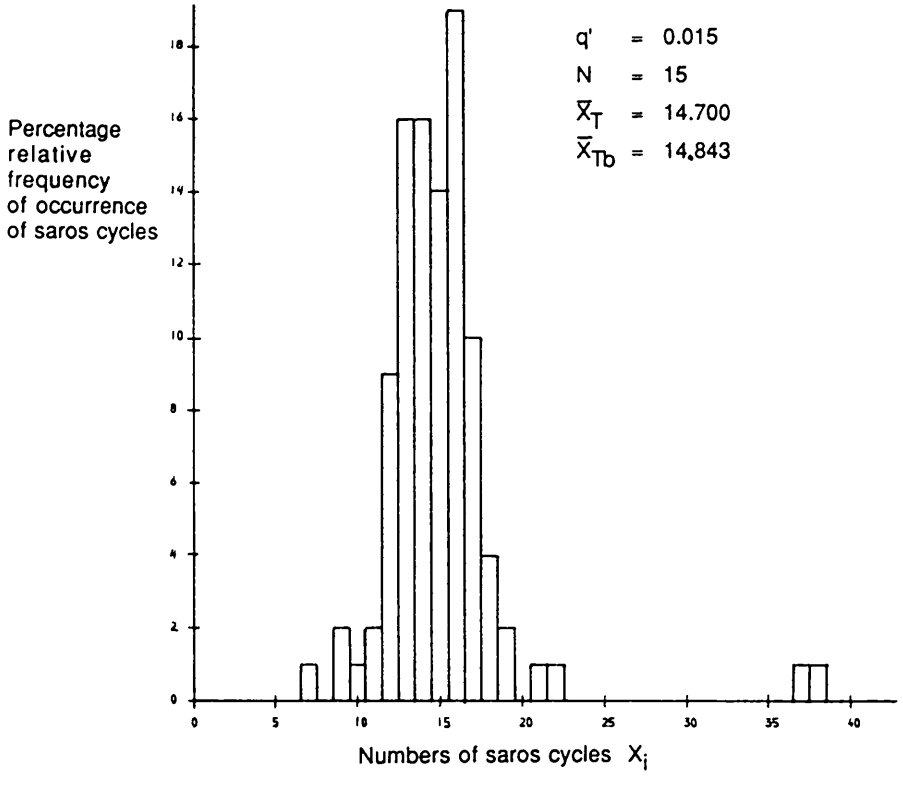
Percentage relative frequency of occurrence of saros cycles
q' = 0.015
N = 15
$\bar{X}_T$ = 14.700
$\bar{X}_{Tb}$ = 14.843
(b)
Numbers of saros cycles X_i

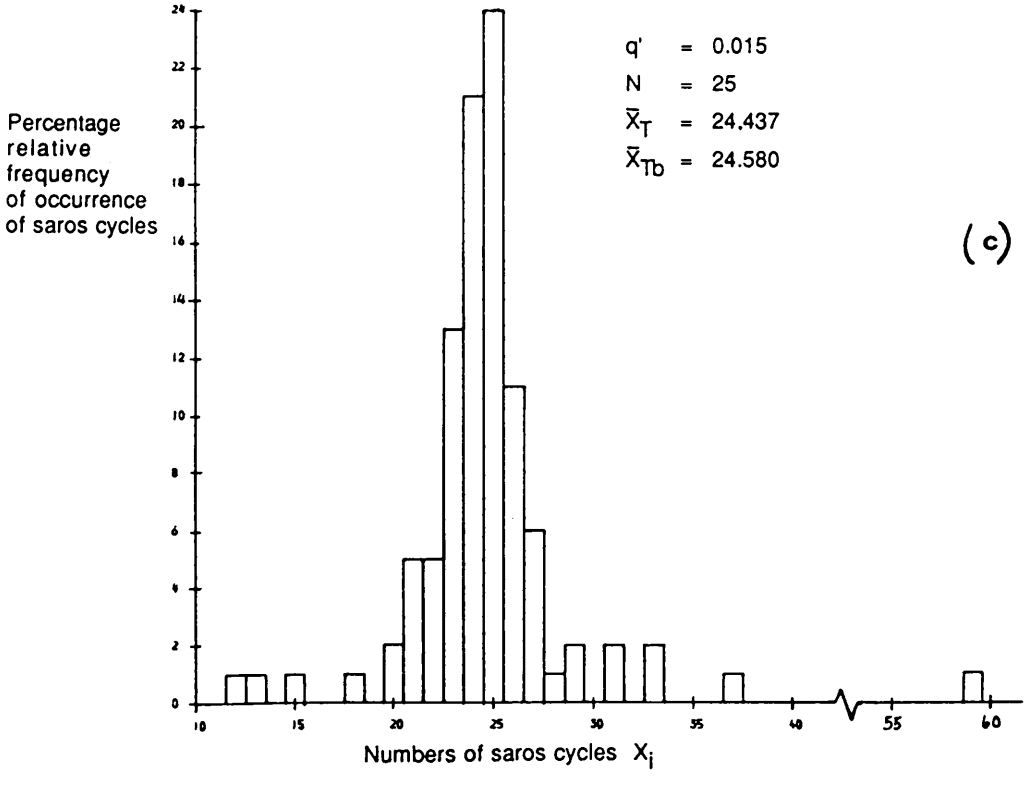
Percentage relative frequency of occurrence of saros cycles
q' = 0.015
N = 25
$\bar{X}_T$ = 24.437
$\bar{X}_{Tb}$ = 24.580
(c)
Numbers of saros cycles X_i

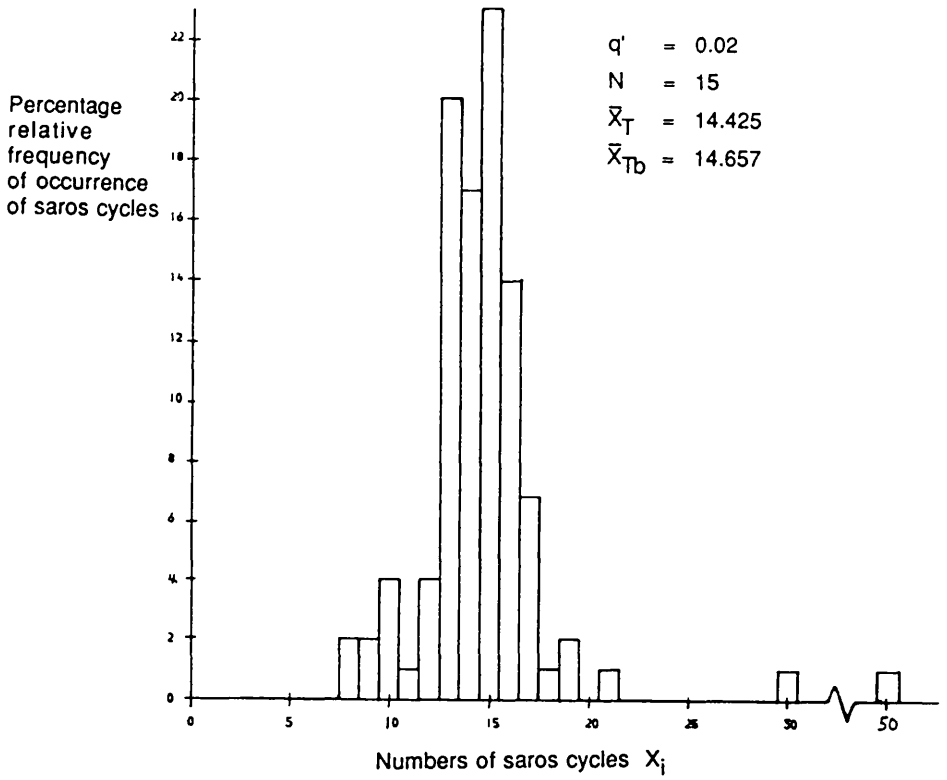
Percentage relative frequency of occurrence of saros cycles
q' = 0.02
N = 15
$\bar{X}_T$ = 14.425
$\bar{X}_{Tb}$ = 14.657
0 2 4 6 8 10 12 14 16 18 20 22
0 5 10 15 20 25 30 50
Numbers of saros cycles X_i

(d)

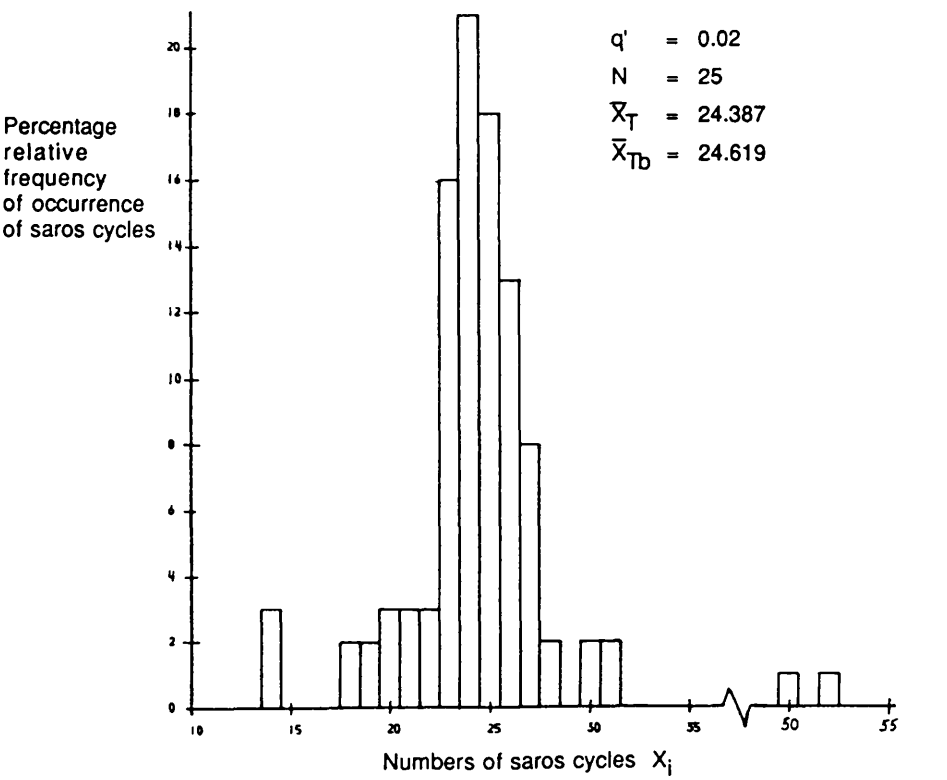
Percentage relative frequency of occurrence of saros cycles
q' = 0.02
N = 25
$\bar{X}_T$ = 24.387
$\bar{X}_{Tb}$ = 24.619
0 2 4 6 8 10 12 14 16 18 20
10 15 20 25 30 35 50 55
Numbers of saros cycles X_i

(e)

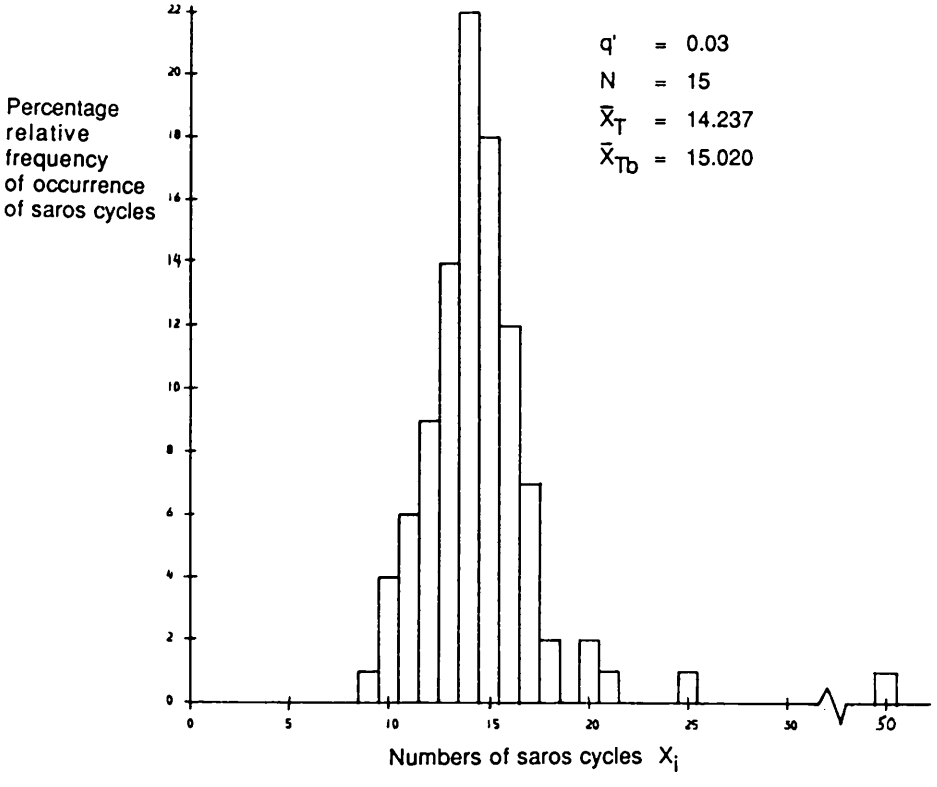
Percentage relative frequency of occurrence of saros cycles
q' = 0.03
N = 15
$\bar{X}_T$ = 14.237
$\bar{X}_{Tb}$ = 15.020
Numbers of saros cycles X_i

(f)

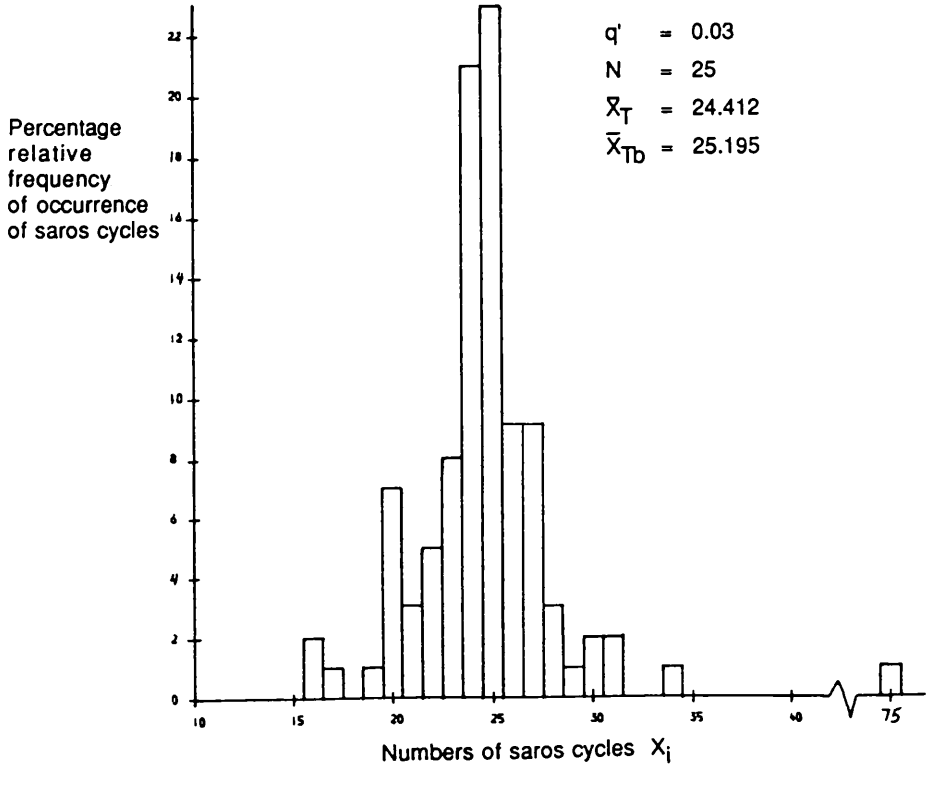
Percentage relative frequency of occurrence of saros cycles
q' = 0.03
N = 25
$\bar{X}_T$ = 24.412
$\bar{X}_{Tb}$ = 25.195
Numbers of saros cycles X_i

(g)

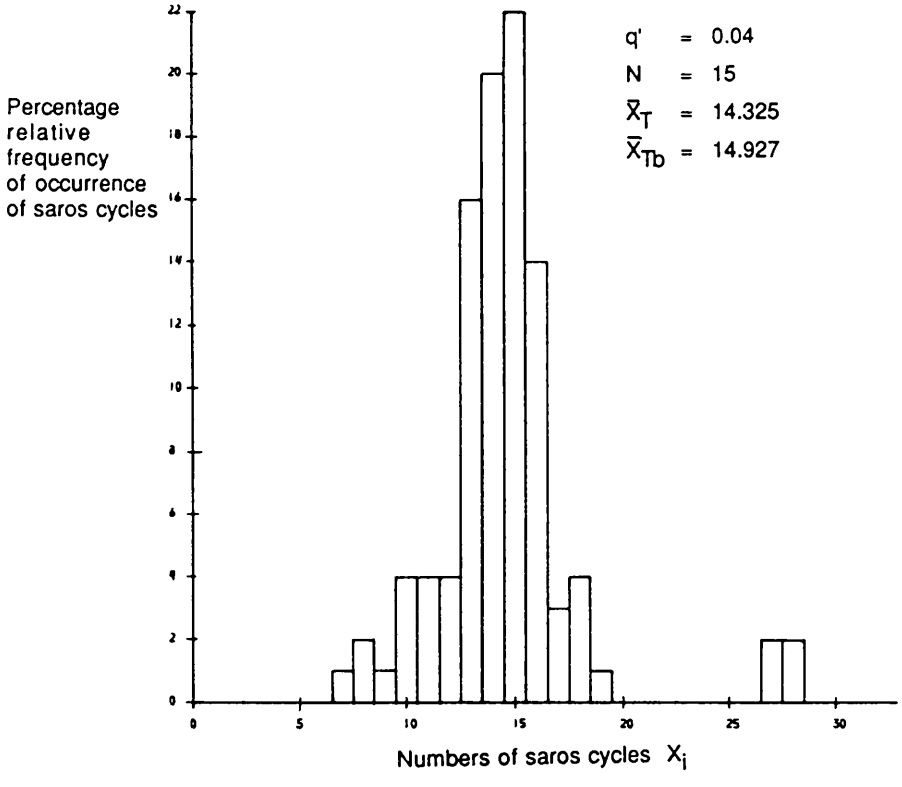
Percentage relative frequency of occurrence of saros cycles
q' = 0.04
N = 15
$\bar{X}_T$ = 14.325
$\bar{X}_{Tb}$ = 14.927
Numbers of saros cycles X_i

(h)

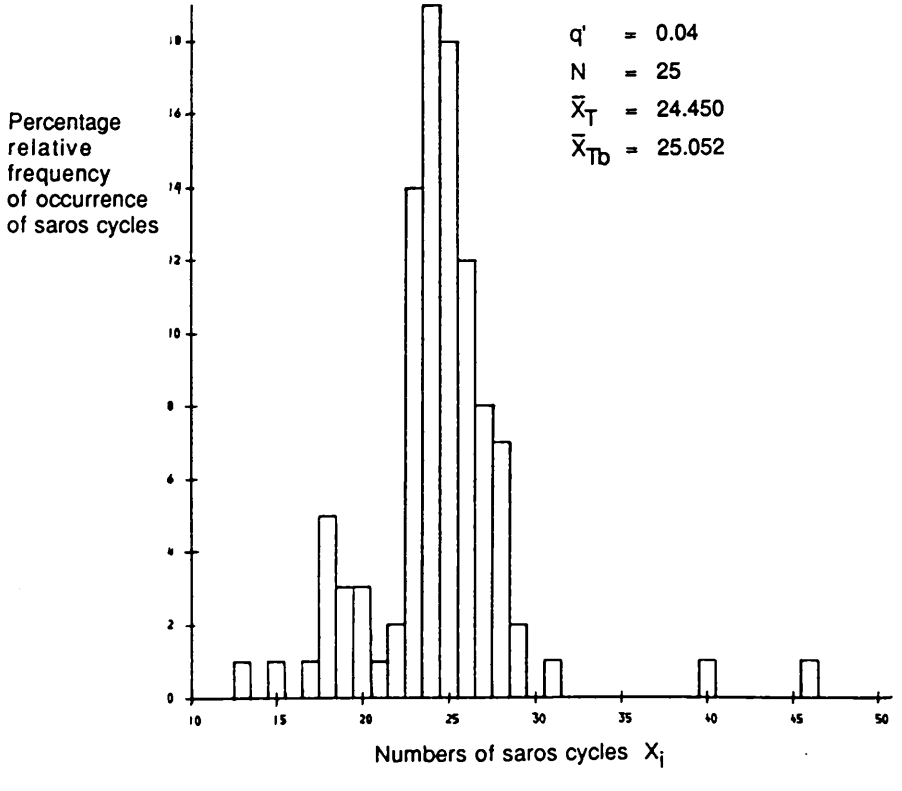
Percentage relative frequency of occurrence of saros cycles
q' = 0.04
N = 25
$\bar{X}_T$ = 24.450
$\bar{X}_{Tb}$ = 25.052
Numbers of saros cycles X_i

(i)

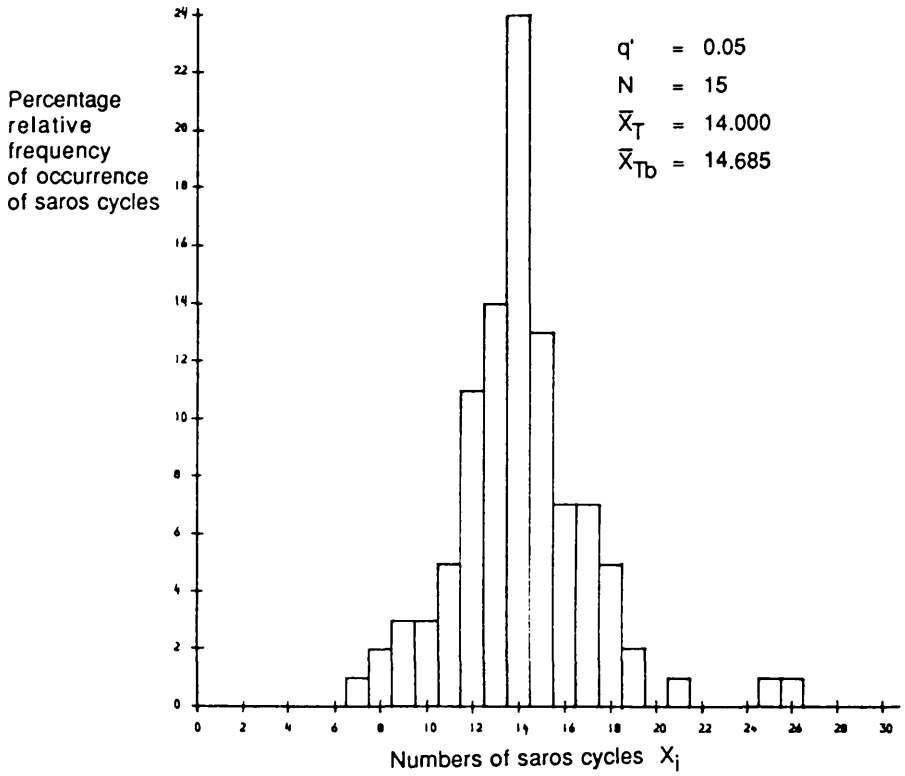
Percentage relative frequency of occurrence of saros cycles
q' = 0.05
N = 15
$\bar{X}_T$ = 14.000
$\bar{X}_{Tb}$ = 14.685
Numbers of saros cycles X_i

(j)

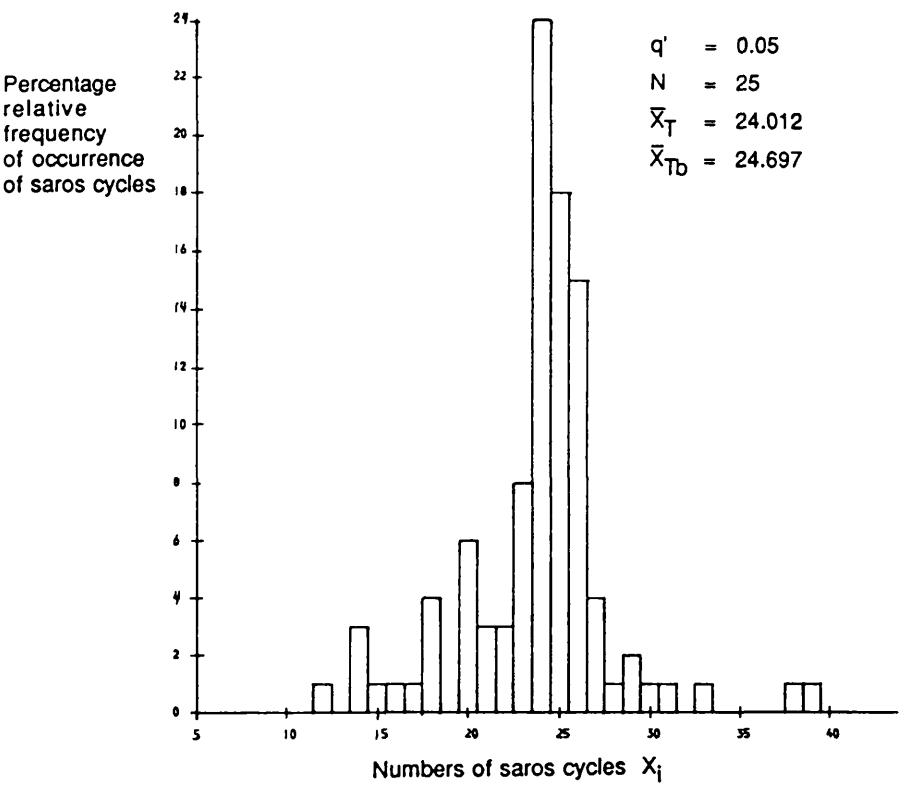
Percentage relative frequency of occurrence of saros cycles
q' = 0.05
N = 25
$\bar{X}_T$ = 24.012
$\bar{X}_{Tb}$ = 24.697
Numbers of saros cycles X_i

(k)

Relative accuracy q'	Expected mean no. of saros cycles $\mu = 3q'^2 A_{max}/T_2'$	10 % trimmed statistics				
		$\bar{X}_T$	s_T	t_T	S_k	K
0.01	10	9.500	1.185	-3.773	0.250	2.204
	15	14.500	1.547	-2.891	0.455	2.478
0.015	10	9.712	1.744	-1.474	−0.091	2.263
	15	14.700	1.957	-1.371	−0.071	1.867
	20	19.487	1.540	-2.978	0.318	2.367
	25	24.437	2.024	-2.486	−0.125	2.689
	30	29.475	2.308	-2.034	−0.135	3.119
0.02	10	9.600	1.715	-2.086	−0.099	2.391
	15	14.425	1.774	-2.899	0.054	2.135
	20	19.550	2.050	-1.964	−0.396	2.790
	25	24.387	2.105	-2.603	−0.148	2.646
	30	29.200	2.407	-2.973	−0.515	2.992
0.025	10	9.262	1.734	-3.803	−0.154	2.444
0.03	10	9.287	1.773	-3.595	0.156	2.525
	15	14.237	2.067	-3.299	−0.016	2.363
	20	19.550	1.932	-2.083	−0.281	2.218
	25	24.412	2.452	-2.143	−0.541	3.215
	30	29.400	2.251	-2.384	−0.368	2.446
0.04	10	9.425	1.564	-3.289	−0.357	2.057
	15	14.325	2.012	-3.001	−0.282	2.656
	20	19.350	2.579	-2.254	−0.537	2.683
	25	24.450	2.936	-1.676	−0.586	3.686
	30	29.337	3.127	-1.895	−1.019	4.496
0.05	10	9.187	1.769	-4.109	0.250	2.846
	15	14.000	2.187	-4.089	0.154	2.461
	20	19.012	2.690	-3.284	−0.539	3.025
	25	24.012	3.031	-2.914	−1.042	3.785
	30	28.787	3.690	-2.939	−0.758	3.266

Table 7.9 The results of numerical experiments for randomly chosen values of T_2' and T_3', testing the validity of the theory predicting the number of saros cycles expected for a given accuracy q' and upper integer limit of A_{max}.

Underlined values of skewness S_k or curtosis K indicate a lack of normality in the distribution, while an underlined t-statistic t_T suggests a lack of agreement between the predicted mean μ and the observed mean $\bar{X}_T$ at a 95% confidence level. Note, however, that $\bar{X}_T$ is consistently less than μ by a bias of about 0.5.

s_T is the standard deviation of the observed mean $\bar{X}_T$.

As in the metonic cycle case, we find that the 10% trimmed mean number of saros cycles is consistently approximately 0.5 points smaller than our predicted number. Assuming that this bias is due to the values of T_2' and T_3' close to low-number commensurabilities which are not taken into consideration by Equation (7), we remove the statistical bias by performing a linear regression between the 10% trimmed mean $\overline{X}_T$ and the predicted μ numbers of saros cycles for each value of q'. We get:

Accuracy q'	Least squares line fit	r
0.015	$\overline{X}_T = 0.9853\ \mu - 0.1430$	1.0000
0.020	$\overline{X}_T = 0.9832\ \mu - 0.2324$	1.0000
0.030	$\overline{X}_T = 1.0080\ \mu - 0.7832$	1.0000
0.040	$\overline{X}_T = 0.9990\ \mu - 0.6022$	1.0000
0.050	$\overline{X}_T = 0.9842\ \mu - 0.6852$	1.0000

The correlation coefficient r confirms that $\overline{X}_T$ and μ are related by a linear function. That the slope is very nearly +1 suggests that μ would be the expected value of the mean if the biases in the analysis were removed.

As expected, the data for the saros cycle counts does not produce as good a fit to a line of slope one as the data for the metonic cycle counts and the biases are generally larger. This is probably due to the addition of one more period to the period set, which increases the chances of getting the 'non-normal' behavior that occurs when one of the periods falls close to a low-number commensurability. The bias still seems to be a function of q' and it still appears to generally increase negatively as q' increases. Again the differences between the biases may not be statistically signigicant.

The relevant biases are then subtracted from every value of $\overline{X}_T$. Table 7.10 gives the new bias-corrected values for the 10% trimmed mean $\overline{X}_{Tb}$ and t-statistic t_{Tb}.

Accuracy q'	Expected mean no. of saros cycles $\mu = 3q'^2 A_{max}/T_2'$	Bias	Bias corrected 10% trimmed statistics	
			mean $\overline{X}_{Tb}$	t-statistic t_{Tb}
0.015	10	-0.1430	9.855	-0.744
	15		14.843	-0.718
	20		19.630	-2.149
	25		24.580	-1.856
	30		29.618	-1.480
0.02	10	-0.2324	9.832	-0.876
	15		14.657	-1.729
	20		19.782	-0.951
	25		24.619	-1.619
	30		29.432	-2.111
0.03	10	-0.7832	10.070	0.353
	15		15.020	0.087
	20		20.333	1.542
	25		25.195	0.711
	30		30.183	0.727
0.04	10	-0.6022	10.027	0.154
	15		14.927	-0.325
	20		19.952	-0.166
	25		25.052	0.158
	30		29.939	-0.174
0.05	10	-0.6852	9.872	-0.647
	15		14.685	-1.288
	20		19.697	-1.007
	25		24.697	-0.894
	30		29.472	-1.280

Table 7.10 The bias corrected 10% trimmed statistics for the frequency distribution of the number of saros cycles. The appropriate bias has been removed from the results of Table 7.9.

Those values of t_{Tb} which are highlighted fail at the 95% confidence level to show agreement between the observed and predicted means.

Most of the bias-corrected values for the Student's t-test confirm that there is sufficient evidence at a 95% confidence level to believe that the number of saros cycles specified by Equation (7) is the mean number of actual saros cycles, once the bias caused by T_2' or T_3' close to low-number commensurabilities is removed. For counts greater than 1, Equation (7) is a sufficiently accurate method of calculating the number of saros cycles since the bias is of order less than 1 for the range of q' that we are interested in studying. For those final counts which are close to 1, the bias should be taken into consideration when using Equation (7).

If we now take reasonable values for the accuracy q' and upper integer limit A_{max} to be 0.01 and 1000 respectively, and take the period set (T_2', T_3') to have values approximating the ratios of the lunar synodic, anomalistic and nodical periods, ie

$$T_2' = T_A / T_S \approx 0.93$$

$$T_3' = T_N / T_S \approx 0.92$$

we find that the number of expected saros cycles from Equation (7) is, on average, 0.32. Adjusted for a bias corresponding to q' = 0.015, the value becomes even less at 0.28. In other words, for greater than 72% of the values of $\alpha = a/a_1$ that the Moon is driven through, the Moon is likely to have no effective saros cycle to stabilize its orbit against solar perturbations! It should be noted that A_{max}=1000 allows cycles with periods as long as 75 years to be included.

In the next section, we study the effect of tidal evolution on the Saros cycle.

7.6 The Effect of Tidal Evolution on the Saros Cycle

At the present epoch, the Earth-Moon-Sun orbital dynamics do contain a saros cycle; however, because of tidal evolution, this situation may change. What effect does the change in the period set (T_S,T_N,T_A) have on our present Saros cycle? Is tidal friction moving the Moon closer to a perfect saros or further away from one? When will the present Saros be at its best (ie closest to a perfect commensurability) and hence able to produce the best repetition of the relative geometry of the Earth-Moon-Sun system after one Saros period? How long will our present Saros cycle last? What other saros cycles has the Moon moved through in the past and will move through in the future? How do these saros cycles compare with the current one as an effective stabilizing mechanism against solar perturbations? How long do these saros cycles last on average? What happens to the Moon between saros cycles?

We begin to answer these questions by studying how the three satellite periods vary with time, if the Moon is assumed to be moving away from the Earth as a result of tidal interaction only. Equations (8), (9) and (10) show that the lunar synodic, nodical and anomalistic periods depend on the mean motion of the Moon n(t), the rate of change of the longitude of the lunar node $\dot{\Omega}(t)$, and the rate of change of the longitude of the lunar apse $\dot{\varpi}(t)$.

$$T_S = \frac{2\pi}{n - n_1} \tag{8}$$

$$T_N = \frac{2\pi}{n - \dot{\Omega}} \tag{9}$$

$$T_A = \frac{2\pi}{n - \dot{\omega}} \tag{10}$$

Each of these parameters in turn depend on the length of the semi-major axis and thus on time as tidal evolution causes the Moon to spiral outwards.

We first find the mean motion as a function of time. Goldreich and Soter (1966) give the rate of change of the Moon's semi-major axis due to tidal friction as:

$$\frac{da}{dt} = \frac{9}{2}\left(\frac{G}{M_p + m}\right)^{\frac{1}{2}} \frac{R^5}{Q_p'}\, m\, a^{-11/2} \qquad (11)$$

where

R = radius of the Earth

M_p, m = masses of the Earth and Moon respectively

a_1, a = semi-major axes of the Earth and Moon respectively

$$Q_p' = Q_p\left(1 + \frac{19\mu}{2g\rho R}\right)$$

$$\sin 2\varepsilon = \frac{1}{Q_p}$$

ε = tidal lag angle of the Earth

μ = coefficient of rigidity of the Earth

g = surface gravity of the Earth

ρ = mean density of the Earth

If we now do a simple integration of this equation, assuming that all the parameters aside from the Moon's semi-major axis are constant with respect to time, we obtain:

$$a = a_0 [\, 1 + K_1 t \,]^{2/13} \qquad (12)$$

where:

$$K_1 = \frac{117}{4}\left(\frac{G}{M_p + m}\right)^{\frac{1}{2}} \frac{R^5}{Q_p'}\, m\, a_0^{-13/2}$$

A zero subscript denotes a value of the specified parameter at the present time of $t = 0$. Then, using Kepler's third law

$$\left(\frac{n}{n_0}\right)^2 = \left(\frac{a_0}{a}\right)^3$$

we can rewrite Equation (12) as

$$n = n_0 \, [\, 1 + K_1 t \,]^{-3/13} \tag{13}$$

To find the lunar rates of change of the longitudes of the node $\dot{\Omega}$ and apse $\dot{\varpi}$ as functions of time, we use Delaunay's (1872) analytic series for these quantities, expanded in terms of the ratio of the mean motions of the Moon and the Sun:

$$\begin{aligned}\frac{d\Omega}{dt} = -n\Bigg[&\left(\frac{3}{4} - \frac{3}{2}\gamma^2 + \frac{3}{2}e^2 + \frac{9}{8}e_1^2 + \frac{51}{8}\gamma^2 e^2 - \frac{9}{4}\gamma^2 e_1^2 - \frac{21}{64}e^4 + \frac{9}{4}e^2 e_1^2 + \frac{45}{32}e_1^4\right)\nu^2 \\ &- \left(\frac{9}{32} - \frac{27}{16}\gamma^2 - \frac{189}{32}e^2 + \frac{23}{32}e_1^2 + \frac{27}{16}\gamma^4 + \frac{567}{16}\gamma^2 e^2 - \frac{99}{16}\gamma^2 e_1^2 - \frac{675}{256}e^4 - \frac{349}{16}e^2 e_1^2\right)\nu^3 \\ &- \left(\frac{273}{128} - \frac{843}{128}\gamma^2 - \frac{2739}{128}e^2 + \frac{3261}{256}e_1^2\right)\nu^4 \\ &- \left(\frac{9797}{2048} - \frac{7185}{1024}\gamma^2 - \frac{165411}{2048}e^2 + \frac{73423}{1024}e_1^2\right)\nu^5 \\ &- \frac{199273}{24576}\nu^6 - \frac{6657733}{589824}\nu^7 + \left(\frac{45}{32}\nu^2 + \frac{1935}{512}\nu^3\right)\alpha^2\Bigg]\end{aligned} \tag{14}$$

$$\begin{aligned}\frac{d\varpi}{dt} = n\Bigg[&\left(\frac{3}{4} - 6\gamma^2 - \frac{3}{8}e^2 + \frac{9}{8}e_1^2 - \frac{45}{4}\gamma^4 + \frac{69}{8}\gamma^2 e^2 - 9\gamma^2 e_1^2 - \frac{3}{32}e^4 - \frac{9}{16}e^2 e_1^2 + \frac{45}{32}e_1^4\right)\nu^2 \\ &+ \left(\frac{225}{32} - \frac{189}{8}\gamma^2 - \frac{675}{64}e^2 + \frac{825}{32}e_1^2 + \frac{1107}{16}\gamma^4 + \frac{81}{32}\gamma^2 e^2 - \frac{349}{4}\gamma^2 e_1^2 - \frac{2475}{64}e^2 e_1^2\right)\nu^3 \\ &+ \left(\frac{4071}{128} - \frac{3963}{32}\gamma^2 - \frac{31605}{512}e^2 + \frac{61179}{256}e_1^2\right)\nu^4 \\ &+ \left(\frac{265493}{2048} - \frac{335403}{512}\gamma^2 - \frac{1483665}{4096}e^2 + \frac{1767849}{1024}e_1^2\right)\nu^5 \\ &+ \left(\frac{12822631}{24576} - \frac{25291729}{16384}e^2\right)\nu^6 \\ &+ \left(\frac{1273925965}{589824} + \frac{352038885}{1179648}e^2\right)\nu^7 \\ &+ \frac{71028685589}{7077888}\nu^8 + \frac{32145882707741}{679477248}\nu^9 + \left(\frac{45}{32}\nu^2 + \frac{7425}{512}\nu^3\right)\alpha^2\Bigg]\end{aligned} \tag{15}$$

where:

$d\varpi/dt$ = rate of movement of the Moon's pericentre

$d\Omega/dt$ = rate of movement of the Moon's node

n, n_1 = mean motions of the Moon and Sun respectively

e, e_1 = mean eccentricities of the Moon and Sun respectively

a, a_1 = semi-major axes of the Moon and Sun respectively

i = inclination of the Moon's orbit

$\gamma = \sin i/2$

$\nu = n_1/n$

$\alpha = a/a_1$

Note that these expressions reduce to the special case given in Brouwer and Clemence (1961, pg. 322), where e, e_1, γ, and α are assumed to be very small. Since Delaunay's expressions contain only second or higher ordered terms involving these parameters, Brouwer and Clemence have neglected them to produce two series involving an expansion in ν only.

$$\frac{d\Omega}{dt} = -n\left(\frac{3}{4}\nu^2 - \frac{9}{32}\nu^3 - \frac{273}{128}\nu^4 - \frac{9797}{2048}\nu^5 - \ldots\right)$$

$$\frac{d\tilde{\omega}}{dt} = +n\left(\frac{3}{4}\nu^2 + \frac{225}{32}\nu^3 + \frac{4071}{128}\nu^4 + \frac{265493}{2048}\nu^5 + \ldots\right)$$

Brouwer and Clemence give this special case to ninth order in ν for $d\varpi/dt$ and to seventh order in ν for $d\Omega/dt$, using rational coefficients. Tisserand (1894, pg.233) sites the same expressions using fraction coefficients. Both Brouwer and Clemence and Tisserand point out that for the Moon, the terms neglected in this special case are large enough to cause some doubt as to the convergence of the series or at least to cause the series to converge only very slowly. We therefore use Delaunay's complete expression giving the coefficients of ν^n (where n = 2,3, ...) as functions of e, e_1, γ, and α to fourth order.

It should also be noted that the formulae for $\dot{\Omega}$ and $\dot{\varpi}$ previously published by Delaunay in his Théorie du Movement de la Lune, Vol II (1867) are not the same as those published later by him in 1872. As these earlier results do not reduce to those

of Brouwer and Clemence and Tisserand, we take the later version of 1882 to be the correct one.

We now assume that any changes in e, γ and e_1 with respect to time due to tidal or gravitational effects are so small over the time interval being studied that second order terms involving these small changes are negligible compared to terms involving changes in the mean motion. This assumption should be valid provided we avoid studying changes over very long intervals of time. In any case lunar theories like Delaunay's have no guarantee of series convergence for long periods of time and so cannot be expected to give meaningful results in such circumstances.

The substitution of Equation (13) into Delaunay's Equations (14) and (15) will give the rates of change of the lunar node and pericentre as functions of time. Equations (13), (14) and (15) can then be substituted into equations (8), (9) and (10) to give the relationships of the three periods T_S, T_N and T_A with time, assuming that only tidal effects are acting on the lunar orbit. Figures 7.10(a) to (e) show the theoretical relationships of n, a, T_S, T_N and T_A with time, allowing only for tidal disturbances to the Moon's orbit, and keeping e,γ and e_1 constant.

Figures 7.10(a) to (e) The theoretical relationship between

(a) the Moon's semi-major axis a

(b) the Moon's mean motion n

(c) the lunar synodic period T_S

(d) the lunar anomalistic period T_A

(e) the lunar nodical period T_N

and time.

These functions are derived using Kepler's third law, Delaunay's lunar theory for $\dot{\Omega}$ and $\dot{\varpi}$ and tidal theory for a(t).

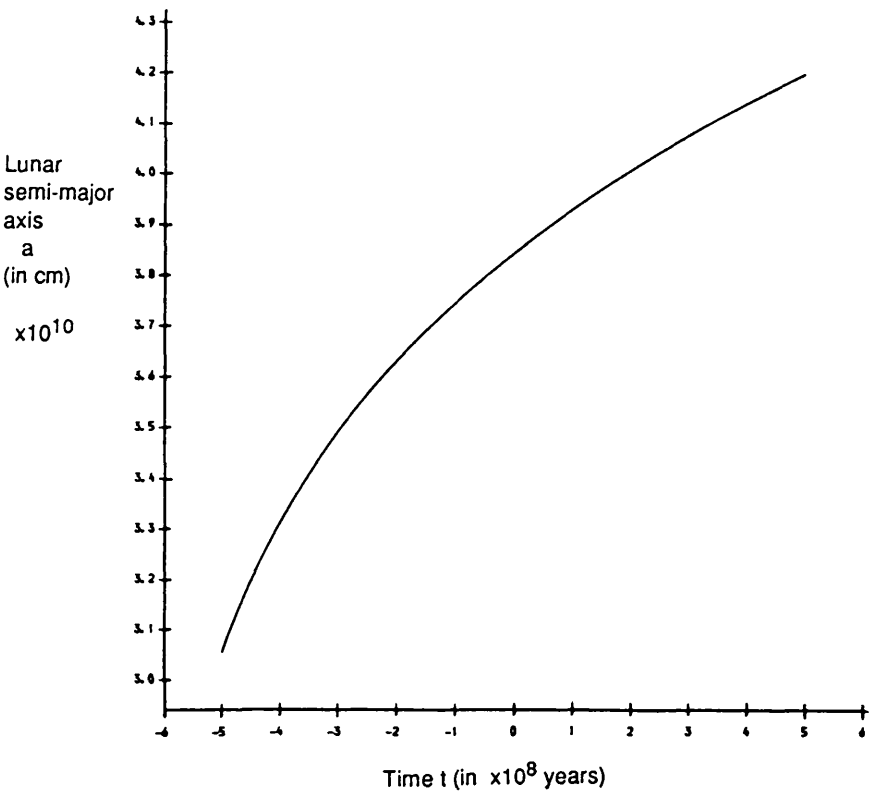

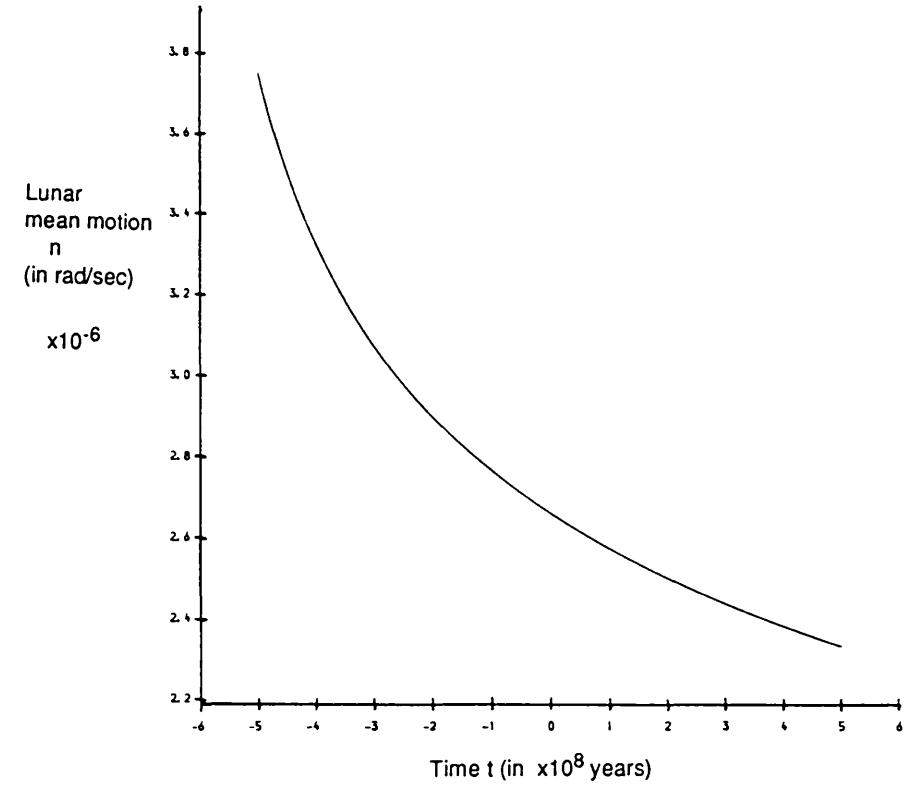
Lunar
mean motion
n
(in rad/sec)
x10-6
3.8
3.6
3.4
3.2
3.0
2.8
2.6
2.4
2.2
-6
-5
-4
-3
-2
-1
0
1
2
3
4
5
6
Time t (in x10^8 years)

(b)

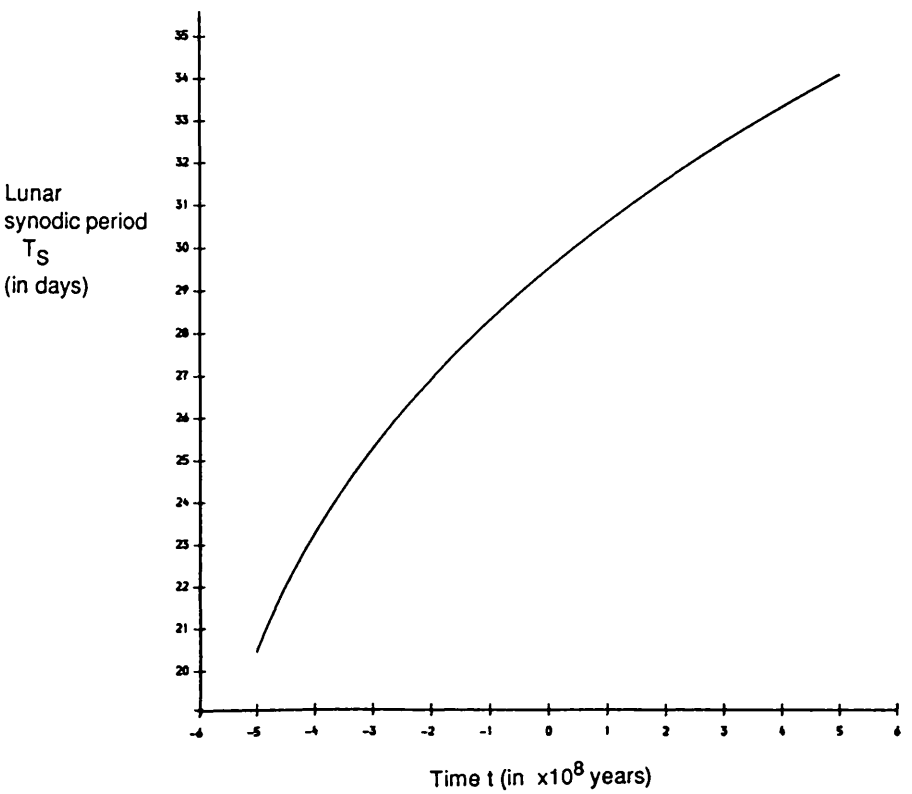
Lunar
synodic period
Ts
(in days)
35
34
33
32
31
30
29
28
27
26
25
24
23
22
21
20
-6
-5
-4
-3
-2
-1
0
1
2
3
4
5
6
Time t (in x10^8 years)

(c)

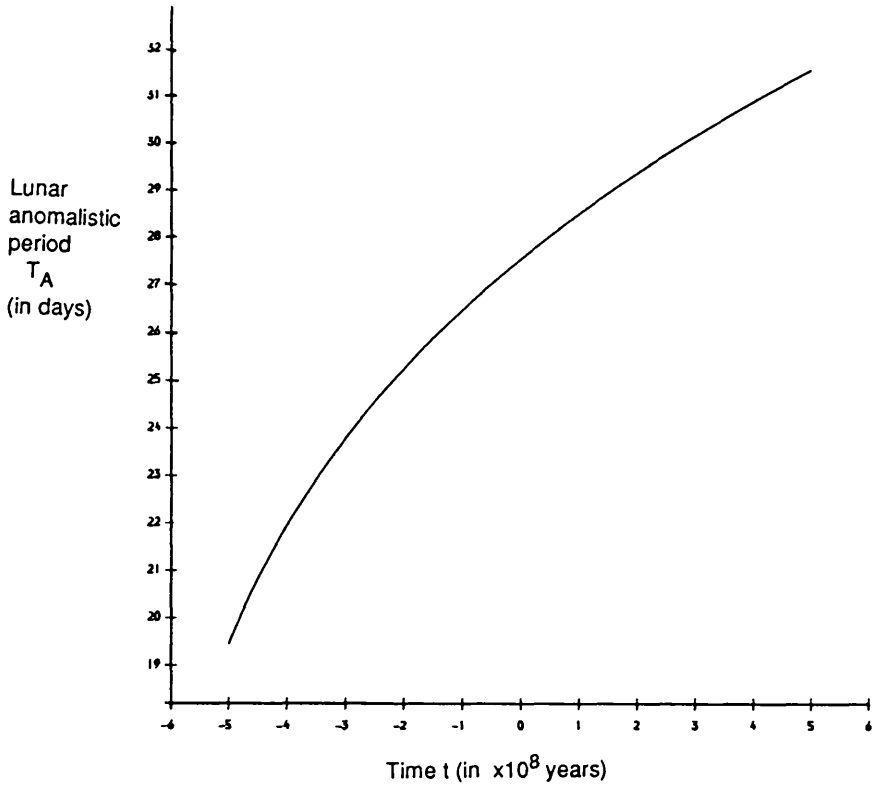
Lunar anomalistic period T_A (in days)
32
31
30
29
28
27
26
25
24
23
22
21
20
19
-6
-5
-4
-3
-2
-1
0
1
2
3
4
5
6
Time t (in x10^8 years)

(d)

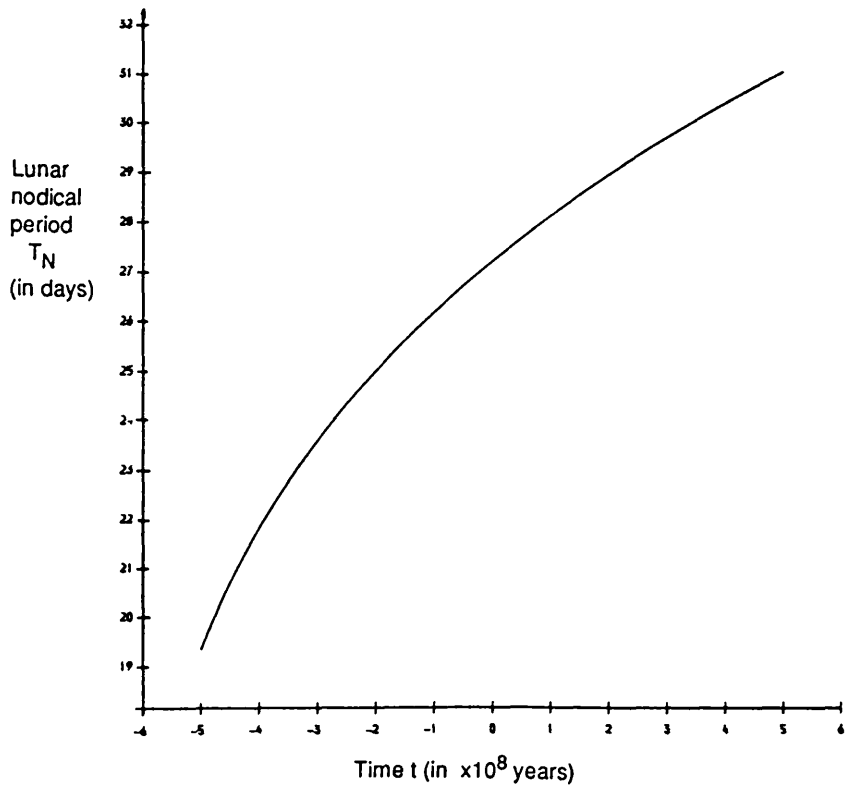
Lunar nodical period T_N (in days)
32
31
30
29
28
27
26
25
24
23
22
21
20
19
-6
-5
-4
-3
-2
-1
0
1
2
3
4
5
6
Time t (in x10^8 years)

(e)

Figures 7.10 are found using the following values for the constants in Equations (13), (14) and (15):

Planet Constants (Earth)

$M_p = 5.98 \times 10^{27}$ g

$R = 6.37812 \times 10^{8}$ cm

$a_1 = 1.49596 \times 10^{13}$ cm

$e_1 = 0.016726$

$n_1 = 1.990987 \times 10^{-7}$ rad/s

$\rho = 5.52$ g/cm^3

$g = 9.8064 \times 10^{2}$ cm/s

$\varepsilon = 2.16$ deg

$\mu = 3 \times 10^{11}$ dynes/cm

Satellite Constants (Moon)

$m = 7.35 \times 10^{25}$ g

$a_0 = 3.844 \times 10^{10}$ cm

$e = 0.05490$

$i = 5.133$ deg

$n_0 = 2.661700 \times 10^{-6}$ rad/s

Other Constants

$G = 6.672 \times 10^{-8}$ dyne cm^2/g^2

The best values for the constants pertaining specifically to the effect of tidal friction on the Moon's orbit are discussed at length in Goldreich and Soter (1966). We use their preferred values. Unfortunately constants such as the tidal lag angle of the Earth ε, the coefficient of rigidity of the Earth μ, and consequently Q_p, are not accurately known. Their uncertainty has caused considerable problems in any attempt

to assign a time scale to the Moon's orbital evolution.

It should be noted that for large time intervals Figures 7.10(a) to (e) probably do not depict the real values of the three periods at the specified times. Even for small times they may not be correct, because of the uncertainty in some of the values of the constants. We have also assumed that these so-called constants remain constant for the time interval that we are studying. If the time intervals are large, this assumption is probably no longer valid. In tidal theory, these complications are traditionally ignored because of a lack of plausible methods for dealing with them.

In any event, our aim is not to find the exact values of the period set (T_S, T_N, T_A) at any given time, but to find an approximate relationship of the period set with time. Thus a possible sequence of saros cycles may be found in order to gain a better understanding of how saros cycles evolve and how often the Moon finds itself in a saros cycle.

It is worth noting that at least for time t = 0 the relationships of T_S, T_N, and T_A with time shown in Figures 7.10 (c) to (e) are very accurate. At time t=0 Delaunay's expressions give:

T_S = 29.530 572 days

T_A = 27.554 562 days

T_N = 27.212 219 days

while the currently accepted values are:

T_S = 29.530 589 days

T_A = 27.554 550 days

T_N = 27.212 221 days

So far in this model, we have assumed that no other perturbations have an accumulative effect on the Moon's orbit over these large time scales. This assumption

could be false if the Moon's orbital dynamics do not include an effective saros cycle to cancel out the large disturbances of the Sun on the Moon's orbit. If the solar perturbations are able to build up before the lunar orbit can find a new saros cycle to stabilize its orbit, the Moon's eccentricity and inclination could change quite dramatically. Any large changes in the eccentricity and inclination due to solar perturbations would invalidate the assumption that the second order terms of e and γ in Delaunay's equations (14) and (15) are constant relative to changes in terms containing the mean motion.

This assumption should, however, be valid for shorter periods of time when solar perturbations have not had time to accumulate. It should certainly be valid for at least the lifetime of our present saros cycle, when solar perturbations are effectively cancelled. Making the assumption for longer times might not be entirely correct, but at least it will provide us with an idea of how the Moon passes from one saros cycle to the next. Even if the initial eccentricity and inclination used to find these saros cycles has changed enough to bring the Moon's orbit into an entirely different set of saros cycles from the ones derived here, it is the fact that tidal friction drives the Moon's orbit through these saros cycles that is important for any stability analysis of the lunar orbit.

A complete study of the saros cycles that the Moon's orbit has evolved through, would require the numerical integration of the Moon's equations of motions taking both the gravitational effects of the Sun and the tidal effects of the Earth into account and allowing for variations in e, i and e_1 due to these effects.

Having found the variation of the three satellite periods with time, we can now evaluate the period set (T_S,T_A,T_N) at successive intervals of time and calculate the saros cycles described by the integer set (A_1,A_2,A_3) which exist for each period set. Here it is important to make the time step small enough in order to discover all the existing saros cycles.

For each saros cycle found, we can also calculate: the discrepancies ε_{12}', ε_{13}', ε_{23}' as functions of time; the beginning t_b of the saros cycle (ie the time when $|\varepsilon_{12}'|$, $|\varepsilon_{13}'|$ and $|\varepsilon_{23}'|$ all first become less than or equal to a given accuracy q'); the end t_e

of the saros cycle (ie the time when $|\varepsilon_{12}'|$, $|\varepsilon_{13}'|$ or $|\varepsilon_{23}'|$ become greater than q'); the duration of the saros cycle $t_d = t_e - t_b$; and the time t_p at which the specified saros cycle is closest to being a perfect saros cycle.

A perfect saros cycle is one where $\varepsilon_{12}' = \varepsilon_{13}' = \varepsilon_{23}' = 0$. Therefore intuitively, a near saros cycle may be taken to be closest to a perfect cycle when its discrepancies are smallest. We can write this mathematically by defining the closest approach of a saros cycle to a perfect saros cycle to occur where the root mean squared of the discrepancies ε^{rms} is at its minimum, viz

$$\varepsilon^{rms} = \sqrt{\varepsilon_{12}^2 + \varepsilon_{13}^2 + \varepsilon_{23}^2}$$

This parameter will then be of use in comparing the abilities of different saros cycles to cancel solar perturbations, since the smaller the value ε^{rms} becomes, the closer the near saros cycle approaches a perfect saros cycle and the better it becomes at cancelling solar perturbations.

Figure 7.11(a) displays the relationship of the discrepancies ε_{12}', ε_{13}' and ε_{23}' with time for the current saros cycle, while Figure 7.11(b) gives the current saros cycle's ε^{rms} as a function of time. If we accept that an accuracy of q' = 0.01 and an upper integer limit of A_{max}=1000 are reasonable restrictions on our definition of a saros cycle, Figures 7.11 provides the following information.

Figures 7.11 The relationships between
(a) the residuals ε_{12}', ε_{13}' and ε_{23}'
(b) the root mean squared sum of the residuals ε^{rms}
and time, for the present saros cycle.

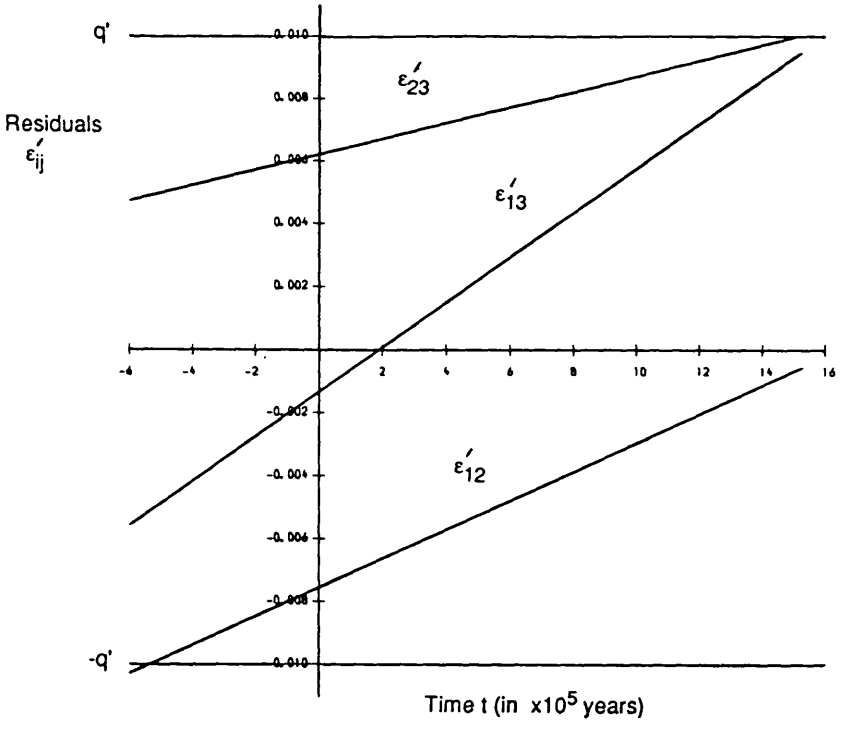
q'
Residuals
ε'_{ij}
ε'_{23}
ε'_{13}
ε'_{12}
-q'
Time t (in x10^5 years)

(a)

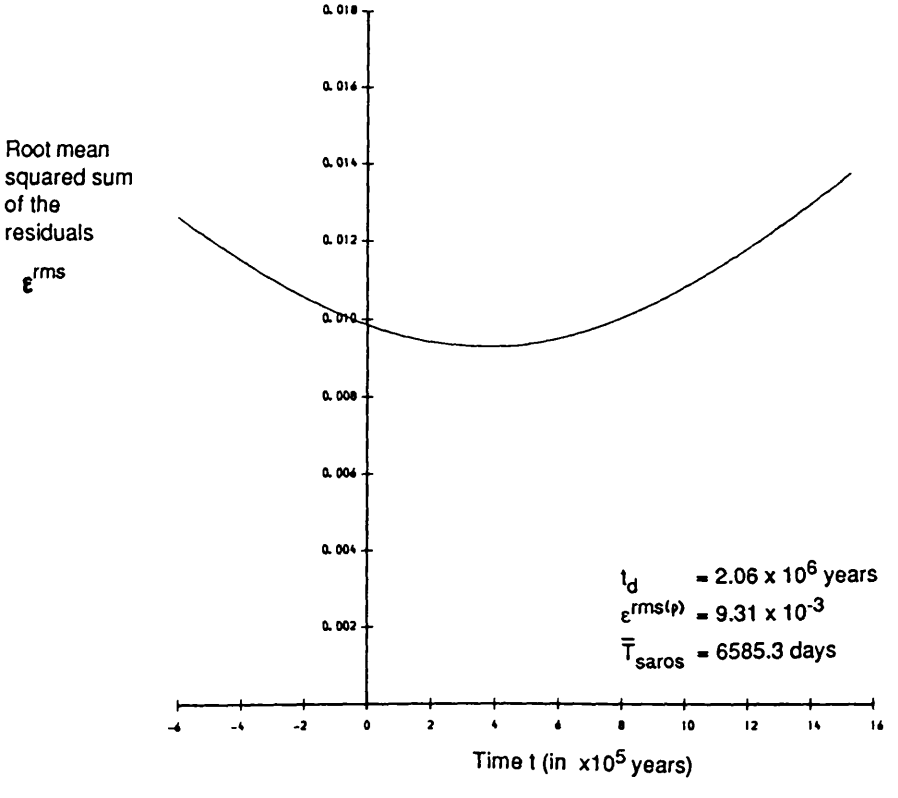
Root mean squared sum of the residuals
ε^{rms}
t_d = 2.06 x 10^6 years
$\varepsilon^{rms(\rho)}$ = 9.31 x 10^{-3}
$\overline{T}_{saros}$ = 6585.3 days
Time t (in x10^5 years)

(b)

The current saros cycle began approximately 5.37×10^5 years ago and is presently improving in its ability to cancel solar perturbations. It reaches its closest approach to a perfect saros cycle in 3.69×10^5 years, where the root mean squared sum of the discrepancies will have decreased to its minimum of $\varepsilon^{rms} = 9.31 \times 10^{-3}$. The present saros cycle will finally be disrupted about 1.52×10^6 years from now, having survived approximately 2.06×10^6 years. Finally, it is the discrepancy ε_{23}' relating T_2' and T_3' (ie the anomalistic and nodical months) which first fails the restriction $|\varepsilon_{ij}'| \leq q' = 0.01$ and consequently puts the Saros cycle outside the accuracy criterion.

Table 7.11 lists the sequence of saros cycles through which the Moon is driven from $t = -5.0 \times 10^7$ years to $t = +5.0 \times 10^7$ years, if only tidal evolution is permitted to change the Moon's orbital elements. In the calculation, a step size of 10^5 years was used. The intervals where no saros cycles occurred were re-analysed with a step size of 10^4 years, but still no new saros cycles appeared. The theoretical beginnings t_b of each saros cycle, their ends t_e, durations t_d, times of cloest approach to a perfect saros cycle t_p, degree of closeness to a perfect saros cycle at this point in time $\varepsilon^{rms(p)}$, and average saros period $T_{saros(p)}$ at time $t = t_p$ are also given.

On average, the saros cycles endure about 8×10^5 years, but they can last as much as 2.2×10^6 years or as little as 1×10^5 years. The saros periods range from about 2,000 days to 27,200 days with an average of 18,200 days. The closest approaches to a perfect saros cycle as measured by the parameter $\varepsilon^{rms(p)}$, range from 0.45×10^{-3} to 13.4×10^{-3}, with an average of 7.61×10^{-3}.

From Table 7.11 we can see that our present saros cycle seems to be particularly effective at stabilizing the Moon's orbit against solar perturbations. It lasts longer than most with a lifetime of 2×10^6 years and its Saros period is the smallest. Our present Saros is, however, not as good as the average saros cycle in Table 7.11, at repeating the geometry of the system every saros period since its $\varepsilon^{rms(p)}$ is larger than average.

Saros cycle			Beginning	Duration	Closest approach to a perfect saros		
					Time	Residual	Period
A_1	A_2	A_3	t_b ($\times 10^5$yrs)	t_d ($\times 10^5$yrs)	t_p ($\times 10^5$yrs)	$\varepsilon^{rms(p)}$ ($\times 10^{-3}$)	T_{saros} (days)
848	908	919	-417.67	1.15	-417.58	12.90	25,028
692	741	750	-393.02	1.06	-393.16	13.16	20,421
847	907	918	-391.59	5.66	-389.05	8.53	24,995
691	740	749	-361.24	7.06	-358.03	8.34	20,393
536	574	581	-353.96	1.03	-354.37	13.34	15,918
535	573	580	-312.90	9.23	-308.69	8.25	15,790
915	980	992	-301.22	6.54	-298.13	5.14	27,006
380	407	412	-282.61	1.38	-283.24	13.38	11,216
759	813	823	-254.46	7.99	-250.71	5.02	22,404
379	406	411	-223.86	13.05	-217.97	8.41	11,188
603	646	654	-183.02	10.25	-178.28	4.63	17,801
826	885	896	-133.48	7.52	-129.48	4.42	24,387
224	240	243	-110.80	4.29	-110.52	12.96	6,614
447	479	485	- 60.37	14.03	- 53.72	3.72	13,199
894	958	970	- 56.86	6.03	- 53.72	7.43	26,398
670	718	727	- 39.35	9.03	- 34.65	5.57	19,784
223	239	242	- 5.37	20.61	3.69	9.31	6,585
738	791	801	45.41	8.23	49.37	5.70	21,795
514	551	558	114.95	10.57	119.95	7.65	15,182
805	863	874	148.66	7.43	152.43	6.17	23,778
291	312	316	199.23	22.20	210.11	1.41	8,597
582	624	632	204.77	11.10	210.11	2.82	17,193
873	936	948	206.62	7.40	210.11	4.22	25,789
650	697	706	281.99	1.60	282.06	12.93	19,204
649	696	705	320.66	5.93	323.46	10.18	19,176
359	385	390	337.53	7.27	340.82	11.40	10,606
717	769	779	373.99	9.17	378.60	0.45	21,167
358	384	389	413.07	5.93	416.63	11.89	10,579
785	842	853	420.89	6.34	424.45	9.12	23,198
426	457	463	487.43	15.64	495.49	2.48	12,591
852	914	926	491.33	7.82	495.49	4.97	25,181

Table 7.11 The saros-type cycles through which the Moon's orbit evolves in the time interval of -5×10^7 years to $+5\times10^7$ years.

Only the effects of tidal friction on the lunar orbit are taken into account. The present Saros cycle is highlighted.

Figures 7.12(a) to (d) parts (i) give a few examples of how the residuals of some of the other saros cycles change with time. Parts (ii) depict their closest approaches to a perfect saros cycle. All the saros cycles listed in Table 7.11 have residuals which are almost linear functions of time, with the result that their ε^{rms} curves are all smooth and contain unique minima.

The saros cycles in Figures 7.12(a) and (b) both have longer than average durations. Figures 7.12(a) show a saros cycle with a smaller than average saros period, smaller than average minimum accuracy, and consequently a larger than average duration. The saros cycle shown in Figures 7.12(b) has a larger saros period and a larger minimum accuracy than the saros cycle in Figures 7.12(a), and as a result has a shorter duration.

Figures 7.12(c) is an example of a saros cycle of reasonably large saros period, but very small minimum accuracy. It consequently has a slightly longer than average duration. Figures 7.12(d), on the other hand, is an example of a saros cycle of relatively small saros period, but very large minimum accuracy. It too has a slightly longer than average duration.

Generally smaller minimum accuracies and saros periods tend to produce longer lasting saros cycles. However, which parameter has the greater influence in the relationship with the duration of the saros cycle, the accuracy or the saros period, is not known.

Figures 7.12(a) to (d) The relationships between

(i) the residuals ε_{12}', ε_{13}' and ε_{23}'

(ii) the root mean squared sum of the residuals ε^{rms}

and time, for each of the following saros cycles

(a) $A_1 = 447$, $A_2 = 479$, $A_3 = 485$

(b) $A_1 = 514$, $A_2 = 551$, $A_3 = 558$

(c) $A_1 = 717$, $A_2 = 769$, $A_3 = 779$

(d) $A_1 = 380$, $A_2 = 407$, $A_3 = 412$

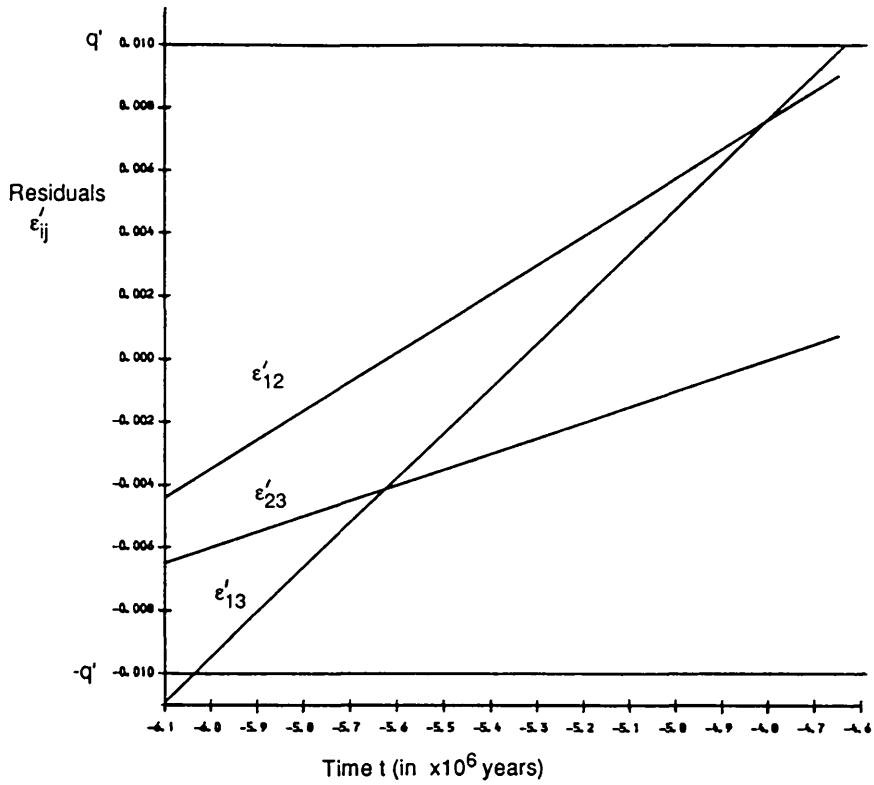
q'
0.010
0.008
0.006
Residuals
ε'_{ij}
0.004
0.002
0.000
ε'_{12}
-0.002
ε'_{23}
-0.004
-0.006
ε'_{13}
-0.008
-q'
-0.010
-5.1 -5.0 -4.9 -4.8 -4.7 -4.6 -4.5 -4.4 -4.3 -4.2 -4.1 -4.0 -3.9 -3.8 -3.7 -3.6
Time t (in x10^6 years)

(a) i

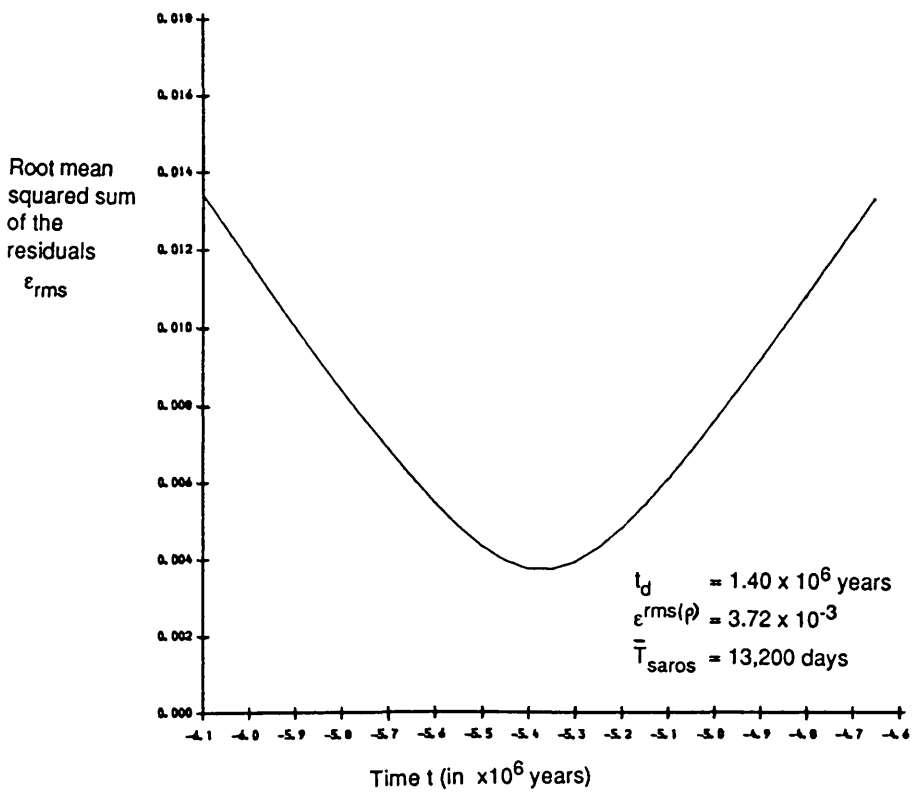
Root mean squared sum of the residuals
ε_{rms}
0.018
0.016
0.014
0.012
0.010
0.008
0.006
0.004
0.002
0.000
t_d = 1.40 x 10^6 years
$\varepsilon^{rms(\rho)}$ = 3.72 x 10^{-3}
$\bar{T}_{saros}$ = 13,200 days
-5.1 -5.0 -4.9 -4.8 -4.7 -4.6 -4.5 -4.4 -4.3 -4.2 -4.1 -4.0 -3.9 -3.8 -3.7 -3.6
Time t (in x10^6 years)

(a) ii

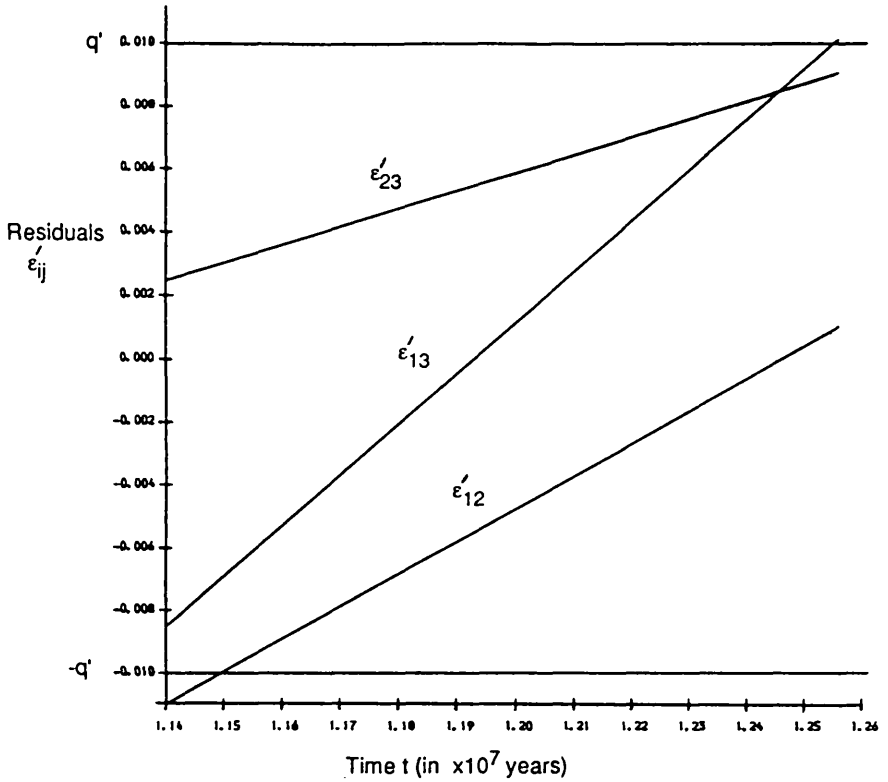
q'
-q'
Residuals
ε'_{ij}
ε'_{23}
ε'_{13}
ε'_{12}
Time t (in x10^7 years)

(b)i

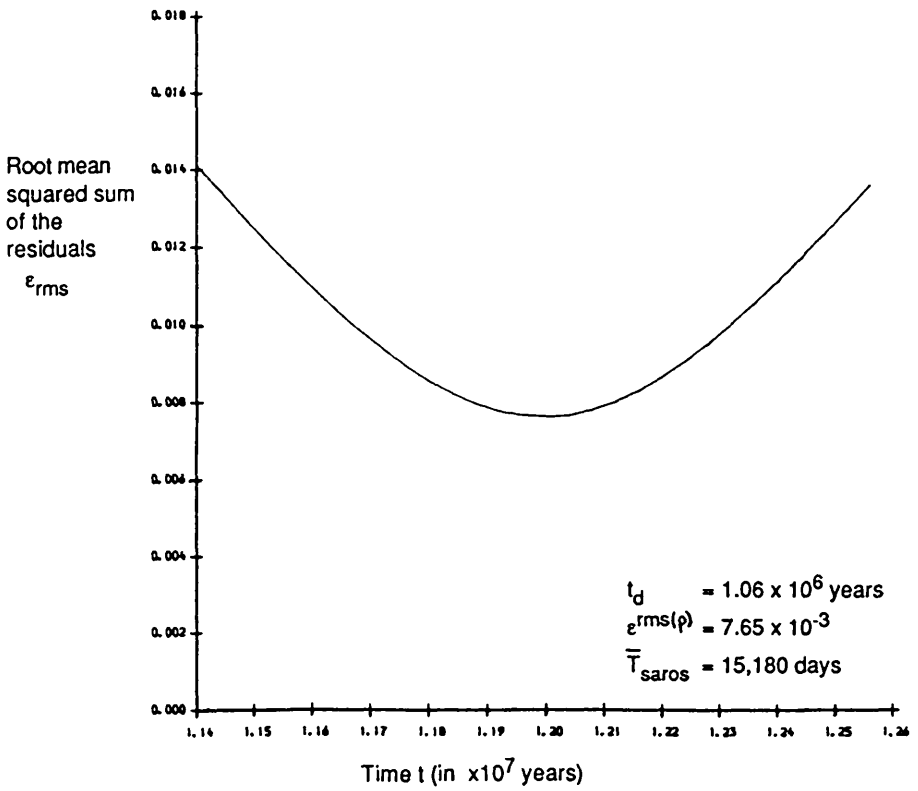
Root mean squared sum of the residuals
ε_{rms}
t_d = 1.06 x 10^6 years
$\varepsilon^{rms(\rho)}$ = 7.65 x 10^{-3}
$\overline{T}_{saros}$ = 15,180 days
Time t (in x10^7 years)

(b)ii

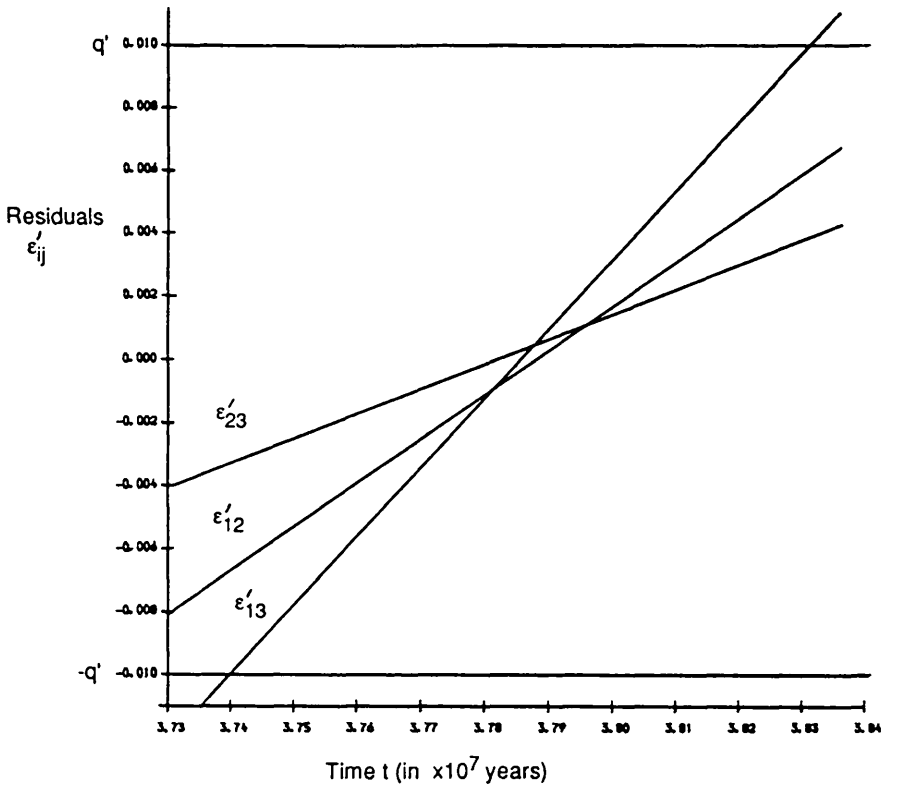
q'
-q'
Residuals
ε'_{ij}
ε'_{23}
ε'_{12}
ε'_{13}
Time t (in x10^7 years)

(c) i

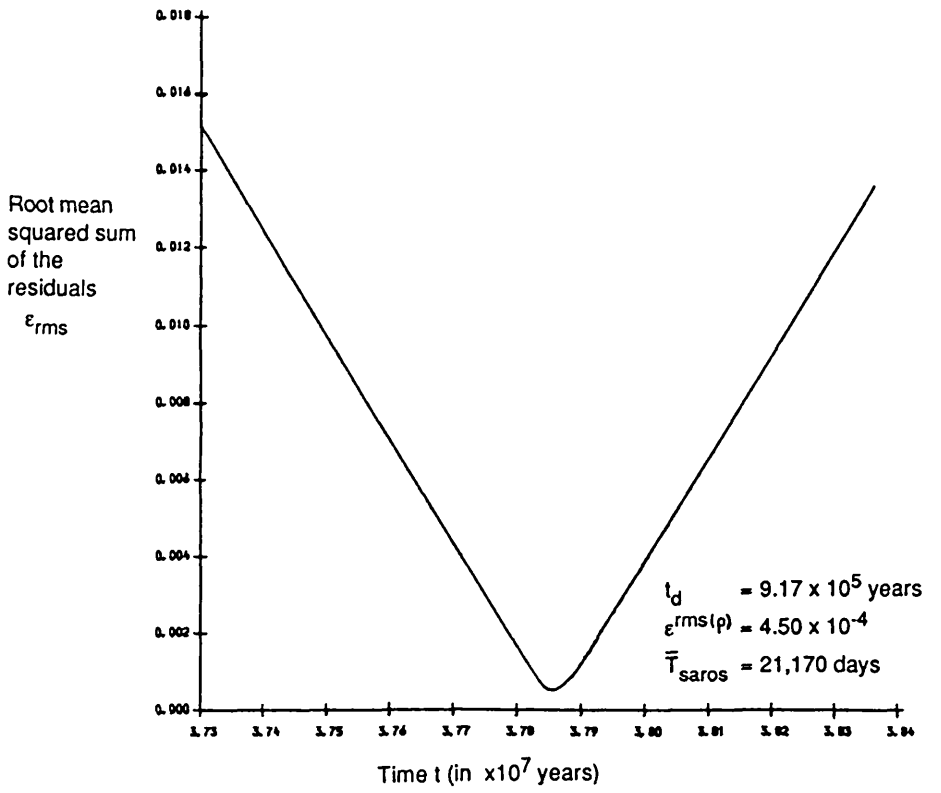
Root mean squared sum of the residuals
ε_{rms}
t_d = 9.17 x 10^5 years
$\varepsilon^{rms(\rho)}$ = 4.50 x 10^{-4}
$\bar{T}_{saros}$ = 21,170 days
Time t (in x10^7 years)

(c) i i

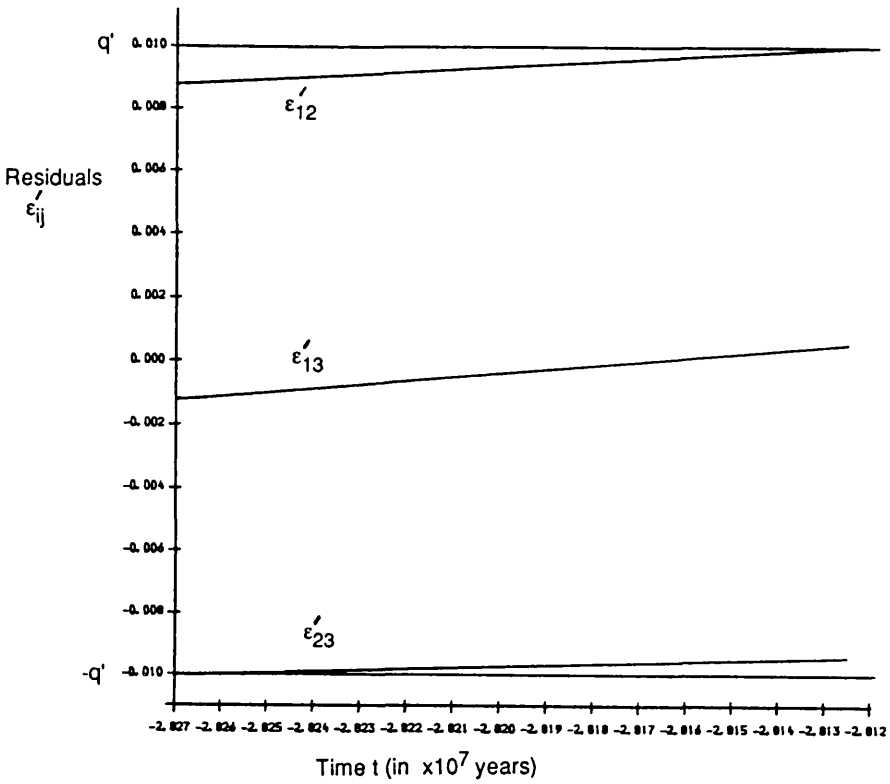
q'
0.010
0.008
0.006
0.004
0.002
0.000
-0.002
-0.004
-0.006
-0.008
-0.010
-q'
Residuals
ε'_{ij}
ε'_{12}
ε'_{13}
ε'_{23}
-2.827 -2.826 -2.825 -2.824 -2.823 -2.822 -2.821 -2.820 -2.819 -2.818 -2.817 -2.816 -2.815 -2.814 -2.813 -2.812
Time t (in $x10^7$ years)

(d) i

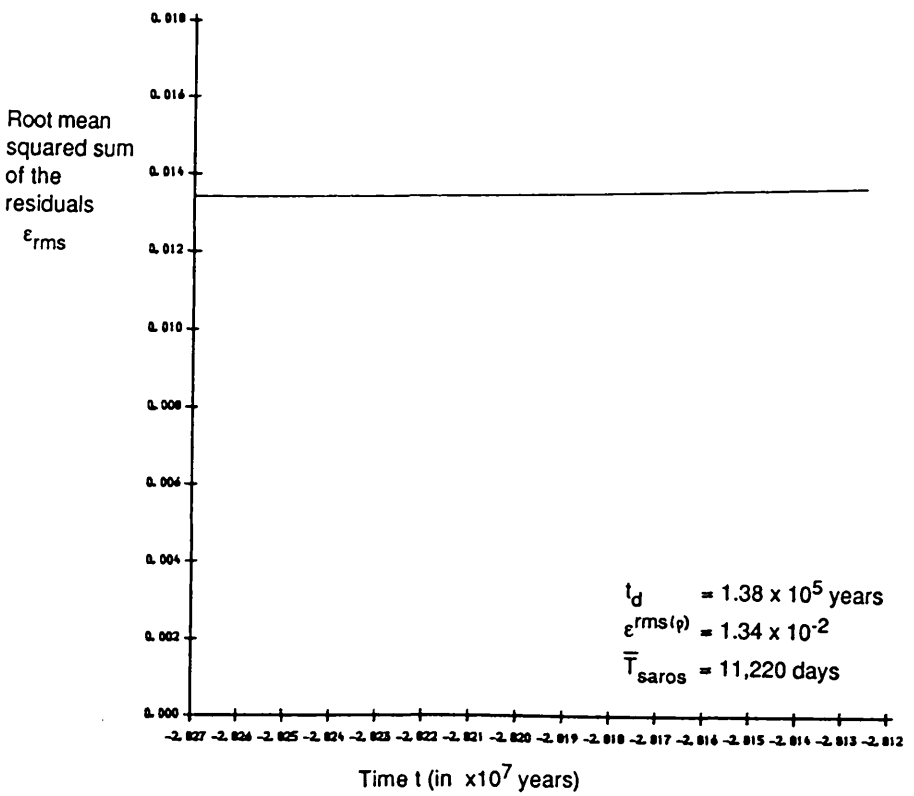
0.018
0.016
0.014
0.012
0.010
0.008
0.006
0.004
0.002
0.000
Root mean squared sum of the residuals
ε_{rms}
t_d = 1.38 x 10^5 years
$\varepsilon^{rms(\rho)}$ = 1.34 x 10^{-2}
$\overline{T}_{saros}$ = 11,220 days
-2.827 -2.826 -2.825 -2.824 -2.823 -2.822 -2.821 -2.820 -2.819 -2.818 -2.817 -2.816 -2.815 -2.814 -2.813 -2.812
Time t (in $x10^7$ years)

(d) i i

Table 7.11 also shows that as is expected from the probability analysis of Section 7.4, the Moon's orbit possesses a saros cycle less than 28% of the time or calculating the proportion of time spent in a saros cycle directly from Table 7.11, for only 25.3% of the time. This proportion is more obviously seen in Figures 7.13 where a horizontal line marks the existence of a saros cycle at the specified time interval on the x-axis. The y-axis gives the period of the saros cycle. It should be remembered, however, that these intervals are calculated taking into account only the effect of tidal evolution on the Moon's orbital elements.

What happens to the Moon's orbit during epochs when tidal friction has taken the Moon into a situation where a saros no longer exists or where only one with a very long period is present, is still uncertain. It seems possible that in such a case, solar perturbations may grow to the point where they change the Moon's orbital elements irreversibly before another saros cycle is found.

All we may suppose at present is that when the Moon finds a good near saros cycle within its orbital dynamics, which it does on a purely random basis about 25% of the time, the orbit is maintained against solar perturbations for the length of time that tidal evolution allows the near saros cycle to exist. Future work will need to be devoted to examining the lunar behavior between saros cycles.

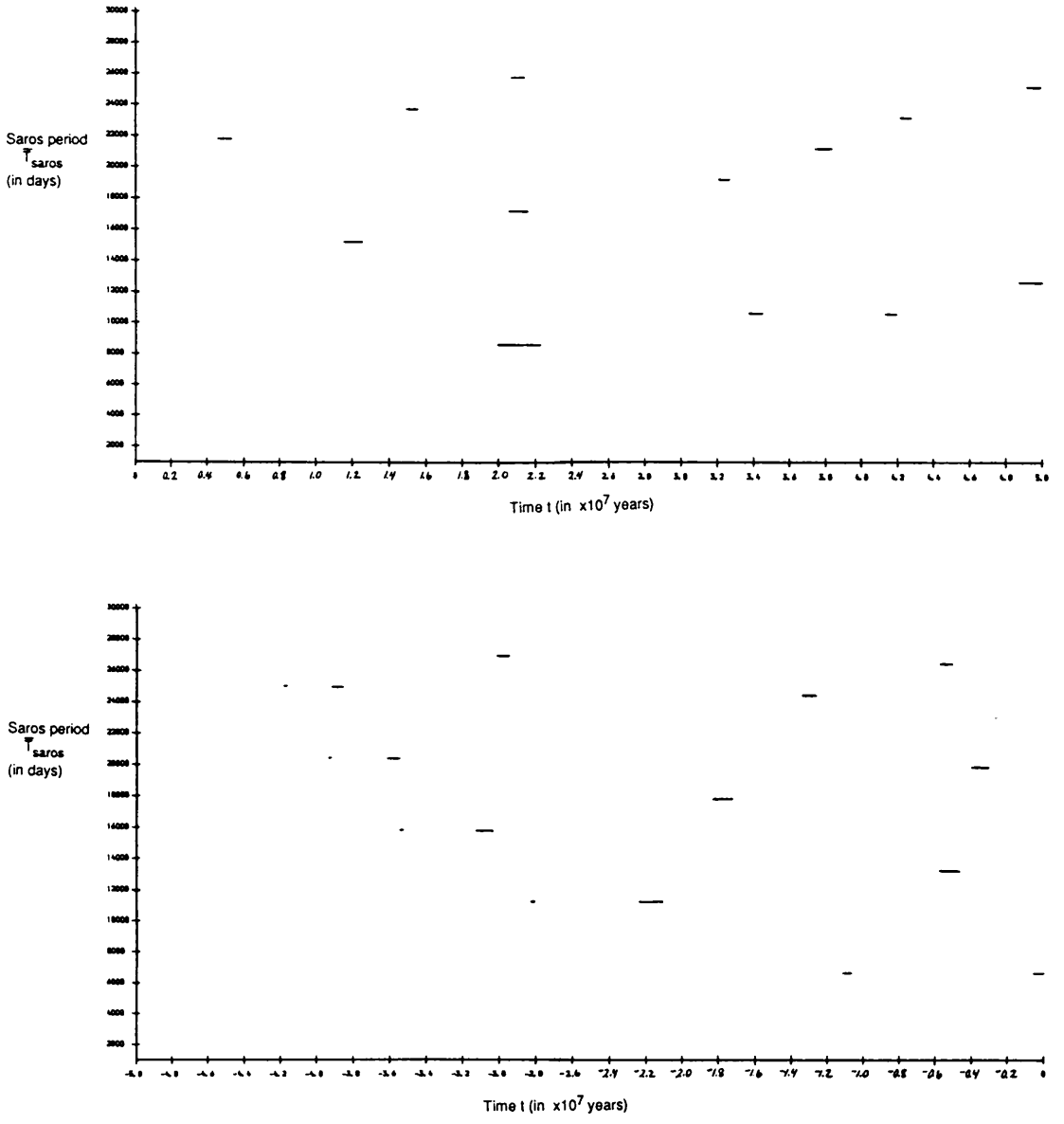

Figures 7.13(a) to (b) The Saros cycles that the Moon is driven through over the time interval of -2.5×10^7 years to $+2.5 \times 10^7$ years, if only tidal evolution is affecting the Moon's orbital elements.

7.7 Conclusions

We have been able to answer quite a few of the questions about the nature of saros cycles, their frequency of occurrence and their possible use as a stability mechanism for the Earth-Moon system against solar perturbations. We now know that, the Moon acting under solar perturbations appears to be moving in a nearly periodic orbit of period equal to one Saros period of 6585.32 days. The Saros period is therefore the natural averaging period by which solar perturbations can be most effectively removed in any research into the long-term evolution of the lunar orbit.

The occurrence of at least two mirror configurations during the Saros cycle ensures that the relative dynamical geometry of the Earth-Moon-Sun system is nearly repeated after one Saros period.

The existence of the Saros mechanism in reversing solar perturbations so effectively may have consequences for temporary lunar stability. If the lunar orbit contains a near saros cycle that is close enough to a perfect saros cycle to repeat the relative dynamical geometry of the Earth-Moon-Sun system accurately, and has a saros period small enough to allow the system to repeat the saros cycle before solar perturbations can grow beyond the point where the system changes irreversibly, the system may remain stable by cancelling solar perturbations over the saros period for as long as tidal evolution allows the saros cycle to persist.

Tidal evolution will, however, eventually destroy the saros cycle and another one must be found by the Moon in order that solar perturbations can be effectively cancelled for the new orbit. If we consider only tidal effects, we can now calculate a possible sequence of saros cycles which might be found in the lunar orbit's evolution. Unfortunately, the lunar orbit has only about a 25% chance of finding such a stabilizing saros cycle.

In general, we find that for a given period set (T_1,T_2,T_3) not close to a low number commensurability, the number N of expected saros cycles is given by the formula:

$$N = \frac{3q'^2}{T_2'} A_{max}$$

where $T_1>T_2>T_3$, $T_2'=T_2/T_1$, q' is the maximum deviation allowed from a perfect saros cycle relative to the largest period T_1, and A_{max} is the largest integer multiple allowed in the saros cycle. If we are analyzing the value of N for a number of period sets of similar value and N is of the order 1, a small fractional bias which depends on the value of q' should be subtracted from the formula to allow for the small number of period sets which lie close to a low number commensurability and are therefore not taken into consideration by the formula.

Without a saros stabilizing mechanism which cancels solar perturbations quickly, the lunar orbital elements could change enough that they may become irreversibly different from their original values. They would then continue to change until the Moon either escapes, collides with the Earth, or finds another good near saros cycle within the system's orbital dynamics to stabilize the new orbital elements.

What happens to the lunar orbit between saros cycles is still uncertain. We have only studied the evolution of the lunar orbit as it is affected by tidal friction alone. A complete study of the effect of the saros cycles on lunar evolution must include both the gravitational effects of the Sun and the tidal effects of the Earth. Future work should involve numerical integrations of the Moon's equations of motion taking both these effects into consideration, while paying particular attention to the relationship between irreversible changes in the orbital elements and the passage of the lunar orbit in and out of saros cycles.

The present work also suggests that a search should be made for other higher order commensurabilities of the saros cycle type occurring, for example, amongst the saturnian and jovian satellites that are highly perturbed by the Sun. Is it possible that the groupings of such satellites are consequences of saros cycles providing at least a temporary cancelling of solar perturbations? If so, high number commensurabilities may prove to play a more important role than has hitherto been accepted, in the whole question of the orbital stability and evolution of highly perturbed planetary satellites.

CHAPTER 8

FUTURE RESEARCH

8.1 Future Lines of Research in the Study of Saros Cycles

8.2 Future Lines of Research in the Study of the Finite-Time Stability Method

"It matters not how straight the gate
How charged with punishment the scroll
I am the master of my fate
I am the captain of my soul."
anonymous

8.1 Future Lines of Research in the Study of Saros Cycles

The research of Chapters 6 and 7 has left us with some unanswered questions and quite a few interesting new problems to study. The following is a short summary of these problems and some suggestions for their investigation.

So far we have studied the nearly periodic behavior of the Saros cycle through the use of eclipse records, the Astronomical Ephemerides or Nautical Almanacs and the JPL Ephemeris. It would be interesting to develop a numerical integration of the elliptic restricted three-body problem in order to study whether or not the Saros phenomenon is basically a three-body mechanism. If it is, the numerical integrations can then be used to simplify the study of the properties of the Saros cycle.

The above study was actually completed while writing this thesis, but will not be discussed in detail here. For a description of the method used and the results found see Supplementary Material, Paper 2. In summary, numerical integrations of the elliptic restricted three-body problem do exhibit a near repetition of the orbital elements after one Saros period, regardless of when the Saros period is chosen to begin. The numerical integrations did simplify the study of the Saros cycle, making it very easy to find the locations of the two mirror configurations which cause the return of the orbital elements to the initial conditions. Many of the well-known lunar cycles such as the two evection cycles of periods 31.81 days and 205.84 days can also be easily seen within the numerically integrated data as being sub-multiples of the Saros period.

The discovery that the Saros cycle is basically a three-body phenomenon, led to the thought that a periodic orbit of period equal to one Saros may exist in the circular restricted three-dimensional three-body lunar problem. Such a periodic orbit could only be found in the circular problem and not the elliptical one because the Saros

cycle does not include a good commensurability with the anomalistic period of the Sun, so that in the elliptical case the Sun has not returned after one Saros period to the same distance from the Earth as it started with.

Recently, we have discovered not one, but a family of eight periodic orbits existing within the vicinity of the Moon's orbit for the circular restricted three-dimensional three-body problem. Again this discovery shall not be discussed at length in this thesis, but a description of the periodic orbits can be found in Perozzi et al (1991).

The set of eight periodic orbits existing near the Moon's orbit have yet to be studied in detail, but future work could include a study of the stability of the new set of periodic orbits using recognized analytical methods. Also the existence of a periodic orbit very near the Moon's orbit could be useful in the development of a new Lunar theory. One of the periodic orbits could be used as an intermediate orbit to which extra perturbative terms could be added to obtain the "true" orbit of the Moon. In doing so a fourier analysis of the periodic orbit would be carried out.

In Section 7.6, we studied the possible sequence of saros cycles that the Moon might evolve through if only tidal interaction is taken into account and if all the orbital elements of the Moon and the Sun, except for the semi-major axis of the Moon, were to remain constants. This experiment should be repeated with the incorporation of the variations in the Moon's orbital eccentricity e and inclination i due to the tidal effects of the Earth. The variation of the Sun's orbital eccentricity e_1 should also be included.

Preliminary calculations suggest that the additions of e(t) and i(t) to the tidal evolution problem produce only small changes in the saros cycle sequence, but that the addition of $e_1(t)$ has a great affect on the sequence. For example, an exploration of the phase space of sin i, e and e_1 in the vicinity of the Saros cycle shows that the small changes in i and e resulting from tidal effects only bring the present Saros cycle closer or further away from a perfect saros cycle. In fact, we can find the values of e and i which produce a perfect saros cycle for a given value of e_1.

Changes in the value of e_1 from its possible minimum of 0 to its possible maximum of approximately 0.067 can, however, cause the Moon's orbit to pass

completely out of the region where the present Saros cycle is considered to be a good saros cycle (ie the region where the near commensurabilities between the three periods T_S, T_A and T_N have errors less than 0.5 days).

The above exploration of the sin i, e and e_1 phase space was performed by varying sin i, e and e_1 while keeping all the other orbital elements constant. Delaunay's expressions for $\dot{\Omega}$ and $\dot{\varpi}$ were then used to calculate the new values of the three periods T_S, T_A and T_N. These values were used to determine the regions in the phase space where the errors between the near-commensurabilities were zero (implying the existence of a perfect saros cycle) and where the errors were less than 0.5 days (implying the existence of a good near saros cycle).

The complete results of these preliminary experiments studying the sin i, e and e_1 phase space near the present Saros cycle will not be included in this thesis, but it is hoped that this material, along with the materials of Chapter 7, will form the bulk of a future paper (ie Perozzi et al, in preparation (a)).

We are still unsure as to what happens to the lunar orbit when it does not contain a good saros cycle for reversing the effects of solar perturbations. The existence of a near saros cycle within the orbital dynamics of the Moon seems to provide at least a temporary stability against solar perturbations for the length of time that tidal evolution allows the near saros cycle to persist. During epochs where no near saros cycles exist within the lunar orbital dynamics, the solar perturbations may accumulate enough to cause irreversible changes in the orbital elements of the Moon's orbit.

It would therefore be very interesting to perform numerical integrations of the elliptical restricted three-body problem using osculating elements for the initial conditions which represent the orbital dynamics of a Moon without a saros cycle. It would be difficult to find such osculating elements, but it may be possible to use instead a set of mean orbital elements taken from one of the gaps in Table 7.11, where no saros cycles were found to exist. After the numerical integration is completed, the mean periods T_S, T_A and T_N over the integration time interval can be computed and used to confirm whether or not the lunar orbit contains a saros cycle. If it doesn't

contain one, the behavior of the orbital elements in this new lunar orbit without a saros cycle can be compared with the behavior of the orbital elements in the elliptical restricted three-body lunar problem containing the present Saros cycle. As a cautionary note, it may be that, due to the growth of solar perturbations, the orbital elements of a lunar orbit without a saros cycle may change quite irregularly. The idea that such orbital elements can have mean values may therefore be nonsense.

Tidal friction should also eventually be added to the elliptical restricted three-body problem. Integration of such a problem would be quite difficult to perform since the perturbations due to tidal friction become noticeable only over very long time spans; however, the results would be of interest in order to study the possible relationship between time intervals when saros cycles do or do not exist within the lunar orbital dynamics and time intervals of temporary stability or instability of the lunar orbital elements.

Finally it has already been remarked that a search for the existence of saros cycles within the orbital dynamics of other satellites, such as the outer satellites of Jupiter and Saturn which are also greatly perturbed by the Sun, should also be made. Two approaches are possible here. The first involves a search through the literature for reasonably accurate values of the mean orbital elements of any of the outer satellites found in the solar system. The mean synodic, anomalistic and nodical periods can then be derived using Delaunay's expressions for $\mathring{\Omega}$ and $\mathring{\varpi}$, which are valid for any planet-satellite-Sun problem. Once we have values for the mean periods, it can be easily checked whether the periods exhibit near commensurabilities of a form similar to the Saros cycle, to within a given accuracy q and maximum integer limit of A_{max}.

The second approach involves a numerical integration of the elliptic restricted three-body problem for each of the satellites using a set of observationally derived osculating orbital elements as the initial conditions. These osculating elements could possibly be obtained from a data base of such satellite observations kept by the Royal Greenwich Observatory. The mean synodic, anomalistic and nodical periods over the integration time interval can then be calculated and again these periods can be used to discover whether or not a saros cycle exists within the orbital dynamics of the satellite.

8.2 Future Lines of Research in the Study of the Finite-Time Stability Method

Chapters 2 to 5 contain some suggestions for further study of the stability of planetary satellites against solar perturbations using the finite-time stability method as it is described in this thesis. These chapters also describe a few ideas for expanding the finite-time stability method to include other problems besides the circular and elliptical coplanar restricted three-body problems. The following is a summary of these possible lines of future research.

If greater computing time becomes available, it would be of interest to find minimum duration contours for a range of imaginary satellites orbiting each of the planets Jupiter, Saturn, Uranus and Mars at the second and third levels of the finite-time stability method. These could then be compared with the equivalent contour graphs found for the first level of the finite-time stability method. The range of satellite eccentricities and semi-major axes ratios which produce large minimum durations for the satellites can then be easily read from each contour graph for each level of the finite-time stability method.

The natural cycle used for the elliptic case in the third level of the finite-time stability method was taken to be one similar to that of the circular case for easier comparison of the two cases. The cycle therefore passed from a closest approach of a conjunction of the satellite and the Sun with the satellite's line of apse to the next closest approach of a conjunction with the satellite's line of apses, regardless of the location of the Sun's line of apse. To be consistent with the finite-time stability method's policy of studying the most pessimistic case, we assumed the Sun's line of apse was always located at right angles to the satellite's line of apse, the worst approximation to a mirror configuration.

With greater computer time, the above study of the elliptical case should be expanded to include a synodic period of the motions of the lines of apses of both the satellite and the Sun. The new level of the finite-time stability method would then involve calculating the largest change in the satellite's eccentricity over a cycle which passed from a closest approach of a conjunction of the satellite and the Sun with a near alignment of the apse lines of both the satellite and the sun, to the next time such an

event occurred.

The finite-time stability method could also be easily expanded to include more general three-dimensional three-body problems. For the restricted three body problem the analytic work similar to that of Chapters 2 to 4 would simply include two more equations of motion referring to the rate of change of the inclination i of the satellite's plane to the ecliptic plane and the rate of change of the longitude Ω of the ascending node. It may also be possible to extend the present finite-time solution of the coplanar restricted problem to include the solution of a more general coplanar problem, such as the problem of two satellites of similar mass orbiting the same planet.

Isolated three-body systems do not actually exist within the solar system. It would be interesting to attempt to extend the finite-time stability method to include problems involving four or more bodies. Finite-time solutions to such problems as a satellite system containing two satellites being disturbed by the Sun may be possible. The main difficulty with such a solution would be the choice of a natural cycle involving all the bodies. The basic cycle could still involve the repetition of a conjunction of the four or more bodies, but such a perfect alignment of the bodies is almost never likely to occur. We would therefore have to study instead, the repetition of near alignments of the bodies to within some given angular distance. This is similar to our study of near saros cycles where the commensurabilites are equal to each other to within a given error q, instead of perfect saros cycles where the commensurabilites are exactly equal to each other.

Finally, perhaps of greatest interest would be the use of the Saros cycle as the basic period in the finite-time stability method applied to the Earth-Moon system perturbed by the Sun. See Section 6.6 for a description of a possible procedure for solving this problem. Other saros cycles may also be found to exist within the orbital dynamics of the outer satellites for which the present finite-time stability method failed to give any meaningful results. The finite-time stability method, using the appropriate saros cycle as a basic period, might then produce more reasonable minimum durations for these satellites.

Appendix A - Statistical Tables

Table 1 - Critical Values z for the Standard Normal Distribution

Table 2 - Critical Values for Student's t Distribution

Table 3 - 95% Confidence Level Points of Skewness and Kurtosis for Approximation to a Normal Distribution

Tables 1 and 2 are reproduced from the statistical tables found in the Appendix Tables of Koopmans' An Introduction to Contemporary Statistics (1981). The original source of each table is given below the respective table.

Table 3 is reproduced from the statistical tables found in Appendix A of Alastair McDonald's Ph. D. thesis entitled Statistical Stability of Three and More Body Hierarchical Systems in Celestial Mechanics (1986). The table was originally computed by A.L. Brooks in the Dept. of Physics and Astronomy, University of Glasgow.

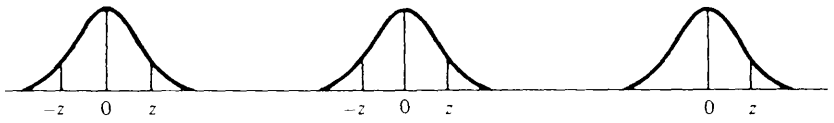

CONFIDENCE INTERVALS $P(\|Z\| \leq z)$	TWO-SIDED TESTS $P(\|Z\| \geq z)$	ONE-SIDED TESTS $P(Z \geq z)$	CRITICAL VALUE **z**
.10	.90	.45	.126
.20	.80	.40	.253
.30	.70	.35	.385
.40	.60	.30	.524
.50	.50	.25	.674
.60	.40	.20	.842
.70	.30	.15	1.036
.80	.20	.10	1.282
.90	.10	.05	1.645
.95	.05	.025	1.960
.98	.02	.01	2.326
.99	.01	.005	2.576
.995	.005	.0025	2.807
.999	.001	.0005	3.290
.9995	.0005	.00025	3.480
.9999	.0001	.00005	3.890
.99999	.00001	.000005	4.420
.999999	.000001	.0000005	4.900

Source: D. B. Owen and D. T. Monk, *Tables of the Normal Probability Integral*, Sandia Corporation Technical Memo 64-57-51 (March 1957).

Table 1 The critical values z for the standard normal distribution.

	PROBABILITY									
	.50	.80	.90	.95	.98	.99	.995	.998	.999	CONFIDENCE INTERVALS
	.50	.20	.10	.05	.02	.01	.005	.002	.001	TWO-SIDED TESTS
ν	.25	.10	.05	.025	.01	.005	.0025	.001	.0005	ONE-SIDED TESTS
1	1.000	3.078	6.314	12.706	31.821	63.637	127.32	318.31	636.62	
2	.816	1.886	2.920	4.303	6.965	9.925	14.089	22.326	31.598	
3	.765	1.638	2.353	3.182	4.541	5.841	7.453	10.213	12.924	
4	.741	1.533	2.132	2.776	3.747	4.604	5.598	7.173	8.610	
5	.727	1.476	2.015	2.571	3.365	4.032	4.773	5.893	6.869	
6	.718	1.440	1.943	2.447	3.143	3.707	4.317	5.208	5.959	
7	.711	1.415	1.895	2.365	2.998	3.499	4.020	4.785	5.408	
8	.706	1.397	1.860	2.306	2.896	3.355	3.833	4.501	5.041	
9	.703	1.383	1.833	2.262	2.821	3.250	3.690	4.297	4.781	
10	.700	1.372	1.812	2.228	2.764	3.169	3.581	4.144	4.537	
11	.697	1.363	1.796	2.201	2.718	3.106	3.497	4.025	4.437	
12	.695	1.356	1.782	2.179	2.681	3.055	3.428	3.930	4.318	
13	.694	1.350	1.771	2.160	2.650	3.012	3.372	3.852	4.221	
14	.692	1.345	1.761	2.145	2.624	2.977	3.326	3.787	4.140	
15	.691	1.341	1.753	2.131	2.602	2.947	3.286	3.733	4.073	
16	.690	1.337	1.746	2.120	2.583	2.921	3.252	3.686	4.015	
17	.689	1.333	1.740	2.110	2.567	2.898	3.222	3.646	3.965	
18	.688	1.330	1.734	2.101	2.552	2.878	3.197	3.610	3.922	
19	.688	1.328	1.729	2.093	2.539	2.861	3.174	3.579	3.883	
20	.687	1.325	1.725	2.086	2.528	2.845	3.153	3.552	3.850	
21	.686	1.323	1.721	2.080	2.518	2.831	3.135	3.257	3.189	
22	.686	1.321	1.717	2.074	2.508	2.819	3.119	3.505	3.792	
23	.685	1.319	1.714	2.069	2.500	2.807	3.104	3.485	3.767	
24	.685	1.318	1.711	2.064	2.492	2.797	3.091	3.467	3.745	
25	.684	1.316	1.708	2.060	2.485	2.787	3.078	3.450	3.725	
26	.684	1.315	1.706	2.056	2.479	2.779	3.067	3.435	3.707	
27	.684	1.314	1.703	2.052	2.473	2.771	3.057	3.421	3.690	
28	.683	1.313	1.701	2.048	2.467	2.763	3.047	3.408	3.674	
29	.683	1.311	1.699	2.045	2.462	2.756	3.038	3.396	3.659	
30	.683	1.310	1.697	2.042	2.457	2.750	3.030	3.385	3.646	
40	.681	1.303	1.684	2.021	2.423	2.704	2.971	3.307	3.551	
60	.679	1.296	1.671	2.000	2.390	2.660	2.915	3.232	3.460	
120	.677	1.289	1.658	1.980	2.358	2.617	2.860	3.160	3.373	
∞	.674	1.282	1.645	1.960	2.326	2.576	2.807	3.090	3.291	

Source: Abridged from Table 12 of *Biometrika Tables for Statisticians*, Vol. 1, edited by E. S. Pearson and H. O. Hartley (London: Cambridge University Press, 1962).

Table 2 The critical values for Student's t distribution.

Sample Size n	Skewness S_k Lower Limit	Standard Error	Upper Limit	Standard Error	Kurtosis K Lower Limit	Standard Error	Upper Limit	Standard Error
3	-0.7047	0.0001	0.7050	0.0001	1.5000	0.0000	1.5000	0.0000
4	-1.0687	0.0018	1.0685	0.0022	1.0667	0.0014	2.2996	0.0008
5	-1.2076	0.0041	1.2130	0.0035	1.2437	0.0011	3.0081	0.0030
6	-1.2390	0.0042	1.2357	0.0056	1.2906	0.0030	3.5173	0.0064
7	-1.2323	0.0056	1.2297	0.0065	1.3279	0.0024	3.8673	0.0093
8	-1.2034	0.0064	1.2080	0.0074	1.3935	0.0020	4.0985	0.0098
9	-1.1868	0.0074	1.1836	0.0060	1.4397	0.0028	4.2820	0.0141
10	-1.1652	0.0070	1.1547	0.0060	1.4795	0.0028	4.4121	0.0158
11	-1.1320	0.0063	1.1360	0.0067	1.5134	0.0026	4.5165	0.0168
12	-1.0994	0.0061	1.1145	0.0062	1.5463	0.0025	4.5457	0.0203
13	-1.0965	0.0046	1.0802	0.0059	1.5806	0.0024	4.6172	0.0196
14	-1.0585	0.0043	1.0561	0.0062	1.6044	0.0023	4.6200	0.0137
15	-1.0354	0.0064	1.0341	0.0061	1.6348	0.0023	4.6140	0.0190
16	-1.0238	0.0061	1.0176	0.0055	1.6615	0.0027	4.6494	0.0113
17	-1.0009	0.0061	0.9969	0.0068	1.6767	0.0029	4.6473	0.0166
18	-0.9684	0.0047	0.9747	0.0049	1.7003	0.0024	4.6374	0.0161
19	-0.9595	0.0048	0.9498	0.0059	1.7249	0.0028	4.6451	0.0190
20	-0.9352	0.0055	0.9291	0.0049	1.7472	0.0028	4.6280	0.0143
21	-0.9174	0.0054	0.9217	0.0054	1.7540	0.0025	4.6258	0.0150
22	-0.9022	0.0053	0.9114	0.0049	1.7764	0.0024	4.6355	0.0159
23	-0.8898	0.0053	0.8991	0.0041	1.7895	0.0030	4.6053	0.0166
24	-0.8719	0.0035	0.8691	0.0045	1.8053	0.0031	4.6122	0.0145
25	-0.8694	0.0042	0.8577	0.0049	1.8267	0.0027	4.5972	0.0145
26	-0.8480	0.0047	0.8452	0.0043	1.8378	0.0025	4.6026	0.0139
27	-0.8382	0.0044	0.8395	0.0046	1.8515	0.0029	4.5982	0.0150
28	-0.8203	0.0046	0.8284	0.0045	1.8605	0.0028	4.5817	0.0153
29	-0.8108	0.0040	0.8089	0.0053	1.8749	0.0025	4.5481	0.0170
30	-0.8015	0.0047	0.7970	0.0041	1.8896	0.0029	4.5591	0.0158
40	-0.7057	0.0040	0.7079	0.0047	1.9863	0.0026	4.4324	0.0121
50	-0.6529	0.0043	0.6438	0.0039	2.0642	0.0025	4.3569	0.0122
60	-0.5946	0.0034	0.5949	0.0029	2.1160	0.0019	4.2440	0.0111
70	-0.5528	0.0031	0.5527	0.0030	2.1684	0.0028	4.1839	0.0100
80	-0.5223	0.0033	0.5208	0.0025	2.2078	0.0025	4.1358	0.0099
90	-0.4913	0.0020	0.4896	0.0026	2.2404	0.0022	4.0789	0.0102
100	-0.4671	0.0022	0.4658	0.0022	2.2664	0.0021	4.0305	0.0105
110	-0.4462	0.0023	0.4477	0.0019	2.2948	0.0020	3.9792	0.0076
120	-0.4313	0.0022	0.4310	0.0026	2.3205	0.0021	3.9442	0.0083

Table 3 The upper and lower limits placed on the skewness and kurtosis of a distribution in order for it to be 'normal' with a 95% confidence level.

References

Allan, R. R.: 1969, *Evolution of Mimas-Tethys Commensurability*, Astron. Jour. **74**, 497.

Andrews, D. F., Biekel, P. J., Hampel, F. R., Huber, P. J., Rogers, W. H. and Tukey, J. W.: 1972, Robust Estimates of Location: Survey and Advances, Princeton Univ. Press, New Jersey.

Applegate, J. H., Douglas, M. R., Gursel, Y., Sussman, G. J. and Wisdom, J.: 1986, *The Outer Solar System for 200 Million Years*, Astron. Jour. **92**, 176.

Arnol'd, V. I.: 1963, *Small Denominators and Problems of Stability of Motion in Classical and Celestial Mechanics*, Russian Mathematical Surveys **18**(6), 86.

The Astronomical Ephemeris: 1898, H. M. S. O., London.

____ 1916, H. M. S. O., London.

____ 1934, H. M. S. O., London.

____ 1952, H. M. S. O., London.

____ 1970, H. M. S. O., London.

Bailey, J.M: 1971, *Origin of the Outer Satellites of Jupiter*, Journal of Geophysical Research **76**, 7827.

Brouwer, D. and Clemence, G.: 1961, Methods of Celestial Mechanics, Academic Press, London.

Brown, E. W. and Shook, C. A.: 1933, Planetary Theory, Cambridge Univ. Press.

Carpino, M., Milani, A. and Nobili, A. M.: 1987, *Long-Term Numerical Integrations and Synthetic Theories for the Motion of the Outer Planets*, Astron. Astrophys. **181**, 182.

Churchhouse, Robert F. editor: 1981, Numerical Methods: Handbook of Applicable Mathematics Vol. III, John Wiley and Sons, Chichester.

Cohen, C. J. and Hubbard, E. C.: 1965, *Libration of the Close Approaches of Pluto to Neptune*, Astron. Jour. **70**, 10.

Cohen, C. J., Hubbard, E. C. and Oesterwinter, C.: 1967, *New Orbit for Pluto and Analysis of Differential Corrections*, Astron. Jour. **72**, 973.

____ 1973, *Elements of the Outer Planets for One Million Years*, Astron. Papers Am. Eph. Naut. Alm. **22**, 1.

Cook, Alan: 1988, The Motion of the Moon, Adam Hilger, Bristol.

Crommelin, A. C. D.: 1901, *The 29-Year Eclipse-Cycle*, The Observatory **24**, 379.

Delambre, J. B. J.: 1817, Histoire de l'Astronomie Ancienne Vol. II, Paris.

Delaunay, M.: 1867, Théorie du Mouvement de la Lune Vol. II, Gauthier-Villars, Paris.

____ 1872, *Note sur les Mouvements du Périgée et du Noeud de la Lune*, Comptes Rendus Herbdomadaires des Séances de L'Académie des Sciences **74**(1), 17.

Dermott, S., Malhotra, R. and Murray, C.: 1988, *Dynamics of the Uranian and Saturnian Satellite Systems: A Chaotic Route to Melting Miranda?*, Icarus **76**, 295.

Dermott, S. and Murray, C.: 1981a, *The Dynamics of Tadpole and Horseshoe Orbits I. Theory*, Icarus **48**, 1.

____ 1981b, *The Dynamics of Tadpole and Horseshoe Orbits II. The Coorbital Satellites of Saturn*, Icarus **48**, 12.

Eginitis, M. D.: 1889, Annales de l'Observatoire Paris Memoires, No. 19.

The Explanatory Supplement to the Astronomical Ephemeris and the American Ephemeris and Nautical Almanac: 1961, H. M. S. O., London.

Goldreich, P.: 1965, *An Explanation of the Frequent Occurrence of Commensurable Mean Motions in the Solar System*, Mon. Not. Roy. Astr. Soc. **130**, 159.

Goldreich, P. and Soter, S.: 1966, *Q in the Solar System*, Icarus **5**, 375.

Greenberg, Richard: 1984, *Orbital Resonances Among Saturn's Satellites*, in Saturn, T. Gehrels and M. S. Mathews editors, Univ. of Arizona Press, Tucson.

Hagihara, Yusuke: 1972a, Celestial Mechanics: Perturbation Theory Vol. II, Part 1, MIT Press, Massachusetts.

____ 1972b, Celestial Mechanics: Perturbation Theory Vol. II, Part 2, MIT Press, Massachusetts.

Hansen, P. A.: 1831, *Untersuchungen uber die gegenseitigen Störungen des Jupiters und Saturns*, eine von Königl, Akad. Wiss. zu Berlin am 8 Juli 1830, gekrönte Preisschrift, Berlin.

____ 1843, Ermittelung der absoluten Störungen in Ellipsen von beliebiger Excentricität und Neigung, Gotha, Schriften der Sternwarte Seeberg.

Haretu, S. C.: 1885, Annales de l'Observatoire Paris Memoires, No. 18.

Heppenheimer, T. A.: 1975, *On the Presumed Capture Origin of Jupiter's Outer Satellites*, Icarus **24**, 172.

Hill, G. W.: 1878, Amer. Jour. Math. **1**, 5.

____ 1890, *A New Theory of Jupiter and Saturn*, Astron. Papers Am. Eph. Naut. Alm. **4**, 11.

Jacobi, C. G. J.: 1836, *Analyse Mathématique*, Comptes Rendus de l'Académie des Sciences **3**, 59.

Kaula, W. M.: 1962, *Development of the Lunar and Solar Disturbing Functions for a Close Satellite*, Astron. Jour. **67**, 300.

Kinoshita, H. and Nakai, H.: 1984, *Motions of the Perihelions of Neptune and Pluto*, Celest. Mech. **34**, 203.

Kolmogorov, A. N.: 1954, Doklady Akademii Nauk SSSR **98**, 527.

Koopmans, Lambert H.: 1981, An Introduction to Contemporary Statistics, Duxbury Press, Boston.

Kuiper, G. P.: 1956, *On the Origin of the Satellites and the Trojans*, in Vistas in Astronomy Vol. 2, A. Beer editor, Pergamon Press, New York.

Laskar, J: 1988, *Secular Evolution of the Solar System Over 10 Million Years*, Astron. Astrophys. **198**, 341.

____ 1989, *A Numerical Experiment on the Chaotic Behavior of the Solar System*, Nature **338**, 237.

Le Verrier, U. J.: 1855, Annales de l'Obs. Paris **1**, 258.

Lidov, M. L.: 1963, *On the Approximated Analysis of the Orbit Evolution of Artificial Satellites*, in Dynamics of Satellites, M. Roy editor, U. S. S. R. Academy of Sciences Publishing House.

McDonald, A. J.: 1986, Statistical Stability of Three and More Body Hierarchical Systems in Celestial Mechanics, Ph. D. Thesis, University of Glasgow.

Marchal, C. and Saari, D. G.: 1975, *Hill Regions for the General Three-Body Problem*, Celest. Mech. **12**, 115.

Message, P. J.: 1976, *Formal Expressions for the Motion of N Planets in the Plane, with the Secular Variations Included, and an Extension to Poisson's Theorem*, in Long-Time Predictions in Dynamics, V. Szebehely and B. D. Tapley editors, Reidel, Dordrecht.

____ 1982, *Asymptotic Series for Planetary Motion in Periodic Terms in Three Dimensions*, Celest. Mech. **26**, 25.

Milani, A.: 1988, *Secular Perturbations of Planetary Orbits and their Representation as Series*, in Long-Term Dynamical Behavior of Natural and Artificial N-Body Systems, A. E. Roy editor, Reidel, Dordrecht.

Milani, A. and Nobili, A. M.: 1983a, *On Topological Stability in the General Three-Body Problem*, Celest. Mech. **31**, 213.

____ 1983b, *On the Stability of Hierarchical Four-Body Systems*, Celest. Mech. **31**, 241.

____ 1984, *Resonance Locking Between Jupiter and Uranus*, Nature **310**, 753.

____ 1985, *Resonant Structure of the Outer Solar System*, Celest. Mech. **35**, 269.

____ 1988, *Integration Error Over Very Long Time Spans*, Celest. Mech. **43**, 1.

Mitchell, Samuel Alfred: 1951, Eclipses of the Sun, 5th ed., Columbia Univ. Press New York.

Moser, J.: 1966, SIAM Review **8**, 145.

____ 1973, Stable and Random Motions in Dynamical Systems, Princeton University Press, Princeton.

____ 1974, *Stability Theory in Celestial Mechanics*, in The Stability of the Solar System and of Small Stellar Systems, Y. Kozai editor, Reidel, Dordrecht.

Murray, C. D., Fox, K., Malhotra, R. and Nicholson, P. D.: 1988, *Secular Perturbations of the Uranian Satellites: Theory and Practice*, Bull. Am. Astron. Soc. **19**(3), 820.

Nacozy, P. E.: 1977, *A Discussion of Long-Term Numerical Solutions of the Jupiter-Saturn-Sun System*, Celest. Mech. **16**, 77.

The Nautical Almanac for the Year 1987, H. M. S. O., London.

The Nautical Almanac for the Year 1988, H. M. S. O., London.

Newcomb, S.: 1865, *Investigations of the Orbit of Neptune*, Smithsonian Contribution to Knowledge, No. 199, Smithsonian Institution, Washington, D. C.

____ 1874, *Investigations of the Orbit of Uranus*, Smithsonian Contribution to Knowledge, No. 262, Smithsonian Institution, Washington, D. C.

____ 1876, *On the General Integrals of Planetary Motion*, Smithsonian Contribution to Knowledge **21**, No. 281, Smithsonian Institution, Washington, D. C.

____ 1882, *The Recurrence of Solar Eclipses*, Astron. Papers of the Am. Eph. **1**, 7.

____ 1891, *Periodic Perturbations of the Longitudes and Radii Vectores of the Four Inner Planets of the First Order as to the Masses*, Astron. Papers Am. Eph. Naut. Alm. **3**, No. 5, 395.

____ 1895a, Astron. Papers Am. Eph. Naut. Alm. **5**, No. 2, 49.

____ 1895b, Astron. Papers Am. Eph. Naut. Alm. **5**, No. 4, 297.

Newhall, X. X.: 1989, *Numerical Representation of Planetary Ephemerides*, Celest. Mech. **45**, 305.

Ovenden, M. W. and Roy, A. E.: 1961, *On the Use of the Jacobi Integral of the Restricted Three-Body Problem*, Mon. Not. Roy. Astron. Soc. **123**, 1.

Pannekoek, A.: 1961, A History of Astronomy, George Allen and Unwin Ltd., London.

Perozzi, E., Roy, A. E., Steves, B. A. and Valsecchi, G. B.: 1991, *Significant High Number Commensurabilities in the Main Lunar Problem*, in Predictability, Stability and Chaos in N-Body Dynamical Systems, A. E. Roy editor, Plenum, New York (in press).

____ *Significant High Number Commensurabilities in the Main Lunar Problem I. The Saros as a Near-Periodicity of the Moon's Orbit*, (submitted to Celest. Mech. Oct. 1990).

____ *Significant High Number Commensurabilities in the Main Lunar Problem II. Saros-Like Cycles for Varied Lunar Orbits*, (in preparation (a)).

____ *A Postscript to a Discovery of the Ancient Chaldeans*, (in preparation (b)).

Pierce: 1849, Astron. Jour. **1**, 1.

Plummer, H. C.: 1918, An Introduction Treatise on Dynamical Astronomy, Cambridge Univ. Press.

Poincaré, H.: 1893, Les Méthodes Nouvelles de la Mécanique Céleste Vol II, Ch. XIII, Gauthier-Villars, Paris.

Roy, A. E.: 1979, *Empirical Stability Criteria in the Many-Body Problem*, in Instabilities in Dynamical Systems, V. Szebehely editor, Reidel, Dordrecht.

____ 1982, *The Stability of N-Body Hierarchical Dynamical Systems*, in Applications of Modern Dynamics to Celestial Mechanics and Astrodynamics, V. Szebehely editor, Reidel,Dordrecht.

____ 1983, *Asymptotic Approach to Mirror Conditions as a Trapping Mechanism in N-Body Hierarchical Dynamical Systems*, in Dynamical Trapping and Evolution in the Solar System, V. V. Markellos and Y. Kozai editors, Reidel, Dordrecht.

____ 1988, Orbital Motion, 3rd ed., Adam Hilger, Bristol.

Roy, A. E., Carusi, A., Valsecchi, G. and Walker, I. W.: 1984, *The Use of the Energy and Angular Momentum Integrals to Obtain a Stability Criterion in the General Hierarchical Three-Body Problem*, Astron. Astrophys. **141**, 25.

Roy, A. E. and Ovenden, M. W.: 1954, *On the Occurrence of Commensurable Mean Motions in the Solar System*, Mon. Not. Roy. Astron. Soc. **114**, 232.

____ 1955, *On the Occurrence of Commensurable Mean Motions in the Solar System II. The Mirror Theorem*, Mon. Not. Roy. Astron. Soc. **115**, 296.

Roy, A. E. and Steves, B. A.: 1988, *A Finite-Time Stability Criterion for Sun-Perturbed Planetary Satellites*, in Long-Term Dynamical Behavior of Natural and Artificial N-Body Systems, A. E. Roy editor, Kluwer Academic Publishers, London.

Roy, A. E., Walker, I. W. and McDonald, A. J. C.: 1985, *Studies in the Stability of Hierarchical Dynamical Systems*, in Stability of the Solar System and its Minor Natural and Artificial Bodies, V. Szebehely editor, Reidel, Dordrecht.

Roy, A. E., Walker, I. W., McDonald, A. J., Williams, I. P., Fox, K., Murray, C. D., Milani, A., Nobili, A., Message, P. J., Sinclair, A. T. and Carpino, M.: 1988, *Project Longstop*, Vistas in Astronomy **32**, 95.

Smart, W. M.: 1953, Celestial Mechanics, Longmans, London.

Stigler, Stephen M.: 1977, *Do Robust Estimators Work With Real Data?*, Annals of Statistics **5**, 1055.

Stockwell, John N.: 1901, *Eclipse-Cycles*, Astron. Jour. **21**, 185.

Sussman, G. J. and Wisdom, J.: 1988, Science **241**, 433.

Szebehely, V.: 1977, *Analytical Determination of the Measure of Stability of Triple Stellar Systems*, Celest. Mech. **15**, 107.

____ 1978, *Stability of Artificial and Natural Satellites*, Celest. Mech. **18**, 383.

____ 1984, *Review of Concepts of Stability*, Celest. Mech. **34**, 49.

____ 1987, *Stability and Modifications of the Hierarchical Restricted Problem of N-Bodies*, an unpublished lecture at the 1987 NATO Advanced Study Institute entitled Long-Term Dynamical Behavior of Natural and Artificial N-Body Systems, Cortina, Italy.

Szebehely, V. and McKenzie, R.: 1977a, *Stability of Planetary Systems with Bifurcation Theory*, Astron. Jour. **82**(1), 79.

____ 1977b, *Stability of the Sun-Earth-Moon System*, Astron. Jour. **82**(4), 303.

Szebehely, V. and Zare, K.: 1977, *Stability of Classical Triplets and of their Hierarchy*, Astron. Astrophys. **58**, 145.

Time-Life Books, editors: 1988, Mysteries of the Unknown: Cosmic Connections, Time-Life Books, Amsterdam.

Tisserand, F.: 1894, Traité de Mécanique Céleste Vol. III, Gauthier-Villars, Paris.

Tukey, John W.: 1960, *A Survey of Sampling From Contaminated Distributions*, in Contributions to Probability and Statistics: Essays in Honor of Harold Hotelling, I. Olkin, S. G. Ghurye, W. Hoeffding, W. G. Madow and H. B. Mann editors, Stanford Univ. Press, Stanford.

Tukey, J. W. and McLaughlin, D. H.: 1963, *Less Vulnerable Confidence and Significance Procedures for Location Based on a Single Sample: Trimming/Winsorization 1*, Sankyā Series A **25**, 334.

Valsecchi, G. B., Carusi, A. and Roy, A. E.: 1984, *The Effect of Orbital Eccentricities on the Shape of the Hill-Type Analytical Stability Surfaces in the General Three-Body Problem*, Celest. Mech. **32**, 217.

Walker, I. W.: 1983, *Stability Criteria in Many-Body Systems IV. Empirical Stability Parameters for General Hierarchical Dynamical Systems*, Celest. Mech. **29**, 149.

Walker, I. W., Emslie, A. G. and Roy, A. E.: 1980, *Stability Criteria in Many-Body Systems I. An Empirical Stability Criterion for Co-rotational Three-Body Systems*, Celest. Mech. **22**, 371.

Walker, I. W. and Roy, A. E.: 1981, *Stability Criteria in Many-Body Systems II. On a Sufficient Condition for the Stability of Coplanar Hierarchical Three-Body Systems*, Celest. Mech. **24**, 195.

____ 1983a, *Stability Criteria in Many-Body Systems III. Empirical Stability Regions for Corotational, Coplanar, Hierarchical Three-Body Systems*, Celest. Mech. **29**, 117.

____ 1983b, *Stability Criteria in Many-Body Systems V. On the Totality of Possible Hierarchical General Four-Body Systems*, Celest. Mech. **29**, 267.

Zare, K.: 1976, *The Effects of Integrals on the Totality of Solutions of Dynamical Systems*, Celest. Mech. **14**, 73.

____ 1977, *Bifurcation Points in the Planar Problem of Three Bodies*, Celest. Mech. **16**, 35.

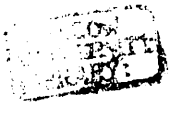

Supplementary Material: Paper 1

A FINITE-TIME STABILITY CRITERION FOR SUN-PERTURBED PLANETARY SATELLITES

A. E. Roy and B. A. Steves,
Department of Physics and Astronomy,
Glasgow University, Glasgow, U.K.

ABSTRACT

The inability of the c^2H stability criterion in the general three-body problem to guarantee Hill (or hierarchical) stability in the case of a planetary satellite perturbed by the Sun when the planet's orbital eccentricity is non-zero leads to the search for a finite-time stability criterion applicable to such cases. Its application to the main satellites of Jupiter, Saturn and Uranus shows that stability lifetimes of at least 10^6 years may be demonstrated for them.

1. INTRODUCTION

In recent years a number of authors (see for example Bozis 1976, Easton 1971 and 1975, Golubev 1968, Marchal 1971, Marchal and Saari 1975, Roy 1979, Roy et al. 1984, Smale 1970, Szebehely and Zare 1977, Valsecchi et al. 1984, Zare 1976, 1977) have made use of the general three-body problem c^2H term, a combination of the total angular momentum c and the total energy H integrals of the system, in order to examine the hierarchical stability (i.e. Hill stability) of a given three-body system. In such a system, two of the bodies, of masses m_1 and m_2, move in disturbed Keplerian elliptic orbits about their common centre of mass, while the third body, of mass m_3, moves in a much larger disturbed Keplerian orbit about the centre of mass of the first two bodies.

If the orbits do not cross, it is possible, by computing c^2H_{crit} from the initial conditions, to show that the binary formed by m_1 and m_2 will never be disrupted by m_3 if $c^2H \leq c^2H_{crit}$. The third body m_3 cannot, in its evolving orbit, cross the changing orbit of m_1 and m_2, though it may escape to infinity. The system is then said to have hierarchical stability. In the restricted three-body problem, moreover, m_2 is a particle of infinitesimally small mass in orbit about m_1 and is disturbed gravitationally by m_3 moving in a circular orbit about m_1. The well-known work of G. W. Hill (1878), utilising the concept of the

surfaces of zero velocity or Hill surfaces derived from the Jacobi integral C, showed that if the surface about m_1 is closed, the particle is prevented from escaping from m_1 and entering into a trajectory about m_2. The particle in this case is customarily said to have Hill stability. In the general three-body problem, the c^2H_{crit} value is equivalent to the value of the Jacobi constant for which the two lobes of the Hill surfaces surrounding each of the massive particles just barely touch. In the general problem, c^2H_{crit} is calculated from the relevant collinear configuration of the three massive particles which is one of three collinear equilibrium configurations dictated by the masses and their linear arrangements (see for example Walker and Roy 1981).

In the restricted problem, it is important to note that, even if there is no guarantee that the massless particle will be kept in orbit about m_1, the particle does not necessarily escape. Its chance of doing so is dictated by its orbital evolution and the width of the 'neck' connecting the now coalesced surfaces about m_1 and m_2 . The escape may be immediate or may take any length of time extending out to an infinitely long period. Similarly, in the general three-body problem, if $c^2H > c^2H_{crit}$, there is no guarantee of hierarchical stability, but the break-up of the original hierarchy (i.e. m_2 is in orbit about m_1 , while m_3 is in a larger orbit about the centre of mass of m_1 and m_2) may occur in a time interval that can vary enormously, depending upon the initial conditions of the system. In a recent series of papers (Roy 1979, 1982, 1983, Roy et al. 1984, Roy et al, 1985, Walker 1983, Walker et al. 1980, Walker and Roy 1983a, 1983b), the existence of a considerable region of empirical stability is demonstrated in cases where $c^2H > c^2H_{crit}$.

Empirical stability, in other words the maintenance of the hierarchy in a general three-body system for a considerable time even when no c^2H guarantee can be given, becomes important in studies of the solar system's sub-systems of bodies. Among such sub-systems are: (1) the Sun and two planets; (2) a planet and two satellites; (3) a planet, its satellite and the Sun.

No example of these three types of sub-systems exists by itself. We are always dealing with an n-body problem where $n>3$ and where there is no analytical guarantee of hierarchical stability. Nevertheless, in these triple systems analytical hierarchical stability can be said to exist until the value of c^2H for such a triple system is brought, by perturbations of other bodies, above the value of c^2H_{crit} for the triple system (see Milani and Nobili 1983a,b). It should be noted that the critical value of c^2H, viz c^2H_{crit}, is a function only of the three masses and therefore is constant. It may be said, then, that a necessary but not sufficient condition for the hierarchical stability of an n-body system, where $n>3$, is that the system's three-body subsystems have c^2H stability.

Now in the solar system, when the values of c^2H_{crit} are computed for examples of types (1) and (2) from the orbital elements and masses, it is found that in all cases c^2H is comfortably less than c^2H_{crit}.

For examples of type (3), namely planet-satellite-Sun systems, $c^2H < c^2H_{crit}$ for all the major satellites of the planets as long as the eccentricities of the planets' orbits about the Sun are neglected. The exceptions to the rule, the retrograde satellites of Jupiter and Saturn, are probably captured bodies. In the case of the Earth's moon, however, the c^2H stability criterion is barely satisfied.

When we take into account the planets' orbital eccentricities, the results change drastically. All planet-satellite-Sun triples (see Valsecchi et al. 1984) fail to satisfy the c^2H hierarchical stability criterion. This result probably shows how restrictive the criterion is rather than indicates the instability of planetary satellites against solar perturbations. A different approach is needed in order to re-examine the problem and the present paper is largely a report on work in progress to find and evaluate such an approach.

2. A FINITE TIME STABILITY CRITERION

Instead of seeking a stability criterion valid for all time, we try to provide one which not only holds in any particular case for a finite time but also provides a means of estimating that time. At first, the approach is illustrated by applying it to the case where the Sun is assumed to move in a circular orbit about the planet, with the satellite having negligible mass. The satellite moves in a disturbed elliptical orbit about the planet in the plane of the Sun's planetocentric orbit. In this case we have the circular coplanar restricted three-body problem. The method is then applied to the case where the Sun is assumed to move in a fixed elliptic orbit about the planet, in other words the elliptic restricted coplanar three-body problem.

2.1 The circular coplanar restricted three-body problem

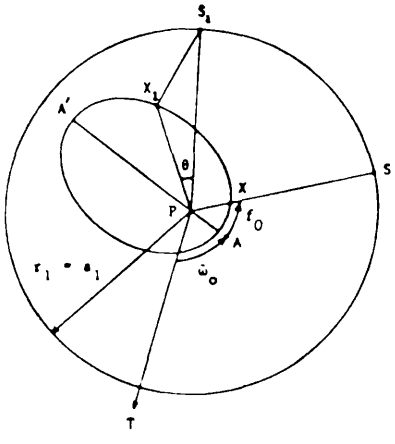

Figure 1: The coplanar circular restricted three-body problem where the planet (P) - satellite (X) system is disturbed by the Sun(S), assumed to be moving in a fixed circular orbit. The initial longitude of the satellite's pericentre $\tilde{\omega}_o$ is arbitrarily chosen to be zero, so that PA lies along ^{o}PT.

In Figure 1 P, S and X denote the positions of the planet, Sun and satellite with PX = r, PS = r_1, XS = Δ and $r << r_1$. Let the osculating orbital elements of the satellite orbit be a (the semi-major axis), e (the eccentricity), $\tilde{\omega}$ (the longitude of pericentre) and ϵ (the mean longitude of the epoch). Let the masses of the planet, Sun and satellite be m, m_1 and m' with m' negligible compred to m and m_1 and with $m << m_1$.

If n and n_1 are the mean motions of the satellite and the Sun respectively then, taking units such that the gravitational constant has the value unity, we have the following relations:

$$n^2a^3 = m+m' \; ; \quad n_1^2 a_1^3 = m_1 + m + m' \; ; \quad r_1 = a_1 = \text{constant.} \qquad (1)$$

The Roy-Walker empirical stability parameters ϵ_{32} and ϵ^{23}(Roy 1979) are given by:

$$\epsilon_{32} = \mu_3 \alpha^3 \quad , \quad \epsilon^{23} = \mu(1-\mu)\alpha^2$$

where $\mu_3 = m_1/(m+m')$, $\mu = m'/(m+m')$, $1-\mu = m/(m+m')$ and $\alpha = a/a_1$. Using Equations 1 and the relation $m' << m << m_1$, the empirical stability ϵ_{32} can be approximated as:

$$\epsilon_{32} \sim (n_1/n)^2 = \nu^2 \; ;$$

the other empirical stability parameter ϵ^{23} is effectively zero.

Let the sidereal periods of the Sun and the satellite be T_1 and T respectively and let their synodic period be T_s. The changes in the satellite's orbital elements due to solar perturbation may be obtained from the Lagrange planetary equations, viz.

$$\frac{da}{dt} = 2\epsilon_{32} \frac{n}{\sqrt{1-e^2}} \{r_1(\frac{1}{\Delta^3} - \frac{1}{r_1^3}) [e \sin f \cos\theta - (1+e\cos f)\sin\theta] - \frac{er}{\Delta^3} \sin f\}$$

$$\frac{de}{dt} = \epsilon_{32}\frac{n}{a}\sqrt{1-e^2}\{r_1(\frac{1}{\Delta^3} - \frac{1}{r_1^3}) [\sin f \cos\theta - (\frac{e(1+\cos^2 f)+2\cos f}{1 + e\cos f})\sin\theta] - \frac{r}{\Delta^3}\sin f\}$$

$$\frac{d\tilde{\omega}}{dt} = -\epsilon_{32} \frac{n\sqrt{1-e^2}}{ae}\{r_1(\frac{1}{\Delta^3} - \frac{1}{r_1^3})[\cos f \cos\theta + (\frac{2+e\cos f}{1+e\cos f})\sin f \sin\theta] - \frac{r}{\Delta^3}\cos f\} \qquad (2)$$

$$\frac{d\epsilon}{dt} = -2\epsilon_{32} \frac{n}{a}\{r_1(\frac{1}{\Delta^3} - \frac{1}{r_1^3}) [(\frac{r}{a} - \frac{3\, e n t \sin f}{2\sqrt{1-e^2}}) \cos\theta + \frac{3a\sqrt{1-e^2}nt}{2r} \sin\theta]$$

$$- \frac{r}{\Delta^3}(\frac{r}{a} - \frac{3ent\sin f}{2\sqrt{1-e^2}})\} + (1 - \sqrt{1-e^2})\frac{d\tilde{\omega}}{dt}$$

Equations (2) may be integrated numerically or solved analytically to a desired degree of approximation. For the present purpose, however, it is advantageous to change the independent variable in Equations 2 from time t to the true anomaly f, and subsequently to θ, the angle between the planetocentric radius vectors of the satellite and the Sun,

(see Figure 1) so that

$$\theta = \ell - \ell_1 = f + \tilde{\omega} - \ell_1$$

where ℓ and ℓ_1 are the longitudes of the satellite and the Sun respectively.

The first step, using the relation

$$r^2 \frac{df}{dt} = h = na^2\sqrt{1-e^2} \quad \text{and setting } a_1 = 1 \text{ so that } \alpha = a,$$

gives

$$\frac{da}{df} = \frac{2\epsilon_{32}}{1-e^2}\left(\frac{r}{a}\right)^2\left\{r_1\left(\frac{1}{\Delta^3}-\frac{1}{r_1^3}\right)\left[e\sin f\cos\theta - (1+e\cos f)\sin\theta\right] - \frac{er}{\Delta^3}\sin f\right\}$$

$$\frac{de}{df} = \frac{\epsilon_{32}}{a}\left(\frac{r}{a}\right)^2\left\{r_1\left(\frac{1}{\Delta^3}-\frac{1}{r_1^3}\right)\left[\sin f\cos\theta - \left(\frac{e(1+\cos^2 f)+2\cos f}{1+e\cos f}\right)\sin\theta\right] - \frac{r}{\Delta^3}\sin f\right\} \qquad (3)$$

$$\frac{d\tilde{\omega}}{df} = \frac{-\epsilon_{32}}{ea}\left(\frac{r}{a}\right)^2\left\{r_1\left(\frac{1}{\Delta^3}-\frac{1}{r_1^3}\right)\left[\cos f\cos\theta + \left(\frac{2+e\cos f}{1+e\cos f}\right)\sin f\sin\theta\right] - \frac{r}{\Delta^3}\cos f\right\}$$

$$\frac{d\epsilon}{df} = \frac{-2\epsilon_{32}}{a\sqrt{1-e^2}}\left(\frac{r}{a}\right)^2\left\{r_1\left(\frac{1}{\Delta^3}-\frac{1}{r_1^3}\right)\left[\left(\frac{r}{a} - \frac{3ent\sin f}{2\sqrt{1-e^2}}\right)\cos\theta + \frac{3nt\sqrt{1-e^2}}{2r}\sin\theta\right]\right.$$

$$\left. -\frac{r}{\Delta^3}\left(\frac{r}{a} - \frac{3ent\sin f}{2\sqrt{1-e^2}}\right)\right\} + \left(1-\sqrt{1-e^2}\right)\frac{d\tilde{\omega}}{df}$$

Equations (3) are exact and can easily be integrated numerically. The second step is then carried out by using the following transformation,

$$\frac{d\sigma}{d\theta} = \left(\frac{d\theta}{df}\right)^{-1}\frac{d\sigma}{df}$$

where $\sigma = a, e, \tilde{\omega}$ or ϵ ; $\quad \frac{d\theta}{df} = 1 - \frac{d\ell_1}{df}$.

ℓ_1 as a function of f can be found through a series expansion. The differential equations $d\sigma/d\theta$ are then integrated analytically after expanding them to the desired degree of approximation about the small values of $\alpha = a/a_1$, e, and $\nu = n_1/n$. Both numerical and analytical integration procedures were applied to the problem as a check on the accuracy of the solutions. In this investigation, we are not interested so much in the exact positions of the bodies at any given time, but rather in the minimum time the Sun requires to render the satellite's orbit parabolic. Up until this point, all the equations and the method of analysis described have been applicable to both the case where the Sun is assumed to move in a fixed circular orbit and the case where the Sun is assumed to move in a fixed elliptical orbit. We now apply the method to the circular case.

Step 1. Suppose that at time t=0 a conjunction PXS occurs at a true anomaly of value f_0. The initial longitude of pericentre $\tilde{\omega}_o$ as measured

from the direction PT, where T is the vernal equinox, can be arbitrarily chosen to be zero (i.e. PA lies along PT), since all initial orientations of the satellite's elliptical orbit with respect to the Sun's circular orbit produce identical configurations. Thus at a conjunction the initial true anomaly of the Sun f_{10} is equal to f_0. The problem now contains four independent initial parameters: the satellite's orbital displacement f_0, the satellite's semimajor axis a, the satellite's eccentricity e, and the mass ratio of the three bodies through

$$\nu = n_1/n \approx \sqrt{\mu_3 a^3} = \sqrt{\varepsilon_{32}} \quad .$$

We wish to obtain the changes Δe, Δa, $\Delta\tilde{\omega}$, $\Delta\varepsilon$ that occur in the elements a, e, $\tilde{\omega}$, ε over one synodic period taken from the opposition of the Sun and the satellite prior to this conjunction, to the opposition immediately after the conjunction. The equations (4) have therefore to be integrated from $\theta = -\pi$ to $\theta = +\pi$. We assume that over one synodic period the satellite's orbital elements remain constant on the right hand sides of equations (4) throughout the integration. r_1 is set equal to a_1 for the circular case. Then, integrating and expanding equation (4) to second order about the small quantities $\alpha = a/a_1$, $\nu = n/n$, and e (i.e. $\alpha^i e^j \nu^k$ where $i+j+k \leq 2$) the following results are obtained:

$\Delta a = 0$

TABLE 1

$\Delta e = \pi\varepsilon_{32} x$

Coefficient	L_o (sin)
$\frac{15}{8} a - \frac{39}{32} a\nu + 4\nu + \frac{40}{3} \nu^2$	1
$-\frac{15}{2} e - \frac{33}{2} e\nu$	2

$e\Delta\tilde{\omega} = \pi\varepsilon_{32} x$

Coefficient	L_o (cos)
$\frac{3}{2} e (1+\nu)$	0
$-\frac{15}{8} a + \frac{39}{32} a\nu - 4\nu - \frac{40}{3} \nu^2$	1
$\frac{15}{2} e + \frac{33}{2} e\nu$	2

$\Delta\varepsilon = \pi\varepsilon_{32} x$

Coefficient	L_o (cos)
$\frac{5}{2} + 7\nu + \frac{23}{2} \nu^2 \frac{15}{2} e^2 - 6a(1+2\nu)$	0
$-\frac{33}{16} ae + 46 e\nu + 12e$	1
$-\frac{27}{2} e^2$	2

where $L_0 = f_0 + 2e\nu \sin f_0 + \ldots\ldots$

The column headed 'Coefficient" contains the coefficient of the sine or cosine term, while the other column contains the coefficients of the arguments of the cosine or sine terms given at the top of the column. For example, the second term in Δe is

$$\pi\varepsilon_{32}\left(- \frac{15}{2} e - \frac{33}{2} e\nu \right) \sin 2 L_0$$

The loss of accuracy incurred when the two nearly equal quantities $1/\Delta^3$ and $1/r_1^3$ are subtracted (see Equations (2) and (3)) is avoided by the binomial expansion:

$$\frac{1}{\Delta^3} - \frac{1}{r_1^3} = \frac{\rho}{r_1^3}\left[3 \cos\theta + \frac{3}{2}\rho(5 \cos^2\theta - 1) + \frac{5}{2}\rho^2(7 \cos^3\theta - 3 \cos\theta)\right.$$

$$\left. + \frac{15}{8} \rho^3(1 - 14 \cos^2\theta + 21 \cos^4\theta)\right] \text{, where } \rho = \frac{r}{r_1}$$

For a well-behaved satellite, Δa is very small. The danger, therefore, to the satellite's stability will arise, not from changes, in a, but from changes in the orbital eccentricity e. If e reaches unity, the satellite will escape or collide with its planet, in the practical case of a finite-sized planet.

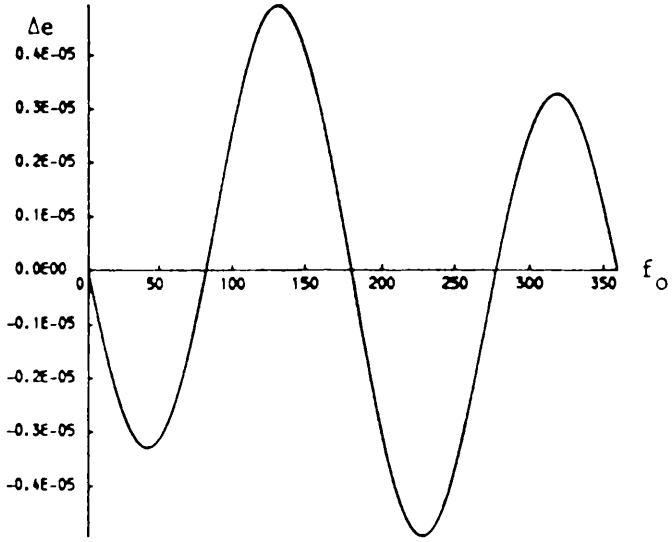

Figure 2: The variation in the change in the satellite's eccentricity Δe over one synodic period for different starting values of the initial conjunction true anomaly f_o, in the case where the Sun is assumed to be moving in a fixed circular orbit. The data used here is that of the Jupiter, Galilean satellite system where $\alpha = 0.0025$, $e = 0.01$ and $\mu_3 = 1{,}100$. Both the numerical and analytical solutions for Δe are shown here to lie virtually on the same curve.

We now sample the size of Δe by repeating the evaluation of Δe for different initial starting values of the conjunction true anomaly f_0. Figure 2 shows the variation in the value of Δe for f_0 values ranging from 0^o to 360^o for both our numerical and analytical solutions. The analytical solution was found to be virtually identical to the numerical solution for typical solar system values of the initial independent parameters α, e and μ_3, the relative differences between the two solutions averaging about 10^{-5}. In particular, Figure 2 shows the results for the Galilean satellites of Jupiter, where α, e and μ_3 are taken to be 0.0025, 0.01, and 1,100 respectively.

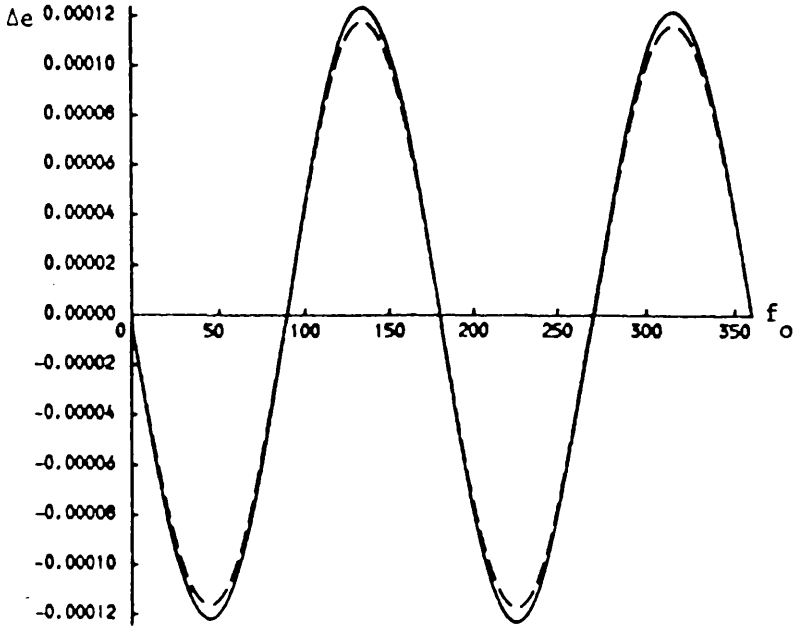

Figure 3: The same parameters, as in Figure 2, are used except that the satellite's eccentricity is now set to e = 0.3. The numerical solution for Δe (dashed curve) is now noticeably different from the analytical solution for Δe (solid curve). At e = 0.3 our analytical solution starts to break down.

Figure 3 shows the variation of Δe as a function of f_0 for the same Jupiter-Galilean satellite system with the exception that now the eccentricity of the satellite's orbit has been increased to e = 0.3. At e = 0.3, we see that the numerical and analytical solutions start to deviate noticeably from each other, having relative differences of about 10^{-2}. Beyond e = 0.3, for typical solar system values for α and μ_3, our analytical solution tends to break down.

Let the maximum size of Δe be Δe_{max}. Through a simple optimization of Δe, we find that the maximum Δe is given by:

Table 2: The Minimum Time needed for solar perturbations to increase a satellite's orbital eccentricity from e_o to e_T.

Planet-Satellite System	α	e	μ_3	e_1	T_s (days)	T_1 (years)	CIRCULAR CASE		ELLIPTICAL CASE	
							T_D (years)	T_c (years)	T_D (years)	T_c (years)
Jupiter-Callisto	0.0025	0.01	1,100	0.05	20	12	4.32×10^2	1.45×10^7	3.72×10^2	Currently being computed
Saturn-Iapetus	0.0025	0.03	3,500	0.06	20	30	9.25×10^1	2.25×10^6	7.73×10^1	
Uranus-Umbriel	0.0003	0.004	23,000	0.05	5	84	3.95×10^3	3.35×10^{10}	3.41×10^3	

$$\Delta e_{max} = \pi \varepsilon_{32} (A_1 - 2A_2 \cos L_o) \sin L_o$$

where

$$\cos L_o = \frac{A_1 - \sqrt{A_1^2 + 32A_2^2}}{8A_2}, \quad \sin L_o = \sqrt{\frac{1}{2} - \frac{A_1}{4A_2} \cos L_o}$$

and where

$$A_1 = \frac{15}{8} a - \frac{39}{32} a\nu + 4\nu + \frac{40}{3} \nu^2, \quad A_2 = \frac{15}{2} e + \frac{33}{2} e\nu$$

Depending on the values of α, e and μ_3 used, $L_0 \approx f_0$ is typically about 135° for $\Delta e \approx \Delta e_{max}$.

Suppose that each successive synodic period adds the Δe_{max} for the current value of e to that current value of e. This supposition is of course ridiculously pessimistic regarding the satellite's projected lifetime in orbit, but gives a first estimate from which to proceed. If our method of calculating Δe is valid for values of e up to $e_T = 0.3$, then the time interval $T_D = NT_S$ can be easily computed, where N is the number of synodic periods needed and T_D is the time taken in order for e to grow from e_0 to e_T under the above pessimistic assumption. Table 2 shows the values of T_D calculated for three separate trial cases in the solar system. For preliminary testing of our method of analysis, values for α, e and μ_3 for the Jupiter, Saturn, Uranus satellite systems have been used which will give the largest Δe_{max} (i.e. we use the largest values of α, e and μ_3) and hence the shortest minimum duration of the planet-satellite system. Thus the initial three trial runs give the calculated minimum durations for all the Galilean satellites, all the satellites of Saturn excluding Phoebe and Hyperion which have highly eccentric orbits and all the satellites of Uranus. Calculations show that for these satellites of Jupiter, Saturn and Uranus, $T_D = NT_S > T_1$, where T_1 is not only the Sun's sidereal period of revolution about the planet, but is also close to the time taken for a conjunction line to make one revolution with respect to the satellite orbit's major axis.

Step 2. Figure 2 shows that as f_0 varies from 0° to 360°, the change in Δe is essentially cyclic. Therefore if the satellite remains in orbit for a length of time T_1 equivalent to f_0 moving through 360 degrees, the net change in e, Δe, will be very much smaller than that computed by the pessimistic summing of the Δe_{max} every synodic period. We define the time T_1 taken for the conjunction line to move through a full cycle of 360 degrees to be the period of a conjunction line cycle. If $T_D > T_1$, we may jump to this next, less pessimistic and more realistic stage of assessment of the minimum time it will take for the eccentricity to increase from e_0 to e_T.

Even if $T_D \sim T_1$ or is less than T_1, there is no guarantee that instability will eventually result. Nevertheless, in this paper we confine our attention to the case $T_D > T_1$.

The analytical theory is now used to map synodic period to synodic period to obtain, for an initial value f_0 of the true anomaly at the first conjunction,

(i) the change of the elements $\Delta\sigma$, where $\sigma = \alpha, e, \tilde{\omega}, \epsilon$ over a complete conjunction line cycle where the revolution is taken with respect to the satellite orbit's major axis,

(ii) the maximum value of e, viz e_{max}, reached within the conjunction line cycle.

Note: If e_{max} exceeds the range of e within which the analytical theory holds, numerical integration of Equations (4) is required during that part of the cycle where e lies outside that range.

It might be thought that we should now choose the f_0 of the first conjunction which gives the largest value of Δe in a conjunction cycle and suppose, in our pessimistic way, that this value of Δe is added onto e every conjunction cycle. This is an unnecessarily pessimistic procedure.

The angle between two consecutive conjunctions is $\phi = n_1 T_s$, so that a conjunction must occur each cycle at an f_0 no more than $\phi/2 = \frac{1}{2} n_1 T_s$ from the pericentre of the satellite's orbit. It is the Δe occurring in a cycle based on a conjunction of true anomaly $f_{0(max)} = \frac{1}{2} \cdot n_1 T_s$ that should be used in the pessimistic summing procedure.

Applying the previous procedure when we summed the Δe_{max} obtained in a single synodic period, but now summing the Δe_{max} change per conjunction cycle, the minimum time $T_c = N' T_1$ it will take for the satellite orbit's eccentricity to grow from e_0 to e_T is computed. It is found that for all major satellites of Jupiter, Saturn and Uranus, $N' >> 1$. Table 2 shows the calculated values of T_c.

By this stage we have effectively applied procedures that have removed the short-period behaviour (i.e. terms with periods in the neighbourhood of the satellite's sidereal period) and also much longer periodic behaviour (terms with periods in the neighbourhood of the Sun's sidereal period). Can we go still further in lengthening the minimum time it will take for the Sun to tear the satellite away from the planet?

Step 3. The Roy-Ovenden mirror theorem states that if a system of point masses moving under their mutual gravitational attractions comes at a particular epoch into a dynamical configuration such that all the relative velocity vectors of the masses are perpendicular to all their corresponding relative radius vectors, then the system's behaviour after that epoch is a mirror image of its behaviour prior to that epoch. Roy and Ovenden (1954) pointed out that in practice only two different kinds of mirror configurations exist. In one configuration, the masses are arranged collinearly, with their velocity vectors perpendicular to the straight line through the masses. In the other configuration, the masses lie in a plane, with their velocity vestors perpendicular to that plane.[1]

---

1. C. Marchal, at a lecture during the proceedings of which this is a record, pointed out that these mirror conditions were known to Poincaré. Though Marchal was unable to give an exact reference, it would seem this is yet another example of the old saying that there are no new discoveries in celestial mechanics, only a failure to read the literature!

In an elliptic orbit, of eccentricity e, the angle γ between the velocity vector $\underset{\sim}{v}$ and the radius vector $\underset{\sim}{r}$ at a true anomaly f is given by

$$\left.\begin{aligned} \sin\gamma &= \frac{1 + e\cos f}{(1 + 2e\cos f + e^2)^{\frac{1}{2}}} \\ \cos\gamma &= \frac{-e\sin f}{(1 + 2e\cos f + e^2)^{\frac{1}{2}}} \end{aligned}\right\} \qquad (5)$$

Obviously γ_{max} occurs when $\cos f = -e$ (i.e. $r = a$).

Also

$$\sin\gamma_{max} = \sqrt{1 - e^2}$$

$$\cos\gamma_{max} = -e$$

Now the angle between two consecutive conjunctions is $\phi = n_1 T_s$ where T_s is the synodic period of the satellite. The maximum angle between the apse line of the satellite's orbit and the first conjunction after it or the last conjunction before it is therefore $\phi/2 = T_s/T_1 \sim \pi n_1/n$ since, for a satellite, $T \sim T_s$.

If we replace γ by $90^\circ + q$ in (5) we have

$$\cos q = \frac{1 + e\cos f}{(1 + 2e\cos f + e^2)^{\frac{1}{2}}}$$

$$\sin q = \frac{e\sin f}{(1 + 2e\cos f + e^2)^{\frac{1}{2}}}$$

where q is the deviation from 90° of the angle between the radius vector and the velocity vector at the true anomaly f. For the conjunctions immediately following or proceeding the pericentre, f is then necessarily small, being given by f_c, where

$$f_c \lesssim \pi\frac{n_1}{n} = \pi\nu .$$

Then for small f_c, $q \sim e\sin f_c \sim e f_c$.

Each time the conjunction line is near the apse line, the system passes through a close approximation to a Roy-Ovenden mirror configuration. Hence whatever has happened to the eccentricity during the first half of a conjunction cycle of duration T_1 must be almost completely reversed in the second half. Now we have seen (Table 2) that for all the major satellites of Jupiter, Saturn and Uranus $T_D = NT_1$ with N being a large number. This means that within the time interval T_D there will occur N conjunction cycles, each cycle of which contains a conjunction occurring near the apse line. Unless the periods of the satellite and the Sun are exactly commensurable, the angle f_c within the period T_D will wander between $-\pi\nu$ and $+\pi\nu$. If N is large, there will be a statistical certainty that a value $f_c \sim \pi\nu/N$ will occur, so that the angle q, the deviation from 90° of the angle between the satellite's velocity vector and radius vector, will be, on at least one occasion when there is a nearest confi-

guration to the apse line, as small as $q \sim e\pi\nu/N$. In fact, an opposition of the Sun and the satellite is just as good as a conjunction as far as a mirror condition is concerned. Likewise a conjunction or opposition near pericentre or apocentre is equally 'useful' in almost reversing completely the perturbations that have been built up by the Sun's gravitational field. Hence we should modify f_c to $\pi\nu/2N$ and thus get

$$q \sim \frac{e\pi\nu}{2N} \quad .$$

If we take typical values of the parameters, say $e = .03$ $\nu = n_1/n = 5 \times 10^{-3}$, $N \sim 40$, then q is no more than 6×10^{-6} rad., or 1.2 arcsec., a deviation from 90^0 so small that the solar perturbations must be almost completely reversed, thus pushing to even longer durations the survival of the satellite in orbit about the planet. Work is in progress to extend the satellite's survival time by this method.

2.2 The elliptic coplanar restricted three-body problem

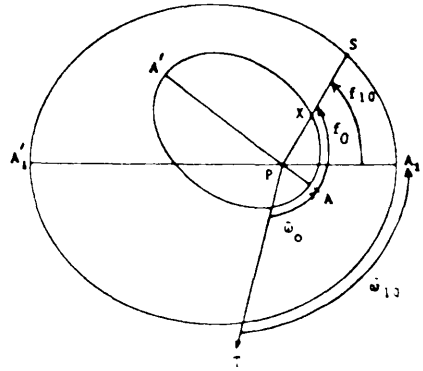

Figure 4: The coplanar elliptical restricted three-body problem where the planet (P)- satellite (X) system is disturbed by the Sun (S), which is assumed to be moving in a fixed elliptical orbit. The initial longitude of the Sun's pericentre $\tilde{\omega}_{10}$ is arbitrarily chosen to be zero, so that PA_1 lies along PT.

In this case the circular orbit of the Sun is replaced by a fixed elliptic orbit centred on the planet (Figure 4). Let the Sun's orbital elements be, in the usual notation, a_1, e_1, $\tilde{\omega}_1$, ε_1. Then we have the usual two-body relations giving the Sun's coordinates and velocity components as functions of these elements and the time t. For example,

$$r_1 = \frac{a_1(1-e_1^2)}{1+e_1\cos f_1} \quad ; \quad V_1^2 = \mu_1\left(\frac{2}{r_1} - \frac{1}{a_1}\right) \quad ; \quad r_1^2 \frac{df_1}{dt} = h_1 = n_1 a_1^2\sqrt{1-e_1^2}$$

and so on. Also, $T_1 = 2\pi/n_1$.

It may be noted in passing that no integral exists for the elliptic coplanar restricted three-body problem, unlike the previous case which possesses the Jacobi integral. We now proceed to follow the steps taken in the circular case.

Step 1. At a conjunction, the true anomalies of the satellite and the Sun are said to be f_0 and f_{10} respectively, while their longitudes of pericentre are $\tilde{\omega}_0$ and $\tilde{\omega}_{10}$ as measured from the direction PT, where T is the vernal equinox. Without loss of generality, since the Sun's orbital major axis if fixed, we can immediately replace PT by PA_1 as the reference direction. This means that $\tilde{\omega}_1 = \tilde{\omega}_{10} = 0$.

Also, at the initial conjunction,

$$f_0 + \tilde{\omega}_0 = f_{10} \quad , \quad \text{or}$$

$$\tilde{\omega}_0 = f_{10} - f_0 .$$

We now have five independent starting parameters, f_0, f_{10}, α,e and ν as opposed to the four parameters f_0,α,e and ν we had in the circular case.

The Lagrange planetary Equations (4), in the form where the independent variable θ is the longitude difference between the radius vectors of the satellite and the Sun are unchanged, but θ is now given by

$$\theta = \ell - \ell_1 = f + \tilde{\omega} - (f_1 + \tilde{\omega}_1) = f - f_1 + \tilde{\omega} .$$

since $\tilde{\omega}_1 = \tilde{\omega}_{10} = 0$.

The expansions giving the net changes $\Delta\sigma$ over one synodic period in the elements $\sigma = a,e,\tilde{\omega},\epsilon$ of the satellite's orbit are now more complicated since the Sun is no longer assumed to be moving in a circular orbit. Nevertheless the $\Delta\sigma$ can be obtained to the desired order of accuracy using the same method as before. The expressions obtained are very long and will not be given in this paper.

This general perturbation theory was tested as before by comparing its results with those given by the numerical integration of the Lagrange's planetary Equations (3). Again we are not concerned with high accuracy. The theoretical integration as compared to the numerical integration remains accurate enough for our purposes, viz. they agree to within an order of five per cent, for all values of e and e_1 up to 0.3.

Then, as before, the maximum value of the net change in e, Δe_{max}, over one synodic period T_s is found from the values of Δe obtained through sample calculations where f_0 and f_{10} are made to range from 0° to 360°. (Figure 5). Figure 5 shows the same variation of Δe with f_0 as in Figures 2 and 3, but for a range of starting initial conjunction true anomalies f_{10} for the Sun where the Sun is assumed to be moving in a fixed elliptical orbit. It is interesting to note that the case where the Sun is assumed to be moving in a fixed circular orbit (as denoted in Figure 5 by the dashed line) is no different from the equivalent elliptical case

but merely falls approximately at the centre of a range of similar curves for the elliptical case.

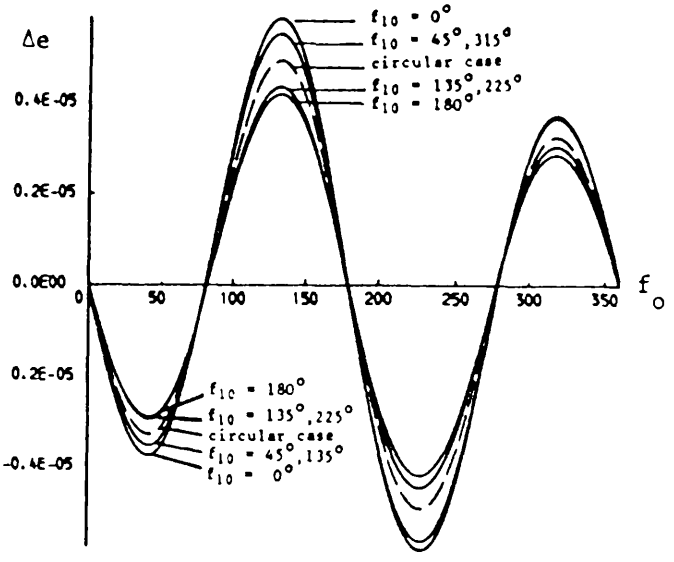

Fgiure 5: The variation in the change in the satellite's eccentricity Δe over one synodic period with the satellite's initial conjunction true anomaly f_0 for given values of the Sun's initial conjunction true anomaly f_{10}, in the case where the Sun is assumed to be moving in a fixed elliptical orbit. The data used here is that of the Jupiter-Galilean satellite system where $\alpha = 0.0025$, $e = 0.01$, $\mu_3 = 1{,}100$ and $e_1 = 0.05$. The dashed curve represents the equivalent case where the Sun is assumed to be moving in a fixed circular orbit. This curve also lies approximately in the same position as the curve for $f_{10} = 90^\circ$, 270° in the elliptical case.

Again, supposing pessimistically that Δe_{max} is added on to the value of e every synodic period and supposing that the change in e because of this addition is taken into account when computing the new value of Δe_{max}, we obtain the minimum time T_D in which the Sun can secularly perturb the satellite's eccentricity from its initial value e_0 to a value e_T taken to be 0.3. It should be noted that T_s is no longer constant but varies about a mean value $\bar{T}_s$.

Again it is found, for all the major satellites of Jupiter, Saturn and Uranus, that $T_D = NT_s$, with $N >> 1$. In particular, $T_D > T_1$ where the Sun's sidereal period T_1 is also approximately the period of revolution of the conjunction line with respect to the satellite's major axis. See Table 2.

Step 2. Since $T_D >> T_1$, we can advance a step further to compute $T_c = N'T_1$. T_c is the minimum time taken by the Sun and N' is the number of the conjunction line cycles needed, to raise the satellite's orbital eccentricity from e_0 to $e_T = 0.3$, if Δe_{max} is now taken to be the net change in e over one cycle of the conjunction line with respect to the

satellite's pericentre. Here, as before, the value of the satellite's true anomaly at the initial conjunction f_0 of the connunction line cycle is taken to be $f_0 = \phi/2 = \frac{1}{2} n_1 T_s$. In choosing Δe's size, we also take, for $f_0 = \frac{1}{2} n_1 T_s$, the maximum value of Δe given by f_{10} in the range $0 < f_{10} < 360^o$, namely $f_{10} = 0^o$. Work is in progress to obtain for the elliptical case, $T_c = N' T_1$ using the method of step 1. As before there appears to be no major differences between the circular and elliptical cases, times T_c of a similar magnitude to those found for the circular case being obtained. Thus, as in the circular case, for the major satellites of Jupiter, Saturn and Uranus, $T_c >> T_1$ which allows us to move on to step 3.

Step 3. At this stage the previous case found in section 2.1 must be modified to include a third step necessitated by the changing angle between the pericentre directions of the satellite's and the Sun's orbits. While the Sun's orbital major axis is fixed, solar perturbations on the satellite cause the satellite's orbital major axis to advance. Let the synodic period of the line of the apses, in other words, the time taken by the satellite's orbital apse line to advance 360^o on the solar orbit's apse line, be $T_{\tilde{\omega}}$. Then

$$T_{\tilde{\omega}} = \frac{2\pi}{\dot{\tilde{\omega}} - \dot{\tilde{\omega}}_1} = \frac{2\pi}{\dot{\tilde{\omega}}} \qquad \text{since } \dot{\tilde{\omega}}_1 = 0$$

We can then write as a rough approximation

$$T_{\tilde{\omega}} = \frac{2\pi\ T_s}{\overline{\Delta\tilde{\omega}}}$$

where $\overline{\Delta\tilde{\omega}}$ is the mean change in $\tilde{\omega}$ over one synodic period of the satellite and is preferably calculated over many conjunction cycles. We expect that, in general,

$$T_s \quad \text{and } T_1 << T_{\tilde{\omega}} << T_c \ .$$

Let $T_{\tilde{\omega}} = MT_1$, where $1 << M << N'$. Then $2N'/M$ is the number of times the two lines of the apses are collinear in the time T_c taken by the Sun to increase the satellite's orbital eccentricity from e_0 to e_T. (Note: The apses are collinear twice in a synodic period of the apses).

Step 4. We now apply the Roy-Ovenden mirror theorem. A perfect mirror configuration would occur if a conjunction or an opposition of the Sun and the satellite occurred with both bodies at pericentre and/or apocentre and the lines of the apses were collinear. This will rarely, if ever, happen.

There will, nevertheless, be occasions when close approaches to mirror configurations take place. Consider an occasion at epoch τ when the apses are collinear. The worst conjunction or opposition for a mirror configuration at this moment would be one that occurred at 90^o from the common apse line. It is obvious that in this case the conjunction or opposition 'spoke' nearest the apses would be occupied by the Sun and

the satellite at a time $t = T/4$ after time τ. By this time the apses would have separated by the small angle $\phi_{\tilde{\omega}}$, given by

$$\phi_{\tilde{\omega}} = \frac{2\pi T_1}{4T_{\tilde{\omega}}} = \frac{\pi}{2}\frac{T_1}{T_{\tilde{\omega}}} .$$

This means there will always be in each apse line cycle a conjunction or opposition within an angle $\phi_{\tilde{\omega}}$ of the apse lines. At that moment, using (7)

$$\sin q \sim e \sin f \sim ef$$

$$q \sim e\,\phi_{\tilde{\omega}} = \frac{\pi e_1 T_1}{2T_{\tilde{\omega}}}$$

But $T_{\tilde{\omega}} = MT_1$, therefore

$$q = \frac{\pi e}{2M} .$$

Now before the Sun can increase the satellite's eccentricity from e_0 to e_T, a time T_c will have elapsed where $T_c = N'T_1$. Unless a hard commensurability exists, therefore, there is a statistical certainty that on at least one occasion in that time, the angle q will be as small as

$$q \sim \frac{\pi e}{2M}\frac{N'}{M} = \frac{\pi e N'}{2M^2}$$

This angle, for the main satellites of Jupiter, Saturn and Uranus, is so small that a very close approach to a mirror configuration is almost certain to occur within a time T_c, resulting in an almost perfect reversal of all solar perturbations. This time of survival of the satellite can then, with confidence, be taken to be very much in excess of the value of T_c computed for that satellite.

A method is now being sought for by the present authors that will use the synodic period of the line of the apses $T_{\tilde{\omega}}$ and the Roy-Ovenden mirror theorem to gain even longer minimum durations for planet-satellite systems under solar perturbations.

3. DISCUSSION AND CONCLUSIONS

In this preliminary account of the application of the finite-time stability criterion method, it is seen that as far as solar perturbations of the major satellites of Jupiter, Saturn and Uranus are concerned the minimum time needed to detach the satellites from their planet is much the same whether the eccentricity of the planet's orbit is taken into account or not.

Preliminary results suggest that the Sun cannot, within the lifetime of the solar system, detach the five major satellites of Uranus from Uranus, even when the eccentricity of Uranus' orbit is included in the problem.

Where the major satellites of Jupiter are concerned, namely Amalthea, Io, Europa, Ganymede and Callisto, the minimum time taken by the Sun to enhance appreciably the eccentricities of their orbits seems to be much longer than any given by previous studies of stability. The minimum duration of Jupiter's satellites is still several orders of magnitude smaller than the age of the solar system, but the present authors hope to lengthen this minimum time appreciably in future work.

In the present paper, the existence of more than one satellite in the satellite system and their effects upon each other has not been taken into account and it would be of some interest, for example, to consider the mediating effects of the Laplace relation on the evolution of the relevant Galilean satellites under solar perturbations.

Saturn's main satellites, Mimas, Enceladus, Tethys, Dione, Rhea, Titan and Iapetus, likewise, seem stable against solar perturbations for millions of years. Again future work may well increase this minimum time.

The Earth's Moon is a complex case and has not been included in the present work, but will hopefully be the subject of a future paper.

It is well-known that the introduction of the eccentricity of the Sun's orbit, by turning the circular restricted coplanar three-body problem into the elliptic restricted coplanar three-body problem, eliminates the possibility of using the Jacobi integral and the resulting solution giving the stability guarantee of a closed Hill surface about the planet. Likewise, in the general three-body problem, the guarantee of $c^2H \leq c^2H_{crit}$ fails for those satellites we have treated, when the solar orbit's eccentricity is taken into account. It would thus appear that the c^2H criterion is far too stringent a test for most of the real cases of interest in the satellite systems and that a more modest search for a simple finite-time stability criterion can produce estimates closer to our beliefs in the long lifetimes in orbit of these objects as supported by planetological studies of their surface histories.

REFERENCES

Bozis, G. (1976). Astrophys. Sp. Sci., 43, 355.
Easton, R. (1971). J. Diff. Eq., 10, 371.
Easton, R. (1975). J. Diff. Eq., 19, 258.
Golubev, V.G. (1968). Doklady Akad. Nauk. SSSR, 180, 308.
Hill, G.W. (1878). Am. J. Math., 1, 129, 245.
Marchal, C. (1971). Astron. Astrophys. 10, 278.
Marchal, C. and Saari, D. (1975). Celest. Mech., 12, 115.
Milani, A. and Nobili, A. (1983a). Celest. Mech., 31, 213.
Milani, A. and Nobili, A. (1983b). Celest. Mech., 31, 241.
Roy, A.E. (1979). Empirical stability criteria in the many-body problem. In V. Szebehely (ed.) Instabilities in Dynamical Systems. Reidel.
Roy, A.E. (1982), The stability of N-body hierarchical dynamical systems In V. Szebehely (ed.), Applications of Modern Dynamics to Celestial Mechanics and Astrodynamics, Reidel.
Roy, A.E. (1983). Asymptotic approach to mirror conditions as a trapping mechanism in N-body hierarchical dynamical systems. In V.V. Markellos and Y. Kozai (eds.).Dynamical Trapping and Evolution in the Solar System. Reidel.
Roy, A.E., Carusi, A., Valsecchi, G. and Walker, I.W. (1984). Astron. Astrophys., 141, 25.
Roy, A.E. amd Ovenden, M.W. (1954). Mon. Not. Roy. Astron. Soc., 114, 232.
Roy, A.E., Walker, I. W. and McDonald, A.J.C. (1985). Studies in the Stability of hierarchical dynamical systems. In V. Szebehely, (ed.) Stability of the Solar System and its Minor Natural and Artificial Bodies. Reidel.
Smale, S. (1970). Invent. Math., 11, 45.
Szebehely, V.G. and Zare, K. (1977). Astron. Astrophys. 58, 145.
Valsecchi, G.B., Carusi, A. and Roy, A.E. (1984). Celest. Mech. 32, 217-230.
Walker, I.W. (1983). Celest. Mech., 29, 149.
Walker, I.W., Emslie, A.G. and Roy, A.E. (1980). Celest. Mech., 22, 371.
Walker, I.W. and Roy, A.E. (1981). Celest. Mech., 24, 195-225.
Walker, I.W. and Roy, A.E. (1983a). Celest. Mech., 29, 117.
Walker, I.W. and Roy, A.E. (1983b). Celest. Mech., 29, 267.
Zare, K. (1976). Celest. Mech., 14, 73.
Zare, K. (1977). Celest. Mech., 16, 35.

Supplementary Material - Paper 2.

(Perozzi, Roy, Steves and Valsecchi, submitted to Celest. Mech. Oct. 1990)

SIGNIFICANT HIGH NUMBER COMMENSURABILITIES IN THE MAIN LUNAR PROBLEM. I: THE SAROS AS A NEAR-PERIODICITY OF THE MOON'S ORBIT

Ettore Perozzi	Telespazio s.p.a. Roma, Italy
Archie E. Roy	University of Glasgow, Scotland
Bonnie A. Steves	Queen Mary and Westfield College University of London, U.K.
Giovanni B. Valsecchi	Istituto di Astrofisica Spaziale Roma, Italy

Abstract

A description is given of certain historically known cycles associated with high-number near commensurabilities among the synodic, anomalistic and nodical lunar months and the anomalistic year. Using eclipse records, the JPL ephemeris and results from three-body numerical integrations, any dynamical configuration of the Earth-Moon-Sun system (within the framework of the main lunar problem) is shown to repeat itself closely after a period of time equal in length to the classical Saros cycle of 18 years and 10 or 11 days. The role played by mirror configurations in reversing solar perturbations on the lunar orbit is examined and it is shown that the Earth-Moon-Sun system moves in a nearly periodic orbit of period equivalent to the Saros. The Saros cycle is therefore the natural averaging period of time by which solar perturbations can be most effectively removed in any search into the long term evolution of the lunar orbit.

Keywords: Moon's Orbit, Saros, Commensurability, Periodic Orbit, Three-Body Problem.

Steves, B.A.: 1990, Finite-Time Stability Criteria for Sun-Perturbed Planetary Satellites, Ph.D. Thesis, University of Glasgow.

Index

1. INTRODUCTION

Several discoveries in ancient times concerning the lunar problem depend upon the almost exact repetition of certain easily observable dynamical configurations. The Metonic cycle ensures that, if a full moon or new moon occurs on a particular date, a full moon or new moon will occur on the same date 19 years later, allowing easy calibration of the lunar phase to the solar calendar. The Saros period of 18 years and 10 (or 11 days depending on the number of leap years in the interval) gives the basic time span for eclipse prediction. Hipparcus (circa 140 B.C.) introduced three additional relationships involving the synodic, anomalistic and nodical (or draconitic) months of the Moon, in an attempt to improve the predictability of events in the Earth-Moon-Sun system. The existence of these cycles depends upon high-number commensurabilities between the mean motions of the Sun and the Moon and the lunar nodical and anomalistic months (see for example Crommelin, 1901; Deslambre, 1817; Mitchell, 1951; Newcomb, 1882).

The interest of the present authors does not, however, lie primarily with the uses made of these cycles for calendar and eclipse predictions, but rather with the dynamical features of the main lunar problem which produce the high order commensurabilities forming the Metonic, Saros and Hipparcus cycles.

Through the use of eclipse records, the relative dynamical geometry of the Earth-Moon-Sun system during eclipses is shown to repeat itself very closely over one Saros period. We then consider the implications of the fact that, although the Saros is a relationship involving mean quantities and therefore "fictitious" bodies, eclipses, which are formed by the real Earth-Moon-Sun system, are still repeated. The closeness of the repetition is surprising considering that the eccentricities of the orbits may cause the Sun and the Moon to be respectively up to ± 2 degrees and 5 degrees from their mean positions.

Discussion is made of a possible mechanism involving mirror configurations, which effectively reverses the solar perturbations acting on the Earth-Moon system over one Saros period. It is then shown, using the refined lunar ephemeris computed at JPL which includes all solar system perturbations, that the dynamical configuration of the Earth-Moon-Sun system at any time, and not just at times of eclipses, is very nearly repeated after one Saros period. Further dynamical characteristics of the Saros cycle are investigated using a numerical integration of the elliptic three-body problem involving the Earth, Moon and Sun.

2. HISTORICALLY KNOWN LUNAR CYCLES

The first lunar cycle of interest, discovered by the Athenian astronomer Meton about 433 BC, was probably already known to the Babylonians, but is referred to today as Meton's Cycle. It depends upon the fact that 235 synodic months of the Moon are almost equal to 19 tropical years. Given that the mean solar tropical year is T_T=365.24220 days, and the lunar synodic month is T_S=29.530589 days, Meton's cycle consists of

$$235\ T_S = 6939.688 \text{ days}; \quad 19\ T_T = 6939.60 \text{ days}$$

The small difference between these two figures (less than two hours), ensures that, if a full moon or new moon occurs on a particular date, full moon or new moon will occur on the same date 19 years later. The existence of the Metonic cycle is related to a high-order commensurability between the mean motions of Sun and Moon. From the Explanatory Supplement to the Astronomical Ephemeris, we have

$$n_S = 0.9856473354\ ^\circ/\text{day}; \qquad n_m = 13.1763965268\ ^\circ/\text{day}$$

where n_S and n_m are the mean motions of Sun and Moon respectively. Then

$$19\ n_m = 250.35154^\circ; \qquad 254\ n_S = 250.35441^\circ,$$

and

$$19\ n_m\ /\ 254\ n_S = 0.9999885$$

The Metonic cycle simplified calendar activities and it was widely used in the medieval calculation of the date of Easter.

The second discovery, the Saros, is attributed to the Babylonians. It is essentially a period of about 6585.32 days, or approximately 18 years and 10 or 11 days, depending on the number of leap years in the interval. The sequence of eclipses occurring within a Saros period is observed to be repeated closely enough for predictions to be surprisingly accurate. In order to show it, we follow the approach described by Roy (1988): in Table 1 are listed the values of the semi-diameters of the Moon and the Sun during eclipses of four different kinds, which recurred approximately every Saros period in the years 1898, 1916, 1934, 1952 and 1970. Data are generated using the JPL ephemeris file.

The eclipses were:

A - a partial eclipse of the Moon
B - a total eclipse of the Sun
C - a partial eclipse of the Moon
D - an annular eclipse of the Sun

The characteristics of each of the four eclipses remain more or less unchanged over the five occasions. From Table 1, we can see that the lunar semi-diameter, which is equivalent to the Moon's geocentric distance, varies only slightly from Saros to Saros. The same is true of the Sun's semi-diameter, even though the ranges within which both lunar and solar semi-diameters can vary are large (Sun 15'.75 - 16'.30; Moon 14'.70 - 16'.73).

If we now look at the full set of relative position and velocity coordinates for the Earth-Moon-Sun system at a particular eclipse epoch and compare these quantities with the corresponding eclipse one Saros period later, we find that, in general, all of them are closely repeated. Specifically, in Table 2, we see that the semi-diameters of the Sun σ_s and the Moon σ_m, the difference between the Sun and the Moon's geocentric longitudes $(\lambda_s - \lambda_m)$ and latitudes $(\beta_s - \beta_m)$, and the daily rates of change of these coordinates, $\dot{\sigma}_s$, $\dot{\sigma}_m$, $(\dot{\lambda}_s - \dot{\lambda}_m)$ and $(\dot{\beta}_s - \dot{\beta}_m)$ return to much the same values after one Saros period. The data in Table 2 describe a partial eclipse of the Moon which occurred on February 10-11, 1952 and recurred one Saros period later on February 21, 1970.

The Babylonians probably discovered the repeatability of eclipses at Saros intervals of time from their eclipse records extending over many centuries. The word "saros" in fact means "repetition" and astronomers since Babylonian times have used the Saros and eclipse records for predicting not only the occurrence of eclipses but also their circumstances.

The near repetition of eclipses is a consequence of the set of high integer near commensurabilities existing between the Moon's synodic, anomalistic and nodical months. Their mean values are:

Synodic (T_S) = 29.530589 days

Anomalistic (T_A) = 27.554551 "

Nodical (T_N) = 27.212220 "

These mean values remain steady over many centuries to within one second even though the actual values of these different months may vary considerably in any one revolution of the Moon,

due to solar perturbations. Then, as is well-known:

$$223\ T_S = 6585.3213 \text{ days}$$

$$239\ T_A = 6585.5375 \text{ "}$$

$$242\ T_N = 6585.3575 \text{ "}$$

This close agreement ensures that the mean geometry of the Earth-Moon-Sun system at the beginning of a Saros is almost exactly repeated at the end. Since there is no commensurability between the mean motions of the Moon and the Sun, the Sun's geocentric radius vector is about ten degrees from its former position. However, it may easily be shown by familiar elementary properties of elliptic orbital motion, that the Sun's radius vector, velocity vector and the angle between them change at most by 1 part in 340 when the solar true anomaly is displaced by 10 degrees.

The close similarity of eclipses separated by a Saros period also means that over any Saros cycle, the perturbations of the Sun on the Earth-Moon system, and in particular the large disturbances in the Moon's semimajor axis, eccentricity and inclination, are almost completely cancelled. The angle between the osculating lunar apse line and the mean one, which can be as large as 20 degrees, is also restored to very near its former value.

Historically, various commentators on the Saros have taken it to refer principally to the commensurability between the synodic month and the nodical month of the Moon. For the purpose of predicting eclipses of the Sun and the Moon, the important factor is the angular distance of the Moon from its nodes at new or full moon. When the Moon's centre is not within 42 arc minutes of the ecliptic, even a partial eclipse is not possible. Thus, even if the anomalistic month was not commensurable with the nodical or synodic months in the Saros interval, eclipse prediction would still be possible. However, the existence of the two additional commensurabilities, only one of which is really independent of the others, ensures that the prediction of the characteristics of the eclipse is also possible.

A commensurability between the synodic month and the solar year allows the prediction of the calendar date at which the Moon's phase and also the Sun's angular diameter are repeated. Eclipses can be predicted when a commensurability exists between the nodical month and the synodic month. If the commensurabity is between synodic and anomalistic months, the phase and angular diameter of the moon are repeated. If exact commensurabilities existed between the length of the year and the lengths of all

three types of months, the same type of eclipse would be repeated on the same calendar date. No such cycle is known (see Table 3).

Various searches have been carried out in the past for more accurate eclipse predicting cycles, which do not necessarily include a commensurability with the anomalistic month. Table 3 contains a summary of historically known lunar cycles. Their names/authors and lengths (in years) are listed in the first section of the table. In order to identify commensurabilities, the cycle length is then taken to be an integral multiple of the synodic month T_S. These integers are given in the column headed T_S. Under T_N (the nodical month) and T_A (the anomalistic month) are given the numbers obtained by dividing the cycle length by T_N and T_A respectively. The proximity of these numbers to integer values is what has led to the recognition of these cycles. The last section of the table gives a synoptic view of the repeatability of observarble events associated with each cycle. More details on this subject can be found in Steves (1990).

3. PERTURBATION REVERSAL BY MIRROR CONFIGURATIONS

We now consider the basic mechanism by which solar perturbations on the Earth-Moon system are largely reversed in a period of one Saros to such an extent that no matter what the dynamical geometry is at any epoch, one Saros later it is very nearly repeated.

It is well-known that if a system of n gravitating point masses ($n \geq 2$) enters a configuration where every radius vector from the centre of mass of the system is perpendicular to every velocity vector, then the behaviour of each body after that epoch will be a mirror repetition of its history before it (Roy and Ovenden 1954). There are two and only two types of configurations possible, one where the bodies are collinear with all their velocity vectors perpendicular to that line, and the other where the bodies occupy a plane with the velocity vectors perpendicular to that plane. A corollary to the mirror theorem states that if a dynamical system passes through two mirror configurations then the system is periodic, its period being twice the time interval between the two mirror configurations.

An isolated mirror configuration event does not guarantee that the system is anywhere near a periodic orbit (e.g. hyperbolic and parabolic orbits). If a second near mirror configuration occurs then by the mirror theorem it would produce a return to the neigbourhood of the first and the system would move for some time along a quasi-periodic orbit. The duration of this orbit would be a function of the departure of the bodies' configuration from exact mirror events.

The Saros has been known to exist for some 2500 years, that is, the relative geometry of the Earth, Moon and Sun is known to have repeated itself closely some 140 times at least. It would therefore appear that there must exist in each Saros a minimum of two near mirror configurations in order that such repetitions should take place.

Consider first the hypothetical case of a perfect Saros where the Earth, Moon and Sun are in a periodic orbit, the Sun's geocentric orbit being circular. Let the period be T_{saros}=6585.3213 days and let the mean synodic, anomalistic and nodical months T_S, T_A and T_A be such that

$$223\ T_S = 239\ T_A = 242\ T_N = 6585.3213 \text{ days} = T_{saros}$$

Let the Sun S, Moon M and Earth E be collinear at new moon, with the Moon at perigee, the lunar orbit's line of nodes also being collinear with the line SME, the ascending node Ω lying in the direction SEΩ (figure 1a). Then at that moment the mutual velocities in the system are perpendicular to the line SME producing a perfect mirror configuration.

Now consider the situation at an epoch T/2 later, when 111.5 T_S, 119.5 T_A, 121 T_N months will have elapsed. The Sun, Moon and Earth are again collinear, though the Moon is now at apogee, it is full moon and the ascending node lies in the direction EΩS (figure 1b). At that moment, the mutual velocities are again at right angles to the line SEM giving a second perfect mirror configuration which will reverse the solar perturbations built up during the first half of the Saros, returning the system at the end of the Saros to a repetition of the mirror configuration that began it.

The Saros however, is not exact and the Sun's geocentric orbit is elliptic. In what follows we consider the observed mean motions of Moon, Sun, lunar perigee and ascending node and show that as far as the Earth-Moon-Sun system's mean behaviour is concerned, any mean configuration of Sun, Moon, lunar apse and node is followed one-half Saros later by a configuration such that if the first is close to a mirror configuration, the second must likewise be.

From the Explanatory Supplement to the Astronomical Ephemeris, pages 98 and 107, we take the following mean motions for the quantities $\mathbb{(}$, A ,Ω , and $\odot$

$$\begin{aligned} \mathbb{(} &= 270.434164^\circ + 13.17639652^\circ\, d \\ A &= 334.329556^\circ + 0.11140408^\circ\, d \\ \Omega &= 259.183275^\circ - 0.05295392^\circ\, d \\ \odot &= 279.696678^\circ + 0.98564733^\circ\, d \end{aligned} \qquad (1)$$

where, $\mathbb{(}$ is the mean longitude of the Moon, measured from the vernal equinox γ to the ascending node N of the lunar orbit and then along the orbital plane to the Moon's mean radius vector, A is the mean longitude of perigee, measured in the same manner as $\mathbb{(}$, Ω is the mean longitude of the ascending node N and $\odot$ is the mean longitude of the Sun. Note that

$$\mathbb{(} = \Omega + \omega + M$$

$$A = \Omega + \omega$$

The quantity d is the number of Julian days elapsed from the epoch JD 2415020.0 or E.T. 1900 January 0.5. Then

$$
\begin{aligned}
(-\odot &= \triangle D = 350.73748^\circ + 12.19074919^\circ\ d \\
(-A &= \triangle A = 296.10461^\circ + 13.06499245^\circ\ d \qquad (2) \\
(-\Omega &= \triangle N = 11.25089^\circ + 13.22935045^\circ\ d
\end{aligned}
$$

In expressions (1) the terms of higher order have been neglected as they are very small for times less than one Saros long.

Consider the values of $\triangle D$, $\triangle A$ and $\triangle N$ at time d and at a time $d+t_1$ where $t_1 = 6585.3213/2 = 3292.6606$ days, that is one-half Saros later. Let the values of $\triangle D$, $\triangle A$ and $\triangle N$ at time d minus the values at time $d-t_1$ be:

$$\delta(\triangle D) = 12.190749 \cdot 3292.6606 \text{ days} = 40139.998^\circ = 179.998^\circ$$

$$\delta(\triangle A) = 43018.587^\circ = 178.587^\circ$$

$$\delta(\triangle N) = 43559.762^\circ = 359.762^\circ$$

Hence if the configuration at time d was at or near to a mirror configuration, lunar major axis collinear with or near to the lunar line of nodes or 90 deg from them, new or full moon at or near to perigee or apogee, a similar configuration must occur one-half Saros later. In Appendix I, we prove that the first mirror configuration will occur before one-half Saros period has passed. Thus, two near mirror configurations will always occur within any interval of one Saros period which implies that the Earth-Moon-Sun dynamical system is moving in a nearly periodic orbit of period equal to one Saros cycle.

4. THE EARTH-MOON SYSTEM AS AN ALMOST PERIODIC ORBIT

If the Earth-Moon system under solar perturbations is close to a periodic orbit of period equal to one Saros, then the near repetition of eclipses is only a special case. Any configuration of Earth, Moon and Sun, after one Saros should be very nearly repeated. A configuration must not only include relative radius vectors but also relative velocity components so that we are essentially considering the dynamical geometry.

In order to test this hypothesis, the following procedure was adopted. An epoch t_1 was chosen randomly, but avoiding the time of a solar or lunar eclipse. Then, using the JPL high-precision numerically integrated planetary and lunar ephemerides (Standish et al, 1976), the relative position and velocity coordinates of the Moon and the Sun are found at this epoch t_1. Specifically, similar to the case described previously where the epoch was taken to be the time of an eclipse, we find the geocentric distance of the Moon r_m, the differences between the Sun and the Moon's geocentric ecliptic longitudes $(\lambda_s-\lambda_m)$ and latitudes $(\beta_s-\beta_m)$ and the daily rates of change of these coordinates $\dot{r}_m$, $(\dot{\lambda}_s-\dot{\lambda}_m)$, $(\dot{\beta}_s-\dot{\beta}_m)$.

We take the value of the Saros period to be approximately T = 6585.3 days and search through the ephemeris within the time interval $t_1 + T \pm 0.5$ days for the time t_2 at which the differences between the relative position and velocity coordinates of the two epochs t_1 and t_2 are minimized. If the relative dynamical geometry of the Earth-Moon-Sun system is repeated after one Saros period, the results should show that a minimum of the differences in the coordinates at epochs t_1 and t_2 does occur at a time approximately equal to the Saros Period and that these differences are very small.

In order to minimize simultaneously the differences between these six coordinates (we did not consider the Sun's geocentric distance as it would introduce a long-term libration with a period of the order $18 \cdot 360/10 = 650$ years, see also section 2), we choose a goodness of fit expression Q, which consists of:

$$Q = \sqrt{\sum_{i=1}^{6} \left[\frac{X_{2i}-X_{1i}}{\triangle X_{maxi}} \right]^2} \qquad (3)$$

where X_{1i} and X_{2i} are the values for one of the relative coordi-

nates at epochs t_1 and t_2 respectively, and i=1 to 6 represents the six relative coordinates r_m, $(\lambda_s-\lambda_m)$, $(\beta_s-\beta_m)$, $\dot{r}_m$, $(\dot{\lambda}_s-\dot{\lambda}_m)$, $(\dot{\beta}_s-\dot{\beta}_m)$ specifying the relative dynamical geometry of the Earth-Moon-Sun system at any given time. The quantity $\triangle X_{maxi}$ is the maximum possible difference between any two values of a given coordinate. We use the the relative discrepancy between the coordinates at epochs t_1 and t_2 (i.e. we normalize each term of eq. (3)) in order to remove the problem of giving more weight in the summation to the larger valued coordinates. For example, the maximum possible difference between two values of r_m is the radial distance at apocentre minus the radial distance at pericentre: $\triangle r_{max} = 2ae$.

We then search through the ephemeris for the time t_2 near t_1+T which minimizes Q. Once it is found, we define the quantity $T^*=t_2-t_1$ as the "osculating" value of the Saros period for that particular epoch t_1. This procedure is repeated for values of t_1 which span two Saros periods, from 1952 to 1988: in total, one hundred values of t_1 were tested. The results are so similar that we give only a sample set of 5 in Table 4. From it we can see that, irregardless of the initial time chosen, the relative positions and velocities of the Moon and the Sun are best repeated after an interval of time close to the classical Saros period, i.e. $T^*\approx T_{saros}=223\ T_S$. The accuracy of the repetition can be deduced from the last two columns of Table 4, where are listed the values of Q which minimized expression (3) and the percentage relative discrepancy P (obtained by dividing Q by the total number of coordinates taken into consideration). From these data it can be stated that, on average, a given relative coordinate of the Earth-Moon-Sun system is repeated approximately one Saros period later to within about 0.5%.

The actual 100 osculating Saros periods found as a function of their starting epoch t_1 are plotted in Fig.2a. They appear rather regularily distributed around the Saros period computed directly from the synodic month: $223\ T_S = 6585.321$ (indicated in Fig.2a by a solid line). In fact the average value of the sample is 6585.320 days, with a standard deviation of 0.03 days.

Traditionally the Saros period is taken to be 6585.321 days, which involves only the synodic month. By adopting the idea of a goodness of fit expression Q to find numerically the Saros period, we have changed its definition (the time interval which minimizes Q); however, the average Saros period found in this manner is remarkably close to the traditional result. This suggests that the synodic month plays the dominant role in driving the system towards the repetition of any particular configuration.

Generally, we can conclude that the relative dynamical geometry of the Earth-Moon-Sun system over one Saros period is repeated at any osculating phase of the period, not just in the mean geometry reference frame, nor at the occurrence of certain particular events (e.g. eclipses). In other words, the perturbations of the Sun on the Earth-Moon system, particularly the large disturbances in the Moon's semimajor axis, eccentricity and inclination, are almost completely cancelled out over a Saros, no matter where it is taken to start. This suggests that the Saros period could have relevance to any question of the stability of the Earth-Moon system against solar perurbations.

5. THE SAROS CYCLE INVESTIGATED BY NUMERICAL INTEGRATION OF THE RESTRICTED ELLIPTIC 3-BODY PROBLEM

Although the rates of change of the perigee and node longitudes of the Moon, whose values play an essential role in the Saros, are affected by many perturbations, by far the largest of these is that due to the Sun (see e.g. Roy (1981), Table 9.2). We can therefore expect to be able to study the main characteristics of lunar cycles like the Saros by just integrating the Moon's motion in the simplified model of the elliptic restricted 3-body problem.

To this purpose we set up a system consisting of the Sun, the Earth moving on a fixed keplerian ellipse with its mass augmented by that of the real Moon, and a massless Moon perturbed by the two former bodies. Initial conditions were taken from the JPL Ephemeris DE-118, and are the positions and velocities of the Earth and Moon at JD 2434000.5. The equations of motion were integrated in cartesian coordinates using the RADAU integrator (Everhart, 1985) to 15th order, on a fast Personal Computer, in order to compute the geocentric elements of the Moon, and its elongation (i.e. the angle Moon-Earth-Sun), over a time interval of about two Saros. The data so collected were then used to form Figures 2b to 4, which illustrate many aspects of the lunar orbit and the Saros.

Figure 2b was obtained using the same procedure as for Figure 2a, but using, instead of the JPL Ephemeris, the data coming from the numerical integration. As can be seen, the average period of the Saros in this case is slightly larger than that of Figure 2a. The reason for this is that the starting position and velocity of the Earth chosen for the integration give an osculating semimajor axis of 0.9997067 AU, instead of the mean value 1 AU. Because the smaller value of the semimajor axis is then used as the semimajor axis of the fixed ellipse of the restricted problem, we must use Delaunay's formulae (Delaunay, 1872) to recompute the synodic month corresponding to this Earth-Moon-Sun system, and take as the new length of the Saros 223 of these synodic months. Performing this computation, and taking into account the different value of the osculating eccentricity of the Earth at the starting date (a minor correction compared to that of the semimajor axis), we get 6585.511 days for the length of the Saros. This value is in agreement with the data in the Figure as their mean value is now 6585.537 ± 0.03 days.

As a check, we have carried out another integration, which begins with the JPL Ephemeris osculating elements corresponding to JD 2433000.5, a date in which the semimajor axis of the Earth was 1.0005252 AU. The data are illustrated in Figure 2c. Delau-

nay's formulae give 6584.901 days as the new length of the Saros, a value which is again in good agreement with the mean value of T^* actually found (6584.850 ± 0.045 days).

Having ascertained that our three-body integration reproduces the Saros cycle reasonably well over the time span covered, thus confirming that basically it is a three-body phenomenon, we can then use the results of the integration to illustrate some major features of the system. Figures 3a to 3e show the degree to which the lunar orbital parameters repeat themselves after one Saros cycle. The graphs have been constructed by superposing each parameter in turn, i.e. the semimajor axis, eccentricity, argument of perigee and longitude of node, using a time delay of one Saros, where the Saros period is taken to be the appropriate one computed from Delaunay's formulae, as explained above. In Figure 3, all the orbital parameters, with the notable exception of the longitude of the node, are well reproduced after an interval of time of one Saros. The longitude of the node behaves differently because its revolution period is, as is well known, 18.6 years, slightly larger than that of the Saros cycle. On the other hand, this only means that eclipses taking place one Saros apart in time will take place with the three-bodies aligned in two different directions with respect to a fixed reference frame. All the other characteristics of the Earth-Moon-Sun configuration are repeated.

We have seen in previous sections that good approximations to mirror configurations can be expected to occur in the Earth-Moon-Sun system, leading to the repetition of the orbital elements shown in Figure 3. Examples of such near mirror configurations can be found rather easily in the integration data. One of them is illustrated in Figure 4a,b. There, in the same style as in Figure 3 (i.e. superposing them after a time delay corresponding to one Saros) are plotted the Moon-Earth-Sun angle, the Moon's true anomaly, and the argument of perigee of the Moon centered at a date corresponding to a near mirror configuration with the three bodies on the same line, and with the Moon at perigee. Note that Figure 3, with its closely repeating orbital elements, has been constructed by centering its time axis on the near mirror of Figure 4.

In connection with the problem of the frequency of occurrency of near mirror configurations, Figure 5 shows the behaviour, again in the style of Figure 3, of the argument of perigee of the Moon when it passes through zero. As one can see, its motion is given essentially by the superposition of three terms: an overall secular rotation with period equal to one third of the Saros length, and two oscillations superimposed on it, which are easily recognized as the well known evection cycles of periods 31.81 days and 205.84 days (these values are computed using again the appropriate Delaunay's formulae). We note that the repeatability of the lunar orbital elements after one Saros, and in particular

that of the argument of perigee illustrated in Figure 5, implies that the two oscillations superimposed on the secular rotation, both due to the evection, must have a mean period that is an almost exact sub-multiple of the Saros period, a fact that has apparently escaped attention in the past. The two evection cycles, in fact, are contained in one Saros almost xactly 207 times (the shortest one) and 32 times (the longest).

An interesting feature of Figure 5 is that any horizontal line intercepts the argument of perigee plot in more than one point; actually the number of interceptions is about ten times more than that. See, for example, in Figure 3, where the argument of perigee passes through zero degrees thirteen times in about 200 days. The consequence of this behaviour is that it is about ten times easier to find a near mirror configuration to within a certain residual angle than it would be if the osculating argument of perigee did not show this large wobbling about its mean value, as was assumed for the worst case analysis of Appendix I.

6. CONCLUSIONS

It has been shown, using the JPL ephemeris and numerical integrations of the elliptic restricted three-body problem, that the existence of the Saros implies a near repetition of the orbital elements in the main lunar problem not only at eclipses, but at any other time during the Saros. It would therefore appear that the Moon moves in a nearly periodic orbit of period equivalent to the Saros and that the Saros is the natural period of time for averaging solar perturbations in any study of the evolution of the Moon's orbit.

It is well-known that the Moon has no analytical guarantee of Hill-type stability against solar perturbations, and so the existence of the Saros mechanism in reversing so efficiently solar perturbations can have consequences with respect to lunar stability.

The numerical integration of the elliptic restricted three-body problem reproduces the Saros phenomenon, showing it to be basically a three-body mechanism. The occurrence of near mirror configurations during the Saros cycle is the mechanism which produces a return to the initial conditions for all parameters, except the longitude of nodes which is shifted by a constant amount. This last fact suggests that if the orbit of the Sun around the Earth is taken to be circular, there should exist a periodic orbit of period one Saros. Preliminary computations indicate that indeed this is the case and it will be the subject of a future paper.

ACKNOWLEDGEMENTS

The early developments of this work have been supported by the Osservatorio Astronomico Collurania (Teramo, Italy).

References

Crommelin A.C.D, 1901. "The 29-Year Eclipse Cycle". The Observatory 24, 379.

Delaunay Ch, 1872. "Note Sur le Mouvements du Perigee et du Noeud de la Lune". Comptes rendus hebdomadaires des Seances de l'Academie des Sciences 74 (1), 17.

Deslambre J.B.J., 1817. "Histoire del l'Astronomie Ancienne", II, 144, Paris.

Everhart E. 1985. "An Efficient Integrator That Uses Gauss-Radau Spacings". In 'Dynamics of Comets: their Origin and Evolution', A.Carusi and G.B.Valsecchi eds, D.Reidel, Dordrecht, 185.

Explanatory Supplement to the Astronomical Ephemeris and the American Ephemeris and Nautical Almanac, 1961. H.M.S.O.

Mitchell S.A., 1951. "Eclipses of the Sun" (5th ed.), Columbia University press, New York.

Newcomb S., 1882. "The recurrence of Solar Eclipses". Astron. Papers of the Amer. Ephemeris 1, 7.

Roy A.E., 1983. "Asymptotic Approach to Mirror Conditions as a Trapping Mechanism in N-Body Hierarchical Dynamical Systems". In 'Dynamical Trapping and Evolution in the Solar System', V.V. Markellos and Y. Kozay eds, D. Reidel, Dordrecht, 277.

Roy A.E., 1988. "Orbital Motion" (3rd ed.). Adam Hilger, Bristol and Philadelphia, 282.

Roy A.E. and Ovenden M.W., 1954. Mon. Not. Roy. Astron. Soc. 114, 232.

Standish E.M., Keesey M.S.W., Newhall X.X., 1976. "JPL Development Ephemeris Number 96". NASA Technical Report 32-1603.

Steves B.A. 1990. "Finite-Time Stability Criteria for Sun-Perturbed Planetary Satellites." PhD Thesis.

Appendix I

THE OCCURRENCE A NEAR MIRROR CONFIGURATION IN ANY PERIOD OF LENGTH ONE-HALF OF A SAROS

In Appendix II, it is shown that the Moon's orbital eccentricity is more effective at producing deviations from perfect mirror configurations at conjunctions and oppositions than the Moon's orbital inclination. We therefore assume, to a first approximation, that the Earth-Moon-Sun system is coplanar.

From simple geometrical considerations, the opposition or conjunction nearest the lunar orbital major axis is the most effective one at reversing perturbations and would be completely effective if it occurred on the axis. The worst possible case would therefore be when both conjunction and opposition occur equidistant from the axis. It may be shown that the time interval between the worst case and one where an opposition or conjunction occurs very close to the major axis is less than one half Saros.

Now it is readily seen that approximately every six months, or every seven synodic months, the rotating Earth-Sun line crosses the lunar apse line, i.e. there occurs a mean opposition and conjunction pair straddling the Moon's orbital major axis. The mean angle between consecutive conjunction and opposition of Sun and Moon has a value given by $n_S T_S/2=14.553368°$. Because the Moon's line of apses is moving in the same direction but at a lower mean rate ($\dot{\bar{\omega}}=0.11140408$ °/day, see equations 1), the maximum possible angle spanned in one half synodic month is reduced by a factor $\dot{\bar{\omega}} T_S/2=1.64491°$. Hence, the worst possible case will be one where the opposition occurs at an angle

$$- \phi_A = -(n_S - \dot{\bar{\omega}}) T_S/4 = -6.454235°$$

behind the apse while the following conjunction occurs at an angle ϕ_A ahead of the moving apse line. Every seven synodic months thereafter, the opposition-conjunction pair straddling the apse line moves at a constant rate in such a way that the opposition occurs nearer and nearer to the apse line while the conjunction departs further and further from it. This movement continues until the conjunction which occurs previous to the opposition is now occurring closer to the apse line than the original conjunction and this new conjunction and the old opposition become the new pair which straddle the apse. The pair slip at a rate of

$$\Theta_S = 7\ T_S\ (n_S - \dot{\bar{\omega}}) - \pi = 0.7185°$$

per seven synodic months. Note that the equation giving the slippage rate is quantized in the sense that the formula is only relevant to the opposition-conjunction pair straddling the apse or, in other words, only valid every seven synodic months. In Table 5 this process is illustrated in detail. Table 5a shows the theoretical analysis of the quantitized rate at which the opposition-conjunction pair straddling the apse moves with respect to the apse, while Table 5b gives the equivalent numerical values for the formulae in Table 5a.

The time interval necessary for the opposition in the "worst" case to reach the apse line is then of the order of

$$\frac{\phi_A}{\Theta_S} \quad (7T_S) = 5.084 \text{ years}$$

which is less than one half Saros period. From a geometrical point of view, the best result of the slippage is that the opposition will be exactly aligned with the apse. At worst, two successive positions of the slipping oppositions will straddle the apse, equidistant from it at an angle $\Theta_S/2=0.35922°$. Even in the worst case, the near mirror configuration therefore deviates from a perfect mirror by a q value (see Appendix II) of only 1.185 arc minutes . Thus, not only will a near mirror configuration occur within any half Saros interval, but also the near mirror configuration which does occur will be a very good one.

Appendix II

THE RELEVANCE OF THE LUNAR ECCENTRICITY AND INCLINATION ON THE OCCURRENCE OF MIRROR CONDITIONS

It can be shown that, in the Earth-Moon-Sun system the eccentricity of the Moon's orbit is more important than the lunar inclination in the formation of mirror configurations and that as a first approximation we can therefore neglect the Moon's inclination and study the occurrence of mirror configurations in the simpler coplanar case.

In an elliptic orbit, the angle τ between radius vector and velocity vector is given by (Roy 1983):

$$\sin \tau = \frac{1 + e \cos f}{\sqrt{(1 + e^2 + 2e \cos f)}}$$

$$\cos \tau = \frac{- e \sin f}{\sqrt{(1 + e^2 + 2e \cos f)}} \quad .$$

e being the eccentricity and f the true anomaly. The deviation of the angle τ from 90 deg is then q, where

$$\sin q = \frac{e \sin f}{\sqrt{(1 + e^2 + 2e \cos f)}}$$

$$\cos q = \frac{1 + e \cos f}{\sqrt{(1 + e^2 + 2e \cos f)}}$$

Note that as f tends to zero or π, q tends to zero and that for small e:

$$\sin q \approx e \sin f$$

In an Earth-Moon-Sun eccentric, coplanar system, the largest possible deviation q_{max} from a mirror configuration, when an opposition or conjunction occurs is caused by the larger eccentricity of the Moon's orbit (e=0.055) and occurs when the opposition or conjunction is located at a true anomaly of $f=\pi/2$ or $3\pi/2$. The maximum deviation q_{max} is therefore approximately equal to 3.15 degrees. For a value of f as small as one degree, q=3.3 arc minutes.

Consider now a circular inclined system where two bodies orbit a third in circular orbits with mutual inclination i. Roy (1983) shows that the deviation p from 90 deg of the angle between the velocity vector of one body and the radius vector of the other is given by

$$\sin p = 1/2\ (1-\cos i)\ \sin 2\Gamma$$

when they are each located at an angle Γ measured along their respective orbital planes from their mutual line of nodes.

For a given i, p is a maximum when $\Gamma = \pi/4,\ 3\pi/4,\ 5\pi/4,\ 7\pi/4$ with

$$\sin p_{max} = 1/2\ (1-\cos i)\ .$$

Using the Moon's mean orbital inclination value of 5.15 deg, we find that p_{max} = 0.1156 deg (or 6.95 arc minutes), a value almost 30 times smaller than the maximum deviation q_{max} possible in the eccentric coplanar case. For a value of 1 as small as 1 deg, p=0.24 arc minutes.

Thus it is clear that the moon's orbital eccentricity is more effective at producing deviations from perfect mirror configurations at conjunctions and oppositions than the moon's orbital inclination.

Table 1: REPEATABILITY OF ECLIPSES (I)

Eclipse Type	Year 1898	1916	1934	1952	1970
A	Jan.7	Jan.19	Jan.30	Feb.10-11	Feb.21
Moon	14.867	14.830	14.808	14.788	14.780
Sun	16.265	16.255	16.235	16.207	16.172
B	Jan.21	Feb.3	Feb.13-14	Feb.25	Mar.7
Moon	16.405	16.423	16.455	16.487	16.527
Sun	16.247	16.225	16.193	16.157	16.113
C	Jul.3	Jul.14	Jul.26	Aug.5	Aug.17
Moon	16.722	16.715	16.718	16.720	16.732
Sun	15.731	15.735	15.748	15.770	15.798
D	Jul.18	Jul.29	Aug.10	Aug.20	Aug.31-Sep.1
Moon	14.765	14.733	14.720	14.708	14.710
Sun	15.739	15.755	15.780	15.810	15.847

(a) Semi-diameters are in arc-minutes.

Table 2: REPEATABILITY OF ECLIPSES (II)

Eclipse Date	$\lambda_s-\lambda_m$	$\dot{\lambda}_s-\dot{\lambda}_m$	$\beta_s-\beta_m$	$\dot{\beta}_s-\dot{\beta}_m$
1952 2 11.02729	179.925°	-10.942°	-0.848°	1.091°
1970 2 21.35467	179.919°	-10.917°	-0.863°	1.087°

Eclipse Date	σ_s	$\dot{\sigma}_s$	σ_m	$\dot{\sigma}_m$
1952 2 11.02729	16'12.4"	-0.18"	14'48.1"	3.85"
1970 2 21.35467	16'10.3"	-0.22"	14'46.9"	3.50"

(a) latitude λ and longitude β are in degrees.
(b) semi-diameters are in minutes and seconds of arc.

Table 3: SUMMARY OF HISTORICALLY KNOWN LUNAR CYCLES

Cycle name	length	Commensurability in T_S	T_N	T_A	Repeatability of C_d	E_{ms}	σ_m	σ_s
Meton	19.000	235			Y	-	-	Y
Saros	18.030	223	241.999	238.992	-	Y	Y	Y
Hipparchus	20.294	251		269.000	-	-	Y	-
Crommelin	57.890	716	777.000		-	Y	-	-
Hipparchus	441.291	5458	5922.999		-	Y	-	-
Hipparchus	689.992	8534	9261.062	9146.004	-	Y	Y	Y

(a) Legend: C_d = Calendar date
E_{ms} = Lunar and Solar eclipses
σ_m = Apparent semi-diameter of the Moon
σ_s = Apparent semi-diameter of the Sun
Y = Yes

Table 4: OSCULATING SAROS PERIODS

Saros Period (days)	Beginning / End	r_m (km)	$\dot{r}_m$ (km/day)	$\lambda_S-\lambda_m$ (deg)	$\dot{\lambda}_S-\dot{\lambda}_m$ (deg/day)	$\beta_S-\beta_m$ (deg)	$\dot{\beta}_S-\dot{\beta}_m$ (deg/day)	Q	P %
6585.32696	1952 2 11.02729	403657.9	-1749.7	179.925	-10.942	-0.848	1.091	0.015	0.19
	1970 2 21.35425	404162.9	-1591.9	179.924	-10.916	-0.864	1.087		
6585.32751	1958 10 20.89109	392136.2	4829.7	254.564	-11.633	-4.980	0.401	0.023	0.29
	1976 10 31.21860	391372.4	4877.1	254.561	-11.677	-4.990	0.397		
6585.27911	1964 7 15.63149	390917.8	5398.4	279.984	-11.755	-5.163	0.227	0.032	0.40
	1982 7 26.91061	389942.7	5522.6	279.978	-11.817	-5.184	0.210		
6585.36501	1974 2 4.86549	359560.4	-2023.8	209.769	-13.991	1.620	1.281	0.004	0.05
	1992 2 16.23050	359473.7	-2206.4	209.769	-14.001	1.611	1.282		
6585.36290	1979 10 31.60589	364882.5	-1481.2	229.510	-13.543	1.011	1.272	0.009	0.11
	1997 11 10.96879	364603.2	-1727.4	229.510	-13.559	0.992	1.276		
6585.32358	1988 6 7.71649	370856.4	1595.6	84.094	-13.086	-0.380	-1.234	0.014	0.17
	2006 6 19.04007	370542.8	1308.2	84.093	-13.112	-0.305	-1.237		

(a) The first two rows correspond to the partial lunar eclipse which occurred on 11 Feb. 1952, for comparison with the other epochs which have been chosen far from eclipses.

Table 5: OPPOSITION-CONJUNCTION PAIR STRADDLING MECHANISM

a

Epoch	Longitude of Sun at		Longitude of Apse	Difference in longitude: Conj./Opp. − Apse
	Conjunction	Opposition		
0		$-\frac{1}{4} n_s T_S$	$-\frac{1}{4} \dot{\omega} T_S$	$-\frac{1}{4} T_S (n_s - \dot{\omega})$
$\frac{1}{2} T_S$	$\frac{1}{4} n_s T_S$		$\frac{1}{4} \dot{\omega} T_S$	$\frac{1}{4} T_S (n_s - \dot{\omega})$
$7\ T_S$		$\frac{27}{4} n_s T_S$	$\frac{27}{4} \dot{\omega} T_S$	$\frac{27}{4} T_S (n_s - \dot{\omega}) - \pi$
$\frac{15}{2} T_S$	$\frac{29}{4} n_s T_S$		$\frac{29}{4} \dot{\omega} T_S$	$\frac{29}{4} T_S (n_s - \dot{\omega}) - \pi$
$14\ T_S$		$\frac{55}{4} n_s T_S$	$\frac{55}{4} \dot{\omega} T_S$	$\frac{55}{4} T_S (n_s - \dot{\omega}) - 2\pi$
$\frac{29}{2} T_S$	$\frac{57}{4} n_s T_S$		$\frac{57}{4} \dot{\omega} T_S$	$\frac{57}{4} T_S (n_s - \dot{\omega}) - 2\pi$
'Slippage' per seven synodic periods: $\Theta_s = 7\ T_S (n_s - \dot{\omega}) - \pi$				

b

Epoch	Longitude of Sun at		Longitude of Apse	Difference in longitude: Conj./Opp. − Apse
	Conjunction	Opposition		
0		- 7.27669°	-0.822457°	- 6.454230°
$\frac{1}{2} T_S$	7.27669°		0.822457°	6.454230°
$7\ T_S$		196.47053°	22.206340°	- 5.735802°
$\frac{15}{2} T_S$	211.02391°		23.851259°	7.172657°
$14\ T_S$		400.21776°	45.235136°	- 5.017374°
$\frac{29}{2} T_S$	414.77113°		46.880050°	7.891085°
'Slippage' per seven synodic periods: $\Theta_s = 0.7185°$				

FIGURE CAPTIONS

Fig.1

This diagram shows the geometrical properties of two subsequent collinear mirror configuration events, separated by one-half Saros period, and occurring at conjunction (a) and opposition (b) respectively. The location of the ascending node of the Moon's orbit is indicated by Ω.

Fig.2

The osculating Saros periods T^* found through the numerical procedure described in section 4 are plotted as a function of the starting date t_1, measured in number of years from the partial lunar eclipse which occurred on 11 Feb. 1952 (JD 2434053.5). The time span covers two Saros periods and the horizontal line marks the Saros value computed using the mean synodic month of the Moon ($T_{saros}=223\ T_S$). The three plots differ only in the source orbital data used: a) JPL-DE118 ephemeris; b) numerical integration of the restricted elliptic three-body problem (starting date JD= 2434000.5); c) same as b) but using a different starting date (JD= 2433000.5). In the last two cases, the mean synodic month line has been drawn according to the value of T_S found using Delaunay's Lunar Theory.

Fig.3

Time evolution of the orbital elements of the Moon in the restricted elliptic three-body problem. In order to stress the almost repetition of the orbital paths separated by one Saros period, the origin of time is zeroed at the beginning of each Saros so that the two lines correspond to two subsequent Saros periods. Note that the separation between the lines becomes often undistinguishable.

Fig.4

The occurrence of mirror configurations can be analized monitoring the evolution in time of the Moon-Earth-Sun angle (indicated as $\triangle\lambda$ in the figure), the Moon's true anomaly (f) and its argument of perigee (ω). A perfect collinear mirror configuration occurs when these three quantities are zero at the same time. Plot (b) is an enlarged view of (a).

Fig.5

Long-term behaviour of the lunar argument of perigee: the evection cycles are clearly recognizable; the two lines have the same meaning as in fig.3.

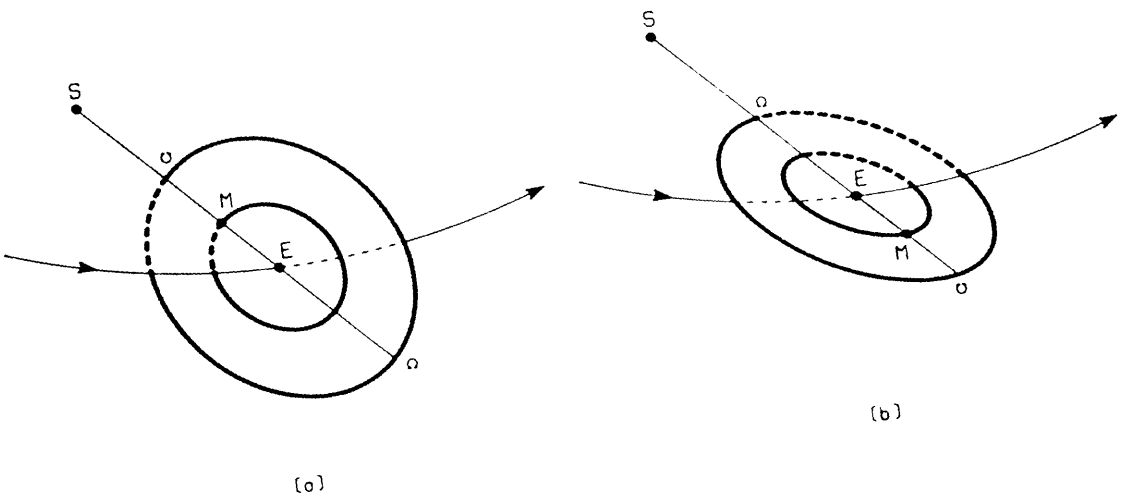

FIGURE 1

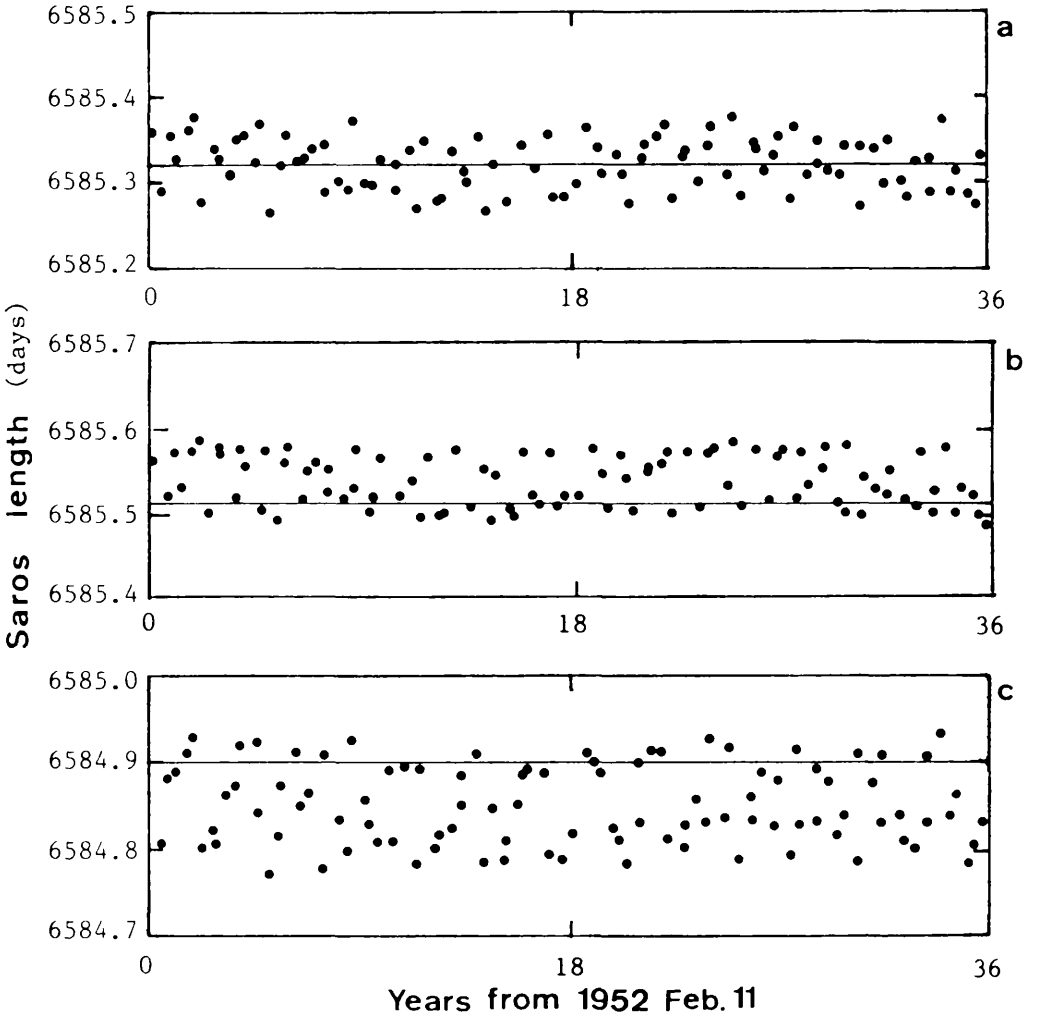
6585.5
6585.4
6585.3
6585.2
a
0
18
36
6585.7
6585.6
6585.5
6585.4
b
0
18
36
6585.0
6584.9
6584.8
6584.7
c
0
18
36
Saros length (days)
Years from 1952 Feb. 11

FIGURE 2

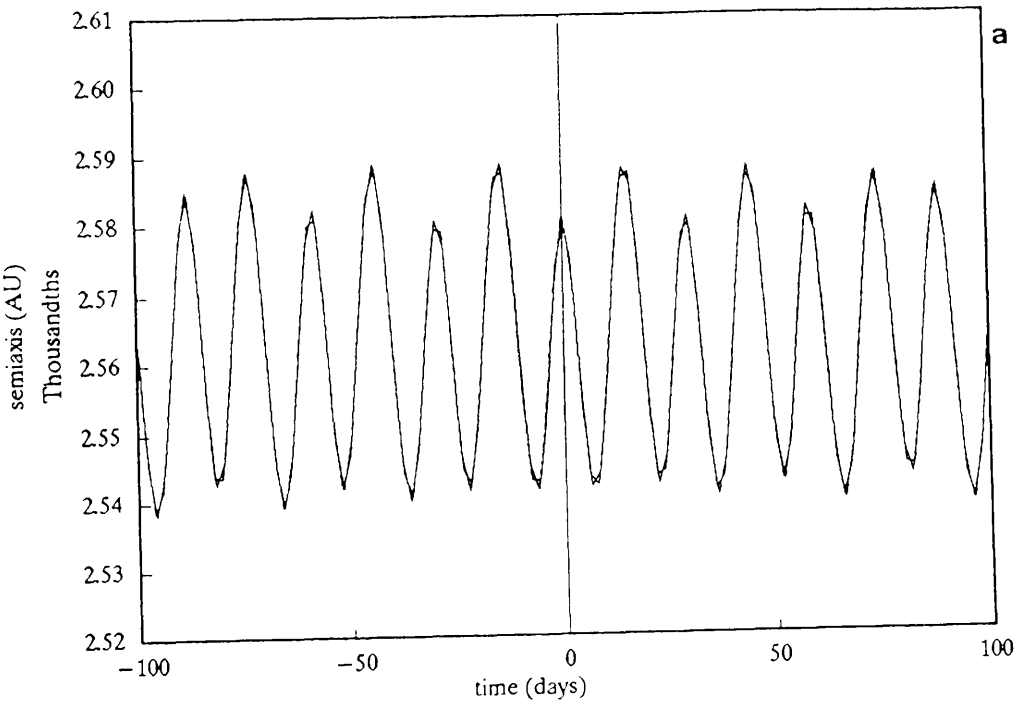
a
2.61
2.60
2.59
2.58
2.57
2.56
2.55
2.54
2.53
2.52
semiaxis (AU)
Thousandths
−100
−50
0
50
100
time (days)

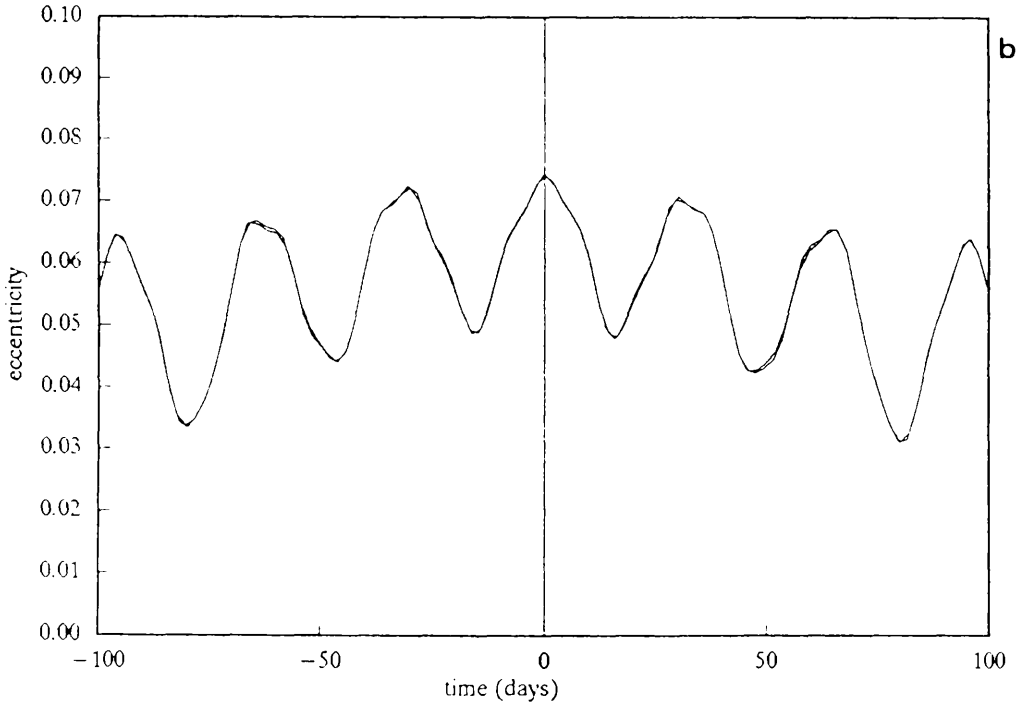
b
0.10
0.09
0.08
0.07
0.06
0.05
0.04
0.03
0.02
0.01
0.00
eccentricity
−100
−50
0
50
100
time (days)

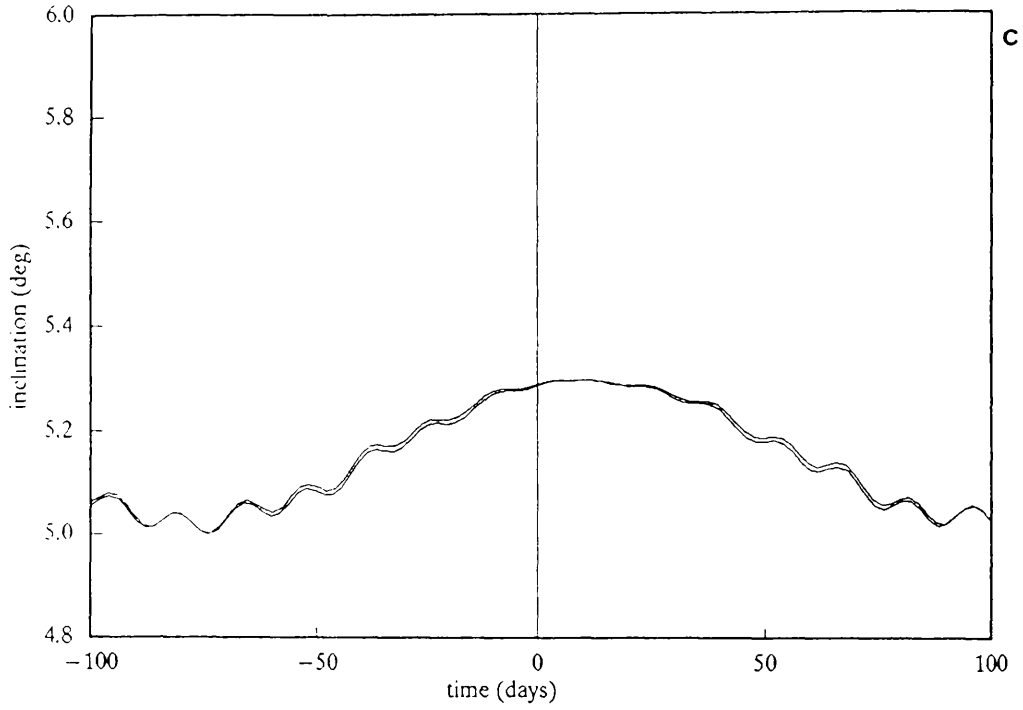
c
6.0
5.8
5.6
5.4
5.2
5.0
4.8
inclination (deg)
−100
−50
0
50
100
time (days)

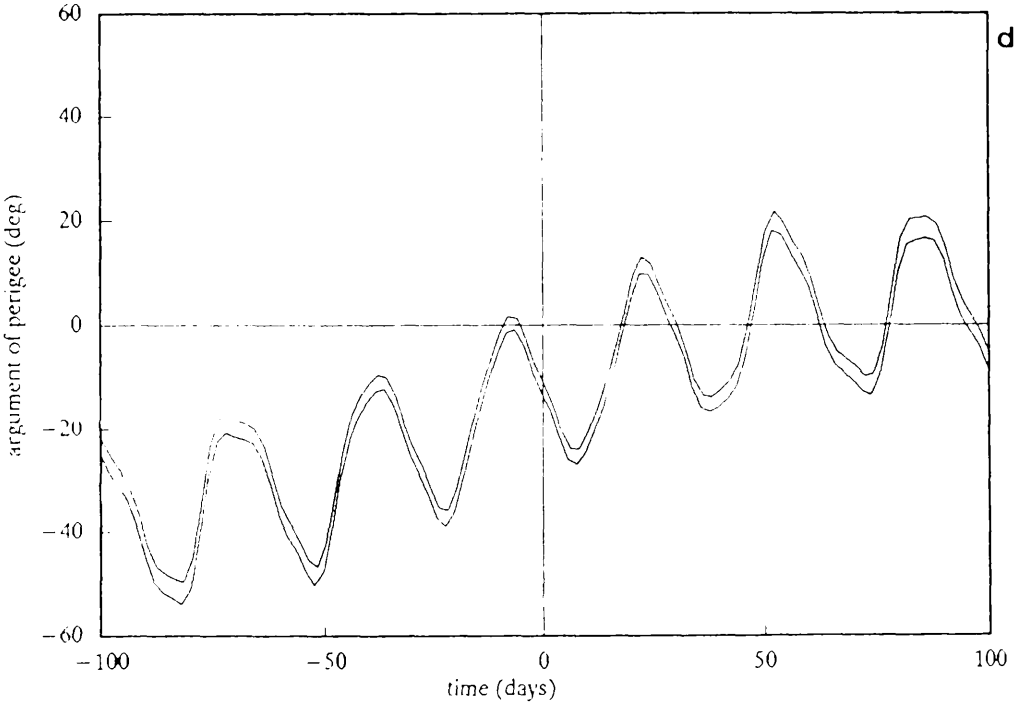
d
60
40
20
0
−20
−40
−60
argument of perigee (deg)
−100
−50
0
50
100
time (days)

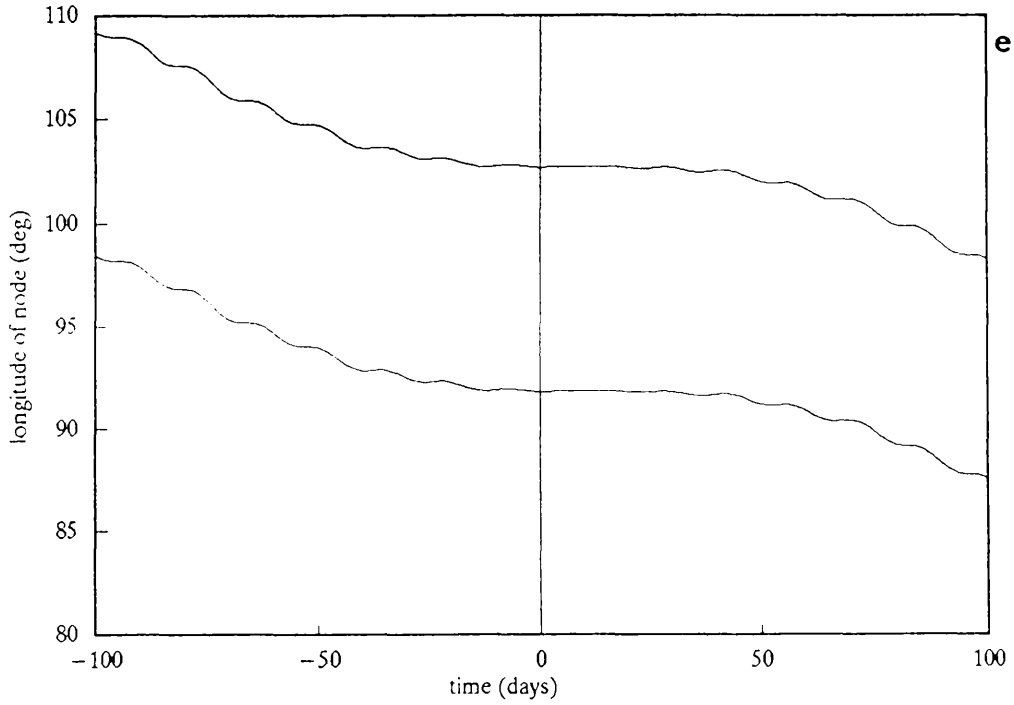
e
110
105
100
95
90
85
80
longitude of node (deg)
−100
−50
0
50
100
time (days)

FIGURE 3 e

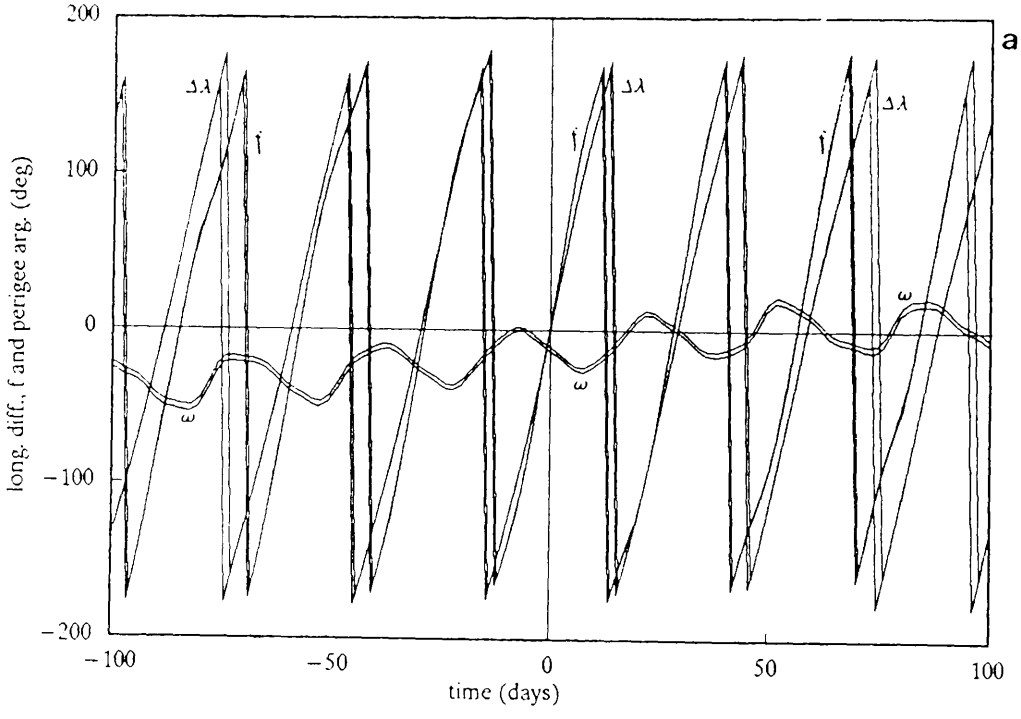
a
200
100
0
−100
−200
−100
−50
0
50
100
time (days)
long. diff., f and perigee arg. (deg)
Δλ
f
ω

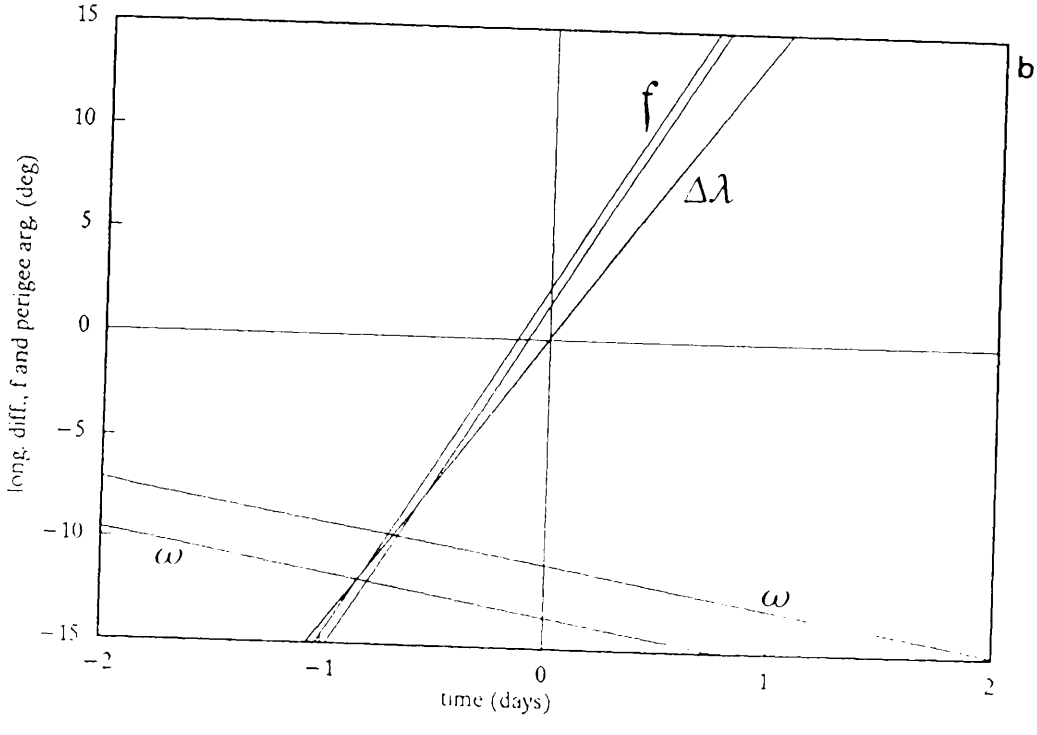
b
15
10
5
0
−5
−10
−15
−2
−1
0
1
2
time (days)
long. diff., f and perigee arg. (deg)
f
Δλ
ω
ω

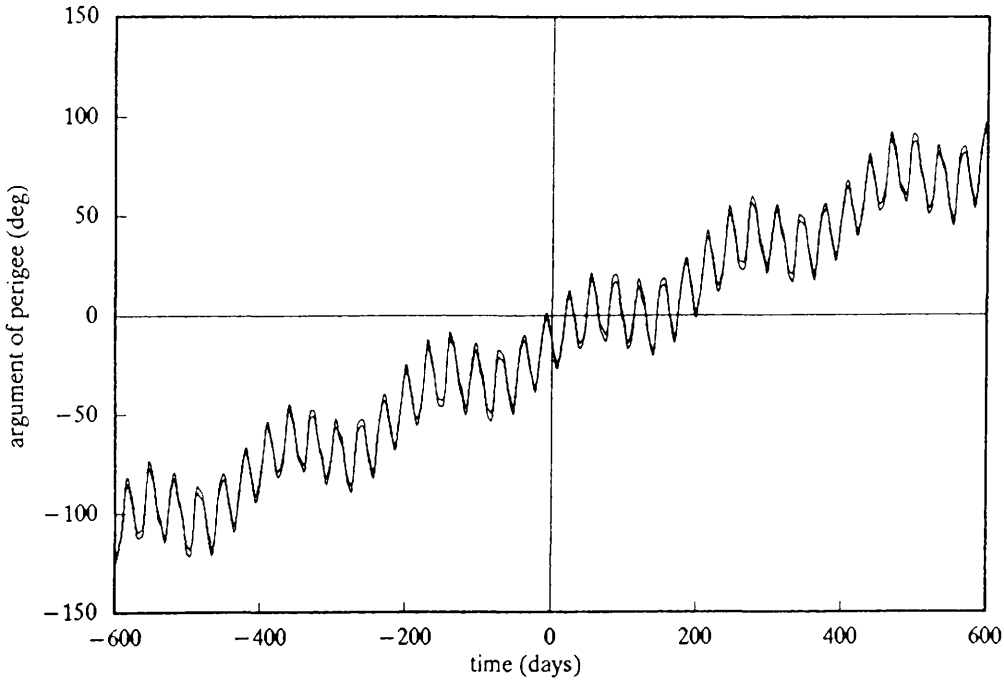
150
100
50
0
−50
−100
−150
argument of perigee (deg)
−600
−400
−200
0
200
400
600
time (days)

FIGURE 5